NASA Reference Publication 1108(02)

1987

Propagation Effects on Satellite Systems at Frequencies Below 10 GHz

A Handbook for Satellite Systems Design

Second Edition

Warren L. Flock

University of Colorado
Boulder, Colorado

National Aeronautics and Space Administration

Scientific and Technical Information Division

Foreword

This Second Edition of the NASA Handbook for Propagation Effects on Satellite Systems at Frequencies Below 10 GHz was prepared by Dr. Warren L. Flock of the Department of Electrical and Computer Engineering of the University of Colorado, under contract to The NASA Jet Propulsion Laboratory. Dr. Flock was also the author of the first edition of the Handbook, NASA Reference Publication 1108, which was published in December 1983 with the same title as this present one.

Both editions of these Handbooks were developed under NASA's Propagation Measurements and Studies Program, which has been involved for two decades in the study of radiowave propagation over earth-space paths. The need for this handbook, as a companion to the earlier handbook for frequencies of 10 - 100 GHz (NASA Reference Publication 1082(03) published in 1983) has become more evident as the eighties have progressed and more and more of the work of the program has been redirected from above 10 GHz to frequencies in the 500 to 2,000 MHz region of the spectrum as interest in mobile-satellite propagation problems has increased.

Dr. Ernest K. Smith, the predecessor of Dr. Faramaz Davarian as Jet Propulsion Laboratory Program Manager, was instrumental in the initial definition and structure of both Handbooks and has coordinated the development and review process.

A second NASA Handbook, published earlier, presents a summary of propagation effects above 10 GHz ("Propagation Effects Handbook for Satellite System Design - A Summary of Propagation Impairments on 10 to 100 GHz Satellite Links with Techniques for System Design", NASA Reference Publication 1082(03), 1983). Together these two documents provide a comprehensive description of propagation factors affecting telecommunications systems involving earth-space links.

A NASA review panel, meeting in September 1986, praised these handbooks and suggested that they be updated every four years, in synchronization with the CCIR cycle. As of this writing about half of the 1986 CCIR Green Books are available, and these include Volume V of Study Group 5, Propagation in Non-ionized Media. This Handbook has been further updated, beyond the originally prepared version of a Second Edition, to better reflect the material of the latest available CCIR Green Books, especially Volume V.

John Kiebler, Manager
Propagation Studies and Measurements Program
NASA Headquarters

PREFACE TO SECOND EDITION

Frequencies below 10 GHz continue to provide a large fraction of satellite service, and new applications, including mobile satellite service and the global positioning system, use frequencies below 10 GHz. As frequency decreases below 10 GHz, attenuation due to precipitation and gases decreases and ionospheric effects increase. Thus the ionosphere, which can be largely neglected above 10 GHz, receives major attention in this handbook. Though attenuation and depolarization due to rain are less severe below 10 GHz than above, they are neverthless still important and constitute another major topic. Emphasis of this handbook is on propagation effects on satellite communications but material that is pertinent to radionavigation and positioning systems and deep-space telecommunications is included as well.

A handbook on propagation effects in the 10-100 GHz range has been prepared under NASA sponsorship* and the present handbook serves a similar purpose for the 100 MHz to 10 GHz range. Much interest is directed at present to frequencies above 10 GHz. The ACTS (Advanced Communications Technology Satellite) program utilizes frequencies near 30 and 20 GHz.

Descriptive background material concerning the various propagation impairments is given in Chapters 1 through 7, and Chapter 9 is devoted to the estimation or calculation of the magnitudes of these effects for use in system design. Link power budget equations and the role of propagation effects in these equations are the subjects of Chapter 10. The final two chapters include some repetition of material presented earlier so that they can be used independently of the earlier chapters to a considerable extent. To avoid excessive duplication, however, references are made in some cases to figures and tables of the earlier chapters. Chapter 8 deals with the complex subject of interference between space and terrestrial systems. Although it draws upon the previous chapters and is pertinent to Chapter 10, the material of Chapter 8 constitutes a distinct and interesting subject of its own.

The handbook is based upon the work of the many investigators cited in the lists of references. Research supported by the Communications and Information Systems Division of the Office of Space Science and Applications of NASA has contributed greatly to knowledge of satellite communications, including the propagation aspects considered here, and is well represented in the reference lists.

I would like to express my appreciation for support and cooperation in the preparation of this handbook to Dr. Ernest K. Smith, RTOP manager at the Jet Propulsion Laboratory while this volume was in preparation, and to Mr. John Kiebler and Dr. Louis J. Ippolito, present and former managers at NASA Headquarters respectively. Also I appreciate the assistance of Dr. Faramaz Davarian, present RTOP manager, Dr. Vahraz Jamnejad, Dr. Arvydas J. Kliore, Mr. Tomas A. Komarek, Mr. Paul Robbins, Dr. Stephen D. Slobin, and Dr. William J. Weber, all with the Jet Propulsion Laboratory, and Mr. Alfred M. Goldman, Jr., formerly with the Laboratory.

In this second edition, updating of the frequency allocations of Chapter 1 has been carried out using information provided by Paul Robbins. Chapter 2 on ionospheric effects received updating but has changed the least. Chapter 3 includes new material on excess range delay and water-vapor radiometers. The subject of modeling of rain attenuation in Chapters 4 and 9 has been updated to include the latest revisions of the CCIR model, and Chu's treatment of depolarization has been featured. The treatment of Rayleigh scattering of Chapter 5 has been reorganized. The material on land-mobile satellite systems in Chapters 6 and 9 has been expanded considerably, and the global positioning system (GPS) is also treated more fully in Chapter 6. Antimultipath techniques and shadowing by trees receive attention in Chapter 6. Noise of terrestrial origin is now treated more adequately in Chapter 7. Chapter 8 on interference has been updated to conform to the latest CCIR treatment. Single sideband systems and spread spectrum systems are topics which have been added to Chapter 10.

*NASA Communications Division, NASA Headquarters, A Propagation Effects Handbook for Satellite Systems Design, A Summary of Propagation Impairments on 10-100 GHz Satellite Links, with Techniques for System Design, Third Edition, June 1983, NASA Reference Publication 1082(03) by L. J. Ippolito, R.D. Kaul, and R.G. Wallace.

TABLE OF CONTENTS

TABLE OF CONTENTS

TABLE OF CONTENTS

INDEX

CHAPTER 1

INTRODUCTION

1.1 PROPAGATION EFFECTS ON SYSTEM PERFORMANCE

1.1.1 Performance of Earth-Space Links

A fundamental requirement for satisfactory satellite communications is the maintenance of a sufficient signal-to-noise ratio. Propagation effects may cause transmission losses which adversely affect this ratio. The received carrier power C on a path of length d is given by

$$C = \frac{P_T G_T A_R}{4\pi d^2 L} \tag{1.1}$$

Here P_T is the power supplied to the transmitting antenna, G_T is the gain of the transmitting antenna, A_R is the effective area of the receiving antenna, and L is a loss factor which includes all losses, including propagation losses, that are not otherwise taken into account. If the losses included in L reduce C to 0.5 of what its value would be in the absence of losses, for example, L would have a value of 2. Transmission losses are commonly specified in terms of the losses exceeded for a certain small percentage, such as 0.01 percent, of a year or worst month.

Equation 1.1 can be converted to

$$C = \frac{P_T G_T G_R}{L_{FS} L} \tag{1.2}$$

where, for the receiving antenna, use has been made of the relation between gain and effective area A_{eff}, namely

$$G = 4\pi A_{eff} / \lambda^2 \tag{1.3}$$

The quantity L_{FS} is the so-called free-space loss and is given by

$$L_{FS} = (4\pi d/\lambda)^2 \tag{1.4}$$

In Eqs. (1.3) and (1.4), λ is wavelength. The noise power X in watts at the receiving antenna terminals is given by

$$X = k\, T_{sys}\, B \tag{1.5}$$

where k is Boltzmann's constant (1.38×10^{-23} J/K), T_{sys} is the system noise temperature (K), and B is bandwidth (Hz). The ratio C/X is given by

$$C/X) = \frac{P_T\, G_T\, G_R}{L_{FS} L k T_{sys} B} = \frac{(EIRP)\, G_R}{L_{FS} L k T_{sys} B} \tag{1.6}$$

where EIRP (effective isotropically radiated power) has been substituted for the product $P_T G_T$. In some cases, however, P_T is taken to be the transmitter or power amplifier output rather than the transmitting antenna input. In that case

$$EIRP = P_T\, G_T \,/\, L_T \tag{1.7}$$

where L_T accounts for losses in switches, filters, cables, or waveguides between the power amplifier and the antenna terminals. The quantity C/X is commonly expressed in dB (decibel) values and then takes the form of

$$(C/X)_{dB} = (EIRP)_{dBW} - (L_{FS})_{dB} - L_{dB} + (G_R/T_{sys}) - k_{dBW} - B_{dB} \tag{1.8}$$

In terminology commonly used, this relation applies to RF (radio-frequency) links and their power budgets. In Eq. (1.8) k is taken to be the product of k as defined above times a 1 K temperature range times a 1 Hz bandwidth so that it has units of dBW (power measured in dB with relation to one watt). Then T_{sys} and B are treated as nondimensional quantities expressed in dB above unity. The L_{FS} value in dB is given by

$$(L_{FS})_{dB} = 10 \log (4\pi d/\lambda)^2 = 20 \log (4\pi d/\lambda) \tag{1.9}$$

The carrier power-to-noise density ratio, C/X_o), where X_o is noise power per Hz , is frequently used. It differs from C/X only by the factor B, representing bandwidth, and is thus given by

$$C/X_o = \frac{(\mathrm{EIRP})\, G_R}{L_{FS} L T_{sys} k} \tag{1.10}$$

Some satellites serve a wide geographical area in which a number of earth stations are located. In such a case the satellite transmitter gain G_T and the corresponding value of EIRP that are used must be the appropriate value. It can not be assumed that the maximum antenna gain, for the center of the main beam, is the value to use. For satellites that are operational or for which antenna designs are available, plots showing contours of constant EIRP may be available (Fig. 10.6). These plots, commonly referred to as footprints, allow selecting the proper value of G_T or EIRP to use.

As the system designer may be required to provide a certain C/X_o ratio over a certain area A_{cov}, it is instructive to show the relation between these parameters and other system parameters. A relation accomplishing this purpose has been supplied by Pritchard (1977) who gives the following expression.

$$A_{cov}\,(C/X_o) \propto P_T A_R / L T_{sys} \tag{1.11}$$

A similar expression involving bandwidth B and C/X is

$$A_{cov}\, B\, (C/X) \propto P_T A_R / L T_{sys} \tag{1.12}$$

Note that these relations show proportionality rather than equality. Pritchard has stressed that Eqs. (1.11) and (1.12) are fundamental to appreciating the essential problems of space communication. They display clearly the roles of L and T_{sys} in determining system performance. L is used here primarily to account for propagation losses but also for pointing error losses, etc. T_{sys} is not strictly a propagation effect but plays a comparable role. A derivation and further discussion of Eq. (1.11) is given in Sec. 10.4.

1.1.2 Determination of Distance and Elevation Angle of Satellite

Satellite orbits are treated analytically by Pratt and Bostian (1986) and Pritchard and Sciulli (1986). A geostationary satellite rotates above the equator with an angular velocity equal to that of the Earth and thus appears stationary with respect to the Earth. We take the altitude of geostationary satellites to be 35,786 km above sea level. Unless an earth station is directly under a satellite, however, the distance d of the satellite will be larger than 35,786 km. The value of d can be established by use of the law of cosines of plane triginometry. Consider first that the earth station is on the same longitude as the subsatellite point at 0 deg of latitude. The subsatellite point is located where a straight line from the satellite to the center of the Earth intersects the Earth's surface. Referrring to Fig. 1.1

$$d^2 = r_o^2 + (h + r_o)^2 - 2\, r_o\, (h + r_0) \cos \theta' \tag{1.13}$$

where θ' is latitude. The equatorial radius of the Earth is 6378.16 km, the polar radius is 6356.78 km, and the mean radius is 6371.16 km (Allen, 1976). To obtain the most accurate value of d, it would be necessary to take into account the departure of the Earth from sphericity, but an approximate value of d can be obtained by taking r_o, the earth radius, to be 6378 km and h, the height of the satellite above the Earth's surface, to be 35,786 km in Eq. (1.13). It may be convenient to divide all terms by $(h + r_o)^2$ or $(42,164)^2$ giving

$$[d/(h + r_o)]^2 = f^2 + 1 - 2f \cos \theta' \tag{1.14}$$

where $f = r_o/(h + r_o) = 0.1513$. Once d is known then all three sides of a triangle are known and the angle ψ can be determined by applying the law of cosines again. The applicable equation is

$$(h + r_o)^2 = d^2 + r_o^2 - 2\, r_o\, d \cos \psi \tag{1.15}$$

The elevation angle θ measured from the horizontal at the earth station is equal to ψ - 90 deg.

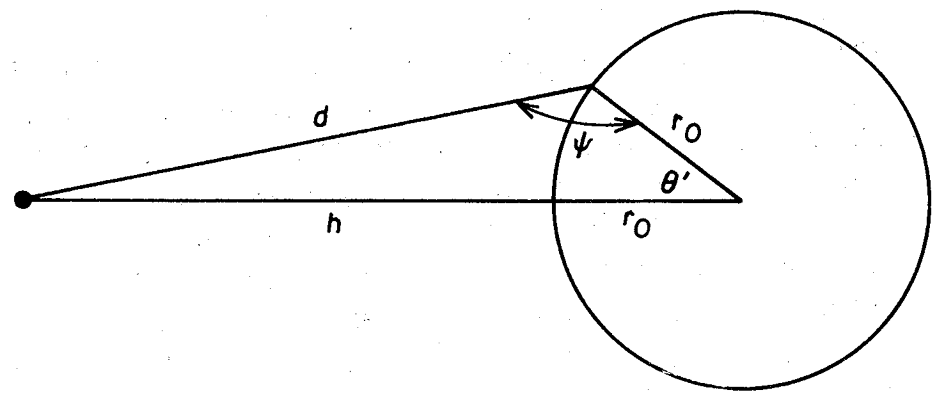

Figure 1.1 Geometry for calculation of distance d of satellite from earth station.

For an earth station not on the same meridian as the subsatellite point, one can use

$$\cos Z = \cos \theta' \cos \phi' \tag{1.16}$$

in Eq. (1.13) in place of $\cos \theta'$ where ϕ' is the difference in longitude between subsatellite point and earth station. Cos Z is the angular distance of a great-circle path for the special case that one of the end points is at 0 deg latitude (Fig. 1.2). Also the expression follows from the "law of cosines for sides" of spherical triginometry (Jordan, 1986). The angle α of Fig. 1.2 for an earth-space path can be determined by using

$$\cos \alpha = \tan \theta' \cot Z \tag{1.17}$$

another relation applying to a right spherical triangle (Jordan, 1986). The angle α is shown in Fig. 1.2a for an earth station located to the east of the subsatellite point. The azimuth angle measured from north in this case would be 180 deg + α. For an earth station location to the west of the subsatellite point as in Fig. 1.2b, the azimuth angle from north is 180 deg - α. As an example, calculations for Boulder, Colorado. latitude 40 deg N, longitude 105 deg W and for Satcom-2, located at 119 deg W, with cos Z = cos 40 deg times cos 14 deg = 0.743, give d = 37,668 km, elevation angle θ = 41.46 deg, and azimuthal angle = 201.2 deg.

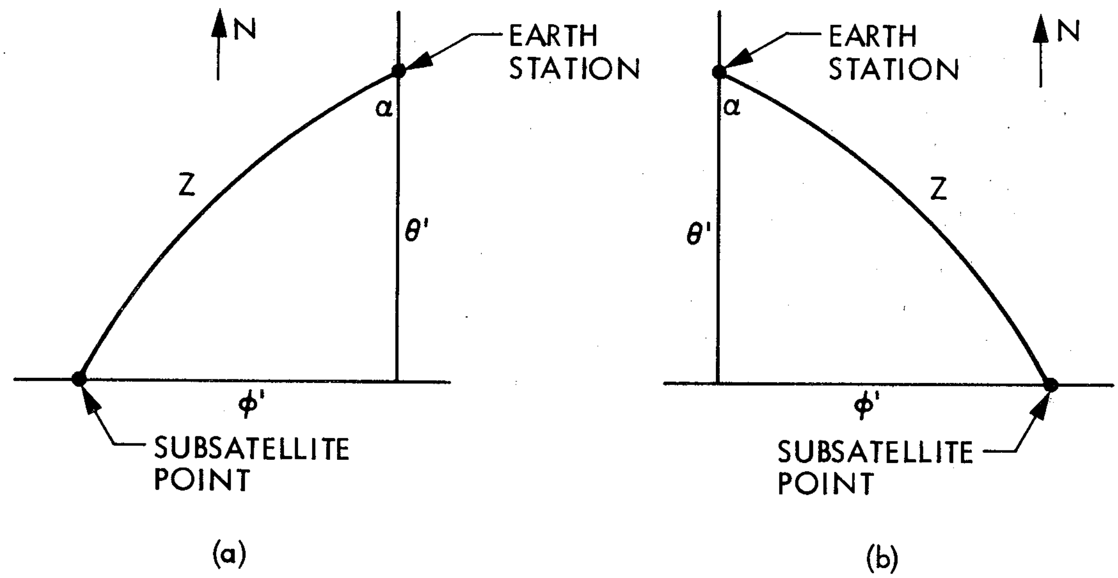

Figure 1.2 Projection of right spherical triangles on Earth's surface.

In Eq. (1.14), r_o was taken as the Earth's equatorial radius, but values of r_o and h can be adjusted for elevations significantly above sea level. Local topography affects the angle of the path above the local horizon and can be taken into account to determine this angle for a particular location. Propagation effects are a function of elevation angle and tend to become more serious with decreasing elevation angle. An elevation angle of 5 deg may be considered to be the minimum elevation angle that should normally be used. The procedure described above for determining distance and elevation and azimuthal angles, essentially the same as that described by Dougherty (1980), is presented as suitable for link analysis and consideration of propagation effects rather than for precise aiming of antennas.

1.13 Propagation and Related Effects

Relatively small margins are utilized for satellite communications, and it is important to use no larger a margin than necessary. Thus it is important to have as accurate information as practical about the propagation factors contributing to L even for the case of effects which might appear to be minor.

Frequencies in roughly the 1 to 4 GHz range tend to be affected only slightly by the Earth's atmosphere, but even in this range it is important to know what the magnitudes of the effects are. Moving to higher frequencies, attenuation and noise due to rain, clouds, and atmospheric gases increase. These effects may become limiting factors above 10 GHz. The ionospheric effects of Faraday rotation, amplitude and phase scintillation, and absorption, on the other hand, become increasingly significant with decreasing frequency.

Depolarization or cross polarization may occur in propagation through the atmosphere or in reflection from terrestrial features. These terms refer to a degradation or change in polarization as from purely vertical linear polarization to linear at an angle slightly different from vertical. This latter polarization is equivalent to a combination of vertical and horizontal polarization. The power converted to the orthogonal polarization may interfere with a channel having that polarization and make less effective the practice of frequency "reuse" (using the same frequency for two orthogonal polarizations in this case). An effect that is important to ranging and navigation systems is the excess range delay, above that encountered in propagation through a vacuum, that is encountered in propagation through the Earth's ionosphere and troposphere.

Electromagnetic radiation emitted by the atmosphere, an important part of sky noise, is not strictly a propagation effect but is closely related and increases when attenuation increases. As is evident from Eqs. (1.11) and (1.12), T_{sys} affects system performance directly. Sky noise contributes to T_{sys}. When using a low noise receiving system, only a slight increase in sky noise may increase T_{sys} significantly. It is important to know T_{sys}, as well as L, as accurately as practical.

A few references of a general nature, concerning either satellite systems or propagation effects, are appropriate for mention here. A comprehensive treatment of satellite communication engineering has been presented by Miya (1981), and Freeman (1981) includes satellite systems, as well as HF radio, line-of-sight terrestrial systems, and troposcatter systems, in his Telecommunication Transmission Handbook. Thompson (1971) prepared an Atmospheric Transmission Handbook covering the range from 3 kHz to 3,000 THz. Recent references on satellite communications have been provided by Feher (1983), Pratt and Bostian (1986), and Pritchard and Sciulli (1986). Hall (1979) presented a summary of tropospheric effects on radio communication, and Ippolito (1986) concentrated on the role of radio wave propagation in satellite communciations. NASA Reference Publication 1082 (Ippolito, Kaul, and Wallace, 1983) treats propagation effects at frequencies above 10 GHz, but many of the concepts and much of the material presented is pertinent to a broader range of frequencies. Evans (1986) has reviewed the development of international satellite communications over the past two decades and considered likely trends in satellite systems as these may evolve with relation to fiber-optic cables.

1.2 FREQUENCY ASSIGNMENTS AND APPLICATION BELOW 10 GHZ

Frequencies below 10 GHz are used for a variety of purposes involving earth-space paths as shown in Table 1.1. The categories of service are actually little different for frequencies above 10 GHz. This handbook treats propagation effects between 100 MHz and 10 GHz, and a listing of frequency allocations for space service in this band is given in Table 1.2. The entries in this table are from the Final Acts of the World Administrative Radio Conference, Geneva, 1979, Volume 1E (ITU, 1982, Revised 1985) for Region 2, which comprises North and South America and portions of the Atlantic and Pacific Oceans. Allocations for Region 1 (Europe, Africa, and Northern Asia) and Region 3 (Southern Asia and the South Pacific, including Australia and New Zealand) are similar but differ in details. The reference includes numerous footnotes giving information about exceptions for particular countries and periods, but information from the footnotes is omitted from Table 1.2 unless otherwise indicated. For brevity we use Uplink and Downlink in place of Earth-to-space and space-to-Earth as in the original publication. Allocations are also given in the Manual of Regulations and Procedures for Federal Radio Frequency Management (NTIA, 1986) and in the FCC Rules and Regulations.

The INTELSAT satellite system uses frequencies near 6 GHz for the uplink and frequencies near 4 GHz for the downlink, and allocations used by INTELSAT are included in Table 1.2 as entries for fixed satellites. Note that a number of space services utilize lower frequencies. Included among these services are space

Table 1.1 Satellite Services (ITU, 1982, Revised 1985)

Aeronautical Mobile Satellite
Aeronautical Radionavigation Satellite
Amateur Satellite
Broadcasting Satellite
Earth Exploration Satellite
Fixed Satellite
Inter Satellite
Land Mobile Satellite
Maritime Mobile Satellite
Maritime Radionavigation Satellite
Meteorological Satellite
Mobile Satellite
Radiodetermination Satellite
Radionavigation Satellite
Space Operations
Standard Frequency and Time Signal Satellite

Table 1.2 Frequency Allocations for Space Services (ITU, 1982, Revised 1985).

Frequency (MHz)	Services
137 - 138	Space Operations and Research (Downlink) Meteorological Satellite (Downlink)
138 - 143.6	Space Research (Downlink)
143.6 - 143.65	Space Research (Downlink)
143.65 - 144	Space Research (Downlink)
144 - 146	Amateur Satellite
149.9 - 150.05	Radionavigation Satellite
267 - 272	Space Operation (Downlink)
272 - 273	Space Operation (Downlink)
322 - 328.6	Radio Astronomy
399.9 - 400.05	Radionavigation Satellite
400.05 - 400.15	Standard Frequency and Time Signal Sat.
400.15 - 401	Meteorological Satellite (Downlink) Space Research and Operation (Downlink)
401 - 402	Space Operation (Downlink) Earth Exploration Satellite (Uplink) Meteorological Satellite (Uplink)
402 -403	Earth Exploration Satellite (Uplink) Meterological Satellite (Uplink)
406 - 406.1	Mobile Satellite (Uplink)
406.1 - 410	Radio Astronomy
460 - 470	Meteorological Satellite (Downlink)
608 -614	Radio Astronomy (Footnote 688) Mobile Satellite (Uplink)
620 -790	Broadcasting Satellite (Footnote 693)

Table 1.2 Frequency Allocations for Space Services (continued).

Frequency (MHz)	Services
806 - 890	Mobile Satellite (Footnotes 699,700,701)
942 - 960	Mobile Satellite (Footnotes 699, 701)
1215 - 1240	Radionavigation Satellite (Downlink)
1240 - 1260	Radionavigation Satellite (Downlink)
1370 - 1400	Space Research (Passive) Earth Exploration Satellite (Footnote 720)
1400 - 1427	Radio Astronomy (1420 MHz H line) Earth Exploration Satellite (Passive) Space Research (Passive)
1427 - 1429	Space Operation (Downlink)
1525 - 1530	Space Operation (Downlink) Earth Exploration Satellite
1530 - 1535	Space Operation (Downlink) Maritime Mob. Sat. (Downlink, Foot. 726) Earth Exploration Satellite
1535 - 1544	Maritime Mobile Satellite (Downlink)
1544 - 1545	Mobile Satellite (Downlink)
1545 - 1559	Aeronautical Mobile Satellite (Downlink)
1559 -1610	Radionavigation Satellite (Downlink)
1626.5 - 1645.5	Maritime Mobile Satellite (Uplink)
1645.5 - 1646.5	Mobile Satellite (Uplink)
1646.5 - 1660	Aeronautical Mobile Satellite (Uplink)
1660 - 1660.5	Aeronautical Mobile Satelllte (Uplink) Radio Astronomy
1660.5 - 1668.4	Radio Astronomy Space Research (Passive)

Table 1.2 Frequency Allocations for Space Services (continued).

Frequency (MHz)	Services
1668.4 - 1670	Radio Astronomy
1670 - 1690	Meteorological Satellite (Downlink)
1690 - 1700	Meteorological Satellite (Downlink)
1700 - 1710	Meteorological Satellite (Downlink)
1718.8 - 1722.2	Radio Astronomy (Footnote 744)
1758 - 1850	Space Operation and Research (Uplink, Footnote 745)
1770 - 1790	Meteorological Satellite (Footnote 746)
2025 - 2110	Space Operation and Research Earth Exploration Satellite (Footnote 747)
2110 - 2120	Space Research (Deep Space Uplink) (Footnote 748) Space Research and Operation (Uplink) (Until 31 Dec. 1990, Footnote 749)
2200 - 2290	Space Research and Operation Earth Exploration Satellite (Footnote 750)
2290 - 2300	Space Research (Deep Space Downlink)
2500 - 2535	Mobile Satellite (Downlink, Footnote 754)
2500 - 2655	Fixed Satellite (Downlink) Broadcasting Satellite
2655 - 2690	Fixed Satellite (Downlink and Uplink) Broadcasting Satellite Earth Exploration Satellite (Passive) Radio Astronomy and Space Research
2690 - 2700	Earth Exploration Satellite (Passive) Radio Astronomy and Space Research
3400 -3500	Fixed Satellite (Downlink)

Table 1.2 Frequency Allocations for Space Services (continued).

Frequency (MHz)	Services
3500 - 3700	Fixed Satellite (Downlink)
3700 - 4200	Fixed Satellite (Downlink)
4202	Standard Frequency and Time (Downlink) (Footnote 791)
4500 - 4800	Fixed Satellite (Downlink)
4800 - 4900	Radio Astronomy
4990 - 5000	Radio Astronomy Space Research (Passive)
5250 - 5255	Space Research
5650 - 5725	Space Research (Deep Space)
5725 - 5850	Fixed Satellite (Uplink)
5830 - 5850	Amateur Satellite (Downlink) (Footnote 808)
5850 - 5925	Fixed Satellite (Uplink)
5925 - 7025	Fixed Satellite (Uplink)
6427	Standard Frequency and Time (Uplink) (Footnote 791)
7125 - 7155	Space Operation (Uplink, Footnote 810)
7145 - 7190	Space Research (Deep Space Downlink) (Footnote 811)
7250 -7300	Fixed Satellite (Downlink) Mobile Satellite (Downlink)
7300 - 7450	Fixed Satellite (Downlink) Mobile Satellite (Downlink)
7450 - 7550	Fixed Satellite (Downlink) Meteorological Satellite (Downlink) Mobile Satellite (Downlink)

Table 1.2 Frequency Allocations for Space Service (continued).

Frequency (MHz)	Services
7550 - 7750	Fixed Satellite (Downlink) Mobile Satellite (Downlink)
7900 - 7975	Fixed Satellite (Uplink) Mobile Satellite (Uplink)
7975 - 8025	Fixed Satellite (Uplink) Mobile Satellite (Uplink)
8025 - 8175	Fixed Satellite (Uplink) Earth Exploration Satellite (Downlink) Mobile Satellite (Uplink)
8175 - 8215	Earth Exploration Satellite (Uplink) Fixed Satellite (Uplink) Meteorological Satellite (Downlink) Mobile Satellite (Uplink)
8215 - 8400	Earth Exploration Satellite (Downlink) Fixed Satellite (Uplink) Mobile Satellite (Uplink)
8400 - 8450	Space Research (Deep Space Uplink)
8450 - 8500	Space Research (Downlink)
9975 - 10025	Meteorological Satellite (Footnote 828)

research, involving the use of telemetry for transmitting data to the Earth, and space operations, including the functions of tracking and command. The frequency ranges of 2110 to 2120 MHz, 2290 to 2300 MHz, 5650 to 5725 MHz, and 8450 to 8500 MHz are listed as being for deep-space research. Plans for the proposed satellite power system for collecting solar energy called for transmission of energy to the Earth at 2450 MHz, but implementation of such a system is questionable.

Parties involved in the development of land-mobile satellite systems in the United States and Canada have wanted to use portions of the 806-890 MHz band that have been held in reserve, but an FCC decision of July 28, 1986 allows only for L-band operation in the United States for land-mobile satellite service. The Aeronautical and Mobile Satellite services will share on an equal basis (co-primary) the 1549.5-1558.5 MHz band for space to mobile platform transmission and the 1651-1660 band for mobile platform to space transmission. The Aeronautical Mobile Satellite service is designated as the primary occupant and Mobile Satellite service will be a secondary service, operated on a non-interference basis, in the 1545-1549.5 MHz band for space to mobile platform operation with 1646-1651 MHz used for mobile platform to space operation. Some of the 806-890 MHz band that was previously held in reserve was allocated to the Public Safety Radio Service, and four MHz (849-851 and 894-896) were kept in reserve.

The version of Table 1.2 of this edition includes a number of entries that were not in the original 1979 version of the table, especially in the 7250-8175 MHz range where Mobile Service was added to the previous listings. NTIA (1986) shows the allocations in this frequency range to be for governmental use in the United States.

Listings or logs of operational or planned geostationary satellites are published from time to time in the COMSAT Review and elsewhere. The texts by Pratt and Bostian (1986) and Pritchard and Sciulli (1986) also include information of this type.

1.3 STRUCTURE OF THE EARTH'S ATMOSPHERE

Earth-space paths traverse both the Earth's troposphere and ionosphere, and the characteristics of the atmospheric regions are thus pertinent to satellite communications.

Troposphere

Temperature decreases with increasing altitude in the troposphere, but temperature inversion layers provide exceptions to this general characteristic. The thickness of the troposphere varies but it extends to about 10 km over the poles and 16 km over the equator. The upper limit of the troposphere is known as the tropopause. A plot of atmospheric temperature versus altitude is shown in Fig. 1.3.

Atmospheric pressure tends to decrease exponentially with altitude in accordance with

$$p = p_o e^{-h/H} \tag{1.18}$$

where h is the height above a reference level where the pressure is p_o. The scale height H is not a constant as it is a function of temperature T, the average mass of the molecules present, and the acceleration of gravity g as indicated by

$$H = kT/mg \tag{1.19}$$

where k is Boltzmann's constant.

The rate of change of temperature with altitude in a dry atmosphere in an adiabatic state (involving no input or loss of heat energy) is given by $dT/dh = -9.8$ deg C/km. The dry adiabatic rate of change of temperature with height is of interest because the stability or instability of the atmosphere is determined in large part by the relative values of the actual rate of change of temperature with altitude and the dry adiabatic rate. If the actual lapse rate of the atmosphere (rate of decrease of temperature with altitude) is 9.8 deg C/km, a parcel of air that is originally in equilibrium with its surroundings and which is then moved upwards or downwards will tend to remain in equilibrium, at the same temperature as its surroundings. The parcel of air will then not be subject to an restraining or accelerating force. Such a lapse rate of temperature is referred to as neutral. If the actual lapse rate of the atmosphere is greater than 9.8 deg C/km, a rising parcel of air will tend to cool only at the adiabatic rate and be warmer than its surroundings. As a result it will be lighter than the air around it and will be accelerated still further upwards. The air in this condition is unstable. If the lapse rate is less than 9.8 deg C/km, a parcel moved upwards will tend to cool at the adiabatic rate and be cooler than its surroundings. Thus it is subject to a force that inhibits vertical motion. A lapse rate less than 9.8 deg C/km is a stable lapse rate.

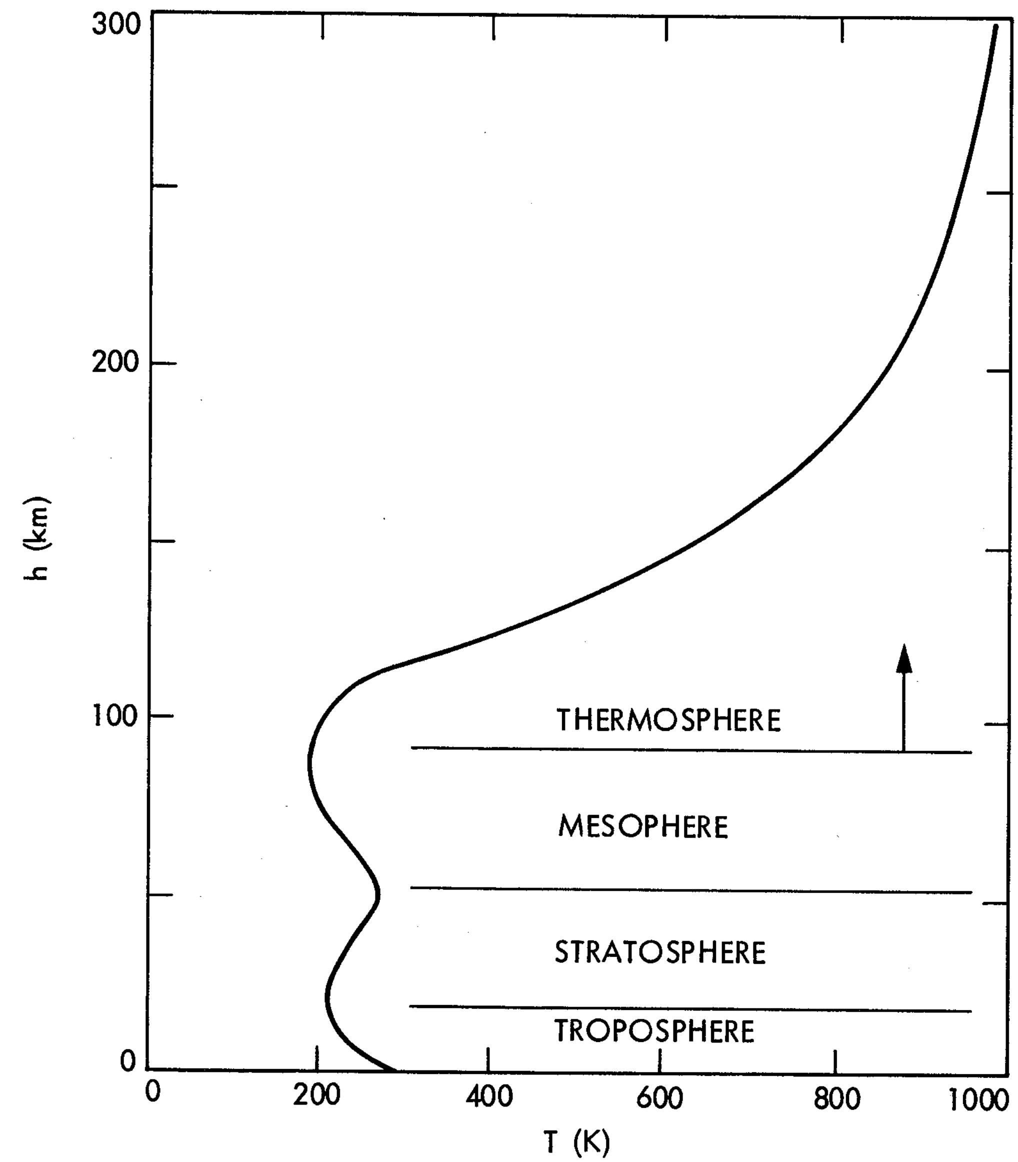

Figure 1.3 Atmospheric temperature versus altitude (values from U.S. Standard Atmosphere, 1976).

In an inversion layer temperature increases with altitude, and such a layer is highly stable. All vertical motions are strongly inhibited in an inversion layer, and pollution emitted below the layer tends to be confined below it. If a source of water vapor exists below an inversion layer, the vapor tends to be confined below the layer also with the result that a large decrease in index of refraction may be encountered in upward passage through an inversion layer. The occurrence of inversion layers may have an important effect on low-angle earth-space communication paths (Secs. 3.2 and 3.3).

Inversions tend to develop at night and in the winter, especially under conditions of clear sky as in the desert at night and in the arctic and subarctic in winter. Inversions may also form when warm air blows over a cool surface such as an ocean surface. Subsiding air is another cause of inversions, and this type of inversion is common because descending air is associated with developing or sempermanent anticyclones. The Pacific coast of the United States lies along the eastern edge of a semipermanent anticyclone that forms in the Pacific; this occurrence is a major factor in causing the pollution problems of the Los Angeles area.

Model atmospheres have been developed to present the best available estimates of the average values of pressure, density, temperature, and other parameters. One such model atmosphere is the U.S Standard Atmosphere (1976). Temperature tends to decrease on the average at a rate of 6.5 deg C/km, which is less than the dry adiabatic rate. When rainfall occurs at the Earth's surface a transition to ice and snow particles tends to occur at the height where the 0 deg C isotherm is reached. Water drops cause much higher attenuation than do ice particles and snow, so the 0 deg C isotherm marks the upper boundary of the region where most attenuation due to precipitation occurs.

Stratosphere, Mesosphere, Thermosphere

Above the troposphere temperature increases with height, to a maximum near 50 km, as a result of the absorption of solar ultraviolet radiation by ozone (Fig. 1.3). This region of increasing temperature with height is known as the stratosphere. The mesosphere, a region of decreasing temperature with height, occurs above the stratosphere and extends to about 85 km.

Above 85 km is the thermosphere, in which temperature again increases with height as a result of the dissociation of atmospheric gases by solar ultraviolet radiation. Above 300 km temperatures change little with height for a considerable distance. Below about 100 km temperature changes little with time, but the temperature above 120 km may vary by nearly a factor of 3 to 1, being highest in the daytime near the peak of the 11-year sunspot cycle.

The characteristic of the thermosphere of most importance to satellite communications is not the temperature structure itself but the ionization that occurs there. On the basis of the ionization, the region is known as the ionosphere. The ionosphere has a lower limit of about 60 km, and it thus includes part of the mesosphere as well as the thermosphere.

Ionosphere

The ionosphere extends from about 60 km to a not very well defined upper limit of about 500 to 2000 km above the Earth's surface. As geostationary satellites operate at an altitude of about 35,786 km, transmissions to and from these satellites pass through the entire ionosphere. The ionosphere, which is ionized by solar radiation in the ultraviolet and x-ray frequency ranges, is an ionized gas or plasma containing free electrons and positive ions so as to be electrically neutral. Only a fraction of the molecules are ionized, and large numbers of neutral molecules are also present. It is the free electrons that affect electromagnetic wave propagation in the frequency range considered in this report (100 MHz to 10 GHz).

Because different portions of the solar spectrum are absorbed at different altitudes, the ionosphere consists of several layers or regions. The layers are not sharply defined, distinct layers, and the transition from one to the other is generally gradual with no very pronounced minimum in electron density in between. Representative plots of electron density are shown in Fig.1.4. Two good sources of further information about the ionosphere are those by Rishbeth and Garriot (1969) and Ratcliffe (1969).

D Region

The D region, the lowest of the ionospheric regions, extends from approximately 50 to 90 km with the maximum electron

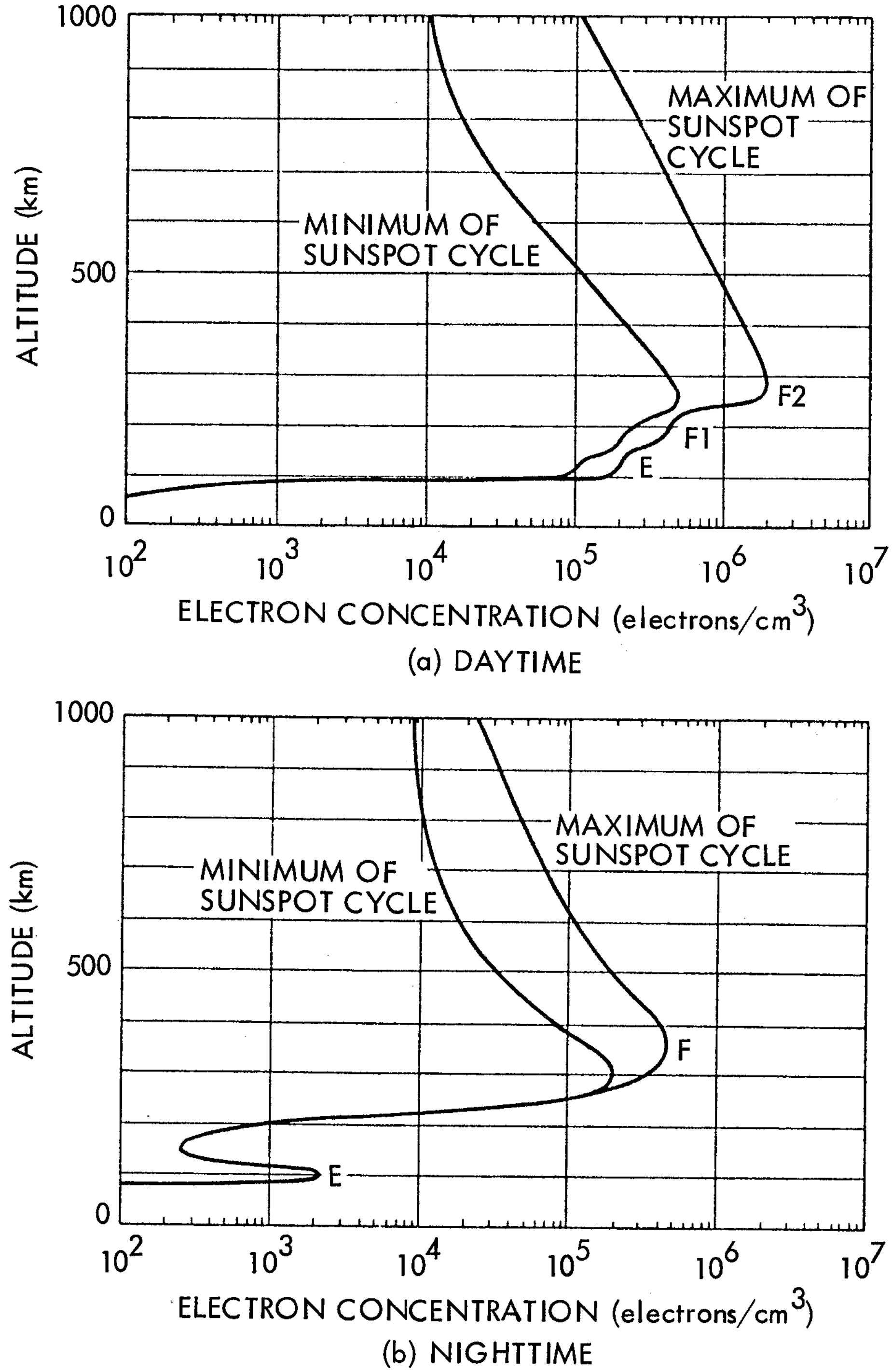

Figure 1.4 Electron density distribution at the extremes of the sunspot cycle (from Hanson, W.B., "Structures of the Ionosphere" in Johnson, F.S. (ed.), Satellite Environment Handbook, Stanford U. Press, 1965).

electron density of about $10^9/m^3$ occurring between 75 and 80 km in the daytime. At night electron densities throughout the D region drop to vanishingly small values.

As the electron concentration in the D region is very low, it tends to have little effect on high-frequency waves. However, attenuation in the ionosphere occurs mainly through collisions of electrons with neutral particles, and as the D region is at a low altitude many neutral atoms and molecules are present and the collision frequency is high. Therefore transmissions in the AM broadcast band are highly attenuated in the day time in the D region, but distant reception improves at night when the D region disappears.

E Region

The E region extends from about 90 to 140 km, and the peak electron concentration occurs between about 100 and 110 km. Electron densities in the E region vary with the 11-year sunspot cycle and may be about $10^{11}/m^3$ at noon at the minimum of the solar cycle and about 50 percent greater at the peak of the cycle. Electron concentrations drop by a factor of about 100 at night. Intense electrical currents flow in the equatorial and auroral ionospheres at E-region altitudes, these currents being known as equatorial and equatorial electrojets. Radio waves are scattered from electron density structure associated with the electrojets at frequencies up to more than 1000 MHz. Backscatter echoes from the auroral electrojets indicate the regions of occurrence of aurora and are referred to as radio aurora. The phenomena of sporadic E, thin, sporadic, often discontinuous layers of intense ionization, occurs in the E region, at times with electron densities well above $10^{12}/m^3$. The E layer is useful for communications, as HF waves may be reflected from the E layer at frequencies which are a function of time of day and period of the sunspot cycle. By causing interference between VHF stations, sporadic E tends to be a nuisance.

F Region

The F region has the highest electron densities of the normal ionosphere. It sometimes consists of two parts, the F_1 and F_2 layers. The F_1 layer largely disappears at night but has peak densities of about $2.5 \times 10^{11}/m^3$ at noon at the minimum of the solar cycle and $4 \times 10^{11}/m^3$ at noon at the peak of the solar cycle. The F_2 layer has the highest peak electron densities of the ionosphere and the electron densities there remain higher at night than in other regions. The peak electron density is in the 200- to 400-km height range and may be between about $5 \times 10^{11}/m^3$ and $2 \times 10^{12}/m^3$ in the daytime and between $1 \times 10^{11}/m^3$ and $4 \times 10^{11}/m^3$ at night. Reflection from the F_2 layer is the major factor in HF communications which formerly handled a large fraction of long-distance, especially transoceanic, communications.

Plasmasphere and Magnetosphere

The upper limit of the ionosphere is not precisely defined but for the purposes of space communications may be taken as 2000 km, this being the upper limit for significant Faraday rotation (Sec.2.2). Above the ionosphere is the plasmasphere or protonosphere, which has an electron content of about 10 percent of the ionospheric content in the daytime and up to 50 percent of the ionospheric content at night, as defined along an earth-space path.

The Earth's magnetic field is confined inside an elongated cavity in the solar wind, that extends to about 10 earth radii in the direction towards the Sun and has a long tail extending to about 50 earth radii or farther in the opposite direction. The boundary of this cavity is known as the magnetopause, and the region inside the boundary, above the ionosphere, is known as the magnetosphere. The magnetosphere can be defined as the region in which the Earth's field dominates the motion of charged particles, in contrast to the ionosphere where collisions play a major role. The Van Allen radiation belts, discovered in 1958 by use of Explorer 1, are in the magnetosphere. The plasmasphere, usually considered to be above the ionosphere (or above 2000 km), is below the Van Allen belts and is the lowest region of the magnetosphere. The plasmasphere is bounded on the upper side at about 4 earth radii at the equator by the plasmapause where the plasma density drops by a factor of 10 to 100 or from about $10^8/m^3$ to $10^6/m^3$.

Irregularities and Disturbed Conditions

A brief description has been provided of the ionospheric layers. Consideration of the ionosphere can be separated into the quiet ionosphere and ionospheric disturbances and irregularities, as occur at times of magnetic storms and essentially every night to some degree in the auroral and equatorial ionospheres. Both propagation in the quiet ionosphere and the effects of disturbances and irregularities are considered in the following Chap. 2.

1.4 NATURAL REGIONS OF THE EARTH, A GLOBAL VIEW OF PROPAGATION EFFECTS

The uneven heating of the Earth's surface by the Sun, the rotation of the Earth and the consequent Coriolis force, and surface features of the Earth determine a characteristic pattern of wind over the Earth. See, for example, a text on meteorology such as that by Donn (1975), p. 238. In good measure because of this pattern, corresponding characteristic patterns of climate, ecosystems, vegetation, tropospheric refractivity (Sec. 3.1), and rainfall (Chap.4) also occur over the surface of the Earth. The living portions of ecosystems are referred to as biotic communities, and the major terrestrial biotic communities are known as biomes. For practical purposes the biomes can be referred to simply as natural regions. Maps of the natural regions of all the continents are included in the Aldine University Atlas (Fullard and Darley, 1969). The climatological, ecological, and geographical characteristics of a region are closely related and are pertinent to satellite communications. Areas of tropical forest, which are rapidly disappearing, can be expected to have heavy rainfall and a high atmospheric water vapor content. The Arctic, on the other hand, has low precipitation and low values of water vapor.

Global models for estimating rainfall statistics have been developed and are discussed in Sec. 4.3.3, where rain rate regions are shown in Figs. 4.8 - 4.10 and Figs. 4.13 - 4.15. The regions shown are in rough correspondence with the natural regions of Fullard and Darley (1969) and also with the Koppen system for classifying climates (Trewartha, 1968). The global models are not very detailed, however, and advantage should be taken of any more detailed information that may be available.

REFERENCES

Allen, C.W., Astrophysical Quantities. London: University of London, Athlone Press, 1978.

Donn, W.L., Meteorology, 4th Ed. New York: McGraw-Hill,1975.

Dougherty, H.T., A Consolidated Model for UHF/SHF Telecommunications Links Between Earth and Synchronous Satellites, NTIA Report 80-45, U.S. Dept. of Commerce, Aug. 1980.

Evans, J.V., "Twenty years of international satellite communications," Radio Sci., vol.21, pp. 647-664, July-Aug. 1986.

Feher, K., Digital Communications, Satellite/Earth Station Engineering. Englewood Cliffs, NJ: Prentice-Hall, 1983.

Freeman, R. L., Telecommunications Transmission Handbook, 2nd Ed., New York: Wiley, 1981.

Fullard, H. and H.C. Darby, Aldine University Atlas. Chicago: Aldine, 1969.

Hall, M.P.M., Effects of the Troposphere on Radio Communications. Stevenage, UK and New York: Peter Peragrinus for IEE, 1979.

Ippolito, L.J., R.D. Kaul, and R.G. Wallace, Propagation Effects Handbook for Satellite Systems Design, A Summary of Propagation Impairments on 10 to 100 GHz Satellite Links with Techniques for System Design, NASA Reference Pub. 1082(03). Washington, DC: NASA Headquarters, 1983.

Ippolito, L.J., Radiowave Propagation in Satellite Communications. New York: Van Nostrand Reinhold, 1986.

ITU (International Telecommunications Union), Final Acts of the World Administrative Radio Conference, Geneva, 1979, Volume 1E, 1982, Revised 1985.

Jordan, E.C. (ed. in chief), Reference Data for Engineers: Radio, Electronics, Computer, and Communications, Seventh Ed., Indianapolis, IN: Howard W. Sams, 1986. (Also in ITT, Reference Data for Radio Engineers, Sixth Ed., 1975.)

Miya, K., Satellite Communication Technology. KDD Bldg. 3-2, Nishi-Shinjuku 2-chome, Shinjuku-ku, Tokyo, Japan, 1981.

NTIA (National Telecommunications and Information Administration), Manual of Regulations and Procedures for Federal Radio Frequency Management. Washington, DC 20230: NTIA, May 1986.

Pratt, T.and C.W. Bostian, Satellite Communications. New York: Wiley, 1986.

Pritchard, W. L. and J.A. Sciulli, Satellite Communication Systems Engineering. Englewooe Cliffs, NJ: Prentice-Hall, 1986.

Ratcliffe, J.A., An Introductdion to the Ionosphere and Magnetosphere. Cambridge: Cambridge University Press, 1972.

Rishbeth, H. and O. K. Garriott, Introduction to Ionospheric Physics. New York : Academic Press, 1969.

Thompson, W.I., Atmospheric Transmission Handbook, Report No. DOT-TSC-NASA-71-6. Cambridge, MA: Transportation Systems Center. Feb. 1971.

Trewartha, G.T., An Introduction to Climate. New York: McGraw-Hill, 1968.

U.S. Standard Atmosphere, 1976, sponsored by NOAA, NASA, USAF. Washington, DC: Supt. of Documents, U.S. Government Printing Office, 1976.

CHAPTER 2

IONOSPHERIC EFFECTS

2.1 PROPAGATION IN HOMOGENEOUS PLASMAS

This chapter includes a brief treatment of ionospheric propagation. The reader interested in a more thorough analysis of this large and interesting subject is referred to treatises by Budden (1951), Davies (1965, 1969), Kelso (1964), and Ratcliffe (1972). An elementary introduction starting with Maxwell's equations was given by Flock (1979).

2.1.1 Characteristic Waves

The Earth's ionosphere is a partially ionized gas or plasma which is rendered anisotropic by the presence of the Earth's magnetic field. The concept of characteristic waves is important in considering the propagation of electromagnetic waves in such a medium. These are the waves which propagate without changing their polarization, by which reference is made to whether a wave is linearly, circularly, or elliptically polarized and, in the case of linear polarization, to the direction of the electric field intensity vector of the wave (e.g. vertical, horizontal, or at an angle between vertical and horizontal). Changing from right circular to left circular polarization, for example, constitutes a change in polarization, and changing the direction of linear polarization also constitutes a change in polarization.

The nature of the characteristic waves that propagate in an anisotropic plasma such as the Earth's ionosphere can be determined by the application of Maxwell's equations. It develops that there are two characteristic waves and that the parameters of the characteristic waves depend upon the direction of propagation with respect to the Earth's magnetic field (the angle θ_B of Fig. 2.1).

<u>Parallel Propagation</u>

For propagation parallel to the Earth's field B ($\theta_B = 0^o$) in the lossless case the two characteristic waves are left and right circularly polarized and have indices of refraction n_ℓ and n_r given by

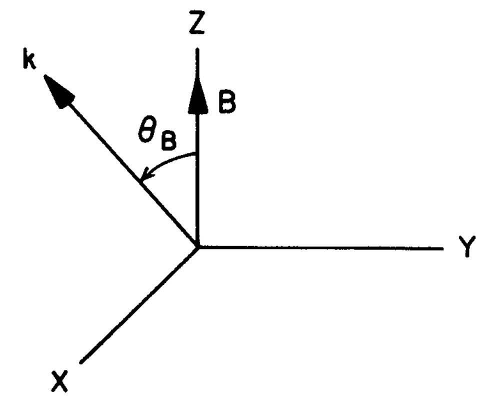

Figure 2.1 Coordinate system for considering propagation at an angle θ_B from the direction of the Earth's field B.

$$n_\ell^2 = K_\ell = 1 - \frac{\omega_p^2}{\omega\,(\omega + \omega_B)} \tag{2.1}$$

and

$$n_r^2 = K_r = 1 - \frac{\omega_p^2}{\omega\,(\omega - \omega_B)} \tag{2.2}$$

K_ℓ and K_r are the relative dielectric constants for the left and right circularly polarized waves. The quantity ω is the angular frequency of the wave and equals $2\pi f$ where f is frequency in Hz, while ω_B is the angular gyrofrequency of the electrons in the plasma and is given by

$$\omega_B = \frac{-qB}{m} \tag{2.3}$$

where B is the Earth's magnetic field in Wb/m^2, $q = -e = -1.6022 \times 10^{-19}$ C is the charge of the electron, and m is the mass of the electron (9.1096×10^{-31} kg). The Earth's field is roughly that of a magnetic dipole, inclined by about 12 deg with respect to the rotational axis, for which the field decreases as the cube of the radius or distance from the center of the Earth. Figure 2.2 shows field values given by a dipole model. For a more accurate model, reference can be made to the International Geomagnetic Reference Field (IGRF) developed by a working group of IAGA (The International Association of Geomagnetism and Aeronomy). A special issue of the Journal of Geomagnetism and Geoelectricity was devoted to the third-generation IGRF model (vol. 34, No. 6, pp. 307-422, 1982), and Appendix 2.2 describes briefly the basis for the IGRF models. A paper by Peddie (1982) in vol. 34 describes the third-generation 1980 model and also the IGRF 1965 and 1975 first- and second-generation models. All of the models include extrapolation ahead, and the third-generation model for 1980 includes extrapolation to 1985. The 1985 or fourth-generation IGRF model was presented in the June 17, 1986 issue of EOS. Numerical values of the 1985 coefficients of the spherical harmonic expansion of the geomagnetic field (Appendix 2.2) are included in this article in EOS.

A description of a computer algorithm for synthesizing the geomagnetic field from values of the spherical harmonic coefficients is given in a paper by Malin and Barraclough (1981). The coefficients of the IGRF models and computer programs for synthesizing field values are also available in the United States from the following sources.

World Data Center A, NOAA
NESDIS/NGDC (E/GC11)
325 Broadway, Boulder, CO 80303

World Data Center A for Rockets and Satellites
Code 601, NASA/Goddard Space Flight Center
Greenbelt, MD 20771

The geomagnetic models archived at the National Geophysical Data Center (NGDC) of NOAA in Boulder are described in a leaflet, Magnetic Field Models, updated in January 1986 and available from the center. Several models in addition to IGRF models are

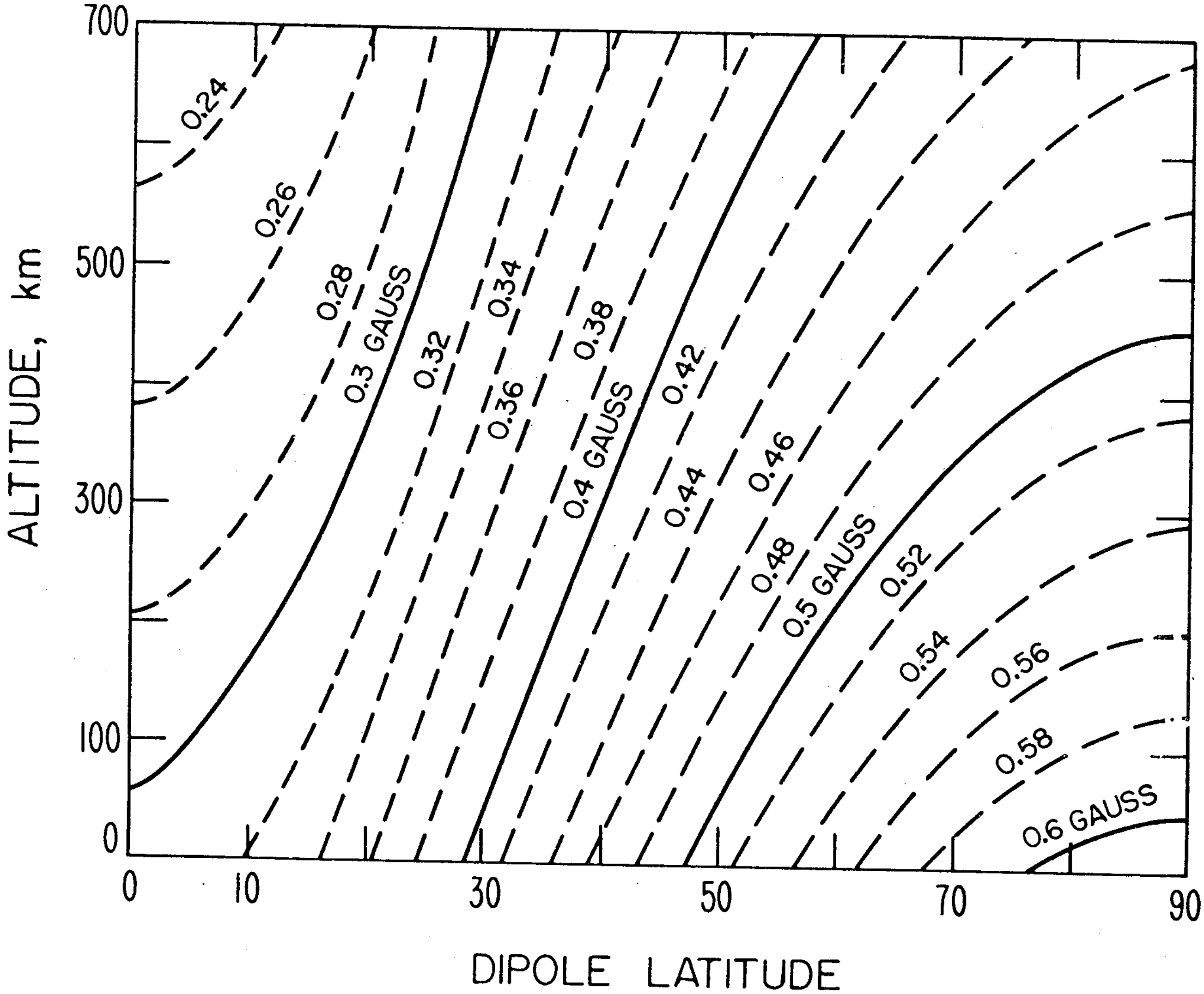

Figure 2.2 Total intensity of the Earth's magnetic field as a function of altitude and dipole latitude, assuming an earth-centered dipole of magnetic moment M = 7.95 x 10^{25} gauss cm^3 (after Smith, 1974).

archived, and, although we referred above to the 1965 model as the first generation IGRF model, the leaflet refers to the IGRF as involving earlier models as well.

The quantity ω_p^2 is the angular plasma frequency squared and can be found by using

$$\omega_p^2 = Nq^2/(m\epsilon_o) \tag{2.4}$$

where N is electron density ($e\ell/m^3$) and ϵ_o is the electric permittivity of empty space (8.854×10^{-12} F/m). For practical applications it may be convenient to convert from angular frequency to frequency in MHz for propagation at HF and higher frequencies. To this end

$$(f_B)_{MHz} = 2.7992 \times 10^4\, B \simeq 2.8 \times 10^4\, B \tag{2.5}$$

with B in Wb/m^2, or $(f_B)_{MHz} \simeq 2.8$ B with B in gauss. Also

$$(f_p)_{MHz} = 8.9788 \times 10^{-6}\, N^{1/2} \tag{2.6}$$

with N the number of electrons per m^3. Then

$$n_\ell = \left[1 - \frac{f_p^2}{f\,(f + f_B)}\right]^{1/2} \tag{2.7}$$

$$n_r = \left[1 - \frac{f_p^2}{f\,(f - f_B)}\right]^{1/2} \tag{2.8}$$

Perpendicular Propagation

For propagation perpendicular to the magnetic field ($\theta_B = 90$ deg) one characteristic wave has its electric field intensity vector directed along the z axis of Fig. 2.1. The index of refraction n_o and relative dielectric constant K_o in this case are given by

$$n_o^2 = K_o = 1 - \omega_p^2/\omega^2 = 1 - f_p^2/f^2 \tag{2.9}$$

which also apply for the case of no magnetic field. The subscript o stands for ordinary; the ordinary wave is unaffected by the magnetic field for perpendicular or transverse propagation. If the electric field intensity is in the y direction in Fig. 2.1 (or in general perpendicular to B), the situation is somewhat more complicated. In this case, the index of refraction n_x and the relative dielectric constant K_x are given by

$$n_x^2 = K_x = K_\ell K_r / K_\perp \tag{2.10}$$

where

$$K_\perp = 1 - \frac{\omega_p^2}{\omega^2 - \omega_p^2}$$

This wave is referred to as the extraordinary wave. The two characteristic waves for propagation perpendicular or transerve to the magnetic field are linearly polarized in the plane perpendicular to the direction of propagation, but it develops that for the extraordinary wave there is a component of electric field intensity in the direction of propagation (the x direction if the transverse component is in the y direction).

2.1.2 Role of Index of Refraction

The index of refraction n of an electromagnetic wave is by definition the ratio of $c \simeq 2.9979 \times 10^8$ m/s, the velocity of an electromagnetic wave in empty space, to v_p, the velocity of the wave in question in the medium. Thus

$$n = c/v_p \tag{2.11}$$

The phase constant β of an electromagnetic wave gives the phase lag of the wave with distance when used in

$$E = E_o e^{-j\beta z} \tag{2.12}$$

for the case of a wave propagating in the z direction and having an electric field intensity E_o at a reference position where $z = 0$. The constant β can be expressed in several ways as shown by Eq. (2.13).

$$\beta = 2\pi/\lambda = \omega/v_p = \beta_o n \tag{2.13}$$

where λ is wavelength and β_o is the phase constant of empty space.

It was shown earlier that the two characteristic waves, for propagation either parallel or perpendicular to the magnetic field, have different values of index of refraction. Thus they have different phase velocities, phase constants, and wavelengths.

2.1.3 Reflection and Refraction

Reflection

Examination of the expressions for relative dielectric constant, Eq. (2.9) for the ordinary wave for transverse propagation for example, reveals that it is possible for the dielectric constant to be negative and that the index of refraction can thus become imaginary. For $\omega > \omega_p$ in Eq. (2.9) n_o is real, but, for $\omega < \omega_p$, n_o is imaginary. An imaginary value of index of refraction determines that β of Eq. (2.12) will also be imaginary so that, instead of a propagating wave as indicated in Eq. (2.12), an evanescent condition will occur so that $E = E_o e^{-\alpha z}$ because the quantity $-j\beta$ of Eq. (2.12) has become $-j\beta_o\ (-j|n|) = -\alpha$. The different possibilities are summarized in Table 2.1.

Table 2.1 Characteristics of n and E(z) Corresponding to Different Relative Values of ω and ω_p.

ω	n	E(z)
$\omega > \omega_p$	real	$E = E_o e^{-j\beta z}$
$\omega = \omega_p$	0	$E = E_o$
$\omega < \omega_p$	imaginary	$E = E_o e^{-\alpha z}$

The condition $E = E_o e^{-\alpha z}$ of Table 2.1 represents a field that attenuates with z, but the attenuation in this case is not dissipative. Instead it involves reflection and reversal of direction as suggested in Fig. 2.3b. In Fig. 2.3 an increase of electron density with height in the ionosphere is assumed. The frequency ω is much greater than ω_p in Fig. 2.3a, and the ray path is essentially unaffected by the ionosphere, whether the path is vertical or oblique. In Fig. 2.3b the condition $\omega < \omega_p$ is reached in the vertical path shown and the ray is reflected. Figure 2.3b suggests the overall result, but the

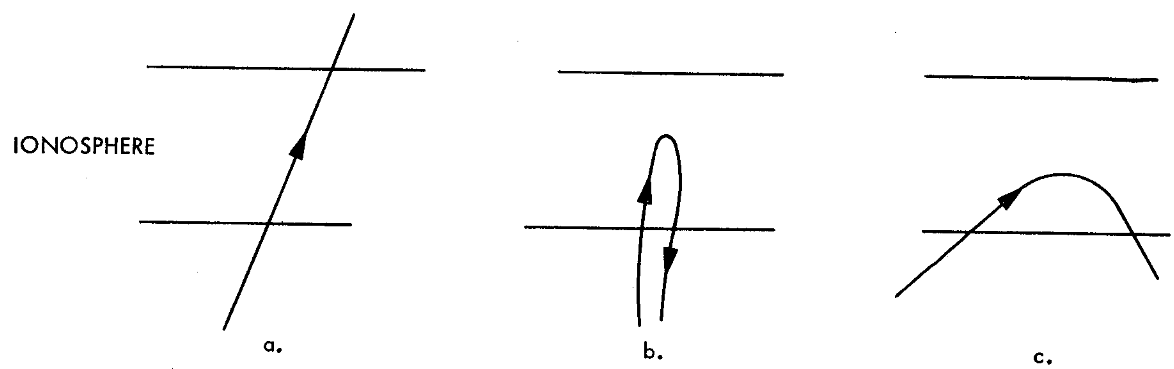

Figure 2.3 Ionospheric ray paths.

a. $\omega >> \omega_p$ throughout.
b. The condition $\omega < \omega_p$ is reached along the ray path.
c. Oblique-incidence path.

reflection process actually takes place over a range of heights, consistent with $E = E_o e^{-\alpha z}$, rather than abruptly at a particular level. Furthermore, if the evanscent region is of limited extent and E still has a significant value at the far side of the region from the source, then a wave of diminished amplitude will be launched and will propagate beyond the evanscent region.

For the ordinary wave ω_p plays the role of a critical frequency with propagation occurring for $\omega > \omega_p$ and not for $\omega < \omega_p$. The situation is similar to propagation in a metallic waveguide having a certain cutoff frequency f_c. In a waveguide propagation occurs for $f > f_c$ and an evanescent condition occurs for $f < f_c$. An evanescent section of waveguide can serve as a waveguide-below-cutoff attenuator. For the left and right circularly polarized waves, Eqs. (2.1) and (2.2) show that the conditions $\omega_p^2 = \omega^2 + \omega\omega_B$ and $\omega_p^2 = \omega^2 - \omega\omega_B$ separate propagating and nonpropagating regions for the left and right circularly polarized waves, respectively.

The above discussion is idealized in that dissipative attenuation does occur to some degree in the ionosphere so that, for $\omega > \omega_p$, $E(z) = E_o e^{-j\beta z} e^{-\alpha z}$ where now α represents dissipative attenuation involving the conversion of electromagnetic energy into heat. The topic of absorption or dissipative attenuation is treated in Sec. 2.7.

Refraction

In Fig. 2.3c a ray is obliquely incident upon the ionosphere and is shown to experience reflection. In this case ω is always greater than ω_p, however, and while the overall result is usually viewed as reflection the process is basically one of refraction. Applying Snell's law with the angle χ measured from the zenith and neglecting the Earth's curvature, $n \sin \chi = n_o \sin \chi_o$ where χ_o is the initial launch angle below the ionosphere and n_o, the index of refraction of the troposphere, is essentially unity. At the highest point in the path of Fig. 2.3c the angle χ is 90 deg. Therefore, at this point $n = \sin \chi_o$. For the ordinary wave and transverse propagation

$$n^2 = 1 - (f_p/f)^2$$

with f_p the plasma frequency and f the operating frequency. Therefore

$$n^2 = \sin^2 \chi_o = 1 - (f_p/f)^2 \tag{2.14}$$

from which $\cos \chi_o = f_p/f$ and

$$f = f_p \sec \chi_o \tag{2.15}$$

This expression gives the maximum frequency, f, which will be reflected, or refracted, from or below a height where the plasma frequency is f_p in the case of a wave having a launch angle of χ_o. If f_p is the peak plasma frequency in the ionosphere then f is the maximum usable frequency, in particular the maximum frequency that will be reflected for a launch angle of χ_o.

The above case can be considered to be an extreme example of refraction. At the frequencies of major interest in this handbook, ionospheric refraction will be of rather minor importance but will cause a slight bending of a ray such that the apparent elevation angle of arrival will be higher than the geometric elevation angle. For satellites well above most of the ionization the error in elevation angle $\Delta\theta$ is given by

$$\Delta\theta = \frac{(R + r_o \sin \theta_o)\, r_o \cos \theta_o}{[h_i\,(2r_o + h_i) + (r_o \sin \theta_o)^2]} \, \frac{\Delta R}{R} \quad \text{rad} \tag{2.16}$$

where θ_o is the apparent elevation angle, h_i is the height of the centroid of the electron content along the path (normally between 300 and 450 km), and ΔR is the range error [Eq. (2.34)]. For sufficiently low elevation angles or for long ranges corresponding to geostationary satellites for which $R > r_o \sin \theta_o$

$$\Delta\theta \simeq \frac{\cos \theta_o}{2\, h_i} \, \Delta R \quad \text{rad} \tag{2.17}$$

As ΔR, the range error, varies with time, the elevation angle error $\Delta\theta$ also varies with time. Furthermore as $\Delta\theta$ is the difference between the true and apparent elevation angles, the apparent elevation angle or direction of arrival varies with time.

These relations were developed by Millman and Reinsmith (1974). Klobuchar (1978) reports that for a frequency of 1.6 GHz, a worst case elevation angle of 5 deg, and a TEC (total electron content) of 10^{19} electrons/m^2, $\Delta\theta$ will be 0.3 mr. Equation (2.33) shows the range error, and therefore the refraction or elevation angle, to vary inversely with frequency squared.

2.1.4 QL Approximation

Propagation can occur at any angle θ_B with respect to the magnetic field, and analysis for the general case is more complex than for strictly parallel or perpendicular propagation. The situation is simplified, however, when the QL (quasi-longitudinal) approximation is applicable. To state this approximation, we use the common practice of defining ω_p^2/ω^2 as X and ω_B/ω as Y. Using these quantities, Eqs. (2.1) and (2.2) take the forms

$$n_\ell^2 = K_\ell = 1 - X/(1 + Y) \tag{2.18}$$

and

$$n_r^2 = K_r = 1 - X/(1 - Y) \tag{2.19}$$

Also defining Y cos θ_B as Y_L and Y sinθ_B as Y_T, the condition for the QL approximation to apply is

$$4(1 - X)^2 Y^2 >> Y_T^2 \tag{2.20}$$

When this approximation applies the characteristic waves for propagation at an angle θ_B with respect to the magnetic field are circularly polarized, as they are for $\theta_B = 0$ deg, and their indices of refraction have the forms

$$n_\ell^2 = K_\ell = 1 - X/(1 + Y_L) \tag{2.21}$$

and

$$n_r^2 = K_r = 1 - X/(1 - Y_L) \tag{2.22}$$

2.1.5 Application to Space Communications

The value of X in Eq. (2.20) is a major factor in determining if the QL approximation applies, and X is defined as ω_p^2/ω^2. For space communications ω tends to be high, X tends to be small, and the QL approximation tends to apply, even for large values of θ_B. Thus the characteristic waves on earth-space paths are normally left and right circularly polarized waves. Also examination of Eqs. (2.1) and (2.2) or (2.21) and (2.22) shows that n_ℓ and n_r have values only slightly less than unity for large values of ω and that these values approach closer to unity and to each other as ω increases. Thus for ω sufficiently large, n_ℓ and n_r are essentially unity, reflection does not occur, and the effect of the ionosphere can be neglected. Such is the case for frequencies above 10 GHz. Moving downward in frequency below 10 GHz, however, one reaches frequencies for which ionospheric effects are important, even though n_ℓ and n_r may still be not far from unity.

In this and the following Secs. 2.2 through 2.4 consideration is given to uniform or homogeneous media, but the ionosphere is characterized by various disturbances and irregularities which affect propagation and which are also most important for lower frequencies. These irregularities and their effects are treated in Secs. 2.5 through 2.7.

2.2 FARADAY ROTATION

Analysis of the propagation of a linearly polarized high-frequency wave in the ionosphere shows that it experiences rotation of the plane of polarization such that a wave that is launched with vertical polarization, for example, does not remain vertical. Depending on the frequency, length of path in the ionosphere, and orientation with respect to the Earth's magnetic field, the amount of rotation may vary from a negligible amount to amounts in excess of 360 deg to many complete rotations. The basis for such rotation, known as Faraday rotation, is that a linearly polarized wave consists of left and right circularly polarized components which have different indices of refraction. That such is the case can be visualized with the aid of Fig. 2.4.

Consider that E_ℓ and E_r are the electric field intensity vectors of left and right circularly polarized waves. Small auxiliary arrows are used to indicate the direction of rotation for E_ℓ and E_r for a right-handed coordinate system with z, the direction of propagation, extending out of the plane of the page. E_ℓ and E_r are the circularly polarized components of a linearly polarized wave having its electric field intensity in the x direction. Figure 2.4a shows an instant when E_ℓ and E_r both lie on the x axis, and Fig.2.4b shows conditions an instant later. It can be recognized that as the two vectors rotate their projections on the y axis cancel and the sum of their projections on the x axis provide cosinusoidal variation of the amplitude of E, with E always lying along the x axis. Note that as E varies cosinusoidally, E_ℓ and E_r maintain constant lengths.

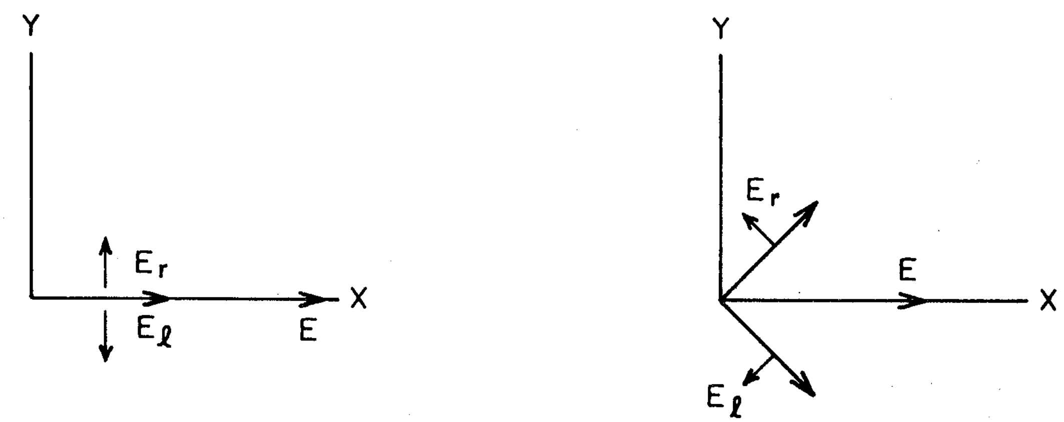

(a) (b)

Figure 2.4. Illustration suggesting how circularly polarized waves combine to form a linearly polarized wave.

As the vectors E_ℓ and E_r propagate in the z direction, they continue to rotate with angular velocity ω in their respective directions but the phases of the rotations lag in accordance with the factors $e^{-j\beta_\ell z}$ and $e^{-j\beta_r z}$. The indices n_ℓ and n_r have different values and therefore β_ℓ and β_r have different values, in accordance with Eq. (2.13). Thus after propagating a distance z, the rotations are no longer symmetrical about the x axis, and the field intensity E no longer lies along the x axis but at an angle ϕ from the original x axis where, for the case of a uniform ionosphere

$$\phi = (\beta_\ell z - \beta_r z)/2 \tag{2.23}$$

[More generally $\phi = \int (\beta_\ell - \beta_r)/2 \; dz$, with β_ℓ and β_r functions of position along the path.] The parameter β_ℓ is larger than β_r but its lag in phase of rotation is in the right circular direction. Thus Fig. 2.5 shows a possible condition after propagation through some distance z, namely rotation of **E** through an angle ϕ in the right circular direction.

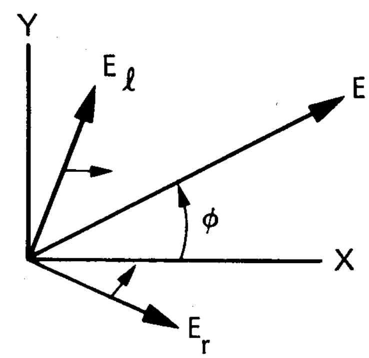

Figure 2.5. Faraday rotation through an angle ϕ from the conditions of Fig. 2.4.

Consider now propagation at an angle θ_B with respect to the magnetic field when the QL approximation applies. For sufficiently high frequencies the calculation of rotation can be simplified by noting that

$$\frac{\beta_o(n_\ell - n_r)}{2} = \frac{\beta_o}{2}\left[\left\{1 - \frac{X}{1+Y_L}\right\}^{1/2} - \left\{1 - \frac{X}{1-Y_L}\right\}^{1/2}\right]$$

$$\simeq \frac{\beta_o}{2}\left[1 - \frac{X}{2\,(1+Y_L)} - 1 + \frac{X}{2\,(1-Y_L)}\right] = \frac{\beta_o}{2} X Y_L \tag{2.24}$$

The electron density and magnetic field along the path will in general not be uniform but total rotation can be determined by first defining the differential rotation $d\phi$ in an increment of path length $d\ell$ and then integrating along the length of path. Thus

$$d\phi = (\beta_0/2)\, XY_L\, d\ell \qquad \text{rad} \tag{2.25}$$

and, using the definitions of X and Y_L, the total rotation ϕ in radians along a path is given by

$$\phi = \frac{e^3}{2c\epsilon_0 m^2\omega^2} \int N\, B \cos\theta_B\, d\ell \qquad \text{rad} \tag{2.26}$$

where $e = 1.6022 \times 10^{-19}$ C, $m = 9.1096 \times 10^{-31}$ kg, $c \simeq 3 \times 10^8$ m/s, $\epsilon_0 = 8.854 \times 10^{-12}$ F/m, and $\omega = 2\pi f$. Also

$$\phi = (2.36 \times 10^4/f^2) \int N\, B \cos\theta_B\, d\ell \quad \text{rad} \tag{2.27}$$

with f in Hz, N standing for electrons/m^3, and B. the Earth's field in Wb/m^2. It should be kept in mind that Eqs. (2.24) - (2.27) are approximations that are valid only at sufficiently high frequencies, perhaps above about 100 MHz.

The total rotation can be seen to vary inversely with f^2 and to be proportional to the integral of electron density, weighted by the value of $B \cos\theta_B$ along the path. If it is desired to carry out integration in the vertical direction, letting $d\ell = dh$, but the path is a slant path, a factor sec χ can be introduced inside the integral, where χ is the zenith angle or angle of the path measured from the vertical. B varies inversely with the cube of the radius from the Earth's center and has very low values above about 2000 km, and Faraday rotation is insensitive to ionization above that level. Therefore Faraday rotation measurements of signals from geostationary satellites provide a measure of ionospheric total electron content but not of total electron content along the entire path to a satellite. The region above the ionosphere, above about 2000 km, may have an electron content that is about 10 percent of the ionospheric content in the daytime and 50 percent at night (Davies, Hartmann, and Leitinger, 1977).

For some situations, it is sufficiently accurate to replace $B \cos \theta_B$ in Eq. (2.27) by an average value, namely B_L, and to take it outside the integral. The expression for the Faraday rotation angle then becomes

$$\phi = (2.36 \times 10^4/f^2)\, B_L \int N\, d\ell = (2.36 \times 10^4/f^2)\, B_L\, \mathrm{TEC} \qquad (2.28)$$

with $B_L = \left(\int N B \cos \theta_B\, d\ell \right) / \int N\, d\ell$. The quantity TEC stands for total ionospheric electron content along the path in this case. Equation (2.28) can be inverted to find TEC by use of

$$\mathrm{TEC} = \phi f^2 / (2.36 \times 10^4 B_L) \qquad (2.29)$$

On a fixed path, when the above procedure is applicable, the amount of Faraday rotation depends on TEC, which exhibits a pronounced diurnal variation as well as a variation with the season, solar flare activity, and period of the solar cycle. When the form of the variation of electron density with altitude changes the value of B_L may change also.

A practical consequence of Faraday rotation is that, in the frequency range where Faraday rotation is significant, one cannot transmit using one linear polarization and receive using an antenna with the same linear polarization without a high probability of a significant polarization loss. Among the techniques for avoiding or dealing with the problem are using a sufficiently high frequency that Faraday rotation is negligible, using a receiving antenna that can accept both orthogonal linear polarizations so that no polarization loss occurs, and using circular rather than linear polarization. As a right or left circularly polarized wave is a characteristic wave, it does not change polarization as it propagates and thus presents no problem, as long as both antennas of the link are designed for the same circular polarization. Another possibility, if Faraday rotation is not too great or highly variable, is to vary the orientation of a linear transmitting or receiving antenna to compensate for the Faraday rotation expected along the path, as a function of time of day, season, and period of the sunspot cycle.

As Faraday rotation and group delay and other topics of the following Sec. 2.3 are all functions of TEC (total electron content) along a path, numerical illustrations of Faraday rotation are deferred until Sec. 2.4 which deals with TEC.

2.3 GROUP DELAY, PHASE ADVANCE, DOPPLER FREQUENCY, AND BANDWIDTH COHERENCE

2.3.1 Group Delay

To consider excess ionospheric group delay, or excess range delay, at high frequencies, note that the integral $\int n \, d\ell$, evaluated along a path with n representing index of refraction, gives the true distance along the path if $n = 1$ but gives a value P, sometimes called the phase path length, which is different from the true distance if n does not equal unity. Thus ΔR, the difference between P and the true length R, is given by

$$\Delta R = \int (n - 1) \, d\ell \tag{2.30}$$

Neglecting refraction and considering that $f > 100$ MHz so that $n^2 \simeq 1 - X$,

$$n^2 = 1 - f_p^2/f^2 = 1 - 80.6 \, N/f^2 \tag{2.31}$$

where N is electron density ($e\ell/m^3$) and f is frequency in Hz. Taking X as being small compared to unity as is the case for sufficiently high frequencies ($f > 100$ MHz),

$$n \simeq 1 - X/2 = 1 - 40.3 \, N/f^2 \tag{2.32}$$

For group delay, however, one is concerned with the group velocity rather than phase velocity. As $v_g v_p = c^2$ for ionospheric propagation when $v_p > c$, where v_g is group velocity and v_p is phase velocity, one should use the group refractive index, $n_g = 1 + X/2$. The result is that

$$\Delta R = \frac{40.3}{f^2} \int N \, d\ell \qquad \text{m} \tag{2.33}$$

where ΔR is a positive range error (excess range delay) and is the difference between the true range and that which would be inferred by assuming a velocity of c. (The true range is less than the inferred range.) The excess range delay ΔR corresponds to an error in time or an excess time delay of

$$\Delta t = \frac{40.3}{cf^2} \int N\, d\ell = \frac{1.34 \times 10^{-7}}{f^2} \int N\, d\ell \quad \text{s} \qquad (2.34)$$

where $\int N\, d\ell$ is the TEC (total electron content) along the path. If the TEC is known or can be estimated closely, Δt can be determined from Eq. (2.34).

Use of a second lower frequency allows determining Δt and TEC without any advance information. Let $\Delta t_1 = 40.3\ \text{TEC}/cf_1^2$ where f_1 is the frequency of major interest and let $\Delta t_2 = 40.3\ \text{TEC}/cf_2^2$. Then

$$\delta t = \Delta t_2 - \Delta t_1 = \frac{40.3\ \text{TEC}}{c} \left[\frac{1}{f_2^2} - \frac{1}{f_1^2} \right] \qquad (2.35)$$

It is now possible to solve for Δt_1 which is given by

$$\Delta t_1 = \frac{f_2^2}{f_1^2 - f_2^2}\, \delta t \qquad (2.36)$$

The quantity δt can be readily measured by suitably modulating both carrier frequencies but Δt cannot be measured directly for lack of a suitable reference.

Equation (2.35) can be rearranged to give the value of TEC, i.e.

$$\text{TEC} = \frac{\delta t\, c}{40.3} \frac{f_1^2 f_2^2}{f_1^2 - f_2^2} \qquad (2.37)$$

A procedure has been described for determining Δt at the expense of utilizing a second frequency. Such a correction is important in the case of satellite positioning systems such as the GPS (global positioning system). Using GPS it may be possible to determine position to an accuracy of a few meters, whereas if no allowance is made a TEC of $10^{18}/m^2$ can cause an error of 134 ns or 40 m at a frequency of 1 GHz (Klobuchar, 1978).

Another case where high accuracy is desired is that of the DSN (Deep Space Network) of the Jet Propulsion Laboratory, where it may be desired to determine ranges to spacecraft with an accuracy of 3 m or better. Coded signals are transmitted to spacecraft at S or X band and retransmitted back to the station at X band. Also range measurements are used for determining the declination angle of a spacecraft near zero declination by VLBI techniques. This procedure involves determining the difference in distance to the spacecraft from Goldstone, California and Canberra, Australia. Correction for excess time delay is essential for this purpose.

Equation (2.37), when applied to an earth-space path, gives the TEC along the entire path, in contrast to Faraday rotation measurements which give the electron content of the ionosphere only. Numerical values of time delay are given in Sec. 2.4.

2.3.2 Phase Advance

The presence of the ionosphere advances the phase ϕ of a received signal with respect to the value for unionized air. (Do not confuse phase with Faraday rotation. The same symbol ϕ is used here for these two different phenomena.) The phase advance $\Delta\phi$ can be found by multiplying the excess range delay ΔR by the phase constant $\beta = 2\pi/\lambda = 2\pi f/c$, with the result that

$$\Delta\phi = \frac{40.3\ (2\pi f)}{f^2\ c}\ \mathrm{TEC} = \frac{8.44 \times 10^{-7}}{f}\ \mathrm{TEC} \quad \mathrm{rad} \qquad (2.38)$$

Dividing by 2π gives the value of $\Delta\phi$ in cycles.

$$\Delta\phi = \frac{1.34 \times 10^{-7}}{f}\ \mathrm{TEC} \quad \mathrm{cycles} \qquad (2.39)$$

2.3.3 Doppler Frequency

Frequency and phase are related by

$$f = \frac{1}{2\pi} \frac{d\phi}{dt} \tag{2.40}$$

with f in Hz and ϕ in radians. The Doppler shift in frequency, f_D, corresponding to the phase change of Eq. (2.39) is given by

$$f_D = \frac{1}{2\pi} \frac{8.44 \times 10^{-7}}{f} \frac{d(TEC)}{dt} = \frac{1.34 \times 10^{-7}}{f} \frac{d(TEC)}{dt}$$

In terms of finite quantities

$$f_D = \frac{1.34 \times 10^{-7}}{f} \frac{\Delta(TEC)}{T_c} \tag{2.41}$$

where the TEC changes by Δ(TEC) in the time interval or count time T_c and f_D is the average value during T_c.

2.3.4 Differenced Range versus Integrated Doppler

A technique known as differenced range versus integrated Doppler (DRVID) has been used at the Jet Propulsion Laboratory for obtaining information about changes in columnar electron content (TEC) (Callahan, 1975). The basis for the technique is the difference in group and phase velocities, the group velocity being less than c and the phase velocity being greater than c. In terms of index of refraction,

$$n_g = 1 + 40.3\ N/f^2 \text{ and } n = 1 - 40.3\ N/f^2$$

where n_g is the group index and n is the phase index (which is normally what one refers to when speaking of index of refraction). Total columnar electron content TEC and electron density N are related by TEC = $\int N\, d\ell$, where the integral is taken along the path length.

The Deep Space Network of the Jet Propulsion Laboratory has utilized a system for measuring range delay by the use of two-way transmissions of coded pulse trains. For the time interval between t_o and t, this system provides a value ΔR_g which is a combination of a true change in range, $R(t) - R(t_o)$, and the excess range delay $40.3\ \Delta(TEC)/f^2$. That is

$$\Delta R_g(t, t_o) = R(t) - R(t_o) + \frac{40.3\ \Delta(TEC)}{f^2} \tag{2.42}$$

A similar expression applies for $\Delta R_\phi(t,t_o)$, which is obtained from a phase or Doppler frequency measurement .

$$\Delta R_\phi(t, t_o) = R(t) - R(t_o) - \frac{40.3\ \Delta(TEC)}{f^2} \tag{2.43}$$

The difference $\Delta R_g - \Delta R_\phi$ is designated as DRVID and is given by

$$DRVID\ (t, t_o) = \Delta R_g - \Delta R_\phi = \frac{80.6\ \Delta(TEC)}{f^2} \tag{2.44}$$

The change in TEC, Δ(TEC) can be determined from Eq. (2.44), and if a series of consecutive measurements of this kind are made a record of the variation of TEC can be constructed. Note that the absolute value of TEC can not be determined by this method but that the effects of motion of the spacecraft and of the troposphere are canceled out as n_g and n are the same in the troposphere.

The quantity ΔR_ϕ can be obtained from the expression, in terms of finite increments of phase and time, for Doppler frequency f_D, namely

$$f_D = \frac{1}{2\pi} \frac{\Delta\phi}{T_c} \tag{2.45}$$

and from the expression relating $\Delta\phi$ and ΔR_ϕ, which is

$$\Delta\phi = \frac{2\pi}{\lambda_o} \Delta R_\phi \tag{2.46}$$

By substituting Eq. (2.46) into Eq. (2.45), $\Delta\phi$ can be eliminated, with the result that

$$f_D = \frac{1}{\lambda_o} \frac{\Delta R_\phi}{T_c} \quad \text{or} \quad \Delta R_\phi = f_D \lambda_o T_c \tag{2.47}$$

2.3.5 Bandwidth Coherence

The rate of change of time delay with frequency, or the time-delay dispersion, is found by taking the derivative of Eq. (2.34) yielding

$$\frac{dt}{df} = \frac{-80.6}{cf^3} \int N\, d\ell = \frac{-2.68 \times 10^{-7}}{f^3} \text{TEC} \tag{2.48}$$

The rate of change of phase angle with frequency, or the phase dispersion, is found by taking the derivative of Eq. (2.38) giving

$$\frac{d\phi}{df} = \frac{-8.44 \times 10^{-7}}{f^2} \text{TEC} \tag{2.49}$$

The effect of dispersion is to introduce distortion into broadband signals.

2.4 ELECTRON CONTENTS OF IONOSPHERE AND PLASMASPHERE AND THEIR EFFECTS

Faraday rotation measurements on satellite-to-Earth paths provide values of the electron content of the ionosphere, and group delay measurements give the total electron content (TEC) along the entire path. By taking the difference of the total and ionospheric values, the electron content of the plasmasphere or protonosphere is obtained. Most electron content data refer to ionospheric values, but data for the plasmasphere as well have been reported by Davies, Hartman, and Leitinger (1977), Klobuchar and Working Group (1978), and Davies (1980).

The ionospheric TEC shows pronounced diurnal variations consistent with the production of ionization by solar radiation in the daytime and the decay of ionization at night. Extreme values of the ionospheric TEC are given by Klobuchar (1978) as $10^{16}/m^2$ and $10^{19}/m^2$; $10^{18}/m^2$ is generally regarded as the maximum zenith value. Zenith values of ionospheric TEC refer to the electron content of a vertical column having a cross section of one square meter and extending to the height of the plasmasphere. Representative curves showing the diurnal variation of TEC for an invariant latitude of 54 deg are given in Fig. 2.6. Invariant latitude equals $\cos^{-1}(1/L)^{1/2}$ and refers to the magnetic field line that is at a distance L, measured in earth radii, from the center of the Earth at the magnetic equator. The data were obtained at Sagamore Hill, MA using 136 MHz signals from ATS-3.

One effect of TEC is to produce excess group time delay. Plots showing ionospheric time delay as a function of TEC and frequency are shown in Fig. 2.7. A worldwide model giving ionospheric time delay at a frequency of 1.6 GHz is shown in Fig. 2.8. Typical values of Faraday rotation as a function of ionospheric TEC and frequency for a northern mid-latitude earth station viewing a geostationary satellite near the station meridian are shown in Fig. 2.9. Using Fig. 2.6 together with Figs. 2.7 and 2.9 provides information about the diurnal variation of TEC and how this variation affects time delay and Faraday rotation. Ionospheric disturbances and irregularities and the solar cycle also cause variations in these parameters that may be important in some cases.

Table 2.2 gives a summary of ionospheric effects at frequencies from 100 MHz to 10 GHz. Included are the effects of Faraday rotation, time delay, refraction, and dispersion that have already been mentioned and values for absorption and variation in direction of arrival.

Table 2.2 Estimated maximum ionospheric effects in the United States for one-way paths at an elevation angle of about 30 deg [derived from CCIR Reports 565-3 (CCIR, 1986a), 263-4, 263-5, and 263-6 (CCIR, 1986b).]

Effect	100 MHz	300 MHz	1 GHz	3 GHz	10 GHz
Faraday rotation	30 rot.	3.3 rot.	108°	12°	1.1°
Excess time delay	25 μs	2.8 μs	0.25 μs	0.028 μs	0.0025 μs
Refraction	$\leq 1^{\circ}$	<7 min	≤0.6 min	<4.2 s	≤0.36 s
Variation in direction of arrival	20 min	2.2 min	12 s	1.32 s	0.12 s
Absorption (auroral and polar cap)	5 dB	1.1 dB	0.05 dB	6×10^{-3} dB	5×10^{-4} dB
Absorption (mid latitude)	<1 dB	0.1 dB	<0.01 dB	$<1\times10^{-3}$ dB	$<10^{-4}$ dB
Dispersion	0.4 ps/Hz	0.015 ps/Hz	0.0004 ps/Hz	1.5×10^{-5} ps/Hz	4×10^{-7} ps/Hz

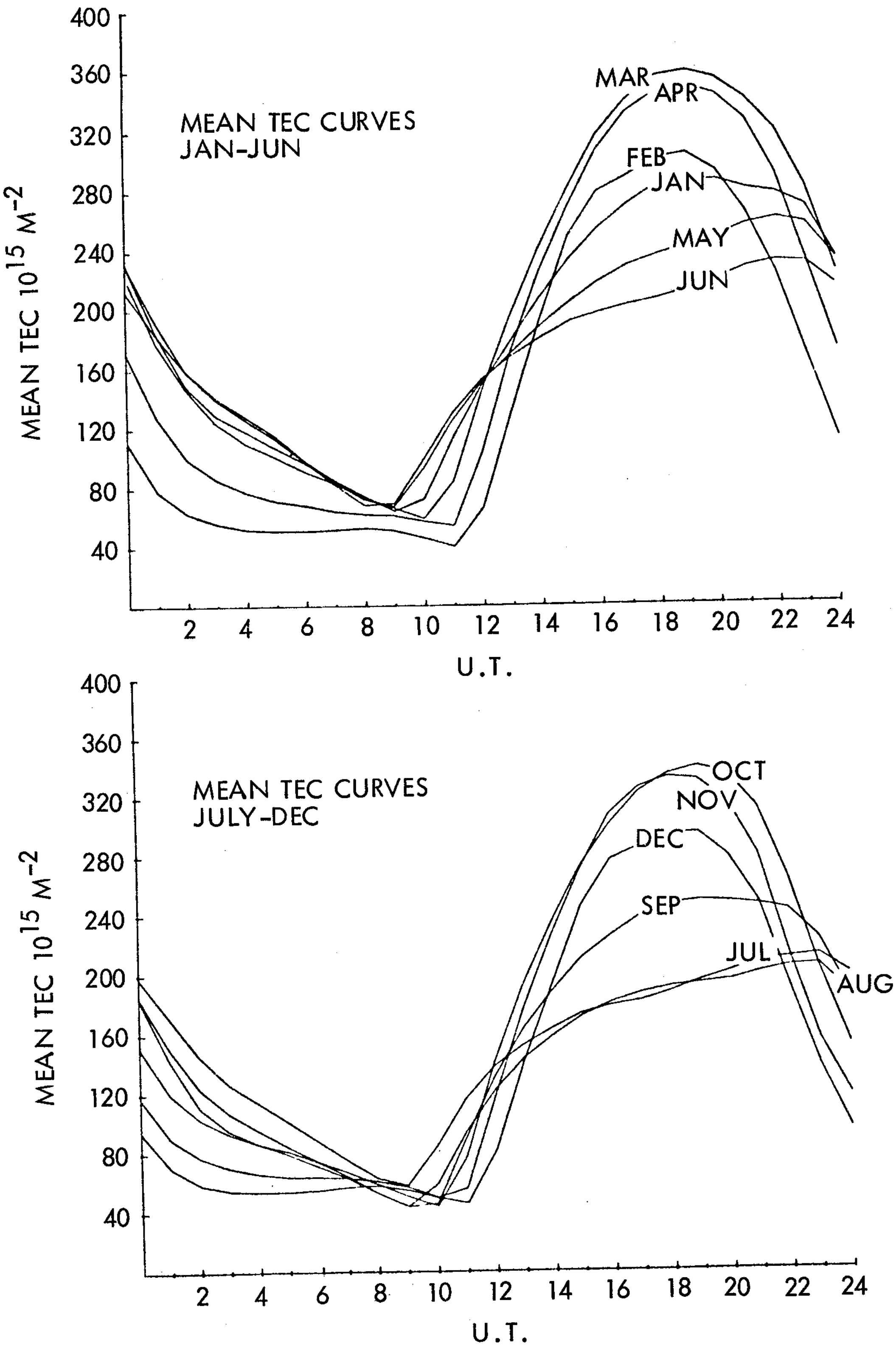

Figure 2.6 Diurnal variations in TEC, mean monthly curves for 1967 to 1973 as obtained at Sagamore Hill, MA (after Hawkins and Klobuchar, 1974).

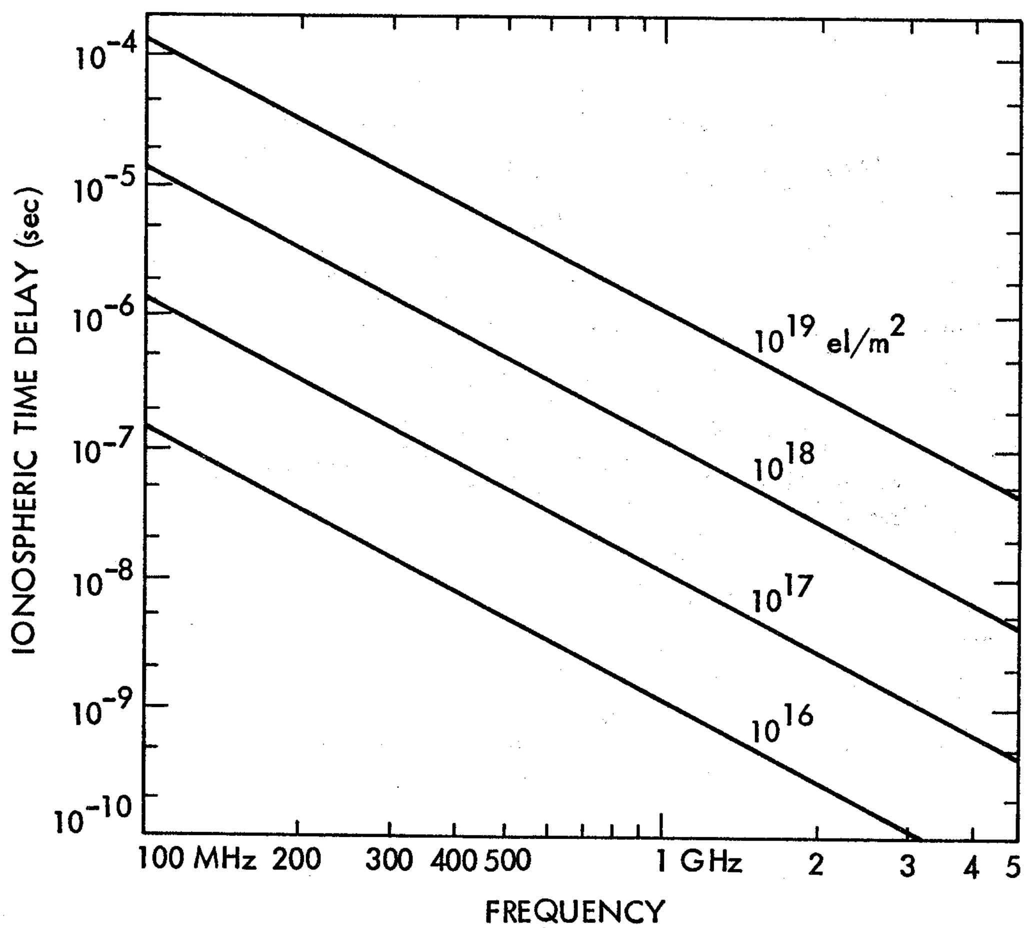

Figure 2.7. Ionospheric time delay as a function of ionospheric TEC and frequency (after Klobuchar, 1978).

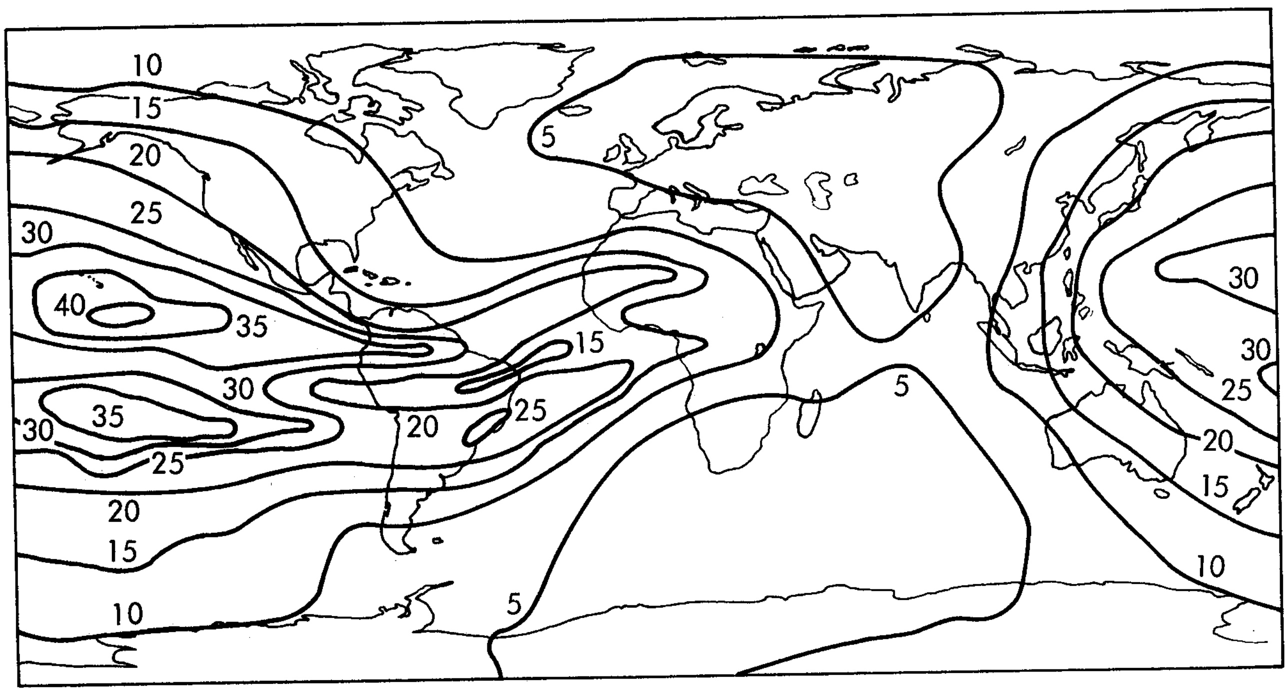

Figure 2.8. Ionospheric time delay in nanoseconds at a frequency of 1.6 GHz, based on the Bent model of ionospheric TEC (after Klobuchar, 1978).

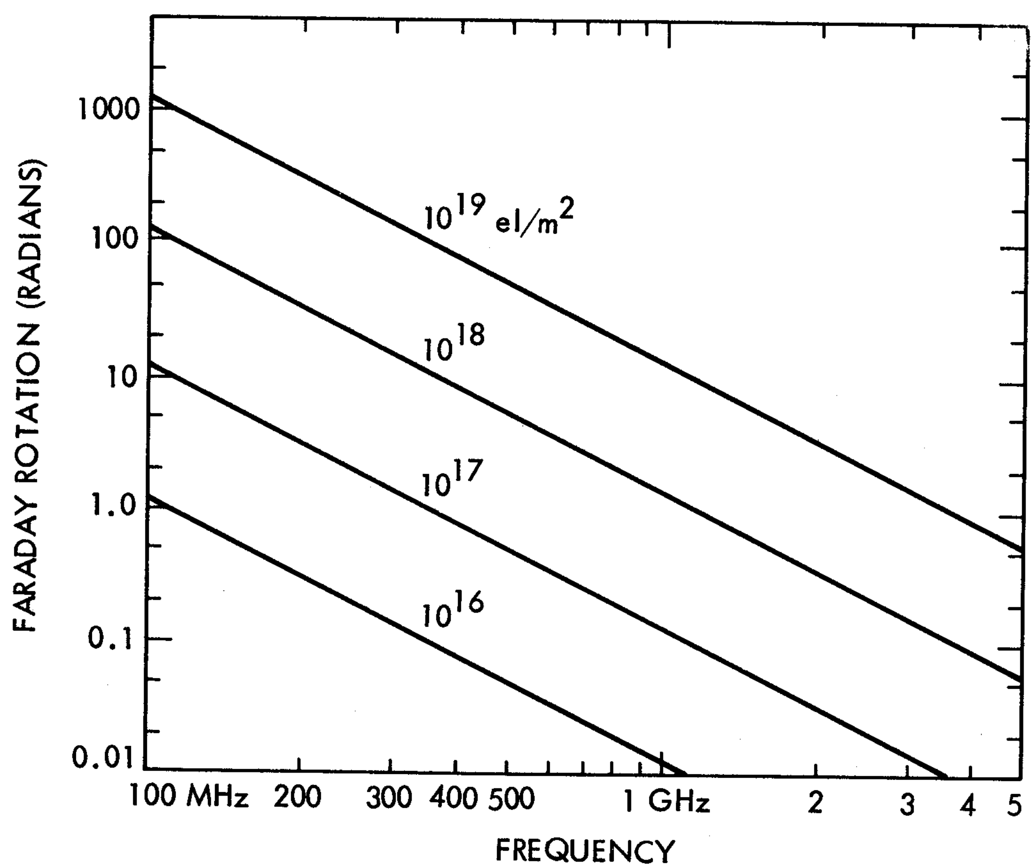

Figure 2.9. Faraday rotation as a function of ionospheric TEC and frequency (after Klobuchar, 1978).

2.5 IONOSPHERIC DISTURBANCES AND IRREGULARITIES

2.5.1 Equatorial Ionosphere

Because of atmospheric solar and lunar tidal forces and heating by the Sun, horizontal movements or winds occur in the ionosphere. As a result, electric fields are developed by the dynamo effect, described by $\mathbf{E} = \mathbf{v} \times \mathbf{B}$, where $\mathbf{E}$ is electric field intensity, $\mathbf{v}$ is the velocity of the charged particles of the ionosphere, and $\mathbf{B}$ is the Earth's magnetic field. (This is a vector relation and $\mathbf{E}$ is perpendicular to both $\mathbf{v}$ and $\mathbf{B}$.) The electric fields in turn drive a current system in the ionosphere which involves two systems of current loops in the daytime hemisphere, one in the northern hemisphere and one in the southern hemisphere. The currents flow counterclockwise in the northern hemisphere and clockwise in the southern hemisphere so that the currents of both systems flow from west to east near the geomagnetic equator. It develops that the conductivity becomes high over a restricted range of altitude in this equatorial region. In addition the equatorial ionosphere is favorably situated to intercept solar radiation, which is the main agent causing ionization in the ionosphere. As a result of the factors mentioned, a strong, concentrated current, known as the equatorial electrojet, flows at heights from 90 to 130 km in the E region of the equatorial ionosphere. Electron density irregularities and variations associated with the electrojet cause scattering of electromagnetic waves which are incident upon and propagate through this region. Strong radar backscatter echoes are received from the equatorial electrojet. The Jicamarca Radar Observatory near Lima, Peru, operating at a frequency near 50 MHz, has provided a large amount of information concerning the equatorial ionosphere. It can record both discrete echoes from E and D irregularities and weak incoherent-scatter echoes from the entire ionosphere (Evans, 1969, Farley, 1963, Balsley, 1969).

The occurrence of plasma bubbles (McClure et al., 1977) has been an object of investigation since Woodman and La Hoz (1976) reported the appearance of rising plume-like structures, using the Jicamaraca radar. The bubbles typically have a width of 100 km and electron densities 1 to 2 orders of magnitude less than the surroundings (Heron, 1980). Such bubbles are considered further in Sec. 2.6.

2.5.2 Auroral Ionosphere

Energetic particle precipitation into the auroral ionosphere causes the visible aurora, excess ionization which attenuates and scatters radio waves, and concentrated electrical currents known as auroral electrojets. The currents in turn cause characteristic variations in the geomagnetic field. These phenomena occur in the form of an oval (Fig. 2.10) which surrounds but is eccentric with respect to the Earth's magnetic dip pole, with the oval center displaced by about 3 deg toward the dark hemisphere (Akasofu, 1968). The oval is fixed approximately with respect to the Sun, and the Earth rotates beneath the oval. The term auroral zone is applied to the area that is swept out by the midnight portion of the auroral oval, where auroral activity occurs essentially every night to some degree. The concept of the auroral oval has been reviewed recently by Feldstein (1986).

The excess ionization occurs prominently in the E region and can be regarded as a variety of sporadic E. Intense radar backscatter or radar auroral echoes can be received at HF, VHF, and UHF frequencies. The irregularities in ionization are field aligned, having a considerable extent along the Earth's magnetic field lines and a small extent perpendicular to the lines. The line of sight to the echoing region must be close to perpendicular to the magnetic field to receive VHF-UHF echoes which must therefore be at ranges of 500-900 km in Alaska. An auroral radar facility at Anchorage, Alaska has transmitted data to the NOAA-USAF Space Environment Services Center in Boulder, Colorado. HF waves experience sufficient refraction in the auroral ionosphere to achieve perpendicularity without being launched originally in the perpendicular direction. An ionospheric trough, namely a region of reduced ionization, separates the auroral and mid-latitude ionospheres. This trough appears to be linked by magnetic field lines to the plasmapause of the magnetosphere (Sec. 1.3).

The riometer (relative ionospheric opacity meter) has been a valuable tool for studying the auroral and polar ionospheres. It operates typically at a frequency of 30 MHz and, by recording the amplitude of cosmic noise, monitors auroral and polar-cap activity and the associated attenuation experienced by radio waves propagating through the auroral ionosphere. An incoherent scatter radar facility at Chatanika, Alaska near Fairbanks, has been in

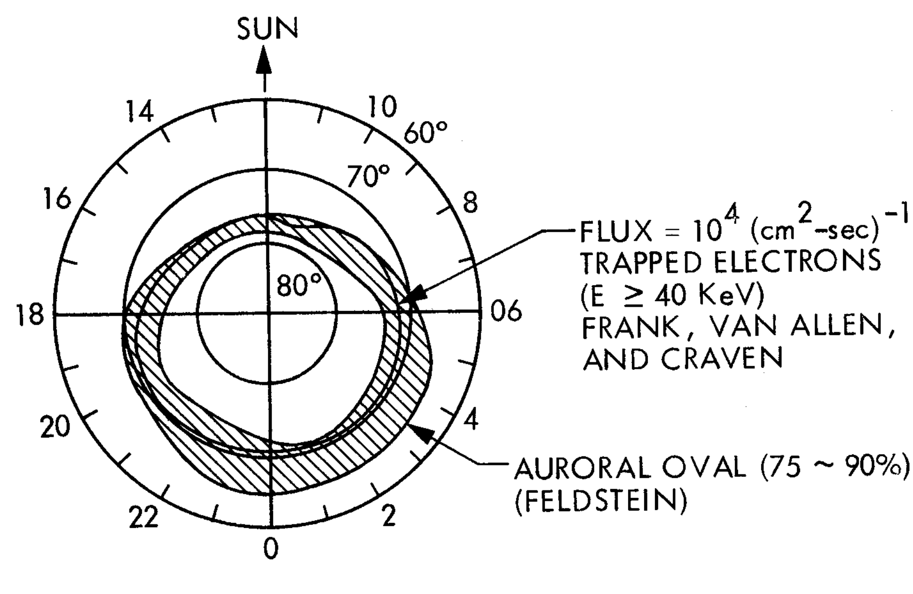

Figure 2.10. The auroral oval (Akasofu, 1968).

operation since about 1972 and has provided extremely valuable information about the auroral ionosphere (Leadabrand et al., 1972; Baron, 1974; Hunsucker, 1974). Auroral absorption is considered further in Sec. 2.7.

2.5.3 SID'S and Ionospheric Storms

The equatorial and auroral ionospheres are characterized by irregularities and disturbed conditions on a more or less continuous basis, but varying as to degree and subject to diurnal variation. The mid-latitude ionosphere exhibits less activity and disturbance generally but is subject to the effects of solar flares and sporadic E. Auroral activity is also enhanced by flare activity.

The effects of solar flares can be divided into the categories of simultaneous and delayed. The simultaneous effects result from the radiation of X-rays from the flares. X-rays propagate with the velocity c, the velocity of light. The simultaneous effects are known as sudden ionospheric disturbances (SID's), a term which covers a variety of phenomena including SWF (shortwave fadeout), SCNA (sudden cosmic noise absorption), SPA (sudden phase anomaly) and SFD (sudden frequency deviation). These effects tend to be important at HF frequencies. Phase ϕ and frequency f are related by

$$f = \frac{1}{2\pi} \frac{d\phi}{dt} \tag{2.50}$$

and if a change in phase occurs, a corresponding change in the frequency of the recorded signal also occurs. The change in frequency is similar to that encountered in reflection from a moving object and the term Doppler frequency is applied in both cases. Solar X-rays affect primarily the D region of the ionosphere.

Delayed effects from solar flares are caused by particles which are emitted from the Sun and may take 20 to 40 or more hours to reach the Earth. The particles cause magnetic and ionospheric storms (Rishbeth and Garriott, 1969), which can result in blackout at HF frequencies and also cause variations in phase and Doppler frequency. Ionospheric storms strongly affect the F region of the ionosphere. Magnetic storms are manifested by large irregular variations in the magnitude and direction of the Earth's magnetic field, as recorded on magnetometers, and are accompanied by ionospheric storms.

It is not always possible to make a clear distinction betweer quiet ionospheric conditions and the disturbed conditions of magnetic storms. Some magnetic activity and associated ionospheric effects, especially the TID's and spread F discussed in the following subsection, tend to occur to some degree nearly every night even in temperate latitudes.

2.5.4 Traveling Ionospheric Disturbances and Spread F

Traveling ionospheric disturbances (TID's) propagate as acoustic-gravity waves in the Earth's ionosphere (Hines, 1974). These waves involve variation in pressure and corresponding variations in electron density. Measurements of the Faraday rotation of signals from satellites indicate a cyclical variation in total electron content as TID's propagate though an earth-space path. TID's frequently appear to originate in the auroral zone and to propagate toward the equator. The condition of spread F is commonly associated with TID's (Booker, 1979). Spread F manifests itself and was originally identified on ionosonde records, which are made by vertically pointing radar systems whose frequency is varied periodically from about 0.5 to 25 MHz. Under quiet ionospheric conditions, the traces on an ionosonde record have the form shown in Fig. 2.11. In an ionogram, the virtual height of reflection is plotted as a function of frequency. The symbols f_o and f_x in Fig. 2.11 stand for penetration frequencies of the ionospheric layers (E, F_1, and F_2) for the "ordinary" and "extraordinary" waves. The highest penetration frequency shown, f_xF_2, is about 7 MHz. Waves at higher frequencies pass through the ionosphere without reflection. A main point for present purposes is that the traces are relatively clean and distinct, although those of Fig. 2.11 have been redrawn to provide greater clarity.

When spread F occurs, the trace for the F region is broken up into a multiplicity of separate traces. Spread F has been divided into two main types, which are range spreading and frequency spreading. Range spreading involves two or more traces having different virtual heights well below the penetration frequency as in Fig. 2.12a. The high-frequency portions of the traces are branched or blurred in frequency spreading as in Fig. 2.12b. Spread F occurs for the largest percentage of time in equatorial and auroral latitudes, but as mentioned previously tends to occur nearly every night in temperate latitudes to some degree as well. It is positively correlated with magnetic activity at high latitudes and negatively correlated at low latitudes (Rishbeth and Garriott, 1969).

2.5. Polar-cap Absorption

Very energetic protons or solar cosmic rays, which may reach the Earth in only 15 minutes to several hours after a flare, are associated with some intense solar flares. These particles are guided by the Earth's magnetic field to the polar regions, above about 64 deg in geomagnetic latitude, where they cause polar-cap absorption. Such polar-cap absorption events occur most frequently near the peak of the sunspot cycle and tend to last for several days. When the polar regions have periods of both daylight and darkness, the absorption decreases significantly at night with respect to daytime values. The auroral oval partially overlaps the equatorward edge of the region where polar-cap absorption occurs, and both polar-cap and auroral absorption can occur in the auroral zone. An illustration of polar-cap absorption is given in Sec. 2.7.

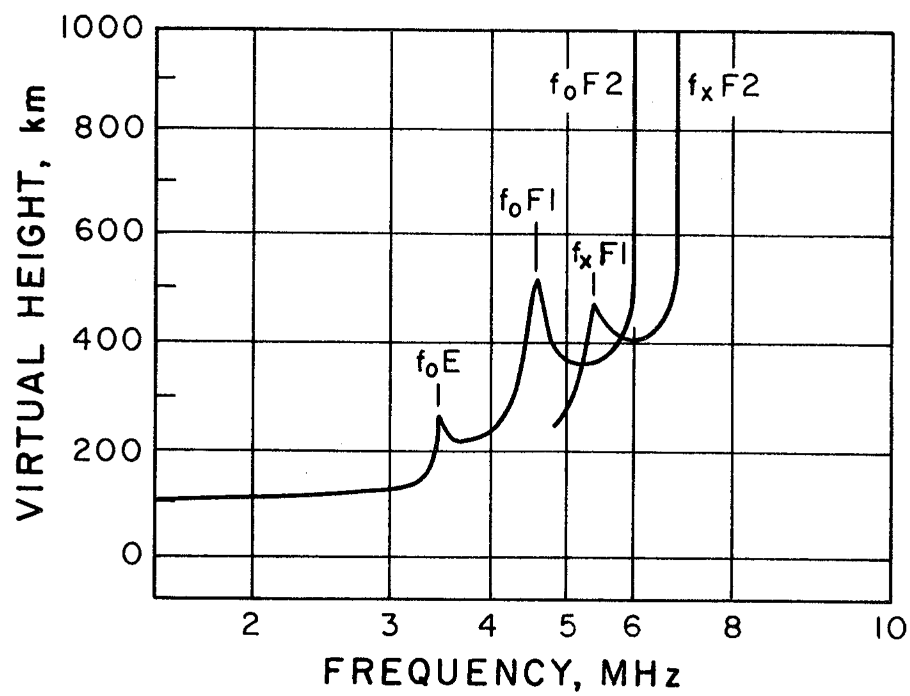

Figure 2.11. Ionospheric traces under quiet ionospheric conditions, Washington, DC. June 3, 1962 (after Davies, 1969).

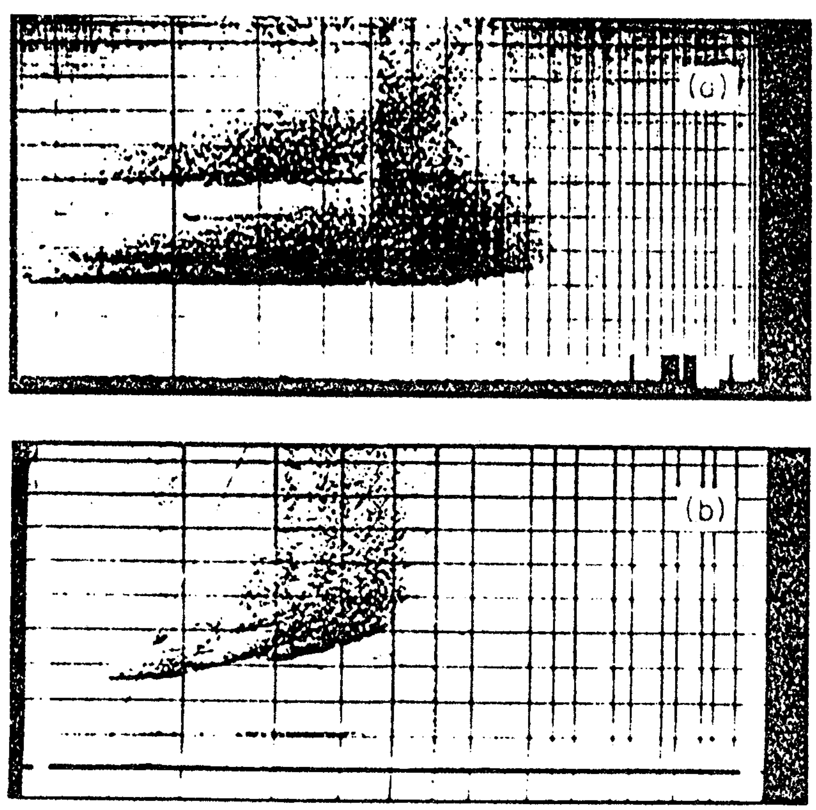

Figure 2.12. Ionograms showing spread-F. a. Range spreading. b. Frequency spreading. Virtual height versus frequency. (Davies, 1965).

2.6 IONOSPHERIC SCINTILLATION

2.6.1 Introduction

Irregular variations or scintillations of the amplitude of radiowaves from radio stars were first recorded by Hay, Parsons, and Phillips (1946) who reported variations in the amplitude of signals from Cygnus and Cassiopeia at 36 MHz. At first, it was thought that the emissions from the stars might be varying with time, but records obtained simultaneously from stations separated by 200 km showed no similarity whereas when the receiver separation was only about 1 km the records were closely similar (Smith, 1950; Little and Lovell, 1950). These results showed that the scintillations were not caused by the stars but were of localized origin, and it was concluded that their source was in the ionosphere. The scintillations were attributed by Hewish (1952) to a diffraction pattern formed at the ground by a steadily drifting pattern of irregularities in the ionosphere at a height of about 400 km. According to Aarons, Whitney, and Allen (1971), the irregularities are mostly in the F layer at heights predominantly from 225 to 400 km.

With the advent of satellites, scintillations of signals from such spacecraft were also observed (Yeh and Swenson, 1964). The signals from radio stars are incoherent and broadband and allow the recording of amplitude and angle-of-arrival scintillations but not phase scintillations. Coherent, monochromatic signals from spacecraft have the advantage of allowing the recording of phase scintillations and spectral broadening as well as amplitude scintillations (Crane, 1977; Woo, 1977; Smith and Edelson, 1980). The early observations of scintillations were at comparatively low frequencies and, on the basis of the assumed form of decrease of scintillation intensity with frequency, it was expected that frequencies as high as those of the 4 and 6 GHz bands planned for the INTELSAT system would be free from scintillation effects. It developed, however, that scintillation occurs at 4 and 6 GHz at equatorial latitudes (Craft and Westerlund, 1972; Taur, 1973).

Scintillation may involve weak scattering or strong scattering. The strongest scattering is observed in the equatorial and auroral regions, especially the equatorial areas. The resulting scintillation is corresponingly intense and extends to higher frequencies than elsewhere. Scintillation tends to be weak at temperate latitudes. Maximum scintillation occurs at night in all three regions. The pattern of occurrence is suggested in Fig. 2.13. It is generally agreed that the weak mid-latitude scintillation is due to diffractive scattering, and it has sometimes been assumed that such is the case for all scintillation. Certain analyses of strong scattering, including that responsible for scintillation at microwave (SHF) frequencies, however, have led to conclusions that such scintillation must be caused by a higher portion of the atmosphere, in particular the plasmasphere (Booker, 1975) or by a different mechanism, namely refractive scattering rather than diffractive scattering (Crain, Booker, and Ferguson, 1979). The refractive scattering is said to be caused by ionization structure in the form of "holes" or "bubbles" that are perpendicular to the line of sight. Refractive scattering is considered to involve irregularities of scale larger than the Fresnel scale, and diffractive scattering is assumed to involve irregularities having sizes near the Fresnel scale.

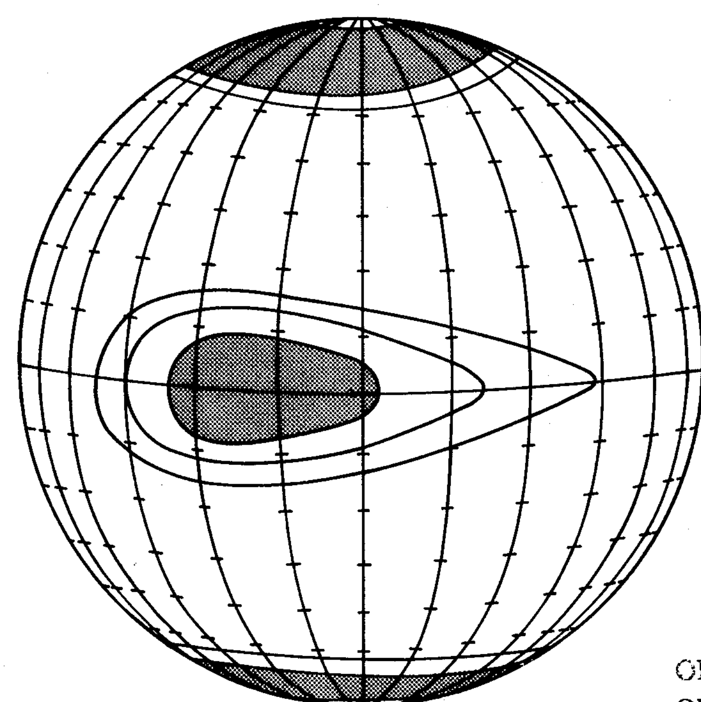

Figure 2.13. Pattern of ionospheric scintillation (CCIR, 1986b).

Several measures or indices of scintillation have been used. Attention was given to the subject of indices by Briggs and Parkin (1963) who introduced indices designated by S, S_1, S_2, and S_4. The index S_4, representing the standard deviation of received power divided by the mean value is said to be the most useful of the several indices (Klobuchar and Working Group (1978). It is given by

$$S_4 = \frac{1}{\overline{E^2}} \left[\overline{(E^2 - \overline{E^2})^2} \right]^{1/2} \tag{2.51}$$

where E is field intensity. A similar index, m, is defined as the ratio of rms fluctuation to mean value of power.

The index SI has been proposed as a convenient approximate measure of scintillation (Whitney, Aarons, and Malik, 1969). It is defined by

$$SI = \frac{P_{max} - P_{min}}{P_{max} + P_{min}}$$

where the P's represent power. In order to avoid overemphasizing extreme conditions, it is recommended that the third peak down from the maximum and the third minimum up from the absolute minimum be used to define P_{max} and P_{min}.

The parameter τ_c, the fade coherence time, is pertinent to digital communications. If τ_c is long compared to the time interval corresponding to one bit, the average bit error can be computed in terms of S_4. It has been stated that knowledge of S_4, τ_c, and a rough measure of coherence bandwidth are what is needed for considering the effect of scintillation on transionospheric communication systems (Klobuchar and Working Group, 1978).

2.6.2 Theoretical Background

Discussions of ionospheric scintillation may refer to Fresnel scale sizes and distances. To introduce these concepts, consider a path of length d between transmitting and receiving locations. At distances d_T from the transmitter and d_R from the receiver, the first Fresnel zone radius F_1 is given by (Appendix 2.1)

$$F_1 = \left(\frac{\lambda\, d_T\, d_R}{d} \right)^{1/2} \tag{2.52}$$

All the elements of radiation passing through the first Fresnel zone have components of electric field intensity that add constructively. If the distance to the transmitter d_T becomes very large compared to d_R, d_T approaches d and the first Fresnel zone radius is given by

$$F_1 = (\lambda\, d_R)^{1/2} \tag{2.52a}$$

The first Fresnel zone is circular in cross section and has an area of πF_1^2. Converting to different symbols, corresponding to irregularities that occur with a radius or scale size L about equal to F_1 at a height $h = z$ above a point of observation Eq. (2.52a) becomes

$$L = (\lambda\, z)^{1/2} \tag{2.52b}$$

Upon rearrangement, one obtains

$$z = L^2/\lambda \tag{2.53}$$

In Eqs. (2.52b) and (2.53), L takes the place of F_1 and z takes the place of d_R. In some cases, one may wish to know the Fresnel distance z corresponding to a certain value of L. In other applications, one may wish to know the Fresnel scale size L corresponding to a certain distance z. If d_T is not sufficiently large to justify using Eq. (2.52b), one can revert to Eq. (2.52).

Some analyses of ionospheric scintillation are based on consideration of scattering in an ionospheric layer or screen containing identical roughly isotropic or ellipsoidal irregularities of scale size L, as in Fig. 2.14. Let the irregularities of the layer be characterized by ΔN, the deviation in electron density from that of surroundings. The corresonding deviation Δn in index of refraction n can be determined by use of Eq. (2.33) to be given by

$$\Delta n = -40.3\ \Delta N/f^2 \tag{2.54}$$

Therefore

$$\overline{(\Delta n)^2} = 1.624 \times 10^3\ \overline{(\Delta N)^2}/f^4 \tag{2.55}$$

where the overbars indicate mean values. The phase change $\Delta\phi$ in traversing a single irregularity of size L is

$$\Delta\phi = (2\pi/\lambda)\ (L\ \Delta n) \tag{2.56}$$

where $2\pi/\lambda$ is the phase constant. Equation (2.55) can be written in an alternative form as

$$\frac{\overline{(\Delta n)^2}}{n} = \frac{1}{4\pi^2}\ r_e^2\ \lambda^4\ \overline{(\Delta N)^2} \tag{2.57}$$

where r_e is the classical electron radius (2.82×10^{-15} m). Using this form and considering a layer of thickness D rather than a layer of negligible thickness, the total mean square phase fluctuation $\overline{(\Delta\phi)^2}$ in a layer of thickness D at a zenith angle χ is given by Booker (1975) as

$$\overline{(\Delta\phi)^2} = 4\ r_e^2\ \lambda^2\ \overline{(\Delta N)^2}\ L\ D \sec\chi \tag{2.58}$$

Note that n of Eq. (2.57) is essentially unity and that Δn can be either a positive or negative quantity. The classical electron radius, r_e, is given in terms of other quantities by $r_e = \mu_o e^2/4\pi m$, (CRC, 1972) where $\mu_o = 4\pi \times 10^{-7}$ H/m is the magnetic

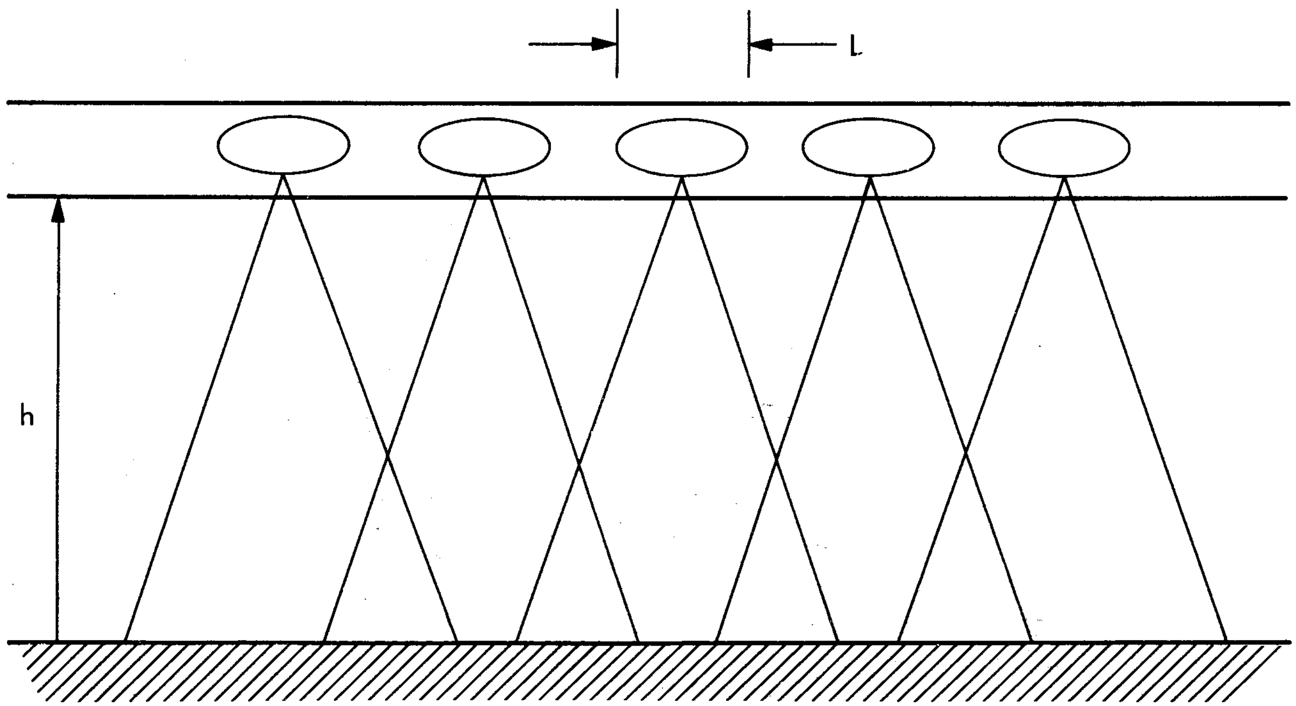

Figure 2.14. Layer of irregularities of scale size L.

permittivity of empty space and e and m are the charge and mass of the electron, respectively. It is not essential that the quantity classical electron radius be introduced into Eqs. (2.57) and (2.58). Instead one can employ Eq. (2.54) and $f = c/\lambda$ giving directly the result the that $|\Delta n|^2 = (4.484 \times 10^{-16})^2 \ \lambda^4 \ |\Delta N|^2$. [A check of the numerical coefficient of $|\Delta N|^2$ shows that it equals $r_e^2/4\pi$.]

Only phase variations occur immediately below the layer of Fig. 2.14, but amplitude variations develop farther below the layer. The distance h that is required for amplitude fluctuations to develop is in the order of the Fresnel distance $z = L^2/\lambda$ of Eq. (2.53). In particular, if $h > \pi L^2/\lambda$ amplitude fluctuations are said to develop (Booker, 1975). The phasor diagram of Fig. 2.15 can help to visualize the association of phase and amplitude fluctuations The parameter A represents the undisturbed component of field intensity

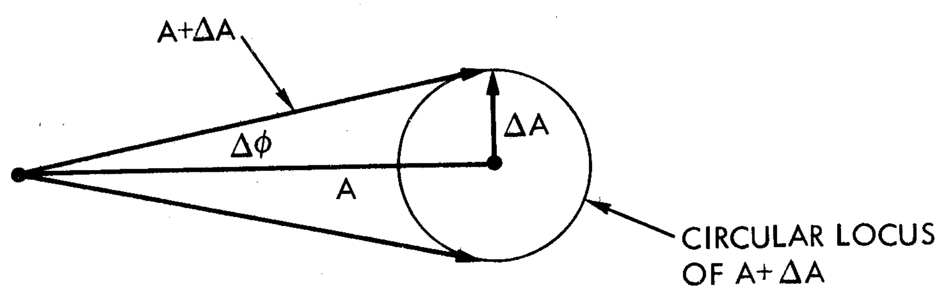

Figure 2.15 Phasor illustration of amplitude and phase variations.

and $\overline{(\Delta A)^2} = \overline{(\Delta\phi)^2}\, A^2$ so that

$$\overline{(\Delta A/A)^2} = \overline{(\Delta\phi)^2} \tag{2.59}$$

in the fully developed case. In the diagram ΔA represents a quantity that adds with random phase to A to produce amplitude variations.

Using results obtained by Bowhill (1961) but expressing relations in his own notation, Booker (1975) obtained the following expressions for phase and amplitude scintillations for weak scattering. The relations are in terms of $Z = \pi L^2/\lambda$.

$$\overline{(\Delta\phi)^2} = 4\, r_e^2\, \lambda^2\, \overline{(\Delta N)^2}\, LD \sec\chi\, \frac{1 + 0.5\,(h \sec\chi/Z)^2}{1 + (h \sec\chi/Z)^2} \tag{2.60}$$

$$\overline{(\Delta A/A)^2} = 4\, r_e^2\, \lambda^2\, \overline{(\Delta N)^2}\, LD \sec\chi\, \frac{0.5\,(h \sec\chi/Z)^2}{1 + (h \sec\chi/Z)^2} \tag{2.61}$$

when $h \sec\chi \gg Z$

$$\overline{(\Delta\phi)^2} = \overline{(\Delta A/A)^2} = 2\, r_e^2\, \lambda^2\, \overline{(\Delta N)^2}\, LD \sec\chi \tag{2.62}$$

when $h \sec\chi \ll Z$

$$\overline{(\Delta\phi)^2} = 4\, r_e^2\, \lambda^2\, \overline{(\Delta N)^2}\, LD \sec\chi \tag{2.63}$$

$$\overline{(\Delta A/A)^2} = \frac{2}{\pi^2}\, r_e^2\, \lambda^4\, \overline{(\Delta N)^2}\, \frac{h^2}{L^3}\, D \sec^3\chi \tag{2.64}$$

These relations are said to explain weak mid-latitude scintillation for parameters in the order of L = 800 m (scale size of Fig. 2.14), D = 200 km (thickness of ionosphere), and h = 300 km (height to center of ionosphere). In the analysis outlined above, a layer of substantial thickness is considered, but in other treatments the layer is replaced by an equivalent two-dimensional screen. Thus scintillation may be discussed in terms of a diffracting screen model (Cronyn, 1970). For present purposes, we will not distinguish between scattering by a layer or a screen.

For the theory of weak scattering to apply, it has been assumed that the phase variation introduced by the ionosphere is restricted to about 1 radian. For this condition, the amplitude variations observed at the ground are considered to correspond to the pattern of irregularities in the ionosphere, for irregularities below a certain size. If the phase variation is greater than 1 radian, the correspondence breaks down (Lawrence, Little, and Chivers, 1974). The amplitude scintillation index tends to increase with distance below the ionospheric layer but remains less than unity for weak scattering. The amplitude scintillation index for strong scattering can reach a value of unity and saturate or limit at that value, whereas phase scintillation does not reach a saturation point but continues to increase if the intensity of scattering continues to increase. An analysis by Rino and Fremouw (1977) indicated that phase variations are commonly in excess of 1 radian even when amplitude scintillation is weak.

The total field intensity at the ground is the sum of an unperturbed component and the perturbations in field intensity due to irregularities as in Fig. 2.15. The generation of perturbations can be understood in terms of electrical currents that flow in the irregularities due to the incident field intensity. Because of these currents, having a density different than that of the surrounding ionosphere, the irregularities act like antennas having roughly conical radiation patterns as suggested in Fig. 2.14. The beamwidth of the conical beams is about λ/L, the larger the irregularity the narrower the beamwidth and vice versa. At an observing point at a distance d below the layer where $d \ll z = L^2$, with z the Fresnel distance corresponding to the scale length L, only one beam is intercepted and only phase variations are recorded. For larger distances, the cones of radiation overlap and conditions for interference and consequent amplitude scintillations occur.

Assuming weak scattering and a pattern of ionospheric irregularities drifting horizontally, the above discussion indicates qualitatively how amplitude scintillations develop. A further question, however, is under what conditions will the amplitude scintillations correspond to and allow determination of the sizes of the irregularities. An additional requirement, if this condition is to be met, is that, as mentioned above, the irregularities must not be too large. In particular, the irregularities must not fill more than the first Fresnel zone. Radiation from the even Fresnel zones interferes with that from the odd zones (Appendix 2.1) and this condition introduces effects that preclude the identification of irregularities having scale sizes larger than $(\lambda z)^{1/2}$ [Eq. (2.52b)]. Phase scintillations, however, are not so limited and can be used to detect irregularities over a large range of scale sizes. Also they do not saturate but cover a wide dynamic range.

The temporal and spatial fluctuations of phase and amplitude are related to the power spectrum and autocorrelation function of electron density variations, the power spectrum and autocorrelation function being Fourier transforms of each other (Beckmann, 1967). Early analyses assumed a Gaussian form for the power spectrum (Briggs, and Parkin, 1963), but Rufenach (1972) assumed a power-law form. The relation between irregularity size ℓ_x and the corresponding frequency of temporal phase variation depends on the velocity of the moving pattern of irregularities. Assuming the pattern to be moving in the x direction with velocity v_x, $\ell_x = v_x T = v_x/f$ and $f = v_x/\ell_x$. The frequency f is that of the temporal variation in signal phase corresponding to a periodicity in electron density of ℓ_x, and T is the period of the temporal variation. The vector velocity of the moving pattern of irregularities can be determined by the use of three spaced antennas when the direction of the velocity is originally unknown (Coles, 1978).

The model involving diffraction in an ionospheric screen or layer has been widely employed to analyze scintillation, but it has been asserted that it may not be suitable if the irregularities are not confined to a sufficiently thin layer and if amplitude variations already occur at the lower boundary of the layer. First-order perturbation solutions of the scalar wave equation, based on the Rytov approximation or the method of smooth perturbations presented by Tatarski (1967,1971) are said to provide a means of treating the general case (Jokipii, 1973; Woo and Ishimaru, 1973, 1974; Crane, 1977; Ishimaru, 1978). The diffracting screen or layer model has been defended as being convenient and accurate for treating ionospheric scintillation (Bramley, 1977) and has been used by Rino (1979a.b) in his analysis of scintillation. Some proponents of the Rytov approximation say that the diffracting screen model gives good results in some cases but not in others, whereas the Rytov approximation is applicable generally. Some proponents of the diffracting screen model say that it gives good results, that it involves concepts equivalent to the use of a lumped-constant equivalent circuit for treating transmission problems, and that the Rytov approximation does not always correctly predict observed scintillation characterisics.

2.6.2 Effect of Source Size, Interplanetary Scintillations

Star twinkle in visible light but, because of their larger angular size, planets do not. The same effect of size occurs for radio waves. The reduction in scintillation when the source has an angular width greater than a certain value is due to the fact that the diffraction pattern on the ground is the convolution of the point-source pattern and the brightness distribution of the source. For weak scattering, the angular width of the source $\Delta\theta$ must be less than the angular width of the irregularities as seen from the ground if scintillation is to develop. The relation used by Lawrence, Little, and Chivers (1964) is that

$$\Delta\theta < L/2\pi d \tag{2.70}$$

for scintillation to occur, where L is the scale size of the irregularities and d is the distance to the irregularities. For strong scattering, they take

$$\Delta\theta < L/2\pi d\phi \tag{2.71}$$

for scintillation to be evident, where ϕ is the magnitude of the average phase change in radians and is greater than 1 radian. The effect of source size was recognized by Briggs (1961). Typically, radio sources must be smaller than about 6 to 10 minutes of arc if ionospheric scintillation is to develop.

In recording signals from radio sources of very small size along paths passing close to the Sun, Hewish, Scott, and Wills (1964) observed scintillations having short periods, typically around 1 s, which is small compared with the periods, typically around 30 s, that had been associated with ionospheric scintillations up to that time. For such short-period scintillations to be recorded, the sources must have angular widths of about 0.5 second or arc or less. (The angular extent of sources can be determined by interferometry techniques.) On the basis of the relations embodied in Eqs. (2.70) and (2.71) and taking into account that the signal paths passed through the solar wind close to the Sun, it was concluded that the scintillations were of interplanetary origin. An account of the early observations of interplanetary scintillation (IPS) has been provided by Cohen (1969). The use of IPS has become an important means for obtaining information about the solar wind (Woo, 1975,1977).

Before IPS were recognized, it was noted that radio-star signals that passed near the Sun expérienced angular broadening (Hewish, 1955). What was actually observed was a decrease in signal amplitude. This decrease could not be explained on the basis of absorption or refraction but only on the basis of angular broadening due to scattering by electron density irregularities. Angular broadening has been vividly illustrated as such by two-dimensional displays produced by a radio heliograph operating at 80 MHz (Blessing and Dennison, 1972). The radioheliograph, having a beamwidth at the zenith of 3.9 min, produces a 2 deg square-area picture of the sky every second.

When Pioneer 6, having a stable monochromatic signal was occulted by the Sun, another effect, spectral broadening, was observed (Goldstein, 1969). To record spectral broadening, the sidebands of the spacecraft signal are eliminated by filtering and only the pure carrier is recorded. Spectral broadening causes the carrier which originally has an exceedingly narrow width in frequency to be broadened in frequency. The phenomena may be caused by the Doppler shift of elements of radiation that are scattered from electron density irregularities or by amplitude scintillation or by a combination of both mechanisms.

2.6.4 Observed Characteristics of Scintillation

Scintillation tends to be most intense in equatorial, auroral, and polar latitudes and to have a general pattern of occurrence as shown in Fig. 2.13 (Aarons, Whitney, and Allen, 1971; CCIR, 1986b). Table 2.3 gives examples of observed percentages of occurrence of scintillation at frequencies of 137 and 254 MHz. The table includes K_p values, which are measures of magnetic activity, and shows that scintillation increases with K_p at sub-auroral and auroral latitudes.

The unexpected occurrence of scintillation at microwave frequencies at equatorial latitudes is illustrated for 6 GHz in Fig. 2.16 by Taur (1973), who presented further examples of the same type. Equatorial scintillation is often characterized by a sudden onset, and its occurrence varies considerably with location within the equatorial region. Basu et al. (1980) obtained data at 1.54 GHz at Huancayo, Peru for a 20-month period in 1976-1977 using the MARISAT satellite. Scintillation generally occurs after sunset and before midnight, with maximum intensities in roughly Feb.-March and Sept.-Oct. (Fig.2.17). Aarons et al. (1981a) obtained data at 1.54 GHz during the peak of the sunspot cycle in 1979 and 1980 from Huancayo; Natal, Brazil; and Ascension Island. Peak-to-peak fading greater than 27 dB was recorded at Ascension Island, and 7-9 dB were recorded at Huancayo and Natal. The latter two locations are close to the magnetic equator in what in known as the electrojet region. Ascension Island is at approximately 17 deg S dip latitude and is in the equatorial anomaly, namely the region from about 15 to 20 deg north and south of the magnetic dip equator where electron densities are higher than at the geomagnetic equator itself (Rishbeth and Garriot, 1969). Additional information about scintillation in the equatorial anomaly has been presented by Mullen et al. (1985). Scintillation greater than 30 dB at 1.5 GHz and 7 dB at 4 GHz was observed. Fan and Liu (1983) describe studies of GHz equatorial scintillations in the Asian region. Peak-to-peak fluctuations up to 14 dB were recorded. Aarons (1985) and Franke and Liu (1985) have modeled equatorial scintillation, with particular attention given to observations at Huancayo and Ascension Island, respectively.

Mid-latitude scintillation shows a well-established maximum near midnight, corresponding to the occurrence of spread F.

Table 2.3 Percentage of occurrence of scintillation (CCIR, 1982, 1986b). (a) ≥ 10 dB peak to peak, equatorial latitudes

Location	Frequency	Day	Night
		(400-1600 LT)	(1600-400 LT)
Huancayo, Peru	137 MHz	3	14
	254 MHz	2	7
		(600-1800 LT)	(1800-600 LT)
Accra, Ghana	137 MHz	0.4	14

(b) ≥ 12 dB peak to peak at 137 MHz, subauroral and auroral lat.

Location	K_p	Day (500-1700 LT)	Night (1700-500 LT)
Sagamore Hill, MA	0 to 3+	0	1.4
	> 3+	0.1	2
Goose Bay, Labrador	0 to 3+	0.1	1.8
	> 3+	1.6	6.8
Narssarssuaq, Greenl.	0 to 3+	2.9	18
		19	45

(c) ≥ 10 dB peak to peak at 254 MHz, auroral latitudes

Location	K_p	Day (600-1800 LT)	Night (1800-600 LT)
Goose Bay, Labrador	0 to 3+	0.1	0.1
	> 3+	0.3	1.2
Narssarssuaq, Greenl.	0 to 3+	0.1	0.9
		2.6	8.4

LT: Local Time

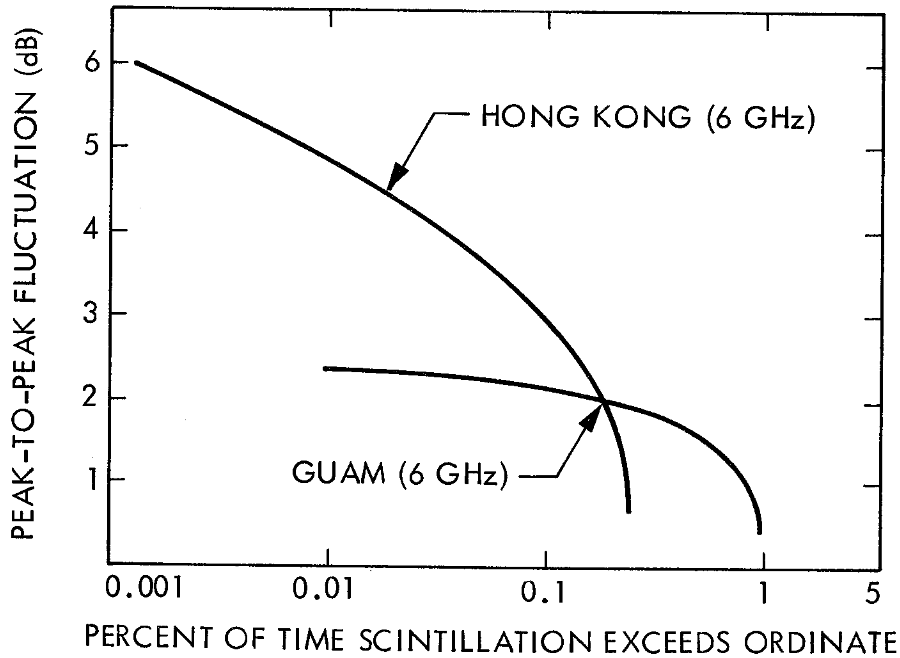

Figure 2.16. Scintillation, Guam and Hong Kong (Taur, 1973).

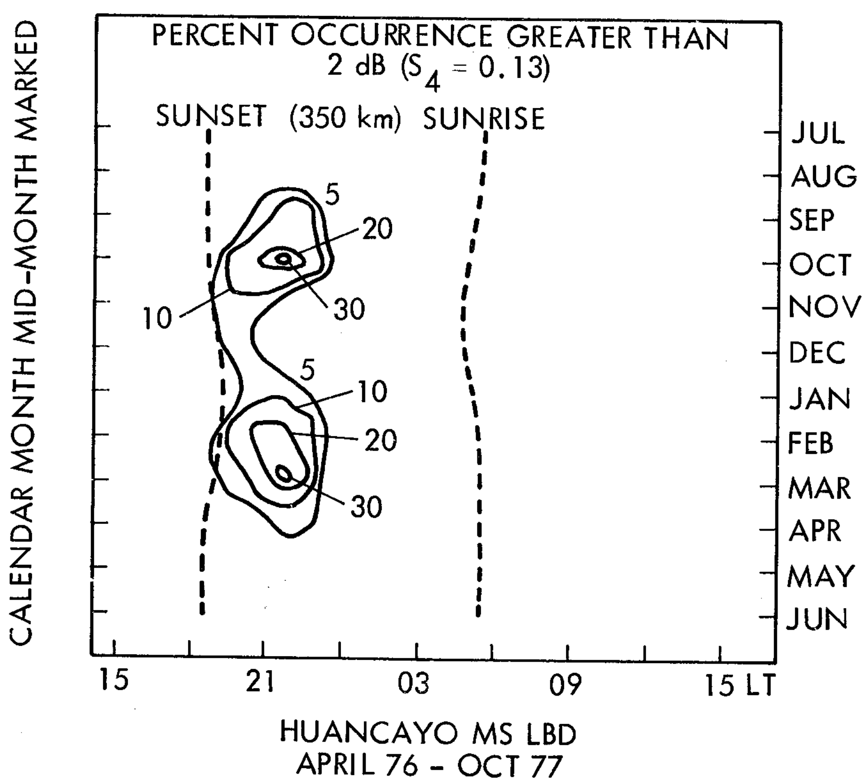

Figure 2.17. Monthly percentage of scintillations ≥ 2 dB, Huancayo, MARISAT, 1.54 GHz, (Basu et al., 1980).

Scintillation at middle latitudes is generally not intense, but some cases of severe scintillation have been recorded in Japan. During a magnetic storm on March 27, 1979, peak-to-peak scintillation of 18, 10, 15, and 3.5 dB were recorded at 136 MHz and 1.7, 4, and 12 GHz, respectively, on different paths in and around Japan (Minakoshi et al. 1981). Another report from Japan of severe scintillation, in this case of 1.5 GHz signals, has been provided by Karasawa et al. (1985). Signals from a MARISAT satellite over the Indian Ocean at an elevation angle of 17.3 deg were utilized. Fluctuations lasting for a long period and sometimes exceeding 30 dB peak-to-peak in the equinoctial month were observed and shorter spike-like scintillations were also evident.

Scintillation increases at high latitudes, the increase beginning near the region of the ionospheric trough. In the auroral oval, both discrete and diffuse aurora, as shown by Defense Meteorological Satellite images, have been correlated with scintillation at 136-137 MHz (Martin and Aarons, 1977). Frihagen (1971), using 40 MHz transmissions, has reported two regions of peak scintillation activity at high latitudes, one corresponding to the auroral oval and one above 80 deg geomagnetic latitude over the polar cap. Aarons et al. (1981b) have prepared plots showing percentages of occurrence of scintillation greater than 10 dB in the polar cap at Thule, Greenland at a frequency of 250 MHz. Buchau et al. (1985) relate 250-MHz scintillation to ionospheric structures in the polar cap. S. Basu et al. (1985) report the first long-term measurements of phase scintillations at high latitude at 250 MHz. The median and 90th percentile values of rms phase deviation at 250 MHz for an 82 second detrend interval are 2 and 6 rad, respectively, at both auroral and polar cap locations.

Measurements by Fremouw et al. (1978) employing 10 frequencies between 137 and 2891 MHz transmitted from a satellite in a high-inclination orbit and recorded at equatorial and auroral latitudes (Ancon, Peru; Kwajalein Island; and Fairbanks, Alaska) showed an $f^{-1.5}$ variation of the intensity of amplitude scintillations with frequency for S_4 less than 0.4 and an f^{-1} variation of phase scintillation with frequency. The more recent HiLat mission, utilizing satellite P83-1 with a 10-frequency radio beacon, had the objective of obtaining quantitative information on the spatial and temporal spectra of high-latitude amplitude and phase scintillation. The satellite was launched on June 27, 1983 from Vandenberg Air Force base. Early results of this mission have been presented by Fremouw et al. (1985).

Amplitude scintillations result in reduction of signal-to-noise ratio for a fraction of the time. Phase scintillations may or may not be important depending on the type of system. For digital systems, phase scintillations may be unimportant if the bit rate is much greater than the scintillation rate. Phase scintillations tend to be important for radio navigation systems such as GPS and for synthetic-aperture radars. For positioning systems phase scintillation results in range jitter and consequent loss of precision in range (Rino, Gonzalez, and Hessing, 1981; Yeh and Liu, 1979) as increments of phase $\Delta\phi$ and corresponding changes in apparent range ΔR_ϕ are related by $\Delta\phi = (2\pi/\lambda_o)\ \Delta R_\phi$ [Eq. (2.46)]. Loss of signal coherence is another possible effect from scintillation (Rino, Gonzalez, and Hessing, 1981). Loss of coherence across a band as narrow as 11.5 MHz at UHF was observed by Fremouw et al. (1978).

Amplitude scintillations can be described by use of power spectra, autocorrelation functions, cumulative probability distributions, fade-duration distributions, and plots showing message reliability (Whitney and Basu, 1977). Power spectra have been presented by a number of authors including Rufenach (1972), Crane (1976), and Whitney and Basu (1977). Examples of power spectra are shown in Figs. 2.18. Cumulative probability distributions show the percentage of time that signal amplitude exceeds specified dB values. The Nakagami-m distribution shows good agreement with observed distributions (Whitney and Basu, 1977; Fremouw et al., 1978; Panter, 1972). For the m of this distribution equal to unity (not to be confused with the scintillation index m), the distribution is a Rayleigh distribution.

The power spectra, cumulative probability distributions, etc. contain detailed information about scintillation characteristics, but frequently one is primarily interested in certain parameters such as

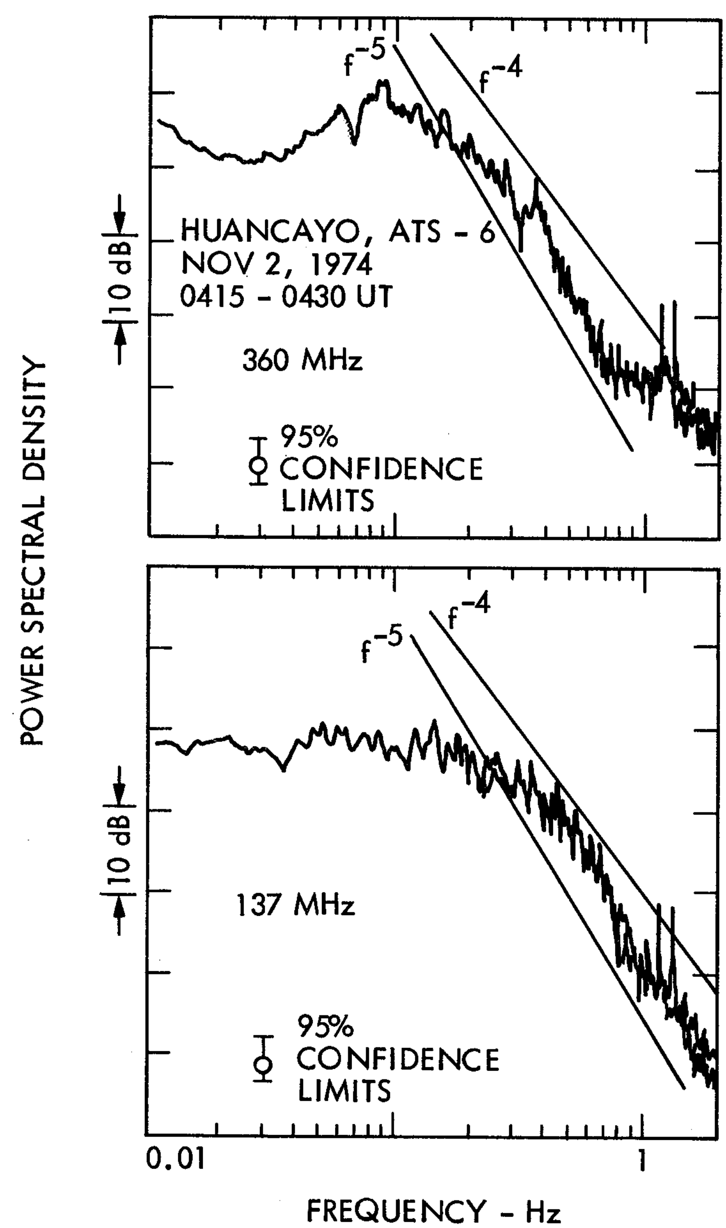

Figure 2.18. Typical power spectra for intense scintillations; S_4 = 0.78 at 360 MHz, S_4 = 0.94 at 137 MHz (Whitney and Basu, 1977).

mean value, standard deviation, scintillation index, and coherence time. The index S_4 is the ratio of standard deviation to mean value. Coherence time τ_c can be obtained from plots of the autocorrelation function and is the time for this function to decrease from unity to some specified value such as 0.5 or 1/e. Whitney and Basu (1977) used 0.5 in their analysis of scintillation data. For predicting bit error rate, the form of the probability distribution function is needed.

In CCIR Report 263-6, values of the fading period of scintillation are given (CCIR, 1986b). The period varies over a large range and can be as long as several minutes. The fading period of GHz scintillation varies from 2 to 15 seconds.

2.7 ABSORPTION

Attenuation was not included in discussing the characteristic waves and Faraday rotation in previous sections, but waves propagating in the ionosphere experience dissipative attenuation which becomes increasingly important with decreasing frequency. A principal mechanism of attenuation is collisions of free electrons with neutral atoms and molecules. An electromagnetic wave propagating in a plasma imparts an ordered component of velocity to the electrons but the electrons lose some of the associated energy in the collision process. Hence the electromagnetic wave is attenuated. The attenuation coefficient α, determining the rate of decrease of electric field intensity with distance in accordance with $e^{-\alpha z}$ for the left circularly polarized wave, is given, using conventional magneto-ionic theory, by

$$\alpha_\ell = \frac{Nq^2 \upsilon}{2m\epsilon_o n_r c\,[(\omega + \omega_B)^2 + \upsilon^2]} \quad \text{Nepers/m} \qquad (2.72)$$

where υ is the collision frequency. For the right circularly polarized wave, the corresponding expression is

$$\alpha_r = \frac{Nq^2 \upsilon}{2m\,\epsilon_o n_r c\,[(\omega - \omega_B)^2 + \upsilon^2]} \quad \text{Nepers/m} \qquad (2.73)$$

All quantities are in SI units. N is in electrons/m^3; q, the electron charge, equals 1.6022×10^{-19} C; m = 9.1096×10^{-31} kg; $\epsilon_o = 8.854 \times 10^{-12}$ F/m; n_r is the real part of the index of refraction; c = 2.9979×10^8 m/s; $\omega = 2\pi f$ with f in Hz; and υ is collision frequency in Hz. When attenuation is taken into account, the index of refraction becomes complex and is a function of collision frequency as well as electron density. The value of the real part n_r can be calculated precisely, based on assumed values of N and υ, but if losses are slight n_r has essentially the same value as for the lossless case, for which $n = n_r$ and is entirely real. Note that ω appears in the denominator and that for $\omega \gg \omega_B$, where ω_B is angular gyrofrequency, and $\omega \gg \upsilon$, attenuation varies inversely with ω^2. The frequencies used for space communication are generally sufficiently high that attenuation does vary inversely with frequency squared and n_r does have the same value as in the lossless case. Also, n_r approaches unity as frequency increases.

For frequencies above about 30 MHz or for transverse propagation of the ordinary wave, the attenuation constant varies inversely with frequency squared and takes the simpler form

$$\alpha = \frac{Nq^2 \upsilon}{2m\epsilon_o n_r c\, \omega^2} \quad \text{Nepers/m} \tag{2.74}$$

To obtain attenuation in dB/m, the value of α in Nepers/m can be multiplied by 8.686.

For oblique paths, total attenuation is proportional to sec χ/f^2, where χ is the zenith angle, for frequencies above 30 MHz (CCIR, 1986b). Attenuation tends to be low at the frequencies used for space communications, the highest attenuations occurring under conditions of auroral and polar-cap absorption.

Table 2.4 shows values of auroral absorption at a frequency of 127 MHz as published in CCIR Report 263-6 (CCIR, 1986b). In a typical night of auroral activity at Fairbanks, Alaska, long quiet auroral arcs appear to the north before midnight. These progress southward and may reach close to the zenith by 23 h local time. One or two westward traveling folds or surges in the otherwise quiet arcs may have been observed by this time. Between 23 h and 02 h the auroral forms become widespread and active in the sky, this phase being known as the auroral breakup. After the breakup, patchy, luminous forms appear in the sky. Quiet arcs may then reappear as the opening phase of a second cycle of activity. Auroral absorption is usually greatest in the breakup and post-breakup periods.

Figure 2.19 shows illustrative hypothetical plots of absorption during a polar-cap absorption event at 30 MHz, as could be derived from riometer events. The top curve applies in the summer when sunlight occurs for 24 hours a day. The other two curves for equal periods of day and night show a pronounced diurnal variation in absorption. The decrease in absorption at night is due to the decreased density of free electrons that occurs when solar radiation is absent.

Table 2.4 Auroral Absorption at 127 MHz, dB (CCIR, 1986b).

	Elevation Angle	
Percentage of time	20°	5°
0.1	1.5	2.9
1	0.9	1.7
2	0.7	1.4
5	0.6	1.1
50	0.2	0.4

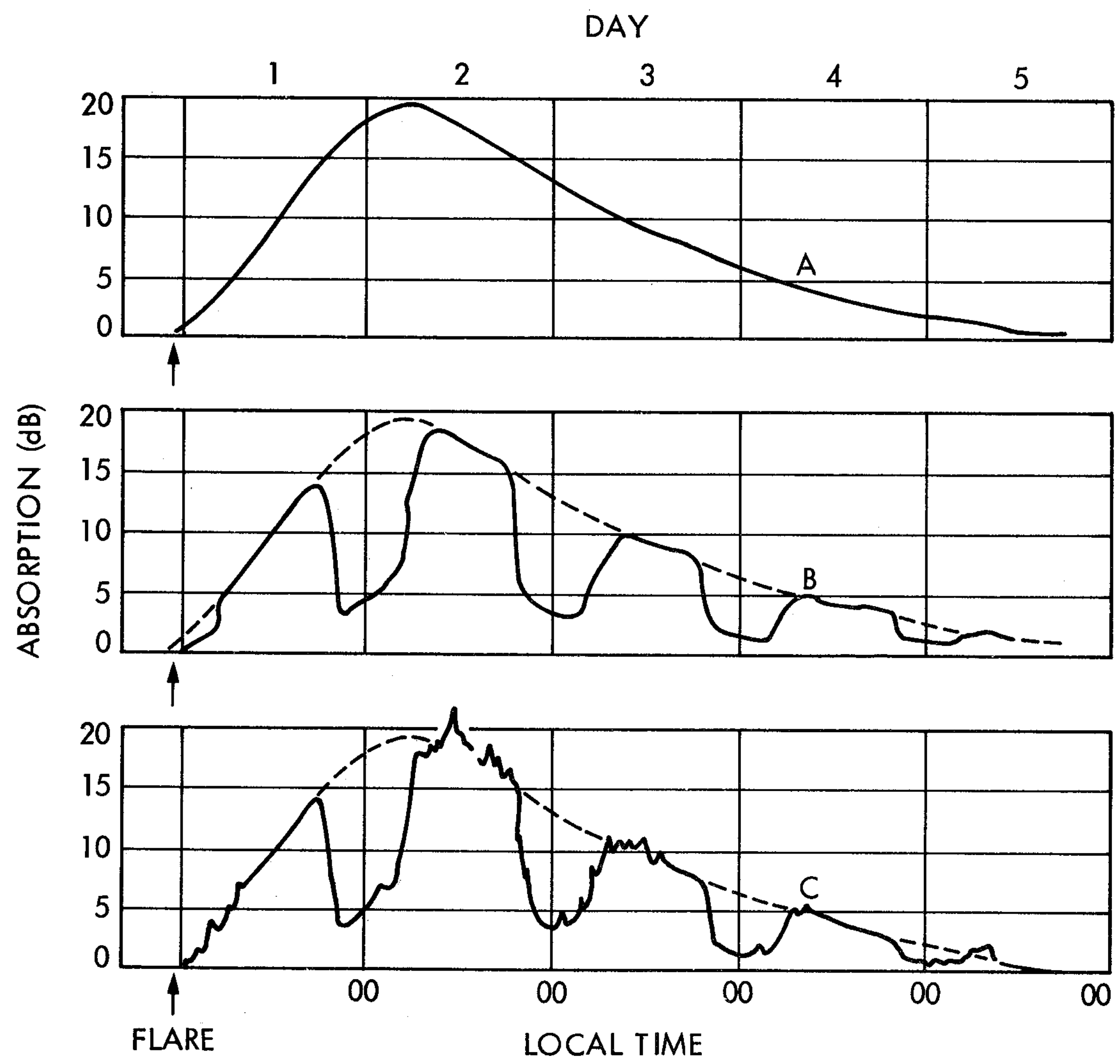

Figure 2.19. Hypothetical model showing polar cap absorption following a major solar flare as expected to be observed on riometers at approximately 30 MHz. (CCIR, 1986b).

A: High latitudes, 24 h of daylight.
B: High latitudes, equal day and night.
C: Auroral zone.

2.8 TRANSIONOSPHERIC PROPAGATION PREDICTIONS AND CORRECTIONS

For some satellite systems advance estimates of ionospheric parameters in the planning stage are sufficient, but for other systems continuously updated long-term (e.g. monthly) or short-term (e.g. daily) predictions may be needed. Furthermore, real-time or near-real-time values of ionospheric parameters may be required in some cases.

The problem of ionospheric predictions was considered in a conference devoted to solar-terrestrial predictions (Donnelly, 1978). Included in the proceedings of the conference is a report treating transionospheric propagation predictions (Klobuchar and Working Group, 1978). It is stated in the working group report that monthly values of TEC can probably be predicted within ±20 percent for regions where a time history of TEC exists. However, even if monthly mean values could be predicted perfectly accurately, short-term variations from the monthly mean values would still present a problem. Much of the difficulty arises from the ionospheric effects of geomagnetic storms. Theoretical capabilities were not considered to be capable of predicting storm-related TEC behavior, and prediction procedures based on morphological data are the only alternative. The report discusses the problem and possible remedies.

Faraday-rotation data from linearly polarized 137-MHz beacons of the geostationary satellites ATS-1, SIRIO, and Kiku-2 have been used by the Jet Propulsion Laboratory to measure TEC and determine ionospheric corrections to range and Doppler data used for Voyager spacecraft navigation (Royden et al., 1980). By taking the difference between TEC values determined by Faraday rotation and TEC values from dual-frequency transmissions from Voyager (2295 MHz in the S band and 8415 MHz in the X band), the electron content of the path beyond the ionosphere is also determined. The electron content beyond the ionosphere includes that of the plasmasphere and the solar plasma. In passing by the moon Io of Jupiter, electrons in its atmosphere contributed to the total electron content along the path and made possible a comparison of

C-2

experimental results and theoretical models of the electron density surrounding Io. A two-frequency technique involving time-delay measurements for determining TEC, in order to correct for its effects, was described in Sec. 2.3.1.

In addition to the periodical literature, URSI (International Scientific Radio Union), the CCIR (International Radio Consultative Committee), and the series of Ionospheric Effects Symposia are good sources of information about the ionosphere and its effects. U.S. Commission G, Ionospheric Radio and Propagation of URSI, usually participates in two URSI meetings per year in the United States, and URSI holds international General Assemblies every three years. Volume VI of Recommendations and Reports of the CCIR and the CCIR working groups which contribute to it treat Propagation in Ionized Media. The fifth Ionospheric Effects Symposium (IES) was held in May, 1987 in Springfield, Virginia, sponsored by the Naval Research Laboratory, the Office of Naval Research, the Air Force Geophysics Laboratory, and the Army Center for Communications. The May/June 1985 issue of Radio Science was devoted to papers presented at the 1984 IES, and several of these are cited in this chapter.

REFERENCES

Aarons, J., J.P. Whitney, and R.S. Allen, "Global morphology of ionospheric scintillations," Proc. IEEE, vol. 59, pp. 159-172, Feb. 1971.

Aarons, J. et al., "Microwave equatorial scintillation intensity during solar maximum," Radio Sci., vol. 10, pp. 939-945, Sept.-Oct. 1981a.

Aarons, J. et al., "VHF scintillation activity over polar latitudes," Geophys. Res. Lett., vol. 8, pp.277-280, 1981b.

Aarons, J., "Construction of a model of equatorial scintillation intensity," Radio Sci., vol. 20, pp. 397-402, May-June 1985.

Akasofu, S.I., Polar and Magnetospheric Subsystems. New York: Springer-Verlag, 1968.

Balsley, B.B., "Some characteristics of non-two-stream irregularities in the equatorial electrojet," J. Geophys. Res., vol. 74, pp.2333-2347, May 1, 1969.

Baron, M.J., "Electron densities within aurorae and other auroral E-region characteristics," Radio Sci., vol. 9, pp.341-348, Feb. 1974.

Basu, S. et al., "Long-term 1.5 GHz amplitude scintillation measurements at the magnetic equator," Geophys. Res. Lett., vol. 7, pp. 259-262, April 1980.

Basu, S. et al., Morphology of phase and intensity scintillations in the auroral oval and polar cap," Radio Sci., vol.20, pp. 347-356, May-June1985.

Beckmann, P. Probability in Communication Engineering. New York: Harcourt, Brace, and World, 1967.

Blesing, R.G. and P.A. Dennison, "Coronal broadening of the Crab Nebula 1969-1971: observations," Proc. Astron. Soc. Australia, vol.2, pp. 84-86, March 1972.

Booker, H.G., "The role of the magnetosphere in satellite and radio-star scintillation," J. Atmos. Terr. Phys., vol. 37, pp.1089-1098, Aug. 1975.

Booker, H.G., "The role of acoustic gravity waves in the generation of spread-F and ionospheric scintillation," J. Atmos. Terr. Phys., vol. 41, pp. 501-515, May 1979.

Bowhill, S.A., "Statistics of a radio wave diffracted by a random ionosphere," J. of Research of NBS, vol. 65D, pp. 275-292, May-June 1961.

Bramley, E.N., "The accuracy of computing ionospheric radio-wave scintillation by the thin-phase-screen approximation," J. Atmos. Terr. Phys., vol.39, pp. 367-373, March 1977.

Briggs, B.H., "The correlation of radio star scintillations with geomagnetic disturbances," Geophysical J., vol. 5, pp. 306-317, Oct. 1961.

Briggs, B.H. and I.A. Parkin, "On the variation of radio star and satellite scintillations with zenith angle," J. Atmos. Terr. Phys., vol. 25, pp. 339-365, June 1963.

Buchau, J. et al., "Ionospheric structures in the polar cap: their origin and relation to 250-MHz scintillation," Radio Sci., vol. 20, pp. 325-338, May-June 1985.

Budden, K.G., Radio Waves in the Ionosphere. Cambridge: Cambridge U. Press, 1961.

Callahan, P.S. , "Columnar content measurements of the solar-wind turbulence near the sun," Astrophys. J., vol. 199, pp. 227-236, July 1, 1975.

CCIR, Report 263-5, 1982. [Earlier version of CCIR, 1986b.]

CCIR, Report 565-3, "Propagation data for broadcasting from satellites," in Volume V, Propagation in Non-ionized Media, Recommendations and Reports of the CCIR, 1986. Geneva: Int. Telecomm. Union, 1986a.

CCIR, Report 263-6, "Ionospheric effects upon earth-space propagation," in Volume VI, Propagation in Ionized Media, Recommendations and Reports of the CCIR, 1986. Geneva: Int. Telecomm. Union, 1986b.

Cohen, M.H., "High-resolution observations of radio sources," Annual Rev. of Astron. and Astrophys., vol. 7, pp. 619-664, 1969.

Coles, W.A., "Interplanetary scintillations," Space Sci. Rev., vol. 21, pp. 411-425, 1978.

Craft, H.D. and L.H. Westerlund, "Scintillations at 4 and 6 GHz caused by the ionosphere," 10th Aerospace Sci. Meeting, AIAA Paper No. 72-179, 1972.

Crain, C.M., H.G. Booker, and J.A. Ferguson, "Use of refractive scattering to explain SHF scintillations," Radio Sci., vol. 14, pp. 125-134, Jan.-Feb. 1979.

Crane, R.K., "Spectra of ionospheric scintillations," J. Geophys. Res., vol. 81, pp. 2041-2050, May 1, 1976.

Crane, R.K., "Ionospheric scintillation," Proc. IEEE, vol. 65, pp. 180-199, Feb. 1977.

CRC (Weast, R.C. ed.), Handbook of Chemistry and Physics, 52nd Edition, p. F189. Cleveland, OH: Chemical Rubber Co., 1972.

Cronyn, W.M., "The analysis of radio scattering and space-probe observations of small-scale structure in the interplanetary medium," Astrophys. J., vol. 161, pp. 755-763, Aug. 1970.

Davies, K., Ionospheric Radio Propagation. Washington, DC: Supt. of Documents, U.S. Government Printing Office, 1965.

Davies, K., Ionospheric Radio Waves. Waltham, MA: Blaisdell Pub. Co., 1969.

Davies K., G.K. Hartmann, and R. Leitinger, "A comparison of several methods for estimating columnar electron content of the plasmasphere," J. Atmos. Terr. Phys., vol. 39, pp. 571-580, May, 1977.

Davies, K., "Recent progress in satellite radio beacon studies with particular emphasis on the ATS-6 radio beacon experiment," Space Sci. Rev., vol. 25, pp. 357-430, April 1980.

Donnelly, R. F. (ed.), Solar Terrestrial Predictions Proceedings, Volumes 1-4. Boulder, CO: Environ. Res. Labs., NOAA, 1978.

Evans, J.V., "Theory and practice of ionospheric study by Thomson scatter radar," Proc. IEEE, vol. 57, pp. 496-530, April 1969.

Fang, D.J. and C.H. Liu, "A morphological study of gigahertz scintillation in the Asian region," Radio Sci., vol. 18, pp. 241-252, 1983.

Farley, D.T., "A plasma instability resulting in field-aligned irregularities in the ionosphere," J. Geophys. Res., vol. 68, pp. 6083-6097, Nov. 15, 1963.

Feldstein, Y.I., "A quarter of a century with the auroral oval," EOS, vol. 67, Oct. 7, 1986.

Flock, W.L., Electromagnetics and the Environment: Remote Sensing and Telecommunications. Englewood Cliffs, NJ: Prentice-Hall, 1979.

Franke, S.J. and C.H. Liu, "Modeling of equatorial multifrequency scintillation," Radio Sci., vol. 20, pp. 403-415. May-June, 1985.

Fremouw, E.J., et al., "Early results from the DNA wideband satellite experiment - complex signal scintillation," Radio Sci., vol. 13, pp. 167-187, Jan.-Feb. 1978.

Fremouw, E.J., et al., "The HiLat satellite mission," Radio Sci., vol. 20, pp. 416-424, May-June 1985.

Frihagen, J., "Occurrence of high latitude ionospheric irregularities giving rise to satellite scintillation," J. Atmos. Terr. Phys., vol. 33, pp. 21-30, 1971.

Goldstein, R.M., "Superior conjunction of Pioneer 6," Science, vol. 166, pp. 598-601, 31 Oct. 1969.

Hawkins, G.S. and J.A. Klobuchar, "Seasonal and diurnal variations in the total electron content of the ionosphere at invariant latitude 54 degrees," AFCRL-TR-74-0294. Bedford, MA: Air Force Camb. Res. Labs., 28 June 1974.

Hay, J.S., S.J. Parsons, and J.W. Phillips, "Fluctuations in cosmic radiation at radio frequencies," Nature, vol. 158, p. 234, Aug.17, 1946.

Heron, M.L., "Transequatorial propagation through equatorial plasma bubbles - discrete events," Radio Sci., vol. 15, pp. 829-835, July-Aug. 1980.

Hewish, A., "The diffraction of galactic radio waves as a method of investigating the irregular structure of the ionosphere," Proc. Royal Soc. of London, Series A, vol. 214, pp. 494-514, 9 Oct. 1952.

Hewish, A., "The irregular structure of the outer regions of the solar corona," Proc. Royal Soc. of London, Series A, vol. 228, pp. 238-251, 22 Feb. 1955.

Hewish, A., P.F. Scott, and D. Wills, "Interplanetary scintillation of small diameter radio sources," Nature, vol. 203, pp. 1214-1217, Sept. 19, 1964.

Hines, C.O. et al., The Upper Atmosphere in Motion, Geophysical Monograph 18. Washington, DC: A. Geophys. Union, 1974.

Hunsucker, R.D., "Simultaneous riometer and incoherent scatter radar observations of the auroral D region," Radio Sci., vol. 9, pp. 335-340, Feb. 1974.

Ishimaru, A., Wave Propagation and Scattering in Random Media, Vol. 2. New York: Academic Press, 1978.

Jokipii, J.R., "Turbulence and scintillations in the interplanetary plasma," Ann. Rev. of Astron. and Astrophys., vol. 11, pp. 1-28, 1973.

Karasawa, Y., K. Yasukawa, and M. Yamada, "Ionospheric scintillation measurements at 1.5 GHz in mid-latitude region," Radio Sci., vol. 20, pp. 543-551, May-June 1985.

Kelso, J.M., Radio Ray Propagation in the Ionosphere. New York: McGraw-Hill, 1964.

Klobuchar, J.A., "Ionospheric effects on satellite navigation and air traffic control systems," in Recent Advances in Radio and Optical Propagation for Modern Communication, Navigation, and Detection Systems, AGARD Proceedings - LS-93, ISBN 92-835-1280-4. NTIS: Springfield, VA 22161, April 1978.

Klobuchar, J.A. (leader) and Working Group, "B. Trans-ionospheric propagation predictions," in R.F. Donnelly (ed.), vol. 2: Working Group Reports and Reviews of Solar-Terrestrial Predictions Proceedings, pp. 217-245, Boulder, CO: Environ. Res. Labs.,NOAA, 1978.

Lawrence, R.S., C.G. Little, and H.J.A. Chivers, "A survey of ionospheric effects upon earth-space propagation," Proc. IEEE, vol. 52, pp. 4-47, Jan. 1964.

Leadabrand, R.L. et al., "Chatanika, Alaska auroral-zone incoherent scatter facility," Radio Sci., vol. 7, pp. 747-756. July 1972.

Little, C.G. and A.C.B. Lovell, "Origin of the fluctuations in the intensity of radio waves from galactic sources: Jodrell Bank observations," Nature, vol. 165, pp. 423-424, March 18, 1950.

Malin, S.R.C. and D.R. Barraclough, "An algorithm for synthesizing the geostationary field," Computers and Geosci., vol. 7, No. 4, pp. 401-405, 1981.

Martin, E. and J. Aarons, "F layer scintillations and the aurora," J. Geophys. Res., vol. 82, pp. 2717-2722, July 1, 1977.

McClure, J.P., W.B. Hanson, and J.H. Hoffman, "Plasma bubbles and irregularities in the equatorial ionosphere," J. Geophys. Res., vol. 82, pp. 2650-2656, July 1, 1977.

Millman, G.H. and G.M. Reinsmith, An analysis of the incoherent scatter-Faraday rotation technique for ionospheric propagation error correction," General Electric Tech. Inf. Series R 74EMH2, Syracuse, NY, Feb. 1974.

Minakoshi, H. et al., "Severe ionospheric scintillation associated with magnetic storm on March 22, 1979," J. Radio Res. Labs. (Japan), vol. 28, pp. 1-9, 1981.

Mullen, J.P. et al., "UHF/GHz scintillation observed at Ascension Island from 1980 through 1982," Radio Sci., vol. 20, pp. 357-365, May-June 1985.

Panter, P.F., Communication Systems Design. New York: McGraw-Hill, 1972.

Peddie, N.W., "International geomagnetic reference field: the third generation," J of Geomag. and Geoelect., vol. 34, pp. 309-327, 1982.

Ratcliffe, J.A., An Introduction to the Ionosphere and Magnetosphere. Cambridge: Cambridge U. Press, 1972.

Rino, C.L., "A power law phase screen model for ionospheric scintillation, 1. Weak scatter," Radio Sci., vol. 14, pp.1135-1145, Nov.-Dec. 1979a.

Rino, C.L., "A power law phase screen model for ionospheric scintillation, 2. Strong scatter," Radio Sci., vol 14, pp.1147-1155, Nov.-Dec. 1979b.

Rino, C.L. and E.J. Fremouw, "The angle dependence of singly scattered wave-fields," J. Atmos. Terr. Phys., vol. 39, pp. 859-868, Aug. 1977.

Rino, C.L., V.H. Gonzales, and A.R. Hessing, "Coherence bandwidth loss in transionospheric radio propagation," Radio Sci., vol. 16, pp. 245-255, March-April 1981.

Rishbeth, H. and O.K. Garriott, Introduction to Ionospheric Physics New York: Academic Press, 1969.

Royden, H.N., D.W. Green, and G.R. Walson, "Use of Faraday-rotation data from beacon satellites to determine ionospheric corrections for interplanetary spacecraft navigation." COSPAR/URSI Symposium on Scientific and Engineering Uses of Satellite Radio Beacons, Warsaw. Poland, May 19-23, 1980.

Rufenach, C.L., "Power-law wave number spectrum deduced from ionospheric scintillation observations," J. Geophys. Res., vol. 77, pp. 4761-4772, Sept. 1, 1982.

Smith, E.K., A Study of Ionospheric Scintillation as it Affects Satelllite Communication, Office of Telecomm., U.S. Dept. of Commerce, Tech. Memorandum 74-186, Nov. 1974.

Smith, E.K. and R.E. Edelson, "Radio propagation through solar and other extraterrestrial ionized media," JPL Pub. 79-117. Pasadena, CA: Jet Propulsion Lab., Jan. 15, 1980.

Smith, F.G., "Origin of the fluctuations in the intensity of radio waves from galactic sources: Cambridge observations," Nature, vol. 165, pp. 422-423, March 18, 1950.

Tatarski, V.E., Wave Propagation in a Turbulent Medium. New York; McGraw-Hill, 1961.

Tatarski, V.E., The Effects of the Turbulent Atmosphere on Wave Propagation. Springfield, VA: National Technical Information Service, 1971.

Taur, R.R., "Ionospheric scintillation at 4 and 6 GHz," COMSAT Tech. Rev., vol. 3, pp. 145-163, Spring 1973.

Whitney, H.E., J. Aarons, and C. Malik, "A proposed index for measuring ionospheric scintillation," Planet. Space Sci., vol. 7, pp 1069-1073, 1969.

Whitney, H.E. and S. Basu, "The effect of ionospheric scintillation on VHF/UHF satellite communication," Radio Sci., vol. 12, pp. 123-133, Jan.-Feb. 1977.

Woo, R., "Multifrequency techniques for studying interplanetary scintillation," Astrophys. J., vol. 201, pp. 238-248, Oct. 1, 1975.

Woo, R. "Measurements of the solar wind using spacecraft radio scattering observations," in Study of Travelling Interplanetary Phenomena, Shea, M.A. and D.F. Smart (eds.), pp. 81-100. Dordrecht, Holland: D. Reidel Pub. Co., 1977.

Woo, R. and A. Ishimaru, "Remote sensing of the turbulence characteristics of a planetary atmosphere by radio occultation of a space probe," Radio Sci., vol. 8, pp. 103-108, Feb. 1973.

Woo, R. and A. Ishimaru, "Effects of turbulence in a planetary atmosphere on radio occultation," IEEE Trans. Antennas Propagat., vol. AP-22, pp. 566-573, July 1974.

Woodman, R.F. and C. La Hoz, "Radar observations of F-region equatorial irregularities," J. Geophys. Res., vol. 81, pp. 5447-5466, Nov. 1, 1976.

Yeh, K.C., and C. Liu, "Ionospheric effects on radio communication and ranging pulses," IEEE Trans. Antennas Propagat., vol. AP-27, pp. 747-751, Nov. 1979.

Yeh, K.C. and G.W. Swenson, "F-region irregularities studies by scintillation of signals from satellites," Radio Science (Sec. D., J. of Research, National Bureau of Standards), vol. 68D, pp. 881-894, Aug. 1964.

APPENDIX 2.1

FRESNEL ZONES

To obtain expressions for the radii of the Fresnel zones, consider the two paths of Fig. A2.1. TPR is a direct path from the transmitter at T to a receiver at R, and path TSR is longer than TPR. If TSR = TPR + $\lambda/2$ where λ is wavelength, the region within the radius r of the direct path, at the distance d_T from T and d_R from R, is defined as the first Fresnel zone. Let this particular

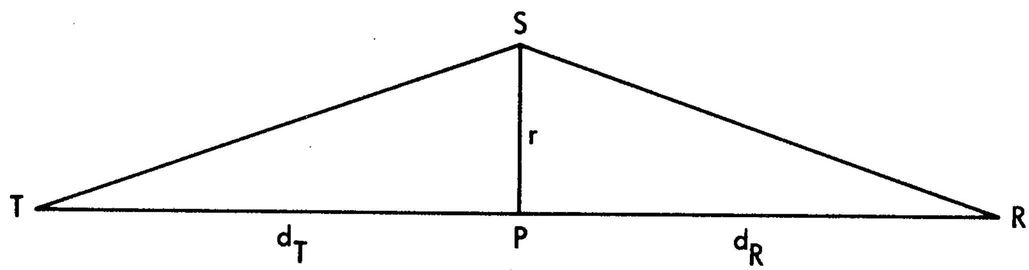

Figure A2.1. Geometry for consideration of Fresnel zones.

value of r be defined as F_1, the first Fresnel zone radius. Considering that the paths are such that TSP and RSP form good approximations to right triangles with $F_1 << d_T$ and $F_1 << d_R$,

$$TS = \sqrt{d_T^2 + F_1^2} = d_T \left[1 + \frac{F_1^2}{2\,d_T^2} \right] \tag{A2.1}$$

and

$$SR = \sqrt{d_R^2 + F_1^2} = d_R \left[1 + \frac{F_1^2}{2\,d_R^2} \right] \tag{A2.2}$$

Setting TPR + $\lambda/2$ = TSR gives

$$d_T + d_R + \lambda/2 = d_T + d_R + \frac{F_1^2}{2\,d_T} + \frac{F_1^2}{2\,d_R} \tag{A2.3}$$

from which

$$\frac{F_1^2}{d_T} + \frac{F_1^2}{d_R} = \lambda \tag{A2.4}$$

and

$$F_1^2 \left[\frac{d_T + d_R}{d_T\, d_R} \right] = \lambda \tag{A2.5}$$

so that

$$F_1 = \sqrt{\frac{\lambda\, d_T\, d_R}{d}} \tag{A2.6}$$

where $d = d_T + d_R$. If TSR = TPR + n $\lambda/2$, then

$$F_n = n^{1/2}\ F_1 \tag{A2.7}$$

All the elements of radiation passing through the first Fresnel zone have components of field intensity that add constructively. Radiation passing through the second Fresnel zone (between $r = F_1$ and $r = F_2$) interferes destructively with that passing through the first zone, and radiation passing through the third zone adds with that through the first. This condition of alternating destructive and constructive intereference continues, radiation from each zone being 180 deg out of phase with that from adjacent zones, but the amplitudes of the contributions decrease with increasing n.

APPENDIX 2.2

EXPANSION OF EARTH'S MAGNETIC FIELD IN SPHERICAL HARMONICS

The Earth's magnetic field can be represented by a scalar magnetic potential as shown by Eq. (A2.8).

$$V = a \sum_{n=1}^{N} \sum_{m=0}^{n} (a/r)^{n+1} \left(g_n^m \cos m\lambda + h_n^m \sin m\lambda\right) P_n^m (\cos \theta) \tag{A2.8}$$

The quantity r is the radial spherical coordinate and a is the mean radius of the Earth (6371.2 km). The quantity λ represents east longitude measured from Greenwich, and θ is geocentric colatitude (the polar angle of spherical coordinates). The northward component of magnetic flux density X_c can be obtained from V by use of

$$X_c = \frac{1}{r} \frac{\partial V}{\partial \theta} \tag{A2.9}$$

and the eastward component Y_c can be obtained from

$$Y_c = -\frac{1}{r \sin \theta} \frac{\partial V}{\partial \lambda} \tag{A2.10}$$

The downward component is given by

$$Z_c = \frac{\partial V}{\partial r} \tag{A2.11}$$

The g's and h's are the coefficients of the spherical harmonic expansion and, as mentioned on p. 2-3, these are given in the June 17, 1986 issue of EOS for the 1985, fourth-generation model.

CHAPTER 3

TROPOSPHERIC CLEAR-AIR EFFECTS

3.1 INDEX OF REFRACTION PROFILE

Propagation in the troposphere is influenced, and in some cases strongly affected, by the variation of the index of refraction with height. By definition, the index of refraction n of a particular type of wave in a given medium is the ratio of c, about 2.9979×10^8 m/s, to the phase velocity of the wave in the medium. The index of refraction of the troposphere is a function of pressure, temperature, and water vapor content as indicated by

$$N = (n - 1) \times 10^6 = \frac{77.6\, p_d}{T} + \frac{72\, e}{T} + \frac{3 \times 10^5\, e}{T^2} \qquad (3.1)$$

where p_d is the pressure of dry nonpolar air in mb (millibars), e is water vapor pressure in mb, and T is temperature in kelvins (Smith and Weintraub, 1953). Because the index n is only slightly greater than 1, the usual practice is to use N units for convenience, with N defined as in Eq. (3.1). N, referred to as refractivity, is seen to vary inversely with temperature and to be strongly dependent on water vapor pressure. The water vapor pressure e, the saturation water vapor pressure e_s, which is a function of temperature (Table 3.1), and relative humidity R.H. are related by $e = e_s$ (R.H.). If Eq. (3.1) is expressed in terms of p, the total pressure, where $p = p_d + e$, it becomes

$$N = \frac{77.6\, p}{T} - \frac{5.6\, e}{T} + \frac{3.75 \times 10^5\, e}{T^2} \qquad (3.2)$$

The last two terms can be combined to give, approximately,

$$N = \frac{77.6\, p}{T} + \frac{3.73 \times 10^5\, e}{T^2} = \frac{77.6}{T}\left(p + \frac{4810\, e}{T}\right) \qquad (3.3)$$

The two forms of Eq. (3.3) are widely used (CCIR,1986a) and give values for N that are accurate within 0.5 percent for the ranges of atmospheric parameters normally encountered and for frequencies below 30 GHz (Crane, 1976). If one wishes to consider the effects of dry air and water vapor separately, however, letting $N = N_d + N_w$ where N_d refers to dry air and N_w to water vapor, Eq. (3.1) should be used with

$$N_d = 77.6\, p_d/T \tag{3.4}$$

and

$$N_w = \frac{72\, e}{T} + \frac{3.75 \times 10^5\, e}{T^2} \tag{3.5}$$

Table 3.1 Saturation Water Vapor Pressure e_s [From List (1984) in Smithsonian Meteorological Tables.]

T (^oC)	e_s (mb)	T (^oC)	e_s (mb)
-30	0.5	18	20.6
-20	1.3	20	23.4
-10	2.9	22	26.4
0	6.1	24	29.8
2	7.1	26	33.6
4	8.1	28	37.8
6	9.3	30	42.4
8	10.7	32	47.6
10	12.3	34	53.2
12	14.0	36	59.4
14	16.0	38	66.3
16	18.2	40	73.8

The absolute humidity or water vapor density in g/m^3, ρ, and e in mb are related (Appendix 3.1) by

$$\rho = 216.5 \, e/T \tag{3.6}$$

The dew point is the temperature at which air is saturated with water vapor, and values of the dew point can be used to determine the saturation water vapor pressure by use of Table 3.1. For example, the highest accepted weather-observatory dew point of 34 deg C [recorded on the shore of the Persian Gulf at Sharjah, Saudi Arabia (U.S. Standard Atmosphere, 1976)] corresponds to a vapor pressure of 53.2 mb and an absolute humidity of 37.5 grams per cubic meter. Although an increase in temperature would cause a decrease in N if water vapor pressure were held constant, the saturation pressure increases rapidly with temperature and the highest values of N therefore occur for high temperatures (and high relative humidities).

The value of N corresponding to the value of e of 53.2 mb at a temperature of 34 deg C, for example, is 467. In nearby desert areas of Saudi Arabia where the relative humidity might approach zero, however, the value of N could approach 256, the value for dry air at the sea level pressure of 1013 mb and the temperature of 34 deg C. The lowest surface values of N tend to occur in high, dry areas where both ρ and e are low. At a height of 3 km, for example, assuming the pressure for a standard atmosphere but a temperature of 273 K, N is 230 with 100 percent relative humidity and 199 with 0 percent humidity. The values of N mentioned above are extreme. Monthly mean values of N at sea level vary between about 290 and 400 within ±25 deg of latitude from the equator, with a somewhat smaller variation elsewhere, and are typically 320 in winter and 340 in summer in the UK (Hall, 1979). In the United States, winter values vary from about 285 to 345 and summer values range from about 275 to 385 (Bean and Dutton, 1966).

Pressure, temperature, and water vapor content all decrease with height above the Earth's surface in the troposphere on the average, but temperature increases with height in temperature inversion layers. Pressure drops off approximately exponentially with height, and the decrease or change of e with height is variable but may be approximately exponential. The refractivity N may also decrease with height in a variable manner but on the average tends to decrease exponentially as described by

$$N = N_s e^{-h/H} \tag{3.7}$$

where N is the refractivity at the height h above the level where the refractivity is N_s. H is the applicable scale height. The change in N in the first km of height above the surface, ΔN, is a parameter of significance. In the average atmosphere as defined by the CCIR, N_s has the value of 315 and ΔN the value of -40 consistent with

$$N = 315\ e^{-0.136\ h} \tag{3.8}$$

with h in km (CCIR, 1986a). Values of N_s and ΔN have been compiled, with N_s sometimes reduced to sea level values. Charts showing these quantities, probability distributions of N_s, water vapor density ρ, etc. have been provided by Bean, Horn, and Ozanich (1960), Bean et al. (1966), and the CCIR (1986a). Figure 3.1 shows annual cycles of N_s for several climatic types.

The exponential model is widely applicable but any reliable data on actual refractivity profiles should be used when available. Such data can be acquired by use of radiosondes or microwave refractometers and often display significant departure from the exponential form. A common cause of non-exponential refractivity profiles is the occurrence of temperature-inversion layers. In an inversion layer, the temperature increases with altitude. Such a layer is highly stable (Sec. 1.3). All vertical motions are strongly inhibited in an inversion layer, and pollution and water vapor existing below the layer tend to be confined below it. Temperature inversions may develop when the loss of heat from the surface of the Earth is not compensated by inputs of heat, the ground being a more efficient radiator than air and therefore cooling more rapidily. Surface and low-level inversions tend to develop at night and in the arctic and subarctic in winter and in locations such as the San Joaquin Valley of California where fog forms under the inversion and prevents surface heating in winter. Inversions may form also when warm air blows over a cool ocean.

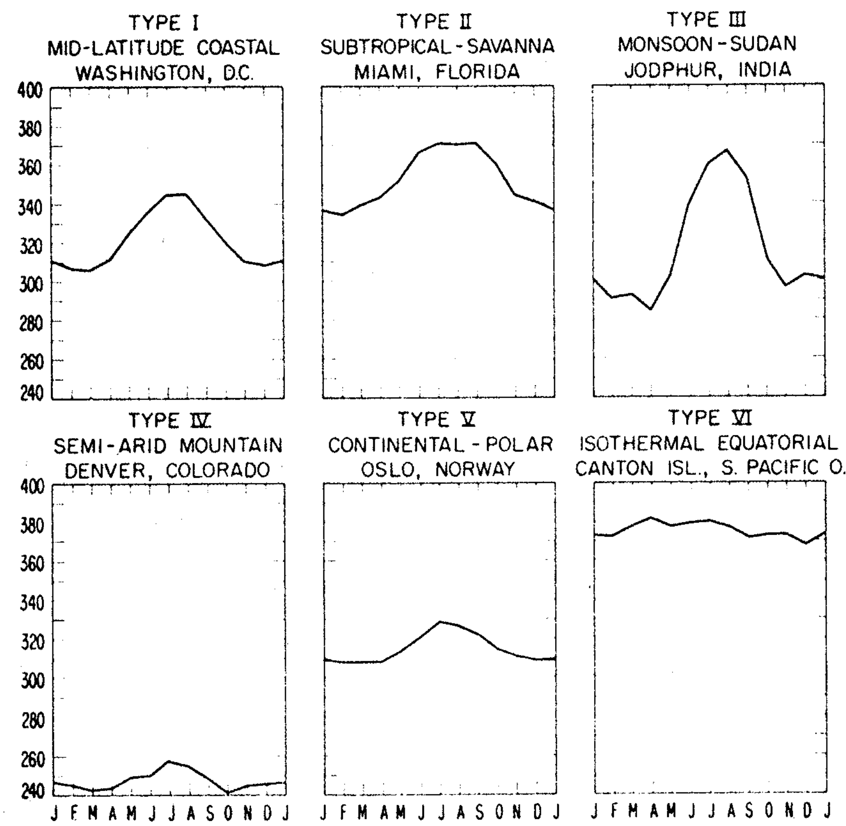

Figure 3.1. Annual cycles of N_s by climatic type (Bean, Horn, and Ozanich, 1960).

Inversions are also caused by subsiding air, and this type of inversion is common because in portions of developing or semipermanent anticyclones the air between about 500 and 5000 m descends at a rate typically about 1000 m/day (Scorer, 1968). The Pacific coast of the United States lies along the eastern edge of a semipermanent anticyclone that forms in the Pacific, and the persistant temperature inversion of the Los Angeles area is caused largely by subsiding air. This air is heated in a process of adiabatic compression but the movement and heating cannot extend to the ground itself, and a temperature inversion is formed at or near the surface.

The occurrence of a high water vapor content underneath an inversion layer may be accompanied by a rapid decrease in water vapor content through the inversion layer. The corresponding N value is also high beneath the layer and drops abruptly through the layer in such a case.

3.2 REFRACTION AND FADING

A practical consequence of the variation of the index of refraction of the troposphere with height is that electromagnetic waves do not travel in straight lines but experience refraction or bending. To treat this phenomenon, consider ray paths which represent paths along which energy is transmitted. An important characteristic of an element of a ray path is its curvature C, defined as $1/\rho$ where ρ is the radius of curvature. It can be shown (Bean and Dutton, 1966; Flock, 1979) that a ray path in a spherically stratified atmosphere has a curvature given by

$$C = -\frac{1}{n}\frac{dn}{dh}\cos\beta \qquad m^{-1} \tag{3.9}$$

where β is the angle of the ray measured from the horizontal. In the troposphere $n \simeq 1$, and for rays having an angle β that is near zero, the expression for C simplifies to

$$C = -\,dn/dh \tag{3.10}$$

This latter form is used for terrestrial line-of sight paths.

The change in direction, or the amount of bending, τ, along a path can be determined by taking $\tau = \int C\, ds$ or $\tau = \sum C\, \Delta s$ where ds is an infinitesmal element of length and Δs is a finite element of length. In a length ds the corresponding bending $d\tau$ is given by

$$d\tau = -\frac{1}{n}\frac{dn}{dh}\cos\beta\; ds \qquad \text{rad} \tag{3.11}$$

But as $dh = \sin\beta\, ds$

$$d\tau = -\frac{dn}{n\tan\beta} \tag{3.12}$$

This form can be used for ray tracing for any arbitrary index of refraction profile and for a path at any angle (Weisbrod and Anderson, 1959; Flock, 1979).

Very-low-angle satellite paths may experience much the same effects as terrestrial line-of-sight paths. To illustrate these effects we use the simple form $C = -\,dn/dh$ for propagation over a spherical earth. In this case the difference in curvature between a ray path and the Earth's surface is given by

$$\frac{1}{r_o} - C = \frac{1}{r_o} + \frac{dn}{dh} \tag{3.13}$$

where r_o is the Earth's radius and $1/r_o$ is the corresponding curvature. To analyze propagation, one can use a geometric transformation such that ray paths become straight lines and the Earth has an effective radius of k times the true radius r_o. Thus

$$\frac{1}{r_o} + \frac{dn}{dh} = \frac{1}{k\,r_o} + 0 \tag{3.14}$$

which maintains the same relative curvature as in Eq. (3.13). The 0 has been included on the right-hand side of Eq. (3.14) to emphasize that it applies to the case that $dn/dh = 0$, for which case the ray paths are straight lines. In terms of N units the relation is

$$\frac{1}{kr_o} = [\,157 + dN/dh\,] \times 10^{-6} \tag{3.15}$$

The relation of Eq. (3.15) is illustrated by Table 3.2.

Table 3.2 Corresponding Values of dN/dh and k.

dN/dh (N/km)	k
157	0.5
78	2/3
0	1.0
-40	4/3
-100	2.75
-157	∞
-200	-3.65
-300	-1.09

Typically, $dN/dh = -40$ and $k = 4/3$, and graphs prepared for $k = 4/3$ have been used for plotting terrestrial microwave paths. However, k can vary over a range of values, and this type of graphical procedure has the shortcoming that a different graph is needed for each k value.

A more efficient procedure is to use a transformation which makes the Earth flat and allows plotting paths for various k values on the same chart. Such plots are made by calculating h' of Fig. 3.2 in accordance with

$$h' = d_1 d_2/(12.75\ k) \qquad \text{m} \qquad (3.16)$$

where d_1 and d_2 are the distances from the two ends of the path (GTE, 1972). The units of Eq. (3.16) are km for d_1 and d_2 and m for h'. The basis for Eq. (3.16) is that $h' = h_{max} - h$ where h_{max} and h are calculated with respect to the center of the path by using, for h for example,

$$h = \ell^2/(12.75\ k) \qquad \text{m} \qquad (3.17)$$

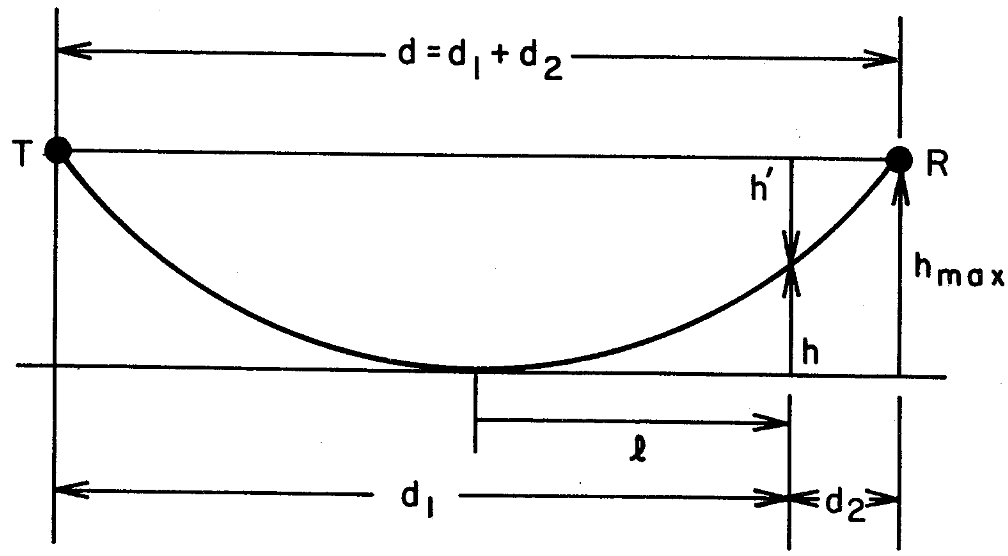

Figure 3.2. Quantities referred to for flat-earth plot.

where ℓ is the horizontal distance from the center of the path, at which point the path is horizontal, to where h is specified. The distance ℓ is in km and h is in m in Eq. (3.17). This expression follows from the construction of Fig. 3.3 where, in contrast to Fig. 3.2, the ray path is straight and the Earth is curved. Here ℓ, r_o, and $r_o + h$ form the three sides of a right triangle. For $h \ll r_o$, it can be determined that

$$h = \ell^2/2r_o \tag{3.18}$$

with all quantities in identical units. For a finite value of dN/dh, however, r_o is replaced by kr_o, and the form of Eq. (3.17) results when ℓ is in km and h is in m.

The effect of the various k values is illustrated in exaggerated form in Figs. 3.4 and 3.5. In Fig. 3.4 all the rays are horizontal at the common point. In Fig. 3.5 ray paths are shown which allow signals from a common transmitter to reach a common receiving location.

It is evident from the above discussion that tropospheric refraction may cause errors in the measurement of elevation angle and variations in angle of arrival which can cause a reduction of

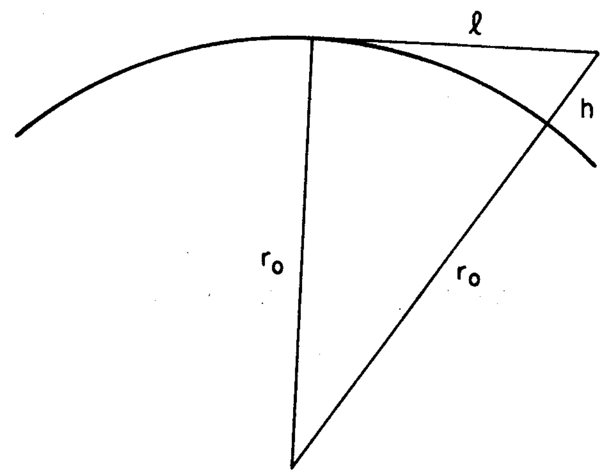

Figure 3.3. Geometry for determining h for initially horizontal ray.

signal amplitude for narrow-beam antennas. Also some degree of beam spreading or defocusing may occur and cause an attenuation of up to about 0.4 dB (Hall, 1979). To visualize how such defocusing occurs, consider a family of relatively closely spaced rays within an antenna beamwidth. The closer the spacing of the rays, the greater the signal intensity is. Defocusing involves a distortion of the ray paths such that the rays are more widely spaced than normally in the region of the receiving antennas.

Various programs for calculating bending have been devised. A simple procedure for calculating bending and elevation angle errors was presented by Weisbrod and Anderson (1959). Bending angles have been calculated by Crane (1976) for different elevation angles and for the 1966 U.S. Standard Atmosphere and an assumed humidity profile. His values are given in Table 3.3. The ray paths extend from the surface to the heights shown, and the heights correspond to the ranges or path lengths shown. The exact values of the bending angles vary depending on atmospheric conditions, but the values of Table 3.3 are representative. Also included are values of range error or excess range (Sec. 3.7). For transmitters or radar targets in the troposphere, the total bending and elevation angle errors are not the same; for astronomical sources and

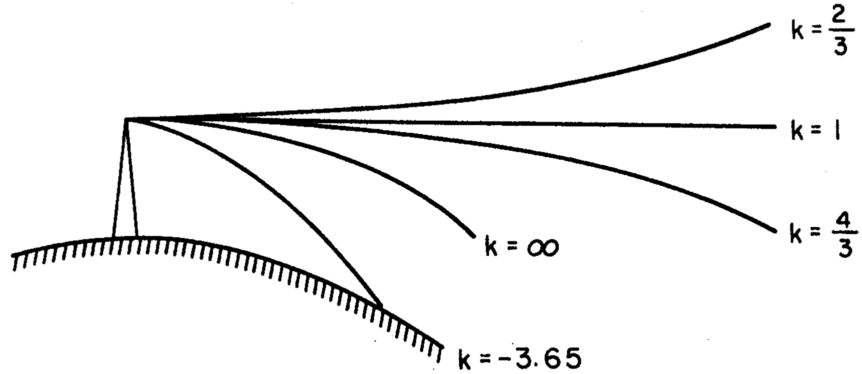

Figure 3.4. Ray paths for several values of k for initially horizontal rays (exaggerated and illustrative only).

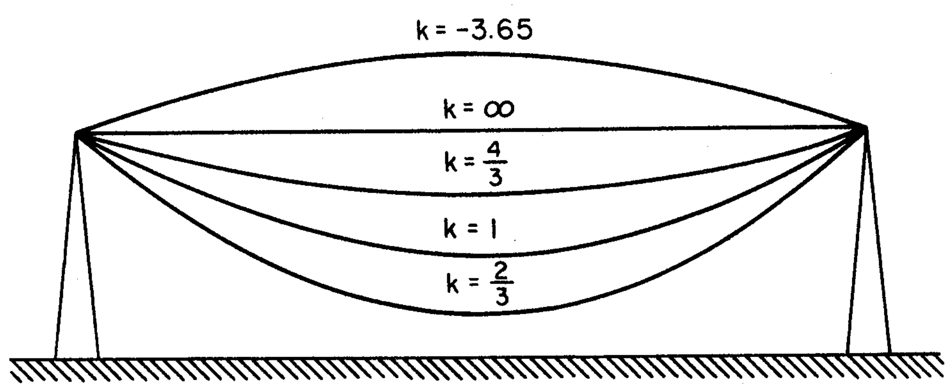

Figure 3.5. Ray paths from a transmitter T to a receiver R for various value of k (exaggerated and illustrative only).

geostationary satellites, the total bending and elevation error angles are identical. Bending takes place largely in the lower troposphere and Crane (1976) has shown that for a horizontally stratified atmosphere the total bending τ is related to surface refractivity N_s by $\tau = a + b\,N_s$, where the coefficients a and b vary with elevation angle and have been tabulated in his paper for Albany, New York. Nearly the same values are said to apply in other circumstances.

A phenomenon of major importance in tropospheric propagation at small angles from the horizontal, especially in the presence of temperature inversions, is the occurrence of severe fading due to multipath propagation. Propagation over more than one path may involve reflection from land and water surfaces and from manmade structures. This type of multipath is considered in Chap. 6. Multipath propagation involving the atmosphere alone, such as suggested in Fig. 3.6, however, also occurs. In terrestrial line-of-sight links, a fading allowance of 30 to 45 dB is commonly assigned for multipath fading. Such paths are often essentially horizontal or at only a slight angle from the horizontal, whereas earth-space paths are usually at rather large angle above the horizontal for which tropospheric fading is much less severe. It is often considered that about 5 to 10 deg is the smallest elevation angle that should be employed for earth-space paths, but there are circumstances for which it may be necessary to operate at lower angles, as at high latitudes. Then atmospheric multipath fading may prove to be as serious as for terrestrial paths.

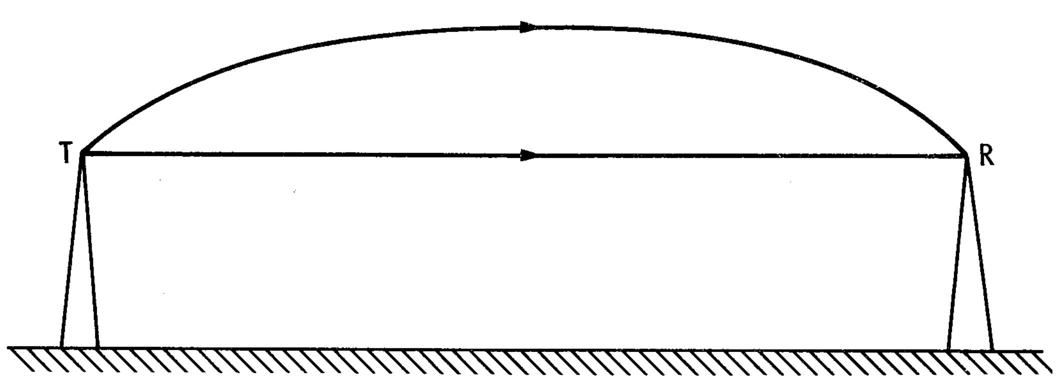

Figure 3.6. Atmospheric multipath propagation.

Table 3.3 Ray Parameters for a Standard Atmosphere[a,b] for Rays from the Surface to Indicated Heights (Crane, 1976).

Initial Elev. Angle (deg)	Height (km)	Range (km)	Bending (mdeg)	Elev.-Angle Error (mdeg)	Range Error (m)
0.0	0.1	41.2	97.2	48.5	12.63
	1.0	131.1	297.9	152.8	38.79
	5.0	289.3	551.2	310.1	74.17
	25.0	623.2	719.5	498.4	101.0
	80.0	1081.1	725.4	594.2	103.8
5.0	0.1	1.1	2.6	1.3	0.34
	1.0	11.4	25.1	12.9	3.28
	5.0	55.2	91.7	52.4	12.51
	25.0	241.1	176.7	126.3	24.41
	80.0	609.0	181.0	159.0	24.96
50.0	0.1	0.1	0.2	0.1	0.04
	1.0	1.3	1.9	1.0	0.38
	5.0	6.5	7.0	4.0	1.47
	25.0	32.6	14.3	10.3	3.05
	80.0	104.0	14.8	13.4	3.13

[a]U.S. Standard Atmosphere Supplements, 1966, Environmental Sci. Serv. Administration, Dept. of Commerce, Washington, DC (1966).

[b]Sissenwine, N., D.D. Grantham, and H.A. Salmela, AFCRL-68-0556, Air Force Cambridge Res. Lab., Bedford, MA (Oct. 1968).

3.3 DUCTING

Ducting is a severe refractive effect involving trapping of a wave in a duct, commonly a surface duct, and possibly propagation for an abnormally long distance. Ducting occurs frequently in some locations, but it is not a reliable means of communication. It can, however, cause interference beyond the horizon, at a location that would otherwise be free from interfering signals (Sec. 8.5; Dougherty and Hart, 1976; Dougherty and Hart, 1979). A necessary condition for ducting to occur is that the refractivity decrease with height at a rate of 157 N units per km or greater. If $dN/dh = -157$ Eq. (3.15) shows that $1/kr_o = 0$, corresponding to $k = \infty$ (Figs. 3.4 and 3.5). A ray that is launched horizontally under this condition remains horizontal at a constant height relative to a spherical surface. If the rate of decrease of N is greater than 157 N/km, a ray may be bent downward to the surface of the Earth as for $k = -3.65$ in Fig. 3.4. Such a path may result in what has been called blackout fading (Hautefeville, et al., 1980).

In such a case no signal reaches the receiving location and the use of space or frequency diversity may not improve the situation. The rays bent downward to the Earth's surface may be reflected upwards, however, and then refracted down to Earth again, etc., giving rise to ducting as illustrated in Fig. 3.7. A second condition for ducting is that the refractivity gradient of -157 N/km or greater be maintained over a height range of a number of wavelengths.

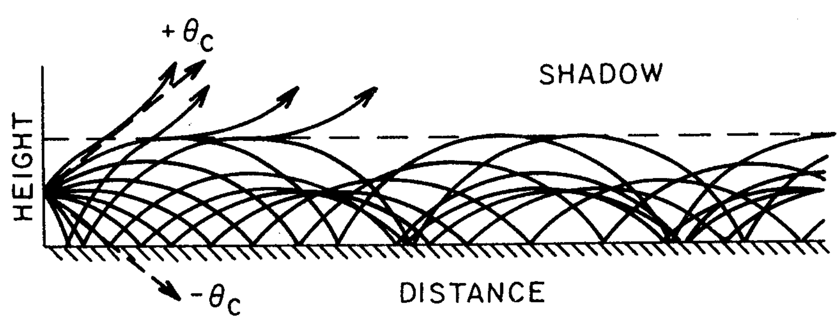

Figure 3.7. Example of ducting.

Ducting constitutes a mechanism for interference between earth stations and terrestrial line-of-sight systems and is considered further in Sec. 8.3.3. The free-space loss L_{FS} when expressed in dB as in Eq. (1.9) depends on distance as 20 log d, but for propagation in a duct the corresponding loss contribution is 10 log d. The reason is that in free space energy spreads out uniformly in all directions, but in a duct energy is constrained and spreads out in only two dimensions.

3.4 ATMOSPHERIC TURBULENCE

In addition to the variation of index of refraction with height, the index also exhibits variations associated with atmospheric turbulence. The theory of turbulence indicates that it develops from wind shear, that turbulence is introduced in the form of large turbulent eddies or blobs of scale size L_o, and that energy is transferred from larger to smaller eddies throughout an inertial subrange corresponding to eddies of size ℓ where $L_o \geq \ell \geq \ell_o$. For eddies smaller than ℓ_o, viscous effects dominate and turbulent energy is dissipated. The process is suggested by Fig. 3.8. Associated with the turbulent eddies or blobs is a corresponding time-variable structure of temperature, water-vapor density, and index of refraction.

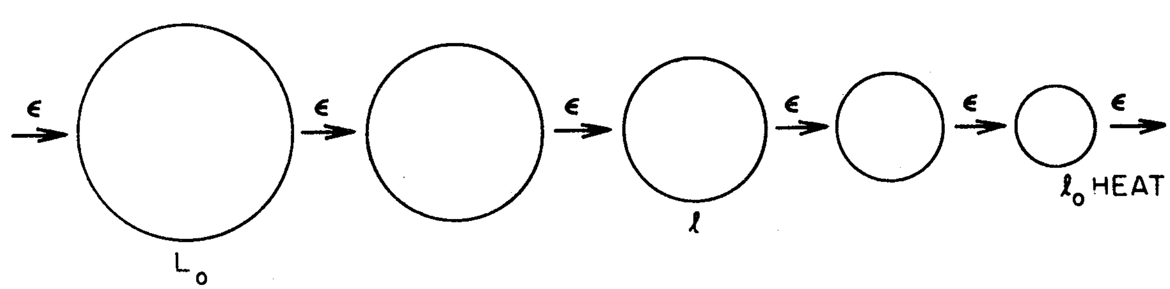

Figure 3.8. Illustration of the transfer of energy at the rate ϵ from large eddies to smaller eddies.

The quantity C_n^2 is a measure of the intensity of the index of refraction variations associated with turbulence. In particular

$$C_n^2 = \overline{(n_1 - n_2)^2} \tag{3.19}$$

where n_1 and n_2 are values of the index of refraction at two locations a distance of 1m apart. The overbar indicates an average value of the quantity below it, namely $(n_1 - n_2)^2$. The atmosphere is normally turbulent to some degree, but the occurrence of turbulence is not uniform and a layered structure of turbulence tends to occur.

The turbulent structure of the index of refraction of the troposphere is believed to be largely responsible for the scatter of electromagnetic waves that is the basis for troposcatter communication systems and radar clear-air echoes. Scatter of this type is known as Bragg scatter and is due to the structure of the index of refraction that has a periodicity of λ' where

$$\lambda' = \lambda/[2 \sin (\theta/2)]$$

with λ the electromagnetic wavelength and θ the scattering angle as shown in Fig. 3.9. The range of eddy size is large, and scatter from turbulence can be expected to occur over a wide range of frequencies and wavelengths.

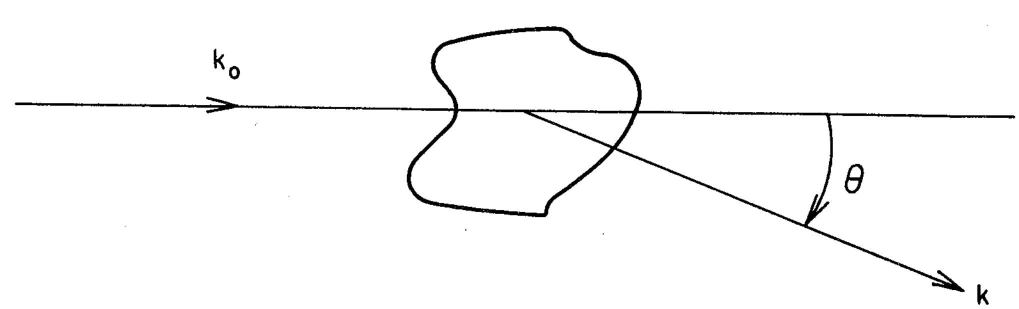

Figure 3.9. Scattering geometry.

For satellite communications, interest lies in the effect of turbulence on forward propagation through turbulent regions. The effects of forward propagation include amplitude fluctuations or scintillations, phase fluctuations, and angle-of-arrival variations.

3.5 AMPLITUDE VARIATIONS DUE TO REFRACTION AND TURBULENCE

It is not always easy to assess the relative importance of amplitude variations due to the large-scale profile of refractivity and due to small-scale structure associated with turbulence, either in advance planning or after the fact. Certain treatments of propagation emphasize one topic, and other studies deal with the other. In designing terrestrial line-of-sight links multipath fading associated with the refractivity profile receives attention, and effects of turbulence are largely ignored (GTE-Lenkurt, 1972). For earth-space paths the emphasis tends to be on effects due to turbulence (Theobold and Kaul, 1978).

The amplitude variations due to turbulence are smaller in general than those due to multipath propagation, as discussed in Sec. 3.2, tend to occur more rapidly or at higher frequencies, and are commonly referred to as scintillation. Such scintillation increases in amplitude with frequency (Thompson et al., 1975). For brevity we will henceforth refer to multipath fading for effects due to large-scale variations in refractivity and to scintillation for effects due to turbulence. Earth-space paths are at higher elevation angles than for terrestrial paths. Even paths at what are considered to be low angles for satellite communications tend to be at larger angles than those of terrestrial paths, for which severe multipath fading may occur. Also multipath fading, while severe at certain times of day and certain seasons in regions subject to strong temperature inversions, does not occur uniformly over large areas or unformly with time. Earth-space paths tend to experience scintillation associated with turbulence more than multipath fading, especially at larger elevation angles and higher frequencies.

Low-angle satellite paths, however, can encounter both scintillation and multipath fading, and refractive multipath effects may dominate at low angles. On a path in Hawaii at an elevation angle of 2.5 deg that simulated a low-angle earth-space at frequencies from 10 to 49 GHz, for example, Thompson et al. (1975) recorded both fades of more than 20 dB and scintillation of several dB in amplitude.

Measurements of 4 and 6 GHz signals at the very small elevation angle of one deg at Eureka in the Canadian arctic, some of which are summarized in Table 3.4, show effects that are probably due primarily to refractive multipath fading. Eureka is at a latitude of 180 deg on Ellesmere Island.

Table 3.4 6 GHz Margins for Tropospheric Fading at Eureka, Northwest Territories, Canada, Elevation Angle $\simeq$ 1 Degree (Strickland, et al., 1977).

Time Duration	Reliability 90%	99%	99.9%
Worst two hours	8.0 dB	18.0 dB	28.0 dB
Worst summer day	6.8 dB	15.5 dB	24.5 dB
Worst summer week (5 day)	5.4 dB	13.0 dB	22.0 dB
Worst month (July, 15 days)	3.8 dB	10.8 dB	20.3 dB

Amplitude fluctuations and phase and angle-or-arrival variations due to turbulence are treated by Theobold and Kaul (1978), who include an example for a path at 28.56 GHz and an elevation angle of 10 deg. They predict a signal loss of 0.12 dB for clear weather, which is a small effect. Both the effects due to turbulence and the possibility of refractive fading would increase if the angle decreased below 10 deg. As noted earlier, Thompson et al. (1975) recorded larger scintillation of several dB at an angle of 2.5 deg in Hawaii.

3.6 GASEOUS ATTENUATION

A microwave absorption peak due to water vapor occurs at 22.235 GHz and peaks due to oxygen occur near 60 GHz and 118 GHz (CCIR, 1986b; Van Vleck, 1951; Waters, 1976; Liebe, 1985). Below 10 GHz absorption caused by atmospheric gases is small. Sea level values of the attenuation constant due to oxygen and water vapor are shown in Figure 3.10. Vertical one-way attenuation values from sea level for frequencies above 1 GHz are shown in Fig. 3.11. Attenuation values for paths at elevation angles θ above 10 deg are equal to the vertical values divided by $\sin\theta$, in a horizontally stratified atmosphere. The treatment by Smith (1982) of attenuation caused by atmospheric gases extends to frequencies below 10 GHz, and the thorough discussion by Liebe (1985) also includes examples for frequencies below 10 GHz.

Equation (3.20), based on the VanVleck-Weisskopf line shape, gives an expression for the sea level attenuation constant, or specific attenuation, in dB/km, due to oxygen for frequencies less than 57 GHz, with frequency f in GHz (CCIR, 1986b).

$$\alpha_o = \left[0.00719 + \frac{6.09}{f^2 + 0.227} + \frac{4.81}{(f-57)^2 + 1.50} \right] f^2/10^3 \quad \text{dB/km} \tag{3.20}$$

The attenuation caused by atmospheric gases plays a role in the determination of coordination distance for interference due to ducting and scatter from rain, and the same equation, but stated as applicable for frequencies less than 40 GHz, is given in Chap. 8 as Eq. (8.24). A complicated line structure appears between 57 and 63 GHz (CCIR, 1986b). Such details can only be shown if an appropriate frequency scale is used. For water vapor, a corresponding expression, neglecting an absorption line near 320 GHz is

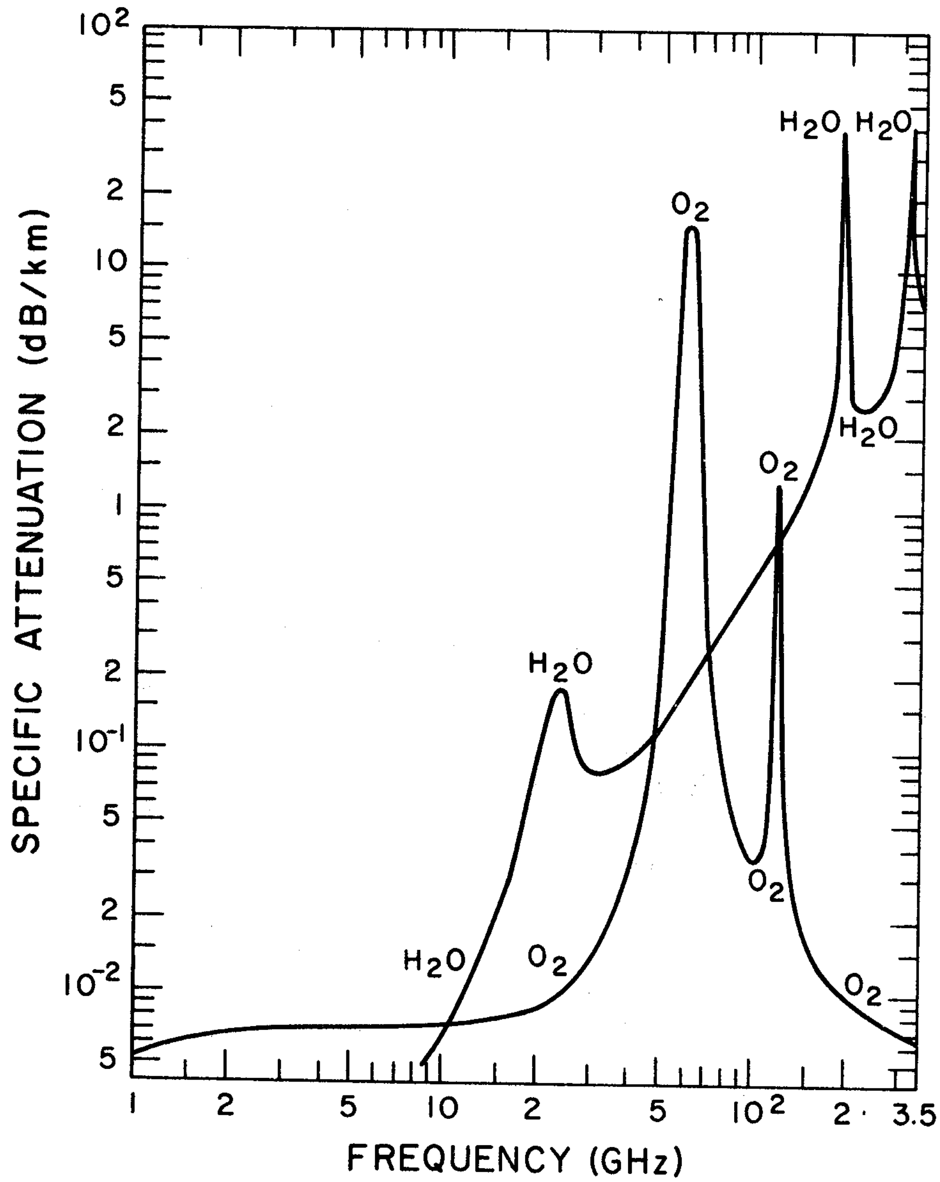

Figure 3.10. Attenuation constant for atmospheric gases for p = 1013 mb, T = 15 deg C, and ρ = 7.5 g/m³ (CCIR, 1986b).

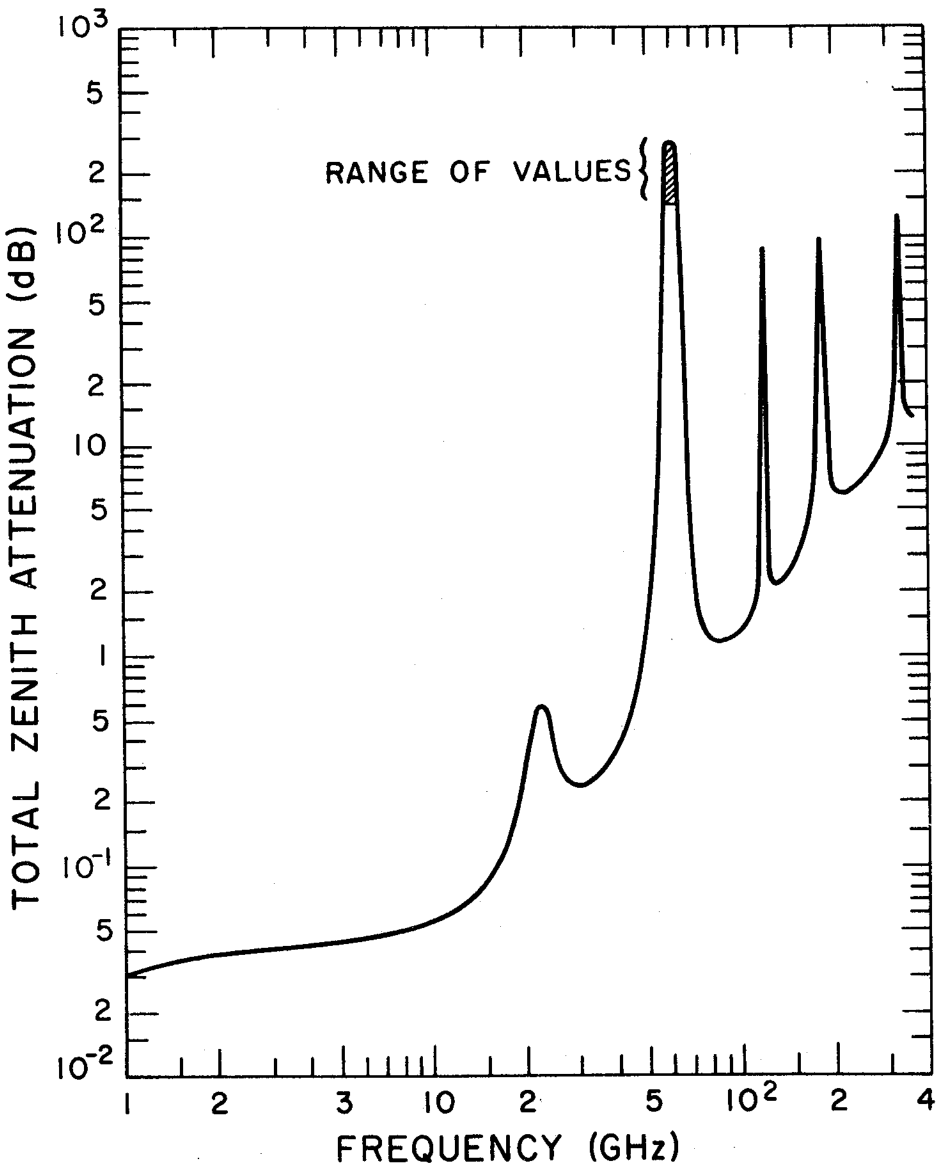

Figure 3.11. Total zenith attenuation at ground level for p = 1013 mb, T = 20 deg C, and $\rho = 7.5$ g/m^3 (CCIR, 1986b).

$$\alpha_w = \left[0.067 + \frac{2.4}{(f-22.3)^2 + 6.6} + \frac{7.33}{(f-183.5)^2 + 5} \right] f^2\rho/10^4 \tag{3.21}$$

with α_w in dB/km. The quantity ρ is water vapor density in g/m^3.

An approximate expression for total attenuation A_a due to atmospheric gases for elevation angles $\theta > 10$ deg (CCIR, 1986b) is

$$A_a = \frac{8\alpha_o + 2\alpha_w}{\sin\theta} \quad \text{dB} \tag{3.22}$$

In CCIR (1986c) the relation given is

$$A_a = \frac{\alpha_o h_o e^{-h_s/h_o} + \alpha_w h_w}{\sin\theta} \quad \text{dB} \tag{3.23}$$

where h_o is a characteristic distance for oxygen and is 6 km for $f < 57$ GHz and $h_w = 2.2 + 3/[\,(f-22.3)^2 + 3\,]$ km for water vapor. The quantity h_s is the height in km of the earth station above sea level, and α_o and α_w are surface (sea level) attenuation constants for oxygen and water vapor.

3.7 TROPOSPHERIC EFFECTS ON RANGE, PHASE, AND DOPPLER FREQUENCY

Range to a target is commonly determined by radar techniques by assuming that electromagnetic waves propagate with the velocity c, about 2.9979×10^8 m/s. The velocity of c corresponds to an index of refraction of unity. In the troposphere, however, the index of refraction, n, is slightly greater than unity with the result that the velocity of an electromagnetic wave is slightly less than c. A range error then results if the velocity c is assumed. The slight error in range is unimportant in many applications but may be important in other situations. In practice, when high accuracy in range is desired, an effort is made to estimate as accurately as possible the excess range delay (the amount by which the indicated range exceeds the true range) in order to correct for it (Flock, Slobin, and Smith, 1982).

Since 1983 the velocity of electromagnetic waves, c, has been taken to be the exact value of 299 792 458 m/s. The fractional uncertainty of c of $\pm 4 \times 10^{-9}$ that was previously stated is no longer applicable (Jennings, Evenson, and Knight, 1986). Along with specifying the above value of c, the meter was redefined to be consistent with c. Length and wavelength are now based on the same physical standard as time and frequency. When using time-of-propagation ranging techniques the time to distance conversion does not now increase uncertainty , as it tended to when the value of c was considered to have the fractional uncertainty stated above.

For the ionosphere (Sec. 2.3.1), the range error ΔR can be determined by taking $\int (n - 1) d\ell$ along the path. For the troposphere, however, calculations are usually carried out by using the quantity $N = (n - 1) \times 10^6$. (In the ionospheric analysis, N stands for an entirely different quantity.) One may choose to treat dry air and water vapor separately. For dry air, making use of Eq. (3.3) for a zenith path,

$$\Delta R_d = 10^{-6} \int N_d \, d\ell = 10^{-6} \int (77.6 \, p_d/T) \, dh \quad \text{m} \qquad (3.24)$$

with ΔR_d the range delay due to dry air in m. The pressure p_d is in mb, h is height in m, and T is temperature in kelvins. Pressure in the troposphere tends to decrease exponentially as indicated by $p = p_o e^{-h/H}$ [Eq. (1.18)], where H is the scale height kT/mg or RT/Mg, k is Boltzmann's constant, g is the acceleration of gravity (about 9.8 m/s^2 at the Earth's surface), R is the gas constant [8.3143×10^3 J/(K kg mol)], M is the mass of a kg mol, and m is the mass of an individual molecule. ($M/m = 6.025 \times 10^{26}$, which corresponds to Avogadro's number but applies to a kg mol rather than a gram mol.) Using the form of H involving R with

M = 28.9665 from Table 3 of the U.S. Standard Atmosphere, 1976, treating T as if it were a constant, and employing the value of g utilized by Hopfield (1971) corresponding to the height at 500 mb at 45 deg latitude (namely, 9.7877 m/s²).

$$\int_0^{\infty} p_d \, dh = \int_0^{\infty} p_o \, e^{-h/H} \, dh = p_o H = p_o RT/(Mg) = p_o T \, 29.326$$

Substituting the value of the integral into Eq. (3.24) and identifying p_o as p_{od}, the surface pressure of dry air

$$\Delta R_d = 2.2757 \times 10^{-3} \, p_{od} \tag{3.25}$$

with p_{od} in mb. If p_{od} is 1000 mb, for example, ΔR has the value of 2.28 m. The delay is directly proportional to the surface pressure of dry air and independent of the temperature profile. Hopfield (1971) has examined the applicability of this relation and has concluded that it allows determining the range error due to dry air on a zenith path to an accuracy of 0.2 percent or about 0.5 cm.

As H is a function of temperature and temperature varies with height, the exponential form $p_d \, e^{-h/H}$ with H a constant should only be assumed to apply over a limited height range. If account is taken of the variation of H with altitude, however, the integral of Eq. (3.24) can be represented as a summation of integrals over layers of limited thickness for which the values of T can be treated as a constants. If this procedure is followed, T will cancel out of all the integrals and the same result will be obtained as shown by Eq. (3.25).

The delay caused by water vapor is considerably smaller than that for dry air, but total water vapor content along a path is variable and not predictable with high accuracy from the surface water vapor pressure or density. Therefore, water vapor is responsible for a larger error or uncertainty in range than is dry air. The expression for N_w, the contribution to refractivity of water vapor, is given by Eq. (3.5), but N_w can be expressed in terms of water vapor density ρ instead of water vapor pressure e, by using $e = \rho T/216.5$ [Eq. (3.6)], and then takes the form

$$N_w = 0.3323\,\rho + 1.731 \times 10^3\,\rho/T \qquad (3.26)$$

from which

$$\Delta R_w = 10^{-6} \int N_w\,d\ell = 3.323 \times 10^{-7} \int \rho\,d\ell + 1.731 \times 10^{-3} \int (\rho/T)\,d\ell \quad \text{m} \qquad (3.27)$$

Alternatively, the total excess range delay can be separated into ΔR_1 and ΔR_2 corresponding to the two terms of Eq. (3.3). This procedure has the practical advantages that it is easier to measure total pressure than the pressure of dry air and that only one simple term is needed to determine each quantity whereas two dissimilar terms are involved in estimating ΔR_w. Following this procedure

$$\Delta R_1 = 2.2757 \times 10^{-3}\,p_o \quad \text{m} \qquad (3.28)$$

where p_o is now the total surface pressure and

$$\Delta R_2 = 1.731 \times 10^{-3} \int (\rho/T)\,d\ell \quad \text{m} \qquad (3.29)$$

The value of the integral can be determined from radiosonde data if ρ and T vary only with height above the surface and not horizontally to a significant degree within the limits of the path.

Accumulation of sufficient data from radiosondes can provide a basis for a statistical description of the range error due to water vapor and for formulating models that may apply to particular locations. Radiosonde data are available from only certain locations, however, and it may be impractical to use radiosondes regularly and routinely for determining range errors due to water vapor. Aircraft instrumented with microwave refractometers can provide more accurate data on ρ and T.

Another approach is to employ microwave radiometry to estimate the value of ΔR_2. This approach is based on the expression for brightness temperature T_b observed when a source at a temperature of T_s is viewed through an absorbing medium having a variable temperature T. T_b is given by (Waters, 1976, Wu, 1977)

$$T_b = T_s e^{-\tau_\infty} + \int_0^\infty T\,\alpha\,e^{-\tau}\,d\ell \qquad (3.30)$$

with $\tau_\infty = \int_0^\infty \alpha \, d\ell$ and $\tau = \int \alpha \, d\ell$ where α is the variable attenuation constant (scattering neglected) at the frequency employed. The expression for T_b takes a simpler, and perhaps more familiar, form when T is constant or when an effective value T_i can be employed. In this case

$$T_b = T_s e^{-\tau} + T_i (1 - e^{-\tau}) \tag{3.31}$$

A problem with the radiometer method is that oxygen and perhaps liquid water contribute to α as well as water vapor. Use of a suitable pair of frequencies allows separating the effects of gaseous and liquid water to a reasonable degree, and the effect of oxygen can also be separated out (Staelin et al., 1977; Wu, 1977; Claflin, et al., 1978). Frequencies of 22.235 and 31.4 GHz have been used, 22.325 GHz being more sensitive to water vapor than liquid water by a factor 2.5 and 31.4 GHz being more sensitive to liquid water than vapor by about a factor of 2.

By using Eq. (3.30) for the two different frequencies, and with the terms involving T_s replaced by constants as T_s due to cosmic sources is small (about 2.7 K), a term $\int W(\ell) \, \rho/T \, d\ell$ is obtained where $W(\ell)$ can be made to have a nearly constant known value by a suitable choice of frequencies and other refinements described in the paper by Wu (1977). This approach to water-vapor radiometers has the appeal of being based on the physics of the problem and gives $\int \rho/T \, d\ell$ rather than the water-vapor content alone, $\int \rho \, d\ell$, which is what some other water-vapor radiometers were designed to provide.

A recent analysis of water-vapor radiometers for determining excess range delay has been prepared by Gary, Keihm, and Janssen (1985) who carried out simulation studies. Microwave brightness temperatures and excess range delay were calculated from radiosonde-based profiles of atmospheric parameters. A statistical retrieval technique was used to obtain retrieval coefficients relating path delay to observables (brightness temperature, surface-air temperature, pressure, and absolute humidity) for various combinations of frequencies. The relation used is

$$\Delta R = C_o + \sum C_i * O_i \tag{3.32}$$

where O_i represents the observables and C_o and C_i are computed by a least squares minimization technique involving the covariance matrices of the observables and path delay. Studies were included for which the surface observables were not included and for which only surface observables were used. Using three frequencies, 20.6, 22.2, and 31.4 GHz gives a small improvement over performance obtained by using only 20.6 and 31.4 GHz. Using surface values gives a modest improvement over results obtained by not using surface values. Surface values alone can be used but performance provided in this way is worse by a factor of 3 to 10 than that achievable by using radiometers. It is reported that it should be possible to correct path delay caused by water vapor with an accuracy better than 0.5 cm for zenith paths.

The exact value of ΔR_2 in a particular case depends on the value of the integral appearing in Eq. (3.29), but an indication of a representative magnitude of ΔR_2 can be obtained by assuming an exponential decrease of N_2 with a scale height H of 2 km. It is of interest that the value obtained in this way is the same as if N_2 were constant up to the height H and zero beyond. Assuming a vapor density ρ of 7.5 g/m^3 at the surface and a temperature of 280 K, the corresponding values of e and N_2 at the surface are 9.70 mb and 46.15 respectively. Then for a vertical path

$$\Delta R_2 = 10^{-6} \int_0^\infty 46.15\, e^{-h/2000}\, dh = 10^{-6} (46.15) (2000)$$

$$= 0.0923 \text{ m} = 9.23 \text{ cm}$$

An extreme value of ΔR_2, corresponding to the highest accepted weather-observatory values of e and ρ of 53.2 mb and 37.5 g/m^3 at the temperature of 34 deg C and assuming an exponential decrease of N_2 with a scale height of 2 km, is 42.1 cm, for a vertical path.

Once a ΔR value is known, a corresponding phase angle ϕ can be determined by use of

$$\Delta\phi = \Delta R\, \beta = \Delta R\, (2\pi/\lambda) \qquad \text{rad} \qquad (3.33)$$

where β is the phase constant and is equal to $2\pi/\lambda$. The doppler frequency error f_D associated with the range and phase errors is given by

$$f_D = \frac{1}{2\pi} \frac{\Delta\phi}{\Delta t} \tag{3.34}$$

where the rate of change of phase with time is involved. Thus f_D involves the rate of change of refractivity along the path. The value given by Eq. (3.34) may also depend in practice to some extent on the interval of time Δt used to measure $\Delta\phi$.

For paths at an elevation angle θ of about 10 deg or greater, the range delay equals the vertical or zenith value divided by $\sin \theta$. That is,

$$\Delta R(\theta) = \Delta R/\sin \theta \tag{3.35}$$

Table 3.3 shows values of $\Delta R(\theta)$ or range error for elevation angles of 0, 5, and 50 deg, based on the 1966 Standard Atmosphere for 45 deg N latitude in July and including an assumed humidity-profile model. These values represent total delay due to both the dry component of air and water vapor. Note the large values of range error for 0 and 5 deg.

The widely used constants provided by Smith and Weintraub (1953) have been employed for calculating refractivity in this chapter. When extreme precision is important, reference can be made to values provided by Thayer (1974).

The excess range delay due to the troposphere (and stratosphere) has also been treated by Saastamoinen (1972). He developed the following expression, which takes account of dry air, water vapor, and atmospheric refraction.

$$\Delta R = 2.277 \times 10^{-3} \sec z \,[p + (1255/T + 0.05)e - 1.16 \tan^2 z] \tag{3.36}$$

The quantity z is the zenith angle and the other quantities have the same meaning as previously in this chapter.

The number 2.277×10^{-3} differs slightly from 2.2757×10^{-3} of Eq. (3.28) because Saastamoinen used a 1963 expression for refractivity by Essen and Frome rather than the expression used elsewhere in this chapter by Smith and Weintraub (1953). Also he used 9.784 m/s^2 for g rather than 9.7877 m/s^2 as in the derivation of Eq. (3.28). He included an expression for g as a function of latitude ϕ and station height H above sea level, namely

$$g = 9.784 \; (1 - 0.0026 \cos 2\phi - 0.00028\, H) \; m/s^2 \qquad (3.37)$$

However he asserted that because of limitations of the ranging process it was sufficiently accurate to use 9.784 m/s^2 for g for all latitudes and station heights. For a pressure of 1013 mb and a zenith path the factor 2.277×10^{-3} of Eq. (3.36) gives a value of 2.3066 m for excess range delay, compared with 2.3053 m for ΔR_1 when Eq. (3.28) is utilized.

The quantity 2.277×10^{-3} [1255/T + 0.05] e of Eq. (3.36) is suitable for obtaining illustrative or approximate values of the additional excess range delay due to water vapor. For a temperature T of 280 K and water vapor pressure e of 9.70 mb, this quantity gives an excess range delay of 10.01 cm. The assumption of a particular exponential profile for illustrating the delay due to water vapor earlier in this section gave a delay of 9.23 cm for the same values of T and e. Part of the difference is due to the fact that in the treatment of this chapter no term like the coefficient 0.05 of Eq. (3.28) is recognized because if total pressure is used for ΔR_1 of Eq. (3.28) the remaining delay due to water vapor ΔR_2 is given by only a single term. But if 0.05 is eliminated from Eq. (3.36) the delay of 10.01 cm is reduced only to 9.90 cm.

3.8 EXCESS RANGE DELAY IN LASER RANGING

This handbook does not attempt to treat optical propagation, but, because it is of interest to persons concerned with tropospheric excess range delay at microwave frequencies to know what the corresponding situation is at optical frequencies, we include this mention of laser ranging. The clear air is dispersive at optical frequencies,and the group refractivity $N_g = (n_g - 1) \times 10^6$ affects excess range delay. The following expression for N_g is given by Abshire and Gardner (1985) and credited to Marini and Murray.

$$N_g = 80.343\, f(\lambda)\, p/T - 11.3\, e/T \qquad (3.38)$$

The quantities p, T, and e have the same meaning and are in the same units (mb for p and e, K for T) as in the previous expressions for radio frequencies. The term $f(\lambda)$ describes the variation of N_g with wavelength and has the form of

$$f(\lambda) = 0.9650 + 0.0164/\lambda^2 + 0.000228/\lambda^4 \qquad (3.39)$$

with λ in μm. The dispersive nature of the atmosphere allows the possibility of two-color (two-frequency) laser ranging such that

$$\Delta R_1 = \gamma\, (R_2 - R_1) \qquad (3.40)$$

$$\text{with } \gamma \simeq \frac{f\,(\lambda_1)}{f\,(\lambda_2 - \lambda_1)}$$

where the subscripts 1 and 2 refer to the two frequencies, R_2 and R_1 are the measured ranges at the two frequencies, and ΔR_1 is the excess range delay at frequency one. Note that the procedure is similar to that described for ionospheric propagation (Sec. 2.3.1), for which the use of two frequencies allows solving for the TEC and the time and range delays at the two individual frequencies.

REFERENCES

Abshire, J. B. and C. S. Gardner, "Atmospheric refractivity corrections in satellite laser ranging," IEEE Trans. Geosci. Remote Sensing, vol. GE-23, pp. 414-425, July 1985.

Bean, B. R. and E. J. Dutton, Radio Meteorology. Washington, DC: Supt. of Documents, U.S. Government Printing Office, 1966.

Bean, B. R., J. D. Horn, and O. M. Ozanich, Climatic Charts and Data of the Radio Refractive Index for the United States and the World, National Bureau of Standards Monoagraph 22. Washington, DC: Supt. of Documents, U.S. Government Printing Office, Nov. 25, 1960.

Bean, B. R., B. A. Cahoon, C. A. Samson, and G. D. Thayer, A World Atlas of Atmospheric Radio Refractivity, ESSA Monograph 1. Washington, DC: Supt. of Documents, U.S. Government Printing Office, 1964.

CCIR, "Radiometeorological data," Report 563-3, Vol. V, Propagation in Non-ionized Media, Recommendations and Reports of the CCIR, 1986. Geneva: Int. Telecomm. Union, 1986a.

CCIR, "Attenuation by atmospheric gases," Report 719-2, Vol. V, Propagation in Non-ionized Media, Recommendations and Reports of the CCIR, 1986. Geneva: Int. Telecomm. Union, 1986b.

CCIR, "Propagation data and prediction methods required for Earth-space telecommunication systems," Report 564-3, Vol. V, Propagation in Non-ionized Media, Recommendations and Reports of the CCIR, 1986. Geneva: Int. Telecomm. Union, 1986c.

Claflin, E. S., S. C. Wu, and G. M. Resch, "Microwave radiometer measurement of water vapor path delay: data reduction techniques," in DSN Progress Report 42-48, Jet Propulsion Laboratory, Pasadena, CA, Sept.-Oct. 1978.

Crane, R. K., "Refraction effects in the neutral atmosphere," in Methods of Experimental Physics, Vol. 12, Astrophysics, Part B: Radio Telescopes (M. L. Meeks, ed.), pp. 186-200. New York: Academic Press, 1976.

Dougherty, H. T. and B. A. Hart, Anomalous Propagation and Interference Fields, Report 76-107, Department of Commerce, 1976.

Dougherty, H. T. and B. A. Hart, "Recent progress in duct propagation predictions," IEEE Trans. Antennas Propagat., vol. AP-27, pp. 542-548, July 1979.

Flock, W. L., Electromagnetics and the Environment: Remote Sensing and Telecommunications. Englewood Cliffs, NJ: Prentice-Hall, 1979.

Flock. W. L., S. D. Slobin, and E. K. Smith, "Propagation effects on radio range and noise in earth-space telecommunications," Radio Sci., vol. 17, pp. 1411-1424, Nov.-Dec. 1982.

Gary, B. L., S. J. Keihm, and M. A. Janssen, "Optimum strategies and performance for the remote sensing of path delay using ground-based microwave radiometer," IEEE Trans. Geosci. Remote Sensing, vol. GE-23, pp. 479-484, July 1985.

GTE Lenkurt, Engineering Considerations for Microwave Communication Systems. San Carlos, CA: GTE Lenkurt, Inc., 1972.

Hall, M. P. M., Effects of the Troposphere on Radio Communications. Stevenage, UK and New York: Peter Peregrinus (on behalf of IEE), 1979.

Hautefeville, M. A. et al., "Duct fading - is Senegal an isolated case?," Telecomm. Jour., vol. 47, pp. 517-525, 1980.

Hopfield, H. S., "Tropospheric effect on electromagnetically measured range: prediction from surface weather data," Radio Sci., vol. 6, pp. 357-367, March 1971.

Jennings, D. A., K. M. Evenson, and D. J. E. Knight, "Optical frequency measurements," Proc. IEEE, vol. 74, pp. 168-179, Jan. 1986.

Liebe, H. J., "An updated model for millimeter wave propagation in moist air," Radio Sci., vol. 20, pp. 1069-1089, Sept.-Oct. 1985.

List, R. J., Smithsonian Meteorological Tables, Sixth Revised Ed., 5th Reprint, Washington, DC: Smithsonian Institution, 1984.

Resch, G. M., "Water vapor - the wet blanket of microwave interferometry," in Atmospheric Water Vapor (A. Deepak, T. D. Wilkerson, L. H. Ruhnke, eds.), pp. 265-282. New York: Academic Press, 1980.

Saastomoinen, J., "Atmospheric correction for the troposphere and stratosphere in radio ranging of satellites," in Geophys. Monogr. Ser., vol. 15, The Use of Artificial Satellites for Geodesy, ed. by S.W. Henriksen et al., pp. 247-251, AGU, Washington, DC.

Smith, E.K. and S. Weintraub, "The constants in the equation for atmospheric refractive index at radio frequencies," Proc. IRE, vol.41, pp. 1035-1037, August 1953.

Smith, E. K., "Centimeter and millimeter wave attenuation and brightness temperature due to atmospheric oxygen and water vapor," Radio Sci., vol. 17, pp. 1455-1464. Nov.-Dec. 1982.

Staelin, D. H. et al., "Microwave spectroscopic imagery of the earth," Science, vol. 197, pp. 991-993, Sept. 2, 1977.

Strickland, J. I., R. I. Olsen, and H. L. Werstivk, "Measurements of low angle fading in the Canadian Arctic," Ann. Telecomm., vol. 32, pp. 530-535, 1977.

Thayer, G. D., "An improved equation for the radio refractive index of air," Radio Sci., vol. 9, pp. 803-807, Oct. 1974.

Theobold, D. M. and R. Kaul, "Prediction of signal fluctuations and low angle fading on earth-space paths," in Prediction of Millimeter Wave Propagation Effects on Earth-Space Paths (10-100 GHz), ORI, Inc., Section IV, Greenbelt, MD: NASA Goddard Space Flight Center, 1978.

Thompson, M. C., L. E. Wood, H. B. Janes, and D. Smith, "Phase and amplitude scintillations in the 10 to 40 GHz band," IEEE Trans. Antennas Propagat., vol. AP-23, pp. 792-797, Nov. 1975.

U. S. Standard Atmosphere, 1976, sponsored by NOAA, NASA, USAF. Washington, DC: Supt. of Documents, U.S. Government Printing Office, 1976.

Van Vleck, J. H., "Theory of absorption by uncondensed gases," in Propagation of Short Radio Waves, Vol. 13, Radiation Lab. Series (D. E. Kerr, ed.), pp. 649-664. New York: McGraw-Hill, 1951.

Waters, J. W., "Absorption and emission by atmospheric gases," in Methods of Experimental Physics, Vol. 12, Astrophysics, Part B: Radio Telescopes (M. L. Meeks, ed.), pp. 142-176. New York: Academic Press, 1976.

Weisbrod, S. and L. J. Anderson, "Simple methods for computing tropospheric and ionospheric refractive effects on radio waves," Proc. IRE, vol. 47, pp. 1770-1777, Oct. 1959.

Wu, S. C., "Frequency selection and calibration of a water vapor radiometer," in DSN Progress Report 42-43, Jet Propulsion Laboratory, Pasadena, CA, pp. 67-81, Nov.-Dec., 1977.

CHAPTER 4

ABSORPTION, SCATTER, AND CROSS POLARIZATION CAUSED BY PRECIPITATION

4.1 MIE AND RAYLEIGH THEORIES FOR ATTENUATION

Raindrops cause attenuation of radio waves by both absorption and scatter. Absorption involves dissipation of some of the energy of an electromagnetic wave as heat. Scatter involves diversion of some of the energy of the wave into directions other than the forward direction. In the case of a beam of electromagnetic radiation, energy is scattered out of the beam. The term extinction is applied to the sum of absorption and scatter. Attenuation constants can be defined for extinction, absorption, and scatter such that

$$\alpha_{ext} = \alpha_{abs} + \alpha_{sca} \tag{4.1}$$

where the α's are attenuation constants and can be identified by their subscripts.

Analysis of absorption and scatter by rain drops has often been based upon the assumption of spherical drop shape, but the recent tendency is to take account of the nonspherical form of drops. For drops that are sufficiently small compared to wavelength, Rayleigh theory applies, but for drops that have sizes comparable to wavelength the more complicated Mie theory, or refinements of it, must be used. Drops with radii $\leq$ 170 μm are essentially spherical, whereas drops with radii betweem 170 and 500 μm are closely approximated by oblate spheroids. (An oblate spheroid is formed by rotating an ellipse about its shortest axis.) Between 500 and 2000 μm, drops are deformed into asymmetric oblate spheroids with increasingly flat bases, and drops $\geq$ 2000 μm develop a concave depression in the base which is more pronounced for the largest drop sizes (Pruppacher and Pitter, 1971). The ratio of the minor to major axes of oblate spheroid drops is equal to $1 - a$, where a is the radius in cm of a spherical drop having the same volume. Figure 4.1 shows an example of the shape of a very large drop.

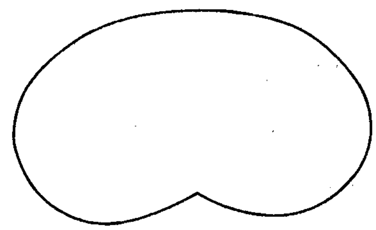

Figure 4.1. Form of a very large raindrop (Pruppacher and Pitter, 1971).

The total or extinction power-density attenuation constant α_p for rain can be expressed as

$$\alpha_p = \int_a N(a)\ C_{ext} \left[n_c, a/\lambda_o\right] da \qquad (4.2)$$

where a summation is indicated over all drop radii a, n_c is the complex index of refraction of water which is a function of temperature and frequency, and λ_o is wavelength in air. C_{ext} is an extinction coefficient and is shown as being expressed as a function of n_c and a/λ_o. N(a) da represents the number of drops per cubic meter in the size interval da and is determined by the drop size distribution which is a function of rain rate. [N(a) has units of m^{-4}, and N(a) da has units of m^{-3}.] Distributions of drop sizes have been determined empirically, the most widely used and tested distribution being the Laws and Parsons (1943) distribution. The Marshall and Palmer (1948) distribution is also well known. The Laws and Parsons data (Table 4.1) obtained by collecting rain drops in pans of flour do not provide N(a) da, but M(a) da, the fraction of the total volume of water striking the ground due to drops of a given size. To determine N(a) da, one must use M(a) da and also v(a), the limiting terminal velocity of raindrops as a function of size, in

$$N(a)\,da = \frac{M(a)\,da\,R}{v(a)\,a^3\,15.1} \tag{4.3}$$

Here R is rain rate in mm/h, v(a) is in m/s, a is in cm, M(a) is nondimensional, and N(a) da is in m^{-3}. The Laws and Parsons data are obtained for a finite, rather than infinitesmal, value of da of 0.025 cm, and Eq. (4.2) is thus evaluated in practice as a summation instead of an integral. Values of v(a) are given in Fig. 4.2.

The Marshall and Palmer distribution, made by making measurements on dyed filter papers, has the form of

$$N(R,a) = N_o\, e^{-ca} \tag{4.4}$$

where R is rain rate and a is drop radius. N and N_o are sometimes stated in units of cm^{-4}, corresponding to the number of drops per cm^3 in a size range of one cm in radius. In these units N_o has the value of 0.16. If a is in cm and R is in mm/h

$$c = 82\, R^{-0.21} \tag{4.5}$$

The number of drops in a volume V, in units of cm^3, having radii between a and a + da is given by N da V. The Laws and Parsons distribution can also be approximated by an equation of the form of Eq. (4.4).

The determination of C_{ext} has been commonly based on the Mie theory for spherical drops (Kerr, 1951; Kerker, 1969; Zufferey, 1972). In this case C_{ext} has the form of

$$C_{ext}\left(n_c, a/\lambda_o\right) = (\lambda_o^2/2)\ \mathrm{Re} \sum_{n=1}^{\infty} (2n+1)\,(a_n + b_n) \tag{4.6}$$

where λ_o is wavelength in air and a_n and b_n are coefficients involving spherical Bessel and Hankel functions of complex arguements. C_{ext} and S_o, which gives the amplitude of the forward scattered wave, are related by

Table 4.1 Laws and Parsons Distribution Giving the Percent of Volume Reaching Ground Contributed by Drops of Various Sizes.*

Drop Radius a (mm)	Rain Rate (mm/h) 0.25	1.25	2.5	12.5	25	50	100	150
0-0.125	1.0	0.5	0.3	0.1				
0.125-0.375	27.0	10.4	7.0	2.5	1.7	1.2	1.0	1.0
0.375-0.625	50.1	37.1	27.8	11.5	7.6	5.4	4.6	4.1
0.625-0.875	18.2	31.3	32.8	24.5	18.4	12.5	8.8	7.6
0.875-1.125	3.0	13.5	19.0	25.4	23.9	19.9	13.9	11.7
1.125-1.375	0.7	4.9	7.9	17.3	19.9	20.9	17.1	13.9
1.376-1.625		1.5	3.3	10.1	12.8	15.6	18.4	17.7
1.625-1.875		0.6	1.1	4.3	8.2	10.9	15.0	16.0
1.875-2.125		0.2	0.6	2.3	3.5	6.7	9.0	11.9
2.125-2.375			0.2	1.2	2.1	3.3	6.8	7.7
2.375-2.625				0.6	1.1	1.8	3.0	3.6
2.625-2.875				0.2	0.5	1.1	1.7	2.2
2.875-3.125					0.3	0.5	1.0	1.2
3.125-3.375						0.2	0.7	1.0

*Drop radius interval, da = 0.25 mm. Multiply percentage values by 0.01 to obtain M(a) da, e.g. for 50 mm/h and 1.125-1.375 mm, M(a) da = 0.209.

After J.O. Laws and D.A. Parsons, "The relation of drop size to intensity," Trans. of the A. Geophysical Union, pp. 452-460, 1943.

$$C_{ext}\left[n_c, a/\lambda_o\right] = (4\pi/\beta_o^2)\ \mathrm{Re}\ S_o\left[n_c, a/\lambda_o\right] \qquad (4.7)$$

where β_o is the phase constant $2\pi/\lambda_o$.

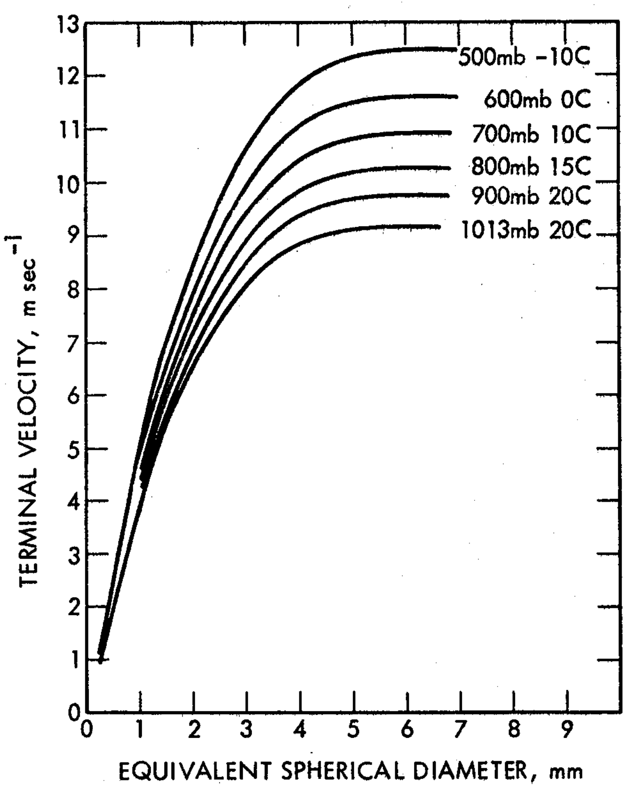

Figure 4.2 Terminal velocity of raindrops at six pressure levels in a summer atmosphere as a function of equivalent spherical diameter. (From Beard, "Terminal velocity and shape of cloud and precipitation drops aloft," J. of Atmospheric Sciences, May 1976.) The pressures 1013, 900, 800, 700, 600, and 500 mb correspond roughly to altitudes of 0, 0.98, 1.95, 3.0, 4.2, and 5.6 km respectively of the U.S. Standard Atmosphere, 1976.

For frequencies of about 3 GHz and less, the Rayleigh approximation can be used instead of the Mie theory. For this case C_{ext} takes the form of

$$C_{ext} = (4\pi^2 a^3/\lambda_o)\ 6K_i/[(K_r + 2)^2 + K_i^2] \qquad (4.8)$$

where K_i is the imaginary part of relative dielectric constant of water and K_r is the real part. The complex index of refraction n_c and complex relative dielectric constant K_c are related by $n_c^2 = K_c$.

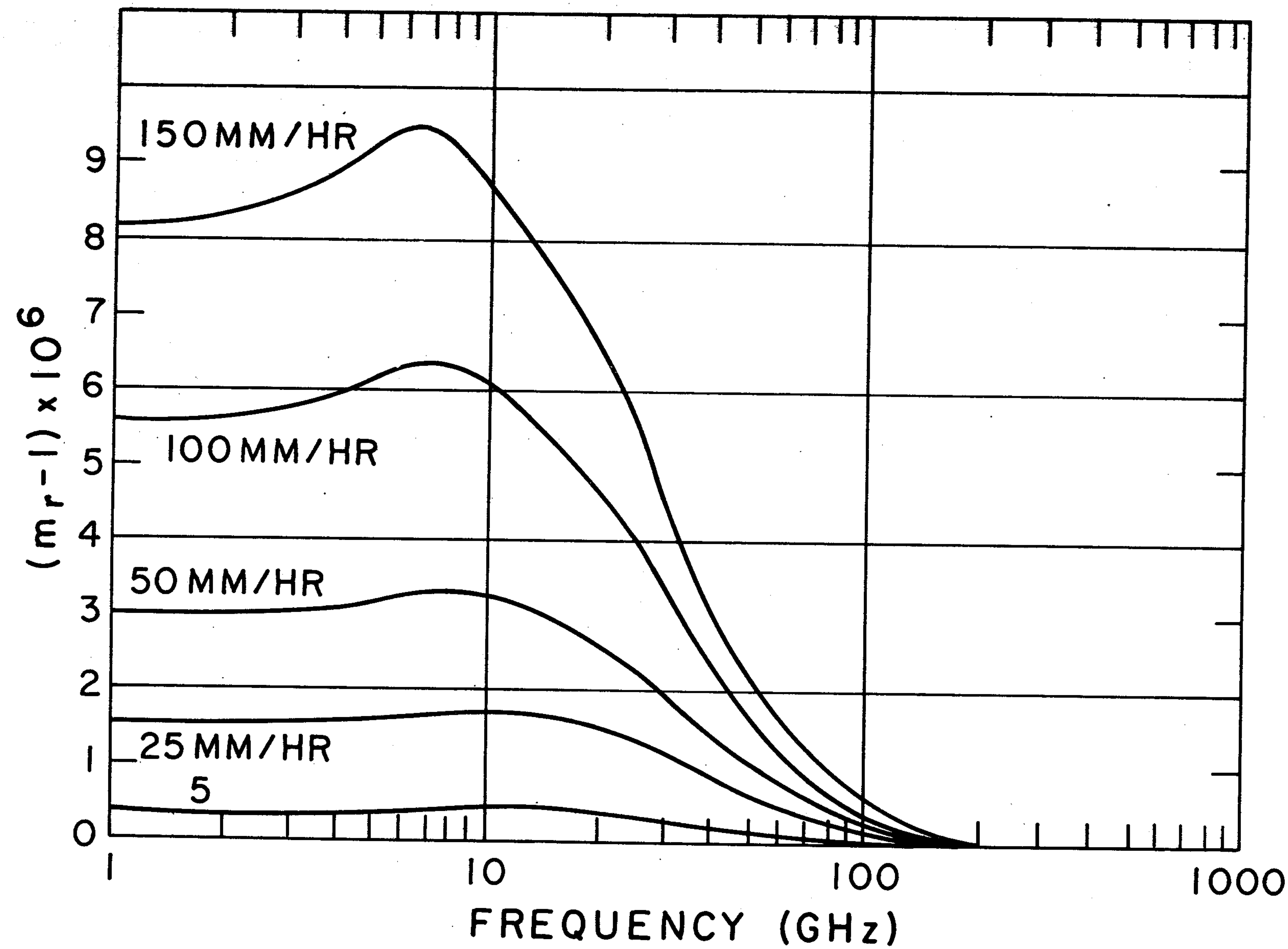

Figure 4.3a. The real part minus unity times 10^6 of the complex index of refraction of rain at 20 deg C (Zufferey, 1972).

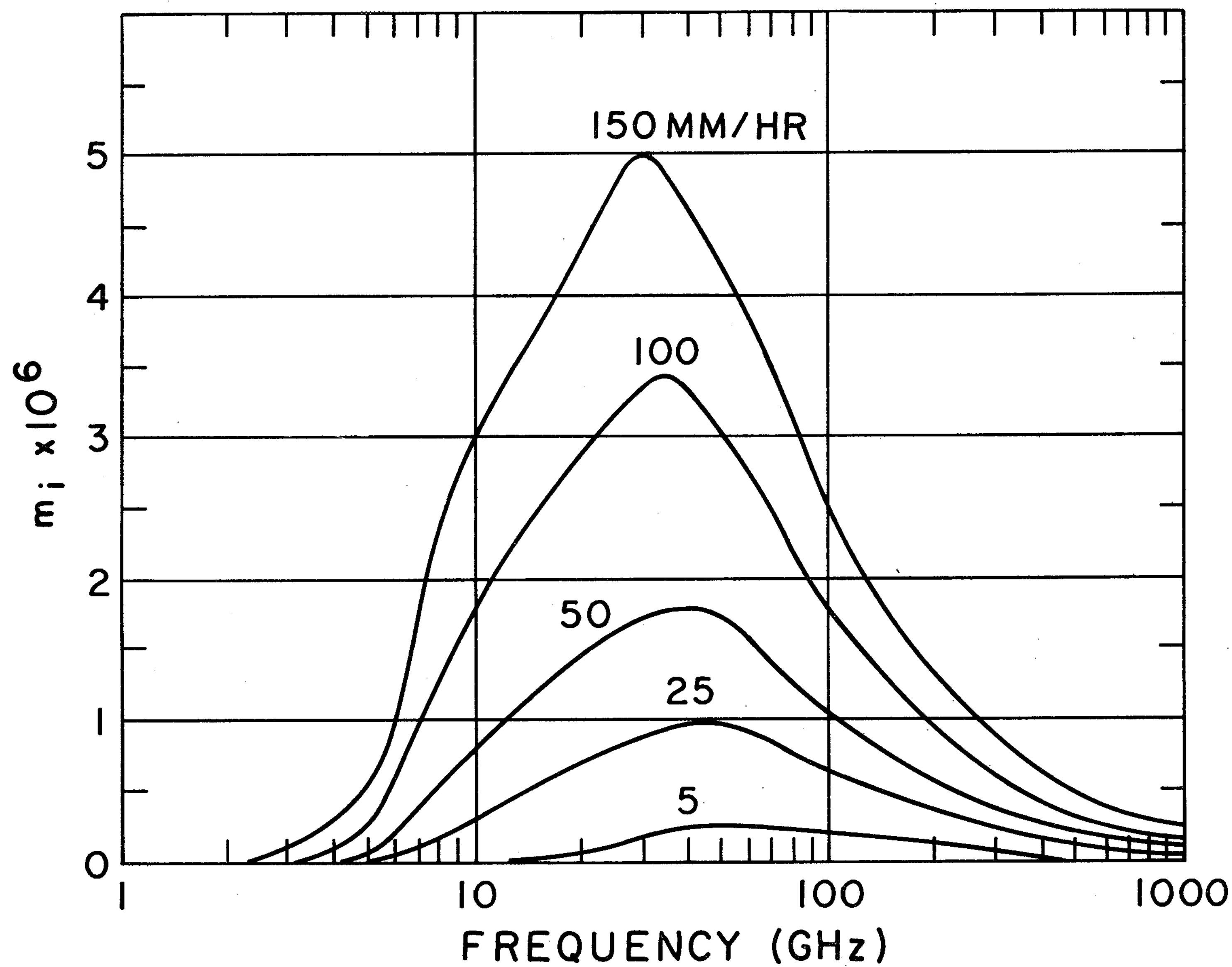

Figure 4.3b. The imaginary part times 10^6 of the complex index of refraction of rain at 20 deg C (Zufferey, 1972).

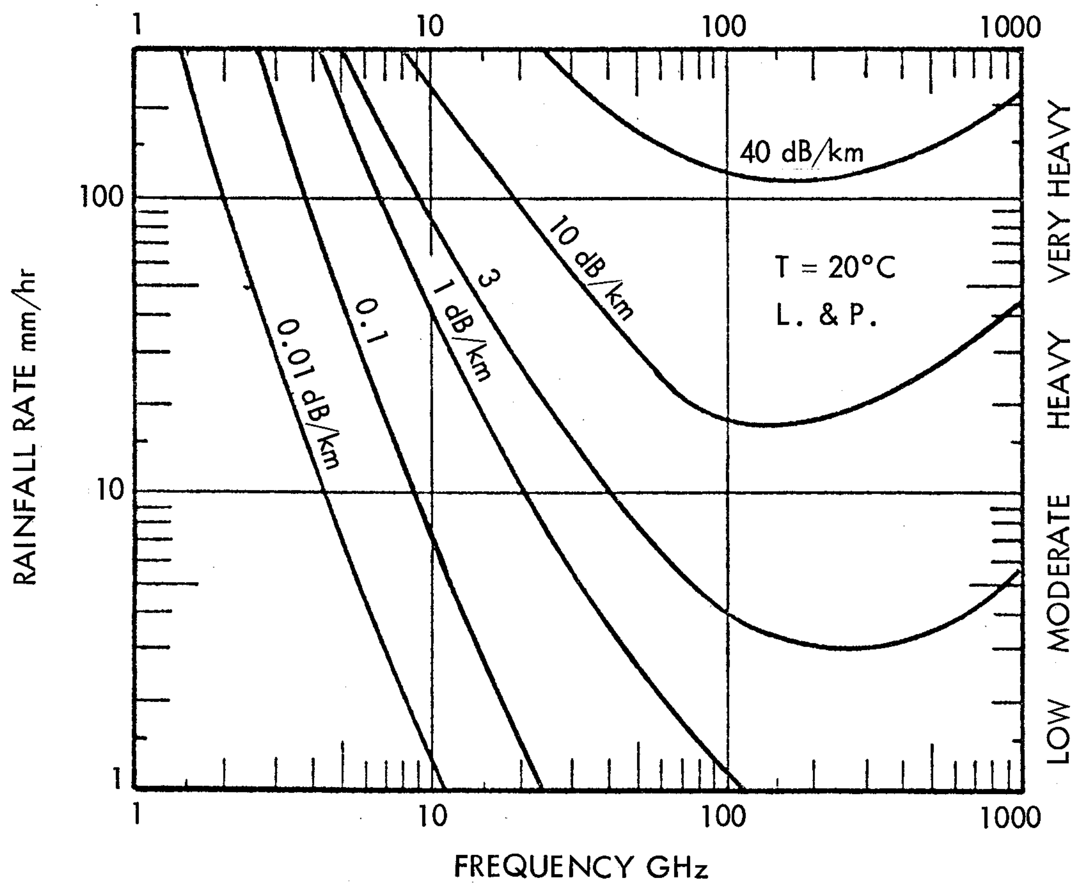

Figure 4.4. Rain rate versus frequency for specific values of attenuation constant (Zufferey, 1972).

An alternative procedure for determining the attenuation constant involves calculating an effective complex index of refraction m_c for the medium in terms of S_o by use of

$$m_c - 1 = j\,(2\pi/\beta_o^3) \int_a N(a)\, S_o \left[n_c, a/\lambda_o\right] da \tag{4.9}$$

This approach has been described by van de Hulst (1957) and Kerker (1969) but early consideration of the concept is attributed by Kerker to an 1899 paper by Rayleigh and 1890 and 1898 papers by Lorenz. The medium in question consists of water drops in empty space. The imaginary part m_i of the complex index m_c determines the field intensity attenuation constant α by use of

$$\alpha = \beta_o\, m_i \qquad \text{Nepers/m} \tag{4.10}$$

The power density attenuation constant α_p is related to the field intensity constant by $\alpha_p = 2\,\alpha$. To obtain attenuation in dB/m multiply α by 8.68 or α_p by 4.34. The phase constant β for the medium can be obtained from $\beta = \beta_o\, m_r$.

Values of the real part minus one and the imaginary part of the complex index m_c are shown in Figs. 4.3a and 4.3b. Plots of rain rate versus frequency for specific values of the attenuation constant are given in Fig. 4.4. These curves show that attenuation increases with rain rate up to about 100 GHz or more.

4.2 EMPIRICAL RELATIONS BETWEEN RAIN RATE AND ATTENUATION

Empirical relations between rain rate and attenuation constant have been developed and are widely used for practical application. In the remainder of this chapter the empirical relations will be primarily what is used to estimate attenuation due to rain. These relations have the form of

$$\alpha_p = a(f)\, R^{b(f)} \tag{4.11}$$

where a and b represent values which are a function of frequency f and R is rain rate in mm/h. The first observation of a relation of this type, but with $b = 1$, is credited to Ryde (1946). Values of $a(f)$ and $b(f)$ have since been determined by several workers including Zufferey (1972) who gave sets of values for light and heavy rain, the dividing line being taken as 10 mm/h. Olsen, Rogers, and Hodge (1978) have analyzed the relation thoroughly and derived tables of values of $a(f)$ and $b(f)$ for the Laws and Parsons and Marshall-Palmer distributions and for the drizzle and thunderstorm distributions of Joss. Their tables include the range from 1 to 1000 GHz for temperatures of 0, 20, and −10 deg C. Values based on the Laws and Parsons distribution for frequencies of 15 GHz and lower for 0 deg C are given in Table 4.2. The values LP_L apply for low rain rates, and LP_H values are for high rates, with some overlap. We take 30 mm/h to be a suitable dividing line and assume that either set of values can be used for that rate. Figure 4.5 shows values of attenuation constant as given in CCIR Report 721-2 (CCIR, 1986a). In addition estimates of the attenuation constant for frequencies below 10 GHz can be taken from Fig. 4.4. For frequencies of 3 GHz or less values of the attenuation constant can be calculated by using Eq. (4.8) for C_{ext}.

The widely used constants provided by Olsen, Rogers, and Hodge (1978) apply to spherical drops for which attenuation is independent of wave polarization. Attenuation for spheroidal drops depends on wave polarization, and Table 4.3 gives values of the constants a and b for vertical and horizontal polarization. Values for arbitrary polarization, including circular, can be derived from those for vertical and horizontal polarization by use of

$$a = [a_H + a_V + (a_H - a_V) \cos^2\theta \cos 2\tau]/2 \qquad (4.12)$$

$$b = [a_H b_H + a_V b_V + (a_H b_H - a_V b_V) \cos^2\theta \cos 2\tau]/2a \qquad (4.13)$$

The subscripts H and V refer to horizontal and vertical polarization. The angle θ is the elevation angle of the path, and τ is the tilt angle of the electric field intensity vector from the horizontal. The angle τ can be taken to be 45 deg for circular polarization. Values for frequencies intermediate between those of Table 4.3 can be obtained by interpolation. Now that information is available to determine a and b for arbitrary polarization, it seems advisable to

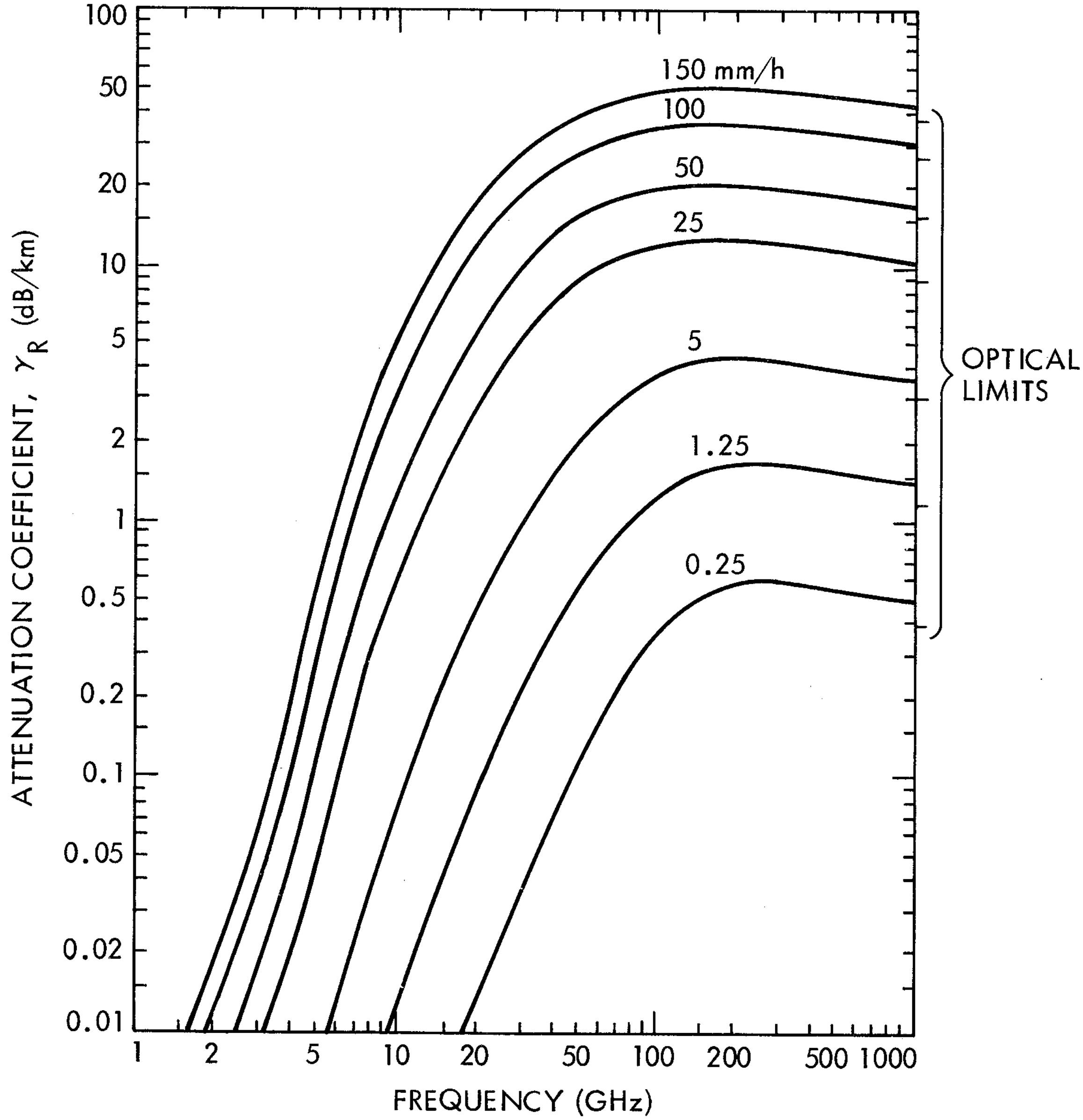

Figure 4.5. Attenuation constant as a function of rain rate and frequency (CCIR, 1986a).

Table 4.2 Values of a and b of Eq. (4.11) from Olsen, Rogers, and Hodge (1978) for T = 0 deg for High and Low Rain Rates.

Freq. (GHz)	a		b	
	LP_L	LP_H	LP_L	LP_H
1.0	6.41×10^{-5}	5.26×10^{-5}	0.891	0.947
1.5	1.45×10^{-4}	1.14×10^{-4}	0.908	0.976
2.0	2.61×10^{-4}	1.96×10^{-4}	0.930	1.012
2.5	4.16×10^{-4}	2.96×10^{-4}	0.955	1.054
3.0	6.15×10^{-4}	4.12×10^{-4}	0.984	1.100
3.5	8.61×10^{-4}	6.42×10^{-4}	1.015	1.150
4.0	1.16×10^{-3}	6.84×10^{-4}	1.049	1.202
5.0	1.94×10^{-3}	1.12×10^{-3}	1.113	1.274
6.0	3.05×10^{-3}	1.99×10^{-3}	1.158	1.285
7.0	4.55×10^{-3}	3.36×10^{-3}	1.180	1.270
8.0	6.49×10^{-3}	5.35×10^{-3}	1.187	1.245
9.0	8.88×10^{-3}	8.03×10^{-3}	1.185	1.216
10	1.17×10^{-2}	1.14×10^{-2}	1.178	1.189
11	1.50×10^{-2}	1.52×10^{-2}	1.171	1.167
12	1.86×10^{-2}	1.96×10^{-2}	1.162	1.150
15	3.21×10^{-2}	3.47×10^{-2}	1.142	1.119

Table 4.3 The Coefficients a and b for Calculating Attenuation for Horizontal and Vertical Polarization (CCIR, 1986a).

Frequency (GHz)	a_H	a_V	b_H	b_V
1	0.0000387	0.0000352	0.912	0.880
2	0.000154	0.000138	0.963	0.923
4	0.000650	0.000591	1.12	1.07
6	0.00175	0.00155	1.31	1.27
8	0.00454	0.00395	1.33	1.31
10	0.0101	0.00887	1.28	1.26
12	0.0188	0.0168	1.22	1.20
15	0.0367	0.0347	1.15	1.13

obtained by interpolation. Now that information is available to determine a and b for arbitrary polarization, it seems advisable to use that information. Values of the well established and somewhat more detailed tables of Olsen, Rogers, and Hodge (1978) are nevertheless included for completeness.

Interest in attenuation due to rain tends to be concentrated at the higher frequencies above 10 GHz where attenuation is the greatest, but the plots of Figs. 4.4 and 4.5 extend below 10 GHz as well. The values from the two figures are in general agreement, both showing that for frequencies of 10 GHz or less and rainfall rates of 100 mm/h or less, the attenuation constant has a value of about 3 dB/km or less. Attenuation constants of this order of magnitude, while less than for higher frequencies, may still be serious, and concern about attenuation due to rain is thus not confined to the higher frequencies but includes all of the X band (8-12 GHz). Attenuation due to rain increases the loss factor L in relations determining the signal-to-noise ratio (Sec. 1.1). It should be kept in mind also that rain increases the systems noise temperature, T_{sys}, as well (Chap.7).

4.3 STATISTICAL ANALYSIS OF ATTENUATION DUE TO RAIN

Procedures for calculating the attenuation constant for propagation through rain as a function of rain rate were described in Secs. 4.1 and 4.2. For predicting the attenuation expected on an earth-space path, one also needs to have a statistical model for the point rainfall intensity at locations or in regions of interest. In particular one generally needs to have an estimate of the rainfall rates that are exceeded for certain small percentages of time. Methods for obtaining rainfall data are described in Sec. 4.3.1. A third need is for a model of the spatial distribution of rainfall, as a function of height and distance from the station, and this topic is treated in Sec. 4.3.2. Finally several models that have been developed for widespread application, in some cases for worldwide use, are described in Sec. 4.3.3.

4.3.1 Rainfall Data

A first step in developing an understanding of the effect of rain on propagation in a particular area may be to obtain raw data on the occurrence of rain there. When sufficient raw data have been accumulated, it can be put into statistical form.

Published data on rain are already available for the United States from the National Climatic Center (Asheville, North Carolina 28801) of the National Weather Service. They supply Hourly Precipitation Data, issued monthly by state (including monthly maximum rainfalls for periods for as short as 15 min for a number of stations in each state); Climatologial Data, issued monthly by state (includes daily precipitation amounts); Climatological Data-National Summary, issued monthly (includes monthly rainfall and greatest rainfall in 24 h); Climatological Data - Annual Summary (includes maximum rainfalls in periods ranging from 5 to 180 minutes); Local Climatological Data, issued monthly (includes hourly rainfall for individual weather stations); and Storm Data, published monthly for the United States. In Canada Monthly Records for Western Canada, Northern Canada, and Eastern Canada and a monthly Canadian Weather Review are available from Supply and Services Canada, Publishing Centre (Hull, Quebec KDA059). Data for a number of other countries are on file at the National Weather Service Library, Room 816, Gramax Bldg., 13th Street, Silver Spring, MD.

Rain gauges are the means used for obtaining most of the National Weather Service rain data. A common type of gauge is supported in a vertical position and has a receiving area ten times the cross section of the measuring tube to facilitate precision in measurement. The amount of precipitation is determined by use of a hardwood measuring stick. Automatic tipping-bucket and universal weighing gauges are in use at National Weather Service stations that are manned by their own personnel (First Order Weather Stations), and chart records from these gauges can be obtained form the National Climatic Center.

If it is deemed advisable to obtain additional data on rainfall or attenuation caused by rain because of lack of detailed published data, a variety of options can be followed if sufficient financial support and manpower are available. One can set up rain gauges of the tipping bucket or weighing type. Radar can monitor precipitation over a wide area using the concepts discussed in Sec. 4.5 for bistatic scatter. For monostatic radar the distances R_1 and R_2 are the same, however, and the scattering volume V is proportional to R^2 for widespread rain, so the ratio of W_R/W_T (received power to transmitted power) is proportional R^{-2} as shown in Eq. (4.14).

$$W_R/W_T = \frac{G^2\,\theta_{HP}\,\phi_{HP}\,c\,\tau\,\pi^3}{1024\,(\ln 2)\,R^2\,\lambda^2}\left|\frac{K_c-1}{K_c+2}\right|^2 Z \tag{4.14}$$

The quantity G is radar antenna gain, θ_{HP} and ϕ_{HP} are the half-power beamwidths of the radar antenna, c is about 3×10^8 m/s, τ is the radar pulse length, λ is wavelength, and K_c is the complex relative dielectric constant of water. Z represents $\sum d^6$ where d is drop diameter and is related to the rain rate R by $Z = 400\ R^{1.4}$ for the Laws and Parsons distribution and $Z = 200\ R^{1.6}$ for the Marshall and Palmer distribution. Equation (4.14) thus allows determining the parameter Z which in turn allows estimating the rain rate R on the basis of the empirical relations given.

Another approach to measuring attenuation due to rain on earth-space paths is to use radiometer techniques. One procedure of this type involves using the Sun as a source. When a source having an effective temperature T_s is viewed through an absorbing medium having an effective temperature of T_i, the observed brightness temperature T_b is given by (Sec. 7.2)

$$T_b = T_s\,e^{-\tau} + T_i\,(1 - e^{-\tau}) \tag{4.15}$$

where τ is referred to as optical depth and is the integral of the the power-density attenuation coefficient along the path, namely $\int \alpha_p\,d\ell$. The temperatures of Eq. (4.15) are measures of power, as kT_bB where k is Boltzmann's constant and B is bandwidth, is power. The first term on the right-hand side of Eq. (4.15) represents the power from the Sun attenuated by the Earth's atmosphere and the second term represents thermal noise emitted by the Earth's atmosphere.

The Sun subtends an angle of 0.5 deg viewed from the Earth, and if the antenna of the radiometer is perfectly aligned with the Sun and the Sun fills the beam, T_s is the effective brightness temperature of the Sun. Otherwise T_s is the average brightness temperature within the antenna beamwidth, as determined by the temperature of the Sun itself and the low background level of about 2.7 K. The object of using Eq. (4.15) is to determine τ due to rain. This can be accomplished by first using the Sun as a source and then switching away from the Sun. The difference between the two values of T_b is $T_s e^{-\tau}$ and if T_s is known then τ is known. T_s can be determined by using the Sun as a source when no rain is present.

If the value of T_i of Eq. (4.15) is known then it is not necessary to use the Sun as a source. Instead one can point away from the Sun and record

$$T_b = T_i (1 - e^{-\tau}) \tag{4.16}$$

from which τ and the corresponding attenuation in dB ($A_{dB} = 4.34 \tau$) can be determined. T_i can be determined originally from measurements using the Sun or in some other way. It tends to be less than the physical temperature where rain is falling because total attenuation is due to scattering as well as absorption. It is only when attenuation is due to absorption alone that T_i can be expected to be equal to actual temperature.

A large amount of data on attenuation due to rain, much of it collected by using beacons on satellites, has been accumulated. The CCIR has established a data bank for earth-space propagation that includes data on rain attenuation (CCIR, 1983a; Crane, 1985a). NASA has sponsored an extensive study program on attenuation due to rain (Kaul, Rogers, and Bremer, 1977; Ippolito, 1978). The Nov.-Dec. 1982 issue of Radio Science was devoted to NASA sponsored propagation studies, including those about rain. Many of the studies of rain have been directed at frequencies above 10 GHz, but a considerable amount involves frequencies not far above (Arnold, Cox, and Rustako, 1981; Nackoney and Davidson, 1982; Vogel, 1982; Bostian, Pratt, and Stutzman, 1986).

4.3.2 Spatial Distribution of Rainfall

1. Vertical Distribution: Temperature decreases with height and precipitation tends to occur as snow rather than rain above the 0 deg C isotherm. Snow causes considerably less attenuation than rain, and it is the length of the path up to the 0 deg C isotherm that largely determines attenuation due to precipitation. Modeling the spatial distribution of rain is difficult and several procedures have been proposed for determining the height extent H of rainfall for estimating attenuation. Figure 4.6 shows curves for what were designated in 1983 as Methods 1 and 2 and also a lower dotted modification of Method 1 for latitudes below 40 deg (CCIR, 1983b). The modification was suggested by parties that thought that the other curves resulted in attenuation values that were excessively high for these latitudes. Method 1, including the dotted modification, and Method 2 have both been replaced, however, and the latest recommended CCIR procedure (CCIR, 1986b,c) is to use the relation given here as Eq. (4.30). This relation is based on 1984 Report 352 of the University of Bradford by Leitao, Watson, and Brussaard, prepared for the European Space Agency. See No. 8 of Sec. 4.3.3 for further discussion of the CCIR models.

2. Horizontal Distribution: Intense rain tends to be localized, and, especially when one is concerned with the high rain rates that are exceeded for small percentages of time, a procedure is needed to account for the fact that high rain rates will very likely not occur along the total length of the path. Some approaches involve determining an effective path length or path reduction factor. The original version of the Global Model (CCIR, 1978) used a path reduction factor $r = \gamma(D)\ R^{-\delta(D)}$ where D is horizontal extent of the path through rain and R is rain rate. This factor is shown graphically in Fig. 4.7. The 1982 CCIR model involves determination of a path reduction factor in an especially simple manner, and this approach has been retained in the latest CCIR report on the subject (CCIR, 1986b). While questions may be raised about this procedure, its simplicity is an advantage. In other cases, an effort is made to model the rain rate that can be expected along the path and to calculate the attenuation accordingly

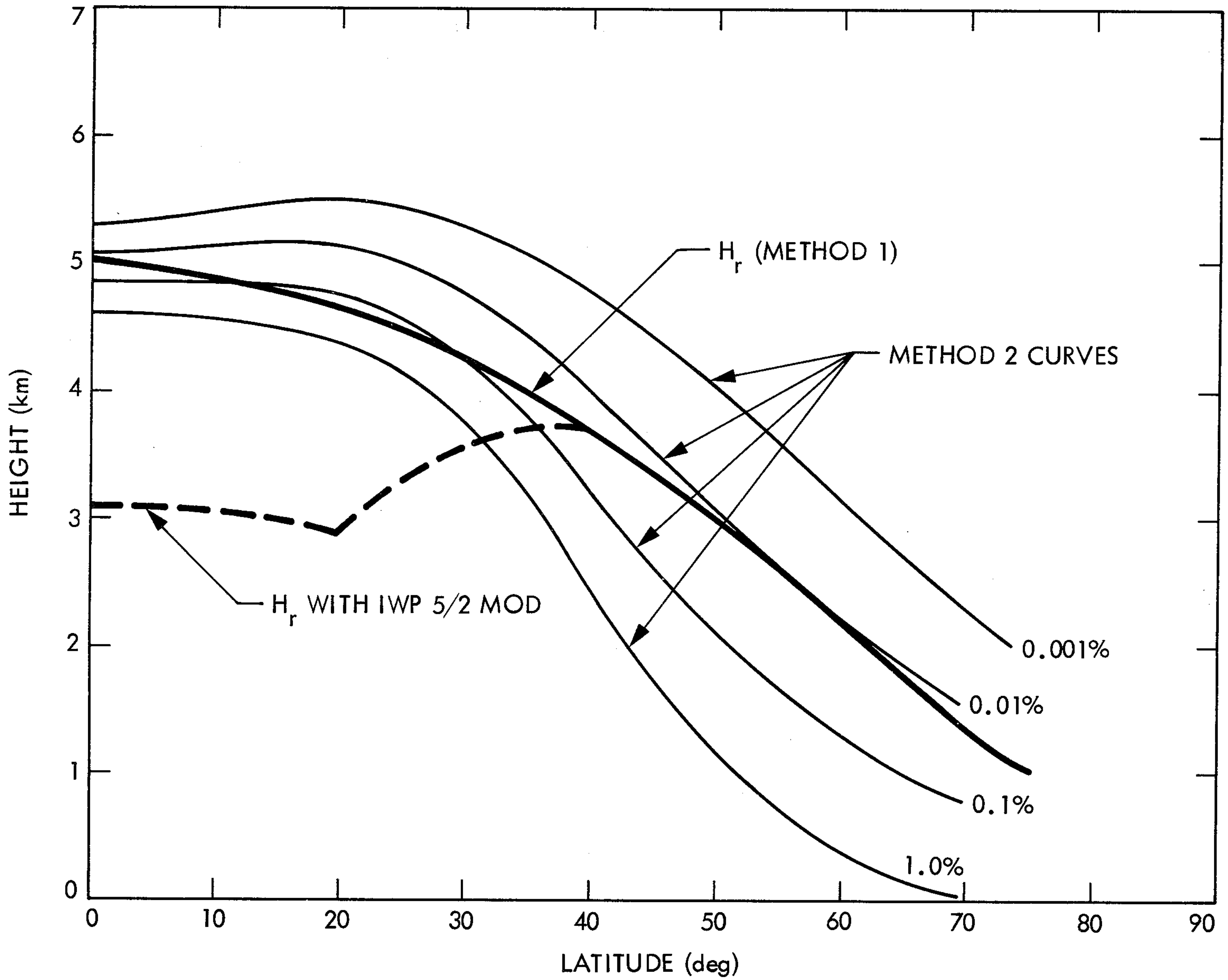

Figure 4.6. Heights of 0 deg C isotherms for Methods 1 and 2 (CCIR, 1983b). The latest recommended procedure, however, utilizes Eq. (4.30).

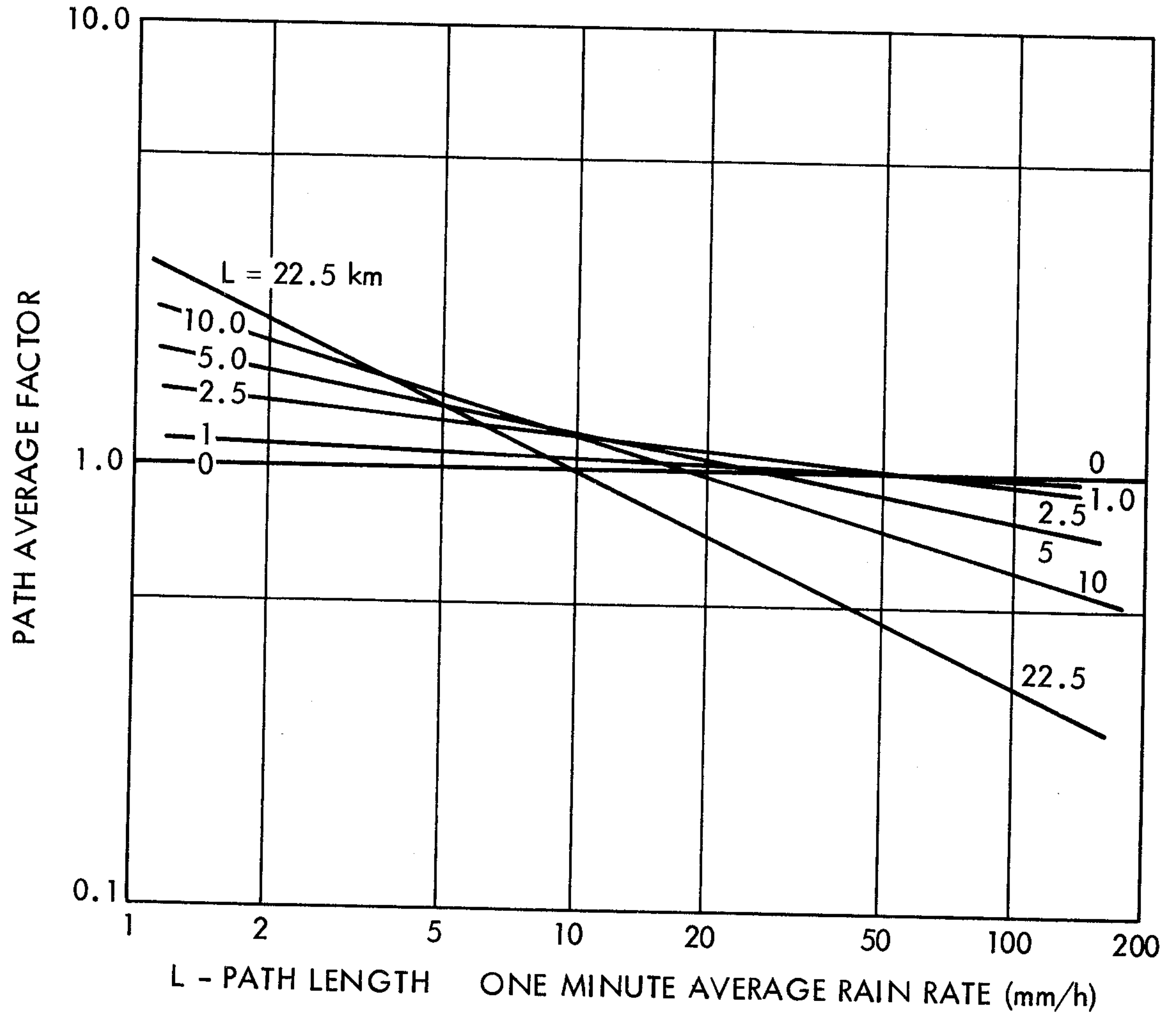

Figure 4.7. Effective path average factor for different path lengths and rates (CCIR, 1978).

Stutzman and Yon, 1986). The two-component model (Crane, 1982, 1985a) starts with an assumed value of attenuation and determines the separate probabilities that the attenuation can be caused by rain cells and surrounding rain debris.

4.3.3 Models of Attenuation Due to Rain

Several models of attenuation due to rain have been developed and refined and updated from time to time. The goal of the models is to provide statistically-based predictions of attenuation, and they encompass the three areas mentioned earlier - statistical data on rain rate, the calculation of the value of the attenuation constant from rain rate, and the spatial distribution of rain.

For locations of First Order Weather Stations in the United States and for locations having similar records elsewhere, data are available to provide statistical descriptions of rainfall. Lin (1977) and Lee (1979) describe and analyze procedures for obtaining the needed statistics from such data, which are published by the National Climatic Center in the United States. Earth stations, however, may well be located elsewhere than where weather stations are found, and for world-wide application it is desirable to divide the Earth into regions having similar rainfall characteristics and to attempt to obtain statistical descriptions of these characteristics. Selection of regions can be done on a large scale in rough accordance with the natural regions of the Earth (Sec. 1.4). A number of variations of such classifications exist. They agree generally on principal features but may disagree on detail and terminology. It has been suggested, however, that classifications made from biological, geographical, or agricultural viewpoints may need some modifications for telecommunications purposes (Segal, 1980). Figures 4.8 and 4.9 show the regions used in the Crane (1980) global model, and Fig. 4.10 shows regions of Canada, consistent generally with the CCIR 1982 model but modified somewhat by Segal (1986). The regions of the CCIR model are shown on a world-wide basis in Figs. 4.13 to 4.15.

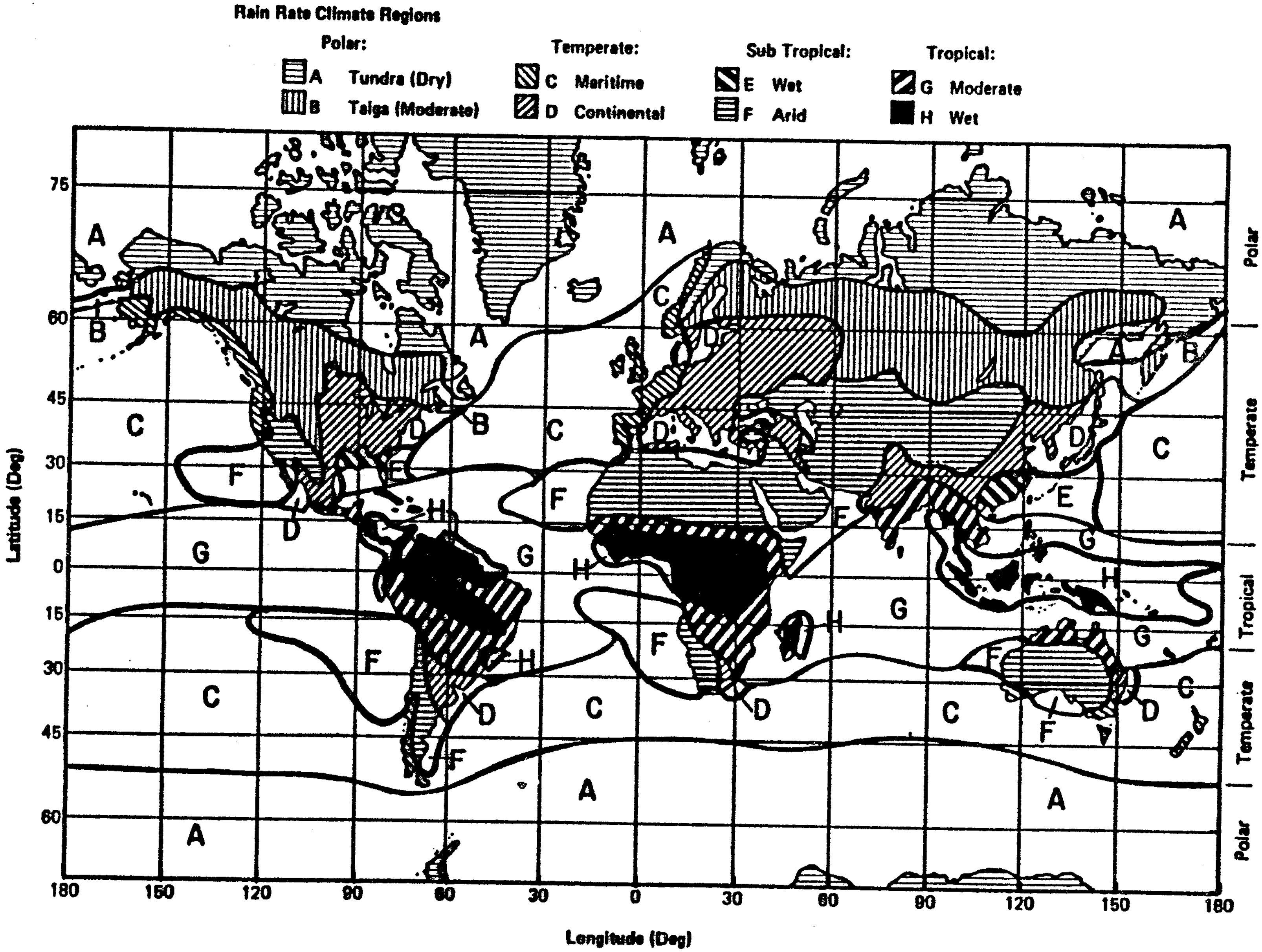

Figure 4.8. Global rain rate regions (Crane, 1980).

ORIGINAL PAGE IS
OF POOR QUALITY

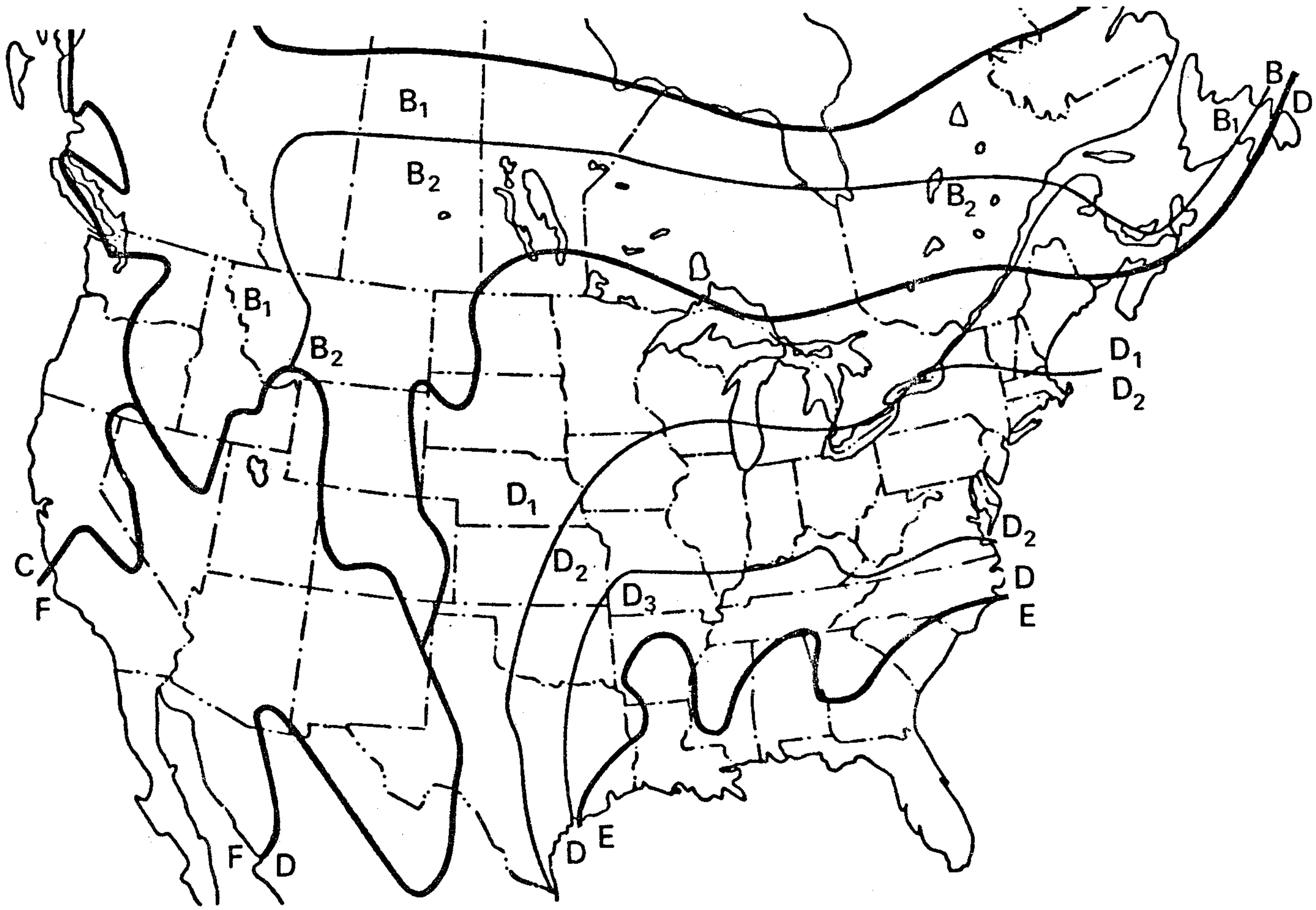

Figure 4.9. Rain rate regions of United States, as used in global model (Crane, 1980).

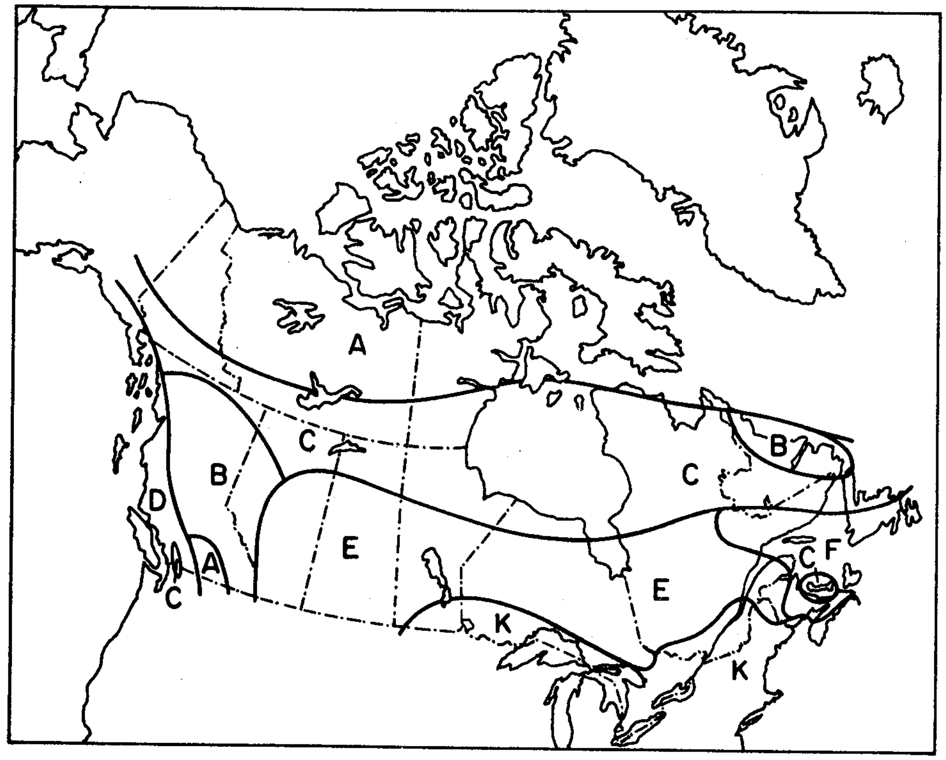

Figure 4.10. Rain rate regions of Canada, as defined by the CCIR and modified by Segal (1986).

The 1980 Global Model of Fig. 4.8 (No. 5 of this Sec. 4.3.3) involves 8 rain rate regions which correspond fairly well to the natural regions of the Earth (Trewartha, 1968; Sec. 1.4). As regions B and D for North America are subdivided, however, the Global Model can actually be considered to involve 11 regions. The modified 1982 CCIR Model (No. 8 of this Sec. 4.3.3) utilizes 14 rain rate regions, and these are based more closely on rain rate alone rather than natural regions. For example, whereas both models designate the arctic and antarctic regions as rain-rate region A, the Global Model restricts designation A to these regions while the CCIR model applies designation A to desert areas as well. Both high-latitude and desert areas have low rainfall, and that is the justification for designating both with the same symbol. The Global Model applies the designation F to deserts, Mediterranean areas, and to some temperate grassland and steppes whereas these three regions are actually quite different. The CCIR model applies the designation E to an even larger area including deserts, the Mediterranean area of southern California, and southern Canada, presumably because these areas may have roughly the same total rainfall. Southern California has hardly any thunderstorm activity, however, whereas the other areas have considerable thunderstorm activity. The type of rain as well as total amount is significant, and more detailed analyses and classifications for the occurrence of rain than those of the world-wide models can very well be utilized, especially for areas characterized by mountain ranges. The occurrence of rain can be very different in both total amount and type on opposite sides of mountain ranges.

Another case for which additional detail is desirable is that of the occurrence of rain as a function of time at given locations. The detail is desirable in order to obtain more reliable statistics about rain rates that are equaled or exceeded for small percentages of time. The averaging process can hide the occurrence of high rain rates for only a minute or a few minutes when rainfall is recorded for periods even as short as five minutes. It has become accepted that a one-minute raingauge integration time is a desirable compromise for recording rainfall. Much time and effort would be required to produce an adequate data base of one minute data, however, and attention has therefore been given to how to estimate one-minute rainfall data from longer-period data (CCIR, 1986c; Segal, 1986).

Characteristics of some of the models of rain attenuation will be described in this section. First we note that a good data base has been accumulated on attenuation due to rain on a number of paths. Analyses have been made of the comparative performance of several of the models to be described by use of this data base with differing conclusions (Crane, 1985a, 1985b; Stutzman and Yon, 1986). The interested reader or person dealing extensively with rain attenuation is advised to read the original papers, as it is not practical to provide detailed descriptions or comparisons showing the relative merits of the models or to provide numerical illustrations of all of them. Instead we include brief discussions of several of the models and use primarily the modified CCIR 1982 model to illustrate how the problem of rain attenuation can be treated. Numerical examples are given in Sec. 9.4. For the United States, however, we tend to favor using the rain-rate regions and values of the 1980 global model. Although the type of rain modeling described here is well developed, the opinion has been stated (Crane at Jan. 1986 meeting of NASA experimenters) that more effort is needed on other topics including fade duration and site diversity predictions.

1. Rice-Holmberg Model

Using a variety of meteorological data, Rice and Holmberg (1973) formulated a model which predicts distributions of t-minute point rainfall rates. The model gives the cumulative number of hours in a year that the rain rate may be expected to exceed a specified value during t-minute periods, e.g. 5-minute periods, etc. The model involves the use of 3 basic parameters which are M, the annual rainfall in mm; β, the average annual ratio of thunderstorm rain to total rain ; and D, the average number of days for which the precipitation exceeds 0.25 mm. M and D are determined directly from recorded data, and β is derived from data on the greatest monthly values in mm and the average number of days with thunderstorms. In considering this model one can set $M = M_1 + M_2$ where M_1 represents thunderstorm or convective rain and M_2 stands for stratiform rain of relatively wide extent and long duration. Convective rain tends to involve high rain rates but only comparatively short periods. The parameter β represents the ratio M_1/M.

2. Dutton-Dougherty Model, Modified Rice-Holmberg Model

The Dutton-Dougherty model predicts total attenuation from precipitation, clouds, and clear air. For attenuation caused by rain it uses a modified Rice-Holmberg model (Dutton,1977). An incentive for modifying the Rice-Holmberg model is that while the original model provides P(R), the percent of time that rainfall rate R is exceeded, given values of R, it is difficult to invert to obtain R, given P(R). That is, if one wishes to determine the rain rate R that is exceeded 0.01 percent of the time, for example, it is difficult to do so by using the original Rice-Holmberg model. The modified Rice-Holmberg model overcomes this problem. Like the original model it uses the 3 parameters, M, β, and D. Stratiform rain is assumed to be uniform up to the rain cloud base and to decrease to zero at the storm top height, while convective rain is assumed to increase slightly, in terms of liquid water content, up to the rain cloud base and to then decrease to zero at the storm top height.

Some results of interest obtained by use of the Dutton-Dougherty model in computer form have been published for Europe (Dougherty and Dutton, 1978) and the United States (Dutton and Dougherty, 1979). The papers provide maps of Europe and the United States that show contours of one-minute rainfall rates in mm/h, corresponding to values equaled or exceeded for 1, 0.1, and 0.01 percent of the time. The papers also include contours of the standard deviation in mm/h of annual rainfall rates corresponding to the percentages mentioned above. Data for 30 years were used for the United States. In 1982, the Dutton-Dougherty model was improved to extend to rain rates exceeded for the low percentage of 0.001 (Dutton, Kobayashi, and Dougherty, 1982). The question of incorporating the concept of effective path length into the model was considered and rejected. Instead a probability modification factor F is retained for modeling the variation of rain intensity in the horizontal direction. This factor multiplies the original percent of time p_o that attenuation of a certain value is expected to obtain a lower value p. For determining the attenuation constant α, an expression like Eq. (4.11) is used except that in place of rain rate R in mm/h the quantity L , liquid water content per unit volume, is employed.

3. Piecewise Uniform Rain Rate Model

The piecewise uniform model (Persinger et al., 1980) is a quasi-physical model developed to eliminate the need for effective path lengths. It involves the assumptions that the spatial rain rate distribution is uniform for low rates but becomes increasingly nonuniform as the peak rain rate increases. Total attenuation A is determined from

$$A = (L/N) \sum_{i=1}^{N} \alpha(R_i) \tag{4.17}$$

where L is the path length which is divided into N equal intervals, α is the attenuation constant corresponding to rain rate R_i of the ith division or cell. Two levels are used in the version reported here, with

$$R_\ell = R_1 \text{ for } 0 \le \ell \le CL, \qquad R_\ell = R_x \text{ for } CL \le \ell < L \tag{4.18}$$

where

$$R_x = R_1 \text{ for } R_1 \le 10 \text{ mm/h}, \quad R_x = R_1(R_1/10)^x \text{ for } R_1 \ge 10 \text{ mm/h} \tag{4.19}$$

In terms of these quantities, the expression for A can be written as

$$A = [\, C\,\alpha(R_1) \; + \; (1 - C)\,\alpha(R_x)\,]\, L \qquad \text{dB} \tag{4.20}$$

Based on experimental evidence for the eastern United States, C is taken to be 0.2 and x is taken to be −0.66. Path length L is found by using a height extent of rain H and a basal length B with H equal to 3.5 km for high latitudes above 40 deg, 4.0 km for mid latitudes, and 4.5 km for low latitudes below 33 deg. The quantity B is taken to be 10.5 km. Then

$$L = H/\sin\theta \text{ for } \theta \ge \theta_o, \qquad L = B/\cos\theta \text{ for } \theta \le \theta_o \tag{4.21}$$

with $\theta_o = \tan^{-1} H/B$ and θ the elevation angle.

4. Radar Modeling

The utility of radar for obtaining rainfall data was mentioned in Sec. 4.3.2, and the radar technique, with emphasis on bistatic scatter, is discussed in Sec. 4.5. Radar contributions to rain-attenuation modeling were described by Goldhirsh and Katz (1979). Data on the intensity of rainfall along a path or over an area and also as a function of height can be obtained.

An extensive amount of radar data have been obtained at Wallops Island, VA by use of the SPANDAR S-band radar, much of it at time that COMSTAR beacon measurements at 28.56 GHz were also being made (Goldhirsh, 1982a). Radar reflectivity Z can be related to rain rate R by

$$R = u Z^{v} \qquad \text{mm/h} \tag{4.22}$$

where u and v are drop-size dependent. A disdrometer, an instrument for measuring drop-size distributions, has been developed and utilized in studies reported here. Values of u and v used for Laws and Parsons and Marshall and Palmer distributions can be derived from Eqs. (4.56) and (4.57). Goldhirsh has shown that the radar data he obtained agreed well with attenuation values measured by use of the COMSTAR beacon. Also he has shown that the radar data can be extrapolated to other locations with good agreement with directly measured data. The radar technique is readily adaptable to space diversity studies, and this application is the subject of a 1982 paper (Goldhirsh, 1982b). The ability to employ radar data for the modeling of both single and joint probability cumulative fade distributions at various path elevation angles and frequencies received attention in a 1984 paper (Goldhirsh, 1984).

5. 1980 Global Model

This model, described by Crane (1980) divides the world into the eight rain-rate regions shown in Fig. 4.8. The United States is covered by five regions, with two, B and D, subdivided as shown in Fig. 4.9. Figure 4.11 or Table 4.4, giving rain rates exceeded for various percentages of time, provide the needed rain rate data. For determining values of attenuation constant α_p use is made of $\alpha_p = aR^b$ where R is rain rate. For Canada, however, we recommend using the regions of Fig. 4.10, supplied by Segal (1986). Rates

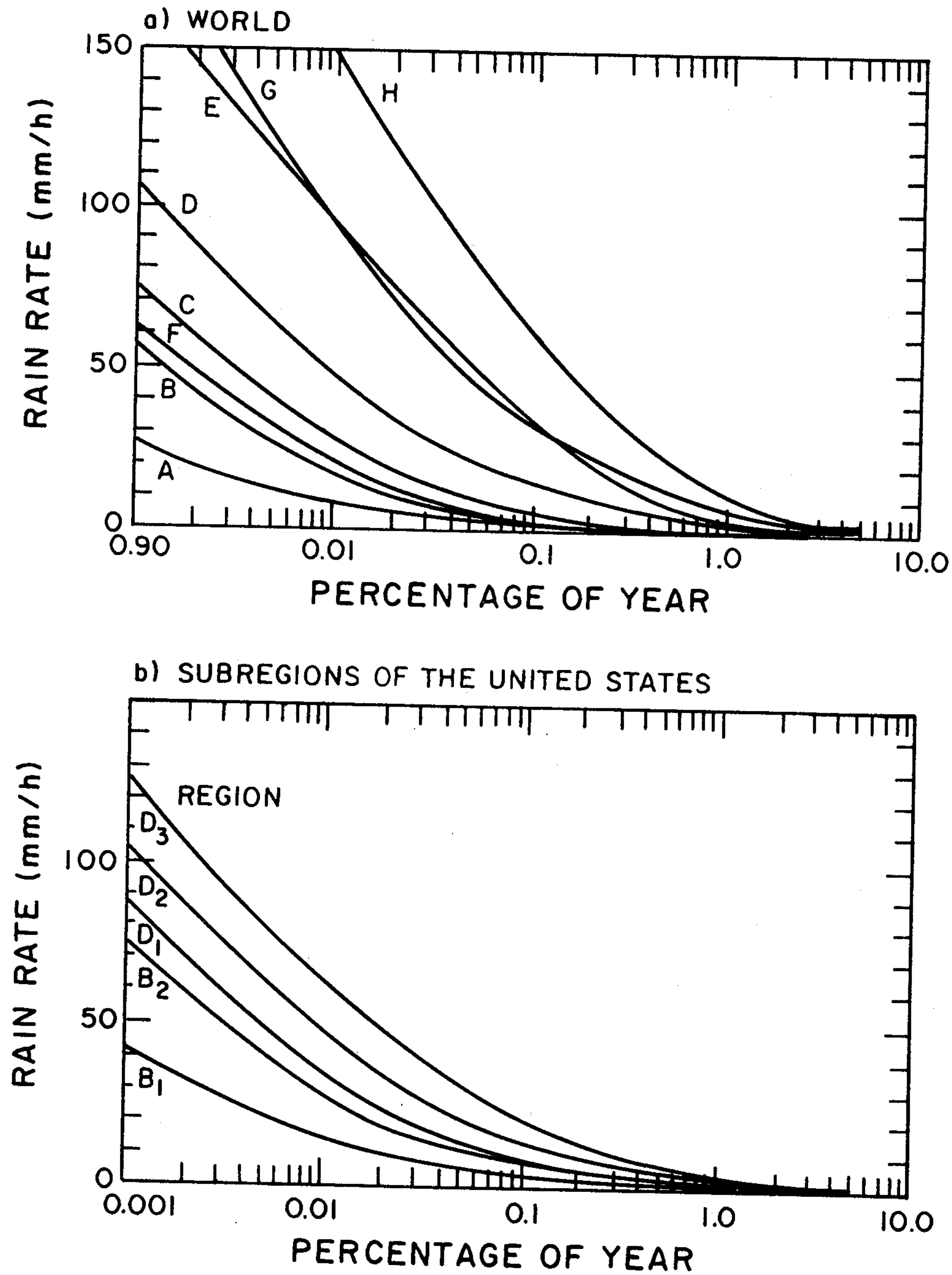

Figure 4.11. Rain rates as a function of percent of year exceeded, for 1980 Global Model.

exceeded as a function of percentage of time for the Canadian regions are shown in Table 4.5. Believing the relation mentioned in Sec. 4.3.2 for the spatial distribution of rainfall to be inadequate because of the nonlinear relation between rain rate and attenuation constant, Crane used numerical differentiation to obtain relative path rain-rate profiles showing that when high point rain rates occur, the most intense rain is found close to the sampling location. When rain rates are low at the sampling location, however, higher rain rates are likely at distances in excess of 6 km away. Approximation of the profiles by exponential functions leads to an expression for attenuation along a horizontal path of length D that involves three such functions as follows.

$$A(R, D) = \alpha R^{\beta} \left[\frac{e^{\mu\beta d} - 1}{\mu\beta} - \frac{b^{\beta} e^{c\beta d}}{c\beta} + \frac{b^{\beta} e^{c\beta D}}{c\beta} \right] \qquad d < D < 22.5 \text{ km} \tag{4.23}$$

$$A(R,D) = \alpha R^{\beta} \left[\frac{e^{\mu\beta D} - 1}{\mu\beta} \right] \qquad 0 < D < d \tag{4.24}$$

with A in dB, R in mm/h, and αR^{β} the expression of Eq. (4.11) but with α and β used in place of a and b.

$$\mu = \frac{\ln (b\, e^{cd})}{d} \quad \text{(d in km)} \qquad b = 2.3\, R^{-0.17}$$

$$c = 0.026 - 0.03 \ln R \qquad d = 3.8 - 0.6 \ln R$$

For elevation angles θ greater than 10 deg, D is given by

$$D = (H_o - H_g)/ \tan\theta \tag{4.25}$$

where H_o is the height of the 0 deg isotherm from the Method II curves of Fig. 4.7 and H_g is the height of the surface. Attenuation A_s along a path of length L is given by

$$A_s = [L\ A(R, D)]/D = [A(R, D)]/ \cos\theta \tag{4.26}$$

for $\theta \geq 10$ deg. For $\theta \leq 10$ deg, see Appendix 4.1. The original

Table 4.4 Rain Rates Exceeded as a Function of Percentage of Year, for Regions A to H of 1980 Global Model.

Percentage of Year	Rain Rates Exceeded (mm/h)											
	A	B_1	B	B_2	C	D_1	$D=D_2$	D_3	E	F	G	H
0.001	29	45	58	70	78	90	108	126	165	66	185	253
0.002	21	34	44	54	62	72	89	106	144	51	157	220.5
0.005	13.5	22	28.5	35	41	50	64.5	80.5	118	34	120.5	178
0.01	10.0	15.5	19.5	23.5	28	35.5	49	63	98	23	94	147
0.02	7.0	11.0	13.5	16	18	24	35	48	78	15	72	119
0.05	4.0	6.4	8.0	9.5	11	14.5	22	32	52	8.3	47	86.5
0.1	2.5	4.2	5.2	6.1	7.2	9.8	14.5	22	35	5.2	32	64
0.2	1.5	2.8	3.4	4.0	4.8	6.4	9.5	14.5	21	3.1	21.8	43.5
0.5	0.7	1.5	1.9	2.3	2.7	3.6	5.2	7.8	10.6	1.4	12.2	22.5
1.0	0.4	1.0	1.3	1.5	1.8	2.2	3.0	4.7	6.0	0.7	8.0	12.0

A percentage of 0.01 of a year corresponds to 53 minutes.

global model used a path reduction factor mentioned in Sec. 4.3.2 and calculated by a procedure like that of the 1982 CCIR model [Eq. (4.33)].

6. Two-Component Model

When using models such as the 1980 Global Model and the 1982 CCIR Model, one first determines the rain rate R that is expected to be exceeded for p percent of the time. The attenuation constant α_p corresponding to R_p is then calculated. The two-component model, however, starts with values of attenuation and determines the separate probabilities of exceeding this attenuation because of convective rain cells on the one hand and widespread rain debris on the other. The name of the model is derived from its recognition and separate treatment of the two types of rain, intense rain in localized cells of the order of a couple of kilometers in diameter and rain of lesser intensity but greater areal extent. Recall that the Rice-Holmberg and Dutton-Dougherty models separated rainfall in a somewhat similar way into thunderstorm or convective rain of generally short duration and stratiform rain of generally wide extent and longer duration.

The two-component model was introduced in 1982 (Crane, 1982). A step-by-step description is given as an appendix in the original paper. A similar treatment of a revised version is given as an appendix in Crane (1985a). Certain features of the model are described in Appendix 4.2 of this handbook.

7. SAM (Simple Attenuation Model)

The simple attenuation model employs the procedure of the 1982 CCIR rain model (No. 8, following) to predict rain rate as a function of percentage of time and calculates the attenuation constant from rain rate by use of the usual empirical relation, Eq. (4.11). The improved version of SAM described in 1986 (Stutzman and Yon, 1986) uses the 1982 CCIR values of a and b for horizontal and vertical polarization, which values also allow determination of a and b for arbitrary polarization [Eqs. (4.12) and (4.13)]. The original SAM model used the a and b values of Olsen, Rogers, and Hodge (1978). A distinctive feature of SAM is its treatment of the spatial distribution of rainfall. Considering that the treatment of this same topic is unnecessarily complicated in the 1980 Global Model, the authors use a simpler assumption about the variation of rainfall with distance from the ground station location. For a rain rate R_o at the station equal to or less than 10 mm/h, the rain rate is assumed to be constant along the path so that

$$R(\ell) = R_o \text{ for } R_o \leq 10 \text{ mm/h}$$

For a rain rate equal or greater than 10 mm/h, $R(\ell)$ is assumed to be given by

$$R(\ell) = R_o\, e^{[-\gamma \ln (R_o/10)\, \ell \cos \theta]}, \quad R_o \geq 10 \text{ mm/h} \qquad (4.27)$$

This expression applies for $\ell \leq L$ where $L = (H - H_o)/\sin \theta$. The expressions for $R(\ell)$ are substituted into

$$A(R_o) = \int_o^L a\, R(\ell)^b \, d\ell$$

leading to the results that

$$A(R_o) = a\, R_o^{\,b} L \qquad R_o \leq 10 \text{ mm/h} \qquad (4.28)$$

$$A(R_o) = a\, R_o^{\,b} \; \frac{1 - e^{[-b\gamma \ln (R_o/10)\, L \cos \theta]}}{b\gamma \ln (R_o/10) \cos \theta}, \quad R_o \geq 10 \text{ mm/h} \qquad (4.29)$$

A value of 1/14 is used for γ in the 1986 version of SAM.

The 1982 CCIR model uses an effective path length equal to L r_p, where r_p is a path reduction factor, and its procedure is actually simpler than SAM in this respect. The CCIR approach is empirical and has been designated as provisional.

8. Modified 1982 CCIR Model

The rain rate regions of the 1982 CCIR model are shown in Figs. 4.13 - 4.15, and the rain-rate values for these regions are given in Table 4.5. In addition, contours of the rain rate exceeded for 0.01 percent of the time are provided in Figs. 9.8 - 9.10. The attenuation constant α_p corresponding to these rain-rate values is found by using aR^b with values of a and b from Table 4.3. The latest revisions of CCIR Reports 563 and 564 give the expression of Eq. (4.30) for determining the height extent H of rain

(CCIR, 1986c,d) For latitudes ϕ less than 36 deg, the height extent of rain H is taken as 4.0 km, and for $\phi \geq 36$ deg one uses

$$H = 4.0 - 0.075\ (\phi - 36^{o})\ \text{km} \qquad \phi \geq 36^{o} \qquad (4.30)$$

In the first edition of this handbook the dotted modification of the Method 1 curve of Fig. 4.6 was recommended, and persons concerned with attenuation from rain at lower latitudes should be alert to the possibility that lower heights than 4.0 km may still be applicable. In either case whether using Eq. (4.30) or Fig. 4.6, the height H to be used is the height equaled or exceeded with a probability of 0.01. The length L though rain is determined by

$$L = H/\sin\theta \quad \text{km} \qquad (4.31)$$

for elevation angles θ greater than 10 deg. For angles less than 10 deg use

$$L = \frac{2\,H}{[\,\sin^2\theta + 2\,(H/a)\,]^{1/2} + \sin\theta} \quad \text{km} \qquad (4.32)$$

where a is effective earth radius.

Attenuation A in dB is determined for the perecentage of 0.01 from

$$A = \alpha_p L\, r_p \qquad (4.33)$$

where α_p and L are discussed above and r_p is an empirical path reduction factor factor given by

$$r_p = \frac{1}{1 + 0.045\,D} \qquad (4.34)$$

where $D = L\cos\theta$ is the horizontal projection of L. Previously the form 90/(90 + 4D) was used; the numerical values of these two expressions are essentially identical. To determine attenuation A_p equaled or exceeded with a probability other than 0.01, the latest recommendation is to use

$$A_p = A_{0.01}\ 0.12\, p^{-(0.546 + 0.043 \log p)} \qquad (4.35)$$

Previously the procedure (CCIR, 1983b) was to use

$$A_p = c\, A_{0.01}\, p^{-d}$$

Values were supplied for the constants c and d and Fig. 4.12 was also given. Although replaced by the CCIR by Eq. (4.35), we retain Fig. 4.12 in this chapter for reference purposes. The original 1982 CCIR model distinguished maritime and continental climates, using what in 1983 became known as Method 1 for maritime climates and Method 2 for continental climates (CCIR, 1983b). Note that Method 1 (original or modified dotted form) provided the height equalled or exceeded with a probability of 0.01 percent. Method 2, however, provided heights for probabilities of 0.001, 0.01, 0.1, and 1 percent. Both Methods 1 and 2 have been replaced with Eq. (4.30) now used for the height of rain H in both cases. The latest procedure nevertheless follows the general plan of Method 1 in that a height is determined only for a probability of 0.01. Then attenuations for other percentages are determined by use of Eq. (4.35).

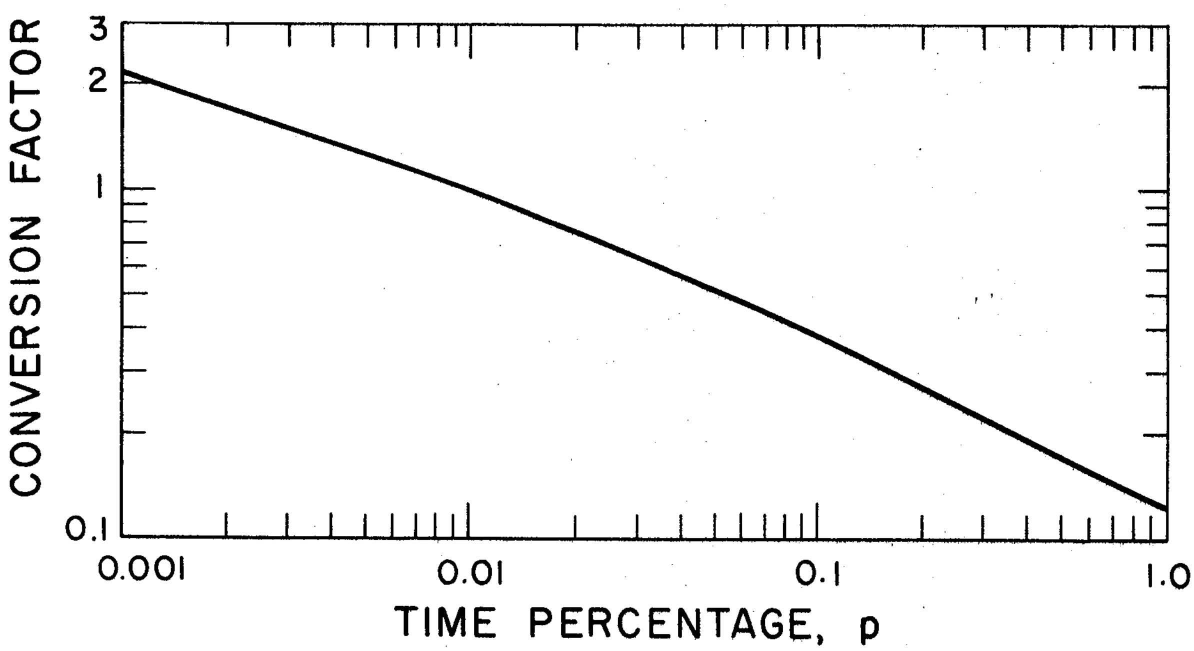

Figure 4.12. Factor cp^{-d} for conversion of the rain attenuation exceeded for 0.01 perecent of the time $A_{0.01}$ to that exceeded for p percent of the time, as given in CCIR (1983b). The latest recommended procedure, however, is to use Eq. (4.35).

Table 4.5 Rain Rates Exceeded as a Function of Percentage of Year, for Regions A to P of 1982 CCIR Model.

Percentage	Rain Rates Exceeded (mm/h)													
of Year	A	B	C	D	E	F	G	H	J	K	L	M	N	P
1.0	-	1	-	3	1	2				2		4	5	12
0.3	1	2	3	5	3	4	7	4	13	6	7	11	15	34
0.1	2	3	5	8	6	8	12	10	20	12	15	22	35	65
0.03	5	6	9	13	12	15	20	18	28	23	33	40	65	105
0.01	8	12	15	19	22	28	30	32	35	42	60	63	95	145
0.003	14	21	26	29	41	54	45	55	45	70	105	95	140	200
0.001	22	32	42	42	70	78	65	83	55	100	150	120	180	250

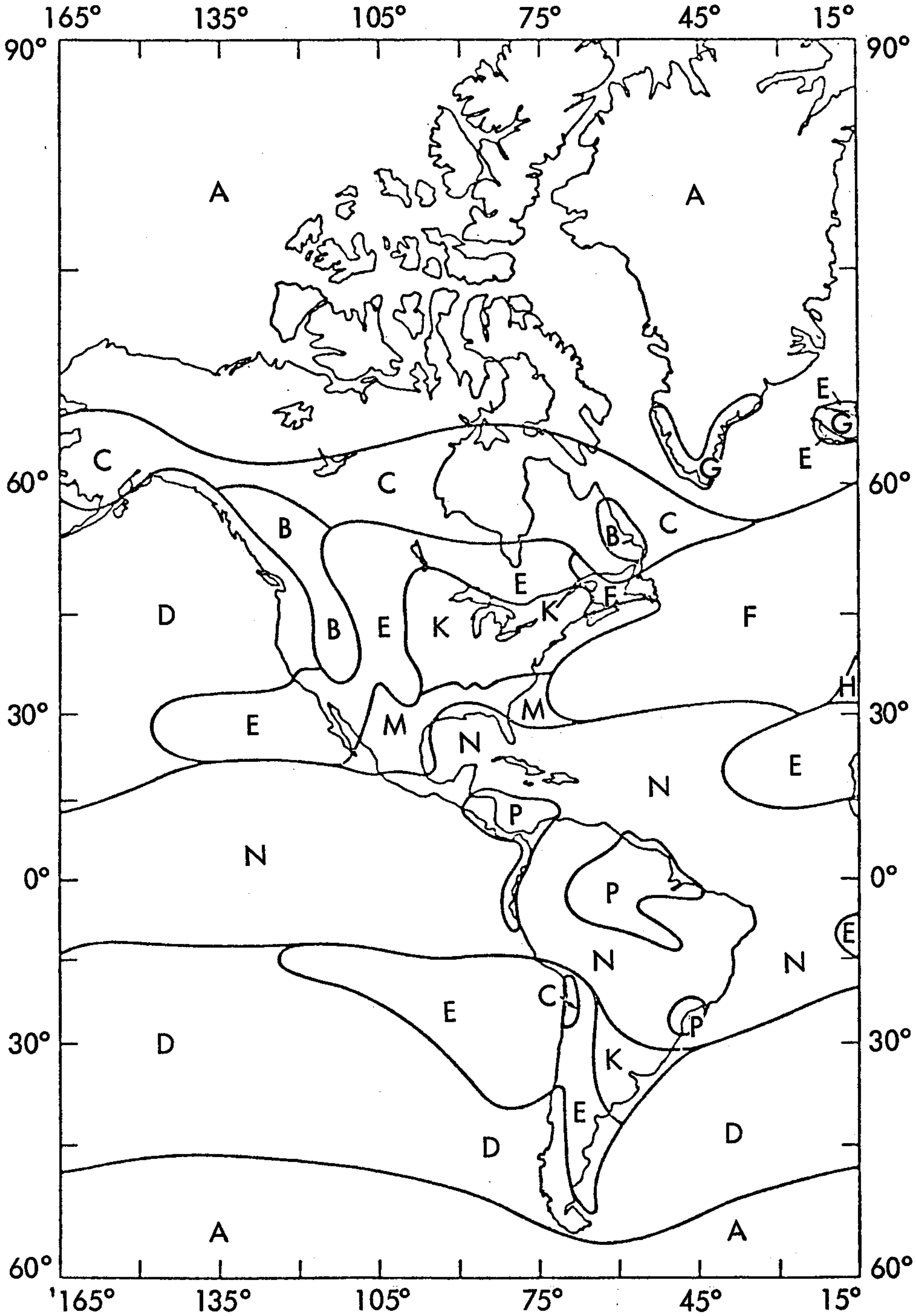

Figure 4.13. Rain-rate regions of the Americas (CCIR, 1986c).

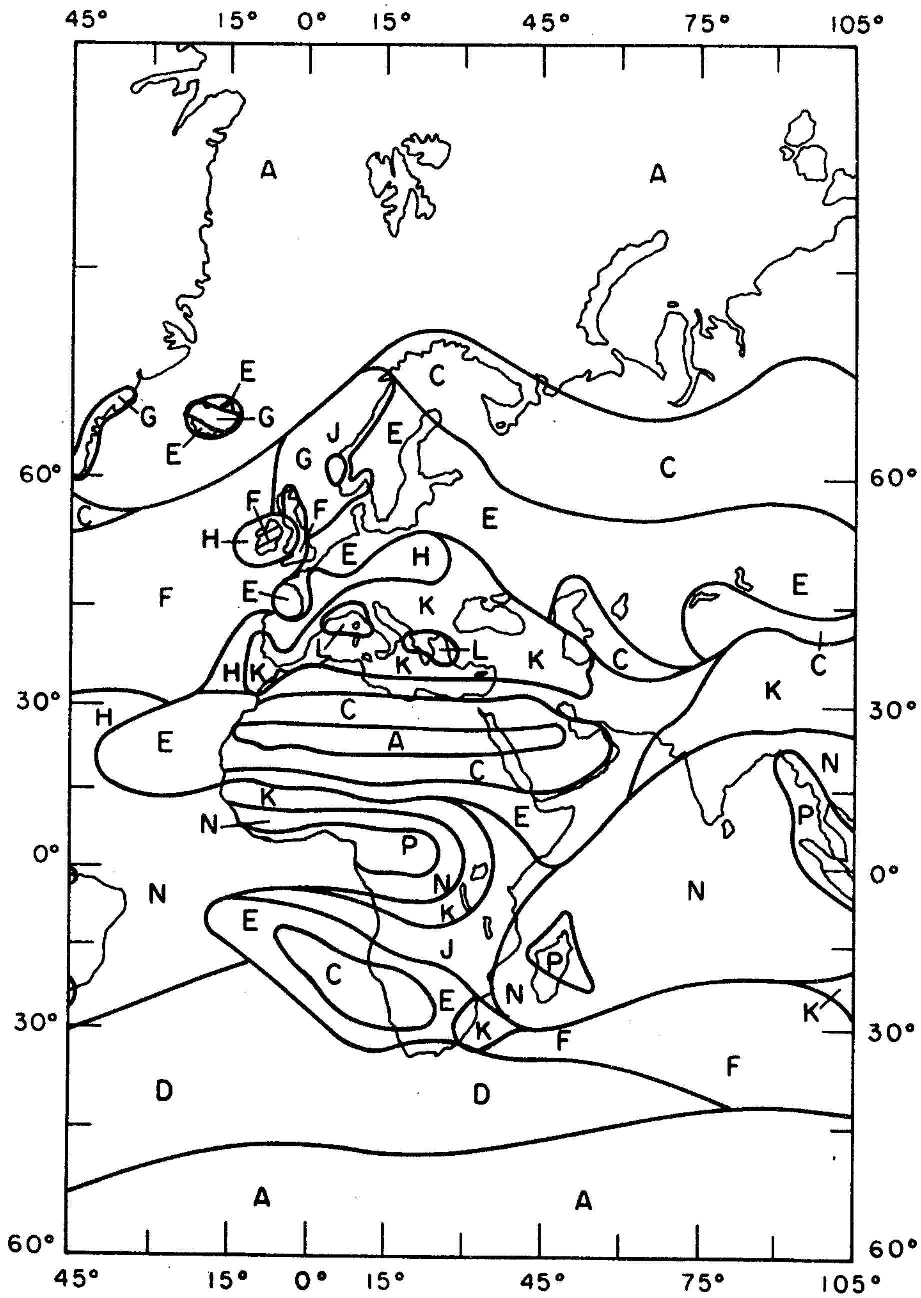

Figure 4.14. Rain-rate regions of Europe and Africa (CCIR, 1986c).

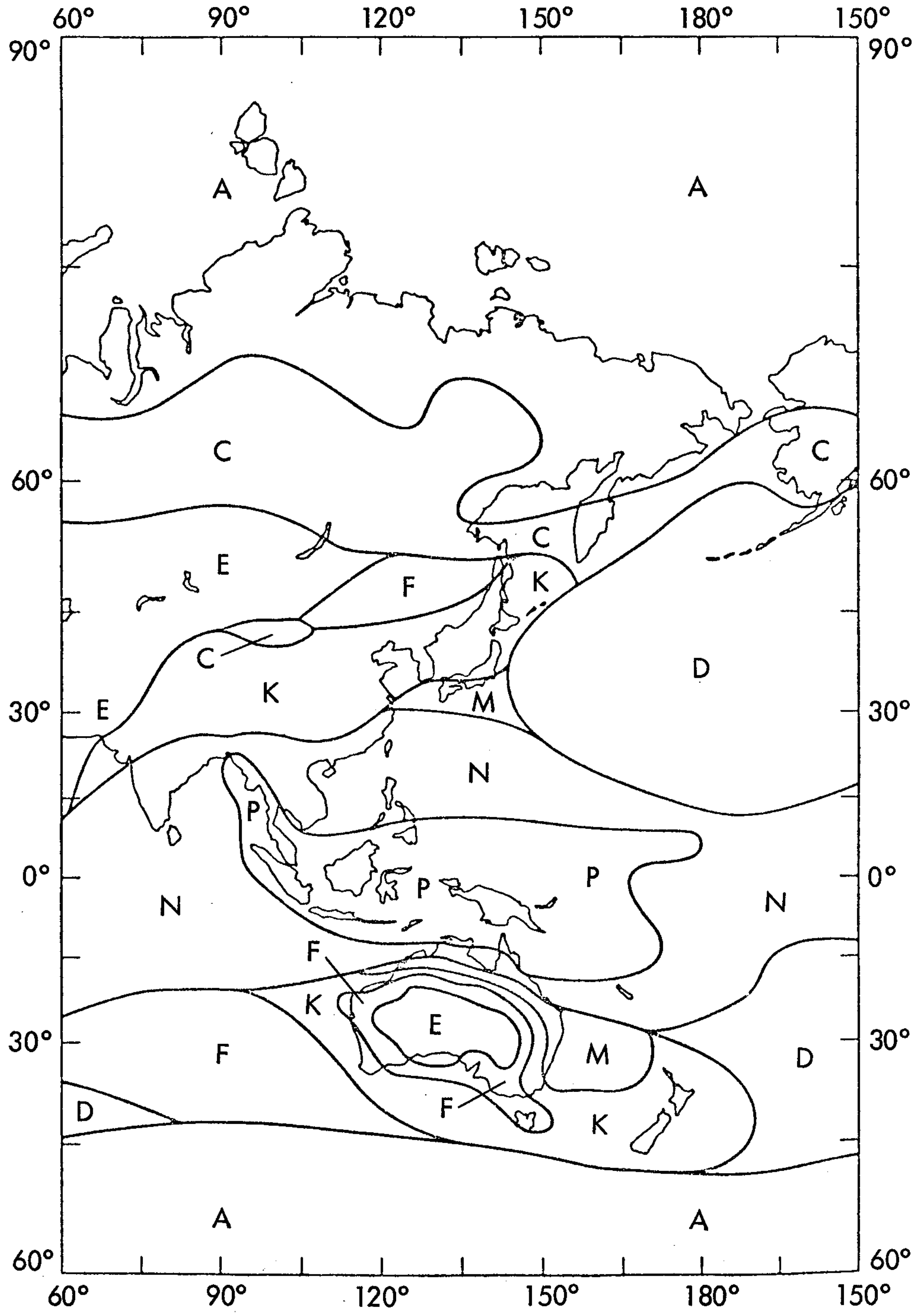

Figure 4.15. Rain-rate regions of Asia and Oceania (CCIR, 1986c).

4.4 DEPOLARIZATION DUE TO PRECIPITATION

The term depolarization refers to a degradation or change in polarization, as from purely vertical linear polarization to linear polarization at an angle slightly different from vertical. This latter condition is equivalent to a combination of vertical and horizontal polarization. Such an effect can be caused by precipitation.

It is highly desirable in many circumstances to be able to use two orthogonal polarizations on the same path, but the ability to do so may be limited to some degree by antenna characteristics or depolarization caused by precipitation or some other phenomena. The two linear polarizations are generally referred to as vertical and horizontal, but for earth-space paths the polarizations tend to be rotated somewhat from the local vertical and horizontal axes (Dougherty, 1980). The two orthogonal circular polarizations are right and left circular polarization (Sec. 2.1.1). Two orthogonal polarizations are sometimes referred to as cross polarizations, and a wave of the opposite or orthogonal polarization that is produced by a process of depolarization is known as a cross-polarized wave. The production of a cross-polarized wave may result in unacceptable interference between orthogonally polarized channels of the same path.

In considering transmission through rain, the ratio of the power of the wanted or copolarized wave to the power of the unwanted or crosspolarized wave is pertinent. Letting E_{11} and E_{22} represent electric field intensities of copolarized waves and E_{12} and E_{21} represent field intensities of crosspolarized or unwanted waves and expressing the ratio in dB, it may have the form of 20 log E_{11}/E_{12}, for example. The first subscript represents either a reference or original polarization, and the second subscript represents an actual (resulting or final) polarization. Thus E_{12} is a field intensity having polarization 2. It may have been derived from a wave of original polarization 1, or polarization 1 may merely be the reference polarization of the system. This kind of ratio is referred to by the term cross polarization discrimination (XPD). For the example mentioned above

$$XPD = 20 \log (E_{11}/E_{12}) \tag{4.36}$$

The use of the term discrimination is pertinent in some cases, but the notation XPD has been used also to describe the polarization of a wave whether a process of discrimination is involved or not. For example, if a receiving system has a linear horizontally polarized antenna but an incident wave is linearly polarized at an angle τ from the horizontal, it may be said that

$$\mathrm{XPD} = 20 \log \cot \tau \qquad (4.37)$$

as $E_{11} = E_o \cos \tau$ and $E_{12} = E_o \sin \tau$, where E_o is a reference intensity and E_{11} and E_{12} are components along horizontal and vertical axes.

Rather than using XPD to describe the state of polarization, use can be made of its reciprocal, depolarization D, which has the form of

$$D = 20 \log (E_{12}/E_{11}) \qquad (4.38)$$

A high XPD value of 40 dB, for example, corresponds to a small depolarization of −40 dB; a low XPD value of 10 dB corresponds to a large depolarization of −10 dB.

Depolarization due to precipitation is caused by the nonspherical shape of rain drops and ice crystals; spherical drops do not cause depolarization. Depolarization would not occur in the case of spheroidal drops either if the field intensity vector of a linearly polarized wave were to lie strictly parallel to either the long or short axes of the drops. In the general case, however, the roughly spheroidal drops tend to be canted or tilted with respect to the electric field intensity vectors. Wind contributes to canting and, even in the case of apparently vertical fall, the drops normally exhibit a distribution of canting angles. Differential attenuation and phase shift of field components parallel to the long and short axes of drops cause depolarization. The effect of differential attenuation is shown in a qualitative way in Fig. 4.16. A circularly polarized wave is equivalent to the combination of two linearly polarized waves that differ by 90 deg in both spatial configuration and electrical phase, and depolarization occurs for circularly polarized waves also. Indeed, it develops that depolarization tends to be worse for circularly polarized waves than for linearly polarized waves.

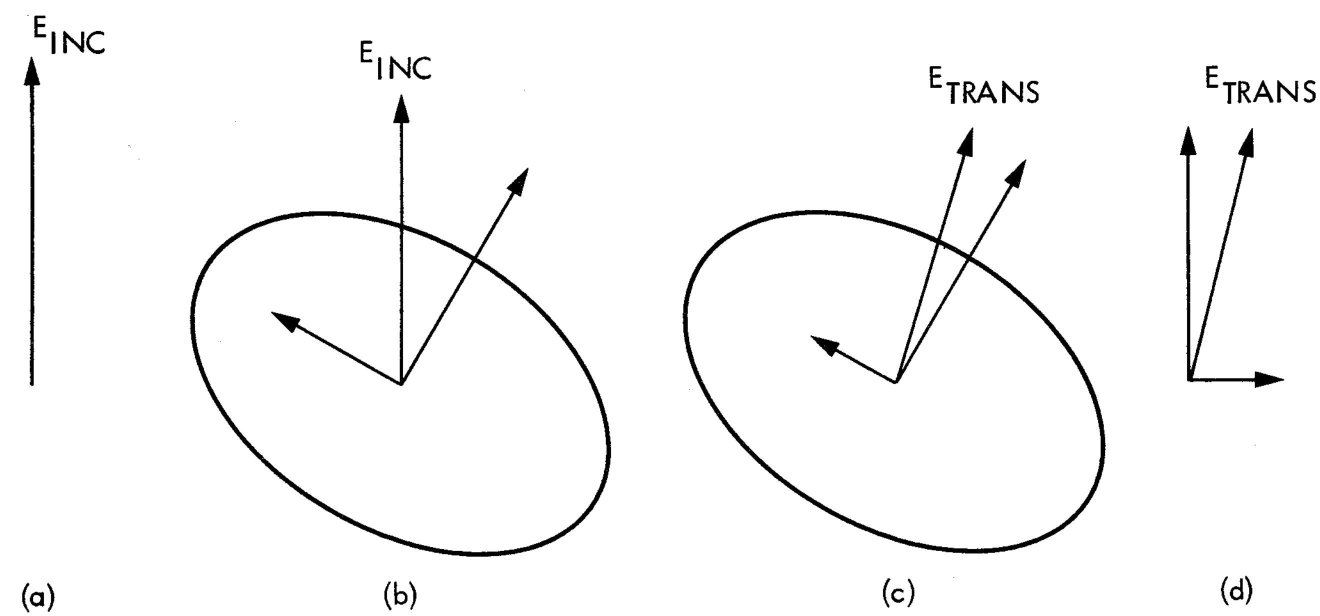

Figure 4.16. An incident vertically polarized wave emerges from rain no longer strictly vertical after experiencing differential attenuation of components parallel to the major and minor axes of raindrops.

Analysis of depolarization D in terms of differential attenuation and phase shift has been presented by Chu (1980). A form for D for circular polarization is

$$D_{cir}\,(\mathrm{dB}) = 10 \log \{ 1/4 \, [\sqrt{(\Delta\alpha)^2 + (\Delta\beta)^2} \; L]^2 \; e^{-4\sigma^2} \} \tag{4.39}$$

where $\Delta\alpha$ is the differential attenuation constant and $\Delta\beta$ is the differential phase constant. The quantity L is the length of the path through rain. A factor of 2 dB is sometimes added to take account of the possible contribution to depolarization of ice particles occurring above the level of the 0 deg C isotherm. When the logarithm of the exponential factor is taken, the result, designated as κ squared, has the form

$$\kappa^2 = 17.37\, \sigma^2 \tag{4.40}$$

with σ in radians or

$$\kappa^2 = 0.0053\, \sigma^2 \tag{4.41}$$

with σ in degrees, where σ is the standard deviation of the raindrop canting angle ϕ, measured from the horizontal, along a path at a particular instant of time. This quantity κ^2 can be set equal to zero as a conservative design procedure (CCIR, 1986d). For linear polarization

$$D_{lin}(\mathrm{dB}) = D_{cir}(\mathrm{dB}) + 10 \log[1/2\, (1 - \cos 4\tau\, e^{-8\sigma^2_m})] \pm \Delta A'/2 \tag{4.42}$$

In this expression τ is the tilt angle from the horizontal of the electric field intensity vector of the linearly polarized wave. The quantity σ_m is the standard deviation in radians of the mean raindrop canting angle ϕ_m from path to path and storm to storm. For σ_m in deg, $8\sigma^2_m$ can be replaced by $\kappa^2_m = 0.0024\, \sigma^2_m$, with 5 deg a suitable value for σ_m. CCIR Report 722-2 (1986d) points out that κ^2 and κ^2_m depend on factors other than the canting angle distribution and should not be thought of as related to canting angle only. The quantity $\Delta A'$ is given by

$$\Delta A' = 5 \log \left(\overline{|a_{vv}|^2 / |a_{hh}|^2} \right) \tag{4.43}$$

where a_{vv} and a_{hh} are attenuation constants for vertical and horizontal polarization. The sign of $\Delta A'/2$ is chosen to give the lowest value of D for quasivertical polarization. In Eq. (4.42), the logarithm of a quantity less than unity is indicated, and this logarithm is therefore negative. The equation thus shows that the depolarization is generally less for linear polarization than for circular polarization. For $\tau = 45$ deg, however, depolarization is essentially the same for linear and circular polarization. The value of τ can be taken as 45 deg for circular polarization, and it is for tilt angles away from 45 deg that linear polarization has an advantage over circular polarization. The distribution of canting angles ϕ is over a range around the horizontal. The angle shown in Fig. 4.16 is exaggerated in order to make the effect of differential attenuation obvious. In Chu's 1980 paper he gives examples of the application of the above relations to extrapolation from measured values of D on one path to values to be expected on other paths.

An alternative form of the right side of Eq. (4.39) for is

$$D_{cir}(\mathrm{dB}) = 20 \log \left[1/2 \sqrt{(\Delta\alpha_o)^2 + (\Delta\beta_o)^2}\ L \cos^2\theta\ e^{-2\sigma^2} \right] \tag{4.44}$$

which is based upon

$$\sqrt{(\Delta\alpha)^2 + (\Delta\beta)^2} = \sqrt{(\Delta\alpha_o)^2 + (\Delta\beta_o)^2}\ \cos^2\theta$$

where $\Delta\alpha_o$ and $\Delta\beta_o$ refer to an elevation angle θ. This equation shows that depolarization decreases with increasing elevation angle.

Values of $\sqrt{(\Delta\alpha_o)^2 + (\Delta\beta_o)^2}$ are given in Fig. 4.17 as a function of rain rate and frequency. That depolarization should decrease with increasing elevation angle can be understood by considering the outline of raindrops as seen from the direction of incident waves at $\theta = 0$ deg and at $\theta = 90$ deg. Differential attenuation and phase are maximum for an elevation angle of 0 deg for which the shape seen looking an incident **k** vector, representing the direction of propagation of an incident wave, is elliptical. At the other extreme for which $\cos\theta = 0$, however, the shape seen when looking along an incident **k** vector at an elevation angle of 90 deg is circular. This symmetrical shape is not conducive to depolarization. Equations (4.42)-(4.44) together with Fig. 4.17 show the dependence of depolarization on rain rate, frequency, polarization, tilt angle, elevation angle, and path length L, which can be determined with the help of Fig. 4.6.

In a later paper (Chu, 1982), the basis is shown for expressing depolarization D and crosspolarization XPD in terms of total attenuation A in dB for frequencies above 10 GHz, as is the case for the common empirical expression for XPD. For this purpose note that $\sqrt{(\Delta\alpha_o)^2 + (\Delta\beta_o)^2}$ is proportional to frequency (Fig. 4.17). Also it develops that total attenuation A in dB is proportional to frequency squared in the 10 to 30 GHz range. Thus $\sqrt{(\Delta\alpha_o)^2 + (\Delta\beta_o)^2}\ L\,f/A$ is a constant. Introducing this constant into Eq. (4.44)

$$D_{cir}(\mathrm{dB}) = 20\log\left[\sqrt{(\Delta\alpha_o)^2 + (\Delta\beta_o)^2}\ L\,f/A\right] - 17.37\,\sigma^2$$

$$- 6.02 - 20\log f + 40\log\cos\theta + 20\log A \qquad (4.45)$$

The term -20 log f appears to correct for the addition of 20 log f into Eq. (4.44) where it did not originally appear, and 20 log A is introduced for the same reason. Keep in mind that A is in dB. The quantities $\Delta\alpha_o$ and $\Delta\beta_o$ refer to an elevation angle of 0 deg, and 40 $\log\cos\theta$ accounts for the $\cos^2\theta$ factor of Eq. (4.44). To convert to XPD one can merely change the signs of the terms. Doing this but taking the first three terms as equal to a constant $(\mathrm{XPD})_o$, one obtains

$$(\mathrm{XPD})_{cir}(\mathrm{dB}) = (\mathrm{XPD})_o + 20\log f_{GHz} - 40\log\cos\theta - 20\log A_{dB} \qquad (4.46)$$

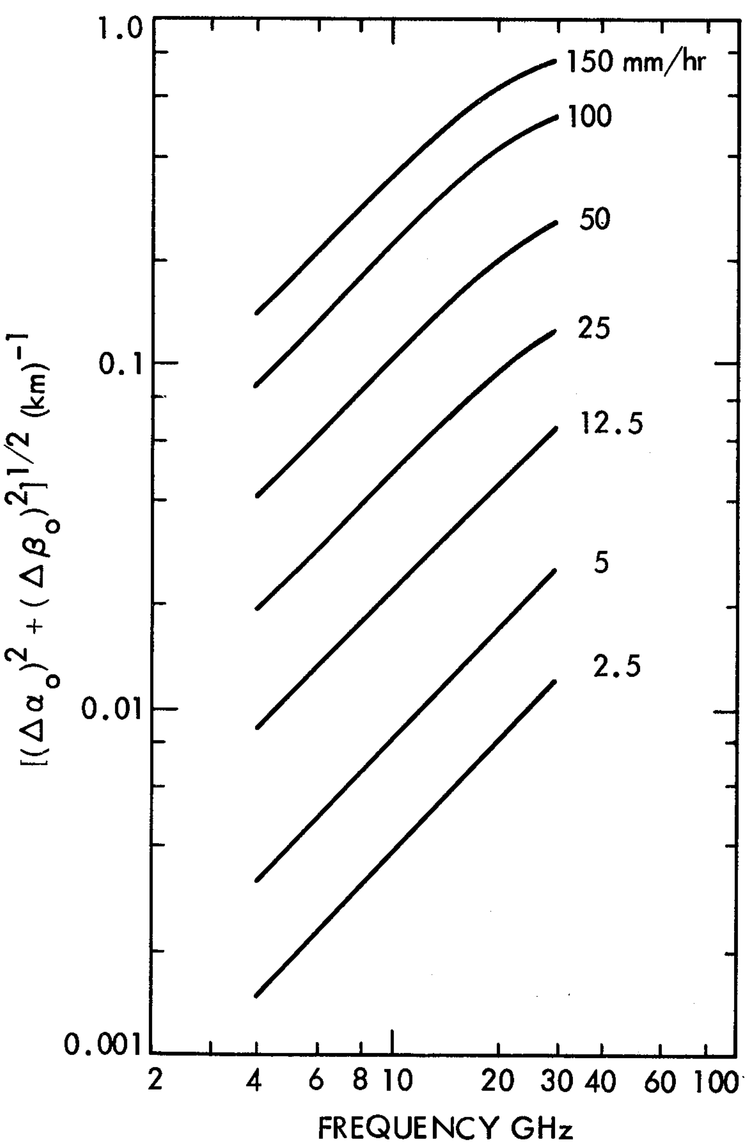

Figure 4.17. Differential propagation constant at zero elevation angle as a function of frequency and rain rate (Chu, 1980).

and

$$(XPD)_{lin}(dB) = (XPD)_{cir} - 10 \log 1/2 \, [\, 1 - \cos 4\tau \, e^{-\kappa_m^2} \,] \pm \Delta A'/2 \quad (4.47)$$

Chu has determined by analysis of experimental data that these relations give satisfactory results with $(XPD)_o$ set equal to 11.5. Thus his form of the equation is

$$(XPD)_{cir}(dB) = 11.5 + 20 \log f_{GHz} - 40 \log \cos\theta - 20 \log A_{dB} \quad (4.48)$$

The quantity $\Delta A'$ of Eq. (4.47) can be converted to the form

$$\Delta A' = 0.15 \, A_{dB} \cos^2\theta \cos 2\tau \quad (4.49)$$

Equation (4.48) is similar to the expression given in CCIR Report 722-2 (CCIR,1986d), namely

$$XPD\ (dB) = 30 \log f_{GHz} - 40 \log \cos\theta - 10 \log [1/2(1 - \cos 4\tau \, e^{-\kappa_m^2})] - 20 \log A_{dB} \quad (4.50)$$

This relation applies to both linear and circular polarization, with τ = 45 deg for circular polarization. Note that the same type of variation with elevation angle and polarization tilt angle is shown in Eqs. (4.47) and (4.48) on the one hand and Eq. (4.50) in the other case. The principal difference in the two treatments is that Eq. (4.48) has $11.5 + 20 \log f_{GHz}$ where Eq. (4.50) has $30 \log f_{GHz}$. Chu (1982) asserts that better agreement is obtained between theory and experiment when $11.5 + 20 \log f_{GHz}$ is used in place of $30 \log f_{GHz}$.

An important point about Eqs. (4.47), (4.48), and (4.50) is that they include a term $-20 \log A_{dB}$, whereas Eqs. (4.39), (4.42), and (4.44) are in terms of differential attenuation and phase. Being able to express XPD in terms of A is a useful step but is only a suitable approach for frequencies above about 8 GHz.

As this handbook refers to frequencies below 10 GHz, it is appropriate to emphasize the application of Eqs. (4.42-4.44) for our purposes. Furthermore these relations have the virtue of being closer to basic physical concepts.

A principal reason why Eq. (4.50) is not suitable for frequencies below about 8 GHz is that differential phase shift tends to play an important role below 8 GHz. Attenuation, and therefore differential attenuation as well, decreases rapidly below 10 GHz, but differential phase shift does not decrease so rapidly. This condition can be understood by reference to Figs. 4.3a and 4.3b. Figure 4.3b shows that the imaginary part, m_i, of the complex index of refraction of a medium containing raindrops, decreases rapidly below 10 GHz. However Fig. 4.3a shows that the real part, m_r, stays nearly constant over a range below 10 GHz.

Occurrences of low values of XPD (or high depolarization) when attenuation is low have been attributed to ice crystals, which cause small attenuation but can degrade XPD. Relations between XPD and attenuation that are developed for rain should not be extended to low values of attenuation for this reason (Bostian and Allnut, 1979). Data on rain depolarization at 4 GHz have been obtained by Yamada et al. (1977). For such relatively low frequencies attenuation values are low and are not useful for predicting XPD either as previously mentioned. A treatment of XPD that differs from that of Eq. (4.50) with respect to dependence on tilt angle τ and canting angle σ and also includes a numerical treatment of the effects of ice crystals is given in CCIR, 1986b. Note that a relation between between κ of Eq. (4.50) and σ is shown following Eq. (4.42).

4.5 BISTATIC SCATTER FROM RAIN

In considering the propagation of signals through a region of rainfall, interest commonly centers on the degree of attenuation of signals propagating in the forward direction. Another effect is that rain scatters energy into all directions, with a resulting potential for interference with earth-space or terrestrial line-of-sight telecommunication systems. Such scatter is referred to as bistatic scatter, using the term bistatic as in radar operations when transmitter and receiver are at different locations.

The process of bistatic scatter can be described as follows. The power density P in W/m^2 at a distance R_1 from a transmitter having a power output of W_T watts and an antenna gain of G_T is given by

$$P = \frac{W_T G_T}{4\pi (R_1)^2} \tag{4.51}$$

At the location where the power density is P, consider a target having a radar cross section of ηV m^2 where η is the cross section per unit volume and V is the total volume taking part in the scattering process. In the present case V is the common volume of the transmitting and receiving antennas as shown in Fig. 4.18.

Considering the common scattering volume to be small so that the distance from the transmitter to any part of it is R_1 and the distance from the receiver to any part of the volume is R_2, the common volume is presumed to radiate isotropically the power incident upon it so that the received power W_R, intercepted by an antenna with an effective area of A_R at the distance of R_2, is given by

$$W_R = \frac{W_T G_T \eta V A_R}{(4\pi)^2 (R_1)^2 (R_2)^2} \tag{4.52}$$

Making use of the relation between gain G and effective area A, namely $G = 4\pi A/\lambda^2$, the equation can be put into the form

$$\frac{W_R}{W_T} = \frac{G_T G_R \eta V \lambda^2}{(4\pi)^3 (R_1)^2 (R_2)^2 L} \tag{4.53}$$

where a loss factor L has been added to take account of attenuation of the incident and scattered waves and any polarization mismatch. Assuming for simplicity that Rayleigh scattering takes place, the cross section per unit volume η is given by

$$\eta = \frac{\pi^5}{\lambda^4} \left| \frac{K_c - 1}{K_c + 2} \right|^2 \sum d^6 \qquad m^2/m^3 \tag{4.54}$$

where K_c is the complex index of refraction of water at the frequency in question and summation is shown over all of the drop diameters d within a unit volume. This summation is commonly represented by the symbol Z so that

$$\eta = \frac{\pi^5}{\lambda^4} \left| \frac{K_c - 1}{K_c + 2} \right|^2 Z \qquad m^2/m^3 \tag{4.55}$$

Empirical relations have been derived between Z and rain rate R. For the Laws and Parsons distribution

$$Z = 400\, R^{1.4} \tag{4.56}$$

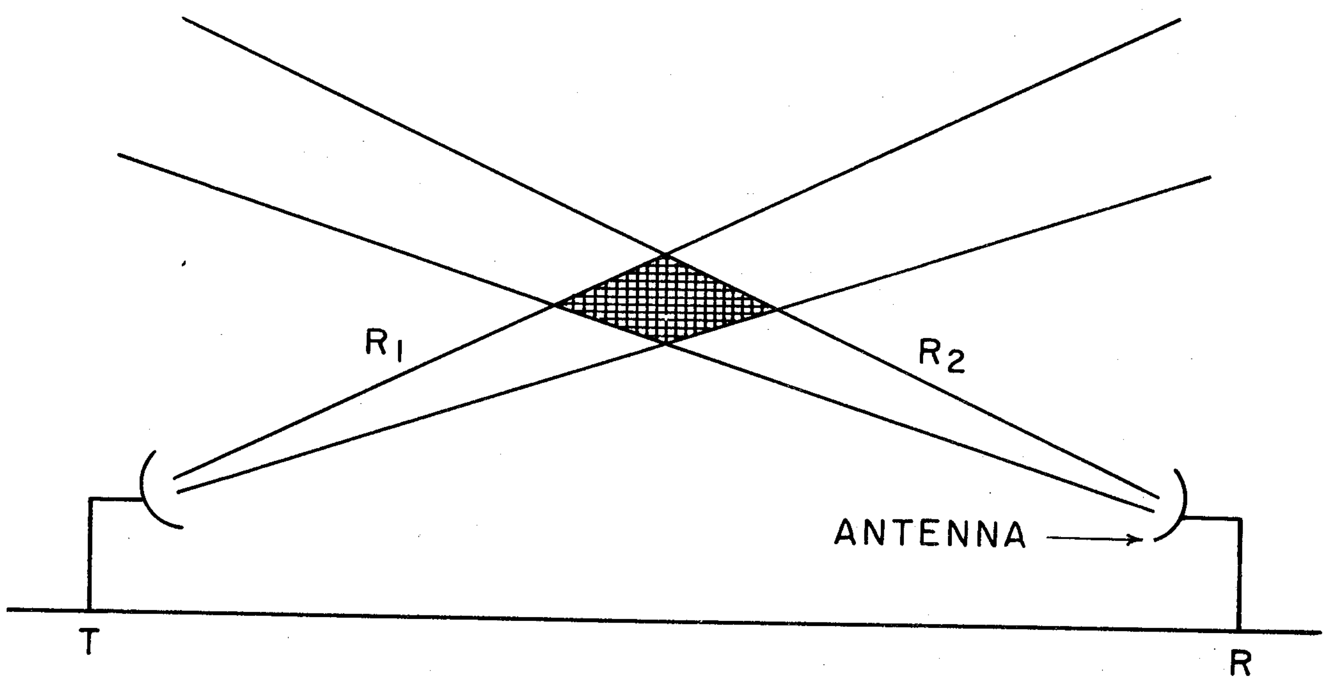

Figure 4.18. The cross-hatched area is a two-dimensional representation of the common volume of the transmitting and receiving antennas.

with Z in mm^6/m^3. Another form of the relation betwen Z and R, which is a slight revision of the relation proposed by Marshall and Palmer and is based on their drop-size distribution is

$$Z = 200\, R^{1.6} \tag{4.57}$$

In monostatic radar observations of rainfall η can be determined from Eq. (4.53) and Z can then be determined from Eq. (4.55) except that for monostatic radar R_1 and R_2 are the same and V is proportional to distance squared so that W_R/W_T varies inversely with distance squared if rain fills the common scattering volume. In Eqs. (4.54) and (4.55), all lengths are in meters. To convert from Z in m^6/m^3 to mm^6/m^3 for use in Eqs. (4.56) and (4.57) multiply by 10^{18}.

For calculation of interfering signal levels one can assume rain rates R and calculate A and η for insertion into Eq. (4.53).

4.6 CONCLUSION

Much of the interest in effects of precipitation on telecommunications has been directed to frequencies above 10 GHz, but the various models of attenuation due to rain are generally applicable below 10 GHz as well. Attenuation and noise due to precipitation may be important for frequencies as low as 8 GHz or lower and may need to be taken into account for frequencies as low as 4 GHz. Depolarization, the production of cross polarized components that have polarizations orthogonal to the original polarizations, increases with attenuation above about 8 GHz. For lower frequencies, differential phase shift rather than differential attenuation tends to make the major contribution to depolarization, and significant depolarization may take place for frequencies as low as 4 GHz. Backscatter from precipitation is important in radar observations at frequencies as low as those of the L band (e.g. 1500 MHz), and bistatic scatter from rain is a potential source of interference for telecommunication system operations at frequencies this low as well as at higher frequencies.

C-3

Water in the form of a thin layer or film over a radome or reflector and as the tiny drops of clouds or fog, as well as in the form of the larger drops of rain, can affect the performance of telecommunications systems. It has been pointed out that a given water content integrated along a path causes more attenuation when the water is in the form of a thin slab than when it occurs as fog or rain. Hogg and Chu (1975) used the water content of a slab 1 mm in thickness, corresponding to a rain of 25 mm/h over a one-km path or fog of 0.1 g/m^3 over a 10-km path, to illustrate this point. Avoiding the use of radomes and using blowers to eliminate water films are means for minimizing system degradation due to water films.

Effects of clouds are considered in the following Chap. 5. Among the effects are a slight range delay, above that due to the gaseous constituents of the atmosphere. The same effect occurs for rain, for which the excess range or time delay can be determined from the real part of the complex index of refraction m_c of Sec. 4.1 by taking $\int \mathrm{Re}\,(m_c - 1)\, d\ell = \int (m_r - 1)\, d\ell$, namely the integral of the real part of m_c minus one over the path. Further consideration of range delay due to liquid water, whether of the tiny drops of fog or the larger drops of rain, can be found in Sec. 5.1.

The companion NASA Reference Publication 1082(03), which applies to frequencies from 10 to 100 GHz, provides extensive coverage of propagation effects caused by rain (Ippolito, Kaul, and Wallace, 1983).

REFERENCES

Arnold, H. W. , D. C. Cox, and A. J. Rustako, "Rain attenuation at 10-30 GHz along earth-space paths: elevation angle, frequency, seasonal, and diurnal effects," IEEE Trans. Commun., vol. COM-29, pp. 716-721, No. 5, 1981.

Bostian, C. W. and J. E. Allnut, "Ice crystal depolarization on satellite-earth microwave radio paths," Proc. IEEE, vol. 126, p. 951, 1979.

Bostian, C. W., T. Pratt, and W. L. Stutzman, "Results of a three-year 11.6 GHz, low-angle experiment using the SIRIO satellite," IEEE Trans. Antennas Propagat., vol. AP-34, pp. 58-65, Jan. 1986.

CCIR, "Rain attenuation prediction," Doc. P/105-E. Geneva: Int. Telecomm. Union, 1978.

CCIR, "Attenuation and scattering by precipitation and other atmospheric particles," Report 721-2 in Vol. V, Propagation in Non-ionized Media, Recommendation and Reports of the CCIR, 1986. Geneva: Int. Telecomm. Union, 1986a.

CCIR, "Propagation data required for space telecommunication systems," Report 564-3 in Vol. V, Propagation in Non-ionized Media, Recommendations and Reports of the CCIR, 1986. Geneva: Int. Telecomm. Union, 1986b.

CCIR, "Radio meteorological data," Report 563-3 in Vol. V, Propagation in Non-ionized Media, Recommendations and Reports of the CCIR, 1986. Geneva: Int. Telecomm. Union, 1986c.

CCIR, "Cross-polarization due to the atmosphere," Report 722-2 in Vol. V, Propagation in Non-ionized Media, Recommendations and Reports of the CCIR, 1986. Geneva: Int. Telecomm. Union, 1986d.

CCIR, "Data bank for earth-space propagation," Doc. 5/19-E, Geneva: Int. Telecomm. Union, 1983a.

CCIR, "Propagation data required for space telecommunication systems," Proposed modification to Report 564-2, Doc. 5/10-E. Geneva: Int. Telecomm. Union, 1983b.

Chu, T. S., "Microwave depolarization of an earth-space path," Bell System Tech. Jour., vol. 59, pp. 987-1007, July-Aug., 1980.

Chu. T. S., "A semi-empirical formula for microwave depolarization on earth-space paths," IEEE Trans. Commun, vol. COM-30, pp. 2550-2554, 1982.

Crane, R. K., "Prediction of attenuation by rain," IEEE Trans. Commun., vol. COM-28, pp. 1717-1733, Sept. 1980.

Crane, R. K., "A two-component rain model for the prediction of attenuation statistics," Radio Sci., vol. 17, pp. 1371-1387, Nov.-Dec.1982.

Crane, R. K., "Comparative evaluation of several rain attenuation prediction models," Radio Sci., vol. 20, pp. 843-863, JulyAug. 1985a.

Crane, R. K., "Evaluation of global and CCIR models for estimation of rain rate statistics," Radio Sci., vol. 20, pp. 865-879, July-Aug. 1985b.

Dougherty, H. T. and E. J. Dutton, "Estimating year-to-year varability of rainfall for microwave applications," IEEE Trans. Commun., vol. COM-26, pp. 1321-1324, Aug. 1978.

Dutton. E. J., Earth-space Attenuation Prediction Procedures at 4 to 16 GHz, OT Report 77-123, May 1977.

Dutton, E. J. and H. T. Dougherty, "Year-to-year varability of rainfall for microwave applications in the U.S.A.," IEEE Trans. Commun., vol.COM-27, pp. 829-832, May 1979.

Dutton, E.J., H. K. Kobayashi, and H. T. Dougherty, "An improved model for earth-space microwave attenuation distribution prediction," Radio Sci., vol. 17, pp. 1360-1370, Nov.-Dec. 1982.

Flock, W. L., Electromagnetics and the Environment; Remote Sensing and Telecommunications. Englewood Cliffs, NJ: PrenticeHall, 1979.

Goldhirsh, J. and I. Katz, "Useful experimental results for earth-satellite rain attenuation modeling," IEEE Trans. Antennas Propagat., vol. AP-27, pp. 413-415, May 1979.

Goldhirsh, J., "Slant path fade and rain rate statistics associated with the COMSTAR beacon at 28.56 GHz for Wallops Island, Virginia over a three-year period," IEEE Trans. Antennas Propagat., vol. AP-30, pp. 191-198, March 1982a.

Goldhirsh, J., "Space diversity performance prediction for earth-satellite paths using radar modeling techniques," Radio Sci., vol. 17, pp. 1400-1410, Nov.-Dec. 1982b.

Goldhirsh, J., "Slant path rain attenuation and path diversity statistics obtained through radar modeling of rain structure," IEEE Trans. Antennas Propagat., vol. AP-32, pp. 54-60, Jan. 1984.

Hogg, D. C. and T. S. Chu, "The role of rain in satellite communications," Proc. IEEE, vol. 63, pp. 1308-1331, Sept. 1975.

Ippolito, L. J., 11.7 GHz Attenuation and Rain Rate Measurements with the Communications Technology Satellite (CTS), NASA Tech. Memo. 80283. Greenbelt, MD: NASA, 1978.

Ippolito, L. J., R. D. Kaul, and R. G. Wallace, Propagation Effects Handbook for Satellite Systems Design, NASA Reference Pub. 1082(03). Washington, DC: NASA Commun. Div., June 1983.

Kaul, R., D. Rogers, and J. Bremer, A Compendium of Millimeter Wave Propagation Studies Performed by NASA, ORI Tech. Report, NASA Contract NAS5-24252, 1977.

Kerker, M., The Scattering of Light and Other Electromagnetic Radiation. New York: Academic Press, 1969.

Kerr, D. E. (ed.), Propagation of Short Radio Waves. Vol. 13, Rad. Lab. Series. New York: McGraw-Hill, 1951.

Laws, J. O. and D. A. Parsons, "The relation of drop size to intensity," Trans. of AGU, pp. 452-460, 1943.

Lee, W. C. Y., "An approximate method for obtaining rain rate statistics for use in signal attenuation estimating," IEEE Trans. Antennas Propagat., vol. AP-27, pp. 407-413, May 1979.

Lin, S. H., "Nationwide long-term rain rate statistics and empirical calculation of 11-GHz microwave rain attenuation," Bell System Tech. J., vol. 56, pp. 1581-1604, Nov. 1977.

Marshall, J. S. and W. M. Palmer, "The distribution of raindrops with size," J. Meterology, vol. 5, pp. 165-166, Aug. 1948.

Nackoney, O. G. and D. Davidson, "Results of 11.7-GHz CTS rain distribution measurments at Waltham, MA," Radio Sci., vol. 17, pp. 1435-1442, Nov.-Dec. 1982.

Olsen, R. L., D. V. Rogers, and D. B. Hodge, "The aR^b relation in the calculation of rain attenuation," IEEE Trans. Antennas Propagat., vol. AP-26, pp. 318-329, March 1978.

Persinger, R. R., W. L. Stutzman, R. E. Castle, and C. W. Bostian, "Millimeter wave attenuation prediction using a piecewise uniform rain rate model," IEEE Trans. Antennas Propagat., vol. AP-28, pp. 149-153, March 1980.

Pruppacher, H. R. and R. L. Pitter, "A semi-empirical determination of the shape of cloud and rain drops," J. Atmos. Sci., vol. 28, pp. 86-94, Jan. 1971.

Rice, P. L. and N. R. Holmberg, "Cumulative time statistics of surface-point rainfall rates," IEEE Trans. Commun., vol. COM-21, pp. 1131-1136, Oct. 1973.

Ryde, J. W., "The attenuation and radar echoes produced at centimetre wavelengths by various meterological phenomena," in Meteorological Factors in Radio-Wave Propagation, pp. 169-189. London: The Physical Society, 1946.

Segal, B., "A new procedure for the determination and classification of rainfall rate climatic zones," URSI Commission F Open Symposium, Lennoxville, Quebec, 26-30 May 1980.

Segal, B., "The influence of raingauge integration time on measured rainfall-intensity distribution functions," to be published in Journal of Atmospheric and Oceanic Tech. vol. 3, Dec.1986.

Stutzman, W. L. and K. M. Yon, "A simple rain attenuation mode for earth-space radio links operating at 10-35 GHz," Radio Sci. vol. 21, pp. 65-72, Jan.-Feb. 1986.

van de Hulst, H. C., Light Scattering by Small Particles. New York: Wiley, 1957.

Vogel, W. J., "Measurements of satellite beacon attenuation at 11.7, 19.04, and 28.56 GHz and radiometric site diversity at 13.6 GHz," Radio Sci., vol.17, pp. 1511-1520, Nov.-Dec. 1982.

Yamada, M., A. Ogawa, O. Furuta, and H. Yuki, "Rain depolarization measurement by using INTELSAT-IV satellite in 4-GHz band at low elevation angle," URSI Commission F Symposium Proc., pp.409-419, LaBaule, France, 1977.

Zuffery, C. H., A Study of Rain Effects on Electromagnetic Waves in the 1-600 GHz Range," M. S. thesis. Boulder, CO: Department of Electrical Engineering, U. of Colorado, 1972 (reprinted in 1979).

APPENDIX 4.1

1980 GLOBAL MODEL

For elevation angles θ less than or equal to 10 deg in the 1980 Global Model, it is stated that D, the horizontal extent of rain, is given by

$$D = E\,\psi \tag{A 4.1}$$

with

$$\psi = \sin^{-1}\left\{\frac{\cos\theta}{H_o + E}\left[(H_g + E)^2 \sin^2\theta + 2E(H_o - H_g) + H_o^2 + H_g^2\right]^{1/2} - (H_g + E)\sin\theta\right\} \tag{A 4.2}$$

The quantity E is the effective earth radius and the value of 8500 km, corresponding to k = 4/3 (Sec. 3.2, Table 3.2) is suggested. H_o is the height of the 0 deg C isotherm, and H_g is the height of the station.

Also for $\theta \leq 10$ deg, the path length L is given by

$$L = \left[(E + H_g)^2 + (E + H_o)^2 - 2\,(E + H_g)\,(E + H_o)\cos\psi\right]^{1/2} \tag{A 4.3}$$

APPENDIX 4.2

TWO-COMPONENT MODEL

The vertical extent of each of the two types of rain considered in the two-component model is taken to be a function of latitude. For convective rain cells, the height H_c is given by

$$H_c = 3.1 - 1.7 \sin [2 (\theta' - 45^o)] \quad \text{km} \qquad \text{(A4.4)}$$

where θ' is latitude. For rain debris the height H_d is given by

$$H_d = 2.8 - 1.9 \sin [2 (\theta' - 45^o)] \quad \text{km} \qquad \text{(A4.5)}$$

The horizontal projections of these heights, D_c and D_d respectively, are found for elevation angles greater than 10 deg from

$$D_c = (H_c - H_o)/ \tan \theta \qquad \text{(A4.6)}$$

$$D_d = (H_d - H_o)/ \tan\theta \qquad \text{(A4.7)}$$

where θ is elevation angle and H_o is station height. More complicated expressions are given for angles less than 10 deg. The horizontal extent W_c of rain cells, taken to be 2.2 km originally, is modeled in the revised version in accordance with

$$W_c = 1.87 R^{-0.04} \quad \text{km} \qquad \text{(A4.8)}$$

and for debris the horizontal variation of rain rate is modeled by

$$W_d = 29.7 R^{-0.34} \quad \text{km} \qquad \text{(A4.9)}$$

The procedure for the two-component model involves determining D_c and D_d as indicated above. Values of attenuation A in dB are used to obtain initial estimates of R, namely R_i, for rain cells, and R_i is used in Eq. (A4.8) to obtain a value for W_c. Likewise an intial value of R. namely R_a, is determined for attenuation A due to debris rain and used to obtain a value for W_d. Adjustments in W_c, R_i, W_d, and R_a are then likely to be required.

For example, W_c is replaced by $W_c' =$ Min of W_c and D_c, and W_d is replaced by $W_d' =$ Min of W_d and D_d. Additionally if $W_c' > W_T$, where W_T is based on modeling of thickness, W_c' is reduced to $W_c'' = W_T$, , and if $W_d' > W_L$, W_d' is reduced to $W_d'' = W_L$, where W_L is based on thickness modeling. Also if $W_c < D_c$ a contribution C of debris rain is added to the effect of the rain cell so that whereas

$$R_i = \left(\frac{0.7\ A \cos\theta}{1.87\ a} \right)^{1/(b-0.04)} \tag{A4.10}$$

$$R_f = \left(\frac{C\ A\ \cos\theta}{W_c'\ a} \right)^{1/b} \tag{A4.11}$$

The parameters a and b are those of $\alpha_p = a\,R^b$ with R the rain rate.

The probability P_f of the path intersecting a rain cell is found from

$$P_f = P_c\,(1 + D_c/W_c'')\ e^{-R_f/R_c} \tag{A4.12}$$

where P_c and R_c are from tables provided and apply to the particular rain-rate region in question. The probability of inrersecting debris is

$$P_g = P_d\,(1 + D_d/W_d'')\ \frac{1}{2}\ \mathrm{erfc}\left(\frac{\ln\,(R_z/R_d)}{2^{1/2}\ S_d} \right) \tag{A4.13}$$

where P_c, R_d, and S_d are from tables and R_z is the final value of debris rain rate. The parameters W_c'' and W_d'' are the final values of what were originally designated as W_c and W_d. Finally the total probability P of attenuation greater than A_{dB} is given by

$$P = P_f + P_g \tag{A4.14}$$

CHAPTER 5

EFFECTS OF SMALL PARTICLES AND BIOLOGICAL MATTER

5.1 CLOUDS AND FOG

5.1.1 Introduction

Clouds, dust, and vegetation and their effects on propagation are the principal topics considered in this chapter. Clouds and fog are both composed of minute water droplets or ice crystals suspended in air. Fog forms near the Earth's surface, and clouds occur at higher levels. Both clouds and fog form through cooling, clouds when air cools adiabatically while rising for example and fog by contact and mixing. Fog also sometimes forms by increase of water content. Clouds are of three basic types - cirrus, cumulus, and stratus (Donn, 1975).

Cirrus clouds are high, thin, separated or detached clouds. They usually form above about 9 km (about 30,000 ft) and consist of thin crystals or needles of ice rather than liquid water. Cumulus clouds are the majestic clouds of summer and fair weather generally. Their base is typically flat and they have considerable vertical extent. Stratus clouds have a large horizontal extent covering all or most of the sky and showing little structure. They tend to have a uniform grey color. If a cumulus or stratus cloud occurs above its normal level, the term alto precedes the name. If a cloud is associated with rain, the term nimbus may be added to the basic name. Thus nimbostratus clouds are rain or snow clouds, and cumulonimbus clouds, which develop from cumulus clouds, are the clouds of thunderstorms. Clouds combining the characteristics of two of the basic types have names such as stratocumulus and cirrostratus.

Drop sizes and liquid water contents in cumulonimbus clouds are given in Table 5.1, adapted from Ludlam (1980). The table show values of drop concentration N, mass density ρ, and mean radius r for particular cumulonimbus clouds, which have relatively large values of liquid water content. The entries are arranged in groups or classes.

Table 5.1 Parameters of Cumulonimbus Clouds (adapted from Ludlam, 1980).

Class	N/cm^3	ρ (g/m^3)	$r(\mu m)$
a	290	0.05	3.45
	590	0.13	3.74
	281	0.65	8.2
b	30	0.03	6.2
	41	0.025	5.26
	85	0.06	5.52
c	229	0.60	8.56
	182	0.95	10.76
	285	0.66	8.21
	220	0.51	8.21
	119	0.70	11.2
d	195	1.6	12.5
	99	5.0	22.9

Fog has four principal categories - radiation fog, advection fog, frontal fog, and upslope fog. Radiation fog forms when the Earth, and the air immediately above it, cools on clear nights. Advection refers to horizontal movement, and advection fog forms when cold air passes over a warm sea surface and when warm moist air passes over a cold surface. The latter mechanism is responsible for about 4/5ths of all maritime fogs (Donn, 1975). Frontal fog is important over the continents and results at a front where warm air moves over cold air. Clouds form in the warm air, and if rain falls from the clouds it will add moisture to the cold air underneath which may already have been humid and near the dew point. The result is the formation of fog in the cold air. Upslope fog forms when humid air ascends a gradually sloping plain as in the interior plains of the United States. Ice fog forms at low temperatures in the order of −34 deg C (−30 deg F) and lower and is aggravated by manmade pollution. Ice fog is a problem in winter in Fairbanks, Alaska (Benson, 1965, 1970).

5.1.2 Rayleigh Scattering

The water droplets of clouds are small compared to wavelength, and Rayleigh scattering theory applies. Relations for η the radar cross section per unit volume; α, the attenuation constant; and β, the phase constant for clouds can be derived by using this theory. A suitable starting point is Laplace's equation $\nabla^2\Phi = 0$ (Ramo, Whinnery, and Van Duzer, 1965), where Φ is scalar electric potential. Although Laplace's equation applies to static fields and we deal here with time-varying conditions, the equation can be applied to the small spherical droplets of clouds in the first stage of analysis because negligible phase shift occurs throughout these droplets.

For the case of a sphere, when no variation with the coordinate ϕ occurs, the solution of Laplace's equation for Φ_1, the potential inside the sphere, is given in spherical coordinates by

$$\Phi_1 = \sum_{n=0}^{\infty} A_n r^n P_n(\cos\theta) \tag{5.1}$$

where r is the radial coordinate, θ is the polar coordinate, and $P_n(\cos\theta)$ is the Legendre polynomial of order n. Outside the sphere

$$\Phi_2 = \sum_{n=0}^{\infty} B_n r^{-n-1} P_n(\cos\theta) - E_o r P_1(\cos\theta) \tag{5.2}$$

where the second term accounts for the applied field E_o. At $r = a$ where a is drop radius, the two expressions can be equated so that

$$(\Phi_1)_{r=a} = (\Phi_2)_{r=a} \tag{5.3}$$

A_n and B_n are coefficients which need to be determined. For a particular value of n, Eq. (5.3) constitutes one equation for two unknowns. A second equation is obtained from

$$(D_{n1})_{r=a} = (D_{n2})_{r=a} \tag{5.4}$$

where D_n stands for the normal component of electric flux density in coulombs/square meter. The values of electric flux density D are related to potential Φ by $E = -\nabla\Phi$ and $D = \epsilon_o K E$ where E is electric field intensity, K is relative dielectric constant, and ϵ_o is the electric permittivity of empty space. The value of K in air outside the drop can be taken as unity, but K is complex and has a magnitude other than unity inside the drop. It turns out that only A_1 and B_1 have nonzero values. All the other A's and B's are zero, and solving for A_1 and B_1 is straitforward. It is B_1 that is of most interest because it gives the field quantities outside the drop. It is found that

$$B_1 r^{-n-1} P_n(\cos\theta) = (E_o a^3/r^2)\left[\frac{K_c - 1}{K_c + 2}\right] \qquad (5.5)$$

Comparing this form with that for an electric dipole (consisting of + and - charges separated by a distance d), it can be seen that a small water drop has an electric dipole moment p_1 given by

$$p_1 = 3V\left[\frac{K_c - 1}{K_c + 2}\right]\epsilon_o E_o \qquad (5.6)$$

where $V = (4/3)\pi a^3$ is the volume of the drop. Note that K has become K_c with the subscript c indicating a complex quantity.

Thus under the influence of an applied field E_o each water droplet is an elementary antenna that radiates energy, and the radiated field can be found by using antenna theory. Knowing the electric dipole moment of the antenna, it is convenient to use the Hertz potential Π, as described in Panofsky and Phillips (1955) for example, to calculate the radiated field intensity E_θ, where θ is measured from the direction of the incident field intensity E_o. The radiated field intensity includes terms decreasing as $1/r$, $1/r^2$, and $1/r^3$, but interest lies in the far-field solution and only the term varying as $1/r$ need be determined. Of course, at this stage the time varying nature of the field quantities is taken into account. The dipole moment p_1 of Eq. (5.6) radiates a far field E_θ given by

$$E_\theta = (3\pi V/\lambda^2 r) \left[\frac{K_c - 1}{K_c + 2}\right] \tag{5.7}$$

and from this expression it is possible to determine a radar cross section σ for a drop by recognizing that

$$P(\pi) = P_{inc}\, \sigma/4\pi r^2 \tag{5.8}$$

where P_{inc} is the incident power density and equals E_o^2/η' and $P(\pi)$ is the radiated power density at an angle of π radians or 180 deg from the direction of the incident wave and equals E_θ^2/η'. The quantity η' is the characteristic impedance of the medium. Equation (5.8) shows that the drop extracts energy from the incident wave in proportion to σ and is assumed to radiate this energy uniformly over a sphere of radius r, thus ignoring the variation of radiated field intensity with θ. Solving for σ, one obtains

$$\sigma = \pi^5/\lambda^4 \left|\frac{K_c - 1}{K_c + 2}\right|^2 d^6 \tag{5.9}$$

where d is drop diameter. To obtain η the radar cross section per unit volume, one sums for all the drops in a cubic meter to obtain

$$\eta = \pi^5/\lambda^4 \left|\frac{K_c - 1}{K_c + 2}\right|^2 \sum d^6 = \pi^5/\lambda^4 \left|\frac{K_c - 1}{K_c + 2}\right|^2 Z \tag{5.10}$$

The other two quantities of interest in this section are α and β, the attenuation and phase constants respectively. To obtain expressions for these, return to the expression for p_1, Eq. (5.6), and make use of the relation from field theory,

$$D = \epsilon_o E + P = \epsilon_o K_m E = \epsilon_o (1 + \chi) E \tag{5.11}$$

where D is electric flux density (C/m^2), E is electric field intensity (V/m), and P is electric dipole moment per unit volume. Here we use K_m to stand for the complex relative dielectric constant of the medium consisting of water droplets in empty space, whereas K_c of Eq. (5.5), etc. stands for the relative dielectric constant of water. The quantity P is found from p_1 by multiplying by the number of drops N per unit volume, assuming all drops to be of equal size and having the same dipole moment. That is

$$P = N p_1 = 3 NV \left[\frac{K_c - 1}{K_c + 2}\right] \epsilon_o E_o \tag{5.12}$$

The complex index of refraction of the medium of water droplets in space, m_c, can be found from

$$m_c^2 = 1 + \frac{P}{\epsilon_o E_o} = 1 + 3 NV \left[\frac{K_c - 1}{K_c + 2}\right] \tag{5.13}$$

The other quantity χ of Eq. (5.11) stands for electric susceptibility and by comparing the two right-hand forms of Eq. (5.11), it is evident that

$$K_m = 1 + \chi \tag{5.14}$$

As we deal with empty droplets in empty space, χ is much less than unity and m_c is given by

$$m_c \simeq 1 + \chi/2 = m_r - j\, m_i \tag{5.15}$$

Knowing m_c, α and β can be found from

$$\alpha = m_i \beta_o \qquad \text{Np/m} \tag{5.16}$$

and

$$\beta = m_r \beta_o \qquad \text{rad/m} \tag{5.17}$$

where β_o is the phase constant of empty space, α is the field intensity attenuation constant of the medium, and β is the phase constant of the medium.

An alternative approach for determining m_c is to use Eq. (4.9) but apply it to particles of fixed size. For the case that $\lambda >> a$, where a is radius, S_o has the form of $j\beta_o\ [(K_c - 1)/(K_c + 2)]\ a^3$ (van de Hulst, 1957). Using Eq. (4.9) with S_o as indicated gives a result for m_c that is identical to that obtained above.

5.1.3 Attenuation

Numerical values of the power attenuation constant for clouds α_p, where $\alpha_p = 2\alpha$, can be found by using

$$\alpha_p = \left\{ 0.4343 \frac{6\pi}{\lambda} \mathrm{Im} \left[- \frac{K_c - 1}{K_c + 2} \right] \right\} \rho_\ell \qquad \text{dB/km} \tag{5.18}$$

where λ is wavelength in cm, I_m indicates the imaginary part of, K_c is the complex relative dielectric constant of water, and ρ_ℓ is the water content of the cloud in g/m³. The quantity K_c is a function of temperature and frequency. It has the value of 78.45 − j11.19 for T = 20 deg C and λ = 10 cm, for example. Table 5.2 shows values of the imaginary part of $-(K_c - 1)/(K_c + 2) = -R$, adapted from Battan (1973) and originally provided by Gunn and East (1954). Equation (5.18) can be used for ice as well as water clouds if the density of ice is taken as 1 g/cm³. Equation (5.18) follows from Eqs. (5.11) through (5.16), if it recognized that

$$N\,V\,\rho_w = N\,V\,1000 = (\rho_\ell)_{kg/m^3} \tag{5.19}$$

where N is the number of drops per cubic meter, V is the volume of a drop, ρ_w is the density of water (1000 kg/m³), and ρ_ℓ is the weight of liquid water in clouds in kg/m³. If ρ_ℓ is to be in g/m³, however, note that

$$(\rho_\ell)_{g/m^3} = 1000\,(\rho_\ell)_{kg/m^3} = 10^6\,N\,V$$

Thus if $(\rho_\ell)_{g/m^3} = 1$, $N\,V = 10^6$. In general NV should be assigned the value of $10^{-6}\,(\rho_\ell)_{g/m^3}$. By multiplying the numerator and denominator of $[-\,(K_c - 1)/(K_c + 2)]$ of Eq. (5.18) by the complex conjugate of the denominator it can be shown that

$$\operatorname{Im}\left\{-\left[\frac{K_c - 1}{K_c + 2}\right]\right\} = \frac{3K_i}{(K_r + 2)^2 + K_i^2} \tag{5.20}$$

An alternative expression for attenuation in a cloud for frequencies from 1 to 50 GHz that does not require knowledge of K_c has the following form (Staelin, 1967).

$$\alpha_p = \frac{(4.343\,\rho_\ell\,10^{0.0122\,(292-T)} - 1 \;(1.16)}{\lambda^2} \tag{5.21}$$

The quantity T is temperature in kelvins and equals 273 plus the temperature in deg C, λ is wavelength in cm, and ρ_ℓ is water content in g/m³.

Values for total attenuation at frequencies of 2.3, 8.5, 10, and 32 GHz as calculated by Slobin (1981) are included in Table 5.3. The model utilized for calculations includes cloud layers having total thickness as shown and also includes the contributions to attenuation due to water vapor and oxygen as well as the larger contributions of water droplets. Values for the combined effect of water vapor and oxygen in a clear atmosphere are also shown for reference (the entry for $\rho_\ell = 0$). The condition of $\rho_\ell = 1$ g/m^3 and a total cloud thickness of 4 km is referred to as a worst case, but it is possible for values of water content as great as 6 g/m^3 or more to occur. See Table 7.1 for a more complete listing, Fig. 9.15 for a map of cloud regions of the United States, and Slobin (1982) for further information.

Table 5.3 shows that attenuation due to clouds at frequencies of 10 GHz and lower is small. It should be noted, however, that the overall effect on signal-to-noise ratio involves both attenuation and the accompanying increase system noise temperature. Also note that the attenuation values are for a zenith path. For the worst case shown in Table 5.3 but for an elevation angle of 10 deg, the attenuation is 0.457/sin 10 deg = 0.457/0.174 = 2.63 dB. Finally the view is taken here that the designer should know closely the magnitudes of the various effects even when they are small.

Table 5.2 Im (-R), adapted from Battan (1973).

Substance	T(°C)	Im (-R), λ = 10 cm	Im (-R), λ = 3.21
Water	20°	0.00474	0.01883
	10°	0.00688	0.0247
	0°	0.01102	0.0335
Ice	0°	9.6×10^{-4}	9.6×10^{-4}
	-10°	3.2×10^{-4}	3.2×10^{-4}
	-20°	2.2×10^{-4}	2.2×10^{-4}

$R = (K_c-1)/K_c+2)$, where K_c is the complex relative dielectric constant.

Table 5.3 Values of Attenuation and Contributions to Noise Temperature of Cloud Models.

ρ_ℓ	Total Thick-ness	S-Band (2.3 GHz) Zenith		X-band (8.5 GHz) Zenith		X-band (10 GHz) Zenith		K_a-Band 32 (GHz) Zenith	
g/m^3	km	T(K)	A(dB)	T	A	T	A	T	A
0.5	2	2.43	0.040	6.55	0.105	8.25	.133	61.00	1.083
0.7	2	2.54	0.042	8.04	0.130	10.31	.166	77.16	1.425
1.0	2	2.70	0.044	10.27	0.166	13.55	.216	99.05	1.939
1.0	3	3.06	0.050	14.89	0.245	19.66	.326	137.50	3.060
1.0	4	3.47	0.057	20.20	0.340	26.84	.457	171.38	4.407
.0	0	2.15	0.035	2.78	0.045	3.05	.049	14.29	0.228

5.1.4 Noise

The contributions to system noise temperature due to clouds, water vapor, and oxygen (primarily clouds) are shown in Table 5.3 also. For considering these values, Eq. (3.25) is repeated below.

$$T_b = T_s e^{-\tau} + T_i (1 - e^{-\tau}) \tag{5.22}$$

The equation applies to the brightness temperature T_b when a source at a temperature of T_s is viewed through an absorbing region having an effective temperature of T_i. The parameter τ represents optical depth, namely the integral of the power attenuation constant along the path. In the case considered here, the first term has a small value and will be neglected. Values of T_i generally range from about 260 K to 280 K. If values for T_i and τ are known or can be assumed then T_b can be calculated.

For example, assume an attenuation of 1 dB and a value of 273 K for T_i. Then noting that

$$A_{dB} = 10 \log L = 10 \tau \log_{10} e = 4.343 \tau \tag{5.23}$$

where A is attenuation and $L = 1/e^{-\tau}$, $\tau = 1/4.343$, $e^{-\tau} = 0.794$, and $T_b = 56$ K. An attenuation of only 1 dB is seen to be associated with a fairly large contribution to system noise temperture. The subject of noise is treated more fully in Chap. 7. Attenuation and noise due to clouds are modest but not insignificant at frequencies of 10 GHz and lower. Table 5.3 includes entries for 32 GHz which illustrate the fact that the effects of clouds are more serious at higher frequencies.

5.1.5 Range Delay

In Sec. 3.7, the excess range delay due to dry air and water vapor was considered. Liquid water in the form of clouds and the larger drops of rain may also make a contribution to range delay. The basis for analyzing the delay due to the liquid water of clouds was developed in Sec. 5.1.2, and Eq. (5.17) for the phase constant of a medium consisting of water droplets in otherwise empty space is applicable. The excess range delay, however, is determined by the difference between the real part of the index of refraction and unity. Thus ΔR due to clouds is given by

$$\Delta R = \int \mathrm{Re}\,(m_c - 1)\, d\ell = \int (m_r - 1)\, d\ell \tag{5.24}$$

Taking the real part m_r of m_c and subtracting unity as indicated in the equation and considering the case of a constant value of m_r over a length L leads to the expression

$$\Delta R = (m_r - 1)L = \frac{3NV}{2}\left[\frac{K_r^2 + K_i^2 + K_r - 2}{(K_r + 2)^2 + K_i^2}\right] L \tag{5.25}$$

This equation can be applied to cloud models to determine representative value of ΔR.

To illustrate the range delay caused by water droplets in a cloud, consider the delay for a zenith path through a cloud 1 km thick and having a water content of 1 g/m³. For a frequency of 3 GHz and a temperature of 20 deg C, it can be determined from curves given by Zuffery (1972) that $n_c = 8.88 - j0.63$ for water. As water has a density of 1 g/cm³, the water content of 1 g/m³ fills only 10^{-6} of a m³ Then NV of Eq. 5.(13) is 10^{-6} and it develops that

$$\mathrm{Re}\,(m_c - 1) = 3/2\,(0.967)\,10^{-6} = 1.45 \times 10^{-6}$$

As a region of uniform water content and a thickness of 1 km is assumed, the integral of Eq. (5.24) simplifies to become the product of $(m_r - 1)$ and 1000 m so that $\Delta R = 0.145$ cm. For f = 10 GHz, $n_c = 8.2 - j1.8$ and the value of ΔR is 0.144 cm, while for f = 30 GHz $n_c = 6 - j2.8$ but ΔR is still about 0.144 cm. The excess range delay in this case is quite insensitive to the values of index of refraction of water n_c and frequency as the index appears in both the numerator and denominator of the expressions for the index of refraction of the medium, m_c, as in Eq. (5.13) where $K_c = n_c^2$. Using the figure of 0.145 cm for a cloud thickness of 1 km and a vertical path but considering instead a cloud 4 km thick and a path at an elevation angle of 10 deg gives a delay of (4) (0.145)/ sin 10 deg = 3.34 cm, which begins to be more impressive. Also while the water content of 1 g/m^3 assumed above is that of a rather dense cloud, the maximum water content has been reported to lie between about 6 and 10 g/m^3.

Raindrops are considerably larger than the small droplets of clouds, and one must generally use Mie scattering theory or refinements of it for analyzing the effects of raindrops. The technique of deriving an equivalent index of refraction m_c for the medium, however, can still be employed. This approach has been utilized most extensively for determining the attenuation constant for rain but can be used to determine $m_r - 1$ as well. Tables giving values of $m_r - 1$ have been provided by Setzer (1970), and Zufferey (1972) has presented such values in graphical form (Fig. 4.3a). Setzer's value for $m_r - 1$ for a rain of 25 mm/h at a frequency of 3 GHz, for example, is 1.8×10^{-6}. The excess range delay in a 1 km path of uniform rain of that rate is 0.18 cm, a value comparable to that for a path through a cloud 1 km in length. Considering a height extent of rain of 4 km , a path at an elevation angle of 10 deg, and rain of 25 mm/h leads to a possible delay of about 4.15 cm. In contrast with attenuation in rain which increases with frequency up to about 150 GHz, excess range delay due to rain decreases above 10 GHz and stays nearly constant below 10 GHz to 1 GHz but with modest maxima in the 6 to 10 GHz range, depending on rain rate (Fig. 4.3a). It appears that the excess range delay in some cases of extensive dense fog or cloud and in some heavy rainstorms may be of significance.

5.2 SAND, DUST, AND OTHER PARTICULATES

Sand and dust storms may reduce visibility to 10 m or less, reach a height of 1 km or more, and extend for hundreds of kilometers over the Earth's surface. Based on extrapolation of laboratory measurements at 10 GHz by Ahmed and Auchterlonie (1975), it has been estimated that the attenuation constant for a particulate density of 10 g/m^3 is less than 0.1 dB/km for sand and 0.4 dB/km for clay (CCIR, 1986a). It was concluded that total attenuation along an earth-space path should normally be less than 1 dB.

An analysis by Bashir, Dissanayake, and McEwan (1980) for 9.4 GHz has included the case of moist sandstorms and, assuming oblate spheroidal particles, has provided different values of attenuation for horizontal and vertical polarizations. Values for attenuation for moist sandstorms were as high as 1.83 dB/km for horizontal polarization. For dry sand the values were about 0.27 dB/km. Values for particulate density per cubic m of air were not given, but information on particle volumes was included. If the particles themselves have densities of 1 g/cm^3, the particulate densities or loading in air would be about 1 g/m^3. Thus particulate densities in the order of 1 to 10 g/m^3 have been assumed for obtaining estimates of attenuation in the cases cited here. Bashir et al. (1980) concluded that attenuation in sandstorms could be a problem for domestic-satellite services in desert areas if sandstorms were encountered at both of two earth stations that were communicating via satellite. The problems of depolarization and interference due to scatter in undesired directions were also considered. The effect of sand storms on microwave propagation has also been analyzed by Chu (1979) and Ghobrial (1980), and Goldhirsh (1982) has presented a unified, quantitative treatment of the effect of dust storms over desert regions on radar operations. The attenuation constant for propagation through dust or sand storms at centimeter wavelengths, as presented by Ghobrial and repeated by Goldhirsh is

$$\alpha_p = \frac{1.029 \times 10^6 K_i N}{[K_r + 2]^2 + K_i^2] \lambda} \sum P_i r_i^3 \qquad \text{dB/km} \tag{5.26}$$

where K_r and K_i are the real and imaginary parts of the complex relative dielectric constant of the dust or sand particles, N is the total number of particles per cubic m, λ is the wavelength, and P_i is the probability that the particle radius lies between r_i and Δr_i. This equation has the form of Eq. (5.18) as modified by use of Eq. (5.20). The effects of sand and dust on radar performance tend to be more serious than for earth-space communications because of the longer paths through sand or dust storms and two-way propagation over such paths.

If optical visibility data and information on particle size are available, estimates can be made of particle density N, taking visibility V_i to be related to attenuation by

$$\alpha_o V_i = 15 \qquad \text{dB} \tag{5.27}$$

where α_o is the optical power density attenuation constant. One must also recognize that for a given fixed size of spherical particle

$$\alpha_o = N C_{ext} \tag{5.28}$$

where C_{ext} is the extinction cross section. In addition use can be made of the normalized cross section $Q_{ext} = C_{ext}/\pi a^2$ where a is particle radius. For optical propagation, Q_{ext} has the value of 2, indicating that the particle affects propagation over a larger area than its physical cross section (because of diffraction as well as reflection and absorption). Using Q_{ext}, the optical power density attenuation constant is given by

$$\alpha_o = N Q_{ext} \pi a^2 = (S Q_{ext} \pi a^2)/(4/3 \pi a^3) = 0.75 S Q_{ext}/a \tag{5.29}$$

where S is the fraction of a unit volume occupied by the particles of interest. Converting to dB/m and letting $Q_{ext} = 2$, the optical constant becomes

$$(\alpha_o)_{dB/m} = 6.5 S/a = 6.5(4/3 \pi a^3)N/a = 27.23 a^2 N \tag{5.30}$$

from which

$$N = \alpha_o/(27.23 a^2) \tag{5.31}$$

Finally letting $\alpha_o = 15/V_i$

$$N = 0.551/(V_i a^2) \tag{5.32}$$

Expressing α_o in dB/km and visibility in km

$$N = 5.51 \times 10^{-4}/(V_i a^2) \tag{5.33}$$

with N the number of particles per cubic meter, V_i the visibility in km, and a the particle radius in meters.

Substituting Eq. (5.33) into Eq. (5.26) and considering only particles of radius a results in

$$\alpha_p = \frac{189}{V_i} \frac{a}{\lambda} \left[\frac{3 K_i}{(K_c + 2)^2 + K_i^2} \right] \tag{5.34}$$

with α_p the microwave attenuation constant in dB/km for propagation through dust and V_i the visibility in km.

Optical data may be available in terms of optical depth τ rather than visibility. In that case it is convenient to have an expression for total attenuation A at microwave frequencies in terms of τ. For this purpose, one can start with Eq. (5.26), as applied to particles of a fixed radius a. Then for N substitute Eq. (5.31) which introduces the optical constant α_o into the equation. Assuming a path of length L and constant conditions along the path, $\alpha_o L = 4.34\ \tau$ as α_o is in dB/km. The resulting equation is

$$A_{dB} = 54.67 \frac{\tau a}{\lambda} \left[\frac{3K_i}{(K_r + 2)^2 + K_i^2} \right] \text{dB} \qquad (5.35)$$

where τ is now in meters (Smith and Flock, 1986).

Many aerosols of natural and manmade origin occur in the Earth's atmosphere and might occasionally have a slight effect on telecommunications on a local scale. Two sources of information on aerosols (particulate matter of the atmosphere) are Clouds and Storms by Ludlam (1980) and Man's Impact on the Global Environment (SCEP, 1970). Most interest in such particulate matter is related to air pollution or scientific considerations. Clearly visible clouds of pollen are given off by pine trees during spring windstorms, and pollen from various plants is a source of hay fever. Measurements in the plume of Mt. St. Helens on May 18, 1980 showed that particle number densities about 9.3 km downwind in the 0.01 to 10 μm diameter range were from 4 to 1000 times the number density in the ambient air. For particles $<$ 2 μm in diameter the mass loading was about 9.5×10^{-5} g/m^3 compared with less than 10^{-7} g/m^3 in the ambient air (Hobbs et al., 1981). Even interplanetary space is not completely empty but is permeated by the solar wind and has a dust content of around 10^{-17} to 10^{-18} g/m^3 (Berman, 1979; Halliday and McIntosh, 1980).

5.3 BIOLOGICAL MATTER

Some background concerning the effect of vegetation and other biological matter on radiowave propagation is included in this section. More recent developments involving earth-space propagation are described in Sec. 6.4 of the following Chap. 6, which deals with land mobile satellite systems. Vegetation can have important effects on radio wave propagation. Flocks of birds are essentially large blobs of water as far as effects on radio waves are concerned and they can attenuate and scatter incident waves. Insects as well as birds are readily detectable by radar means and can have an effect on propagation when they occur in large concentrations, as in the case of swarms of insects in Africa.

Propagation through the vegetation of dense forests and jungles has been treated by considering the forest to be a lossy dielectric having a complex relative dielectric constant K_c and complex index of refraction n_c with $n_c^2 = K_c$ and $n_c = n_r - jn_i$. The attenuation constant for propagation in such a medium is $\beta_o n_i$, where β_o is the phase constant for empty space. Using an alternative form for K_c, namely $K_c = K(1 - j\tan\delta)$, Tamir (1974) reported that measured values of K range from 1.01 to 1.1 and $\tan\delta$ values range from 0.01 to 0.15.

In addition to a direct path through a section of forest, there may be additional rays as shown in Fig. 5.1. In this model TR is the direct path. Rays incident upon the upper boundary at angles equal to or greater than a critical angle θ_c, measured from the perpendicular to the boundary, experience total reflection and energy may thus reach the receiver by a path such as TABR. Waves which skim over the tree tops following a path like TABR are called lateral waves (Tamir, 1984). Some energy may also be reflected from the ground at S and S′ and eventually reach the receiver location. Attenuation on direct paths like TR and reflected paths is very high, and, for other than short paths, propagation is said to be by lateral waves, or by a sky wave for lower frquencies.

Using data from several sources in the frequency range from 100 MHz to 3.3 GHz, LaGrone (1960) found an average excess

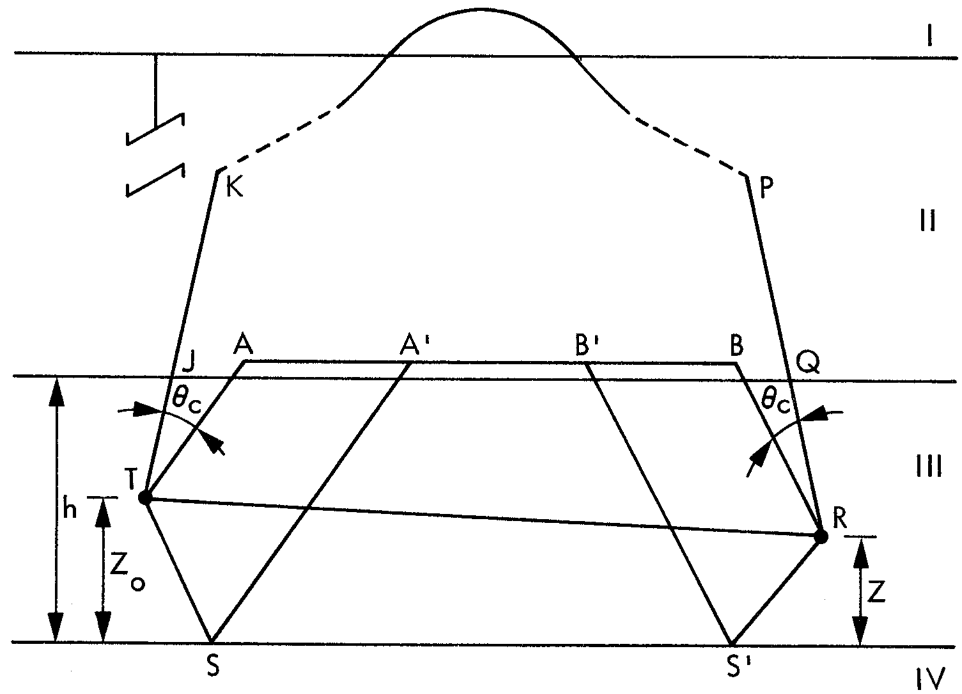

Figure 5.1. Ray paths in an idealized forest environment (Tamir, 1974; CCIR, 1986b).

attenuation constant α of $1.3 \times 10^{-3} f^{0.77}$ dB/m, with frequency f in MHz, for propagation through woodland. Other data for propagation through woodland in the frequency range from 30 MHz to 2 GHz are summarized in Fig. 5.2 (CCIR, 1986b). For propagation over a grove of trees when transmitting and receiving antennas are sufficiently far from the trees, transmission has been found to be primarily by diffraction (LaGrone, 1977). When antennas are closer to small groves of trees less than 400 m in extent, Weissberger (1981) found a relation for attenuation A in dB which in the rounded form decided upon by the CCIR is

$$A = 0.2 \ f^{0.3} d^{0.6} \qquad \text{dB} \tag{5.36}$$

with frequency f in MHz and distance d in m. The proceedings of a workshop on radio systems in forested and/or vegetated environments contain considerable discussion about propagation in such environments (Wait, Ott, and Telfer, 1974). The paper by

Tamir (1974) on lateral waves and a quite comprehensive though brief paper by Hagn (1974) are included in the proceedings of this workshop. Attenuation by individual trees is described in Sec. 6.4, pages 6-47 and 6-48.

Effects of birds and insects on telecommunications can be expected to be localized. In the near vicinities of breeding and wintering birds and along major migration routes in the spring and fall, concentrations of birds could disrupt communications momentarily. Concentrations of sea birds occur in migration and/or summer in arctic and subarctic areas, including the Aleutian and Pribilof Islands, the Bering Strait, Baffin Island, etc. Wintering areas of waterfowl and cranes in North America include the Gulf Coast, southern New Mexico, and interior valleys of California. The areas of bird concentration are commonly in or near wildlife refuges operated by federal agencies. Contact with the U.S. Fish and Wildlife Service in the United States and the Canadian Wildlife Service in Canada would be advisable if consideration is being given to installations near wildlife refuges or other areas of bird concentration. Huge flocks of blackbirds and starlings are sometimes a problem in towns and cities. Large flocks of birds scatter electromagnetic radiation efficiently and have the potential for causing interference between telecommunication systems and between telecommunication and radar systems.

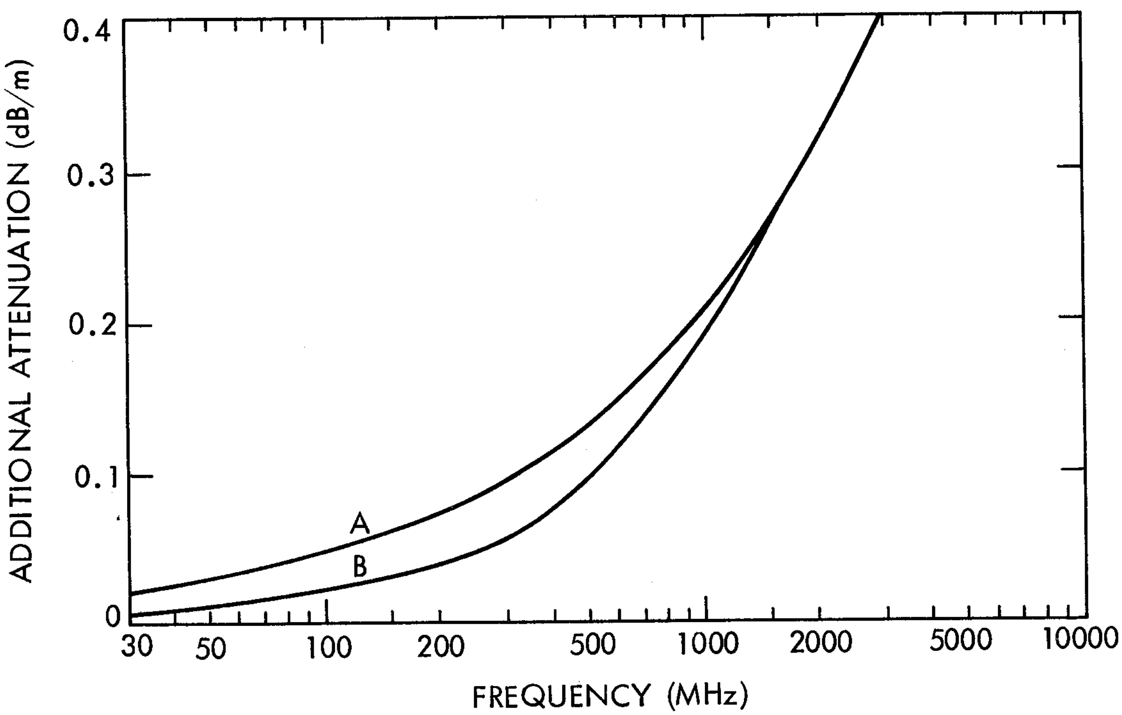

Figure 5.2. Excess attenuation in propagation through woodland (CCIR, 1986b). A: vertical polarization, B: horizontal polarization.

REFERENCES

Ahmed, I.Y. and L.J. Auchterlonie, "Microwave measurements on dust using an open resonator," ELectronics Letters, vol. 12, pp. 445-446, 19 Aug. 1979.

Bashir, S.O., A.W. Dissanayake, and N.J. McEwan, "Prediction of forward scattering and cross polarization due to dry and moist haboob and sandstorms in Sudan in the 9.4 GHz band," Telecomm. J., vol. 46, pp. 462-467, July 1980.

Battan, L.J., Radar Observation of the Atmosphere. Chicago: U. of Chicago Press, 1973.

Benson, C.S., Ice Fog: Low Temperature Air Pollution. Report UAG R-173, Geophysical Institute, U. of Alaska, Fairbanks, AK, 1965.

Benson, C.S., "Ice fog," Weather, vol. 25, pp. 9-18. Jan. 1970.

Berman, A.L., "A Unified Observational Theory for Solar Wind Columnar Turbulence," DSN Progress Report 42-50, pp. 124-131, Jan.-Feb., 1979.

CCIR, "Attenuation by hydrometeors, in particular precipitation, and other atmospheric particles," Report 721-2 in Vol. V, Propagation in Non-ionized Media, Recommendations and Reports of the CCIR, 1986. Geneva: Int. Telecomm. Union, 1986a.

CCIR, "Influence of terrain irregularities and vegetation on tropospheric propagation," Report 236-6 in vol. V, Propagation in Non-ionized Media, Recommendations and Reports of the CCIR, 1986. Geneva: Int. Telecomm. Union, 1986b.

Chu, T.S., "Effects of sandstorms on microwave propagation," Bell Syst. Tech. J., vol. 58, pp. 549-555, Feb. 1979.

Donn, W.L., Meteorology. New York: McGraw-Hill, 1975.

Ghobrial, S.F., "The effect of sandstorms on microwave propagation," Proc. IEEE, vol. 62, pp. 745-553, June 1974.

Goldhirsh, J., "A parameter review and assessment of attenuation and backscatter properties associated with dust storms over desert regions in the frequency range of 1 to 10 GHz," IEEE Trans. Antennas Propagat., vol. AP-30, pp. 1121-1127, Nov. 1982.

Gunn. K.L.S. and T.W.R. East, "The microwave properties of precipitation particles," Quart. J. Roy. Meteor. Soc., vol. 80, pp. 522-545, 1954.

Hagn, G.H., "Electrical properties of forested media," in Workshop on Radio Systems in Forested and/or Vegetated Environments, Wait, J.P., R.H.Ott, and T. Telfer (eds.), pp. I-C-1 to I-C-15, Technical Report No. ACC-ACO-I-74, U.S. Army Communication Command, Fort Huachuca, AZ, Feb. 1974.

Halliday, I. and B.A. McIntosh (eds.), Solid Particles in the Solar System, Symposium No. 90, IAU, Ottawa, Canada, Aug. 27-30, 1979. Dordrecht, Boston: D. Reidel Pub. Co., 1980.

Hobbs, P.W., L.F. Radke, M.W. Eltgroth, D.A. Hegg, "Airborne studies of emission from the volcanic eruptions of Mount St. Helens," Science, vol. 211, pp. 816-818, 20 Feb. 1981.

LaGrone, A.H., "Forecasting television service fields," Proc. IRE, vol. 48, pp.1011, June 1960.

LaGrone, A.H., "Propagation of VHF and UHF electromagnetic waves over a grove of trees in full leaf," IEEE Trans. Antennas Propagat., vol. AP-25, pp. 866-869, Nov. 1977.

Ludlam, F.H., Clouds and Storms, University Park: Pennsylvania State U. Press, 1980.

Panofsky, W.K.H. and M. Phillips, Classical Electricity and Magnetism. Reading, MA: Addison-Wesley, 1955.

Ramo, S.J., J.R. Whinnery, and T. Van Duzer, Fields and Waves in Communication Electronics. New York: Wiley, 1965.

SCEP (Study of Critical Environmental Problems), Man's Impact on the Global Environment. Cambridge, MA: M.I.T. Press, 1970.

Setzer, D.E., "Computed transmission through rain at microwave and visual frequencies," Bell System Tech. J., vol. 49, pp. 1873-1892, Oct. 1970.

Slobin, S.D., Microwave Noise Temperature and Attenuation of Clouds at Frequencies Below 50 GHz. JPL Publication 81-46. Pasadena, CA: Jet Propulsion Lab., 1981.

Slobin, S.D., "Microwave noise temperature and attenuation of clouds: statistics of these effects at various sites in the United States, Alaska, and Hawaii," Radio Sci., vol. 17, 1443-1454, Nov.-Dec. 1982.

Smith E.K. and W.L. Flock, "Propagation through Martian dust at X- and Ka-band," Paper VIII-1, Commission F Open Symposium on Wave Propagation and Remote Sensing, U. of New Hampshire, Durham, NH, July 27-Aug. 3, 1986.

Staelin, D.H., "Measurements and interpretation of the microwave spectrum of the terrestrial atmosphere near 1-centimeter wavelength," J. Geophys. Res., vol. 71, pp. 2975-2881, 1966.

Tamir, T., "Lateral wave applications to radio systems," in Workshop on Radio Systems in Forested and/or Vegetated Environments, Wait, J.R., R.H. Ott, and T. Telfer (eds.), pp. I-B-1 to I-B-7, Technical Report No. ACC-ACO-I-74, U.S. Army Communications Command, Fort Huachuca, AZ, Feb. 1974.

van de Hulst, H.C., Light Scattering by Small Particles. New York: Wiley, 1957.

Wait, J.H., R.H.Ott, and T. Telfer (eds.), Workshop on Radio Systems in Forested and/or Vegetated Environments, Technical Report No. ACC-ACO-1-74, U.S. Army Communications Command, Fort Huachuca, AZ, Feb. 1974. (Distributed by NTIS, Springfield, VA.)

Weissberger, M.A., An Initial Critical Summary of Models for Predicting the Attenuation of Radio Waves by Foliage, ECAC-TR-81-101. Annapolis, MD: Electromagnetic Compatibility Center, Aug. 1981.

Zufferey, C.H., A Study of Rain Effects on Electromagnetic Waves in the 1-600 GHz Range, M. S. thesis. Boulder, CO: Department of Electrical Engineering, U. of Colorado, 1972 (reprinted in 1979).

CHAPTER 6

PROPAGATION EFFECTS ON MOBILE-SATELLITE SYSTEMS

6.1 GROUND WAVES AND EFFECTS OF TERRAIN

Previous chapters have dealt largely with atmospheric effects on radio-wave propagation, the exception being Sec. 5.3 which considers effects of vegetation. Terrestrial telecommunication links and earth-space transmissions, especially at small elevation angles or between satellites and mobile systems, however, may also be influenced by the electrical properties of the Earth's surface and by features of terrain. This section deals with ground waves and obstruction or shadowing by terrain or structures. Section 6.2 treats the physical phenomena of specular reflection and diffuse scatter by the Earth's surface, and Sec. 6.3 relates these phenomena to system design considerations. Sections 6.4, 6.5, and 6.6 give attention to land-mobile, marine-mobile, and aeronautical-mobile systems, and the final Sec. 6.7 describes the Global Positioning System (GPS). All of the major propagation effects on satellite mobile systems (not only the effects of terrain) are given at least brief mention in Secs. 6.4 - 6.7.

6.1.1. Ground Waves

One means by which radio waves propagate from one location to another is by ground waves. In analyzing propagation near the Earth's surface, what are referred to as ground waves are often separated into space waves and surface waves. A space wave consists of the direct wave from transmitter to receiver and the reflected wave, if any, that reaches the receiver after reflection from the Earth's surface. It is the surface wave that is most strongly affected by the electrical properties of the Earth. The attenuation of the surface wave is high and surface wave propagation is limited to short distances for high frequencies. The surface wave is the principal component of the ground wave for frequencies of a few MHz, is of secondary importance at VHF (30-300 MHz), and can be neglected for frequencies greater than 300 MHz (Bullington, 1977).

An approximate expression for the attenuation or loss factor L_s for a surface wave is

$$L_s = \frac{-1}{1 - j2\pi d/\lambda\,(\sin\theta + z)^2} \qquad (6.1)$$

where

$$z = \left(K - j\frac{\sigma}{\omega\epsilon_o} - \cos^2\theta\right)^{1/2} \qquad (6.2)$$

for horizontal polarization and

$$z = \frac{\left(K - j\frac{\sigma}{\omega\epsilon_o} - \cos^2\theta\right)^{1/2}}{K - j\,(\sigma/\omega\epsilon_o)} \qquad (6.3)$$

for vertical polarization. L_s has a maximum value of unity. The expression is most accurate for $L_s \leq 0.1$ and within 2 dB in amplitude in any case but is in error in phase by 180 deg as L_s approaches 1 (Bullington, 1977). In the above expressions $\sigma/\omega\epsilon_o$ can be replaced by its approximate equivalent 60 $\sigma\lambda$. The conductivity σ is in mhos/m, θ is the elevation angle, $\omega = 2\pi f$ where f is frequency, ϵ_o is the electric permittivity of empty space (8.854×10^{-12} F/m), and K is relative dielectric constant. If using 60 $\sigma\lambda$, λ is in m. Surface waves are most important at frequencies below the 100 MHz lower limit of this handbook and in a region within a few wavelengths of the ground. They can be neglected in most applications of microwave mobile communications (Jakes, 1974, where the microwave range is treated as from about 450 MHz to 10 or 20 GHz). A more thorough treatment of surface waves can be found in Jordan and Balmain (1968). Ground-wave propagation at frequencies from 10 kHz to 30 MHz is treated in CCIR Recommendation 368-5 (CCIR,1986a).

6.1.2 Effects of Obstructions

Obstructions along a path in the form of hills and buildings introduce loss with respect to free-space propagation, and the loss varies with time because tropspheric refraction varies with time.

For considering the effect of obstructions, the concept of Fresnel zones is useful. To introduce this topic consider Fig. 6.1 which shows two paths TPR and TSR between a transmitter T and receiver R. TPR is a direct path, and TSR is longer than TPR. If TSR = TPR + $\lambda/2$ where λ is wavelength, the region within the radius r (in the plane perpendicular to TR), at a distance d_T from T and d_R from R, is defined as the first Fresnel zone. The particular value of r in this case is the first Fresnel zone radius and is designated as F_1. The concept can be extended to the case that TSR = TPR + $n\lambda/2$, for which the corresponding Fresnel zone radius can be designated as F_n. The significance of the first Fresnel zone is that all the elements of radiation passing through this zone have components of electric field intensity that add constructively. Radiation passing through the second Fresnel zone (values of r between F_1 and F_2), however, interferes destructively with radiation passing the first Fresnel zone, that passing through the third Fresnel zone adds constructively with that in the first zone but makes a smaller contribution, etc. The process can be understood in terms of Huygen's principle which states that every elementary area of a wavefront can be regarded as a source of secondary spherical waves. When r is small compared to d_T and d_R, it can be determined that

$$F_1 = \sqrt{\frac{\lambda d_T d_R}{d}} \quad \text{m} \tag{6.2}$$

where $d = d_T + d_R$ and all lengths are in meters or that

$$F_1 = 17.3 \sqrt{\frac{d_T d_R}{f\, d}} \quad \text{m} \tag{6.3}$$

if distances are in km, f is measured in GHz, and F_1 is in meters. For the situation that d_T is approximately equal to d the expression for F_1 corresponding to Eq. (6.2) is

$$F_1 = (\lambda d_R)^{1/2} \tag{6.4}$$

The value of F_n is related to that for F_1 by

$$F_n = n^{1/2} F_1 \tag{6.5}$$

One might think that a satisfactory signal amplitude would result on a telecommunications link as long as a direct line of sight from the transmitter to the receiver is provided, but consideration of Huygen's principle suggests that having a direct line of sight may not be sufficient. The analysis of the effect of an obstruction approximating a knife edge is given in texts on optics, for example that by Jenkins and White (1976), and in Jordan and Balmain (1968). The results are conveniently expressed in terms of the ratio h_c/F_1 of path clearance h_c to the first Fresnel zone radius F_1, as in Fig. 6.2. If the edge of the knife-edge obstruction is at the direct line of sight, a loss of 6 dB is encountered. To avoid attenuation a clearance of about 0.6 F_1 is required. Note that Fresnel zone analysis is in terms of field intensity. For zero clearance the total field intensity at the receiver location is reduced to 0.5 of the value for a completely unobstructed path. A reduction of field intensity to 0.5 corresponds to a reduction of power to 0.25 and therefore to the loss of 6 dB. In analyses of diffraction a parameter v equal to $2^{1/2}\, h_c/F_1$ may be utilized and resulting values of attenuation may be plotted as a function of v. The parameter v is used, for example, in CCIR Report 715-2 (CCIR, 1986b) and in Jordan and Balmain (1968).

The field intensity beyond an obstacle is dependent upon the form of the obstacle. The loss due to a knife-edge obstacle at grazing incidence is 6 dB, but the corresponding value for a smooth earth is about 20 dB (Bullington, 1977). Formulas and nomograms for determining the loss due to diffraction by a smooth spherical earth are given in CCIR Report 715-2. This same report discusses propagation over irregular terrain, and Hall (1979) treats this difficult topic. Multiple knife-edge diffraction is the subject of a paper by Deygout (1966). He finds which knife-edge obstacle causes the greatest loss and determines this loss. Then locations and

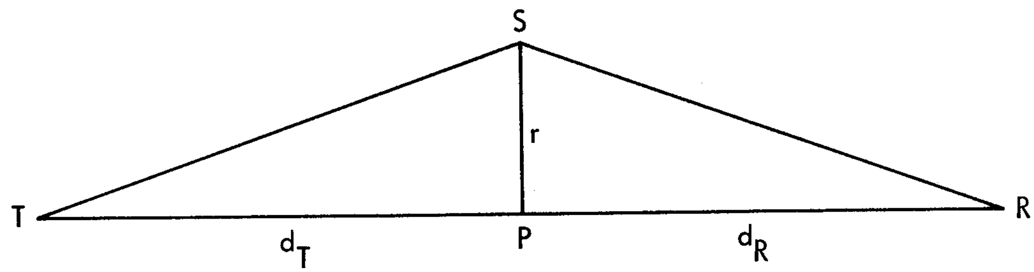

Figure 6.1. Geometry for consideration of Fresnel zones.

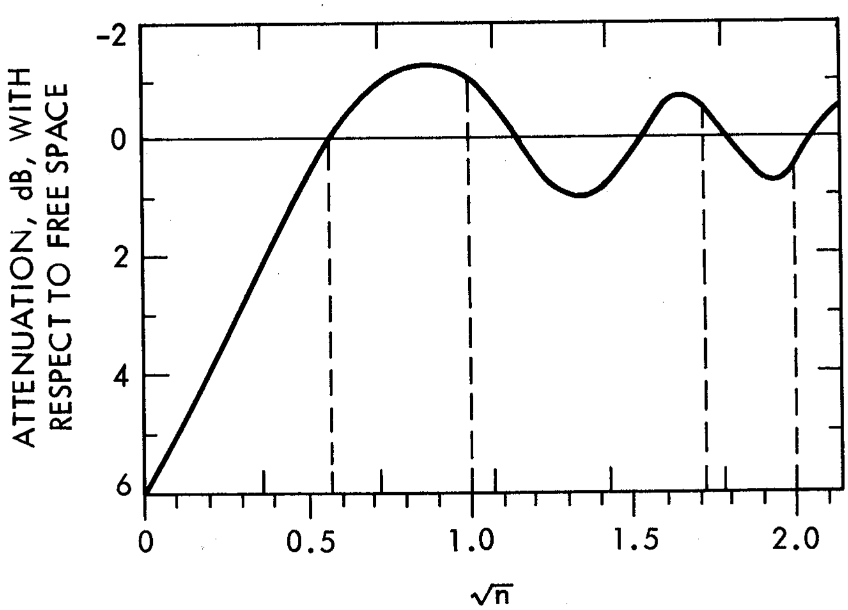

Figure 6.2. Attenuation due to knife-edge diffraction with relation to free space, as a function of $h_c/F_1 = n^{1/2}$ (Hall, 1979).

additional losses are calculated for the other knife-edge obstacles. Assis (1971), noting that the assumption of a knife edge often gives overly optimistic results, employs the approach of Deygout but applies it to the case of rounded obstacles. He provides a set of curves (Fig. 6.3) which give loss as a function of H/F_1, where H is the height of the obstacle above a direct unobstructed path from transmitter to receiver, and a parameter α where

$$\alpha = \lambda^{2/3} r^{1/3}/F_1 \tag{6.6}$$

with λ the wavelength, r the radius of curvature, and F_1 the first Fresnel zone radius. Note that the condition $H/F_1 = -0.6$ corresponds to $h_c/F_1 = 0.6$ and to free space propagation. Also $H/F = 0$ and $\alpha = 0$ is the condition for the loss of 6 dB mentioned for knife-edge diffraction, and $H/F_1 = 0$ and $\alpha = 1.5$ corresponds roughly to the loss of 20 dB mentioned earlier as well. For positive values of H/F_1, corresponding to obstructions extending above the lowest direct unobstructed path, losses are shown to increase above those for H/F_1. An alternative approach to propagation over irregular terrain utilizes an integral equation theory (Ott, 1971) instead of diffraction theory.

It is possible for the signal beyond an obstacle, such as a mountain, to be larger than if the obstacle was not present. This condition occurs due to diffraction alone in the case of a knife-edge obstacle as in Fig. 6.2, where there is a direct line-of-sight path and the obstacle is below the path. We consider now, however, the situation where there is no direct path. This is the case for which the term obstacle gain is normally applied. In this case multipath propagation occurs as in Fig. 6.4, for example, where four paths exist between a transmitter and receiver on the opposite sides of an obstacle. Obstacle gain depends upon the occurrence of favorable phase relations between the signals arriving over the different paths. It can be destroyed by meteorological variations and thus may be subject to fading but can be used to advantage in certain circumstances (Kirby et al., 1955; Hall, 1979). The losses associated with the occurrence of obstacles on mobile communication systems are commonly referred to shadowing losses.

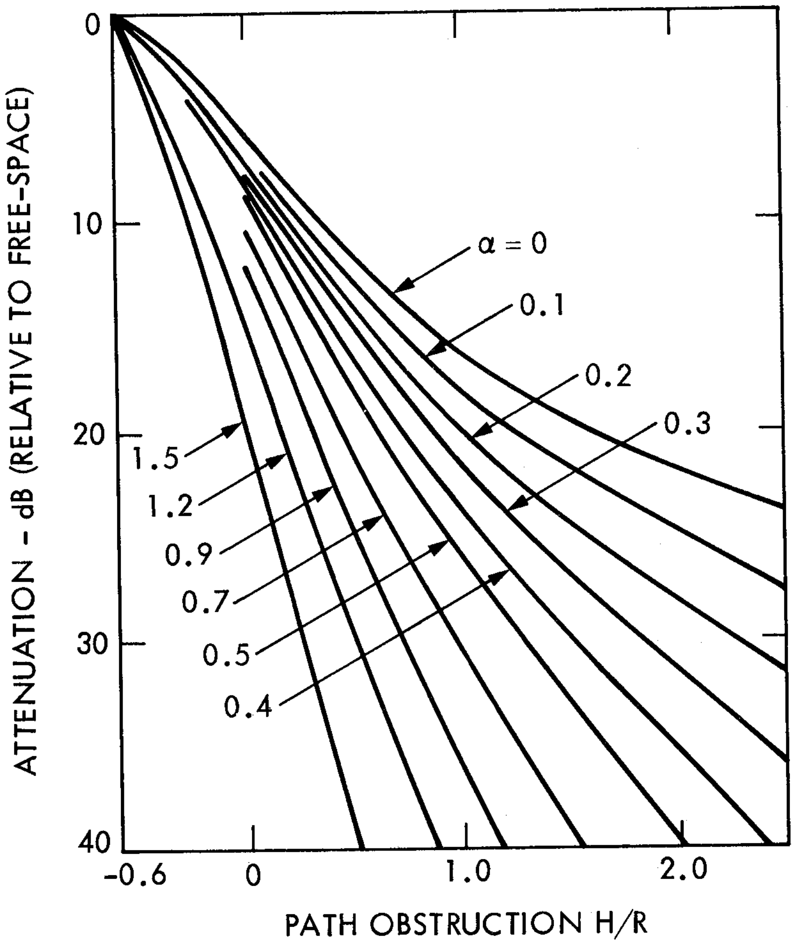

Figure 6.3. Attenuation due to diffraction over obstacles, with relation to free space, as a function of the parameter α and $H/R = H/F_1$ with H the height of the obstacle above a direct unobstructed path (Assis, 1971).

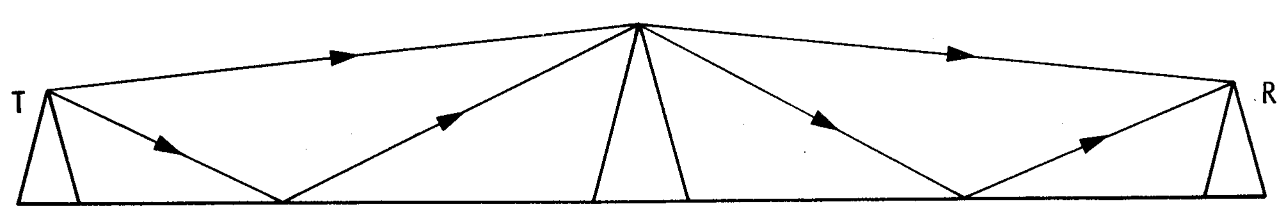

Figure 6.4 Possible ray paths contributing to obstacle gain..

6.2 SPECULAR REFLECTION AND DIFFUSE SCATTER

6.2.1 Introduction

On both earth-space and terrestrial line-of-sight paths, signals may reach a receiving antenna by a direct atmospheric path and by specular reflection and diffuse scatter from the ground. In the following Sec. 6.2.2, expressions are given for total signal amplitude as a function of elevation angle and antenna height for the case of two equal sinusoidal signal components, one traveling over a direct atmospheric path and one experiencing specular reflection from a flat, smooth, perfectly conducting surface. Reflection coefficients for specular reflection from a flat, smooth earth having a finite conductivity are given in Sec. 6.2.3, and surface roughness is taken into account in Sec. 6.2.4. Diffuse scatter is discussed in Sec. 6.2.5, and the factors affecting total signal amplitude are summarized in Sec. 6.2.7.

6.2.2 Multipath Effects

The term multipath refers to a condition in which energy reaches the receiver of a telecommunications system by more than one path. Multipath operation tends to be undesirable, because signals arriving over the different paths tend to arrive with variable relative phase, with the result that they alternately reinforce each other and interfere destructively. The total signal is then characterized by fading involving repeated minima, and the danger exists that the minima will fall below the acceptable signal level. The signals arriving over the different paths also have different time delays which can result in intersymbol interference in digital systems. Multipath propagation may result from reflection from land and water surfaces and manmade structures. Multipath propagation may also arise from atmospheric effects alone, in the absence of reflection from surface features.

Reflections from a plane surface and the total electric field intensity which results when field intensities arriving over two paths are summed can be considered with the aid of Fig. 6.5. The figure shows direct and reflected rays reaching a receiver at a height h_R above a flat, smooth surface at $h = 0$. The transmitter is assumed to be so far away that the two rays can be considered to be parallel at an elevation angle of θ from the horizontal. Assuming also a perfectly conducting surface and horizontal polarization, a 180 deg phase shift will occur upon reflection so that, at $h = 0$, $E_r = -E_i$ where E_r is the field intensity of the reflected wave and E_i is the field of the incident wave of path 2 of Fig. 6.5. The difference in length of paths 1 and 2, $\Delta \ell$, is $2h_R \sin \theta$. If $\Delta \ell = \lambda/2$ (or $n\,\lambda/2$ with n odd), maximum total signal intensity will be recorded as the combination of the 180 deg phase shift on reflection and the phase shift of 180 deg corresponding to $\Delta \ell = \lambda/2$ results in signal reinforcement. If $\Delta \ell = \lambda$ (or $n\lambda/2$ with n even), destructive

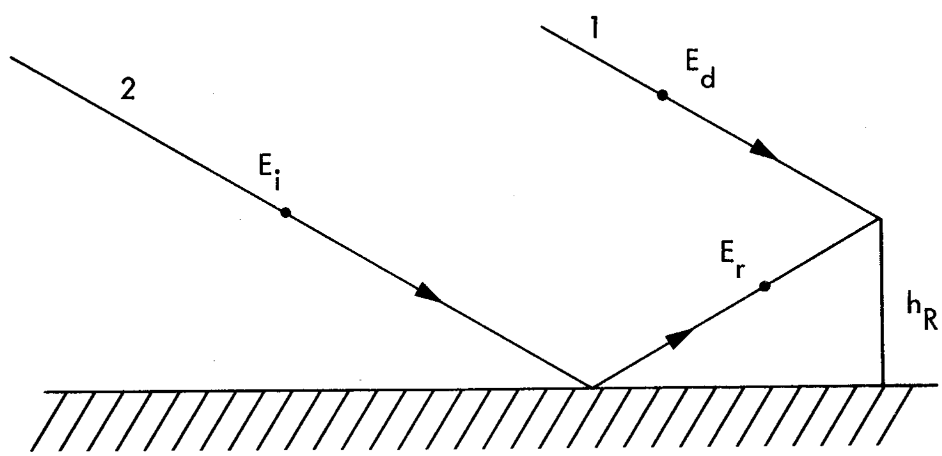

Figure 6.5. Direct and reflected rays for a path employing horizontal polarization (electric-field intensity vectors perpendicular to the plane of the drawing).

interference between the two rays occurs as they then differ in phase by 180 deg. It might seem that satisfactory operation is assured if h_R is chosen so that $\Delta \ell = n\lambda/2$ with n odd. The discussion to this point, however, has neglected the atmosphere. In the Earth's atmosphere the ray paths will be curved to some degree and variable with time so that constructive and destructive interference may take place alternately even for a fixed receiver location and height. In mobile operations, furthermore, the receiver position with respect to reflecting surfaces will vary and the height will not necessarily be optimum at any particular location.

The phase shift ϕ corresponding to the difference in path length $\Delta\ell = 2\, h_R \sin\theta$ is given by

$$\phi = (4\pi h_R \sin\theta)/\lambda \qquad (6.7)$$

where λ is wavelength. If the field intensities E_1 and E_2 of rays arriving over the two paths of Fig. 6.5 have the same amplitude E_0, the total field intensity E (Fig. 6.6) is given by

$$|E| = \left| 2E_o \sin\left(\frac{2\pi h_R \sin\theta}{\lambda}\right)\right| = \left|2E_o \sin\phi/2\right| \qquad (6.8)$$

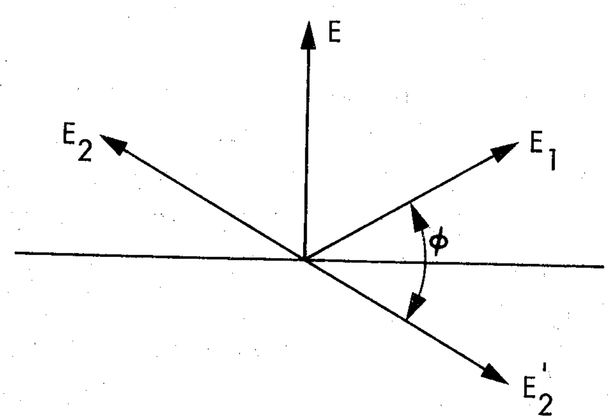

Figure 6.6. Phasor diagram illustrating how field intensities of direct and reflected rays (E_1 and E_2) add to give the total field intensity E.

The two phasors E_1 and E_2 represent field intensities arriving over paths 1 and 2 at the receiver location of Fig. 6.5. In the absence of the phase reversal upon reflection, E_2 would have the direction of E_2'. With phase reversal the vertical components of E_1 and E_2 add to give the result shown. A more general expression for the amplitude of the total signal when the reflection coefficient may be complex and may not have a magnitude of unity is

$$E = E_o \left[(1 - |\rho|)^2 + 4|\rho| \cos^2 (\phi /2) \right]^{1/2} \qquad (6.9)$$

Here $|\rho|$ is the magnitude of the reflection coefficient and ϕ' is the sum of the phase of the reflection coefficient and the phase shift corresponding to the path length difference. This expression is given in Beckmann and Spizzichino (1963, p. 224) except that it is shown there with a plus sign in place of the minus sign. Equation (6.9) shows that the maximum and minimum values of E, E_{max} and E_{min} respectively, are given by

$$E_{max} = E_o (1 + |\rho|), \quad E_{min} = E_o (1 - |\rho|) \qquad (6.10)$$

The result is modified further if the transmitting and receiving antennas have gains that are different for the direct and reflected rays. If the transmitter is on a satellite, only the gains of the receiving antenna will be different for the direct and reflected rays. In that case $|\rho|$ should be replaced by the square root of the ratio of the gain for the reflected ray to the gain for the direct ray. Discrimination against the reflected wave by use of antenna directivity is an important potential means for combating multipath effects. This process is more readily accomplished for large elevation angles than for small elevation angles. In modeling low-elevation angle propagation effects for maritime mobile satellite operations, Fang and Ott (1983) assume that the gain of the particular shipboard antenna considered, having a beamwidth of 12 deg, is reduced in the direction of the reflected wave by

$$e^{-(2\theta/7.22)^2}$$

where θ is the elevation angle in degrees. This expression makes use of the fact that the direction of the reflected ray differs from that of the direct ray by twice the elevation angle. Gain is assumed to be power gain here, as is commonly the case, and the square root is taken to obtain the proper ratio for field intensity.

For terrestrial paths, the analysis of how direct and reflected waves combine to reinforce or interfere destructively can be analyzed with the help of Fig. 6.7. For the case that $d \gg h_T$ and $d \gg h_R$ and for propagation over a flat earth, $\Delta \ell = r_2 - r_1 = 2\pi h_T h_R / d$. The corresponding phase difference ϕ is given by

$$\phi = (2\pi/\lambda)\,(r_2 - r_1) = 4\pi h_T h_R/(\lambda d) \qquad (6.11)$$

For a perfectly conducting surface and assuming equal field intensities E_o for the two paths, it develops that, after taking account of the reversal of phase on reflection,

$$|E| = \left| 2\,E_o \sin\left(\frac{2\pi h_T h_R}{\lambda d}\right) \right| = |2\,E_o \sin(\phi/2)| \qquad (6.12)$$

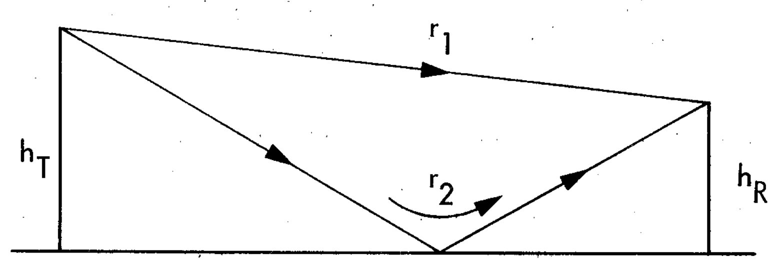

Figure 6.7. Direct and reflected rays for terrestrial path.

The relations for the terrestrial path have been included for comparison with those for an earth-space path. Equation (6.8) can be obtained from Eq. (6.12) by replacing h_T/d by $\sin\theta$.

The approaches shown for earth-space paths can be modified to take account of earth curvature when necessary (Beckmann and Spizzichino, 1963; Flock, 1979). Earth curvature affects the phase relation between direct and reflected rays and may also result in a decrease in the magnitude of the reflected ray. The latter condition tends to be most important for aeronautical-mobile systems and is mentioned again in Sec. 6.5.

The different time delays of the signals arriving over the different paths when multipath propagation occurs also tend to be of most importance for aeronautical systems, for which the differences tend to be greatest. The time delays are also of greater importance for digital systems than for analog systems.

The expressions for field intensity E that have been given in this section apply to stable conditions such that, for constant transmitter and receiver heights and locations, signal amplitude is constant. Reflection from flat, smoooth perfectly conducting surfaces is assumed, and the reflection coefficient therefore has a magnitude of unity. The receiving antenna is assumed to have the same gain for the reflected ray as for the direct ray. In reality, none of these conditions may be fulfilled. In the following Sec. 6.2.3, expressions are given for reflection coefficients for flat smooth surfaces that have finite conductivity. The magnitudes of the reflection coefficients are less than unity and are different for horizontal and vertical polarization in this case. The antenna gain will very likely be at least somewhat less for the reflected wave than for the direct wave. These modifications help to reduce the effect of the reflected wave but fading due to multipath propagation may still occur. If surface roughness is encountered as well, the magnitude of the reflection coefficient for specular reflection tends to decrease further but diffuse scatter as well as specular reflection must then be taken into account.

6.2.3 Reflection Coefficient for Specular Reflection

The complex electric field intensity E_r of the reflected wave on path 2 at $h = 0$ has an amplitude and phase angle that is given by the product of E_i, the electric field intensity of the incident wave at $h = 0$, and the reflection coefficient ρ (Fig. 6.5). Therefore $E_r = \rho E_i$ at $h = 0$ and

$$\rho = E_r/E_i \tag{6.13}$$

where all three quantities may be complex. It is evident that the reflection coefficient determines the amplitude and phase of the reflected wave, with respect to the incident wave.

The reflection coefficent for a smooth surface is a function of the relative dielectric constant K, conductivity σ (mhos/m), elevation angle θ, and angular frequency $\omega = 2\pi f$. For a horizontally polarized incident wave the reflection coefficient ρ_h is given by

$$\rho_h = \frac{\sin\theta - \sqrt{K - j\,\sigma/\omega\epsilon_o - \cos^2\theta}}{\sin\theta + \sqrt{K - j\,\sigma/\omega\epsilon_o - \cos^2\theta}} \qquad (6.14)$$

The angle θ is measured from the horizontal. The symbol ϵ_o represents the electric permittivity of empty space, 8.854×10^{-12} F/m.

The expression for ρ_v the reflection coefficient for "vertical" polarization, meaning for the electric field intensity vectors in the plane of incidence (the plane of the drawing as shown in Fig. 6.8), is

$$\rho_v = \frac{[K - j\,\sigma/\omega\epsilon_o]\sin\theta - \sqrt{K - j\,\sigma/\omega\epsilon_o - \cos^2\theta}}{[K - j\,\sigma/\omega\epsilon_o]\sin\theta + \sqrt{K - j\,\sigma/\omega\epsilon_o - \cos^2\theta}} \qquad (6.15)$$

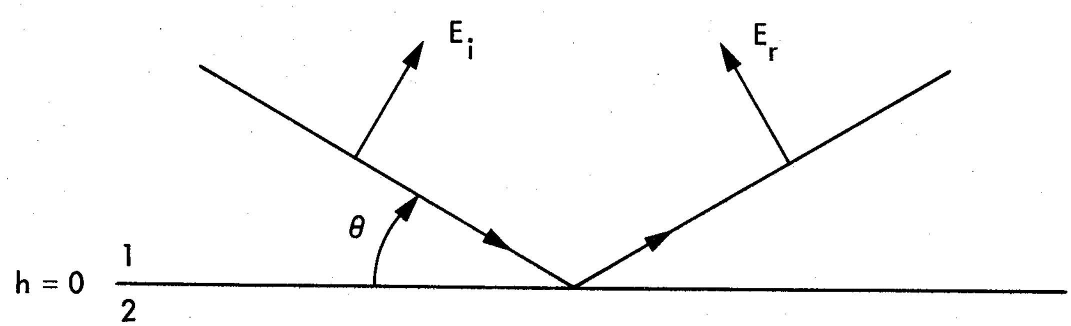

Figure 6.8. Electric field intensity vectors for vertically polarized wave.

Note that the electric field intensity vectors are not strictly vertical unless $\theta = 0$ deg. The field intensities have horizontal components, and the relation between these horizontal components at $h = 0$ is determined by the tangential (horizontal) boundary conditions which apply at this surface. Consistent with Fig. 6.8, it is normally assumed that the vertical components of the field intensities are in the same direction, which means that the horizontal components are automatically taken to be oppositely directed. Thus for a perfectly conducting surface $\rho_v = +1$, consistent with the horizontal components being equal and opposite so that the total tangential field intensity is zero at the surface. Assuming the same perfectly conducting surface and for $\theta = 90$ deg, where horizontal and "vertical" polarizations are indistinguishable, $\rho_h = -1$. The reason for this discrepancy is the different intial assumptions made about the directions of E_i and E_r for the two polarizations. For horizontal polarization they are assumed to be in the same direction, whereas for vertical polarization the horizontal components are assumed to be in opposite directions as mentioned above. As two vectors pointing in the same direction but 180 deg out of phase are equivalent to two vectors pointing in opposite directions but in phase, the two results are compatible. The reflection coefficient ρ_v applies to waves having a vertical component of electric field intensity, and the greatest interest usually lies in the vertical component rather than in the horizontal component. Thus it is appropriate that the sign of ρ_v be chosen to be positive if the vertical component of E_r is in the same direction as that of E_i. The wave to which ρ_h applies is polarized perpendicular to the plane of incidence. The two types of waves are orthogonally polarized, meaning that their electric field intensity vectors are mutually perpendicular. Both have horizontal components but the horizontal component of the wave polarized in the plane of incidence is perpendicular to the horizontal field intensity of the wave polarized perpendicular to the plane of incidence. Plots of ρ_h and ρ_v are given in Fig. 6.9.

An important characteristic of the reflection coefficient for vertical polarization is that in the lossless case ρ_v goes to zero at the Brewster angle θ_p defined by

$$\theta_p = \tan^{-1} (K_1/K_2)^{1/2} \tag{6.14}$$

If medium 1 is air so that $K_1 = 1$

$$\theta_p = \tan^{-1} (1/K_2)^{1/2} \tag{6.15}$$

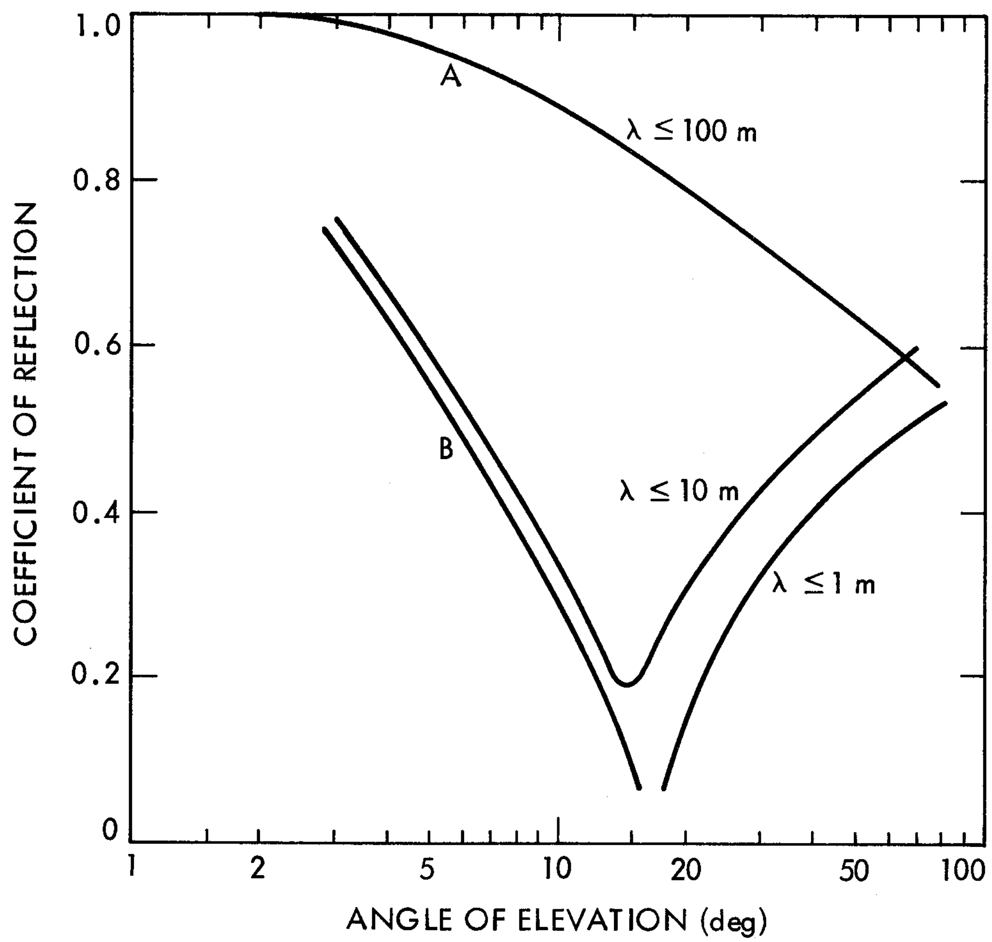

Figure 6.9. Reflection coefficients for plane average ground. A: horizontal polarization; B: vertical polarization (CCIR, 1982). Also see CCIR (1986c).

For σ not equal to zero, a minimum value of $|\rho_v|$ still tends to occur, and as it is $\sigma/\omega\epsilon_o$ that appears in Eq. (6.15) the minimum tends to be quite pronounced for large values of ω. See Sec. 6.2.8 for a discussion of the phase of the reflected signal.

Reflection coefficients for circularly polarized waves can be derived from those for horizontal and vertical polarization. When a circularly polarized wave is reflected, the reflected wave contains in general a component of the original circular polarization and a component of the orthogonal or cross polarization. When a right circularly polarized wave is reflected, for example, both right and left circularly polarized waves result. If the elevation angle is less than the Brewster angle [θ_p of Eq. (6.15)], the original polarization predominates, whereas if the angle is greater than the Brewster angle the cross polarization predominates. It is shown in Appendix 6.1 that the reflection coefficient for the original polarization ρ_c is given by

$$\rho_c = (\rho_h + \rho_v)/2 \tag{6.18}$$

whereas the coefficient giving the cross polarized component ρ_x can be found from

$$\rho_x = (\rho_h - \rho_v)/2 \tag{6.19}$$

6.2.4 Surface Roughness

The discussion of reflection in Secs. 6.2.1 and 6.2.2 assumed a perfectly smooth reflecting surface, consistent with reflection in the forward direction only. If a surface is rough, however, energy is reflected or scattered in other directions as well, with the result that the magnitude of the forward reflection coefficient is reduced. A commonly accepted criterion for roughness is the Rayleigh criterion, which can be explained with the help of Fig. 6.10. Consider two rays A and B such that ray A follows a path longer that of ray B by π rad, the two rays being reflected from locations that differ in height by Δh. As the two rays differ in phase by π rad they interfere destructively for forward reflection. Therefore some of the incident energy is scattered in other than the forward direction. The amount $\Delta \ell$ by which the path length of ray A exceeds that of ray B is given by

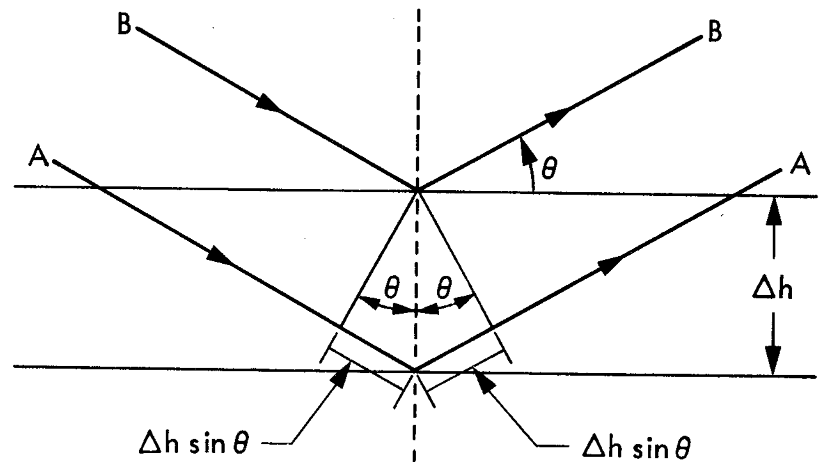

Figure 6.10. Basis for Rayleigh criterion.

$$\Delta \ell = 2\Delta h \sin\theta \tag{6.20}$$

and the corresponding phase difference $\Delta\phi$ equals π so that

$$\Delta\phi = (4\pi/\lambda)\, \Delta h \sin\theta = \pi \tag{6.21}$$

from which

$$\Delta h \geq \frac{\lambda}{4 \sin\theta} \tag{6.22}$$

has been taken as the criterion for roughness (Beckmann and Spizzichino, 1963). Less well established is a criterion for smoothness, but one form has been

$$\Delta h \leq \frac{\lambda}{8 \sin\theta} \tag{6.23}$$

except that 8 is arbitrary and it has been recognized that a larger number may be more appropriate.

The specular reflection coefficients ρ_{hs} and ρ_{vs} for reflection from other than a perfectly smooth surface can be related to the coefficients ρ_h and ρ_v, for example by

$$\rho_{hs} = \rho_h \rho_s \tag{6.24}$$

and

$$\rho_{vs} = \rho_v \rho_s \tag{6.25}$$

where ρ_s is surface roughness factor. A form for ρ_s is

$$\rho_s = e^{-(\Delta\phi)^2/2} \tag{6.26}$$

with

$$\Delta\phi = (4\pi h_s/\lambda) \sin\theta \tag{6.27}$$

where h_s is the rms value of the terrain height irregularities, λ is electromagnetic wavelength, and θ is elevation angle. This relation is the same as that used in Eq. (6.21) except that h_s is now an rms value and $\Delta\phi$ can take any value. However, Miller, Brown, and Vegh (1984) have asserted that the proper form for ρ_s is

$$\rho_s = e^{-(\Delta\phi)^2/2} I_o[(\Delta\phi)^2/2] \tag{6.28}$$

where $I_o[(\Delta\phi)^2/2]$ is the modified Bessel function of $[(\Delta\phi)^2/2]$. This Bessel function has a value of unity or greater and its inclusion results in ρ_s being larger than otherwise.

It has been pointed out by E.K. Smith that the criterion for smoothness of Eq. (6.23) when applied to Eq. (6.26) for surface roughness results in values of ρ_s which are not consistent with a smooth surface. For example, if $\Delta h = \lambda/(8 \sin\theta)$ is used, $\Delta\phi$ becomes $\pi/2$ and the value of ρ_s corresponds to a loss upon reflection of 10 dB. Such a surface can hardly be considered smooth. If $\Delta h = \lambda/(24 \sin\theta)$ is used, $\Delta\phi$ becomes $\pi/6$ and the corresponding loss is about 1.2 dB. This value of Δh gives a more reasonable result, but no great importance can be attached to the precise value of 24.

If the relation of Eq. (6.28), which includes the modified Bessel function, is used, the loss upon reflection for $\Delta\phi = \pi/2$ is reduced from 10 dB to 7.7 dB. For $\Delta\phi = \pi/6$, however, I_o of Eq. (6.28) is close to unity and the loss is about the same (1.2 dB) as when I_o is omitted. It nevertheless seems desirable to include the modified Bessel function for general use and to take as a criterion for smoothness the relation

$$\Delta h \leq \lambda/(A \sin \theta) \tag{6.29}$$

where A can be taken as the value of 24 or greater depending upon what loss upon reflection is deemed appropriate.

As large reflection coefficients for forward reflection tend to be undesirable, the occurrence of high degrees of surface roughness of possible reflecting surfaces can generally be looked upon with favor for telecommunication purposes. In the case of reflection from a rough surface some degree of specular reflection may still take place and diffuse scatter occurs as well. Specular reflection is directional, coherent in phase, and tends to have small fluctuations in amplitude. Diffuse scatter exhibits little directivity, is incoherent in phase, and tends to exhibit larger fluctuations which are Rayleigh distributed (Beckmann and Spizzichino, 1963). Section 6.2.6 gives the form of the Rayleigh probability density function.

6.2.5 Diffuse Scatter

With increasing surface roughness. specular reflection decreases in importance and diffuse scatter increases. Using copolarized circular polarization as an example,

$$\rho_{cd} = \rho_d \, \rho_c \tag{6.30}$$

where ρ_c is the plane-earth reflection coefficient, ρ_d is a coefficient for diffuse scatter, and ρ_{cd} gives magnitude and phase for the diffusely scattered radiation. The same type of relation is assumed to apply to the other polarizations. The value of ρ_d is commonly taken as 0.35, but Fig. 6.11 shows the theoretical distribution in dB for a combination of specular reflection and diffuse scatter for various values of ρ_d. This combination is described by the Rice probability density function [Eq. (6.43)].

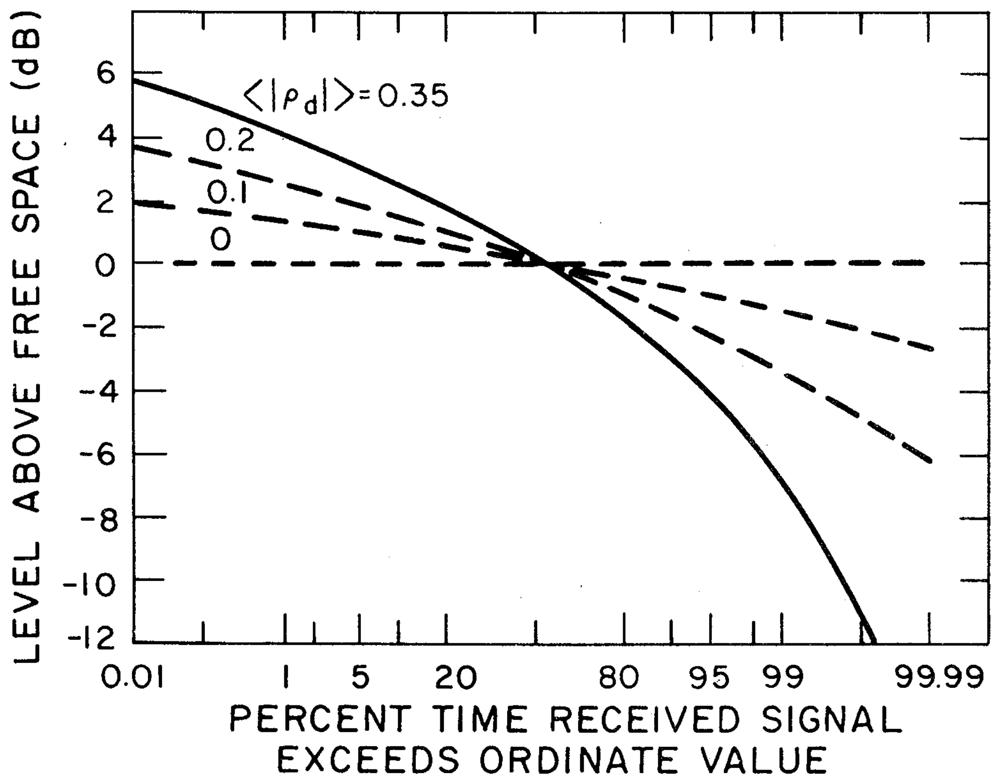

Figure 6.11. Amplitude distributions for signals consisting of specular-reflection and diffuse-scatter components, as a function of diffuse-scatter coefficient ρ_d (Beckmann and Spizzichino, 1963).

6.2.6 Statistical Characteristics of Multipath Signals

In considering the statistics of multipath signals received by moving mobile receivers, a distinction can be made between the rather rapid fluctuations that occur over short distances of a few tens of wavelengths when the mean signal is essentially constant and the slower variations that occur as the vehicle moves over large distances and experiences shadowing losses (Jakes, 1974). For analysing the rapid variations, the received field intensity E(t) can be expressed as the sum of two components that are separated in phase by 90 deg such that

$$E(t) = x(t) \cos \omega t + y(t) \sin \omega t \tag{6.31}$$

The quantities $x(t)$ and $y(t)$ represent the amplitudes of two orthogonal terms, both assumed to have normal or Gaussian distributions with zero mean and the same variance σ^2 such that

$$p(x) = \frac{1}{(2\pi)^{1/2}\,\sigma}\, e^{-x^2/(2\sigma^2)} \tag{6.32}$$

and

$$p(y) = \frac{1}{(2\pi)^{1/2}\,\sigma}\, e^{-y^2/(2\sigma^2)} \tag{6.33}$$

where $p(x)$ and $p(y)$ represent probability densities. Assuming that $p(x)$ are statistically independent, their joint probability density $p(x,y)$ is given by

$$p(x,y) = p(x)\,p(y) = \frac{1}{2\pi\,\sigma^2}\, e^{-(x^2 + y^2)/2\sigma^2} \tag{6.34}$$

It is desirable to know the probability density of the total field intensity amplitude which will be designated by r. The relation between r, x, and y is $r^2 = x^2 + y^2$. To determine $p(r)$, one can begin by using the relation (Beckmann, 1967)

$$p(r,\phi) = p(x,y)\,J \tag{6.35}$$

where J is the Jacobian defined by

$$J = \begin{vmatrix} \dfrac{\partial x}{\partial r} & \dfrac{\partial y}{\partial r} \\[2ex] \dfrac{\partial x}{\partial \phi} & \dfrac{\partial y}{\partial \phi} \end{vmatrix} \tag{6.36}$$

The derivatives shown can be evaluated by noting that

$$x = r\cos\phi \tag{6.37}$$

and

$$y = r\sin\phi \tag{6.38}$$

from which

$$J = \begin{vmatrix} \cos\phi & \sin\phi \\ -r\sin\phi & r\cos\phi \end{vmatrix} = r\,(\cos^2\phi + \sin^2\phi) = r$$

so that

$$p(r,\phi) = \frac{r}{2\pi\sigma^2}\, e^{-r^2/2\sigma^2} \tag{6.39}$$

To obtain p(r) one can integrate with to ϕ from 0 to 2π with the result that

$$p(r) = \frac{r}{\sigma^2}\, e^{-r^2/2\sigma^2} = \frac{2r}{\alpha}\, e^{-r^2/\alpha} \tag{6.40}$$

where $\alpha = 2\sigma^2$ is the mean square value of p(r). This function is known as the Rayleigh probability density function. The forms of the Rayleigh and normal density functions are shown in Fig. 6.12, where b_o takes the place of σ^2 of Eq. (6.40).

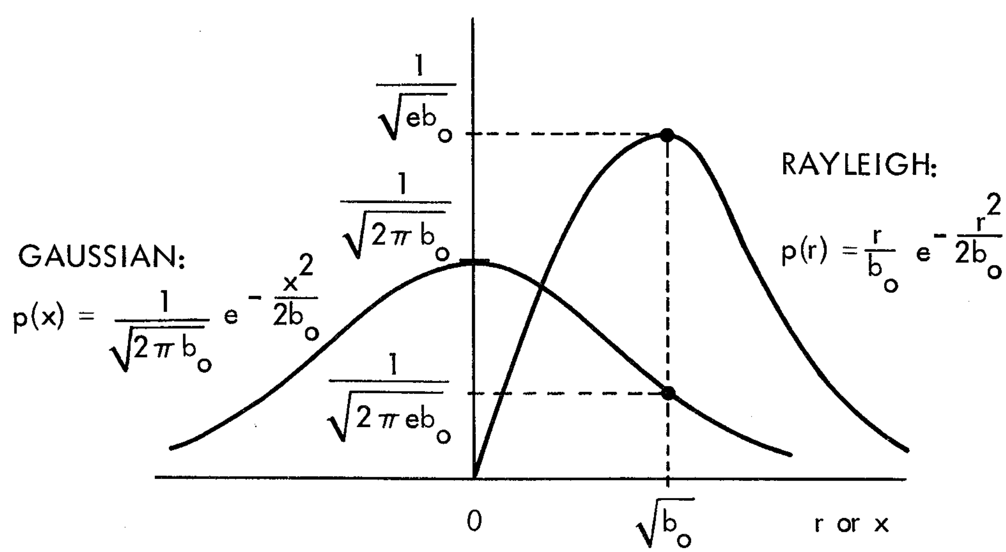

Figure 6.12. Normal and Rayleigh probability density functions (Jakes, 1974).

The probability density for phase in this case $p(\phi)$ is uniform with $p(\phi) = 1/2\pi$ for $0 \leq \phi \leq 2\pi$. Considerable evidence exists to the effect that the signal received by a land mobile receiver in ground-to-ground service is Rayleigh distributed on a local scale. A good approximation to a Rayleigh distribution may occur for as few as four to six multipath components (Schwartz et al., 1966). In some cases when the number of rays is very small, however, the Rayleigh distribution may not apply. The Rayleigh distribution can be considered to be a special case of more general distributions including the m distribution (Panter, 1972) and the Weibull distribution (Beckmann, 1967; Shepard, 1977), and forms of these distributions may be applicable when the Rayleigh distribution is not not.

The logarithmic or decibel forms of the slower deeper variations in mean signal level tend to follow the normal distribution and to have a probability distribution of the form of

$$p(x) = \frac{1}{(2\pi)^{1/2}\,\sigma}\, e^{-(x - x_o)^2/2\sigma^2} \qquad (6.41)$$

where $x = \ln y$ with y being the actual field intensity and $x_o = \ln y_o$ with y_o the mean field intensity. To obtain the probability density of field intensity y one can use $p(x)\,dx = p(y)\,dy$ and note that as $x = \ln y$, $dx = dy/y$ so that $p(y) = p(x)/y$ and

$$p(y) = \frac{1}{(2\pi)^{1/2}\,\sigma\, y}\, e^{-[\ln (y/y_o)]^2/2\sigma^2} \qquad (6.42)$$

This probability density is known as the lognormal probability density function.

The probability density of the sum of a constant vector and a signal following the Rayleigh distribution, such as the sum of the direct line-of-sight and diffuse scatter components for land-mobile satellite transmissions, is the Rice or Rice-Nakagami distribution (Norton et al., 1955; Beckmann and Spizzichino, 1963; Beckmann, 1967). The form given by Beckmann for total electric field intensity r is

$$p(r) = \frac{2r}{\alpha} e^{-(r^2 + c^2)} I_o(2cr/\alpha) \tag{6.43}$$

where c is the field intensity of the constant component, α is the value appearing in the Rayleigh distribution [Eq. (6.40)], and I_o is the modified Bessel function of the first kind and zero order. For application to land-mobile operation it is useful to have an expression for signal power written in terms of K, the ratio of power in the steady component to power in the random or diffuse component. A relation given by Davarian (1985) and utilized by Vogel and Smith (1985), etc. is

$$p(s) = (1 + K) e^{[-s(1 + K) - K]} I_o 2[s(1 + K) K]^{1/2} \tag{6.44}$$

where s is signal power.

Because of its pertinence to satellite or terrestrial land mobile service, attention has been given to combinations of Rayleigh and lognormal fading and Rician and lognormal fading. Rayleigh fading tends to be associated with diffuse scatter, Rician fading with reflection and scatter, and lognormal fading with shadowing by trees, terrain, or structures [Hansen and Meno, 1977; Butterworth, 1985; Loo, 1985; Stutzman, 1985]. Loo (1985) analyzed the sum of Rayleigh and lognormal fading and noted that if the lognormal amplitude is temporarily held constant the resultant probability density is Rician.

6.2.7 Total Signal Amplitude

Factors affecting the total signal amplitude E, arising from the combination of direct and specularly reflected and diffusely scattered waves, can be summarized for linear polarization, using horizontal polarization as an example, by

$$E = E_o \left[1 + g_r(2\theta)\ \rho_s FD\ \rho_h e^{j\phi} + g_r(\theta_d)\ \rho_{hd}\right] \tag{6.44}$$

This expression gives no information about the variation of the parameters with time or how the specular and diffuse components combine but does point out the factors that are involved in determining E, which represents total electric field intensity in volts/meter. The quantity $g_r(2\theta)$ is voltage gain for the specularly reflected wave relative to that for the direct wave, with 2θ indicating that gain refers to an angle that differs by twice the elevation angle θ from that for the direct wave. The factor ρ_s is a roughness factor that is unity or less in magnitude and indicates the degree to which the smooth-earth specular reflection coefficient ρ_h is reduced by surface roughness. F is a factor that can be used to take account of blockage or shadowing by obstacles, including structures, terrain, or vegetation. The theoretical maximum value of F is two, which value would apply if propagation was via only the first Fresnel zone. In practice the value of F is found to be between 0.1 and 1.2 in the majority of cases. D is a divergence factor that takes account of the fact that reflection from a spherical earth tends to result in a decrease in reflected signal intensity as compared to reflection from a flat surface. D is approximately unity for angles θ above about 5 deg. The quantity ϕ represents phase shift due to the difference in path length for the direct and reflected waves. The reflection coefficient ρ_{hd} applies to diffuse scatter, and $g_r(\theta_d)$ stands for voltage gain relative to that for the direct path at an angle θ_d that is an average or effective angle for diffuse scatter Diffuse scatter takes place over a range of angles but θ_d is sometimes taken to be 2θ as for specular reflection.

The phase angle ϕ varies with the height of the receiving antenna above the reflecting surface in accordance with Eq. (6.7). For the simple situation when F = D = 1 and diffuse scatter is negligible, the normalized field intensity will fall within the limits of

$$1 \pm \left[\ |g_r(2\theta)|\ |\rho_{hs}|\ \right] \tag{6.45}$$

where $\rho_{hs} = \rho_h\, \rho_s$ of Eq. (6.44).

For circular polarization similar relations apply but specular reflection in that case results in the production of a cross polarized component as well as a component having the original polarization, as shown by Eqs. (6.18) and (6.19). Antenna gain for the cross polarized component is considerably lower than for the original polarization at the angle of the direct ray, but antenna gains for the specularly generated components may be comparable for large angles away from the direct ray. The antenna may have different phase responses for the two components. For $F = D = 1$ and neglecting diffuse scatter, the normalized output voltage of the antenna falls within the limits of

$$1 \pm [\ |g_{cr}(2\theta)|\ |\rho_{cs}| + |g_{xr}(2\theta)|\ |\rho_{xs}|\ ] \qquad (6.46)$$

where g_{cr} is the antenna voltage gain for the copolarized reflected wave, g_{xr} is the antenna voltage gain for the crosspolarized wave produced by reflection, ρ_{cs} is the rough-surface reflection coefficient for the copolarized wave, and ρ_{xs} is the corresponding coefficient for the crosspolarized wave.

6.2.8 Phase

The phase of the reflected signal, like the amplitude, is a function of relative dielectric constant and conductivity. Values of these parameters for a range of materials, including sea water, fresh water, ice, and ground, are shown as a function of frequency in Recommendation 527-1 (CCIR, 1986d). The phase of the reflection coefficient tends to be close to 180 deg for horizontal polarization for all values of elevation angle. For vertical polarization, the phase tends towards 180 deg for angles less than the Brewster angle [Eqs. (6.14) and (6.15) and Fig. 6.9] and 0 deg for angles greater than the Brewster angle (CCIR, 1986c, Jordan and Balmain, 1968).

6.3 SYSTEM-DESIGN CONSIDERATIONS

6.3.1 Multipath and Fading Measurements

Whereas Sec. 6.2 describes the physical phenomena of specular reflection and diffuse scatter, the present Sec. 6.3 treats related system-design considerations. Data on the effects of reflection and scatter are needed for system design, and Sec. 6.3.1 describes certain measurements that have been carried out in the recent past. Still more recent work conducted to satisfy the needs of land-mobile satellite systems is reported in Sec. 6.4. Section 6.3.2 deals with the techniques of equalization and diversity for combating multipath effects. Techniques applicable to analog and digital narrow-band systems are described in Secs. 6.3.3 and 6.3.4, respectively, and spread-spectrum systems are introduced in Sec. 6.3.5.

Multipath propagation tends to cause signal fading, and data on fading can be accumulated by making measurements of total signal amplitude under multipath-propagation conditions. In this section, however, the term multipath measurement is used in distinction from fading measurement. Fading is taken to refer to variations of signal amplitude under conditions involving no separation or distinction of the multipath components which contribute to fading. By the term multipath measurement, reference is made here to data taken with high time resolution so as to separate and distinguish the multipath signal components. Both multipath and fading data are useful in planning and analyzing performance of mobile communication systems.

One method of making multipath measurements is to transmit very short pulses and to record the signals received over the path of interest. This approach was used by Turin (1980) in a program that involved transmitting 100-ns pulses at carrier frequencies of 488, 1280, and 2920 MHz. Pulses at these three frequencies were transmitted simultaneously at a rate of one per second in urban areas of San Francisco, Oakland, and Berkeley. In such areas, multipath propagation can result from reflections from buildings and other structures as well as from the ground. For a dense, high-rise area, Turin included an illustration showing a signal having a delay of about 3 μs beyond the delay time for a direct line-of- sight path.

The amplitude of the delayed component was greater than that of the direct signal. In addition to field measurements, Turin carried out simulation of multipath propagation and analysis of optimal receiver characteristics for multipath conditions. A problem with the use of short pulses is that as pulse width is reduced peak power must be increased to maintain a sufficient signal-to-noise ratio, and there are practical limits to increasing peak power.

Another approach to multipath measurements involves broadband biphase pseudorandom modulation of the transmitter output and correlation of the received signal with a replica of the transmitted waveform. The use of broadband modulation supplies the needed time resolution and avoids the peak-power problem encountered when using short pulses. The RAKE technique (Price and Green, 1958; Bitzer, 1966; Barrow et al., 1969) involves the use of a tapped delay line as part of the receiving system. The appearance of the delay line and taps on circuit drawings suggests the prongs of a garden rake, and that is the basis for the name of the technique. In the investigations by Barrow et al. of multipath effects associated with tropospheric scatter at 900 MHz, the delay line had ten taps spaced by 0.1 μs and thus covered a total delay of 1 μs. The output of each tap in such a system is correlated with the received signal to obtain data on signal amplitude as a function of time delay τ. The Fourier transform of the correlation functions are taken to obtain power spectral densities $V(\tau,\nu)$ where ν is Doppler frequency. Data are then displayed as three-dimensional plots showing amplitude as a function of time delay and Doppler frequency.

Cox (1973) has carried out studies of propagation at 910 MHz in the urban environment of New York City, the interest being in terrestrial mobile radio service. Some of his work in New York was carried our with a RAKE-like receiver and also presented as three-dimensional plots of signal amplitude as a function of time delay and Doppler frequency. Excess time delays up to about 10 μs were observed but a large fraction of the total signal power occurred for delays of 2 μs or less.

Wideband propagation measurements have been carried out by the Institute for Telecommunication Sciences, National Telecommunications and Information Administration (ITS/NTIA) and the U.S. Army Communications Electronics Command.

Instrumentation development and measurements on 11.8 and 27.2 km line-of-sight paths were conducted by ITS (Espeland, Violette, and Allen, 1984). A system operating at 30.3 GHz utilized biphase modulation by a pseudorandom code at a clock rate of 500 MHz with code lengths of 127 or 32,767 bits. The code rate provided a time resolution of about 2 ns, and the code lengths of 127 and 32,767 bits allowed covering delay spreads of about 0.25 μs and 66.7 μs respectively. Rather than using a tapped delay line as in RAKE receivers, the clock at the receiver operates at a few Hz slower than that of the transmitter with the result that in about a one-second period all bits of the receiver code slide by the received signal. When all the ones and zeros of the two codes or words (receiver and transmitted signal) coincide, a useful output is obtained. One does not need to take the Fourier transform of the correlation function and, if the Doppler frequencies are not of very great interest, one can display signal amplitude as a function of time in a series of two-dimensional plots. In addition to the 30.3 GHz transmissions for which bit error rate (BER) was recorded, coherent CW transmissions were utilized at 11.4, 28.8, and 96.1 GHz.

Measurements emphasizing propagation studies under conditions of irregular terrain and vegetation were carried out cooperatively by ITS and the Army Electronics Command (Hufford et al., 1983; Sass, 1983). In one phase impulses lasting 340 ns were transmitted once a second at frequencies of 600, 1200, and 1800 MHz. Biphase modulation, utilizing a 150 MHz clock rate and a 511-bit code, provided a resolution of better than 10 ns and a measurable delay spread of 3.4 μs.

Results of fading measurements that were carried out to aid in designing land mobile satellite systems are given in Sec. 6.4.

6.3.2 Equalization and Diversity

Equalization is a technique for combating distortion in transmission systems, and space and frequency diversity are measures to ameliorate fading due to multipath propagation, attenuation due to rain, etc. A comprehensive treatment of these topics is not given here, but mention is made of certain aspects.

Amplitude equalization has been commonly used to compensate for distortion caused by differential attenuation of the component frequencies of signals. For digital systems, however, adaptive transversal equalizers that compensate for both amplitude and delay distortion have been used. These equalizers utilize tapped delay lines much like those used in RAKE receivers. Figure 6.13 shows a form of an adaptive equalizer. The signals having delays indicated by $x(t \pm iT)$ feed into amplifiers having gains which can be adjusted to provide an optimum output $h(t)$. The use of such equalizers is not restricted to broadband systems. A definitive tutorial paper on the subject (Qureshi, 1982) refers to the use of adaptive equalizers for combating distortion on lines that are used to transmit digital data at 2400 bps.

Space diversity, which can be accomplished with antenna spacings of one-half wavelength, has received attention as a means of combating fading (Jakes, 1974). Signals from arrays of antennas may be combined by maximal ratio diversity combining which is coherent and adaptive. Yeh and Reudink (1982) have pointed out the virtue of coherent space diversity combining in dealing with interference and advocated its use to achieve efficient spectral utilization. The advantage with respect to interference is that the wanted signals combine coherently while interfering signals combine incoherently. The advantage of space diversity in mobile systems must be weighed against the increased complexity and cost of antenna arrays and circuits for coherent combining.

Spread spectrum systems, described in the following Sec. 6.3.4, provide frequency diversity. Copper and Nettleton (1983) state that a margin of 20 to 30 dB is typically required for multipath fading in narrowband systems, whereas a margin of about 2 to 3 dB may be needed for spread spectrum systems. The basis for the improvement is that all of the frequencies within the broad bandwidth of spread spectrum systems do not fade simultaneously.

The concept of coherence bandwidth is pertinent to consideration of frequency diversity. It was pointed out by Jakes (1974) that electric field intensity under multipath conditions may be represented in the following manner.

$$E_z(\omega,t) = E_o \sum_{n=1}^{N} \sum_{m=1}^{M} C_{nm} \cos\left(\omega t + \omega_n t - \omega T_{nm}\right) \qquad (6.47)$$

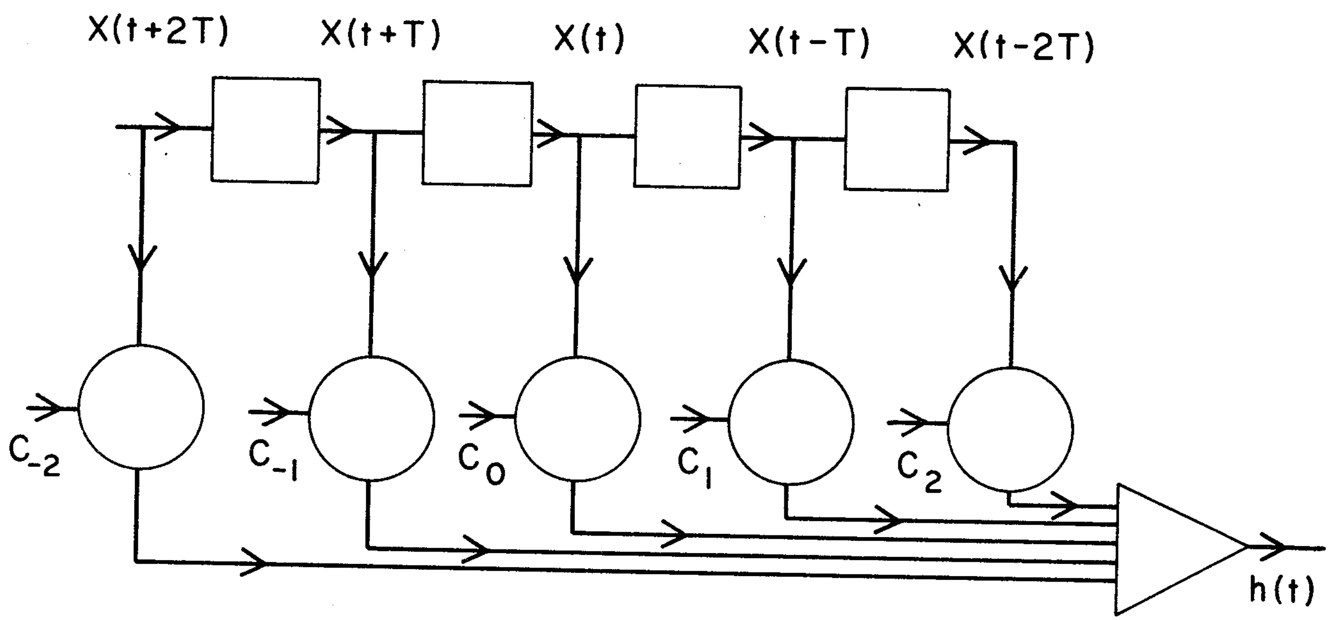

Figure 6.13. Form of adaptive equalizer.

The quantities E_z and E_o are electric field intensities, ω_n is Doppler frequency, and T_{nm} represents time differences between the multipath signal components. The phase ωT_{nm} typically has a value of hundreds of radians, and it can be readily appreciated that a rather small change in angular frequency ω results in a significant change in phase. The analysis by Jakes shows that the coherence bandwidth B_{coh} for the envelope correlation to reach a value of 0.5 is given by

$$B_{coh} = 1/(2\pi\sigma) \tag{6.48}$$

where σ is the time delay spread of the multipath components, as determined by the techniques of Sec. 6.3.1. If σ is 1 μs, for example, B_{coh} is 159 kHz, and if σ is 0.25 μs B_{coh} is 637 kHz. Coherence bandwidths typically vary between about 100 kHz and 1 MHz. Systems having significantly wider bandwidths can provide beneficial frequency diversity.

6.3.3 Narrowband Analog Systems

It is Sec. 6.4 that is devoted specifically to land-mobile systems, but we note here that only a very limited spectrum may be available for these systems. It is important, therefore, to use this spectrum efficiently. Whereas conventional land-mobile systems may utilize a bandwidth of 30 kHz for an audio channel, employing FDMA (frequency-division multiple access), an effort is being made to utilize bandwidths as low as 5 kHz or lower for the same purpose in land-mobile satellite service. Second-generation land-mobile satellite systems may use narrowband digital techniques to acheive operation with 5 kHz channels, but a number of the parties that have applied for licenses for first-generation systems plan to use analog single-sideband systems. In this Sec. 6.3.3, we describe an antimultipath technique that appears to have merit for such service. For a more nearly complete treatment of single-sideband operations see Sec. 10.6. Sec. 6.3.4 mentions digital narrow-band operations briefly and points out that a pilot-tone technique may be advantageous for digital as well as analog narrow-band systems.

One of the possible modulation techniques for audio communication over land-mobile systems is companded single sideband. This technique is efficient in use of bandwidth, and companding reduces the signal-to-noise ratio that would otherwise be required (Sec. 10.6). The use of a transparent tone-in-band (TTIB) pilot tone with feed-forward signal regeneration (FFSR). has been investigated as a means of improving speech quality in mobile radio links subject to fading (Bateman et al., 1985). A notch filter removes a small portion of the audio signal and a tone then occupies the portion removed. The tone-in-band technique contrasts with the tone-above-band approach. FFSR utilizes identical delays in parallel signal and control (pilot-tone) paths to provide improved operation in fading environments. Let the signal at a point in the receiver be represented by

$$y(t) = E\, r(t) \cos [\omega_1 t + \omega_p t + \phi(t)] + S\, r(t) \cos [\omega_1 t + \omega_s t + \phi(t)] \tag{6.49}$$

with $r(t)$ and $\phi(t)$ representing unwanted amplitude and phase modulations. E represents the pilot tone, and ω_p is its angular frequency; S represents the signal, and ω_s is its angular frequency. The audio signal and pilot tone then pass through parallel paths characterized by identical delays and a control signal

$$n(t) = \frac{C}{r(t)} \cos [\omega_o + \phi(t)] \tag{6.50}$$

is developed in the control path, with C a constant and ω_o another IF frequency. Mixing the audio and control signals then results in

$$y_o(t) = \frac{SC}{2} \cos [\omega_s t + (\omega_1 - \omega_o)t\,] \tag{6.51}$$

and, if $\omega_1 = \omega_o$, the desired audio signal is recovered. This technique requires that the frequency of the audio signal and the fading frequencies be separable. As pointed out in Sec. 6.4, such separation appears to be possible as the maximum fading frequency can be expected to be in the order of 150 Hz for carrier frequencies near 850 MHz (Vogel and Smith, 1985).

6.3.4 Narrowband Digital Systems

A pronounced trend towards digital transmission is taking place, and considerable attention is directed towards Integrated Services Digital Networks (ISDN's). A related development for our purposes is that considerable effort is being devoted to achieving near toll quality digital speech at 4800 bps, utilizing 5 kHz channels. Research has been carried out at the Georgia Institute of Technology (Barnwell, 1985), the University of California, Santa Barbara (Gersho, 1985), the Jet Propulsion Laboratory (Townes, 1985; Simon, 1985; and Divsalar, 1985), and at General Electric (1985). Pilot-tone techniques similar to those mentioned in Sec. 6.3.3 for companded single-sideband systems are being considered. General Electric has analyzed both TTIB (Transparent-Tone-In-Band) and TCT (Tone-Calibrated Technique) measures and has asserted that TCT is more bandwidth efficient than TTIB. Linear predictive coding (LPC) is discussed by Townes as one of the narrowband techniques of interest. A description of the various coding methods is outside the scope of this report but persons working with link design and propagation effects should be aware of the work that is going on in this area.

6.3.5 Spread-spectrum Systems

The frequency diversity provided by broadband systems was referred to in the previous Sec. 6.3.2. Broadband systems which achieve their broad bandwidth by use of a signal other than the information being transmitted are defined as spread-spectrum systems. Such systems can be useful for conducting multipath measurements; the systems described in Sec. 6.3.1, other than the narrow-pulse systems, are spread-spectrum systems. Also the Global Positioning System (Sec.6.7) is a spread-spectrum system. Spread-spectrum systems are also useful for communication purposes.

Shannon's law shows the roles of bandwidth B and signal-to-noise ratio S/N in determining communication capacity as indicated by

$$C = B \log_2 (1 + S/N) \tag{6.49}$$

where C is the maximum theoretical communication capacity in bits per second. The value of C given by the equation can not be reached in practice, but the expression correctly indicates that a certain capacity can be achieved by using a high value of S/N and a low value of bandwidth B or vice versa. Spread-spectrum systems utilize a large bandwidth B and therefore operate with a low signal-to-noise ratio. They employ bandwidth expansion factors typically in the order of 100 to 1000 (ratio of transmission bandwidth to signal bandwidth).

The principal ways of spreading the frequency spectrum beyond that of the information content are use of direct sequence (DS), frequency hopping (FH), time hopping, and FM chirp techniques (Dixon, 1976). Attention is given here to the DS and FH techniques. By direct sequence, reference is made to modulation of the carrier by a code sequence. The most common technique is to use 180 deg biphase phase shift keying. The RF bandwidth B after modulation at a 10 Mbps code rate, for example, is 20 Mbps. If the data bandwidth in this case is 20 kbps, the ratio of bandwidths is 2000 or 33 dB. This ratio is referred to as processing gain (PG). Thus

$$PG = 2R_c/R = B/R \tag{6.50}$$

where R is the data bit rate and R_c is the code bit rate. Processing gain B/R relates carrier signal-to-noise ratio C/X and energy per bit to noise power density ratio E_b/N_o after demodulation by

$$E_b/N_o = (C/X)\ (B/R) \tag{6.51}$$

Assuming, for example, that an E_b/N_o ratio of 10 is needed and that B/R is 2000, C/X can be 0.005, corresponding to the signal being buried in noise, and the needed value of E_b/N_o can still be achieved. Figure 6.14 illustrates power spectra of data and spread signals in spread-spectrum systems. One form of a direct sequence spread-spectrum system is shown in Fig. 6.15. Here the carrier is modulated by the information to be conveyed before being modulated by the code sequence. An alternative procedure is to modulate the code sequence by the information. At the receiver a heterodyne arrangement is shown for obtaining the correlation bvetween the code modulated carrier and the receiver code. The signal appears as modulation of the IF frequency at the input and output of the IF amplifier. The demodulation process recovers the narrowband baseband signal. Interference or a signal carried by a different code appears as broadband noise at the output of the mixer, and only a small fraction of this noise passes through the IF amplifier and appears at the demodulator output.

Spectrum is a valuable resource, and it might appear that spread-spectrum systems are wasteful of bandwidth. A major virtue of spread-spectrum systems, however, is that a number of users can employ the same frequency band at the same time by using different codes. The procedure for doing so is referred to as code division multiple access (CDMA). Such CDMA systems provide privacy, but not complete security, as well as freedom from mutual interference for multiple users of the same bandwidth. A principal reason for discussing spread-spectrum systems here, furthermore, is that they constitute a means for combating multipath fading (Sec. 6.3.2). Also some spread-spectrum satellite systems are in use, and propagation effects encountered by such systems deserve consideration. An advantage of CDMA for mobile communications is that each user can be given a code and allowed to enter the system freely, up to some number. Protocol and network management functions can be reduced to a bare minimum as it is not necessary for users to request and receive channel assignments.

RAKE-type receivers, using a tapped delay line as described in Sec. 6.3.1, have application to spread-spectrum systems (Turin, 1980; Proakis, 1983). They are used for selecting, combining, and/or weighting the individual multipath components to provide the optimum signal-to-noise ratio much as for adaptive equalizers (Sec. 6.3.2). For direct sequence spread-spectrum systems to function, close synchronization must be maintained between the transmitter and receiver. The simplest technique for providing synchronization involves the use of a sliding correlator such as that mentioned in Sec. 6.3.1. The sliding correlator operates with a code sequence that has a rate slightly different from that of the transmitter so that the two sequences slip in phase with respect to each other initially but lock in phase when the point of coincidence is reached. In some FH systems no synchronization of the mobile units is required (Cooper and Nettleton, 1978).

Further attention is given to spread-spectrum systems in Sec. 10.7.

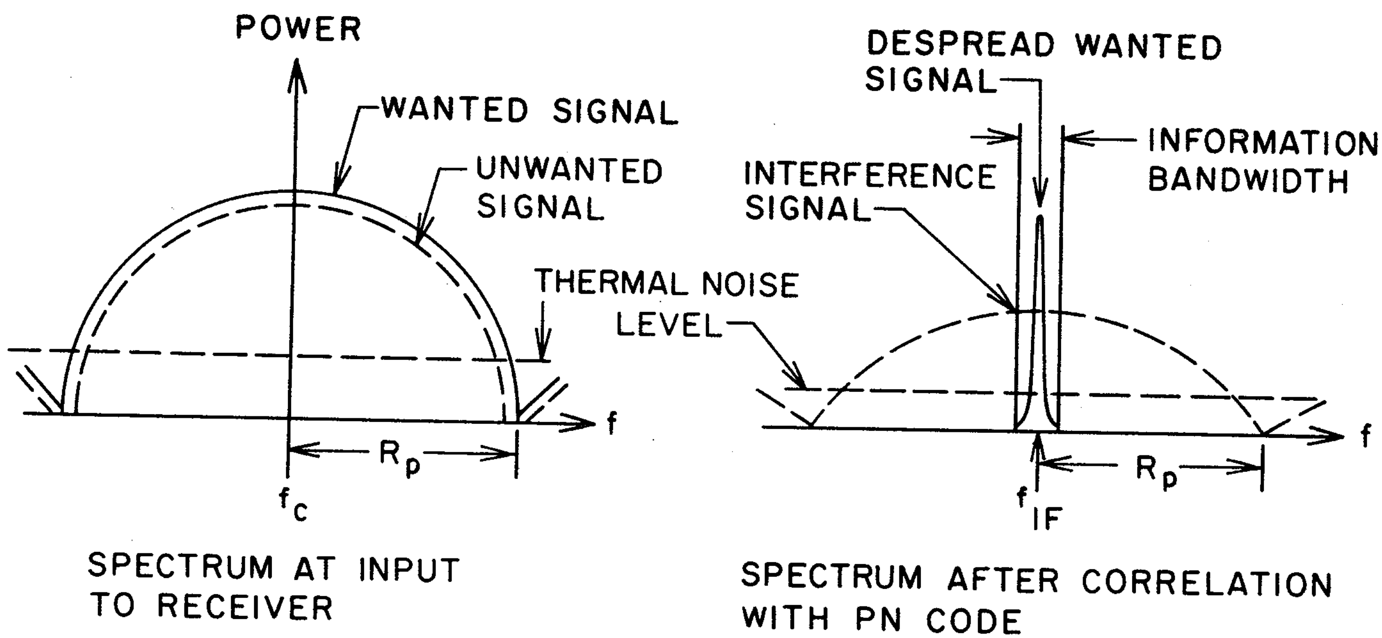

Figure 6.14. Power spectra of wanted and unwanted signals in PN spread-spectrum system.

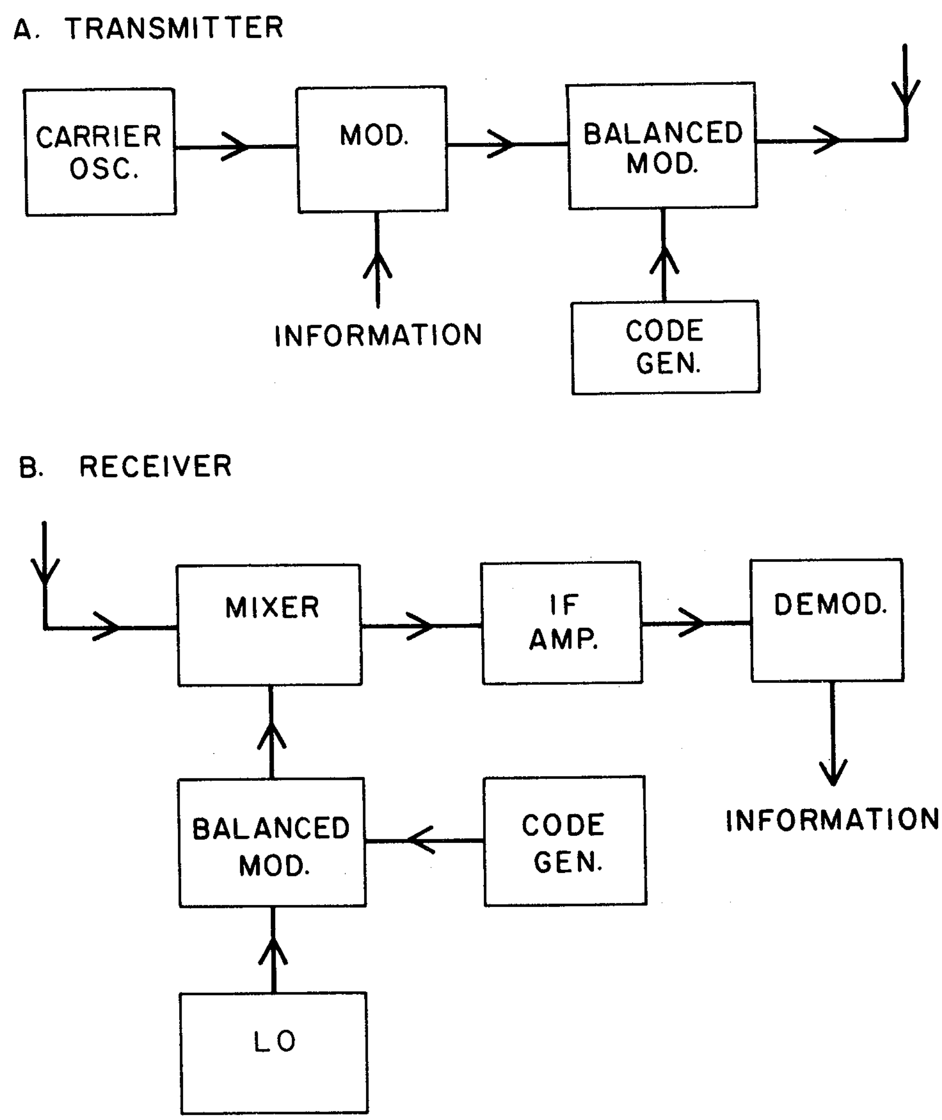

Figure 6.15. Block diagram illustrating direct-sequence spread-spectrum system.

6.4 LAND-MOBILE SATELLITE SYSTEMS

NASA, with the Jet Propulsion Laboratory playing a major role, has been actively carrying out programs to facilitate the implementation of a land-mobile satellite system since about 1980. The concept of a Land Mobile Satellite Service (LMSS) was described by Knouse (1980), and an early design of an LMSS system was prepared by Naderi (1982). Since the beginning close cooperation has taken place between NASA and the Canadian Department of Communications, and Canada has an active Canadian Mobile Satellite program, MSAT (Boudreau and Barry, 1983). In 1985 interest in land-mobile satellite service intensified. A Propagation Workshop on MSAT-X, an experimental program to obtain needed data and develop techniques (Weber and Naderi, 1983), was held at JPL on Jan. 30 and 31, 1985. Industry has shown strong interest, and twelve companies have applied to the FCC for licenses to offer land-mobile service. A Mobile Satellite Industry Briefing at JPL in Nov., 1985 was attended by a large number of investigators and representatives of the companies who applied for licenses. At the time, the FCC had not indicated whether authorization would be granted for operation in portions of the 806 to 890 MHz band or for the L band (about 1500 to 1700 MHz). A July 28, 1986 decision favored the L band, but at the time of writing no licenses have been granted. The companies that have applied have plans for first-generation systems, which will tend to have relatively simple antennas, with many of the companies planning to use analog companded single-sideband modulation. JPL is concentrating attention on research and development on second and third generation systems which may employ large multibeam antennas on the spacecraft and sophisticated digital modulation techniques.

An earth-space path may experience specular reflection and diffuse scatter and resulting fading, as discussed in Sec. 6.2, but fixed earth stations can be designed to minimize such problems. Mobile satellite services are vulnerable to fading from the above causes for two principal reasons. One is that they must operate in a large variety of locations which cannot be selected or prepared in advance. A second major factor contributing to fading is movement of the vehicle. No matter how reliable the signal may be when the vehicle is stationary and in a favorable location, fading becomes a potential problem for a moving vehicle.

Certain measures can be taken to minimize fading. The use of directional antennas which discriminate against reflected rays is one important means. This approach is most effective in the case of satellites at rather high elevation angles, as contrasted to terrestrial services and low-angle satellites. Circular polarization has the favorable features of relatively low reflection coefficients, compared to horizontal polarization, and the fact that reflected rays above the Brewster angle tend to be predominantly cross polarized with respect to incident rays. As receiving antennas are designed for the transmitted polarization, they are insensitive to the orthogonal or cross polarized components of the reflected rays. Thus multipath fading, resulting from interference between direct and reflected rays, is minimized.

Specular reflection and diffuse scatter continue to be of concern to land mobile satellite operations, but certain measurements reported later in this section have tended to shift emphasis to shadowing by roadside trees, especially in the case of two-lane roads. In canyon country or mountainous areas, shadowing by terrain may be important. On broad interstate highways, specular reflection and diffuse scatter may predominate. Effects of vegetation were considered in Sec. 5.3, but the results to be mentioned in this section refer to conditions simulating those of earth-space paths. The situation in this case is quite different from that for propagation from one point to another on the Earth's surface, where the paths are close to horizontal and involve propagation through and/or diffraction over trees as in Fig. 5.2. For earth-space paths the geometry is like that shown in Fig. 6.19.

Measurements were made of signal intensities of transmission from the ATS-6 satellite to mobile receivers at 860 MHz and 1550 Mhz in a number of cities in the United States (Hess, 1980). The data reported were primarily from Denver. The excess path loss for 90 percent spatial coverage for 90 percent of the time for urban areas is about 25 dB and is quite insensitive to frequency. The statement is made that a comparable value for suburban/rural areas is under 10 dB. The probability density of signal intensity is found to be different from that of the Rayleigh distribution. Another study (Brisken et al., 1979) using ATS-1 and ATS-6 satellites determined that ground-reflection multipath and ignition noise affected satellite communications less than terrestrial mobile communications.

Canadian studies of propagation effects on land-mobile satellite service have been described by Butterworth and Mott (1983). A signal source in a helicopter was used in some of their studies. Vogel and Torrence (1984) have carried out measurements of signals received from balloons launched from the NASA high-altitude balloon facility at Palestine, Texas in October, 1983 and January, 1984. Table 6.1 shows some of their results. Shadowing by trees appeared to play a major role in causing the low signal levels shown in the table in the 99 percent column. In November, 1984, another balloon experiment was carried out, this time utilizing a balloon dedicated to the purpose (Vogel, 1985). A summary of propagation considerations related to land-mobile service was prepared by Vogel and Smith (1985).

Some results of measurements made in Canada and Texas are illustrated in Fig. 6.16. Such curves typically consist of two portions, one with the signal dropping rather slowly and the other with the signal dropping more rapidly. The first portion is believed to represent Rician fading, and the second portion is believed to due to lognormal fading caused by shadowing by trees (Butterworth, 1985; Stutzman, 1985). Data in terms of K values (ratio of direct power to multipath power) obtained by Vogel and interpreted by Smith (1986) are shown in Fig. 6.17.

The measurements using helicopters and balloons simulated earth-space propagation. Another useful method of simulation is by use of hardware. The Jet Propulsion Laboratory has designed and implemented an end-to-end hardware simulation of mobile satellite communication links. The simulator includes a propagation path simulator and interference transmitters for investigating propagation effects and interference (Davarian, 1987). Also included are provisions for studying Doppler effects (see following paragraph), band limiting, satellite nonlinearity, and thermal noise.

Table 6.1 Signal Power in dB Relative to Mean as a Function of Elevation Angle θ and Probability, Transmitter in High-altitude Balloon (Vogel, 1984).

Elevation Angle	Probability (percent)		
(degrees)	50	90	99
$10 < \theta < 35$	-1.0	-7.0	-18.0
$10 < \theta < 15$	-1.0	-9.0	-20.5
$15 < \theta < 20$	-1.0	-8.0	-18.5
$20 < \theta < 25$	-1.5	-9.8	-20.3
$25 < \theta < 30$	-0.8	-2.2	-8.2
$30 < \theta < 35$	-0.5	-1.2	-4.5

For $10 < \theta < 35$ and a probability of 99 percent, for example, the signal power is within 18 dB of the mean for 99 percent of the time, or more than 18 dB below the mean for 1 percent of the time.

Attention will now be given to the fading rate encountered under multipath conditions. Consider the situation depicted in Fig. 6.18, where scatter is received predominantly from a particular region. In this case, for a vehicle moving with velocity v, the frequency of the direct signal experiences a Doppler shift f_d given by

$$f_{d_1} = \frac{v_r}{\lambda} = \frac{v_r f}{c} = \frac{v \cos\theta \, f}{c} \tag{6.55}$$

where v_r is the component of velocity parallel to the path, θ is elevation angle, c is the velocity of light, and f is the transmitted frequency. The signal component scattered from the dominant scatterer, however, experiences a shift f_{d_2} given by

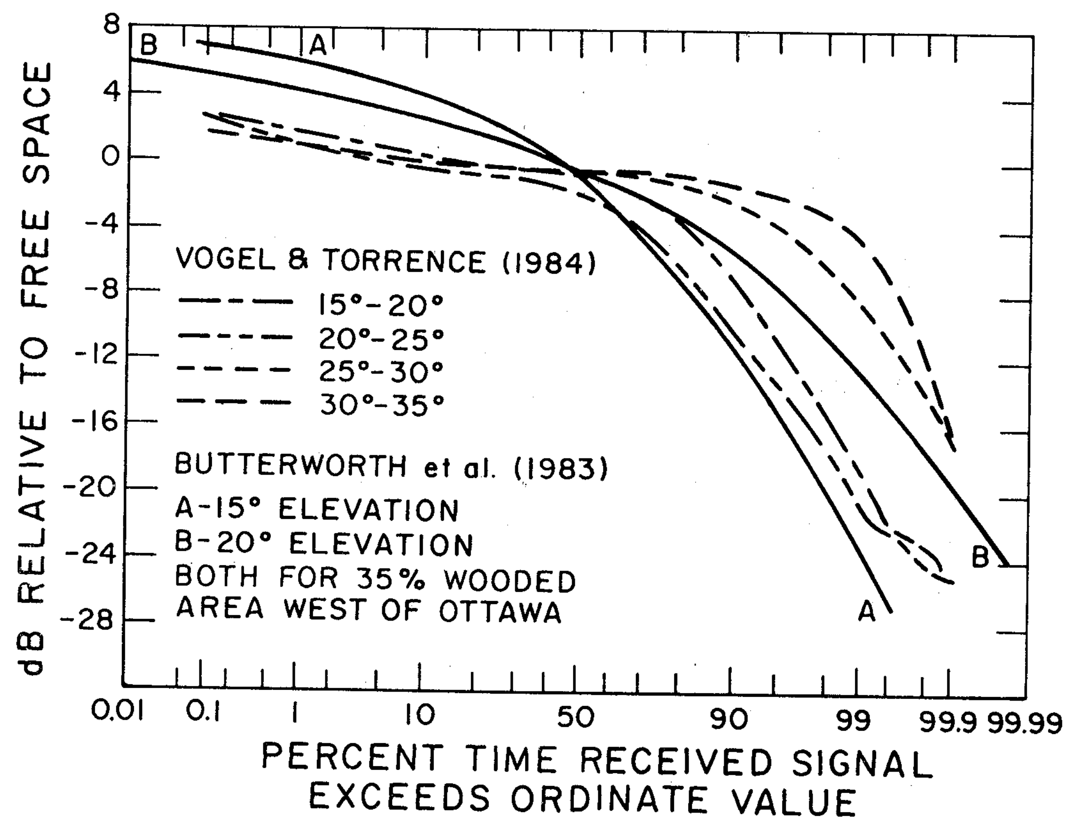

Figure 6.16. Statistical characteristics of simulated land-mobile signals.

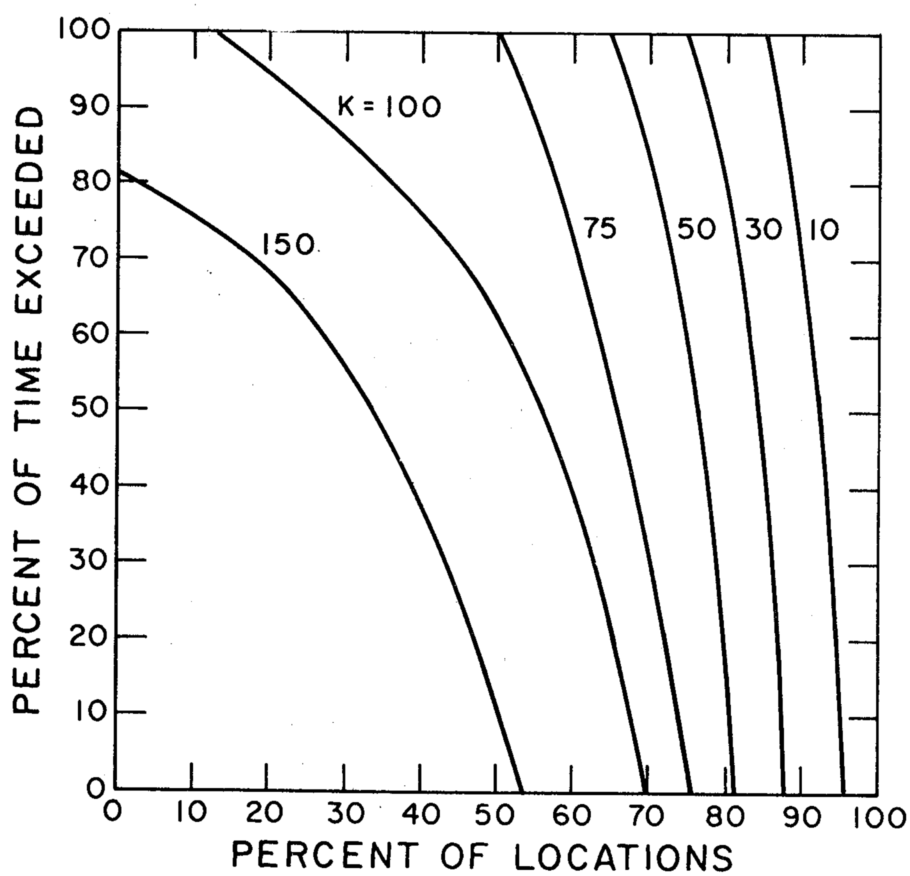

Figure 6.17. K values (ratio of power in steady component of signal to random component) as a function of location and time. Data by Vogel, interpreted by Smith (1986). Example: A K value of 75 is exceeded for about 74 percent of the time in 60 percent of the locations.

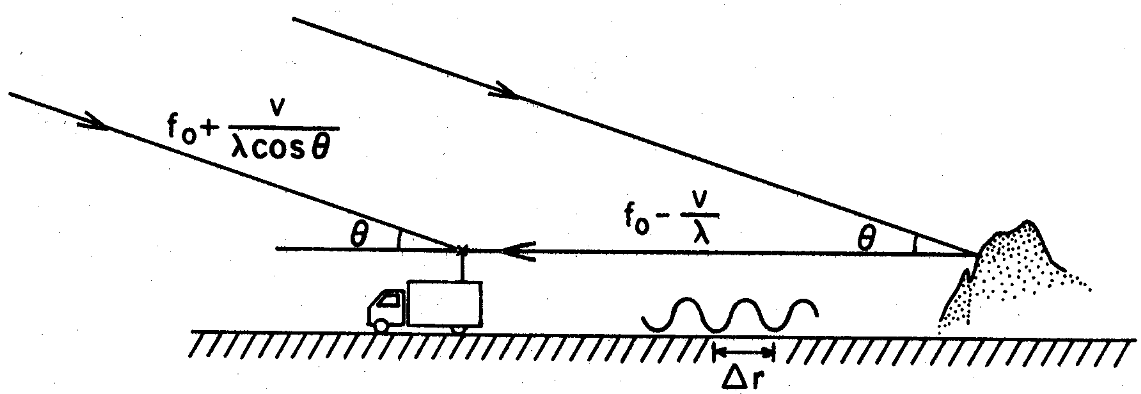

Figure 6.18. Doppler frequencies of land-mobile satellite signals received by moving vehicle.

$$f_{d_2} = -\frac{v\,f}{c} \tag{6.56}$$

so that the difference in the two Doppler shifts Δf is

$$\Delta f = f_{d_1} - f_{d_2} = \frac{v\,f}{c}\,(\cos\theta + 1) \tag{6.57}$$

In the limiting case for which $\theta = 0^{\circ}$

$$\Delta f = 2vf/c = 2v/\lambda \tag{6.58}$$

As in general $f_d = (1/2\pi)\, d\phi/dt$ where ϕ is phase

$$\phi = 2\pi \int \Delta f\, dt \tag{6.59}$$

where ϕ is the difference in phase between the two signal components. It is evident that ϕ varies linearly with time so that at one instant the two signals reinforce each other and at another time they interfere distructively, with the result that signal amplitude varies at the frequency Δf. For $v = 100$ km/h and $f = 850$ MHz, $\Delta f = 157$ Hz from Eq. (6.58). Thus an estimated maximum frequency of fading is 157 Hz. A standing wave of field intensity exists along the roadway with peaks in the standing wave pattern spaced $\lambda/2$ apart in the limiting case or $\lambda/(1 + \cos\theta)$ in general. The above discussion of fading rate follows that by Vogel and Smith (1985).

Measurements of shadowing on tree-lined roads and by single trees have been made by Vogel and Goldhirsh and coworkers at Wallops Island, Virginia and in Maryland using transmitters in drone aircraft or helicopters (Vogel and Goldhirsh, 1986; Goldhirsh and Vogel, 1987). Attenuations of about 2 dB/m at 869 MHz and 2.8 dB/m at 1500 MHz, with total attenuations of 10 to 20 dB, were recorded. The above attenuation constants of 2 to 2.8 dB are larger than those indicated by the use of $\alpha = 0.2\, f^{0.2}\, d^{0.6}$ of Chap. 5. Note, however, that the two situations (Figs. 5.2 and 6.19) are quite different. Most recently the same parties obtained data from canyons in Colorado showing that specular reflection from canyon walls caused fluctuations of ± 3 dB (Vogel and Goldhirsh, 1988).

Other possible propagation and environmental effects on land-mobile service include ionospheric scintillation, man-made noise, and multipath limitations on transmission at high data rates.

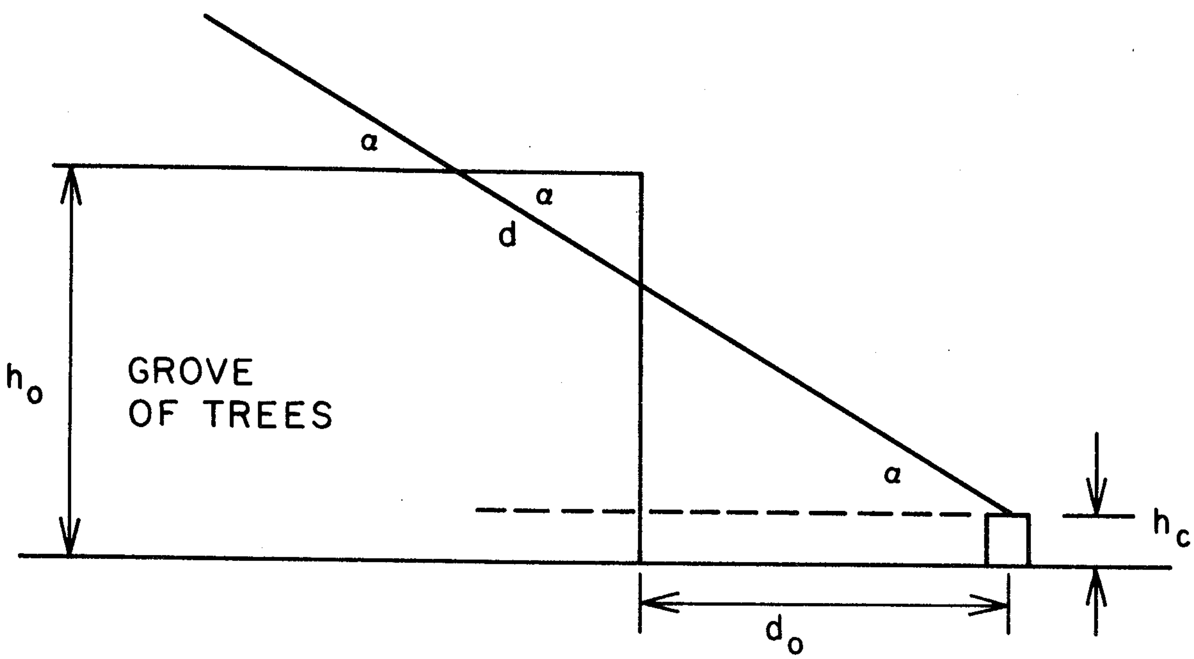

Figure 6.19. Idealized geometry for interception of satellite signal by grove of trees. (Applies to idealized single trees as well as grove).

Extrapolating from data given for 137 MHz (CCIR, 1986i), Smith (1986) estimated that at middle latitudes like that of Hamilton, MA about 2 dB peak-to-peak scintillation might occur for about 2 percent of the time at night at frequencies like 869 and 1500 MHz. At latitudes like that of Goose Bay, Labrador (or southern Alaska) such scintillation might occur for 7 percent of the time, and at latitudes like that of Narssarssuak, Greenland (or northern Alaska) scintillation of this magnitude could occur for 45 percent of the time. For man-made radio noise CCIR Report 258-4 (CCIR, 1986j) gives a formula for noise figure, F_{am}, of $c - d \log f$, with f in MHz for 0.3 to 250 MHz. Values of c and d are given for business, interstate highways, and rural areas. Using the expression beyond its stated limit to obtain an estimate of values for higher frequencies gives noise temperatures as shown in Table 6.2.

Table 6.2. Noise Temperatures for Man-made Noise (Smith, 1986).

Area	c	d	Noise Temperatures (K) 869 MHz	1500 MHz
Business	76.8	27.7	100	22
Interstate Highways	73.0	27.7	42	9
Rural	67.2	27.7	11	2.4

Propagation effects on satellite mobile service are treated in Report 884-1 on maritime mobile service (CCIR, 1986e) and Report 1009 on land mobile service (CCIR, 1986f), both in Volume V, Recommendations and Reports of the CCIR, 1986. In 1982 CCIR Report 884 dealt with both maritime and land mobile service. Volume VIII-3, Recommendations and Reports of the CCIR, 1986 also deals with satellite mobile service, including aeronautical, land, and maritime services. It emphasizes aspects other than propagation. In 1982 these satellite services were treated in sections of one larger Volume VIII devoted to Mobile Service.

6.5 MARITIME-MOBILE SATELLITE SYSTEMS

Maritime-mobile systems must contend with reflection and scatter from the surface of the oceans and seas. Serious ionospheric scintillation may be encountered at geomagnetic latitudes between about 20 deg N and S, especially at frequencies near 1.5 GHz and lower as reported in Sec. 2.6.4. Propagation at low elevation angles tends to present problems over water as well as over land, and serious effects have been reported and analyzed (Fang, Tseng, and Calvit, 1982; Fang and Ott, 1983; CCIR, 1986g).

The electric field intensity at a maritime-mobile receiving antenna, due to signals transmitted from a satellite, is the vector sum of components associated with the direct wave from the satellite, a specularly, coherently reflected wave, and a diffusely, incoherently scattered wave. The magnitude of the reflection coefficient for the specularly reflected wave is decreased below that for a smooth surface by a roughness factor which is described in Sec. 6.2.4 and shown specifically by Eq. (6.28). As the specular reflection coefficient decreases due to increasing roughness, diffuse scatter becomes important. Diffuse scatter is said to be dominant in practice, with normal sea conditions in most areas, but specular reflection plays a role in at least relatively smooth seas.

In CCIR Report 884-1 (CCIR, 1986e), it is assumed that a Rice-Nakagami distribution applies to the combination of a direct wave and diffuse scatter that is observed. In proposed modifications to Report 884, which however were not included in Report 884-1. models of sea surface characteristics as a function of wind speed are used to provide values of the C/M (carrier-tomultipath) ratio in dB versus wind speed for vertical, circular, and horizontal polarization. For small elevation angles, vertical polarization gives a better C/M ratio than circular or horizontal polarization. For large elevation angles, the reflected wave may have predominantly the orthogonal or cross polarization with respect to the circular polarization that is transmitted. The antenna is designed for the transmitted polarization and it discriminates against the orthogonal polarization with the result that circular polarization may have an advantage over vertical and horizontal polarization at large elevation angles. Figures 6.20 and 6.21 show examples of results obtained by use of the models mentioned.

The actual results in a particular case will depend on antenna gain as a function of off-boresight angle and polarization. Figure 6.22 shows reflection coefficients for a smooth plane sea. It can be appreciated that multipath tends to be less of a problem for vertical polarization because reflection coefficients are smaller for this polarization than for horizontal polarization (Fig. 6.22), and the same statement applies for circular polarization for angles less than and not too far above the Brewster angle. Link power budgets for the maritime mobile satellite service are treated in CCIR Report 760-1 (CCIR, 1986h).

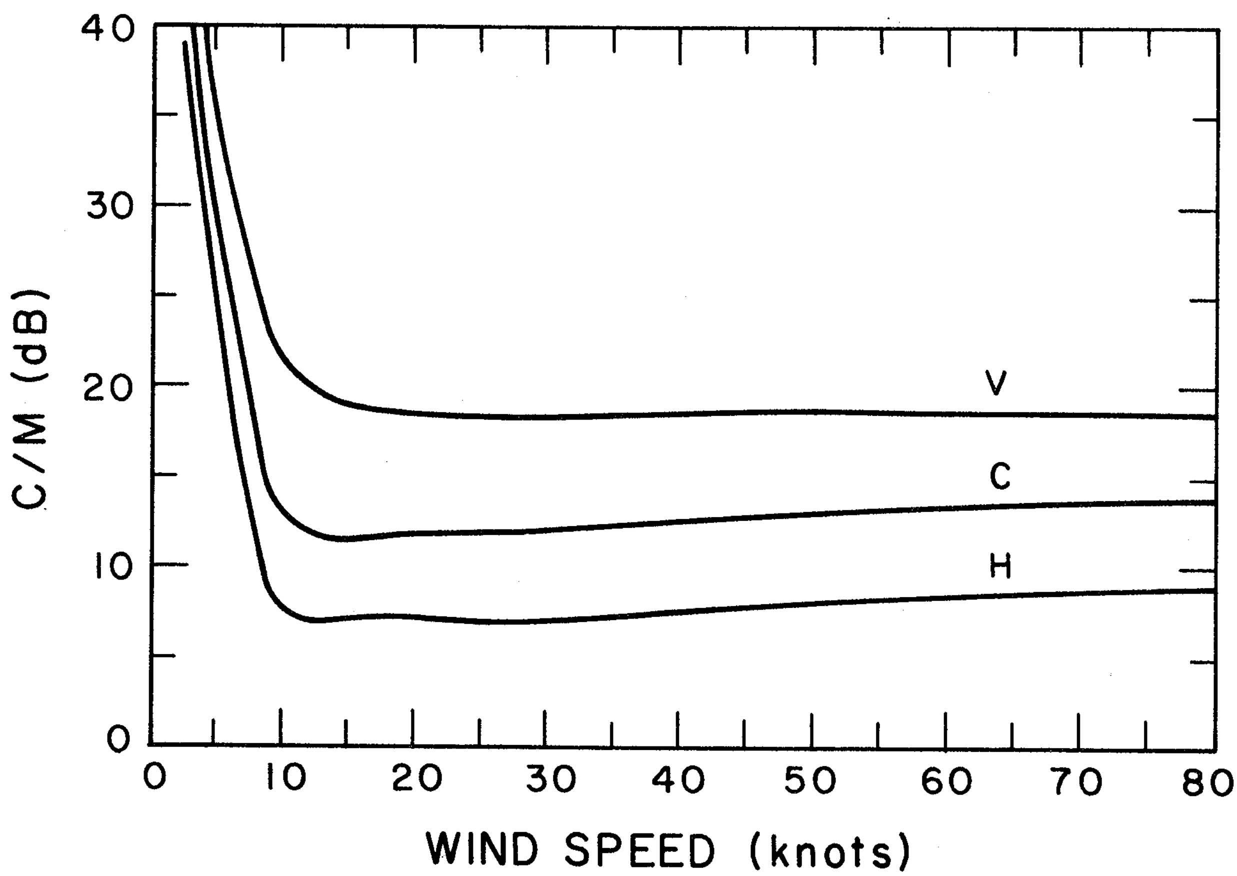

Figure 6.20. C/M ratio versus wind speed for antenna gain of 14 dB and elevation angle of 5 deg (CCIR, 1983).

On February 1, 1982. the International Maritime Satellite Organization (INMARSET) started to provide maritime service (da Silva Curiel, 1983). It took over and expanded the previous MARISAT system which commenced operation in 1976 and provided service for the Atlantic, Pacific, and Indian oceans with three MARISAT satellites. At first INMARSAT used the three MARISAT satellites, but the plan has been to use Maritime Communication Subsystems (MCS) on INTELSAT V satellites or MARECS satellites and to keep the MARISAT satellites as spares. Each satellite receives transmissions at 6 GHz from shore stations and translates them to 1.5 GHz for transmission to ships. Transmissions from ships to satellites are at 1.6 GHz and those from the satellites to the shore stations are at 4 GHz. An allowance of 4 dB for short-term fading was provided for the L-band links in the original MARISAT systems (Lipke et al., 1977).

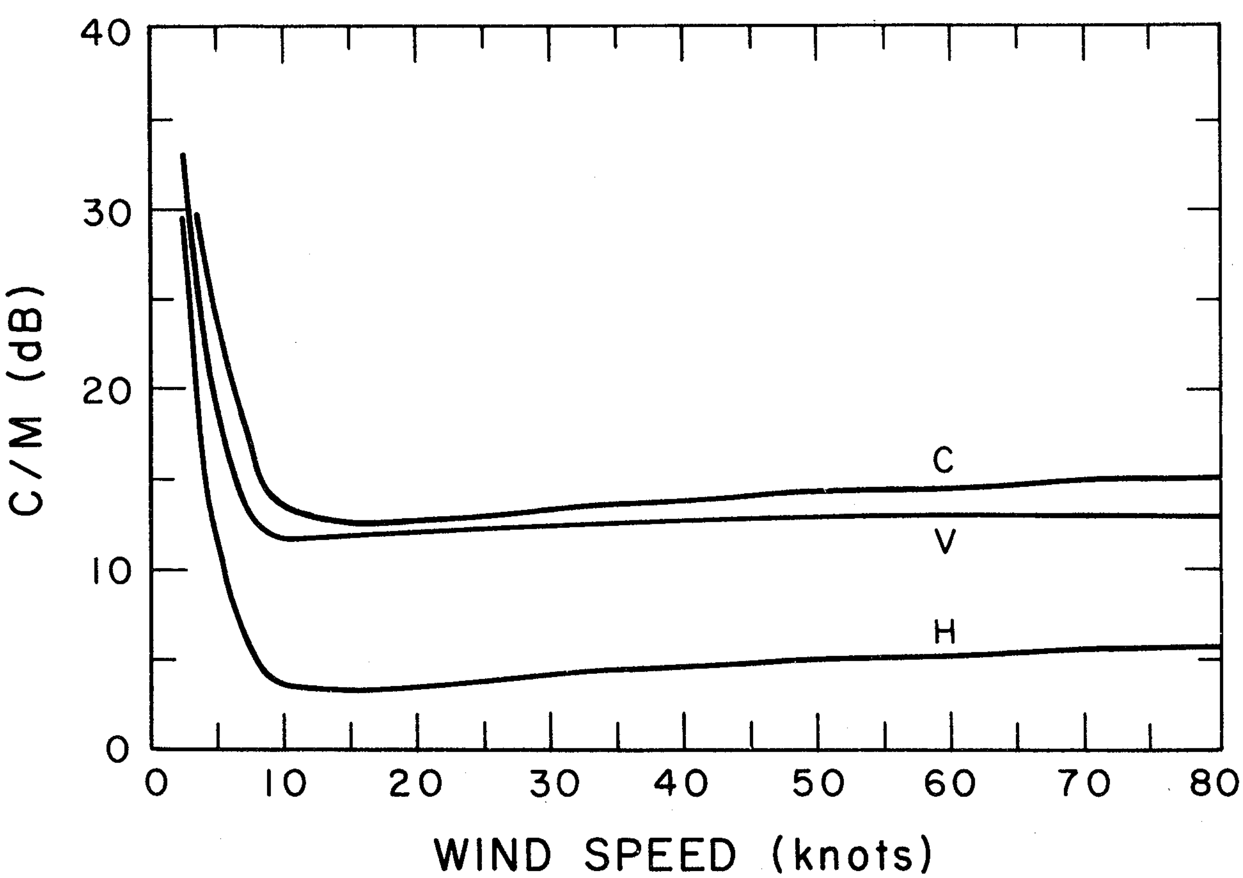

Figure 6.21. C/M ratio versus wind speed for antenna gain of 8 dB and elevation angle of 15 deg (CCIR, 1983).

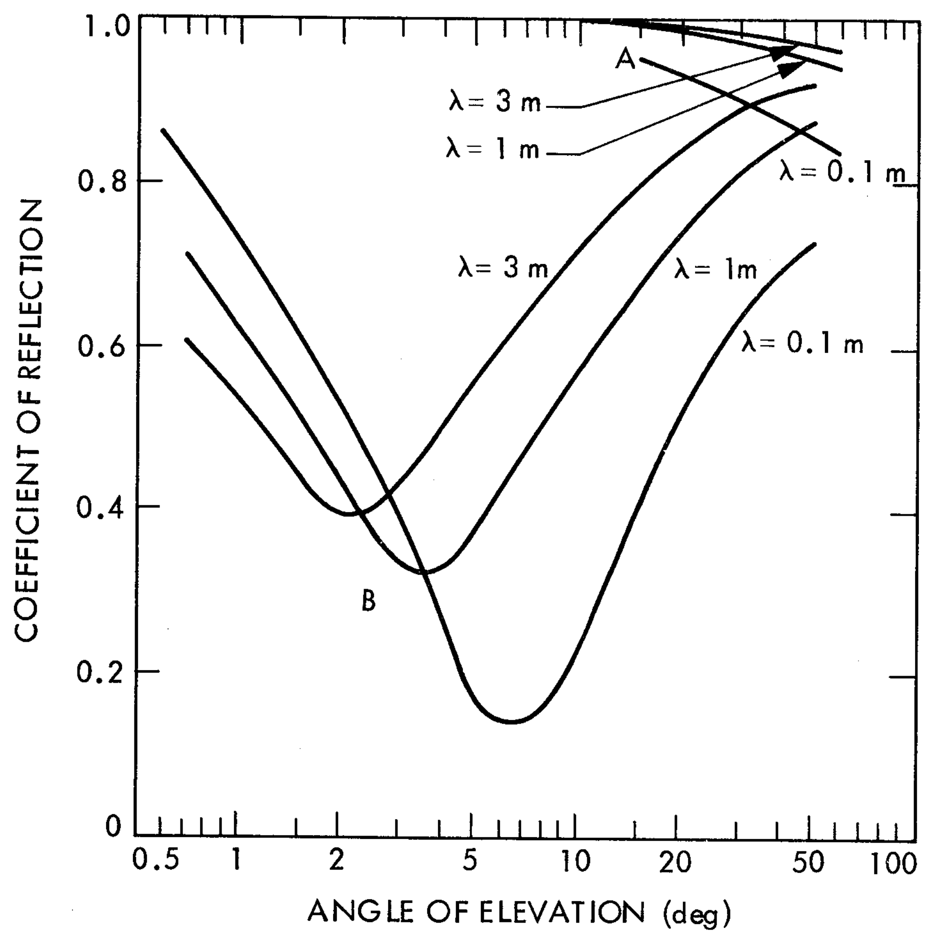

Figure 6.22. Reflection coefficients for smooth plane sea. A: horizontal polarization; B: vertical polarization (CCIR,1982).

6.6 AERONAUTICAL-MOBILE SATELLITE SYSTEMS

Because of the heights at which aircraft fly, aeronautical-mobile satellite operations involve considerations that may not be important for vehicles and ships that are confined to the Earth's surface. For surface operations, multipath propagation is of importance primarily because of the resulting fading. For aeronautical operations, however, time delays of the reflected rays with respect to the direct rays may be of importance as well. The time delay is greatest when an aircraft is directly beneath a satellite. For an aircraft at an altitude of 15 km, for example, the time delay of the reflected ray is 100 μs. For the north Atlantic air routes and a geostationary satellite at 30 deg of longitude, the delay times for aircraft between 8 and 17 km are between about 20 and 60 μs.

Multipath time delays may cause intersymbol interference but the time delays do not cause significant garbling of voice signals. The effect on digital transmission depends on the relative magnitude of the time delay and bit length. When the two periods are comparable, errors may arise unless remedial measures are taken. If the bit period is large compared to the propagation delay and sampling is done at the center of each bit period, problems are minimal.

For small elevation angles and aircraft heights above about 10 km, the reflection from a smooth surface is reduced by the Earth's curvature below the value for a plane earth. The factor by which the reflection coefficient is reduced is known as the divergence factor D (Beckmann and Spizzichino, 1963) and is illustrated in Fig. 6.23 for two different aircraft heights. Aircraft can range over land and sea and also over areas of ice and snow such as the Greenland ice cap and Antarctica. Reflection coefficients for such surfaces, consisting of snow which gradually changes with depth to compact snow and then to ice, are illustrated in Fig. 6.24.

Aircraft in flight pass through the maxima and minima of the interference pattern which is set up by reflection, and they experience fading which is a function of the applicable reflection coefficients. The vertical separation Δh_r between maxima of the

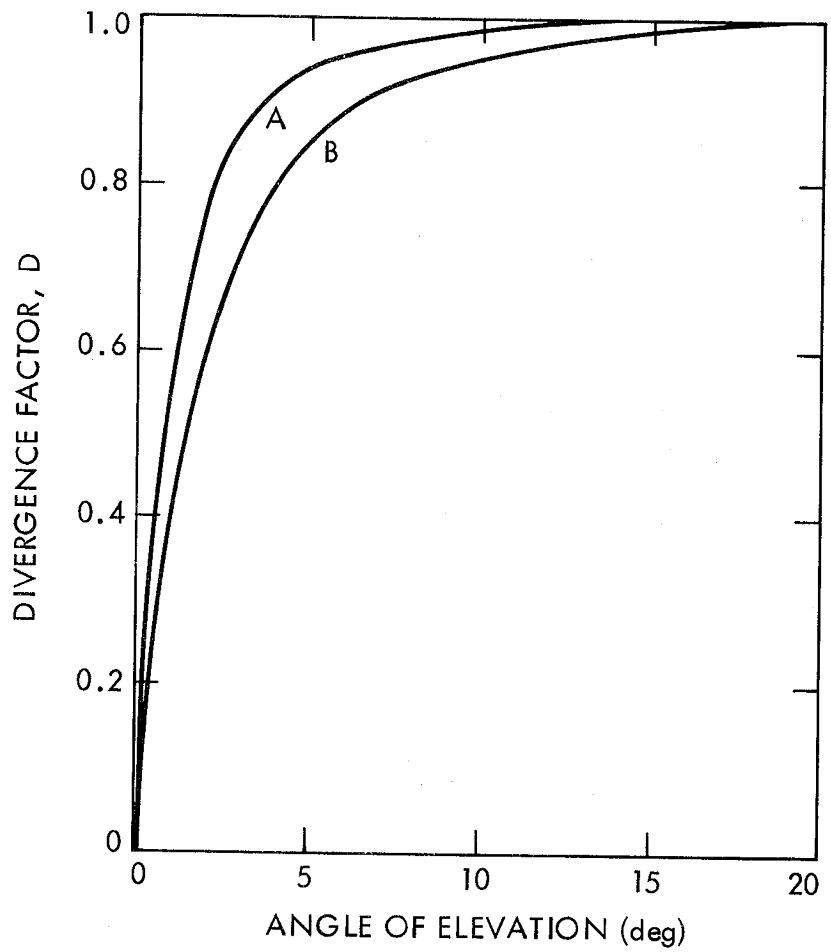

Figure 6.23. Divergence factors, D for reflection from a smooth spherical earth, A: aircraft at 3,000 m; B: aircraft at 10,000 m (CCIR, 1978).

interference pattern can be found from Eq. (6.8), assuming reflection from a plane surface, by setting

$$\frac{2\pi\Delta h_r \sin\theta}{\lambda} = \pi$$

from which

$$\Delta h_r = \frac{\lambda}{2\sin\theta} \tag{6.60}$$

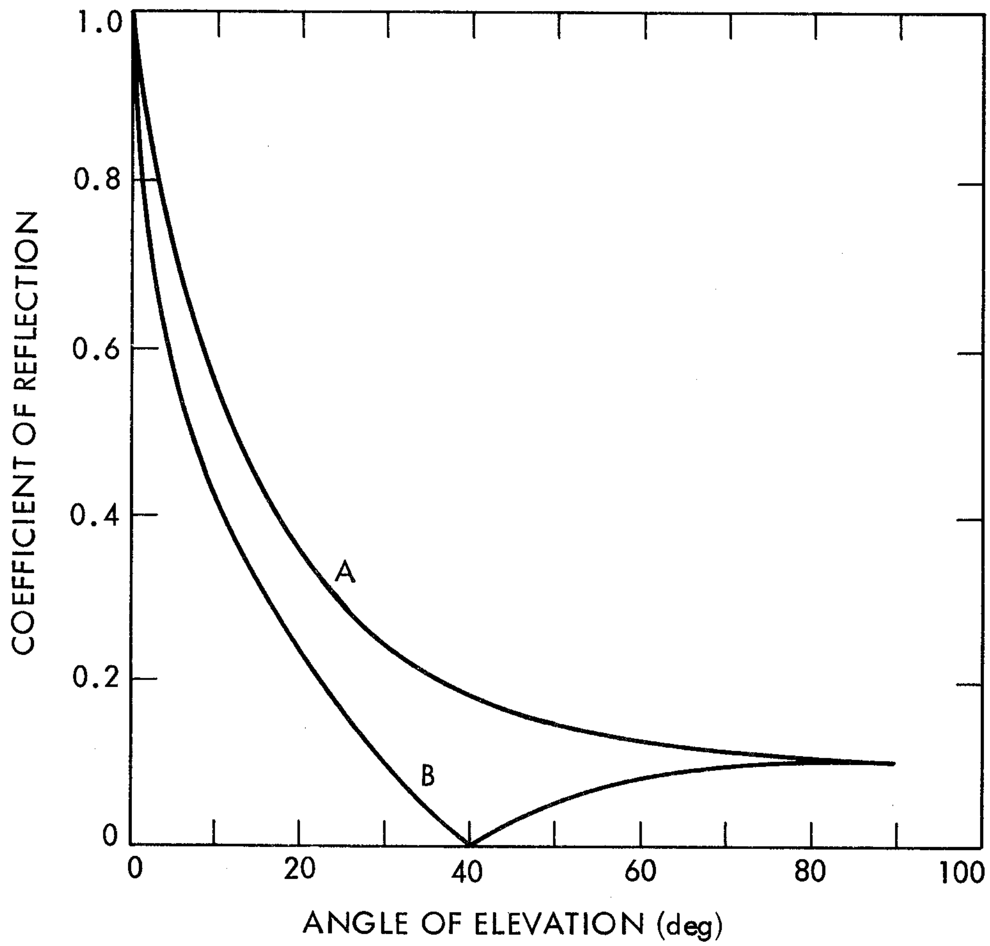

Figure 6.24. Field intensity reflection coefficients for ice caps such as those of Greenland and Antarctica. A: horizontal polarization, B: vertical polarization (CCIR, 1982).

Table 6.2 lists values of Δh_r as determined from Eq. (6.60) for various angles θ. Ascending and descending aircraft pass rapidly

Table 6.2 Vertical Separation Between Maxima of Interference Pattern.

θ (deg)	Δh_r (λ)
2	14.3
4	7.2
8	3.6
15	1.9
30	1.0
60	0.58
90	0.5

through the maxima and minima in the interference pattern. For elevation angles of about 15 deg and greater even aircraft in nominally level flight experience the full range of fading because of limited ability to maintain constant height.

In flight over water the Doppler spectrum of the sea-reflected signal introduces spectral spreading of the received signal, as a function of the elevation angle of the aircraft with respect to the origin of the reflected signal. Values of the measured Doppler bandwidth between points at 1/e of the peak amplitude for L-band transmissions from ATS-5 are shown in Fig. 6.25.

An AEROSAT satellite system specifically designed for aircraft communciations has been proposed but never funded, but at the time of writing the application of satellites to communication with aircraft appears imminent (Sue, 1987). Volumes VIII-1, VIII-2, and VIII-3, Mobile Services, Recommendations and Reports of the CCIR. 1986 include a large number of reports that provide information pertinent to mobile communications, including mobile-satellite communications. Although Report 505-2 (CCIR, 1978) was not updated and included in subsequent cycles of publication, this writer found it to be a useful report. Several of the illustrations used in this chapter appeared in Report 505-2 and then in Report 884 (CCIR, 1982).

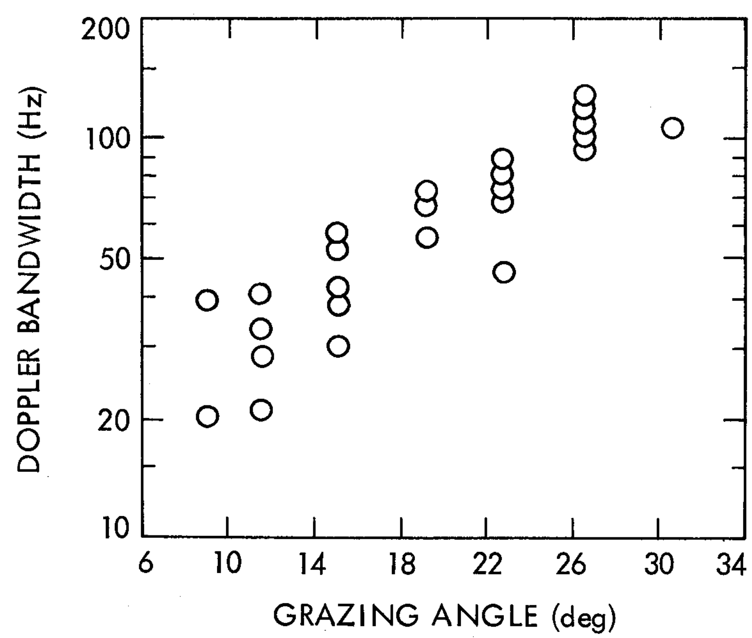

Figure 6.25. Doppler bandwidth as a function of elevation angle, based on 1550 MHz transmissions from the ATS-5 satellite to a 707-type aircraft (CCIR, 1982).

6.7 THE NAVSTAR GLOBAL POSITIONING SYSTEM

The three previous sections have involved consideration of multipath effects that may be important to the three categories of land, maritime, and aeronautical mobile communications services. In addition, the effects are pertinent to radionavigation systems, including the NAVSTAR Global Positioning System (GPS) (Milliken and Zoller, 1978). The system provides three-dimensional position and velocity information to mobile or fixed receivers anywhere in the world whether on land or sea or in the air. Original plans called for 24 satellites in 12-hour orbits at an altitude of 20,183 km in three orthogonal planes (eight in each plane). Budgetary considerations have required a change to operation with a total of 18 satellites (Book, Brady, and Mazaika, 1980). Signals are transmitted at two L-band frequencies, 1575.42 and 1227.60 MHz, to permit correction for ionospheric time delay. The satellites carry precision cesium clocks, and if the user has a precision clock signals from three satellites are sufficient to determine position. A fourth satellite is required for most users, however, who must have a clock of specified accuracy but not a truly precision clock. Each of the two L-band frequencies is a multiple of a 10.23 MHz clock frequency. In particular 154 x 10.23 = 1575.42 and 120 x 10.23 = 1227.60. By making measurements of pseudo range to the four satellites, four equations can be formulated and solved for the four unknowns consisting of three position coordinates and the offset between precision GPS time and time as indicated by the user's clock. The term pseudo range is used because the originally measured quantities are sums of true ranges and offsets due to user time error.

Position determination by use of GPS involves the use of spread-spectrum techniques for separating the signals from a particular satellite from those of other satellites in the field of view and for obtaining precise range values. The signals are received at low levels, usually well below the thermal noise level in the receiver. Each satellite operates with a unique P code, XP_i, which is generated from the product of two PN (pseudonoise) codes, X1(t) and $X2(t + n_iT)$, where T is the 10.23 MHz clock period and n_i takes on values from 0 to 36 (Spilker, 1980). Code X1 has a period of about 1.5 s or 15,345,000 chips and code X2 is 37 chips longer.

If an XP code is allowed to continue without resetting it would have a period without repetition of about 267 days but the code of each satellite is reset to its initial condition every seven days, allowing each satellite a unique seven-day segment of the long code. Thus it can be considered that there is really only one long code and that the different satellites use different parts of it.

Each satellite also transmits a shorter C/A code, $XG(t)$, of 1023 bits or about 1 ms, based on a repetition rate of 1.023 MHz. This code is used for signal acquisition. The C/A code is a Gold code formed as the product of two 1023 bit PN codes, $G1(t)$ and $G2[t + N_i(10T)]$ where T is the period of 10.23 MHz and N_i can take on any of 1023 values. The total signal $SL1(t)$ transmitted on the L1 frequency (1575.42 MHz) is given by

$$SL1_i(t) = A_p\, XP_i(t)D_i(t) \cos(\omega_1 t + \phi) + A_c\, XG_i(t)D_i(t) \sin(\omega_1 t + \phi) \tag{6.61}$$

The A's are amplitudes, XP_i is the P code, XG_i is the C/A code, and $D_1(t)$ carries data at 50 bps on satellite status, satellite position (ephemeris data), errors of the satellite cesium clock, and parameters for correcting for ionospheric excess time delay. The data channel has a 30 s overall frame period and 6 s subframes. The signal $SL2(t)$ at 1227.60 MHz may be modulated by a P code or a C/A code. Assuming modulation by a P code, it has the form of

$$SL2_i(t) = B_p\, XP_i(t)D_i(t) \cos(\omega_2 t + \theta) \tag{6.62}$$

where B_p is amplitude.

Using the 1023 chip $XG_i(t)$, it takes about 45 s or more to establish synchronism of the transmitter and receiver codes. Search must be carried out in both time and frequency as signals from the satellites are Doppler shifted in frequency. The overall time uncertainty is 1023 μs and the frequency uncertainty may be in the order of 10 kHz, compared to an IF bandwidth of 1 kHz. Once the transmitted C/A code has been acquired, the 50 bps data carried by $D_i(t)$ is received. A new HOW word (Hand-Over-Word) that is transmitted every 6 s in the data stream then indicates the correct phase point in the incoming P code, and the user equipment is shifted in phase to synchronize with the incoming P code at the next change in the HOW.

From the propagation viewpoint, ionospheric and tropospheric excess range delay and multipath effects are of practical importance. For the frequencies utilized, ionospheric excess range delay ΔR at the frequency L1 is related to differential range delay δR between the two frequencies by

$$\Delta R = 1.5336 \, \delta R \tag{6.63}$$

The concept of correcting for ionospheric excess range delay by use of two frequencies was presented in Sec. 2.3.1. The ionosphere also modifies Doppler frequency by an amount Δf_{L1} given by

$$\Delta f_{L1} = 3.529 \, \delta f \tag{6.64}$$

for the frequencies utilized, where δf is the differential Doppler frequency between the two frequencies. The 18 GPS satelliltes will be in six oribital planes inclined at 55 deg with respect to the equator and spaced 60 deg in longitude, with three satellites in each oribital plane. The true difference in radial velocity of two satellites, one approaching and one receding from a stationary observer at the north pole where there is zero effect from rotation of the Earth, generates a Doppler frequency difference of 7500 Hz (Spilker, 1980).

Excess range delay due to dry air can be determined and corrected for with high accuracy (Sec. 3.7). The delay due to water vapor is more difficult to determine precisely. Its small magnitude may not be important for routine applications but will be important when high precision is desired, as for geodetic applications. To obtain the highest precision use can be made of carrier phase. This approach requires measures to resolve the inherent ambiguity of multiples of 2π radians in phase (Counselman and Gourevitch, 1981; Brown and Hwang, 1983). One reference reports position errors of 1.2 to 2.7 m due to multipath effects, using standard techniques rather than carrier phase (Milliken and Zoller, 1978). The wide bandwidth of GPS provides frequency diversity and the effect of multipath would be expected to be greater for narrowband operation at the same nominal frequency.

The quantity PDOP (Position Dilution of Precision) represents the ratio of $\Delta p = [(\Delta x)^2 + (\Delta y)^2 + (\Delta z)^2]^{1/2}$ to Δr where Δp is rms position error, expressed in terms of errors in x, y, and z coordinates, and Δr is rms radial range error (Spilker, 1980). It develops that PDOP is likely to have a value of about three or less. If position is to be determined to an accuracy of 10 m, then radial range must be measured to an accuracy of 10/3. Determining the distance between the user's position and that of a satellite involves shifting the phase of the receiver code until maximum correlation is obtained with the incoming signal (Parkinson and Gilbert, 1983). If the phase were to be shifted continuously over a range including that of the maximum signal amplitude, GPS could apparently be used to obtain multipath data (Sec. 6.3.1).

Important impending applications of GPS are to determining satellite orbits and geodetic baselines. The Ocean Topographic Experiment (TOPEX) satellite, scheduled for launch in the early 1990's, will have a GPS receiver on board, and signals from four GPS satellites will be used to determine the position of the satellite (Yunck, Wu, and Lichten, 1985). A differential GPS technique that will be employed will actually involve determining the satellite position with respect to ground receivers at precisely known locations. As suggested by Fig. 6.26, pseudo ranges to two receivers, one on the ground and one in the TOPEX satellite, will be measured. From such a measurement utilizing one GPS satellite, the projection of the distance B between the ground receiver and satellite in the direction of ρ_u of Fig. 6.26 is found. By using four satellites, the magnitude and direction of B is completely determined and the satellite position is thus also known. The differential technique has the advantage of tending to eliminate clock error and errors in positions of the GPS satellites, as their errors are common to both transmission paths along ρ_u and ρ_s of Fig. 6.26. The use of carrier phase will allow determining position rapidly and precisely , and the combination of pseudo range and phase measurements is expected to give better results than either alone. Because the satellite frequencies are not widely separated, it is expected that the use of Eq. (6.54) will not correct for ionospheric delay as precisely as desired, but long-term averaging, the hybrid strategy of using both pseudo range and carrier phase, and simultaneous solutions for both the TOPEX and GPS orbits should allow decreasing the ionospheric as well as other errors to a high degree. Attention is also being given to GPS receiver design, antennas that discriminate against multipath, and the use of water-vapor radiometers to determine the excess range delay due to water vapor.

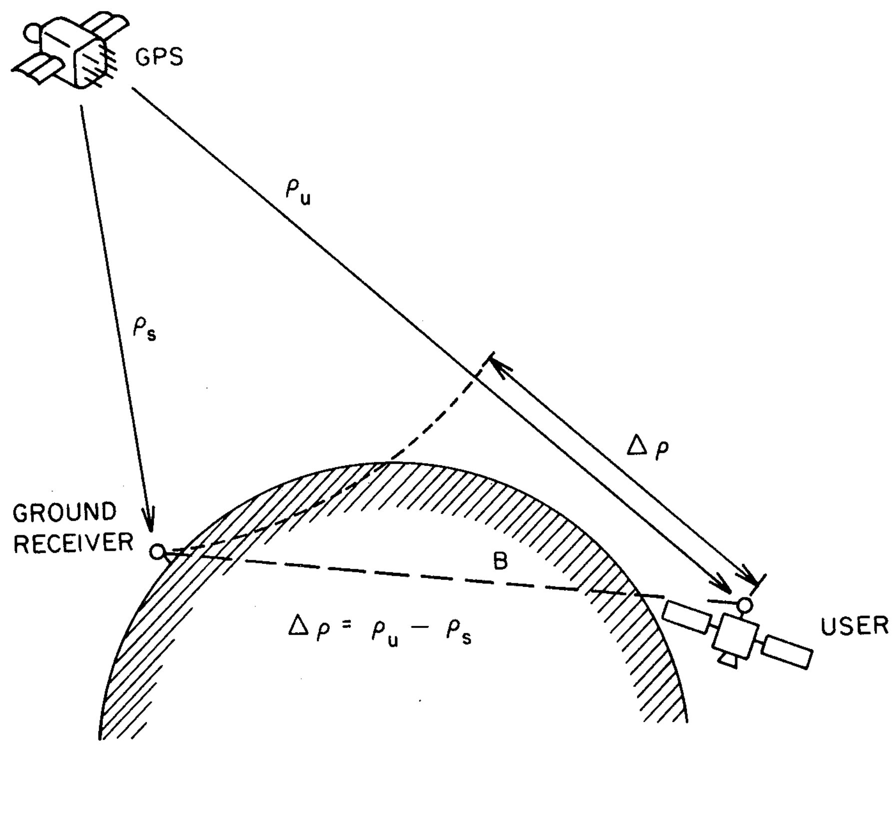

Figure 6.26. Differential technique for utilizing GPS.

REFERENCES

Assis, M. S., "A simplified solution to the problem of multiple diffraction over rounded obstacles," IEEE Trans. Antennas Propagat., vol. AP-19, pp.292-295, March 1971.

Barnwell, T. P. , " Development, design, fabrication, and evaluation of a broadband speech compression system at 4800 bits per second," Session 2, Mobile Satellite Industry Briefing, (viewgraphs) Jet Propulsion Lab., Nov. 13-14, 1985.

Barrow, B. B., L. G. Abraham, W. M. Cowan, and R. M. Gallant, "Indirect atmospheric measurements utilizing rake tropospheric scatter techniques - Part I: The rake tropospheric scatter technique." Proc. IEEE, vol. 57, pp. 537-551, April 1969.

Bateman, A. J., G. Lightfoot, A. Lymer, and J. P. McGeehan, "Speech and data communications over 942 MHZ TAB and TTIB single sideband mobile radio systems incorporating feed-forward signal regeneration," IEEE Trans. Veh. Technol., VT-34, pp.13-21, Feb. 1985.

Beckmann, P., Probability in Communication Engineering. New York: Harcourt, Brace & World, 1967.

Beckmann, P. and A. Spizzichino, The Scattering of Electromagnetic Waves from Rough Surfaces. New York: Macmillan Co. 1963.

Bitzer, D. R., et al., "A rake system for tropospheric scatter," IEEE Trans. Comm., vol. COM-14, pp.496-506, Aug. 1966.

Book, S. A., W. F. Brady, and P. K.Mazaika, "The nonuniform GPS constellation," in IEEE 1980 Position Location and Nav. Sym. Record, pp. 1-8. New York: Inst. of Elect. and Electronic Eng., 1980.

Boudreau, P. M. and A. L. Barry, "The Canadian MSAT program," in Satellite Systems for Mobile Communications and Navigation, pp. 28-32. London & New York: IEE, 1983.

Brisken, A. F., R. E. Anderson, R. L. Frey, and J. R. Lewis, "Land mobile communications and position fixing using satellites," IEEE Trans. Veh. Technol., vol. VT-28, pp. 153-170, Aug. 1979.

Brown, R. G. and P. Y. C. Hwang, "A Kalman filter approach to precision GPS geodesy," Navigation vol. 30, pp. 338-349, Winter, 1983-1984.

Bullington, K., "Radio propagation for vehicular communications," IEEE Trans. Veh. Technol., vol. VT-26, pp. 295-308, Nov. 1977.

Butterworth, J. S. and E. E. Mott, "The characterization of propagation effects for land mobile satellite services," in Satellite Systems for Mobile Communications and Navigation, London and New York: IEE, 1983.

Butterworth, J. S., "Propagation data for land mobile satellite system,", pp. 371-378, Proc. of NAPEX VIII, Jet Propulsion Lab., Pasadena, CA, June 20-21, 1985.

CCIR, "Multipath effects in aircraft-to-satellite communication and radio determination links," Report 505-2 in Vol. VIII, Mobile Services, Recommendations and Reports of the CCIR, 1978. Geneva: Int. Telecomm. Union, 1978.

CCIR, "Propagation data for maritime and land mobile satellite systems above 100 MHz," Report 884 in Vol. V, Propagation in Non-ionized Media, Recommendations and Reports of the CCIR, 1982. Geneva: Int. Telecomm. Union, 1982.

CCIR, Proposed Modifications to Report 884, Propagation Data for Maritime Mobile Satellite Systems for Frequencies Above 100 MHz, CCIR Study Group Doc. 5/102-E, 2 Aug. 1983.

CCIR, "Ground-wave propagation curves for frequencies between 10 kHz and 30 MHz," Recommendation 368-5 in Vol. V, Propagation in Non-ionized Media, Recommendations and Reports of the CCIR, 1986. Geneva: Int. Telecomm. Union, 1986a.

CCIR, "Propagation by diffraction," Report 715-2 in Vol. V, Propagation in Non-ionized Media, Recommendations and Reports of the CCIR, 1986. Geneva: Int. Telecomm. Union, 1986b.

CCIR, "Reflection from the surface of the Earth," Report 1008 in Vol. V, Propagation in Non-ionized Media, Recommendations and Reports of the CCIR, 1986. Geneva: Int. Telecomm. Union, 1986c.

CCIR, "Electrical characteristics of the surface of the Earth," Recommendation 527-1 in Vol. V, Propagation in Non-ionized Media, Recommendations and Reports of the CCIR, 1986. Geneva: Int. Telecomm. Union, 1986d.

CCIR, "Propagation data for maritime mobile-satellite systems for frequencies above 100 MHz," Report 884-1 in Vol. V, Propagation in Non-ionized Media, Recommendations and Reports of the CCIR, 1986. Geneva: Int. Telecomm. Union, 1986e.

CCIR, "Propagation data for land mobile-satellite systems for frequencies above 100 MHz," Report 1009 in Vol. V, Propagation in Non-ionized Media, Recommendations and Reports of the CCIR, 1986. Geneva: Int. Telecomm. Union, 1986f.

CCIR, "Maritime satellite system performance at low elevation angles." Report 920-1 in Vol. VIII-3, Mobile Services, Recommendations and Reports of the CCIR, 1986. Geneva: Int. Telecomm Union, 1986g.

CCIR, "Link power budgets for a maritime mobile satellite service," Report 760-1 in Vol. VIII, Mobile Services, Recommendations and Reports of the CCIR, 1986. Geneva: Int. Telecomm. Union, 1986h.

CCIR, "Ionospheric effects upon earth-space propagation," Report 263-6 in Vol. VI, Propagation in Ionized Media, Recommendations and Reports of the CCIR, 1986. Geneva: Int. Telecomm. Union, 1986i.

CCIR, "Man-made radio noise," Report 258-4 in Vol. VI, Propagation in Ionized Media, Recommendations and Reports of the CCIR, 1986. Geneva: Int. Telecomm. Union, 1986j.

Cooper, G. R. and R. W. Nettleton, "A spread-spectrum technique for high-capacity mobile communications," IEEE Trans. Veh. Technol., vol. VT-27, pp. 264-275, Nov. 1978.

Cooper, G. R. and R. W. Nettleton, "Cellular mobile technology: the great multiplier," IEEE Spectrum, vol. 20, pp. 30-37, June 1983.

Counselman, C. C. and S. A. Gourevitch, "Miniature interferometer terminals for earth surveying: ambiguity and multipath with Global Positioning System," IEEE Trans. Geosci. Rem. Sens., vol. GE-19, pp. 244-252, Oct. 1981.

Cox, D. C., "910 MHz urban mobile radio propagation: multipath characteristics in New York City," IEEE Trans. Comm., vol. COM-21, pp. 1188-1194, Nov. 1973.

da Silva Curiel, A., "The first generation INMARSAT system," in Satellite Systems for Mobile Communication and Navigation, pp. 1-7. London & New York: IEE, 1983.

ɪavarian, F., "Fade margin calculation for channels impaired by Rician fading," IEEE Trans. Veh. Technol. vol. VT-34, pp. 41-44, Feb. 1985.

Davarian, F., "Channel simulation to facilitate mobile-satellite communications research," IEEE Trans. Comm., vol COM-35, pp. 47-56, Jan. 1987.

Deygout, J., "Multiple knife-edge diffraction of microwaves," IEEE Trans. Veh., Technol. Vol. 480-489, July, 1966.

Divsalar, D. "Trellis coded modulation for 4800 bps and 9600 bps in 5 kHz channels," Session 2, Mobile Satellite Industry Briefing (viewgraphs), Jet Propulsion Lab., Nov. 13-14, 1985.

Dixon, R. C., Spread Spectrum Systems, New York: Wiley, 1976.

Espeland, R. H., E. J. Violette, and K. C. Allen, Atmospheric Channel Performance Measurements at 10 to 100 GHz, NTIA Report 84-149, U. S. Department of Commerce, April 1984.

Fang, D. J., T. S. Tseng, and T. O. Calvit, "A low elevation angle propagation measurement of 1.5-GHz satellite signals in the Gulf of Mexico," IEEE Trans. Ant. Propagat., vol. AP-30, pp. 10-15, Jan. 1982.

Fang, D.J. and R.H. Ott, "A low elevation angle L-band maritime propagation measurement," in Satellite Systems for Mobile Communications and Navigation, pp. 45-50. London and New York: IEE, 1983.

Flock, W. L., Electromagnetics and the Environment: Remote Sensing and Telecommunications. Englewood Cliffs, NJ: Prentice-Hall, 1979.

General Electric, "Pilot tone calibration techniques," Session 2, Mobile Satellite Industry Briefing (v iewgraphs), Jet Propulsion Lab., Pasadena, CA, Nov. 13-14, 1985.

Gersho, A., "Development, design, fabrication, and evaluation of a broadband speech compression systems at 4800 bits per second," Session 2, Mobile Satellite Industry Briefing (viewgraphs), Jet Propulsion Lab., Nov. 13-14, 1985.

Goldhirsh, J. and W.J. Vogel, "Roadside tree attenuation measurements at UHF for land mobile-satellite systems,"IEEE Trans. Antennas Propagat., vol. AP-35, pp. 589-596, May 1987.

Hall, M.P.M., Effects of the Troposphere on Radio Communication. Stevenage, U. K. and New York: Peter Peregrinus for IEE, 1979.

Hansen, F. and F. I. Meno, "Mobile fading - Rayleigh and lognormal superimposed," IEEE Trans. Veh. Technol., vol. VT-26, pp. 332-335, Nov. 1977.

Hess, G. C., "Land-mobile satellite excess path loss measurements," IEEE Trans. Veh. Technol., vol.VT-29, pp. 290-297, May 1980.

Hufford, G. A. et al. Wideband Propagation Measurements in the Presence of Forests, CECOM 82-CS029-F, U. S. Army Communications-Electronics Command, Fort Monmouth, NJ 07703, Jan. 1983.

Jakes, W. C., Microwave Mobile Communications. New York: Wiley, 1974.

Jenkins, F. A. and H. E. White. Fundamentals of Optics, 4th ed. New York: McGraw-Hill, 1976.

Jordan, E. C. and K. C. Balmain, Electromagnetic Waves and Radiating Systems. Englewood Cliffs, NJ: Prentice-Hall, 1968.

Kirby, R. S., H. T. Dougherty, and P. L. McQuate, "Obstacle gain measurements over Pikes Peak at 60 to 1,046 Mc,"Proc. IRE, vol. 43, pp. 1467-1472, Oct. 1955.

Knouse, G. H., "Terrestrial land mobile satellite considerations, NASA plans and critical issues," IEEE Trans. Veh. Technol. vol. VT-29, pp.370-374, Nov. 1980.

Lipke, D. W. et al., "MARISAT - a maritime satellite communication system," COMSAT Technical Rev., vol. 7, pp.351-392, Fall 1977.

Loo, C., "A statistical model for a land mobile satellite link," IEEE Trans. Veh. Technol. vol. VT-34, pp. 122-127, Aug. 1985.

Miller, A. R., R. W. Brown, and E. Vegh, "New derivation for the rough-surface reflection coefficient and for the distribution of sea-wave elevations," IEE Proc., vol. 131, Part H, pp. 114-116, April 1984.

Milliken, R. J. and C. J. Zoller, "Principle of operation of NAVSTAR and system characteristics," Navigation, vol. 25, pp. 95-106, Summer 1978.

Norton, K. A., P. L. Rice, and L. E. Vogler, "The use of angular distance in estimating transmission loss and fading rate for propagation through a turbulent atmosphere over irregular terrain," Proc. IRE, vol. 43, pp. 1488-1526, Oct. 1955.

Ott, R. H., "An alternative integral equation for propagation over irrregular terrain," Radio Sci., vol. 6, pp. 429-435, 1971.

Parkinson, B. W. and S. W. Gilbert, "NAVSTAR: Global Positioning System - ten year's later," Proc. IEEE, vol. 71, pp. 1177-1186, Oct. 1983.

Panter, P. F., Communication Systems Design. New York: McGraw-Hill, 1972.

Price, R. and P. E. Green, "A communication technique for multipath channels," Proc. IRE, vol. 46, pp. 555-570, March 1958.

Proakis, J. G., Digital Communications. New York: McGraw-Hill, 1983.

Qureshi, S. "Adaptive equalization," IEEE Commun. Mag., vol. 20, pp. 9-16, March 1982.

Sass, P. F., "Propagation measurements for UHF spread spectrum mobile communications," IEEE Trans. Veh. Technol., vol. VT-32, pp. 168-176, May 1983.

Schwartz, M., W. R. Bennett, and S. Stein, Communication Systems and Techniques. New York: 1966.

Simon, M. K. "Digital modulation for narrow-band fading satellite channels," Session 2, Mobile Satellite Industry Briefing (viewgraphs), Jet Propulsion Lab., Pasadena, CA, Nov. 23-14, 1985.

Sheperd, N. M., "Radio wave loss deviation and shadow loss at 900 MHz," IEEE Trans. Veh. Technol., vol. VT-26, pp. 309-313, Nov. 1977.

Smith, E. K., "Multipath, trees, scintillation, and noise," unpublished presentation at NAPEX IX, U. of Colorado, Boulder, CO, Jan. 16, 1986.

Spilker, J. J., "GPS signal structure and performance characteristics," Navigation, vol 25, pp. 121-146, Summer 1978. (Also pp. 29-54 in Global Positioning System, Papers published in Navigation, vol. 1, 1980).

Stutzman, W. , "PELMOSS modeling," pp. 343-363 in JPL D-2619, Proc. of NAPEX VIII, June 20, 1985 at U. of British Columbia; Jet Propulsion Lab., Pasadena, CA, Aug. 26, 1985.

Sue, M.K. (ed.), An Aeronautical Mobile Satellite System, Part I, Executive Summary; Part II, Technical Report. Pasadena: Jet Propulsion Laboratory, September 1, 1987.

Townes, S. A., "Near toll quality digital speech at 4800 bps," Session 2, Mobile Satellite Industry Briefing (viewgraphs), Jet Propulsion Lab., Pasadena, CA, Nov. 13-14, 1985.

Turin, G. L., "Introduction to spread-spectrum antimultipath techniques and their application to urban digital radio," Proc. IEEE, vol. 68, pp. 328-353, March 1980.

Vogel, W. J., Land mobile radio propagation measurements at 869 and 1501 MHz," pp. 261-281 in JPL D-2619, Proc. of NAPEX VIII, June 20, 1985 at U. of British Columbia; Jet Propulsion Lab., Pasadena, CA, Aug. 26, 1985.

Vogel, W. J. and G. W. Torrence, Measurements Results from a Balloon Experiment Simulating Land Mobile Satellite Transmissions, Elect. Eng. Research Lab., U. of Texas, Austin, TX 78758, 30 April 1984.

Vogel, W. J. and E. K. Smith, Propagation Considerations in Land Mobile Satellite Transmission, MSAT-X Report No. 105, Jet Propulsion Lab., Pasadena, CA, 24 Jan. 1985.

Vogel, W. J. and J. Goldhirsh, "Tree attenuation at 869 MHz derived from remotely piloted aircraft measurements," IEEE Trans. Antennas Propagat., vol. AP-34, pp. 1460-1464, Dec. 1986.

Vogel, W. J. and J. Goldhirsh, "Fade measurements at L-band and UHF in mountainous terrain for land mobile satellite systems," IEEE Trans. Antennas Propagat., vol. AP-36, Jan. 1988.

Weber, W. J. and F. Naderi, "NASA mobile satellite experiment (MSAT-X)," in Proc. Nat. Electronics Conf., Chicago, IL, 1983, vol. 37, pp. 328-330, 1983.

Yeh, Y. S. and D. O. Reudink, "Efficient spectrum utilization for mobile radio systems using space diversity," IEEE Trans. Comm., vol. COM-30, pp. 447-455, March 1982.

Yunck, T. P., S-C. Wu, and S. M. Lichten, "A GPS measurement system for precise satellite tracking and geodesy," J. Astronautical Sciences, vol. 33, pp. 367-380, Oct.-Dec. 1985.

APPENDIX 6.1

REFLECTION COEFFICIENTS FOR CIRCULAR POLARIZATION

An electric field intensity vector $\mathbf{E}$ of arbitrary polarization can be expressed in terms of either circular or rectangular components as indicated by

$$\mathbf{E} = E_R\,\mathbf{a}_r + E_L\,\mathbf{a}_\ell = E_x\,\mathbf{a}_x + E_y\,\mathbf{a}_y \tag{A6.1}$$

where E_R, E_L, E_x, and E_y are in general complex quantities. The $\mathbf{a}$'s represent unit vectors, with $\mathbf{a}_r$ a vector of unit length that is rotating in the right circular direction with angular ω where ω is the angular wave frequency. The unit vector $\mathbf{a}_\ell$ represents a unit vector rotating in the left circular direction, and $\mathbf{a}_x$ and $\mathbf{a}_y$ are unit vectors in the x and y directions. The unit vectors $\mathbf{a}_r$ and $\mathbf{a}_\ell$ can be expressed in terms of $\mathbf{a}_x$ and $\mathbf{a}_y$ by

$$\mathbf{a}_r = \mathbf{a}_x - j\mathbf{a}_y, \qquad \mathbf{a}_\ell = \mathbf{a}_x + j\mathbf{a}_y \tag{A6.2}$$

If these definitions of $\mathbf{a}_r$ and $\mathbf{a}_\ell$ are substituted into Eq. (A6.1), it develops that

$$E_R + E_L = E_x \tag{A6.3}$$

and

$$E_R - E_L = jE_y \tag{A6.4}$$

These two equations can be treated as two equations for two unknowns, E_R and E_L. Solving for these quantities by use of determinents or otherwise,

$$E_R = \frac{E_x + jE_y}{2} \tag{A6.5}$$

and

$$E_L = \frac{E_x - jE_y}{2} \tag{A6.6}$$

The field components E_x and E_y are total field components, and the relations apply to any combination of right and left circularly polarized waves and also when only right or left circular waves are present. For example, consider that only a right circular wave is present. For this case, $E_y = -jE_x$,

$$E_R = \frac{E_x + j(-jE_x)}{2} = E_x , \qquad (A6.7)$$

and

$$E_L = \frac{E_x - j(-jE_x)}{2} = 0 \qquad (A6.8)$$

Consider further that a right circular wave is incident upon a flat, smooth surface. Using the subscript i to refer to the incident wave, it can be determined from Eq. (A6.7) that $E_{Ri} = E_{xi}$. Next consider the wave resulting from reflection of this incident right circular wave. Taking E_x to refer to the horizontal component of the reflected wave, E_x is given by

$$E_x = \rho_h E_{xi} = \rho_h E_{Ri} \qquad (A6.9)$$

where ρ_h is the reflection coefficient for horizontal polarization. Likewise for E_y, the vertical component of the reflected wave,

$$E_y = \rho_v E_{yi} = \rho_v (-jE_{xi}) = -j\rho_v E_{Ri} \qquad (A6.10)$$

Thus for the reflected wave, using Eq. (A6.5),

$$E_R = \frac{\rho_h E_{Ri} + j(-j\rho_v E_{Ri})}{2}$$

and

$$E_R = \frac{\rho_h E_{Ri} + \rho_v E_{Ri}}{2} \qquad (A6.11)$$

Finally divide both sides of Eq. (A6.11) by E_{Ri} and identify E_R/E_{Ri} as ρ_c, the reflection coefficient for the copolarized component of the reflected wave. The result is that

$$\rho_c = E_R/E_{Ri} = \frac{\rho_h + \rho_v}{2} \qquad (A6.12)$$

The same substitutions can be made in Eq. (A6.6) and one can divide by E_{Ri} again but now E_L/E_{Ri} represents ρ_x, the reflection coefficient giving the crosspolarized component of the reflected wave. Following this approach

$$E_L = \frac{\rho_h E_{Ri} - j(-j\rho_v E_{Ri})}{2} = \frac{\rho_h E_{Ri} - \rho_v E_{Ri}}{2}$$

and

$$\rho_x = E_L/E_{Ri} = \frac{\rho_h - \rho_v}{2} \qquad \text{(A6.13)}$$

If consideration is given to an incident left circularly polarized wave, and the type of procedure utilized above is employed again but it is recognized that $E_{yi} = jE_{xi}$ and $E_y = j\rho_v R_{Li}$ for left circular polarization, the same relations, namely Eqs. (A6.12) and (A6.13), are obtained.

The basic relations of Eqs. (A6.1) through (A6.6) are given in a number of references, for example Weeks (1964). A combination of right and left circularly polarized waves constitutes an elliptically polarized wave having an axial ratio (A.R.) given by

$$\text{A.R.} = \frac{|E_R| + |E_L|}{|E_R| - |E_L|} \qquad \text{(A6.14)}$$

This ratio represents the ratio of the major axis of the polarization ellipse to the minor axis. The angle of the major axis of the ellipse, with respect to a reference axis, is halfway between instantaneous positions of the right and left circular components, consistent with Eq. (2.23) for Faraday rotation.

CHAPTER 7

RADIO NOISE

7.1 SYSTEM NOISE TEMPERATURE

7.1.1 Basic Concepts of Electrical Noise

Electrical noise is developed in resistors or conductors, due to the random motions of electrons. The available noise power p at the terminals of a resistor in a one Hz bandwidth at radio frequencies is independent of the value of the resistance and frequency and is given by

$$p = kT \qquad \text{W/Hz} \qquad (7.1)$$

where k is Boltzmann's constant (1.381×10^{-23} J/K) and T is temperature in kelvins (K). The noise power P in a bandwidth B in the radio frequency range is therefore given by

$$P = kTB \qquad \text{W} \qquad (7.2)$$

with B in Hz. The standard reference value, $T_o = 290$ K, is normally used for T in noise power calculations.

If a receiver or amplifier has a resistive input impedance, the noise power at the output terminals of the receiver will be

$$P = gkT_oB + P_i \qquad \text{W} \qquad (7.3)$$

where g is the power gain of the amplifier and P_i is noise which is generated internally within the amplifier. The noise performance of an amplifier can be measured by use of a noise figure F where F is defined by the relation

$$F = P_{out}/(gP_{in}) \qquad (7.4)$$

with the subscripts representing output and input and with $P_{in} = kT_oB$. Alternatively, a noise temperature T_R can be used to describe the noise performance of the receiver such that

$$P_{out} = gk\,(T_o + T_R)\,B \qquad \text{W} \qquad (7.5)$$

Making use of Eqs. 7.3-7.5, it can be established that

$$F = 1 + T_R/T_o \qquad (7.6)$$

and

$$T_R = T_o (F - 1) \qquad \text{K} \qquad (7.7)$$

An advantage of using T_R as a measure of the noise introduced by a receiver is that it refers to the input terminals of the receiver and is additive with respect to temperatures representing other noise sources that may be applied to the receiver input terminals, as in Eq. (7.5).

Consider next a resistive or dissipative attenuator at the temperature T_o. In many applications, one simply considers the power output of the attenuator to be the input power times the power "gain" g_a of the attenuator so that $P_{out} = P_{in} g_a$. It is convenient when working with noise to use a noise temperature in place of noise power itself. Following that practice in this case

$$T_{out} = T_{in}\, g_a \qquad \text{K} \qquad (7.8)$$

A resistive attenuator, however, does more than attenuate. It adds noise as well, and it is advantageous to refer this noise to the input terminals of the attenuator in the same way that noise is referred to the input terminals of an amplifier or receiver. To carry out this procedure, it is necessary to determine the input temperature of an attenuator such that the temperature accounts for the noise generated by the attenuator and is consistent with Eq. (7.8). The advantage is, as with amplifiers, that this noise temperature is additive with respect to noise temperatures representing other sources of noise that may be applied to the input of the attenuator. Then one can use Eq. (7.8) for an attenuator with T_{in} representing the sum of the attenuator input noise temperature and a temperature representing all other noise sources, if any, that may be present (Fig. 7.1). It develops that for an attenuator by itself

$$T_{in} = (\ell_a - 1)\, T_o \qquad \text{K} \qquad (7.9)$$

and

$$T_{out} = (1 - g_a)\, T_o \qquad \text{K} \qquad (7.10)$$

with $\ell_a = 1/g_a$. If an antenna which introduces noise corresponding to the temperature T_A is connected to the input terminals of the attenuator then

$$T_{in} = T_A + (\ell_a - 1)\, T_o \qquad \text{K} \qquad (7.11)$$

and

$$T_{out} = T_A g_a + (1 - g_a)\, T_o \qquad \text{K} \qquad (7.12)$$

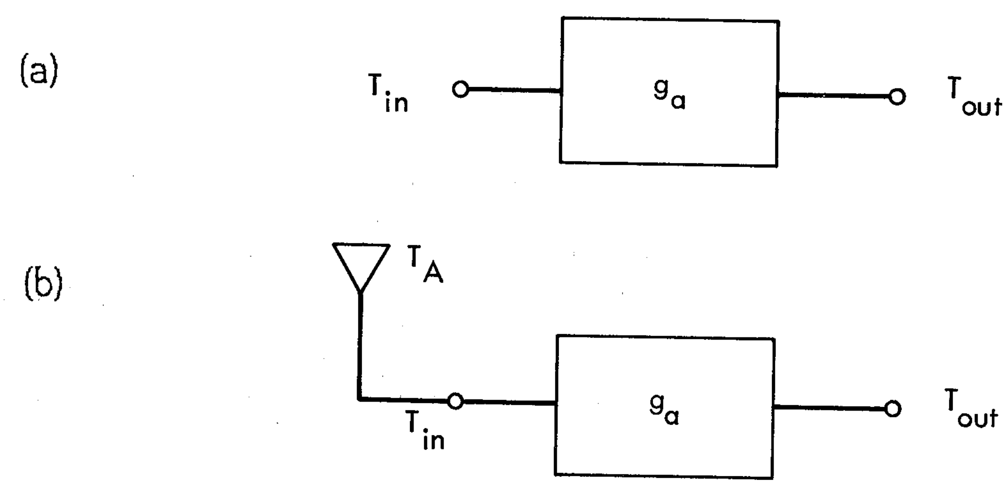

Figure 7.1. Concept of noise temperature of attenuator. For both situations $T_{out} = T_{in}\, g_a$. In Fig.(7.1a), no input is connected to the attenuator and $T_{in} = (\ell_a - 1)\, T_o$. In Fig. (7.1b), $T_{in} = T_A + (\ell_a - 1)\, T_o$, where T_A is the antenna noise temperature.

One additional basic relation is needed in order to define system noise temperature. Consider a system consisting of two separate parts connected in series as in Fig. 7.2.

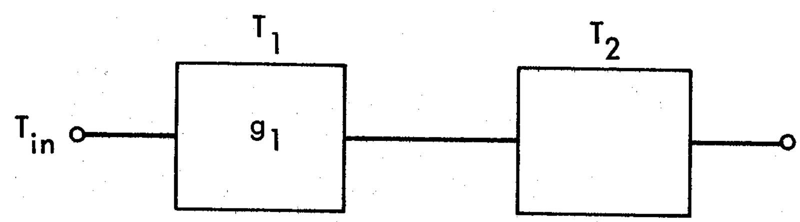

Figure 7.2. System of two parts connected in series and having temperatures of T_1 and T_2.

It develops that

$$T_{in} = T_1 + T_2/g_1 \tag{7.13}$$

If g_1 is the gain of an amplifier and is much greater than unity, T_1 plays a greater role in determining T_{in} than T_2. Each of the two parts of the system may be an amplifier, attenuator, or combination of these. The concept illustrated by Eq. (7.13) can be extended to additional stages. For example, for a system of three parts, $T_{in} = T_1 + T_2/g_1 + T_3/g_1g_2$.

7.1.2 System Noise Temperature

Following Kraus (1986), system noise temperature T_{sys} is defined in Fig. 7.3, suggesting a telecommunication receiving system including an antenna having a noise temperature of T_A, a

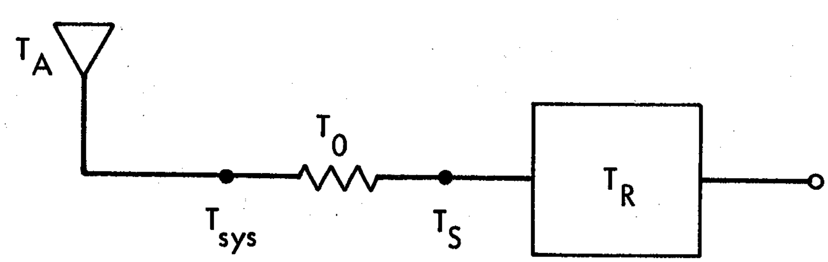

Figure 7.3. Locations where T_{sys} and T_s are defined.

dissipative transmission line which acts as an attenuator at a temperature of $T_a = T_o$, and a receiver having a noise temperature of T_R. T_{sys} is defined as the temperature at the antenna terminals and is given by

$$T_{sys} = T_A + (\ell_a - 1)\, T_o + \ell_a\, T_R \qquad \text{K} \qquad (7.14)$$

Noise introduced by the antenna is accounted for by T_A. Then follows a term representing the input temperature of an attenuator at a physical temperature of T_o [corresponding to T_1 of Eq. (7.13)]. Finally, $\ell_a T_R$ corresponds to T_2/g_1 of Eq. (7.13) as $\ell_a = 1/g_a$.

Some analyses of telecommunication links make use of T_s, defined as at the receiver terminals, rather than T_{sys}. It is simple to convert from T_{sys} to T_s by using

$$T_s = T_{sys}\, g_a \qquad \text{K} \qquad (7.15)$$

resulting in

$$T_s = T_A g_a + (1 - g_a)\, T_o + T_R \qquad \text{K} \qquad (7.16)$$

Either T_{sys} or T_s can be used if carrier and noise powers are defined at the same location, either antenna or receiver terminals. Noise power X at the antenna terminals if given by

$$X = k\, T_{sys}\, B \qquad \text{W} \qquad (7.17)$$

and at the receiver terminals by

$$X = k\, T_s\, B \qquad \text{W} \qquad (7.18)$$

Note that if $g_a = \ell_a = 1$, corresponding to zero attenuation between the antenna and receiver

$$T_{sys} = T_s = T_A + T_R \qquad (7.19)$$

The effective noise temperature of the antenna T_A is not its physical temperature but accounts for all the noise, including sky noise and noise of terrestrial origin, that appears at the output terminals of the antenna. The term sky noise includes noise emitted by the constituents of the Earth's atmosphere, namely gases, hydrometeors, and any other matter such as dust. It also includes extraterrestrial noise emitted by the Sun, Moon, planets, and universe, including the 2.7 K component which fills space. Terrestrial noise may be picked up by the side lobes or as a result of antenna spillover and blockage, in the case of the earth-station antenna. The main lobe, however, of a satellite-borne antenna is usually pointed at the Earth and receives noise of terrestrial origin. Interfering signals can also be considered to constitute noise which contributes to T_A.

The system noise temperature can be decreased by placing a preamplifier at the antenna terminals. In that case, for a system otherwise the same as that of Fig.7.3,

$$T_{sys} = T_A + T_{pre} + \frac{(\ell_a - 1)T_o + \ell_a T_R}{g_{pre}} \qquad (7.20)$$

For this procedure to be most effective, the noise temperature of the preamplifier, T_{pre}, must be low and its gain, g_{pre}, should be high. The contributions to T_A are considered in the following section.

7.2 ATMOSPHERIC CONTRIBUTIONS TO NOISE TEMPERATURE

The principal types of naturally occurring radio noise, generated externally to the receivers of telecommunication systems, are the noise of lightning discharges (commonly referred to as atmospheric noise), cosmic noise, thermal radiation from the atmosphere and nearby terrain and objects, and noise from the Sun, Moon, and distant planets. Noise from lightning predominates for frequencies below about 20 MHz, and cosmic noise tends to be most important between about 20 and 1000 MHz. Above 1000 MHz, atmospheric thermal noise tends to predominate, when the antenna points into space and not towards the Sun or other discrete source. Noise from lightning occurs mainly at frequencies below the range of this handbook and cosmic noise is considered in Sec. 7.3. Attention is directed in this section to atmospheric thermal noise.

A basic relation concerning noise applies to the noise temperature T_b recorded when observing a noise source, represented by a temperature T_s, through an absorbing region. The relation for the zenith is

$$T_b = T_s e^{-\tau_\infty} + \int_0^\infty T(h)\ \alpha(h)\ e^{-\tau}\, dh \qquad (7.21)$$

with

$$\tau_\infty = \int_0^\infty \alpha(h)\ dh$$

and

$$\tau = \int_0^h \alpha(h)\ dh$$

with $\alpha(h)$ the absorption coefficient expressed as a function of height h (Waters, 1976). When T(h) is a constant, a change of the variable of integration made by noting that $\alpha(h)$ dh equals $d\tau$ allows carrying out the integration and obtaining the simpler form (with $\tau = \tau_\infty$)

$$T_b = T_s e^{-\tau} + T_i\ (1 - e^{-\tau}) \qquad (7.22)$$

The first term of Eq. (7.22) shows that the noise source beyond the absorbing region is attenuated by a factor of $e^{-\tau}$. The second term represents atmospheric thermal noise which may be generated whether there is a noise source T_s beyond the absorbing region or not. If τ is zero, corresponding to no absorption, the second term is zero. If attenuation due to scattering occurs as well as absorption, Eq. (7.22) may need to be modified such that $\alpha(h)$ represents absorption only. However, Eq. (7.22) may still be used as it is, with $\alpha(h)$ representing extinction even when there is scattering, if an appropriate, effective temperature T_i can be determined. In this case, T_i will be less than the actual physical temperature of the absorbing region.

One procedure for determining T_i involves alternately pointing at the Sun and away from the Sun. The difference in the two values of T_b give $T_s\, e^{-\tau}$ which allows determining $T_i\,(1 - e^{-\tau})$ also. By recording T_b when pointing at the Sun with no obvious absorbing region present (no clouds or precipitation) and correcting for the small absorption due to gases, one can then determine T_s itself for the Sun. Knowing T_s allows determining $e^{-\tau}$. Finally, as all the other quantities of Eq. (7.22) are known by now, T_i can be determined as well.

Extraterrestrial noise corresponding to a noise temperature of 2.7 K is always present and this small value can be accounted for or ignored, in the latter case and in the absence of any other known source resulting in

$$T_b = T_i\,(1 - e^{-\tau}) \tag{7.23}$$

The value of the effective temperature T_i will be different at different times and locations, but taking it as 280 K appears to give generally good results in temperate regions. Wulfsberg and Altshuler (1972) found that 284 K was a suitable value for Hawaii. In other cases, where scattering was thought to be significant, lower temperatures such as 273 or 260 K have been used.

Figure 7.4 shows the estimated ratio of the extinction (total attenuation) constant to the absorption constant for a 12 mm/h rain model and for a cloud model. According to this figure, scattering is not important for clouds for frequencies below 50 GHz but is significant for rain of this intensity above about 5 GHz. Figure 7.5 shows a plot of Eq. (7.23) for $T_i = 280$ K and also the relation $T_b = 60\, A_{dB}$.

For low-noise systems, the decrease in signal-to-noise ratio C/X due to noise is larger than the accompanying decrease due to signal attenuation, for attenuation up to about 10 dB. This condition is illustrated by Fig. 7.6 which is based upon Eq. (7.23) with $T_i = 280$ K. To understand the basis for Fig. 7.6, consider

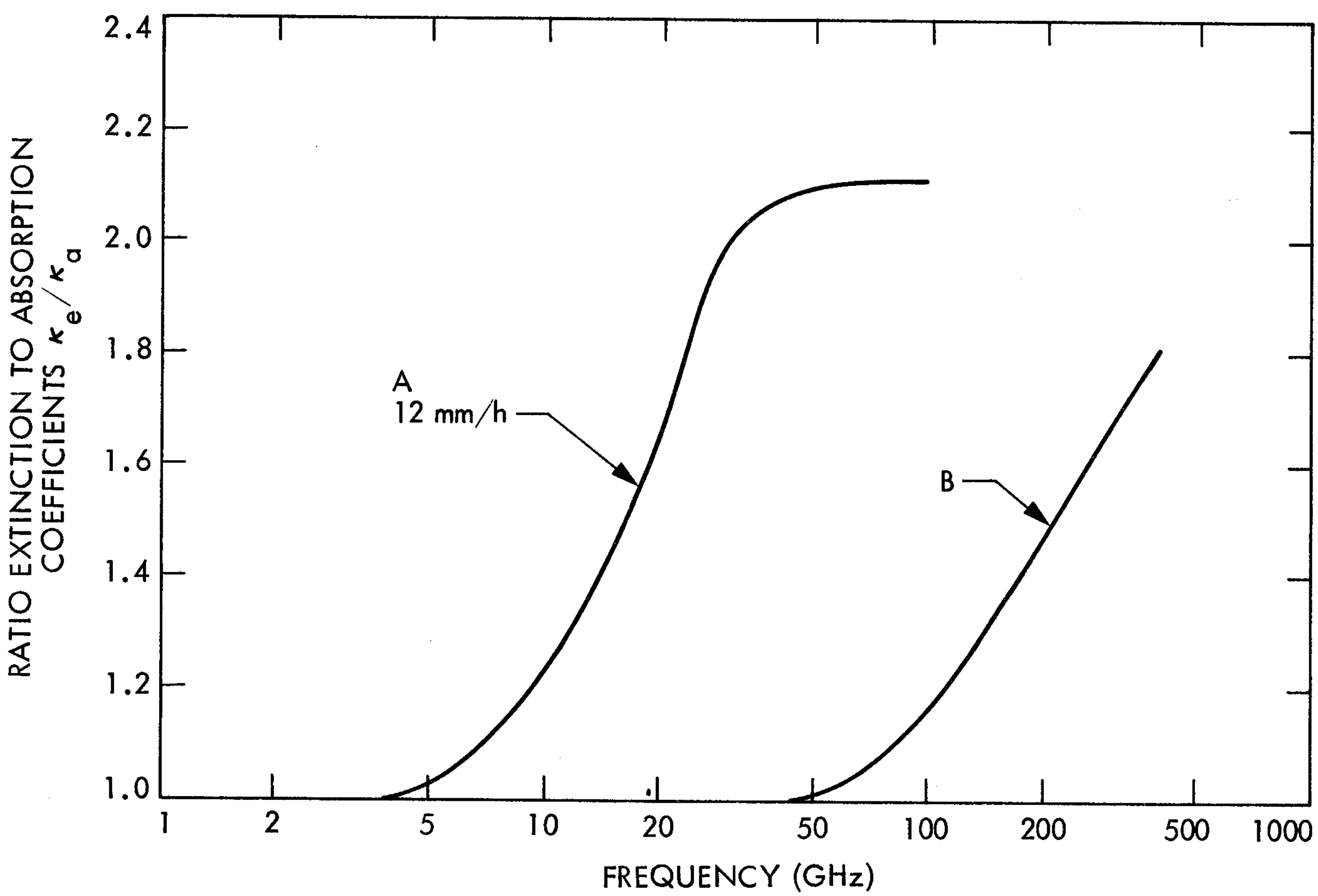

Figure 7.4. Ratio of extinction to absorption coefficients for a rain model (A) and a cloud model (B) (CCIR,1981).

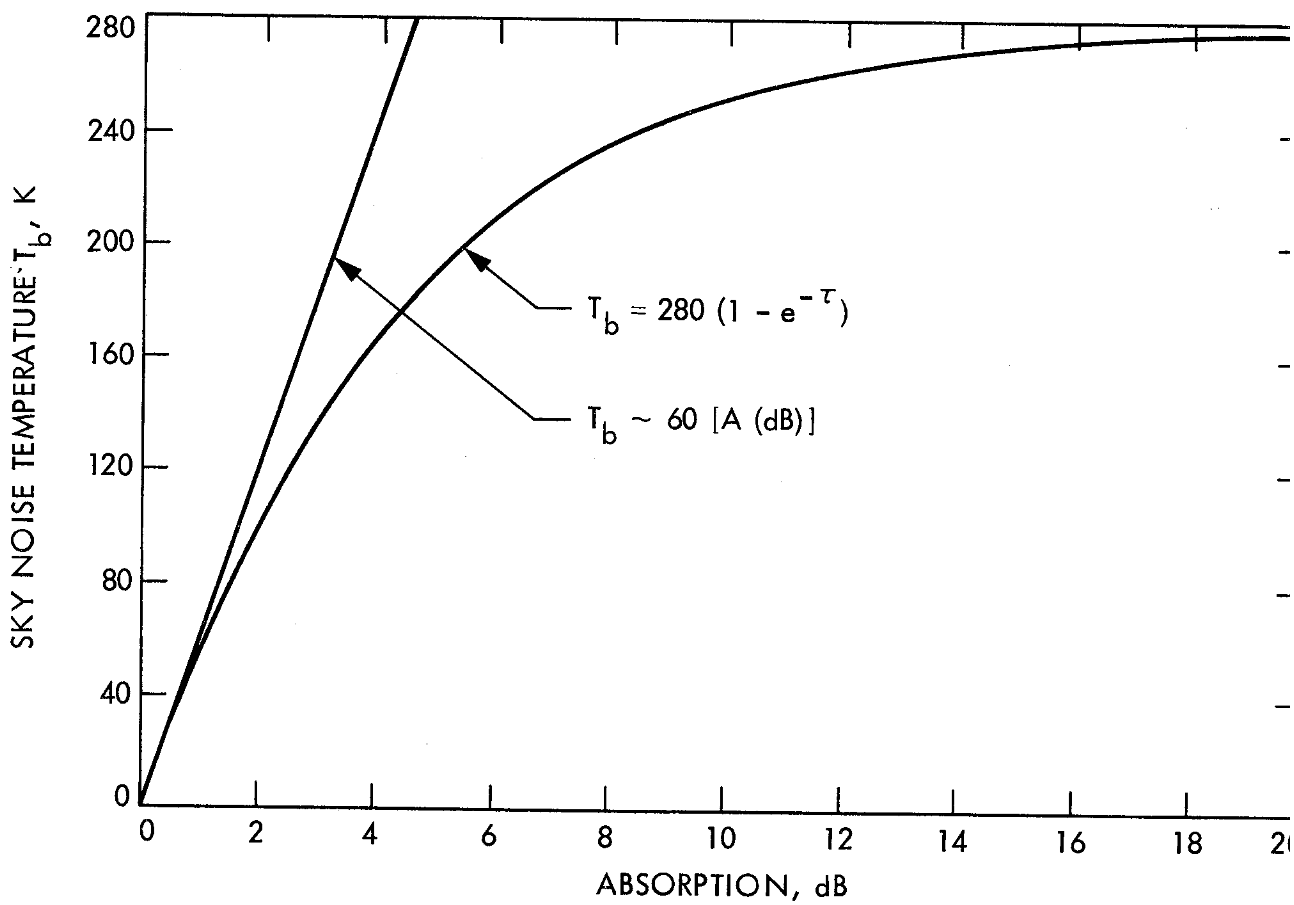

Figure 7.5. Sky noise temperature T_b due to absorbing region, assuming T_i = 280 K (CCIR, 1981).

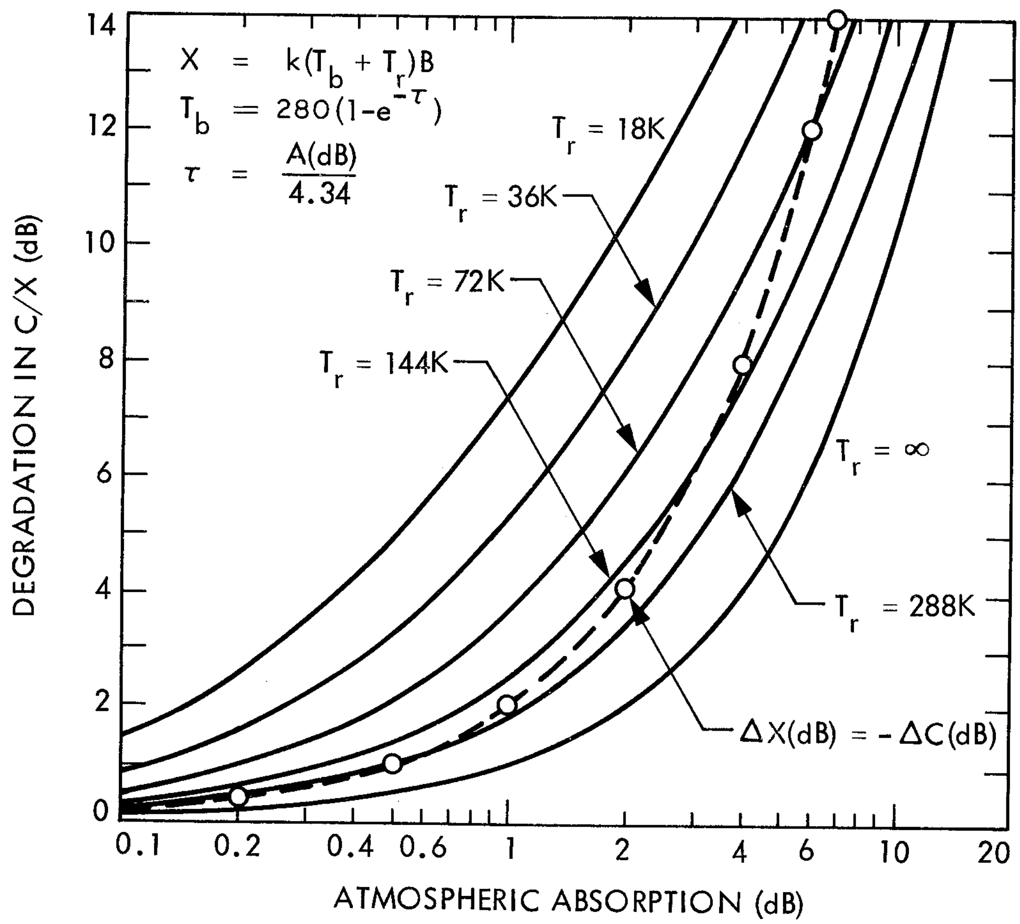

Figure 7.6. Degradation in signal-to-noise ratio, C/X, versus atmospheric absorption, for various values of T_1 (taking T_1 as equal to T_r).

that the signal power C is reduced by the factor of $e^{-\tau}$ by the rain or other source of attenuation that is being considered. The noise power X will be increased at the same time from $X_1 = kT_1B$ to $X_2 = kT_2B$ because of the same absorbing region. The noise power X_2 is related to T_1, T_2, and T_b of Eq. (7.23) by

$$X_2 = k\,(T_b + T_1)\,B = kT_2B \tag{7.24}$$

The optical depth τ is related to attenuation A in dB by

$$\tau = A_{dB}/4.34 \qquad (7/25)$$

where $4.34 = 10 \log_{10} e$. Using the above relations it develops that

$$\Delta(C/X)_{dB} = \Delta A_{dB} + 10 \log (T_2/T_1) \tag{7.26}$$

where $\Delta(C/X)_{dB}$ is the value of the decrease in C/X.

The dotted line in Fig. 7.6 divides the figure into two regions. To the left and above this line, the decrease in C/X due to the increase in noise is greater than the decrease ΔA_{dB} due to attenuation. The reverse is true to the right and below the line. For example, if $T_1 = T_R = 18$ K as may occur in the NASA-JPL Deep Space Network, absorption of 1 dB will result in an increase of noise power of about 6.5 dB and a total decrease of C/X of 7.5 dB. For large earth stations of the type used for some satellite communications, T_1 may be between 50 and 100 K, for which a 1 dB increase in absorption will result in a 2 to 3.3 dB increase in noise and a 3 to 4.3 decrease in C/X.

Attenuation due to gases of the troposphere was illustrated in Sec. 3.6, and attenuation caused by rain was discussed in Chap. 4. Some values of attenuation and noise due to clouds were given in Sec. 5.1.3, and a more extensive set of such values is given in Table 7.1 (Slobin, 1981, 1982). For low noise systems, especially for frequencies above about 10 GHz but also for frequencies as low as 8.5 GHz, clouds are an important source of noise. The values of Table 7.1 apply for zenith paths (elevation angle of 90 deg). Attenuation for elevation angles θ less than 90 deg but greater than 10 deg can be obtained from

$$A(\theta) = A_{zenith}/\sin\theta \qquad \text{dB} \tag{7.27}$$

TABLE 7.1 Sample Cloud Models and S-, X-, K_A-Band Zenith Effects (Slobin, 1981, 1982).

Case	Lower Cloud				Upper Cloud				Remarks	S-Band (2.3 GHz) Zenith		X-Band (8.5 GHz) Zenith		X-Band (10 GHz) Zenith	
	Density g/m^3	Base km	Top km	Thick-ness km	Density g/m^3	Base km	Top km	Thick-ness km		T(K)	A(dB)	T(K)	A(dB)	T(K)	A(dB)
1	-	-	-	-	-	-	-	-	Clear Air	2.15	.035	2.78	0.45	3.05	.049
2	0.2	1.0	1.2	0.2	-	-	-	-	Thin Clouds	2.16	.036	2.90	.047	3.22	.052
3	-	-	-	-	0.2	3.0	3.2	0.2		2.16	.036	2.94	.048	3.28	.053
4	0.5	1.0	1.5	0.5	-	-	-	-		2.20	.036	3.55	.057	4.12	.066
5	-	-	-	-	0.5	3.0	3.5	0.5		2.22	.037	3.83	.062	4.50	.073
6	0.5	1.0	2.0	1.0	-	-	-	-	Medium Clouds	2.27	.037	4.38	.070	5.27	.084
7	-	-	-	-	0.5	3.0	4.0	1.0		2.31	.038	4.96	.081	6.06	.098
8	0.5	1.0	2.0	1.0	0.5	3.0	4.0	1.0	Heavy Clouds	2.43	.040	6.55	.105	8.25	.133
9	0.7	1.0	2.0	1.0	0.7	3.0	4.0	1.0		2.54	.042	8.04	.130	10.31	.166
10	1.0	1.0	2.0	1.0	1.0	3.0	4.0	1.0		2.70	.044	10.27	.166	13.35	.216
11	1.0	1.0	2.5	1.5	1.0	3.5	5.0	1.5	Very Heavy Clouds	3.06	.050	14.89	.245	19.66	.326
12	1.0	1.0	3.0	2.0	1.0	4.0	6.0	2.0		3.47	.057	20.20	.340	26.84	.457

Notes:

1) Clear and cloud models as described in text
2) Cases 2-12 are clear air and clouds combined
3) Antenna located at sea level
4) Heights are above ground
5) No cosmic background or ground contribution considered
6) T(K) is atmospheric noise temperature at zenith
7) A(dB) is atmospheric attenuation along vertical path from ground to 30 km above ground

For lower elevation angles, the following expression has been used.

$$A(\theta) = \frac{2\,A_{zenith}}{\sin^2\theta + 0.00235 + \sin\theta} \quad \text{dB} \qquad (7.28)$$

Figure 7.7 shows values of noise temperature for a clear atmosphere having a water vapor density of 7.5 g/m^3 (CCIR,1986). For a zenith path (θ = 90 deg), the noise values are small for frequencies of 10 GHz and lower. Note, however, that for angles of about 10 deg and less the noise temperature values tend to be significant. For θ = 0 deg, as for a terrestrial path, the noise temperature becomes about 140 K at 10 GHz. Atmospheric and other types of natural radio noise are treated in a mini-review by Flock and Smith (1984).

7.3 EXTRATERRRESTRIAL NOISE

7.3.1 Introduction

While studying atmospheric noise from thunderstorms, Jansky, an engineer with the Bell Telephone Laboratories, first identified radio noise of extraterrestrial origin (Jansky, 1932. 1933). The identification was made while conducting direction-finding observations at a frequency of 20.5 MHz. Three sources of noise were recorded -- noise from nearly thunderstorms, noise from distant thunderstorms, and noise of cosmic or extraterrestrial origin. The cosmic noise came from a region having a right ascension angle near 18 h and a declination angle near -10 deg, which is the direction of the center of the Galaxy. Jansky noted that the extraterrestrial noise was often the limiting factor with respect to the detection of weak signals in the frequency range he was working in.

Reber followed up on Jansky's work by constructing and operating a receiving system having a 9.5 m paraboloidal reflector in his backyard in Wheaton, Illinois. Utilizing a frequency of 160 MHz, he constructed the first radio map of the Milky Way (Reber, 1940). Later he investigated the intensity distribution of cosmic noise at 480 MHz (Reber, 1948).

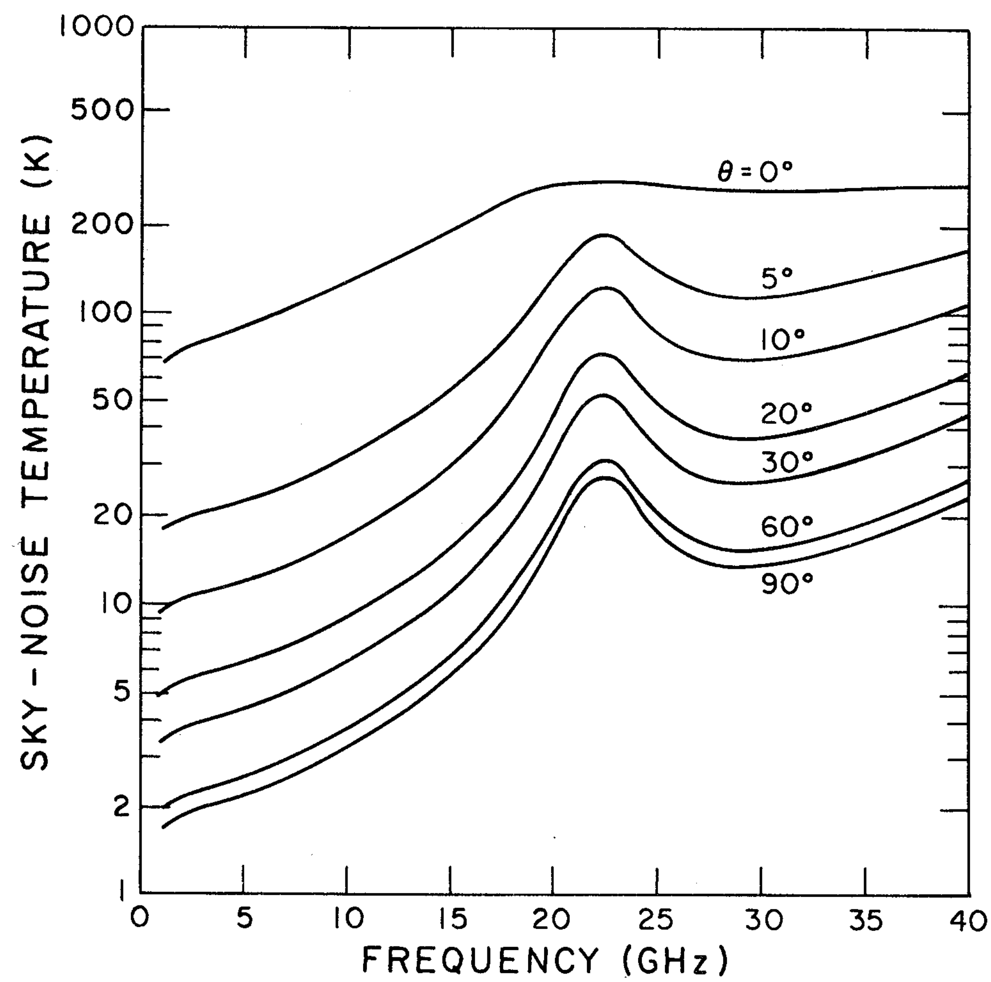

Figure 7.7. Sky-noise temperature for a water vapor density of 7.5 g/m^3 as a function of elevation angle θ (CCIR, 1986).

The first recorded recognition of radio emission from the Sun was made in 1942 by Hey (1946), who was concerned with radio noise causing interference to 5-m radars in southern England during World War II. Jamming by German forces was suspected at first in a particular case in February 1942, but it was concluded that the noise was associated with a large sunspot. Later in the same year, Southworth (1945) of the Bell Telephone Laboratories observed thermal emission from the quiet Sun at centimeter wavelengths. Reber (1944) did not succeed in detecting the Sun by radio means until 1943-1944, as at frequencies of a few hundreds of MHz the Milky Way appears brighter than the Sun when viewed with a broad-beam antenna at radio frequencies.

The first observation of emission from a discrete radio source other than the Sun, namely from Cygnus A. was made by Hey, Parsons, and Phillips (1946). The identification as a discrete source was originally made for the wrong reason. Emission from the source was thought to vary in amplitude as mentioned when introducing the subject of ionospheric scintillation (Sec. 2.6.1). Observations by Bolton and Stanley (1948), utilizing the resolution obtained by interference between direct and reflected rays at a location on a cliff overlooking the the sea, however, showed that the source was indeed discrete, in fact confined to 8 min of arc. Their observations were made mainly at 100 MHz, for which they reported that the source had an effective temperature of 4×10^6 K. In the same year, Ryle and Smith (1948), utilizing a frquency of 80 MHz, identified another strong discrete radio source, Cassiopeia A.

The brightness of the sky at radio frequencies does not correspond to that at optical frequencies, and it has been difficult to identify radio sources with visible objects. The first such identification was made by Bolton, Stanley, and Slee (1949), who identified the radio source Taurus A with the Crab Nebula, the expanding shell of the supernova of 1054 A.D. The prediction in 1945 by van de Hulst of emission by neutral hydrogen at 1421 MHz (Kraus, 1966) and the subsequent detection of such emission by Ewan and Purcell (1951) at Harvard was an important development. The emission by neutral hydrogen is due to a hyperfine transition between two states corresponding to the electron spin being parallel or antiparallel to the spin of the nucleus (the proton). The probability of spontaneous emission of this type is very low, but the extent of interstellar space is so vast that the total amount of emission by hydrogen in space is sufficient to be observable in our galaxy and also in nearby galaxies.

Since the early developments mentioned above many discrete sources of radio emission have been identified and much progress has been made in mapping and cataloguing both discrete sources and background radiation. Interesting histories of the radio observations of extraterrestrial sources have been given by Shklovsky (1960) and Hey (1983), and a valuable thorough account of radio astronomy has been prepared by Kraus (1986). Radio sources are useful for calibrating radio telescopes and, in discussing this topic, Wielebinski (1976) has presented a list of radio sources. The proceedings of IAU Symposium No. 74 include reports on a number of efforts in the mapping of radio sources (Jauncey et al., 1977), and treatments of radio sources have been presented by Fomalont (1981), Kellerman and Pauliny-Toth (1981), and Miley (1981).

The discovery by Penzias and Wilson (1965) of microwave background radiation corresponding to about 3 K in temperature was an important development which earned the Nobel Prize for them (Wilson, 1979). The radiation is believed to be relict radiation from the formation of the universe. It displays a high degree of isotropy, varying by only about 0.003 K in 24 hours. Shakeshaft and Webster (1968) analyzed the values of microwave flux at 12 different frequencies as reported by various observers. They concluded that the values were in agreement with blackbody radiation from matter at 2.68 K, and a value of 2.7 K is commonly assigned to microwave background radiation.

7.3.2 Thermal Emission

Radio noise may be due to thermal or non-thermal emission and may cover a continuum of frequencies or occur at a discrete line frequency. Thermal emission from blackbodies obeys the Rayleigh-Jeans law in the radio-frequency range so that the noise power w received from a uniform source is given by

$$w = (2kT/\lambda^2)\,\Omega_s \qquad \text{W/m}^2\text{/Hz} \qquad (7.29)$$

where k is Boltzmann's constant (1.38×10^{-23} J/K), T is temperature in kelvins, λ is wavelength in m, and Ω_s is the solid angle in steradians subtended by the source. It can be seen that w varies inversely with wavelength squared or with λ to the -2 power. The exponent n of λ is known as a spectral index (Kraus, 1966). A hot blackbody emits thermal radiation and thus tends to be a strong emitter at infrared and optical frequencies but a weak emitter at radio frequencies.

Emission from neutral hydrogen is line emission (most prominently at the discrete frequency of 1421 MHz), but emission from ionized hydrogen, such as occurs near hot stars, is a form of thermal emission. The thermal radiation comes from free electrons experiencing acceleration, as when deflected in passing near a proton. The spectral index for ionized hydrogen can range from 0 to -2. Flux from a region of ionized hydrogen is as described by Eq. (7.29) but T can be either a constant for which $n = -2$ or can vary as wavelength squared for which $n = 0$. Recall that the brightness temperature T_b when viewing a region of intrinsic brightness T_i having an optical depth of τ is given by

$$T_b = T_i\,(1 - e^{-\tau}) \tag{7.30}$$

For a region containing free electrons τ is inversely proportional to frequency squared or directly proportional to wavelength squared, and for high frequencies (e.g. 3 GHz) for which τ is very small

$$T_b \simeq T_i \tau \propto T_i \lambda^2$$

Then T of Eq. (7.29) becomes T_b and is proportional to wavelength squared so that $n = 0$. For lower frequencies for which τ is large $T_b \simeq T_i$, w varies inversely with λ^2, and $n = -2$.

7.3.3 Non-thermal Emission

The mechanism believed to be responsible for most non-thermal emission is synchrotron radiation. This form of radiation occurs when high velocity electrons follow spiral paths in magnetic fields (Jackson, 1962; Kraus. 1986). The electrons may be cosmic ray particles having relativistic velocities. Alven and Herlofson (1950) first suggested that the intense radio emission at low frequencies is due to synchrotron radiation. Consider a relativistic electron moving in a circular orbit. Under this condition, radiation from the electron is concentrated in a narrow cone of width θ which is pointed in the direction of the instantaneous velocity, as suggested in Fig. 7.8. An observer in this direction will observe a short burst of linearly polarized radiation, with its electric field intensity vector oriented as shown in the illustration. Such radiation has a broad frequency spectrum. The spectral index for synchrotron radiation derived from cosmic-ray particles tends to be around 0.75 so that the power density of the radiation, w, is proportional to $\lambda^{0.75}$. Note that unlike the case for thermal emission, the spectral index for non-thermal emission is positive. Table 7.2 gives flux densities w and spectral indices for certain strong discrete sources of radio noise at frequencies indicated in the table.

Line emission from neutral hydrogen is a form of nonthermal emission. It has provided a picture of the spiral structure of our galaxy. Cassiopeia A, in our galaxy, the most intense discrete source of radio noise in the sky other than the Sun is a nonthermal

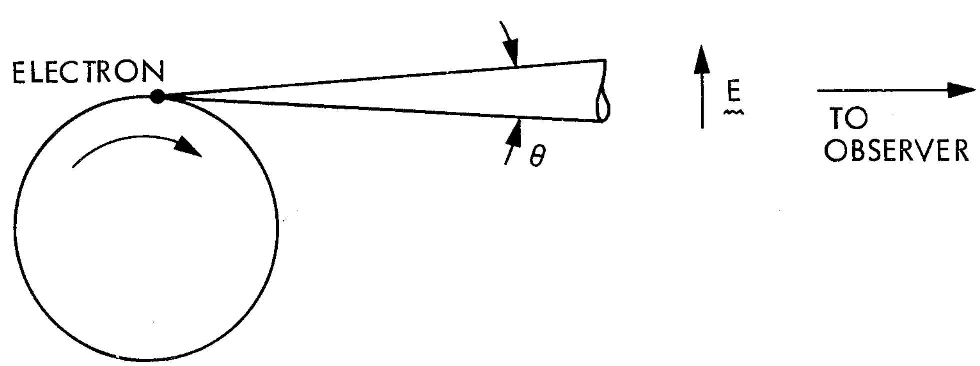

Figure 7.8. Beam of radiation from a very high velocity electron.

Table 7.2 Flux Densities and Spectral Indices for Some Nonthermal Sources (Kraus, 1986).

Source	Noise Power Density, w (Janskys)[1]	Frequency (MHz)	Spectral Index
Cassiopeia A	11,000	178	0.77
Cygnus A	8,700	178	≃0.6
Crab nebula	1,000	1,000	0.27
Virgo A	580		0.83
Cygnus loop	300	100	0.4 - 0.5

[1] One Jansky (Jy) = 10^{-26} W/m²/Hz.

source. Cassiopeia A is a remnant of a supernova believed to have occurred in about 1700. The crab nebula is a remant of a supernova listed in Chinese chronicles as having occured on July 4, 1054. The Cygnus loop is also a supernova remnant. Cygnus A, the second most intense noise source other than the Sun, is a double galaxy outside our own that has a total radio power output of 10^{38} W. Virgo A is a galaxy having a radio power output of 10^{35} W.

7.3.4 The Sun, Moon, and Planets

The Sun emits as a blackbody with a temperature near 6000 K in the optical range, but at radio frequencies (below about 30 GHz) the emission from the quiet Sun is greater than that for a blackbody at this temperature and emission from the disturbed Sun is much greater yet at radio frequencies. Radiation at a particular frequency f, where $f \simeq f_p$, comes mostly from a layer located just above a critical layer having a plasma angular frequency $\omega_p = 2\pi f_p$ given by

$$\omega_p^2 = \frac{Nq^2}{m\epsilon_0}$$

where N is electron density, q is electron charge, m is electron mass, and ϵ_0 is the electric permittivity of empty space (Sec. 2.1).

As N decreases with altitude, the lower frequencies are emitted from higher regions of the solar corona. The Sun appears larger and brighter at radio frequencies than for visible frequencies. The equivalent blackbody temperature for radio frequencies may be 10^{11} K or higher (Kraus, 1986). Note that ω_p is the same quantity that appears in $K = 1 - \omega_p^2/\omega^2$, where $K = n^2$ is the relative dielectric constant for the ordinary wave in a plasma [see Eq. (2.9)].

Radio emission from the Sun can be classified into three components, that from the quiet Sun, a slowly varying component from bright regions, and bursts from transient disturbances such as solar flares (Kundu, 1965; Elgaroy, 1977). The slowly varying component is most prominent in the 3 to 60-cm wavelength range. Emission at 10.7 cm has been recorded for many years at Ottawa, Canada. Data from observatories recording radiation at 3, 10.7, 21, and 43 cm and 169 MHz are included in the Solar-Geophysical Data reports issued by NOAA, Boulder, Colorado. Bursts are classified into centimeter bursts, decimeter bursts, and bursts at meter and decameter wavelengths. The latter are further divided into Types I, II, III, IV, and V.

Centimeter-wave bursts have a rapid rise in intensity and a slower decline and cover essentially a smooth continuum of frequencies. The more complex decimeter bursts show a great variety of fluctuations superimposed on the continuum. Type I or noise storm radiation consists of a slowly varying, broadband enhancement of the normal solar radiation on which a series of bursts near 5 MHz are superimposed. The enhanced radiations last from hours to days, and the bursts last from a fraction of a second to several seconds. The radiation is strongly cirularly polarized. Type II and III bursts are intense events whose frequencies drift lower at rates of about 1 MHz/s and 20 MHz/s respectively. Type IV bursts cover a smooth continuum of frequencies having wavelengths from centimeters to decameters and last from about 10 minutes to a few hours. Type V bursts are also continuum events but last only for seconds to minutes and are usually limited to meter wavelengths.

When the beam of a receiving antenna comes close to the Sun, the noise due to the Sun increases in a manner dependent upon the characteristics of the antenna pattern and the relative positions of the Sun and the antenna beam. Figure 7.9 shows the recorded increase in system noise temperature for the 64-m, S-band antenna of the Deep Space Network of the Jet Propulsion Laboratory when tracking Pioneer 8 (Nov. 1968, near the solar maximum).

Radio emission from the Moon was first detected, at a wavelength of 1.25 cm, by Dicke and Beringer (1946). The mean brightness temperature fo the Moon for the S and X bands is about 240 K (JPL, 1977), and the Moon has the rather large angular size of about 0.5 deg. The observed temperature at microwave temperatures varies slightly with the phase of the Moon, reaching a maximum about 3.5 days after full moon. As for the general case, the noise temperature of an antenna that is pointed at the Moon is the average temperature for the beam. If other sources of noise can be neglected, the average temperature is about

$$240\ (\Omega_{moon}/\Omega_{antenna})\ \text{if}\ \Omega_{moon} < \Omega_{antenna}$$

where Ω_{moon} the solid angle of the Moon is $(\pi/4)\ \theta^2_{moon}$, with θ_{moon} the angular width of the Moon, and $\Omega_{antenna}$ is the solid angle of the antenna [as a rough rule of thumb about $(4/3)\ \theta_{hp}\phi_{hp}$, where the latter angles are half-power beamwidths].

Emission from the planets is of much interest from the viewpoint of radio science, the intense, sporadic, and fluctuating emission of Jupiter being especially noteworthy. Equation (7.30) gives the relation used by JPL (1977) for estimating the increase T_{p1} in system noise temperature due to certain planets at the S and X bands, assuming the planets fall within the antenna beamwidth.

$$T_{p1} = \frac{S_0\,\lambda^2}{8\pi k R^2}\,G\,e^{-2.77\,(\theta^2/\theta^2_{hp})} \tag{7.30}$$

In Eq. (7.30), S_0 is the flux density in W/m²/Hz at a range of 1 AU (1.5×10^{11} m), R is the range of the planet in AU, k is Boltzmann's constant, λ is wavelngth, G is antenna gain modified to include atmospheric attenuation, θ is the planet-earth-probe angle in deg, and θ_{hp} is the half-power beamwidth of the antenna in deg. The flux densities S_o in Janskys at 1 AU for some planets are given in Table 7.3.

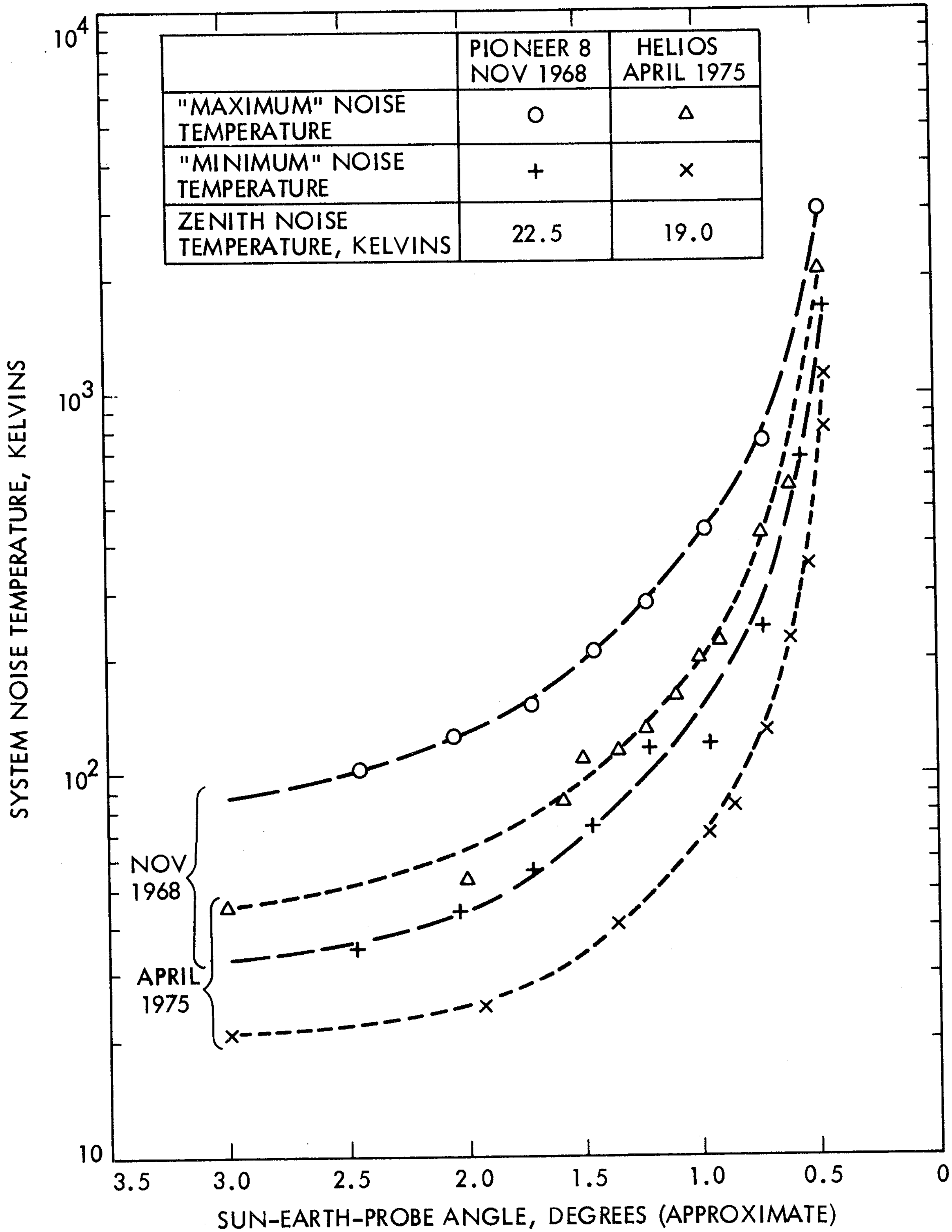

Figure 7.9. System noise temperature vs. sun-earth-probe angle at S band for 64-m antenna stations, from measured data (JPL, 1977).

Table 7.3 Flux Density S_o in Janskys (Jy) at One AU.
($1\ \mathrm{Jy} = 10^{-26}\ \mathrm{W/m^2/Hz}$.)

Planets	S Band	X Band
Venus	0.53	7.4
Mars	0.050	0.68
Saturn	14	170
Jupiter	91 to 118	330

7.3.4 Satellite Operations

A radio map of our galaxy at a frequency of 200 MHz for a beamwidth of 17 deg is shown in Fig. 7.10. The plot is in galactic coordinates and is quite symmetrical with respect to the galactic equator. A noise temperature of 1200 K is shown for the center of the Galaxy. Figure 7.11 shows a similar plot, but for a frequency of 250 MHz and in celestial coordinates, with the zero declination angle corresponding to the Earth's equator. For geostationary satellites the corresponding values of declination δ are restricted to about ±8.7 deg. [For an earth station at the highest possible latitude of about 81.3 deg for communicating with a geostationary satellite, $\delta = \sin^{-1} 6356/(35{,}786 + 6356) = 8.7$ deg where 6356 is the polar radius and 35,786 km is the altitude of a geostationary satellite.] Haslam et al. (1982) have surveyed the radio sky at 408 MHz with an angular resolution of 0.85 deg. Plots of the results of this survey, smoothed to 5 deg angular resolution, are included in CCIR (1986).

The contours of Fig. 7.11 are in units of 6 K above 80 K, the value of the coldest parts of the sky. For an 18 h right ascension angle and 0 deg declination, for example, the value from Fig. 7.11 is 37 and the brightness temperature is 302 K at 250 MHz. To estimate the brightness temperature at a higher frequency note that brightness B of blackbodies at radio frequencies is given by

$$B = 2kT/\lambda^2 \qquad \mathrm{W/m^2/Hz/rad^2} \qquad (7.32)$$

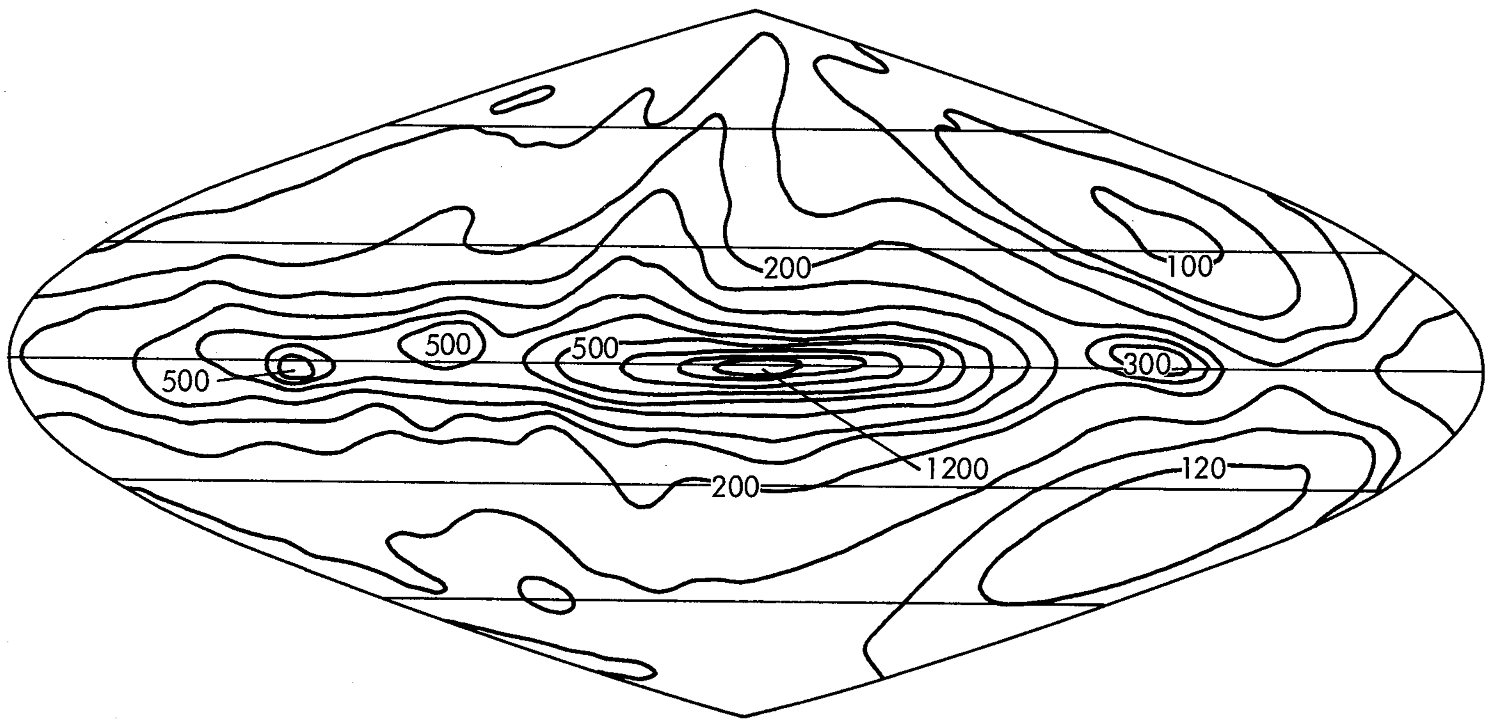

Figure 7.10. Radio map of the Galaxy at $\lambda = 1.5$ m obtained with a 17° beamwidth. The numbers on the contours are radio brightness temperature (K). The galactic centre lies at the centre of the map. The horizontal lines are marked at intervals of 30° of galactic latitude. (After Droge and Priester, 1956).

ORIGINAL PAGE IS OF POOR QUALITY

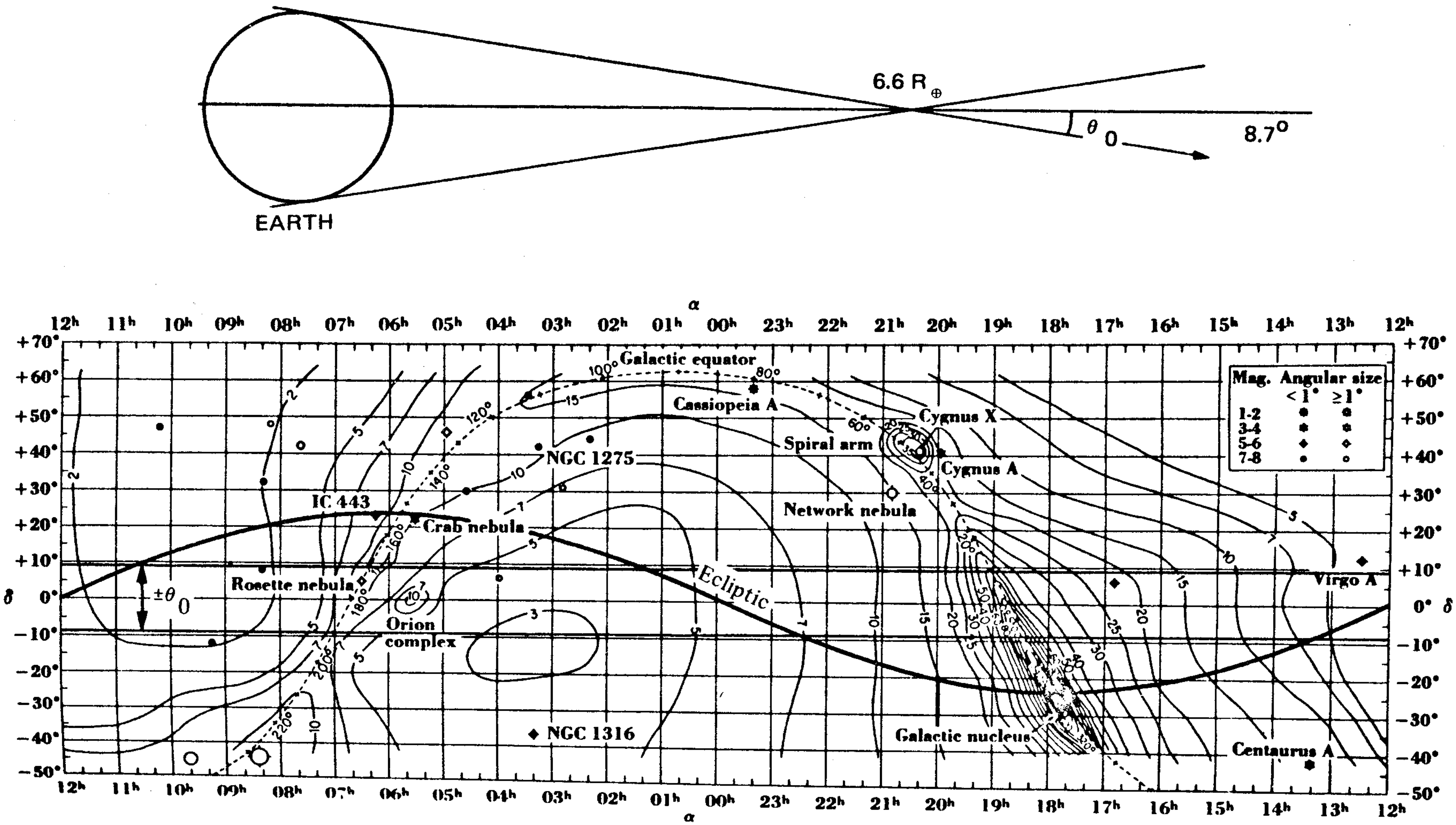

Figure 7.11. Radio sky at 250 MHz as a background for that part of the celestial sphere of interest in earth-satellite telecommunications using the geostationary orbit (CCIR, 1981; Kraus, 1966).

It can be shown that an antenna receiving radiation from a blackbody, assuming that it fills the antenna beam, will receive the power per Hz, w, given by (Flock, 1979)

$$w = kT \qquad \text{W/Hz} \qquad (7.33)$$

For the case of nonthermal radiation, an equivalent blackbody temperature can be assigned even though blackbody-radiation theory does not apply. If the spectral index for nonthermal radiation is 0.75 and T of Eq. (7.32) is to be defined as an equivalent blackbody brightness temperature so that the Rayleigh-Jeans law can be utilized, then T must vary as $\lambda^{2.75}$ or $f^{-2.75}$ (Smith, 1982a). On this basis the brightness temperature at a microwave frequency can be determined from T for 250 MHz (referred to as f_0) by

$$T_b(f_i) = T_b(f_0)\,(f_i/f_0)^{-2.75} + 2.7 \qquad \text{K} \qquad (7.34)$$

For example, if $f_i = 1$ GHz

$$T_b = 302\,(4)^{-2.75} + 2.7 = 9.4 \text{ K}$$

while for $f_i = 4$ GHz

$$T_b = 302\,(16)^{-2.75} + 2.7 = 2.8 \text{ K}$$

The quantity 2.7 K represents the microwave background radiation investigated by Penzias and Wilson (1965), and T_b for $f_i = 4$ GHz is close to this microwave background level. The brightness temperatre T_b in the situation being considered is a strong function of frequency and decreases to a very low value in the S band.

For frequencies above 2 GHz, the extraterrestrial sources of importance are the Sun and a few non-thermal sources such as Cassiopeia A, Cygnus A and X, and the Crab Nebula (CCIR, 1986). Examination of Fig. 7.10, however, shows that the non-thermal sources mentioned are not of concern for geostationary satellites as these sources fall outside the range for δ of ± 8.7 deg. For deep space missions, the value of δ can be near ±23.5 deg, corresponding to the ecliptic, or larger and somewhat larger values of noise may be encountered than for geostationary satellites.

7.3.5 Quasars and Pulsars

Quasars are distant galaxies that look like stars on photographs but are characterized by very large Doppler shifts (redshifts) such that their spectra were not recognized originally. The radio source 3C 48 was first located in 1960, and it was after the discovery of a similar source 3C 273 in 1963 that the large redshifts and corresponding high receding velocities were identified by noting that the observed emission spectrum was that of hydrogen except that it was shifted in frequency by a large amount. The high velocities indicate that quasars (quasi-stellar objects) are at great distances. In order to be seen at such distances, they have to emit extremely high powers at optical frequencies. Many quasars also emit large quantities of radiation at radio frequencies.

Pulsars are considered to be rotating neutron stars which emit radio-frequency or x-ray radiation in the form of a narrow beam, so that an observer on the Earth records short pulses at a regular repetition rate. Jocelyn Bell first identified pulsar signals on Cambridge radio-telescope records of interplanetary scintillation in late 1967. Short pulses, 0.016 second in duration were observed every 1.33730115 second. In 1968 David Staelin and Edward Reifenstein found a pulsar in the middle of the Crab Nebula, a remant of the 1054 supernova. Pulse periods of most pulsars range from 0.033 to 3.7 seconds with a median value of 0.65 second (Hey, 1983).. Pulse lengths are always a few percent of the corresponding pulse periods.

The discoveries of quasars and pulsars were extremely exciting to radio astronomers, and both quasars and pulsars are of great scientific interest. They are mentioned here because they contribute to radio noise. The quasars 3C 273, mentioned above, and 3C 279 occur within the ±8.7 deg range of declination of most importance to satellite communications (Wielebinski, 1976). Quasars, pulsars, and related phenomena are treated in texts on astronomy (e.g. Abell, 1982) and in a number of more specialized publications of both a semipopular and more strictly scientific nature (Shipman, 1980; Hey, 1983).

7.4 NOISE OF TERRESTRIAL ORIGIN

The receiving antenna of an uplink to a satellite points at the Earth and for that reason is commonly assumed to have a noise temperature of 250 to 290 K. Actually the noise temperature is generally lower and is not determined entirely by the Earth alone. To consider the situation further refer to Fig. 7.12 and Eq. (7.35).

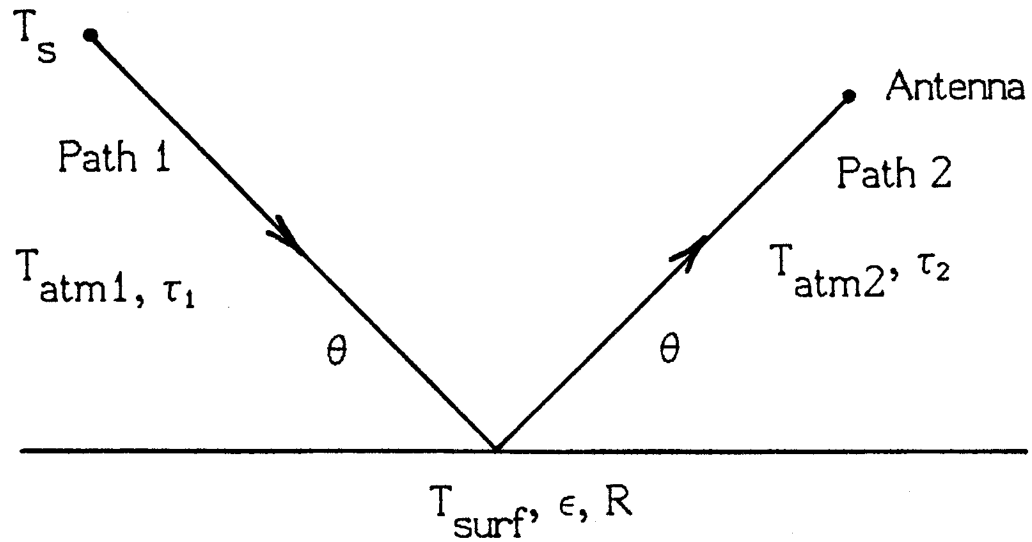

Figure 7.12. Contributions to the brightness temperature T_{b2} recorded by a downward pointing satellite or radiometer antenna (CCIR, 1986).

The brightness temperature T_{b2} recorded by the downward pointing antenna of Fig. 7.12 has the form of

$$T_{b2} = T_{atm2} + (\epsilon T_{surf} + R T_{b1}) e^{-\tau_o} \qquad (7.35)$$

where T_{atm2} accounts for the emission from the atmosphere along path 2, T_{surf} is the actual surface temperature, and T_{b1} is the brightness temperature observed when looking from the ground along path 1. The quantity ϵ is the emissivity of the surface, and R, the power reflection coefficient for radiation incident on the surface, equals ρ squared where ρ is the appropriate reflection coefficient for horizontal, vertical, or circular polarization, etc. of Chap. 6

[Eqs. (6.14), (6.15), (6.18, 6.19]. The optical depth τ_o applies to path 2, from the Earth's surface to the receiving antenna.

Kirchoff's law of radiation theory states that the emissivity ϵ of a surface is equal to its absorptivity α. Both quantities have maximum values of unity. The quantity ϵ represents the fraction of the potential blackbody radiation that is emitted, and α represents the fraction of the incident radiation that is absorbed. For radiation incident upon a surface, the fraction α is absorbed and the fraction R is reflected, where R is the power reflection coefficient. Thus $\alpha + R = 1$, and since $|\alpha| = |\epsilon|$

$$\epsilon + R = 1 \tag{7.36}$$

We deal here with the general case of paths at any elevation angle θ, whereas Eq. (7.21) applies to a zenith path, but otherwise T_{b1} has the form of Eq. (7.21), which is commonly written in the simpler manner of Eq. (7.22). In the present case

$$T_{b1} = T_s e^{-\tau_\infty} + T_{atm1} = T_s e^{-\tau_\infty} + \int_o^\infty T(r)\, \alpha(r)\, e^{-\tau_1(r)} dr \tag{7.37}$$

where the surface is located at $r = 0$, $h = 0$ with r the distance along path 1 and h the height. T_{atm1} accounts for atmospheric emission along path 1. Similarly

$$T_{atm2} = \int_o^{antenna} T(r)\, \alpha(r)\, e^{-\tau_2(r)} dr \tag{7.38}$$

In Eqs. (7.37) and (7.38)

$$\tau_\infty = \int_o^\infty \alpha(r')\, dr' \tag{7.39}$$

$$\tau_1(r) = \int_o^r \alpha(r')\, dr' \tag{7.40}$$

$$\tau_2(r) = \int_r^{antenna} \alpha(r')\, dr' \tag{7.41}$$

$$\tau_o = \int_o^{antenna} \alpha(r')\, dr' \tag{7.42}$$

In the limited frequency range between about 3 to 10 GHz for which atmospheric absorption and emission and extraterrestrial noise may not be significant

$$T_{b2} \simeq \epsilon T_{surf} \tag{7.43}$$

A similar relation is sometimes shown with a term $R\ T_s$ added. Note that $\epsilon = 1 - R = 1 - \rho^2$ and that ϵ therefore depends on wave polarization, elevation angle, the dielectric constant and conductivity of the surface, and surface roughness, as the field intensity reflection coefficient ρ was shown in Chap. 6 to depend on these quantities. For the case of sea water, ρ and ϵ depend on salinity and temperature. The brightness temperature at normal incidence on sea water is shown in Fig. 7.13 as a function of salinity and temperature.

Although T_{b2} is merely noise when telecommunications are being considered, it can be employed to obtain data on phenomena such as sea-surface temperature, for example. Also sea ice and sea water can be distinguished by the higher brightness temperature of sea ice (235 to 240 K for first-year ice and about 210 to 230 K for multiyear ice). Multifrequency radiometry is needed to remove atmospheric and surface roughness effects in order to obtain sea-surface temperature in the general case, and a number of Scanning Multifrequency Microwave Radiometers (SMMR's) have been flown on various missions, the more recent ones on Seasat and Nimbus-7 having frequencies of 6.63, 10.69, 18.0, 21.0, and 37.0 GHz. The microwave radiometers compete with infrared radiometers which have greater spatial resolution and sensitivity but are limited by clouds. Another difference is that emissivity is higher and less variable with sea state and elevation angle at infrared frequencies.

Njoku and Smith (1985) have computed the microwave antenna temperature of the Earth as seen from the geostationary orbit as a function of longitude and frequency. Values ranging from 60 to 240 K have been found. They used an average surface temperature of 292 K and an emissivity of 0.93 for land resulting in a brightness temperature of 272 K for land. A cloud cover of 50 percent with 2.5 g/cm^2 of water vapor was assumed. Brightness temperatures of water are considerably lower than those of land as shown in Fig. 7.14. The brightness temperature at geostationary orbit depends on the fraction of the antenna beam filled by land and the fraction filled by water. The lowest land fraction 0.17 at 160 deg W and the

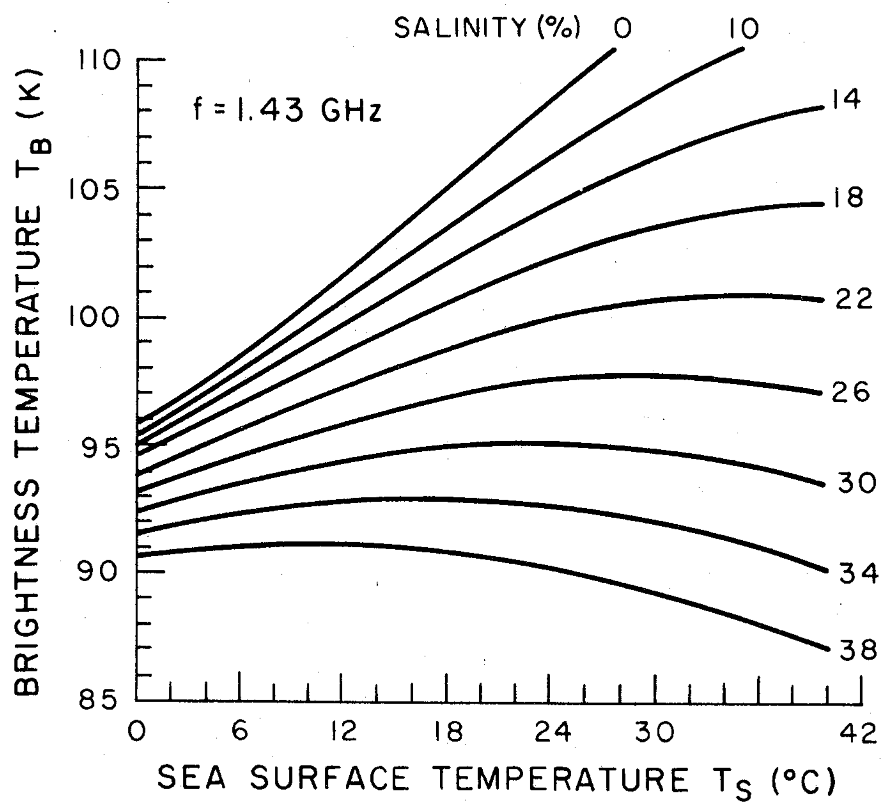

Figure 7.13. Brightness temperature at normal incidence as a function of surface temperature and salinity at a frequency of 1.43 GHz, after Swift (1980).

highest, 0.46 at 30 deg E, correspond to the lowest and highest brightness temperatures, respectively. It is stated that a value of antenna temperature as low as 60 K at 1 GHz can result from antenna efficiencies of around 0.5 to 0.6. The efficiency affects signal intensity as well as noise and is said to not result in a decrease of signal-to-noise ratio, but the true value of antenna temperature should nevertheless be recognized. Antenna temperatures as seen from the geostationary orbit are shown in Fig. 7.14. Note that whereas Fig. 7.12 applies to the case of narrow antenna beamwidths for which a specific elevation angle can be defined, the calculation of brightness temperature from the geostationary orbit assumed that the Earth filled the antenna beam and involved determining resulting average brightness temperatures.

For the case of a downlink from a satellite, the sidelobes and backlobe of the earth-station receiving antenna pick up small amounts of radiation from the Earth. Thus the Earth provides at least a slight contribution to the noise temperature of even a high-quality earth-station antenna. The magnitude of the contribution must usually be determined empirically. Any object in the field of view of an antenna contributes to antenna noise temperature unless it is a perfect conductor. In determining the level of microwave background radiation, Penzias and Wilson (1965) found in a particular case an antenna temperature of 6.7 K when the antenna was pointed to the zenith, of which 2.7 K was cosmic relict radiation, 2.3 K was of atmospheric origin, and 0.9 K was judged to be due to ohmic losses in the antenna and back-lobe response. The latter value is for a very high-efficiency horn antenna and can be considered to be an absolute minimum value.

Noise of terrestrial origin may be natural or man-made. Consideration of man-made radio noise is outside the scope of this handbook. A useful treatment has been provided by Skomal (1978). Chapters are included in his text about noise from automobiles, electric-power systems, and industrial, scientific, and medical sources. Data on man-made noise in the 300 kHz to 250 MHz range are included in CCIR Report 258 (Volume VI, Propagation in Ionized Media), and maximum and mimimum levels of radio noise, including man-made noise, are given in CCIR Report 670 (Volume I, Spectrum Utilization and Monitoring).

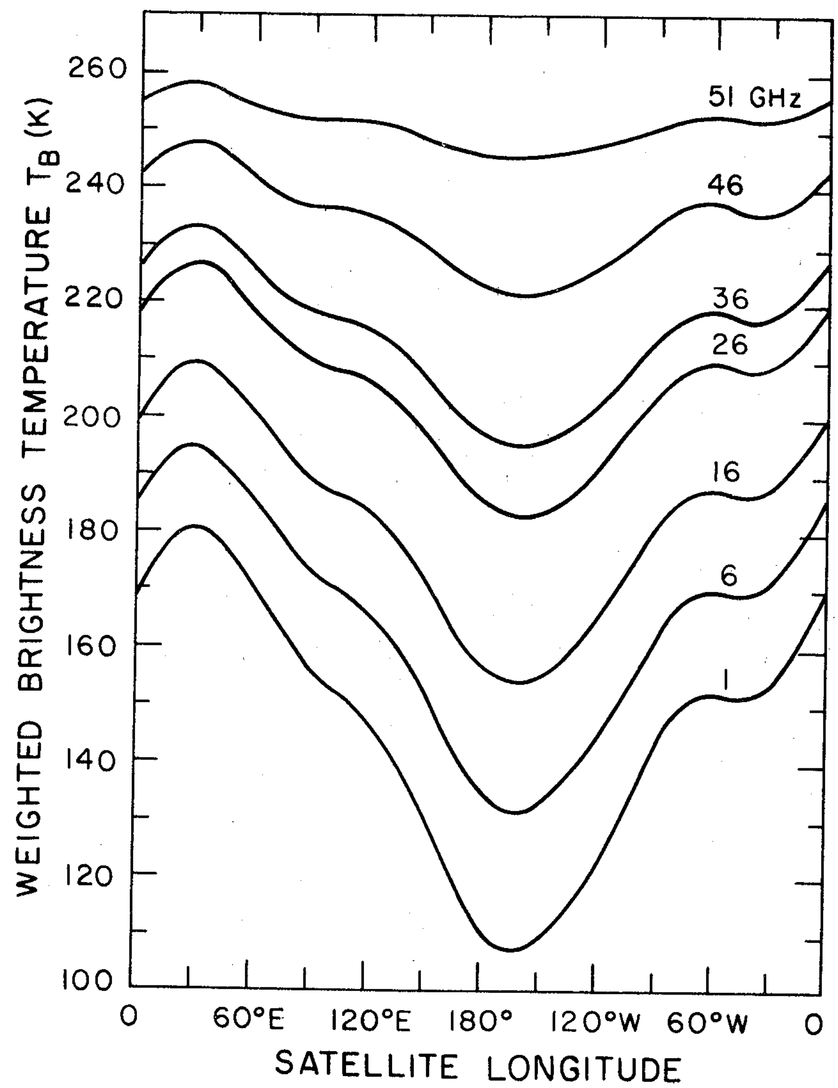

Figure 7.14. Brightness temperature of the Earth as a function of longitude as viewed from the geostationary orbit at frequencies between 1 and 51 GHz. The curves apply to the U.S. Standard Atmosphere, with a columnar content of 2.5 grams/cm^2 of water vapor and 50 percent cloud cover. The normalized earth-coverage antenna pattern is given by $G(\theta) = -3\ (\theta/8.715)^2$ dB for $0 \leq \theta \leq 8.175$ deg where θ is the angle off boresight (Njoku and Smith, 1985).

REFERENCES

Abell, G.O., Exploration of the Universe. Philadelphia: CBS College Publishing, Saunders College Publishing, 1982.

Alfven, H. and N. Herlofson, "Cosmic radiation and radio stars," Phys. Rev., vol. 78, p. 616, 1950.

Bolton, J.G. and G.J. Stanley, "Variable source of radio frequency radiation in the constellation of Cygnus," Nature, vol. 161, pp. 312-313, Feb. 28, 1948.

Bolton, J.G., G.J. Stanley, and O.B. Slee, "Positions of three discrete sources of galactic radio-frequency radiation," Nature, vol. 164, pp. 101-102, July 16, 1949.

CCIR, Draft Revision of Report 564-1 (Mod.1), CCIR Study Group 5 Document 5/34, April 9, 1981.

CCIR, "Radio emission from natural sources above about 50 MHz," Report 720-2, Vol. V, Propagation in Non-ionized Media, Recommendations and Reports of the CCIR, 1986. Geneva: Int. Telecomm. Union, 1986.

Dicke, R.H. and R. Beringer, "Microwave radiation from the Sun and Moon," Astrophys. J., vol. 103, p. 375, 1946.

Droge, F. and W. Priester, "Durchmusterun der allgemeinen radiofrequenz-strahlung bei 200 MHz," Z. Astrophys., vol. 40, pp. 236-248, 1956.

Elgaroy, E.O., Solar Noise Storms. Oxford, New York: Pergamon Press, 1977.

Ewen, H.I. and E.M. Purcell, "Radiation from galactic hydrogen at 1420 Mc/s," Nature, vol. 168, pp. 356-357, Sept. 1, 1951.

Flock, W.L., Electromagnetics and the Environment: Remote Sensing and Telecommunications. Englewood Cliff, NJ: Prentice-Hall, 1979.

Flock, W.L. and E.K. Smith, "Natural radio noise -- a mini-review," IEEE Trans. Antennas Propagat., vol. AP-32, pp. 762-767, July 1984.

Fomalont, E.B., "Extended radio sources," in Origin of Cosmic Rays, IAU Symposium No. 94, Setti, G. et al. (eds.), pp. 111-128. Dordrecht, Netherlands: D. Reidel, 1981.

Haslam, C.G.T. et al., "A 408 MHz all-sky continuum survey. II. The atlas of contour maps." Astron. Astrophys. Supp., vol. 47, pp. 1-143, Jan. 1982.

Hey, J.S., "Solar radiations in the 4 to 6 meter radio wavelength band," Nature, vol. 157, p.47, 1946.

Hey, J.S., The Radio Universe, 3rd Ed. Oxford, New York: Pergamon Press, 1983.

Hey, J.S., S.J. Parsons, and J.W. Phillips, "Fluctuations in cosmic radiation at radio frequencies," Nature, vol. 158, p. 234, Aug. 17, 1946.

Jackson, J. D., Classical Electrodynamics, 2nd Ed. New York: Wiley, 1975.

Jansky, K.G., "Directional studies of atmospherics at high frequencies," Proc. IRE, vol. 20, pp. 1920-1932, Dec. 1932.

Jansky, K.G., "Electrical disturbances apparently of extraterrestrial origin," Proc. IRE, vol. 21, pp. 1387-1398, Oct. 1933.

Jauncey, D.L. (Ed.), Radio Astronomy and Cosmology. IAU Symposium No. 74, Dordrecht, Netherlands: D. Reidel, 1977.

JPL, Deep Space Network/Flight Project Interface Design Handbook, Document 810-5, Rev. D, Sec. TC1-40. DSN Telecommunications Interfaces, Atmospheric and Environmental Effects, Jet Propulsion Laboratory, Pasadena, Ca, 15 Dec. 1977.

Kellerman, K.I. and I.I.K. Pauliny-Toth, "Compact radio sources," in Annual Rev. Astron. Astrophys., vol. 19, pp.373-410. Palo Alto, CA: Annual Reviews, 1981.

Kraus, J.D., Radio Astronomy, 2nd edition. Powell, Ohio 43065: Cygnus-Quasar Books, 1986. (The first edition of 1966 was also useful in the preparation of this chapter.)

Kundu, M. R., Solar Radio Astronomy. New York: Interscience Pub., 1965.

Miley, G., "The structure of extended extragalactic radio sources," in Annual Rev. Astron. Astrophys., vol. 18, pp. 165-218. Palo Alto, CA: Annual Reviews, 1981.

Njoko, E.G. and E.K.Smith, "Microwave antenna temperature of the earth from geostationary orbit," Radio Sci., vol. 20, pp. 591-599, May-June 1985.

Penzias, A.A. and R.W. Wilson, "A meaurement of excess antenna temperature at 4080 Mc/s," Astrophys. J., vol. 142, pp. 419-421, 1965.

Reber, G., "Cosmic static," Proc IRE, vol. 142, pp. 68-70, Feb. 1940.

Reber. G., "Cosmic static," Astrophys. J. vol. 100, pp. 279-287. Nov. 1944.

Reber. G., "Cosmic static," Proc. IRE, vol. 36, pp.1215-1218, Oct. 1948.

Ryle, M. and F.G. Smith, "A new intense source of radio-frequency radiation in the constellation of Cassiopeia," Nature, vol. 162, pp. 462-463, Sept. 18, 1948.

Shakeshaft, J.R. and A.S. Webster, "Microwave background in a steady state universe," Nature, vol. 217, pp. 339,340, Jan. 27, 1968.

Shipman, H.L., Black Holes, Quasars, and the Universe, 2nd Ed. Boston: Houghton Mifflin, 1980.

Shklovsky, I.S., Cosmic Radio Waves, English translation by R.B. Rodman and C.M. Varsavsky. Cambridge, MA: Harvard U. Press, 1960.

Skomal, E.N., Man-Made Radio Noise. New York: Van Nostrand, 1978.

Slobin, S.D., Microwave Noise Temperature and Attenuation of Clouds at Frequencies Below 50 GHz, JPL Publication 81-46, Pasadena, CA: Jet Propulsion Lab., 1981.

Slobin, S.D., "Microwave noise temperature and attenuation of clouds: statistics of these effects at various sites in the United States, Alaska, and Hawaii," Radio Sci., vol. 17, pp. 1443-1454, Nov.-Dec. 1982.

Smith, E.K., "The natural radio noise source environment," Proc. of 1982 IEEE Int. Sym. on Electromagnetic Compatibility, Santa Clara, CA (Sept. 6-8, 1982). New York: IEEE, 1982a.

Smith, E. K., "Centimeter and millimeter wave attenuation and brightness temperature due to atmospheric oxygen and water vapor," Radio Sci., vol. 17, pp. 1455-1464, Nov.-Dec. 1982b.

Southworth, G.D., "Microwave radiation from the sun," J. Franklin Inst., vol. 239, p. 285, 1945.

Swift, C.T., "Passive remote sensing of the ocean - a review," Bound. Layer Meteorol., vol. 18, pp. 25-54, 1980.

Waters, J.W., "Absorption and emission by atmospheric gases,' in Methods of Experimental Physics, vol. 12, Astrophysics, Part B: Radio Telescopes (M.L. Meeks, ed.), pp. 82-97. New York: Academic Press, 1976.

Wilson, R.W., "The cosmic microwave background," Rev. Mod. Phys., vol. 51, pp. 433-445, July 1979.

Wulfsberg, K.N. and E.E. Altshuler, "Rain attenuation at 15 and 35 GHz," IEEE Trans. Antennas Propagat., vol. AP-20, pp. 181-187, March 1972.

CHAPTER 8

PROPAGATION EFFECTS ON INTERFERENCE

8.1 INTRODUCTION

As a result of the congestion of the frequency spectrum and the geostationary orbit and the related widespread use of frequency sharing, consideration of interference has assumed an important role in earth-station siting and other aspects of telecommunication-system design. Interference may arise between terrestrial systems, between terrestrial and space systems, and between space systems. Attention is given here to interference involving space systems, whether between space systems or between space and terrestrial systems. Space-system earth stations, which commonly transmit high power and have sensitive receivers, may cause interference to terrestrial systems when transmitting and may be interfered with by terrestrial systems when receiving. In addition, one earth station may interfere with another. Also, earth stations may receive interfering, unwanted transmissions, as well as wanted signals, from satellites. Likewise satellites may receive interfering transmissions from other than the intended earth station, and terrestrial systems may receive interference from space stations. In Sec. 8.2, some basic considerations are presented concerning the signal-to-interference ratio for a single wanted transmission and a single interfering transmission arriving over a direct path.

In considering the problem of interference to or from an earth station, analysis may be separated into two stages. In the first, a coordination area surrounding the earth station is determined. This area, based on calculating coordination distances in all directions from the earth station, is defined such that terrestrial stations outside the area should experience or cause only a negligible amount of interference. To determine coordination distances information on transmitter powers, antenna gains, and permissable interference levels is needed. For the earth station, the gain towards the physical horizon on the azimuth considered is used. When considering interference due to scatter from rain, it is assumed that the beams of the two antennas intersect in a region where rain is falling. The coordination procedure is thus based on unfavorable assumptions with respect to mutual interference.

After the coordination area has been established, potential interference between the earth station and terrestrial stations within the coordination area can be analyzed in more detail. In this stage of analysis, the actual antenna gains of the terrestrial stations in the directions toward the earth station will be used. Also, it is determined whether the beams of the earth station and terrestial stations truly do intersect, in considering scatter from rain. Terrestrial stations within the coordination area may or may not be subject to or cause significant intereference depending on the factors taken into account in the second stage of analysis.

Two propagation modes are considered for determining coordination area. One involves propagation over near-great-circle paths, and one involves scatter from rain. Coordination distances d_1 and d_2 are determined for the modes and the larger of the two values is used as the final coordination distance. Determination of the two distances is considered in Secs. 8.3 and 8.4. Interference between space stations and terrestrial systems is discussed in Sec. 8.5. Procedures for interference analysis are summarized in Sec. 8.6, and certain practical matters about the siting of earth stations are discussed in Sec. 8.7.

From the propagation viewpoint, interference between terrestrial systems and earth stations is concerned very much with transhorizon propagation. In the late 1950's and early 1960's, transhorizon propagation became of considerable interest as a means of communication over long distances. The rather weak but consistent troposcatter signals were and are utilized for this purpose. The stronger but sporadic signals due to ducting and rain scatter do not occur for the high percentages of time needed for reliable communication, and much of the interest in transhorizon propagation at present is related to interference. Ducting and rain scatter contribute to the higher levels of interfering signals that occur for small percentages of time, and they are highly important in interference analysis (Crane, 1981). The occurrence of ducting is vividly displayed on PPI radar screens showing ground clutter echoes. At times ducting causes ground clutter or targets to appear at considerably greater ranges than normal. Actually there is no fixed normal appearance of the radar screen, as the maximum range at which ground-clutter echoes appear fluctuates continuously.

In this chapter, attention is given to propagation effects on interference and to determination of coordination area, with emphasis on basic concepts. Additional details are given in Appendix 8.1. CCIR Reports 569, 724, and 382 (CCIR, 1986a, b, c) and Appendix 28 to Radio Regulations (ITU, 1982) treat these topics and have been utililized in the preparation of this chapter. Person carrying out coordination analysis should refer to these reports, especially to Appendix 28 for legal purposes; all of the charts, tables, and other details of the reports are not reproduced here. Instead an effort is made to provide explanatory background material and summaries of procedures for use as an introduction and reference on interference analysis. The material in the CCIR reports is subject to a continuing process of revision and updating as a comparison of reports for 1978, 1982 and 1986 indicates.

The procedure described in Appendix 28 of Radio Regulations must be followed in determining coordination area if legal requirements are to be met. The material of Appendix 28 concerning coordination area is essentially the same as that of CCIR Report 382. Study Groups 4 (Fixed Service Using Communication Satellites) and 9 (Fixed Service Using Radio-Relay Systems) have primary responsibility for coordination area; Report 382 is in Volume 9, prepared by Study Group 9. Reports 569 and 724, prepared by Study Group 5 (Propagation in Non-ionized Media), represent its input to the coordination problem. As this handbook is concerned primarily with propagation effects, we describe the approaches of Reports 569 and 724 as well as the procedures of Report 382 and Appendix 28.

8.2 THE SIGNAL-TO-INTERFERENCE RATIO

The signal-to-noise ratio C/X of a telecommunication link was given in Chap. 1 in the form of

$$(C/X)_{dB} = (EIRP)_{dBW} - (L_{FS})_{dB} - L_{dB} + (G_R/T_{sys})_{dB} - k_{dBW} - B_{dB} \qquad (8.1)$$

In this section, attention is given to a corresponding signal-to-interference ratio, C/I. To consider this ratio, first separate EIRP into P_T and G_T where EIRP stands for effective isotropic radiated power, P_T represents the transmitted power, and G_T represents transmitting antenna gain. Also the loss factor L_{dB} can be separated into $A(p,\theta)$, attenuation in dB expressed as a function of percentage of occurrence p and elevation angle θ, and the factor $-20 \log \delta$ representing polarization mismatch (Dougherty, 1980). As δ varies form 0 to 1, $-20 \log \delta$ is a positive quantity. Separating EIRP and L as indicated, C_{dBW} by itself becomes

$$C_{dBW} = (P_T)_{dBW} + (G_T)_{dB} + (G_R)_{dB} - (L_{FS})_{dB} - A(p,\theta) + 20 \log \delta \tag{8.2}$$

For I_{dBW}, the interfering power arriving over a direct path, a similar expression applies, namely

$$I_{dBW} = (P_{Ti})_{dBW} + (G_{Ti})_{dB} + (G_{Ri})_{dB} - (L_{FS})_{dB} - A_i(p,\theta) + 20 \log \delta_i \tag{8.3}$$

where the subscript i refers to the interfering signal. The quantity G_{Ti} represents the gain of the antenna of the interfering transmitter in the direction of the affected receiving system. A similar interpretation applies to the other terms. Interference due to scatter from precipitation will be considered in Sec. 8.3. On the basis of Eqs. (8.2) and (8.3), the C/I ratio may be expressed as follows.

$$\begin{aligned}(C/I)_{dB} = {} & (P_T)_{dBW} - (P_{Ti})_{dBW} + (G_T)_{dB} - (G_{Ti})_{dB} \\ & + (G_R)_{dB} - (G_{Ri})_{dB} + 20 \log (d_i/d) \\ & + A_i(p,\theta) - A(p,\theta) + 20 \log (\delta/\delta_i)\end{aligned} \tag{8.4}$$

The term 20 log (d_i/d) arises from the L_{FS} free-space basic transmission loss terms which have the form of $(4\pi d/\lambda)^2$, where d is distance. In Eq. (8.4), d is the length of the path of the wanted signal and d_i is the length of the path of the interfering signal.

For analyzing transmissions from space to Earth or vice versa, the polarization mismatch factor δ equals cos θ where θ is a polarization mismatch angle to which there may be three contributions such that

$$\theta = \theta_o + \theta_i + \theta_r \tag{8.5}$$

The angle θ_o arises from geometrical considerations and can be determined from

$$\theta_o = \delta B - \alpha\, \delta A \tag{8.6}$$

with δB, the difference in back azimuths between the service path (to the intended earth station) and the interfering path (to the earth station being interfered with). The back azimuth is the angle to the earth station measured from the north-south meridian of the subsatellite point. The factor δA represents the difference in azimuths of the two earth stations, azimuth in this case being measured at the earth station as the angle from geographic north to the great circle path from the earth station to the subsatellite point (Fig. 8.1). The quantity α depends on the great circle distance Z between the earth stations. On this topic, we follow the treatment by Dougherty (1980) and reproduce two of his illustrations showing θ_o as a function of B and A (Fig. 8.2) and B and Z as a function of earth station latitude and longitude with respect to the subsatellite point (Fig. 8.3).

The angle θ_i represents the Faraday rotation of a linearly polarized wave that may take place in propagation through the ionosphere. The concept of Faraday rotation is not applicable to circularly polarized waves. The relation for θ_i used by Dougherty (1980) is

$$\theta_i = 108^{\circ}/f^2 \tag{8.7}$$

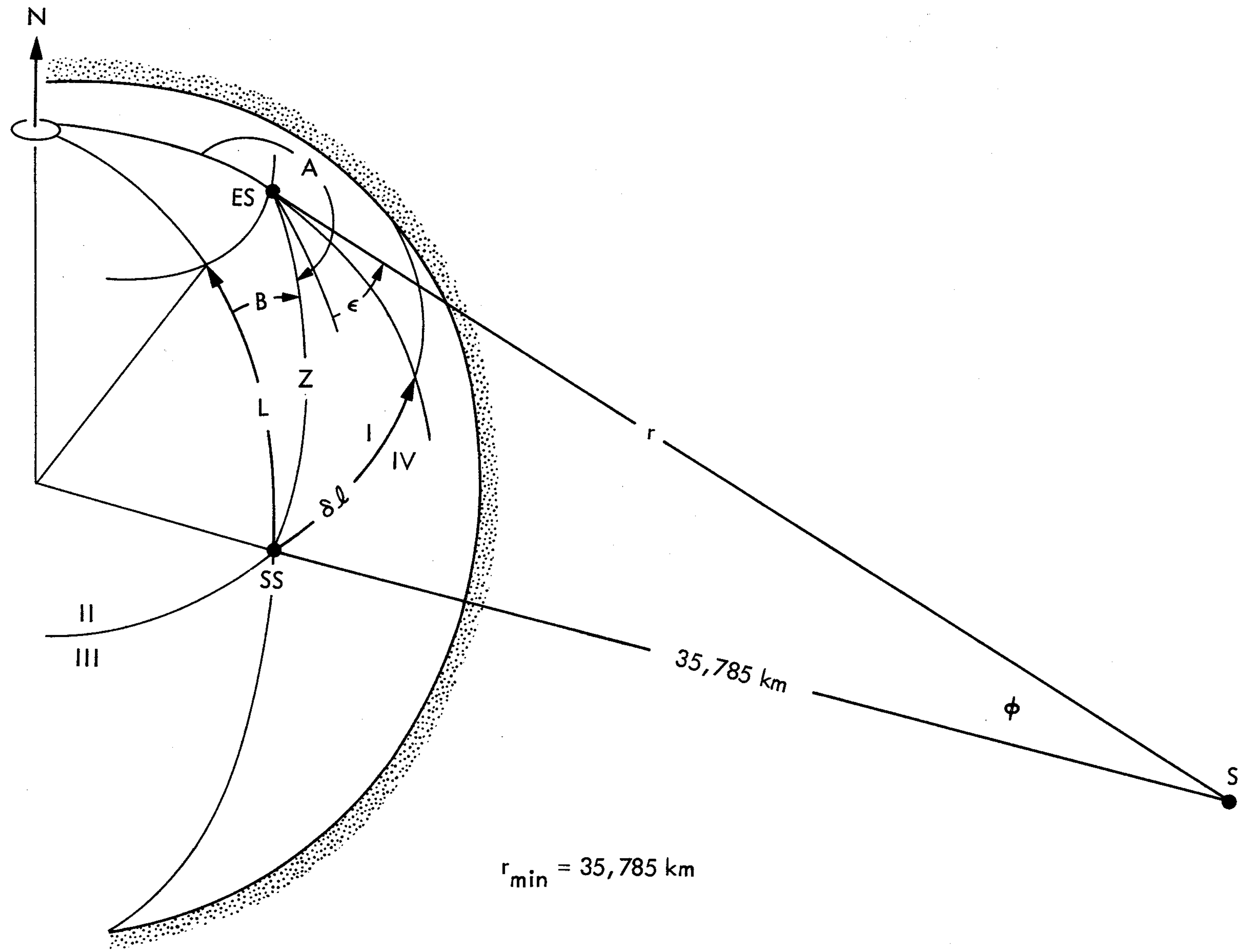

Figure 8.1. Synchronous satellite geometry (Dougherty, 1980).

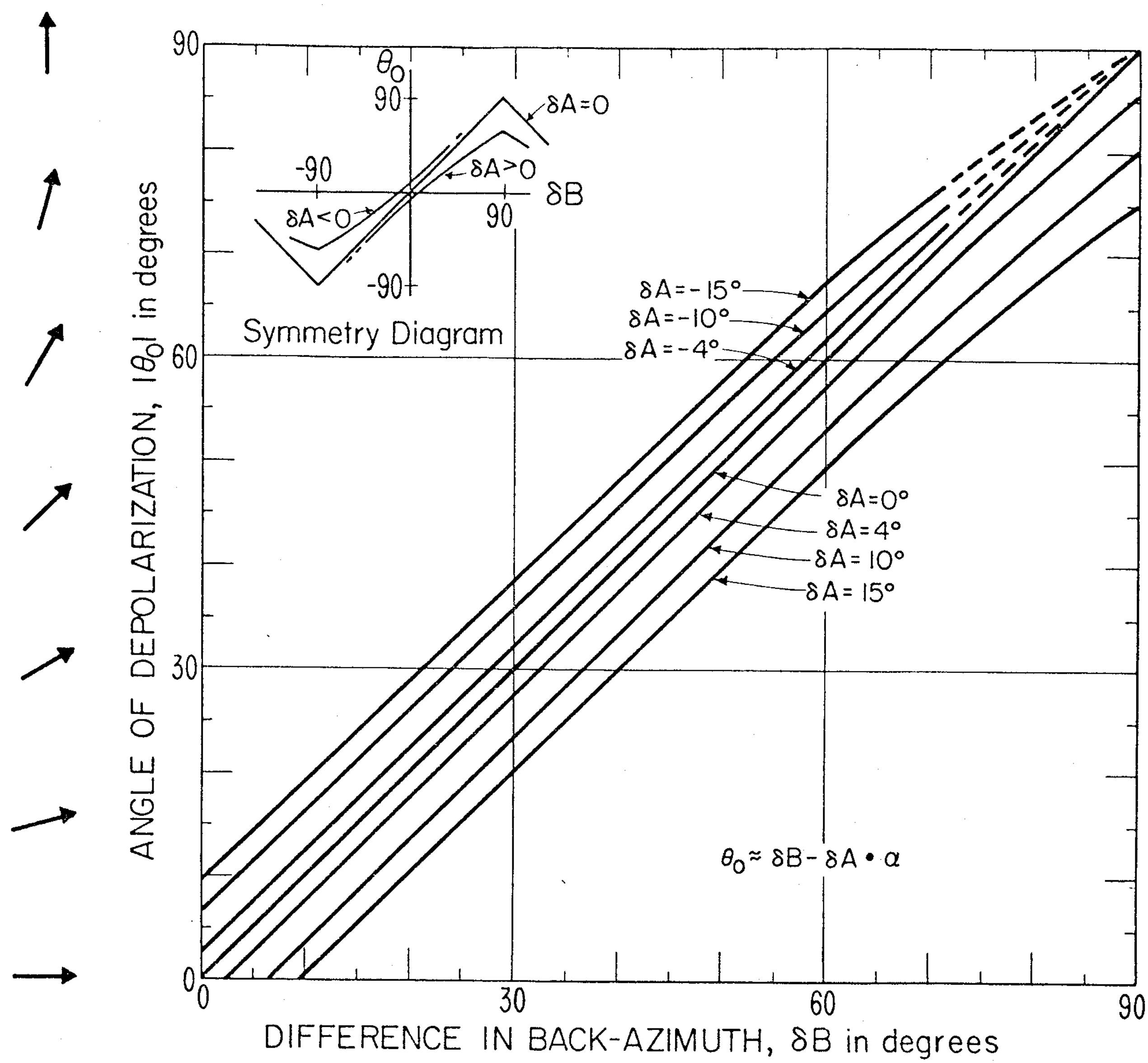

Figure 8.2. The depolarization angle for linear polarization for a potential interference situation (Dougherty, 1980).

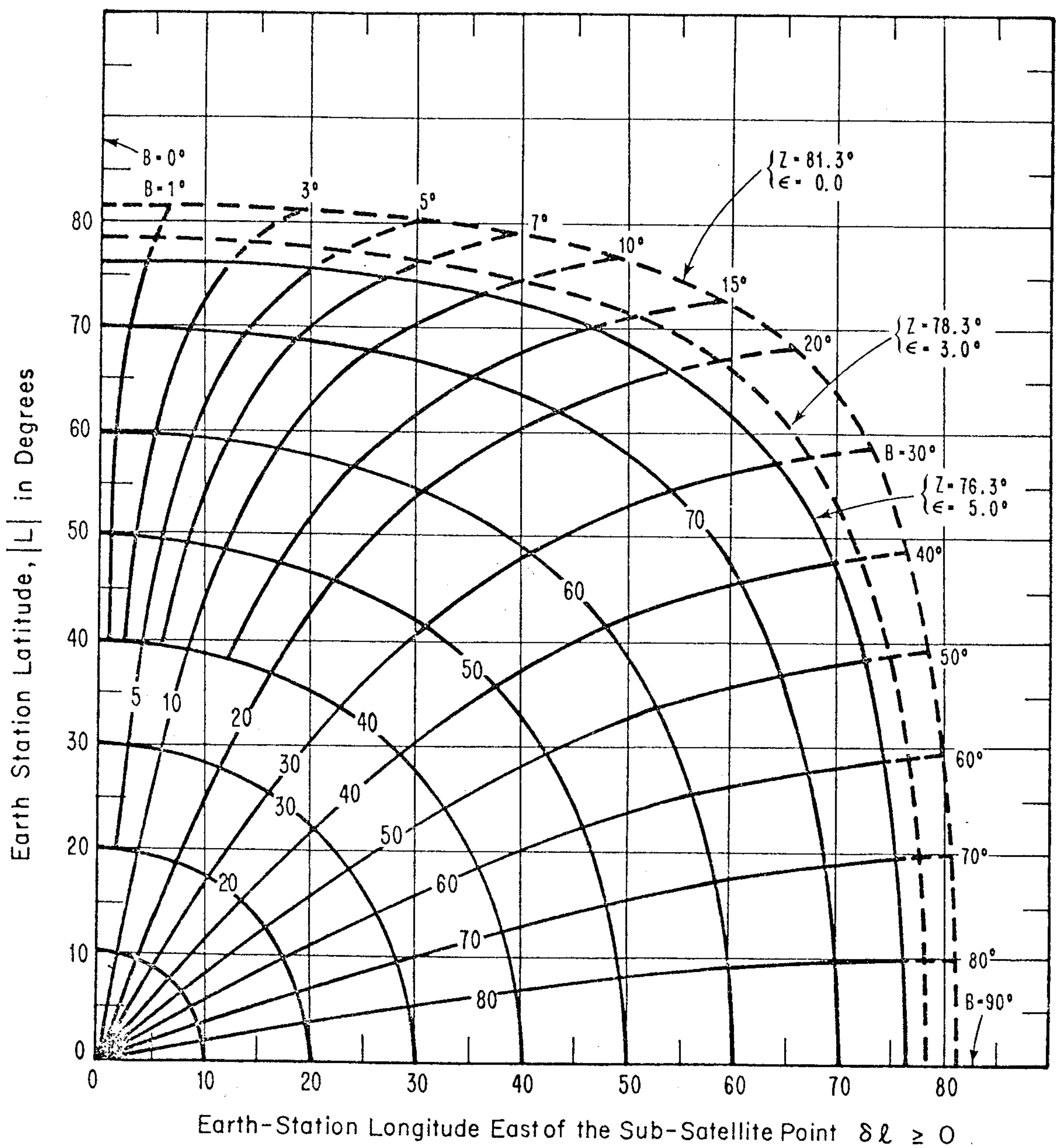

Figure 8.3. The great-circle arc (Z) and back-azimuth (B, from SS to ES) as a function of the earth-station (ES) latitude L and degrees of longitude ($\delta\ell$) east of the sub-satellite point (SS) (Dougherty, 1980).

with f the frequency in GHz. This value of θ_i corresponds to the maximum one-way effect of the ionosphere for an elevation angle of 30 deg. The subject of Faraday rotation is treated in Sec. 2.2. The angle θ_r represents the possible rotation of the electric field intensity due to depolarization caused by precipitation or other effect. By definition , the cross polarization discrimination (XPD) is given by

$$XPD = 20 \log (E_{11}/E_{12})$$

where E_{11} is the amplitude of the copolarized signal (having the original polarization and after taking account of any attenuation along the path) and E_{12} is the amplitude of the orthogonally polarized signal produced by depolarization. The angle θ_r is $\tan^{-1} E_{11}/E_{12}$.

For determining the values of $A(p, \theta)$ and δ in Eqs. (8.2) and (8.3), one evaluates the service path under unfavorable conditions, using the loss occurring for a small percentage of the time, corresponding to $p = 0.01$ percent, for example. The interference path, however, is evaluated with the minor losses occurring for, say, 50 percent of the time. This practice takes into account such possibilities as the wanted signal propagating through an intense rain cell while the unwanted signal follows a path which misses the rain cell and encounters negligible attenuation.

8.3 COORDINATION AREA BASED ON GREAT CIRCLE PROPAGATION

8.3.1 Basic Concepts

For determining coordination area, attenuation needs to be estimated for the two modes of propagation of interfering signals (CCIR, 1986a,b,c). Propagation mode one (mode 1), referring to propagation over a direct near-great-circle path, occurs essentially all of the time to some degree. The second propagation mode (mode 2) is primarily via scatter from rain and may occur infrequently. In this section some general considerations are presented, and propagation mode 1 is discussed. Scatter from rain (mode 2) is treated in Sec. 8.4.

In system planning, it is generally required to estimate the relatively intense interference level which is exceeded for some small percentage, p of the time (e.g., $p = 0.01$ percent) and also perhaps the interference level exceeded for about 20 percent ($p = 20$ percent) of the time. Corresponding to high interference levels are low values of basic transmission loss L_b (Fig. 8.4). Note that in considering attenuation due to rain (Chap.4) concern was directed to the small percentages of time for which maximum values of attenuation occur. Here the concern is for the small percentages of time for which the highest interfering signal intensities occur.

The total loss factor, L_t, relating the transmitted interfering power, P_{ti}, and the received interfering power, P_{Ri}, is defined by

$$L_t = P_{Ti}/P_{Ri} \tag{8.8}$$

An expression for the basic transmission loss, L_b, referred to above can be obtained by a modification of Eq. (1.2), namely from $P_{Ri} = P_{Ti}G_{Ti}G_{Ri}/L_{FS}L$. Identifying $L_{FS}L$ as L_b,

$$L_b = L_{FS}\,L = \frac{P_{Ti}\,G_{Ti}\,G_{Ri}}{P_{Ri}} \tag{8.9}$$

where L_{FS} is the free-space basic transmission loss and L represents other system losses. In decibel values referring to p percent of the time Eq. (8.8) becomes

$$[L_t(p)]_{dB} = (P_{Ti})_{dBW} - [P_{Ri}(p)]_{dBW} \tag{8.10}$$

and Eq. (8.9) becomes

$$[L_b(p)] = (P_{Ti})_{dBW} + (G_T)_{dB} + (G_R)_{dB} - [P_{Ri}(p)]_{dBW} \tag{8.11}$$

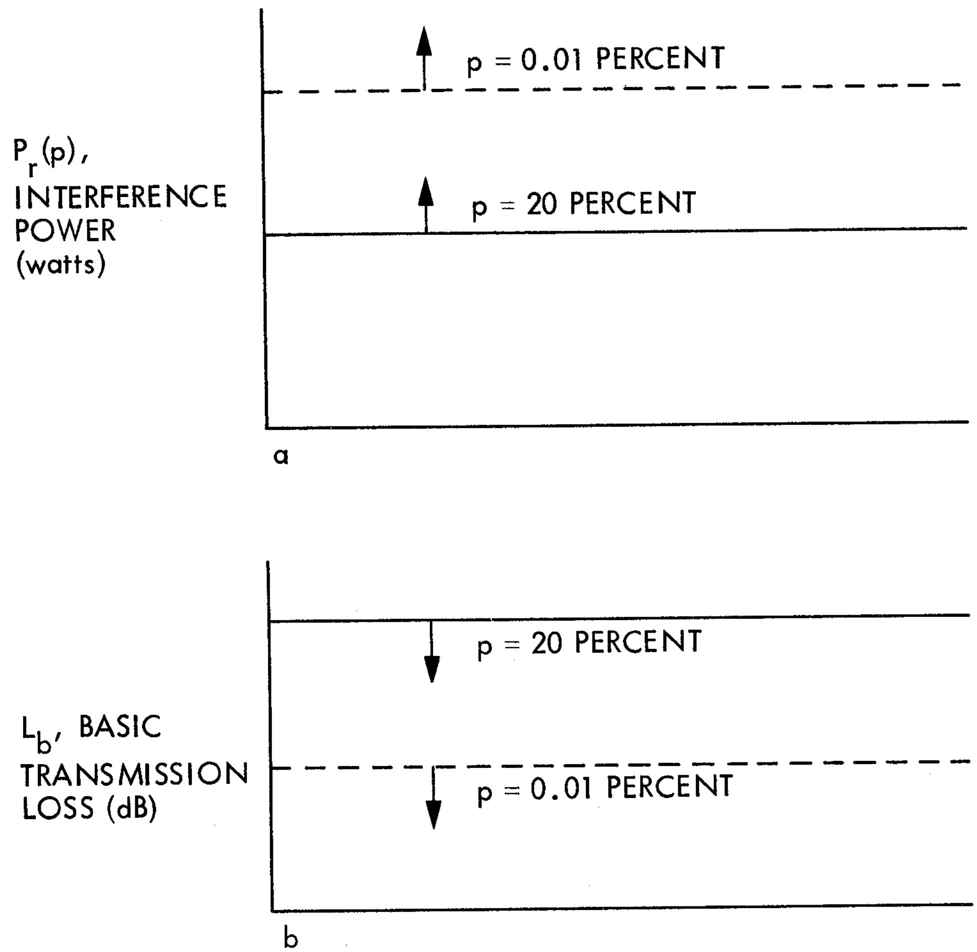

Figure 8.4. Correspondence between interference level and basic transmission loss. The interfering signal power will be above a certain level for 0.01 percent of the time, as suggested by the arrow extending upwards from the dotted line of Fig. 8.4a. The high interference levels above the dotted line of Fig. 8.4a correspond to the low values of basic transmission loss below the dotted line of Fig. 8.4b. For 20 percent of the time, the interference level will be above the solid line of Fig. 8.4a, and the corresponding values of basic transmission loss will be below the solid line of Fig. 8.4b.

In Eqs. (8.10) and (8.11), $P_{Ri}(p)$ is the maximum permissable interfering power level to be exceeded for no more than p percent of the time. Further information about permissible interference levels is given in Appendix 8.1. The gains G_T and G_R are the gains of the transmitting and receiving antennas. For determining coordination distance, the horizon gain at the azimuth in question is used for the earth-satellite station and the maximum gain is used for the terrestrial station. From Eq. (8.9), it can be seen that if $G_T = G_R = 1$ then $L_b = P_{Ti}/P_{Ri}$. For this reason, L_b is said to be the loss that would occur between isotropic antennas.

The basic transmission loss L_b is seen to be the product of L_{FS} and L. For a line-of-sight path and for frequencies below 10 GHz, L_b is roughly but not necessarily exactly equal to L_{FS}. In any case, L_{FS} makes a major contribution to L_b The free-space transmission loss was introduced in Sec. 1.1.1 and defined by

$$L_{FS} = (4\pi d/\lambda)^2 \tag{8.12}$$

where d is distance from the transmitting to receiving locations and λ is wavelength. At higher frequencies, the dissipative attenuation associated with water vapor and oxygen may make significant contributions to L_b. Attenuation of the interfering signal due to rain is not included in L_b for the low values of p normally considered in applying Eq. (8.11) as $L_b(p)$ then represents the low values of basic transmision loss that can be tolerated for only small percentages of time. When considering interfering signals, high values of L_b can be readily tolerated. It is the low values of L_b that are of concern. In terms of decibel values, Eq. (8.12) can be written as

$$(L_{FS})_{dB} = 20 \log(4\pi) + 20 \log d - 20 \log \lambda \tag{8.13}$$

where d and λ are in meters. Commonly, however, L_{FS} is expressed in terms of frequency f rather than wavelength λ. By replacing λ by c/f where $c = 2.9979 \times 10^8$ m/s, one obtains

$$(L_{FS})_{dB} = -147.55 + 20 \log f + 20 \log d \tag{8.14}$$

If f is expressed in GHz rather than Hz, a factor of 180 dB must be added to the right-hand side of Eq. (6.13), and if d is expressed in km rather than m an additional factor of 60 dB must also be included, with the result that

$$(L_{FS})_{dB} = 92.45 + 20 \log f_{GHz} + 20 \log d_{km} \tag{8.15}$$

8.3.2 Line-of-Sight Paths

Although L_b may equal L_{FS} approximately for frquencies below 10 GHz for a certain range of values of p, in the absence of horizon or obstacle effects, the actual received interfering signal on even a clear line-of-sight path fluctuates due to the effects of atmospheric multipath propagation, scintillation, and defocusing and may be greater or less than L_{FS}. Thus although L of Eq. (8.9) has been referred to as a loss factor, it must be able to assume values either greater or less than unity if it is to be applicable to the situation considered here. The variation of the received level P_{Ri} with time provides the basis for specifying P_{Ri} as a function of p. For line-of-sight paths, L can be expressed as $A_o + A_d - G_p$ and L_b is given by

$$(L_b)_{dB} = (L_{FS})_{dB} + A_o + A_d - G_p \tag{8.16}$$

where A_o is attenuation in dB due to oxygen and water vapor. (See Fig. 3.10 for attenuation due to oxygen. That due to water vapor can be neglected below about 15 GHz.) The coefficient A_d represents attenuation due to defocusing in dB, and G_p is an empirical factor in dB given by Table 8.1 for paths of 50 km or greater (CCIR, 1986a).

Table 8.1 G_p of Eq. (8.16) versus percent of time p exceeded.

p (percent)	0.001	0.01	0.1	1
G_p (dB)	8.5	7.0	6.0	4.5

For distances shorter than 50 km, the values of G_p can be proportionally reduced. To estimate the signal exceeded for percentages of the time between 1 and 20, CCIR Report 569 recommends adding 1.5 dB to the value of L_{FS} (thereby increasing L_b by 1.5 dB with respect to what it would be otherwise). The coefficient G_p can be taken to be zero for $p = 20$ percent and greater.

Attenuation due to defocusing results when the variation of refractivity with height dN/dh (Sec. 3.2) itself varies with height so that rays at different heights experience different amounts of bending. Rays representing energy propagation, rays which were originally essentially parallel for example, may then become more widely separated than otherwise and signal intensity is consequently reduced. It develops that the variation of dN/dh with height h is proportional to ΔN, the decrease in refractivity N in the first km above the surface. Figure 8.5 shows attenuation due to defocusing as a function of ΔN and elevation angle θ (CCIR, 1986d).

A given path may be a clear line-of-sight path for certain values of dN/dh (Sec. 3.1) but may have part of the first Fresnel zone obstructed for other values of dN/dh. The effect of obstruction is considered in Sec. 8.3.3.

8.3.3 Transhorizon Paths

Major attention in the analysis of interference between terrestrial systems and earth stations of space systems is directed to transhorizon propagation. The term transhorizon path refers to a path extending beyond the normal radio horizon for which diffraction is a relevant propagation mechansim, as distinquished from a clear line-of sight path at one extreme and a strictly troposcatter path at the opposite extreme. For transhorizon paths, a diffraction loss term A_s(dB) must be added to the free-space loss L_{FS}. In addition, account must be taken of ducting and super-refraction which can be expected to occur for some percentage of the time.

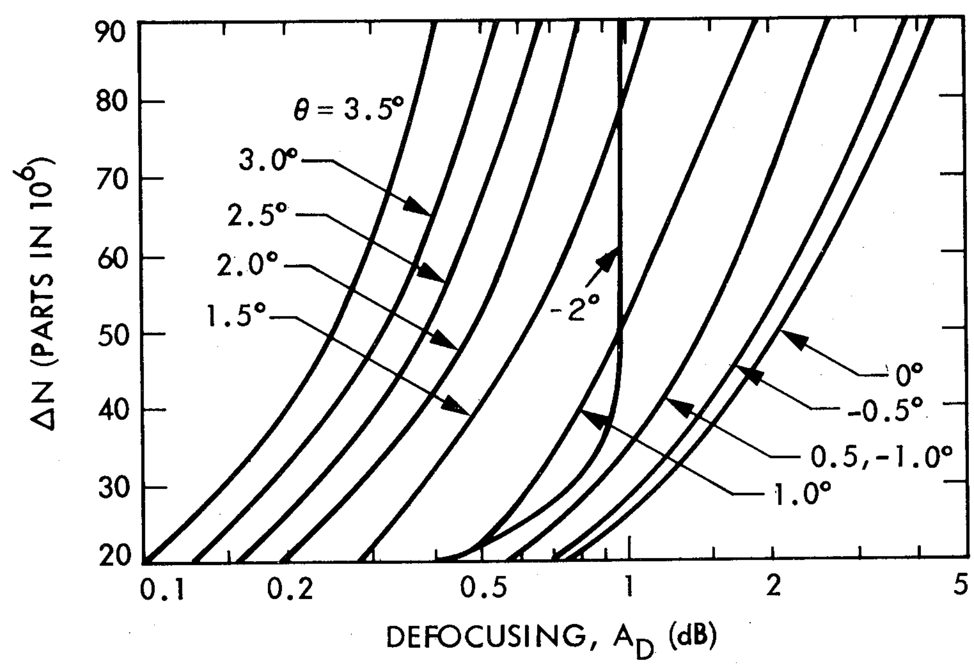

Figure 8.5. Defocusing on near-horizontal paths as a function of ΔN (the decrease in refractivity in the first km) for various values of grazing angle θ (CCIR, 1986d).

A relation for the basic transmission loss L_b between transmitting and receiving terminals which are both immersed in a duct is (CCIR, 1982; CCIR, 1986a but with 92.5 instead of 92.45)

$$(L_b)_{dB} = 92.45 + 20 \log f_{GHz} + 10 \log d_{km} + A_c + (\gamma_d + \gamma_o + \gamma_w)\, d_{km} + A_s \tag{8.17}$$

This equation includes terms like those of Eq. (8.17) for L_{LS} except that 10 log d appears instead of 20 log d. The basis for using 10 log d is that a wave in a duct is constrained in the vertical direction and spreads out only horizontally, whereas in free space a wave spreads in both directions. Because L_b for a duct includes 10 log d rather than 20 log d, L_b tends to be significantly less than L_{FS}. The quantity A_c represents a coupling loss that takes account of the fact that not all the rays leaving the transmitting antenna are trapped within the duct. The γ's are attenuation constants, γ_d being a duct attenuation constant reported to have a theoretical minimum value of 0.03 dB/km (Dougherty and Hart, 1979). The constants γ_o and γ_w represent attenuation due to oxygen and water vapor, respectively . The quantity A_s takes account of loss caused by obstacles along the path. CCIR Report 382-5 (CCIR, 1986c) and CCIR Report 724-2 (CCIR, 1986b), however, use, for L_b for ducting,

$$(L_b)_{dB} = 120 + 20 \log f_{GHz} + \gamma\, d_{km} + A_h \tag{8.18}$$

The term γ includes the γ's of Eq. (8.17), and A_h is a modified form of A_s of Eq. (8.17). Equation (8.17) has the advantage of being closely related to the physical phenomena involved, but it has the computational disadvantage of having a term involving the logarithm of distance and also a term that is linear with distance. One needs to solve for d, the coordination distance for great-circle propagation, and for this purpose Eq. (8.18) has the advantage of having only a term that is linear with distance. The basis for the conversion from Eq. (8.17) to (8.18) is that the term 10 log d can be approximated by

$$10 \log d_{km} = 20 + 0.01\, d_{km} \qquad 100 \text{ km} < d < 2000 \text{ km} \qquad (8.19)$$

Also the coupling loss A_c of Eq. (8.17) has been assigned the value of 7.5 dB whereas in CCIR Report 569-3 (CCIR, 1986a) this loss is given by a table showing it as varying from 6 to 11 dB over water and coastal areas and 9 to 14 dB over inland areas. The value of 120 is obtained by setting 92.45 equal to 92.5 and noting that 92.5 + 20 + 7.5 = 120. The coefficient 0.01 of Eq. (8.19) is included as part of the γ of Eq. (8.18), and γ is then given by

$$\gamma = 0.01 + \gamma_d + \gamma_o + \gamma_w \qquad (8.20)$$

The quantity A_s of Eq. (8.17), expressed in dB, has the form of

$$A_s = 20 \log [\, 1 + 6.3\, \theta\, (f\, d_h)^{1/2}\,] + 0.46\, \theta\, (f\, Cr)^{1/3} \qquad (8.21)$$

where f is frequency in GHz, d_h is distance to the horizon in km, θ is elevation angle in deg above the horizon, and Cr is the radius of curvature of the horizon. If d_h is set equal to 0.5 km and Cr is taken to be 10 m, one obtains the horizon angle correction A_h of Eq. (8.18), namely

$$A_h = 20 \log (\, 1 + 4.5\, f^{1/2}\, \theta\,) + f^{1/3}\, \theta \qquad (8.22)$$

Figure 8.6 shows A_h as a function of elevation angle and frequency.

The factor γ_d is given by (CCIR, 1986b)

$$\gamma_d = [\, c_1 + c_2 \log (\, f + c_3\,)\,]\, p^{c_4} \qquad \text{dB/km} \qquad (8.23)$$

where the c's have different values for four different zones and are given in Table 8.2. The frequency f is in GHz, and p is percentage of time.

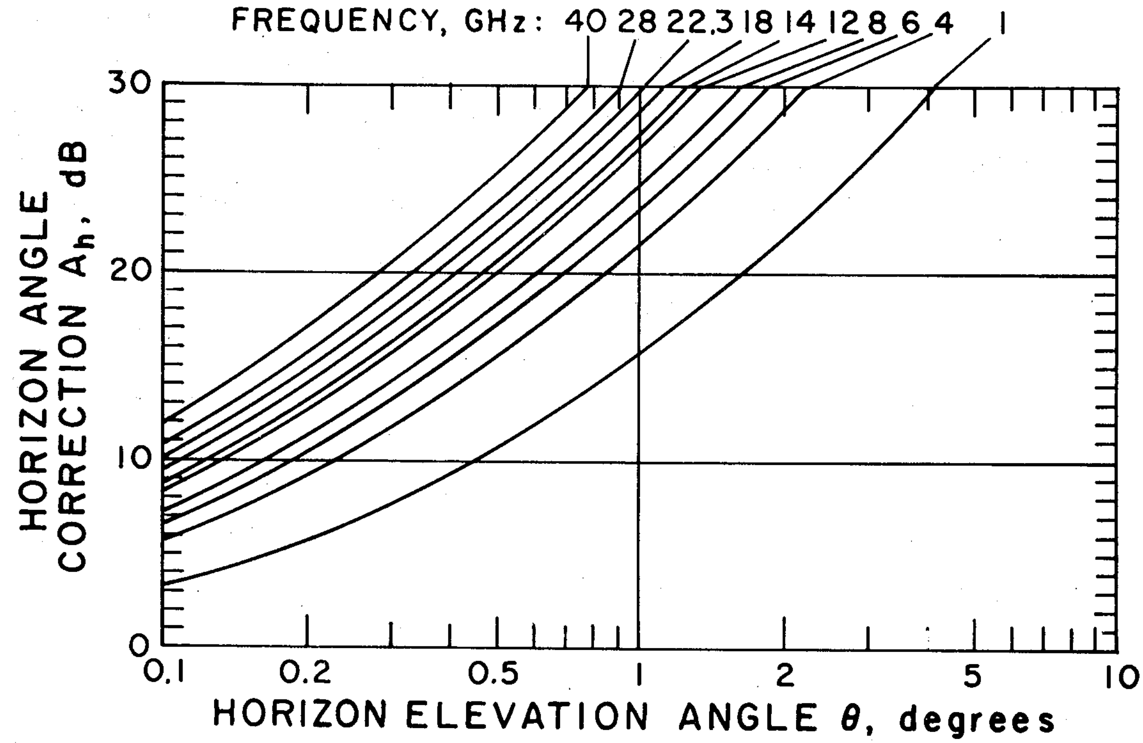

Figure 8.6. The horizon angle correction, A_h, Eq. (8.22).

Table 8.2 Values of Constants for Determination of γ_d.

	c_1	c_2	c_3	c_4
Zone A1	0.109	0.100	-0.10	0.16
Zone A2	0.146	0.148	-0.15	0.12
Zone B	0.050	0.096	0.25	0.19
Zone C	0.040	0.078	0.25	0.16

The zones referred to in Table 8.2 are

Zone A1: Coastal land and shore areas, adjacent to zones B or C, up to an elevation of 100 m relative to mean water level, but limited to a maximum distance of 50 km from the nearest zone B or C area.

Zone A2: All land, other than coastal land and shore areas.

Zone B: "Cold" seas, oceans, and other substantial bodies of water, encompassing a circle 100 km in diameter at latitudes greater than 23.5 deg N or S, but excluding all of the Black Sea, Caribbean Sea, Gulf of Mexico, Mediterranean Sea, Red Sea, and the sea from the Shatt-al-Arab to and including the Gulf of Oman.

Zone C: "Warm" seas, oceans, and other substantial bodies of water, encompassing a circle 100 km in diameter, and including in their entirety the bodies of water mentioned as being excluded from zone B.

The constant γ_o for oxygen is given in CCIR Report 724-2 (CCIR, 1986b) in dB/km for $f < 40$ GHz by

$$\gamma_o = \left[0.00719 + \frac{6.09}{f^2 + 0.227} + \frac{4.81}{(f - 57)^2 + 1.50} \right] f^2/10^3 \qquad (8.24)$$

Attenuation due to water vapor can be neglected for frequencies less than 15 GHz, and the expression for γ_w is therefore not given here.

CCIR Report 724-2 includes plots for a graphical solution for coordination distance for ducting, or great-circle propagation. We do not include these illustrations here, but Eq. (8.18) can be solved algebraically for the distance d by making use of the accompanying information about the parameters appearing in it.

Troposcatter signals, resulting predominantly from inhomogeneous scattering by random fluctuations of the index of refraction of the atmosphere, are normally weaker than the interfering signals due to ducting and super-refraction. However, the tropospheric scatter signals may be dominant for percentages of time between about 1 and 50 percent and for percentages less than one when high site shielding (A_h values of 30 dB and greater) is encountered.

8.4 COORDINATION AREA FOR SCATTERING BY RAIN

For considering interference due to scatter from rain, one can start with a slightly modified version of Eq. (4.53) which refers to bistatic scatter from rain. Inverting this relation to obtain a total loss factor L_t, using G_T, G_{ES}, R_T, and R_{ES} to refer to the gains of the terrestrial and earth-station antennas and their distances from the region of rain scatter, and replacing W_T and W_R by P_{T_i} and P_{R_i} results in

$$L_t = \frac{P_{T_i}}{P_{R_i}} = \frac{(4\pi)^3 R_T^2 R_{ES}^2 L}{G_T G_{ES} \eta V \lambda^2} \tag{8.25}$$

In this expression, L is a loss factor (greater than unity if truly a loss), V is the common scattering volume, and η is the radar cross section per unit volume. For Rayleigh scattering η has the form of

$$\eta = \frac{\pi^5}{\lambda^4} \left| \frac{K_c - 1}{K_c + 2} \right|^2 Z \qquad m^2/m^3 \tag{8.26}$$

where K_c is the complex dielectric constant of water and is a function of frequency and temperature. When expressed in mm^6/m^3, the quantity Z is related to rainfall rate R in mm/h for a Laws and Parsons distribution of drop sizes by the empirical expression

$$Z = 400 R^{1.4} \tag{8.27}$$

Physically, Z represents $\sum d^6$ where d is the drop diameter and the summation is carried out for all of the drops in a unit volume. For frequencies higher than 10 GHz for which Rayleigh scattering does not apply, an effective of modified value of Z, designated as Z_e, is used for coordination distance calculations.

Usually the earth-station antenna has a smaller beamwidth than the terrestrial antenna. Assuming that such is the case and noting that the scattering volume V is defined by the antenna with the smallest beamwidth, V is given approximately by

$$V = (\pi/4)\, \theta^2\, R_{ES}^{\,2}\, D \tag{8.28}$$

where θ is the beamwidth of the earth-station antenna, R_{ES} is the distance from the earth station to the common scattering volume V, and D is the extent of the common scattering volume along the path of the earth-station antenna beam. Assuming a circular aperture antenna for which the beamwidth θ is given approximately by λ/d where d is diameter and making use of the relation between effective antenna area A and gain G, namely $G = 4\pi A/\lambda^2$, it develops that $\theta^2 = \pi^2/G$ and

$$V = \pi^3\, R_{ES}^{\,2}\, D/\,(4\, G_{ES}) \tag{8.29}$$

Substituting for η and V in Eq. (8.25) and recognizing that in η $|(K_c - 1)/(K_c + 2)|$ has a value of about 0.93 (Battan, 1973),

$$L_t = \frac{4^4\, R_T^{\,2}\, L\, \lambda^4}{G_T\, D\, \lambda^2\, \pi^5\, (0.93)\, Z} \tag{8.30}$$

Combining the numerical factors of Eq. (8.30) and replacing λ by c/f results in

$$L_t = \frac{0.9\, R_T^{\,2}\, c^2\, L}{f^2\, G_T\, D\, Z} \tag{8.31}$$

Note that R_{ES} and G_{ES} have dropped out of the expression for L_t but that R_T and G_T remain. Taking logarithms results in

$$(L_t)_{dB} = -0.46 + 20 \log R_T + 169.54 + 10 \log L - 20 \log f - 10 \log G_T - 10 \log D - 10 \log Z$$

$$(L_t)_{dB} = 199 + 20 \log (R_T)_{km} + 10 \log L - 20 \log f_{GHz} - 10 \log D_{km} - 10 \log Z_{mm^6/m^3} - 10 \log G_T \tag{8.32}$$

The number 199 is arrived at from 169.54 - 0.46 + 60 - 30, where +60 is introduced when replacing R_T in m by R_T in km and

−30 is introduced when replacing D in m by D in km. Changing from f in Hz to f in GHz and from Z in m^6/m^3 to Z in mm^6/m^3 introduce two 180 dB factors of opposite sign which cancel out. The relation of Eq. (8.32) can be modified to express D and Z in terms of rain rate R. The distance D is taken to be given by

$$D = 3.5 \ R^{-0.08} \tag{8.33}$$

based on modeling of rain cells and assuming an elevation angle of 20 deg as a conservative assumption. For Z, assuming a Laws and Parsons distribution of drop sizes,

$$Z = 400 \ R^{1.4} \tag{8.34}$$

Taking 10 log D, one obtains 5 - 0.8 log R , and taking 10 log Z gives 26 + 14 log R. Subtracting 26 + 5 from 199 leaves 168, and combining the log R terms results in −13.2 log R. The resulting equation derived from Eq. (8.32), after also specifying the contributions to L, is

$$(L_t)_{dB} = 168 + 20 \log (R_T)_{km} - 20 \log f_{GHz} - 13.2 R$$
$$- 10 \log G_T - 10 \log C + \gamma_o r_o + \Gamma \tag{8.35}$$

The quantity C accounts for attenuation in the common scattering volume. The expression for C given in CCIR Report 724-2 (CCIR, 1986b) is

$$C = [2.17/(\gamma_r D)] \ (1 - 10^{-\gamma_r D/5}) \tag{8.36}$$

where γ_r is the attenuation constant for rain for vertical polarization [Eq. (4.11)]. D, the path through rain is defined by Eq. (8.33), and $\gamma_o r_o$ is attenuation due to oxygen. The distance

r_o is an effective distance equal to 0.7 R_T + 32 km for $R_T < 340$ km and otherwise 270 km. The quantity Γ represents attenuation due to rain outside the common scattering volume. It is given by a rather complicated expression in CCIR Report 724-1 and in the following form in the Report 724-2 (CCIR, 1986b).

$$\Gamma = 631 \, k \, R^{\alpha - 0.5} \ 10^{-(R+1)^{0.19}} \tag{8.37}$$

In Eq. (8.37), kR^{α} is the same quantity as aR^{b} of Eq. (4.11). It is stated that this expression gives the largest value of Γ for intermediate rain rates. This behavior is in contrast to that of Report 724-1 which shows attenuation increasing continuously with rain rate.

Equation (8.37) can be solved for R_T, the distance from the common scattering volume to the terrestrial station. The distance R_T, however, is not the rain-scatter coordination distance d_2, as R_T is not measured from the earth station. The center of the circle representing the locus of R_T (scatter is assumed to occur equally in all directions from the common scattering volume) is displaced from the earth station by Δd which is a function of elevation angle θ where

$$\tan\theta = \frac{h}{\Delta d} = \frac{(R_T - 40)^2}{17{,}000\,\Delta d}$$

and

$$\Delta d = \frac{(R_T - 40)^2 \cot\theta}{17{,}000} \qquad (8.38)$$

The basis for this relation is shown in Fig. 8.7. The grazing ray from the terrestrial transmitter is assumed to graze the horizon at a distance of 40 km, and a k factor of 4/3 (Sec. 3.2) is assumed.

The expression in CCIR Report 382-5 (CCIR,1986c) that corresponds to Eq. (8.35) has the same form except that a gain G_T of 42 dB is assumed and 168 - 42 = 126 so that, for $f \leq 10$ GHz,

$$(L_t)_{dB} = 126 + 20\log(R_T)_{km} - 20\log f_{GHz} - 13.2\log R$$
$$- 10\log C + \gamma_o r_o + 10\log B \qquad (8.39)$$

where 10 log B takes the place of Γ but has the form of Γ for CCIR Report 724-1 (CCIR, 1982).

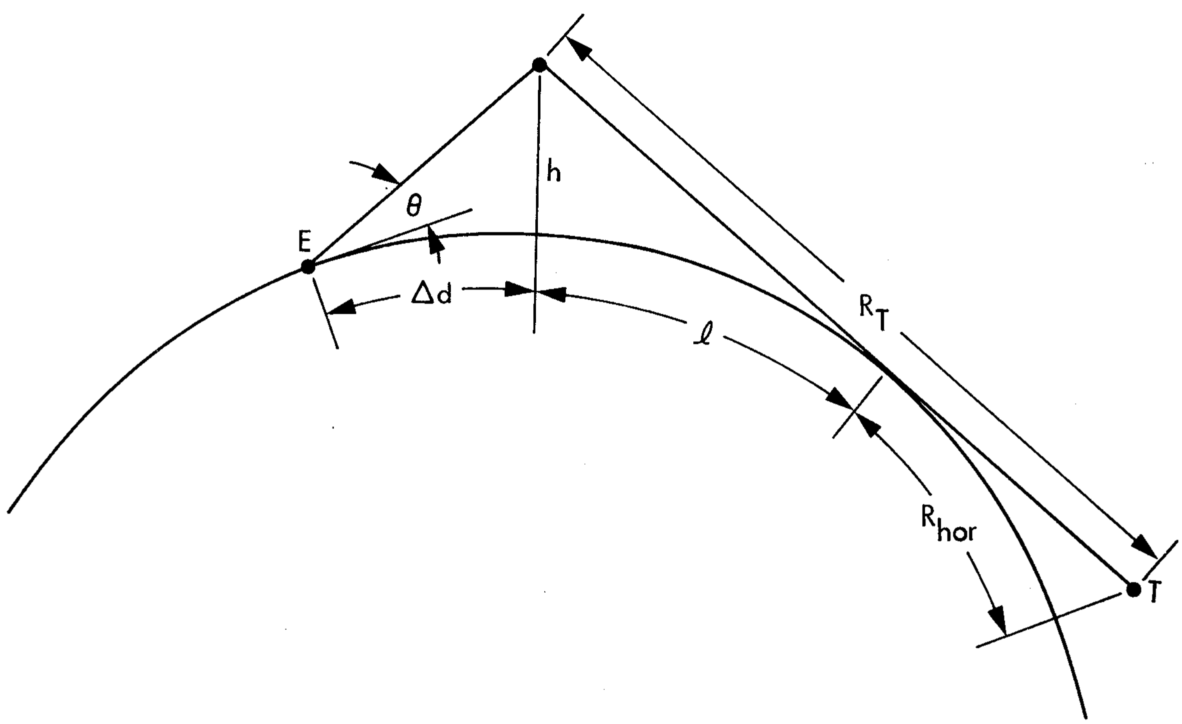

Figure 8.7. Rain scatter involving a transhorizon path from a terrestrial station T. A grazing ray at the horizon will reach a height of $\ell^2/2kr_0 = (R_T - R_{hor})^2/2kr_0$ at the distance $R_T - R_{hor}$ from where the ray is tangential to the Earth's spherical surface. The elevation angle θ corresponding to this height h, as seen from the earth station E, is $\tan^{-1} h/\Delta d$.

Another variation of the equation for interference caused by scatter from rain is

$$[L_2(0.01)]_{dB} = 131 - 20 \log (R_T)_{km} - 20 \log f_{GHz} - 10 \log C$$
$$+ \gamma_o r_o - 14 \log R + (R_t - 40)^2/17{,}000 - 10 \log D_{km} \qquad (8.40)$$

This equation was in the 1978 version of CCIR Report 382 and also in Appendix 28 in 1982. The loss in this case is for a percentage of occurrence of 0.01. The 10 log D_{km} term is retained as such and the "5" referred to following Eq. (8.34) does not appear, so the numerical coefficient of Eq. (8.40) is 131 rather than 126. Also the quantity Z is assumed to decrease at a rate of 1 dB/km, and this decrease is accounted for by subtracting h of Eq. (8.38) from Z $[h = (R_T - 40)^2/17{,}000]$. As it is $-10 \log Z$ that occurs in the original equation, Eq. (8.40) includes +h.

8.5 INTERFERENCE BETWEEN SPACE AND SURFACE STATIONS

Interference between a space station and one on the Earth's surface may take place, for example, when an earth station receives unwanted transmisions from an interfering satellite as well as wanted transmissions from the satellite that serves the earth station. The analysis of Sec. 8.2, presented there as an introduction to the analytical aspects of interference, applies directly to this case, and some additional considerations follow. Because the spacings of satellites in the geostationary orbit may be as close as 2 deg, limitations on the uplink and downlink antenna gains off axis have been prescribed by the FCC. Uplink antenna gain is limited to $32 - 25 \log \theta$, where θ is the off-axis angle in degrees, for values of θ of 1 deg and greater. For downlinks, the corresponding expression is $29 - 25 \log \theta$. A different approach to combat interference, however, is to use the spread-spectrum technique. Small earth-station antennas can then be employed and discrimination against unwanted signals can be obtained by using code-division multiple access.

Scatter from rain, which was not considered in Sec. 8.2 but may also cause interference, can be analyzed by a modification of the approach of Sec. 8.4 with R_T and G_T now taken to refer to the interfering satellite transmitter rather than to a terrestrial transmitter.

Solar power satellites, which would intercept solar energy and transmit energy to the Earth's surface as microwave radiation at a frequency of 2450 MHz according to preliminary plans, present a potential interference problem for communication satellite systems. According to one analysis (CCIR, 1986d) based on likely harmonic content, the interfering signal scattered from rain, even at the fourth harmonic, would be comparable with the signal level received in the fixed satellite service.

In the absence of precipitation, the signal on a line-of-sight path from a satellite will be attenuated by the atmospheric gases and perhaps by defocusing but may experience a gain due to multipath and scintillation effects, for a small fraction of the time, as mentioned in Sec. 8.3.2. The gain due to multipath effects and scintillation may be assumed to be zero for elevation angles above 5 deg and percentages of time greater than one percent (CCIR, 1986d).

8.6 PROCEDURES FOR INTERFERENCE ANALYSIS

8.6.1 Introduction

Previous sections of this chapter have outlined the theoretical basis for interference analysis, with emphasis on basic concepts. In this Sec. 8.6, practical considerations, including procedures for determining coordination distance, are summarized.

The procedures for interference analysis are subject to continuing development and updating. The procedures of Appendix 28 of Radio Regulations (ITU, 1982) carry legal authority, but they may be revised in the future. (Resolution No. 60 of WARC-79 called for a revision in Appendix 28, and the 1982 version of Report 382, utilizing certain data from Reports 724, 563, and 569, has been proposed as a basis for any changes in the radio regulations). The differences in the treatments of the several CCIR reports are in detail and refinement and relate to what losses need to be taken into account and how to achieve the necessary compromise between a satisfactory degree of accuracy on the one hand and convenience and practicality on the other. A basic problem is that the phenomena must be treated in a largely empirical way and the available data bases are limited.

8.6.2 Off-axis Antenna Gain

For calculating the predicted intensity of a terrestrial interfering signal at an earth station or of an interfering signal from an earth station at a terrestrial station, it is necessary to know the gain of the earth station antenna at the horizon at the azimuth of the terrestrial station (or for determining coordination distance at all azimuthal angles). To determine the gain, one must first find the angle of the horizon from the axis of the main antenna beam at the azimuth of interest. For the case that the horizon is at zero elevation angle, the horizon angle ϕ, measured from the axis of the antenna beam, is found by applying the law of cosines for sides of a spherical triangle, namely

$$\cos\phi = \cos\theta_s \cos(\alpha - \alpha_s) \tag{8.41}$$

where θ_s is the elevation angle of the satellite the earth station is servicing , α_s is the azimuth of the satellite, and α is the azimuthal angle of interest. If the horizon is at an elevation angle θ, the corresponding relation becomes

$$\cos\phi = \cos\theta \cos\theta_s \cos(\alpha - \alpha_s) + \sin\theta \sin\theta_s \tag{8.42}$$

Having determined ϕ, it remains to specify a value for the antenna gain at this angle. If the actual antenna gain is known as a function of ϕ, it should be used. If the gain is not known and the antenna diameter to wavelength ratio D/λ is 100 or greater, the following relation, from CCIR Reports 391-5, (CCIR,1986f) and 382-5 and Appendix 28 of Radio Regulations, can be used for angles ϕ in degrees greater than that of the first side lobe

$$G = 32 - 25\log\phi \quad \text{dB} \tag{8.43}$$

If the D/λ ratio is less than 100, the corresponding relation is

$$G = 52 - 10\log(D/\lambda) - 25\log\phi \tag{8.44}$$

The same sources give relations between the maximum gain G_{max} and D/λ, that in Report 382-5 and Appendix 28 being

$$20 \log D/\lambda = G_{max} - 7.7 \quad \text{dB} \qquad (8.45)$$

More preciesly and completely than stated above, Report 382-5 and Appendix 28 give the following set of relations for $D/\lambda \geq 100$.

$$G(\phi) = G_{max} - 2.5 \times 10^{-3} \; (D\phi/\lambda) \qquad 0 < \phi < \phi_m \qquad (8.46a)$$

$$G(\phi) = G_1 \qquad \phi_m < \phi < \phi_r \qquad (8.46b)$$

$$G(\phi) = 32 - 25 \log \phi \qquad \phi_r < \phi < 48^o \qquad (8.46c)$$

$$G(\phi) = -10 \qquad 48^o < \phi < 180^o \qquad (8.46d)$$

where $\phi_m = (20\lambda/D) \; (G_{max} - G_1)^{0.5}$ deg

$$\phi_r = 15.85 \; (D/\lambda)^{-0.6}$$

$$G_1 = 2 + 15 \log D/\lambda \qquad (\text{gain of first side lobe}) \qquad (8.47)$$

For $D/\lambda \leq 100$

$$G(\phi) = G_{max} - 2.5 \times 10^{-3} \; (D\phi/\lambda)^2 \qquad 0 < \phi < \phi_m \qquad (8.48a)$$

$$G(\phi) = G_1 \qquad \phi_m < \phi < 100\lambda/d \qquad (8.48b)$$

$$G(\phi) = 52 - 10 \log D/\lambda - 25 \log\phi, \quad 100\lambda/D < \phi < 48^o \qquad (8.48c)$$

$$G(\phi) = 10 - 10 \log D/\lambda \qquad 48^o < \phi < 180^o \qquad (8.48d)$$

For satellite antennas, CCIR Report 558-3 (1986g) gives the following relations:

$$G(\phi) = G_{max} - 3(\phi/\phi_o)^2 \qquad \phi_o < \phi < a\,\phi_o \qquad (8.49a)$$

$$G(\phi) = G_{max} + L_s \qquad a\,\phi_o < \phi < 6.32\,\phi_o \qquad (8.49b)$$

$$G(\phi) = G_{max} + L_s + 20 - 25(\phi/\phi_o) \qquad 6.32\phi_o < \phi < \phi_1 \qquad (8.49c)$$

$$G\,\phi) = 0 \qquad \phi_1 < \phi \qquad (8.49d)$$

where ϕ_o is one half the 3 dB beamwidth and ϕ_1 is the value of ϕ when $G_{max} = 0$. The parameter "a" has the values of 2.58, 2.88, and 3.16 when L_s, the required near-in side-lobe level relative to the peak, has the values of -20, -25, and -30 dB, respectively.

8.6.3 Procedures for Determining Coordination for Great Circle Propagation

For determining coordination distances d_1 for great circle propagation, it is necessary to first determine the basic transmission loss, L_b, as defined by Eq. (8.11), that can be tolerated for the percentage of time specified (commonly 0.01 percent and perhaps 20 percent as well). The allowable value of L_b is based primarily on factors other than propagation. The quantity $P_{Ri}(p)$ should be taken to be the maximum permissable interference level for p percent of the time. Consideration of this level is primarily outside the scope of this handbook, but material from Appendix 28 of the Radio Regulations that refers to it is reproduced as Appendix 8.1 The quantity G_T refers to the antenna gain of the transmitting interfering station. If the interfering station is an earth station, the gain towards the physical horizon on the azimuth in question is to be used. If the interfering station is a terrestrial station, the maximum expected antenna gain is to be used. The quantity G_R refers to the gain of the station that is interfered with If the station is an earth station, the gain towards the horizon on the azimuth in question is to be used. If the station experiencing interference is a terrestrial station, the maximum expected antenna gain is to used. Relations for estimating off-axis antenna gain were given in the previous Sec. 8.6.2. For determining coordination distance for installation of an earth station, one can intially determine coordination distance in all directions without regard to locations of terrestrial stations. In a second stage of analysis after coordination distance has been determined, the locations and gains of the terrestrial stations towards the earth station can be utilized to determine if an interference problem truly exists.

Having decided on a value for L_b, one can solve for distance d of Eq. (8.17) from CCIR Report 724-2 (1986b) or for distance d of

Eq. (8.18). In Eq. (8.20), we show the coefficient γ of Eq. (8.18) as including a factor of 0.01 in addition to γ_d, γ_o, and γ_w based on Report 724-2 (CCIR, 1986b). CCIR Report 382-5 (CCIR, 1986c) and Appendix 28 of Radio Regulations, however, do not, to our knowledge at the time of writing, include this factor of 0.01. Yet Appendix 28 carries legal authority. A person engaged in determining coordination distances should obtain a copy of the latest version of Appendix 28 and follow whatever instructions it includes. Note that antenna gains were taken into account in determining the value of L_b of Eqs. (8.17 and (8.18) but do not appear explicitly in either of the two equations. The coordination distance found from these equations is designated as d_1. The reports cited include descriptions of procedures for use when great-circle paths cross more than one zone.

For zones B and C (Sec. 8.3.3), if coordination distances turn out to be greater than the values in Table 8.3, the values in the table should be used instead as the coordination distance.

Table 8.3 Maximum Coordination Distance d_1.

	Percent of Time			
Zone	0.001	0.01	0.1	1.0
B	2000 km	1500 km	1200 km	1000 km
C	2000 km	1500 km	1200 km	1000 km

8.6.4 Procedures for Determining Coordination Distance for Rain Scatter

For determining the coordination distance d_2 for scatter by rain, one must first find the total transmission loss L_t that can be tolerated for some specified percentage of time, commonly 0.01. This loss factor represents the ratio of the transmitted interfering power to the received interfering power as shown in Eqs. (8.10) and (8.25). In addition, or alternatively, certain approaches including that of CCIR Report 382-5 and Appendix 28 of the Radio

Regulations, utilize the normalized loss L_2 which is based upon the assumption that the terrestrial antenna in question has a gain of 42 dB. The loss L_2 is reduced by 42 dB with respect to L_t for this reason. For finding the value of L_t, use the definition of L_t of Eq. (8.10). It is necessary to find values for P_{Ti} and to determine $P_{Ri}(p)$, considering it as the maximum permissable interference level for p percent of the time, and the procedure for doing this, the same procedure as when working with great circle propagation, is given in Appendix 8.1. Note that, unlike the case for Eq. (8.11), antenna gains do not appear in Eq. (8.10). Antenna gains G_{ES} and G_T do appear, however, in Eq. (8.25) which shows the factors determining L_t [as distinct from the quantities needed to define L_t, which is what Eq. (8.10) shows].

When the required loss factor has been found, then one must determine the rainfall rate R in mm/h that applies for the specified percentage of time for the location or climatic region being considered. If appropriate long-term data are available for the location in question, it can be used. Otherwise one must use one of several models which show the rain rates exceeded as a function of percentage of time for the various geographical regions of the world.

Several such models are described in Sec. 4.3.3, and values of R, as a function of percentage of time exceeded, are given in Table 4.4 for the 1980 Global Model (No. 5 of Sec. 4.3.3) for regions defined for the United States in Fig. 4.9. The CCIR model, described in CCIR Reports 563-3 (CCIR, 1986e) and 724-2 (CCIR, 1986b) is also included in Sec. 4.3.3 as No. 8. Data concerning this model are presented in two ways. The regions of the world utilized are shown in Figs. 4.13 - 4.15, and Table 4.5 shows the corresponding rain rates as a function of percentage of time exceeded. In addition, Figs. 9.8 - 9.10 from Report 563-3 show contours of fixed values of R that are exceeded for 0.01 percent of the time. The CCIR regions for Canada as modified by Segal are shown in Fig. 4.10.

Once the values of L_t and R have been settled on, one can solve for the value of R_T, the distance of the rain scatter region from the terrestrial station, by use of Eqs. (8.32),(8.35), (8.39), or (8.40). Equation (8.40) is that utilized in Appendix 28 of Radio Regulations and must be followed if legal requirements are to be met. Refer directly to Appendix 28 in that case.

The value of R_T is the radius of a circle centered on the region of rain scatter. The center of this circle is displaced from the earth station by the distance Δd of Eq. (8.38), and d_2, the coordination distance from the earth station to the circle at the azimuth under consideration.

If coordination distances for rain scatter turn out to be greater than those shown in Table 8.4, the values of the table should be used instead.

Table 8.4 Maximum Rain Scatter Distances (km).

	Latitude (deg)				
Percent of time	0-30	30-40	40-50	50-60	60-70
1.0	360	340	290	260	240
0.1	360	340	310	290	260
0.01	370	360	340	310	280
0.001	380	370	360	340	300

8.7 SITING OF EARTH STATIONS

The siting of earth stations in basins or valleys surrounded by hills is highly advantageous for minimizing radio interference. It is recommeded in CCIR Report 385-1 (1986h), however, that the angles of elevation of obstructions should not excced about 3 deg in order to ensure maximum satellite availability. Where sufficient natural shielding cannot be found, artificial shielding may be desirable. Radar fences built for suppression of signals at low elevation angles have provided 20 dB of protection (Crane, 1981). Placement of the earth station antenna in a pit is reported in CCIR Report 390-5 (1986i) to have provided 25 dB of protection in the 4 and 6 GHz fixed satellite bands. Ducting has the potential for producing the highest-level interference fields, but the effect of ducting can be reduced by the measures mentioned. Other siting precautions mentioned in Report 385-1 include avoiding line-of-sight paths between earth stations and interfering transmitters, avoiding locating the earth station with less than a 5 deg discrimination angle at the interfering transmitter between the path to the earth station and the main beam of the interfering transmitter antenna, and maintaining a minimum distance of 50 km when shielding of 3 to 4 deg is available. A distance of only 20 km is said to be sufficient when the shielding has an elevation angle of 10 deg.

Reflections from aircraft can cause interference, and earth stations should preferably not be located near areas of especially heavy aircraft traffic. In the Federal Republic of Germany, some 19,000 events attributed to aircraft reflections were observed during a period of 10,000 hours on a 1.9 GHz troposcatter link 420 km in length. The average basic transmission loss on this link was about 236 dB but for 0.1, 0.02, and 0.005 percent of the time the losses were 216, 213, and 210 dB respectively. The low levels of loss attributed to aircraft (CCIR, 1986a) show the advisability of considering potential interference due to reflections from aircraft.

Although apparently not mentioned in the literature, reflections from flocks of birds can also cause interference, and the vicinity of major waterfowl refuges or flyways should be avoided if possible. As far as the reflection of electromagnetic waves is concerned, birds are like large blobs of water. They are thus effective scatterers of electromagnetic waves and readily detectable by radar at L band (e.g. 1.5 GHz) and higher (Eastwood, 1967). Migrating birds commonly fly at altitudes up to about 3.6 km or higher.

REFERENCES

Battan, L. J., Radar Observations of the Atmosphere . Chicago: University of Chicago Press, 1973.

CCIR, "Propagation data required for the evaluation of coordination distance in the frequency range 1 to 40 GHz," Report 724-1, Vol. V, Propagation in Non-ionized Media, Recommendations and Reports of the CCIR, 1982.. Geneva: Int. Telecomm. Union, 1982.

CCIR, "The evaluation of propagation factors in interference problems between stations on the surface of the earth at frequencies above about 0.5 GHz," Report 569-3, Vol. V, Propagation in Non-ionized Media, Recommendations and Reports of the CCIR,1986. Geneva: Int. Telecomm. Union, 1986a.

CCIR, "Propagation data required for the evaluation of coordination distance in the frequency range 1 to 40 GHz," Report 724-2, Vol. V, Propagation in Non-ionized Media, Recommendations and Reports of the CCIR, 1986. Geneva: Int. Telecomm. Union, 1986b.

CCIR, "Determination of coordination area," Report 382-5, Vols. IV and IX- Part 2, Fixed Service Using Radio Relay Systems. Frequency Sharing and Coordination Between Systems in the Fixed Satellite Service and Radio-relay Systems, Recommendations and Reports of the CCIR, 1986. Geneva: Int. Telecomm. Union, 1986c.

CCIR, "Propagation data required for evaluating interference between stations in space and those on the surface of the earth," Report 885-1, Vol. V, Propagation in Non-ionized Media, Recommendations and Reports of the CCIR, 1986. Geneva: Int. Telecomm. Union, 1986d.

CCIR, "Radiometeorological data," Report 563-3, Vol. V, Propagation in Non-ionized Media, Recommendations and Reports of the CCIR, 1986. Geneva: Int. Telecomm. Union, 1986e.

CCIR, "Radiation diagrams of antennas for earth stations in the fixed satellite service for use in interference studies and for the determination of a design objective," Report 391-5, Vol. IV - Part 1, Fixed Service Using Communication Satellites, Recommendations and Reports of the CCIR, 1986. Geneva: Int. Telecomm. Union, 1986f.

CCIR, "Satellite antenna patterns in the fixed satellite service," Report 558-3, Vol. IV, Fixed Service Using Communication Satellites, Recommendations and Reports of the CCIR, 1986. Geneva: Int. Telecomm. Union, 1986g.

CCIR, "Feasibility of frequency sharing between systems in the fixed satellite service and terrestrial radio services. Criteria for the selection of sites for earth stations in the fixed satellite service," Report 385-1, Vol. IV, Fixed Service Using Communication Satellites, Recommendations and Reports of the CCIR, 1986. Geneva: Int. Telecomm. Union, 1986h.

CCIR, "Earth station antennas for fixed satellite service," Report 390-5, Vol. IV, Fixed Service Using Communication Satellites, Recommendations and Reports of the CCIR, 1986. Geneva: Int. Telecomm. Union, 1986i

Crane, R. K., "A review of transhorizon propagation phenomena," Radio Sci., vol. 16, pp. 649-669, Sept.-Oct. 1981.

Dougherty, H. T., A Consolidated Model for UHF/SHF Telecommunication Links Between Earth and Synchronous Satellites, NTIA Report 80-45, U. S. Dept. of Commerce, Aug. 1980.

Dougherty, H. T. and B. A. Hart, "Recent progress in duct propagation predictions," IEEE Trans. Antennas Propagat., vol. AP-27, pp. 542-548, July 1979.

Eastwood, E. Radar Ornithology. London: Methuen, 1967.

ITU (International Telecommunications Union), Appendix 28, Method for the Determination of the Coordination Area Around an Earth Station in Frequency Bands Between 1 GHz and 40 GHz, Radio Regulations, Edition of 1982. Geneva: Int. Telecomm. Union, 1982.

APPENDIX 8.1

PERMISSIBLE LEVEL OF INTERFERING EMISSION

Information on the permissible level of interfering emission that is included in Appendix 28 of Radio Regulations (ITU, 1982) is reproduced below. Reference is made in the following material to two tables containing detailed listing of parameters for the various frequency bands. These tables are not included here, but notes 1 through 4 discuss the parameters and provide information about their magnitudes.

2.3 *Derivation and tabulation of interference parameters*

2.3.1 *Permissible level of the interfering emission*

The permissible level of the interfering emission (dBW) in the reference bandwidth, to be exceeded for no more than p% of the time at the output of the receiving antenna of a station subject to interference, from each source of interference, is given by the general formula below:

$$P_r(p) = 10 \log (kT_e B) + J + M(p) - W \tag{3}$$

where:

$$M(p) \equiv M(p_0/n) = M_0(p_0) \tag{4}$$

with:

- k: Boltzmann's constant (1.38×10^{-23} J/K);
- T_e: thermal noise temperature of the receiving system (K), at the output of the receiving antenna (see *Note 1*);
- B: reference bandwidth (Hz) (bandwidth of the interfered-with system over which the power of the interfering emission can be averaged);
- J: ratio (dB) of the permissible long term (20% of the time) interfering emission power to the thermal noise power of the receiving system, referred to the output terminals of the receiving antenna (see *Note 2*);

Reprint

p_0: percentage of the time during which the interference from all sources may exceed the permissible value;

n: number of expected entries of interference, assumed to be uncorrelated;

p: percentage of the time during which the interference from one source may exceed the permissible value; since the entries of interference are not likely to occur simultaneously: $p = p_0/n$;

$M_0(p_0)$: ratio (dB) between the permissible powers of the interfering emission, during p_0% and 20% of the time, respectively, for all entries of interference (see *Note 3*);

$M(p)$: ratio (dB) between the permissible powers of the interfering emission during p% of the time for one entry of interference, and during 20% of the time for all entries of interference;

W: equivalence factor (dB) relating interference from interfering emissions to that caused by the introduction of additional thermal noise of equal power in the reference bandwidth. It is positive when the interfering emissions would cause more degradation than thermal noise (see *Note 4*).

Tables I and II list values for the above parameters.

In certain cases, an administration may have reason to believe that, for its specific earth station, a departure from the values associated with the earth station, as listed in Table II, may be justified. Attention is drawn to the fact that for specific systems the bandwidths B or, as for instance in the case of demand assignment systems, the percentages of the time p and p_0 may have to be changed from the values given in Table II. For further information see § 2.3.2.

Note 1: The noise temperature, in kelvins, of the receiving system, referred to the output terminals of the receiving antenna, may be determined from:

$$T_e = T_a + (e - 1)\,290 + eT_r \tag{5a}$$

where:

T_a: noise temperature (K) contributed by the receiving antenna;

e: numerical loss in the transmission line (e.g. a waveguide) between antenna and receiver front end;

T_r: noise temperature (K) of the receiver front end, including all successive stages, referred to the front end input.

For radio-relay receivers and where the waveguide loss of a receiving earth station is not known, a value of $e = 1.0$ is to be used.

Note 2: The factor J (dB) is defined as the ratio of total permissible long term (20% of the time) power of interfering emissions in the system, to the long term thermal radio frequency noise power in a single receiver. In the computation of this factor, the interfering emission is considered to have a flat power spectral density, its actual spectrum shape being taken into account by the factor W (see below). For example, in a 50-hop terrestrial hypothetical reference circuit, the total allowable additive interference power is 1 000 pW0p (CCIR Recommendation 357-3) and the mean thermal noise power in a single hop may be assumed to be 25 pW0p. Therefore, since in a frequency-division multiplex/frequency modulation (FDM/FM) system the ratio of a flat interfering noise power to the thermal noise power in the same reference band is the same before and after demodulation, J is given by the ratio 1 000/25 expressed in dB, i.e. $J = 16$ dB. In a fixed-satellite service system, the total allowable interference power is also 1 000 pW0p (CCIR Recommendation 356-4), but the thermal noise contribution of the down-link is not likely to exceed 7 000 pW0p, hence $J \geq -8.5$ dB.

In digital systems interference is measured and prescribed in terms of the bit error rate or its permissible increase. While the bit error rate increase is additive in a reference circuit comprising tandem links, the radio frequency power of interfering emissions giving rise to such bit error rate increase is not additive, because bit error rate is not a linear function of the level of the radio frequency power of interfering emissions. Thus, it may be necessary to protect each receiver individually. For digital radio-relay systems operating above 10 GHz, and for all digital satellite systems, the long term interference power may be of the same order of magnitude as the long term thermal noise, hence $J = 0$ dB. For digital radio-relay systems operating below 10 GHz, long term interference power should not decrease the receiver fade margin by more than 1 dB. Thus the long term interference power should be about 6 dB below the thermal noise power and hence $J = -6$ dB.

Note 3: $M_0(p_0)$ (dB) is the "interference margin" between the short term (p_0%) and the long term (20%) allowable powers of an interfering emission.

For analogue radio-relay and fixed-satellite systems in bands between 1 GHz and 15 GHz, this is equal to the ratio (dB) between 50 000 and 1 000 pW0p (17 dB).

In the case of digital systems, system performance at frequencies above 10 GHz can, in most areas of the world, usefully be defined as the percentage of the time p_0 for which the wanted signal is allowed to drop below its operating threshold, defined by a given bit error rate. During non-faded operation of the system, the desired signal will exceed its threshold level by some margin M_s which depends on the rain climate in which the station operates. The greater this margin, the greater the enhancement of the interfering emission which would degrade the system to threshold performance. As a first order estimate it may be assumed that, for small percentages of the time (of the order of 0.001% to 0.003%), the level of interfering emissions may be allowed to equal the thermal noise which exists at the demodulator input during faded conditions. Thus, M_0 in Tables I and II may, for digital systems operating above 10 GHz, be assumed to be equal to the fade margin M_s of the system. For digital radio-relay systems operating below 10 GHz it is assumed that the short term power of an interfering emission can be allowed to exceed the long term power of the interfering emission by an amount equal to the fade margin of the system minus J, i.e. 41 dB, where $J = -6$ dB.

Note 4: The factor W (dB) is the ratio of radio frequency thermal noise power to the power of an interfering emission in the reference bandwidth when both produce the same interference after demodulation (e.g. in a FDM/FM system it would be expressed for equal voice channel performance; in a digital system it would be expressed for equal bit error probabilities). For FM signals, it is defined as follows:

$$W = 10 \log \left\{ \frac{\text{Thermal noise power at the output of the receiving antenna in the reference bandwidth}}{\text{Power of the interfering emission at the radio frequency in the reference bandwidth, at the output of the receiving antenna}} \times \frac{\text{Interference power in the receiving system after demodulation}}{\text{Thermal noise power in the receiving system after demodulation}} \right\} \tag{5b}$$

The factor W depends on the characteristics of the wanted and the interfering signals. To avoid the need for considering a wide range of characteristics, upper limit values were determined for the factor W. When the wanted signal uses frequency modulation with r.m.s. modulation indices which are greater than unity, W is not higher than 4 dB. In such cases, a conservative figure of 4 dB will be used for the factor W in (3), regardless of the characteristics of the interfering signal. For low-index FDM/FM systems a very small reference bandwidth (4 kHz) implies values of W not greater than 0 dB. In such cases, a conservative figure of 0 dB will be used for W in (3), regardless of the characteristics of the interfering signal.

When the wanted signal is digital, W is usually equal to or less than 0 dB, regardless of the characteristics of the interfering signal.

CHAPTER 9

ESTIMATION OF PROPAGATION IMPAIRMENTS

9.1 INTRODUCTION

Background material on the various propagation effects on satellite communications has been presented in previous chapters, and in this chapter further attention is devoted to consideration of the magnitudes of the effects for use in system design. Illustrative numerical examples are given. The phenomena are treated in essentially the same order as in Chaps. 1 through 7. Thus ionospheric effects are considered first. Table 9.1 (same as Table 2.2) provides a summary of ionospheric effects (not including ionospheric scintillation).

9.2 IONOSPHERIC EFFECTS

9.2.1 Faraday Rotation: Determination of Longitudinal Component of Magnetic Field.

Many satellite communication systems employ circularly polarized waves and therefore need not be concerned about Faraday rotation. Some satellites transmit linearly polarized waves which are subject to Faraday rotation, however, and attention is given here to its estimation. One reason for using linearly polarized transmission may be to obtain information about ionospheric total electron content (TEC) which contributes to excess range delay and other effects in addition to Faraday rotation. At high frequencies, Faraday rotation along a path is given in SI units by

$$\phi = \frac{2.36 \times 10^4}{f^2} \int N\, B \cos \theta_B \, d\ell \qquad \text{rad} \qquad (9.1)$$

where ϕ is the Faraday rotation angle in radians, f is frequency in Hz, N is electron density in electrons/m^3 (eℓ/m^3), B is magnetic flux density of the Earth's field, and θ_B is the angle between the path and the B vector. The SI unit for B is the tesla (T), also commonly referred to as Webers/m^2 (Wb/m^2). Evaluation of the integral involves the values of N, B, and cos θ_B along the path, but for some situations, for geostationary and orbiting earth satellites, it is sufficiently accurate to replace $B \cos \theta_B$ by an average or effective value $\overline{B}_L$ and take it outside the integral. Then the relation has the form of

$$\phi = \frac{2.36 \times 10^4 \, \overline{B}_L}{f^2} \int N \, d\ell = \frac{2.36 \times 10^4 \, \overline{B}_L}{f^2} \, (\mathrm{TEC}) \quad \mathrm{rad} \qquad (9.2)$$

where

$$\overline{B}_L = \frac{\int N \, B \cos \theta_B \, d\ell}{\int N \, d\ell} \qquad \mathrm{T \ or \ Wb/m^2} \qquad (9.3)$$

Table 9.1 Estimated maximum ionospheric effects in the United States for one-way paths at an elevation angle of 30 deg (same as Table 2.2).

Effect	100 MHz	300 MHz	1 GHz	3 GHz	10 GHz
Faraday rotation	30 rot.	3.3 rot.	108°	12°	1.1°
Excess time delay	25 μs	2.8 μs	0.25 μs	0.028 μs	0.0025 μs
Refraction	$\leq 1^\circ$	<7 min	≤ 0.6 min	<4.2 s	≤ 0.36 s
Variation in direction of arrival	20 min	2.2 min	12 s	1.32 s	0.12 s
Absorption (auroral and polar cap)	5 dB	1.1 dB	0.05 dB	6×10^{-3} dB	5×10^{-4} dB
Absorption (mid latitude)	<1 dB	0.1 dB	<0.01 dB	$<1 \times 10^{-3}$ dB	$<10^{-4}$ dB
Dispersion	0.4 ps/Hz	0.015 ps/Hz	0.0004 ps/Hz	1.5×10^{-5} ps/Hz	4×10^{-7} ps/Hz

A variation of this procedure has been employed by Davies who used

$$\phi = \frac{8.44 \times 10^{-7}}{f^2} \int f_L \, N \, d\ell \qquad \text{rad}$$

$$\phi = \frac{8.44 \times 10^{-7}}{f^2} \, \overline{F} \; (\text{TEC}) \qquad \text{rad} \qquad (9.4)$$

with $\overline{F}$ defined by

$$\overline{F} = \frac{\int N f_H \cos\theta_B \, d\ell}{\int N \, d\ell} \qquad (9.5)$$

As the electron gyrofrequency f_H in Hz equals 2.8×10^{10} B and $(2.8 \times 10^{10}) \times (8.44 \times 10^{-7}) = 2.36 \times 10^{4}$, the two variations are seen to be compatible. The values of TEC obtained by use of Eqs. (9.2) and (9.4) are values for slant paths. If it desired to determine TEC values for equivalent vertical paths, one may use

$$\phi = \frac{2.36 \times 10^{4}}{f^2} \, \overline{M} \; (\text{TEC}) \qquad \text{rad} \qquad (9.6)$$

with

$$\overline{M} = \frac{\int N B \cos\theta_B \sec\chi \, dh}{\int N \, dh} \qquad (9.7)$$

where χ is the zenith angle and dh represents an element of length in the vertical direction (Titheridge, 1972). Davies (1980) has pointed out that the use of an effective vertical content is advantageous when comparing contents over different paths but may be somewhat misleading because there may be no existing vertical path that has the inferred vertical content.

Equations (9.3), (9.5), and (9.7) show what the values of $\overline{B_L}$, $\overline{F}$, and $\overline{M}$ represent but in practice it is generally considered that for $\overline{B_L}$, for example, the value of B_L ($B \cos\theta_B$) at a height such as 400 or 420 km represents a sufficiently good approximation to $\overline{B_L}$

The approach to be used to estimate Faraday rotation depends on the degree of accuracy required. If only a very rough estimate is needed one may refer to Table 9.1 or Fig. 9.1 if an estimate of TEC is available. If somewhat greater accuracy is needed, it may be advisable to determine a value for B_L for the path and to then use Eq. (9.2) for calculating Faraday rotation as a function of TEC. In determining B_L, one has a choice of using a simple dipole model of the Earth's field or more sophisticated models. The dipole model is useful for preliminary estimates or when funding, facilities, or location do not justify the use of more accurate models. The need for a more accurate model than the dipole model tends to be greater at low geomagnetic latitudes than at the higher latitudes. It should be recognized in any case that Faraday rotation is proportional to ionospheric TEC, which is highly variable, and high accuracy in determining B_L may not be justifiable. Also the use of a fixed value of B_L introduces errors and if the highest precision is desired one should theoretically evaluate Faraday rotation by using the integral formulation or by use of a summation obtained by separating the ionosphere into layers of known or assumed values of N, B, and cos θ_B.

The view is taken here that it is useful in some cases to use the value for B_L at 400 km obtained by using a dipole model for the Earth's field, and a procedure for doing so is presented as Appendix 9.1. If one wishes to be assured of greater accuracy than about 25 percent for determining B_L, one can make use of the spherical harmonic coefficients of the International Geomagnetic Reference Field (EOS, June 17, 1986) and a computer algorithm for synthesizing the geomagnetic field such as that by Malin and Barraclough (1981). A special issue of the Journal of Geomagnetism and Geoelecticity (vol. 34, no. 6, 1982) was devoted to the international field. Also the Environmental Data and Information Service (EDIS) of NOAA, Boulder, Colorado can supply values of B_L based on the International Geomagnetic Reference Field. The following Example 9.1, however, illustrates the calculation of B_L at 400 km using a dipole model. The example uses the procedure of Appendix 9.1.

Example 9.1 Determination of B_L

Considering an earth station at Fairbanks, Alaska (65 deg N, 148 deg W) and a geostationary satellite at 148 deg W (on the same geographic meridian), this example illustrates how to find a value for B_L for evaluating Faraday rotation, using the dipole model of the Earth's field. In the example the geographic coordinates of the intersection of the dipole axis and the Earth's surface in the northern hemisphere are taken as 78.8 deg N and 70.9 deg W (Dawson and Newitt, 1982).

From Eqs. (A9.17) and (9.18) with $\theta'_g = 65^o$, $\theta'_p = 78.8^o$, and

$$\phi_g - \phi_p = 148^o - 70.9^o = 77.1^o,$$

$$\theta'_m = 63.279^o \text{ N (geomagnetic latitude)}$$

$$\phi_m = 66.373^o \text{ W (geomagnetic longitude)}$$

Using the procedure described with the aid of Fig. A9.1 and Eq. (A9.14), the path from the earth station to the satellite is found to intercept the 400-km level at a latitude of 56.013 deg N. The geomagnetic coordinates of this point, found by using Eqs. (A9.17) and (A9.18) again, now with $\theta'_g = 56.013$ deg, are

$$\theta'_m = 56.889^o \text{ N}$$

$$\phi_m = 85.945^o \text{ W}$$

From Eqs. (A9.3), (A9.5), and (A9.6), using B_o as 0.32 G (10,000 G = 1 Wb/m^2) and a/r = 6378/(6378 + 400),

$$H = 0.141 \text{ G}, \quad Z = 0.433 \text{ G}, \quad F = 0.455 \text{ G}$$

and

$$F = 0.433\, a_r + 0.146\, a_\theta$$

Converting to rectangular coordinates by using Eqs. (A9.20) and (A9.21)

$$F = 0.0251\, \mathbf{a}_x + 0.354\, \mathbf{a}_y + 0.286\, \mathbf{a}_z .$$

Next one needs to determine $\mathbf{d} = \mathbf{S} - \mathbf{G}$, where S is the geostationary satellite position and G is the earth-station position. For **S**, $\theta'_m = 2.485$ deg and $\phi = 77.338$ deg from Eqs. (A9.17) and (A9.18), with $\theta'_g = 0$ deg. Measuring distances in earth radii with the satellite at 6.6 radii and expressing in rectangular coordinates by use of Eqs. (A9.22 - A9.24),

$$S = 1.445\,\mathbf{a}_x + 6.433\,\mathbf{a}_y + 0.286\,\mathbf{a}_z$$

For G, $\theta'_m = 63.279^\circ$ and $\phi_m = 66.373^\circ$ and, with **G** at a distance of 1 earth radius from the center of the Earth,

$$G = 0.180\,\mathbf{a}_x + 0.412\,\mathbf{a}_y + 0.893\,\mathbf{a}_z$$

Then for $\mathbf{d} = \mathbf{S} - \mathbf{G}$ one obtains

$$\mathbf{d} = 1.265\,\mathbf{a}_x + 6.021\,\mathbf{a}_y - 0.607\,\mathbf{a}_z$$

Next using $\mathbf{F}\cdot\mathbf{d} = Fd\cos\theta_B$

$$1.988 = 2.813 \cos\theta_B$$

$$\cos\theta_B = 0.707,\ \theta_B = 45.03^\circ.$$

Finally

$$B_L = F\cos\theta_B = 0.322\ G = 3.22 \times 10^{-5}\ \mathrm{Wb/m^2}. \quad \leftarrow\!\!---$$

In this example the earth station and satellite are at the same longitude. If they are not, Eqs. (A9.15) and (A9.16) and the adjacent explanation can be used to find the latitude and longitude of the 400-km intercept.

9.2.2 Propagation Effects Directly Dependent on TEC

The total electron content (TEC) along a path is the number of electrons in a column one square meter in cross section (electrons/m^2 or eℓ/m^2) that coincides in position with the path. The TEC of the ionosphere has a pronounced diurnal variation as illustrated in Fig. 2.6 and also varies with solar activity, especially with geomagnetic storms which may result from solar activity. Faraday rotation, excess time delay and associated range delay, phase advance, and time-delay and phase-advance dispersion are directly proportional to TEC. Most ionospheric effects, in fact, tend to be proportional to TEC.

9.2.2.1 Faraday Rotation

The angle of Faraday rotation is proportional to TEC as indicated by Eq. 9.2, which is repeated below. The theory of Faraday rotation was developed in Sec. 2.2, and Eq. 9.2 was further justified in Sec. 9.2.1 which was devoted primarily to consideration of B_L, the longitudinal component of the Earth's magnetic field.

$$\phi = \frac{2.36 \times 10^4}{f^2} \overline{B_L}\ \mathrm{TEC}$$

For systems using linear polarization, uncompensated Faraday rotation can cause a polarization mismatch loss of 20 log δ, where $\delta = \cos\theta_i$ and θ_i is the polarization mismatch angle. This angle may equal the Faraday rotation angle ϕ but may also be less than ϕ, if a certain value of ϕ was anticipated and compensated for but the actual value of ϕ was different. In addition to the diurnal variations of Faraday rotation and the variations with the solar cycle, rapid variations, having periods of fractions of a minute, are also sometimes observed. At Ascension Island at the equatorial anomaly crest, rapid variations of about 90 deg at 136 MHz were observed at the same time that intense scintillation was recorded on 1.54 GHz MARISAST transmissions (Lee et al., 1982). Although Faraday rotation can sometimes be troublesome or at least must be taken into account to ensure satisfactory system performance, it can be a valuable tool for determining ionospheric TEC which causes excess time delay that is important to radionavigation and positioning satellite systems. Representative values of Faraday rotation are shown in Fig. 9.1 as a function of frequency and TEC.

9.2.2.2 Excess Time and Range Delay

The excess time delay Δt due to the TEC along a path is given by

$$\Delta t = \frac{40.3\ \mathrm{TEC}}{cf^2} = \frac{1.34 \times 10^{-7}\ \mathrm{TEC}}{f^2} \quad \mathrm{s} \qquad (9.8)$$

and the excess range delay ΔR due to the TEC is specified by

$$\Delta R = (40.3/f^2)\ \mathrm{TEC} \qquad (9.9)$$

In Eqs. (9.8) and (9.9), f is frequency in Hz and TEC is total electron content in $e\ell/m^2$. It is evident that determination of Δt and ΔR requires information about TEC.

Figure 9.2 shows time and range delay as a function of frequency for a one-way path for TEC values of 10^{17} and 10^{18} $e\ell/m^2$. Sometimes a known or estimated value of TEC is available for a vertical path and it is desired to estimate delay for a path as a function of elevation angle. Figure 9.3 shows the excess range delay or error as a function of elevation angle for a TEC of 10^{18} $e\ell/m^2$ on a vertical path for frequencies of 100 MHz, 400 MHz, and 1200 MHz (Millman, 1980).

9.2.2.3 Phase Advance

The phase advance $\Delta\phi$ of an electromagnetic wave with respect to the value of phase for propagation through a vacuum is also directly proportional to TEC as expressed by

$$\Delta\phi = \frac{8.44 \times 10^{-7}}{f}\ \mathrm{TEC} \quad \mathrm{rad} \qquad (9.10)$$

The change in phase associated with a change in TEC may be of interest. For example, one may wish to relate the change in phase due to a traveling ionospheric disturbance (TID) to the change in TEC. Using $\delta\phi$ for the change in phase associated with an increment $\Delta(\mathrm{TEC})$ in TEC,

$$\delta\phi = \frac{8.44 \times 10^{-7}}{f}\ \Delta(\mathrm{TEC}) \quad \mathrm{rad} \qquad (9.11)$$

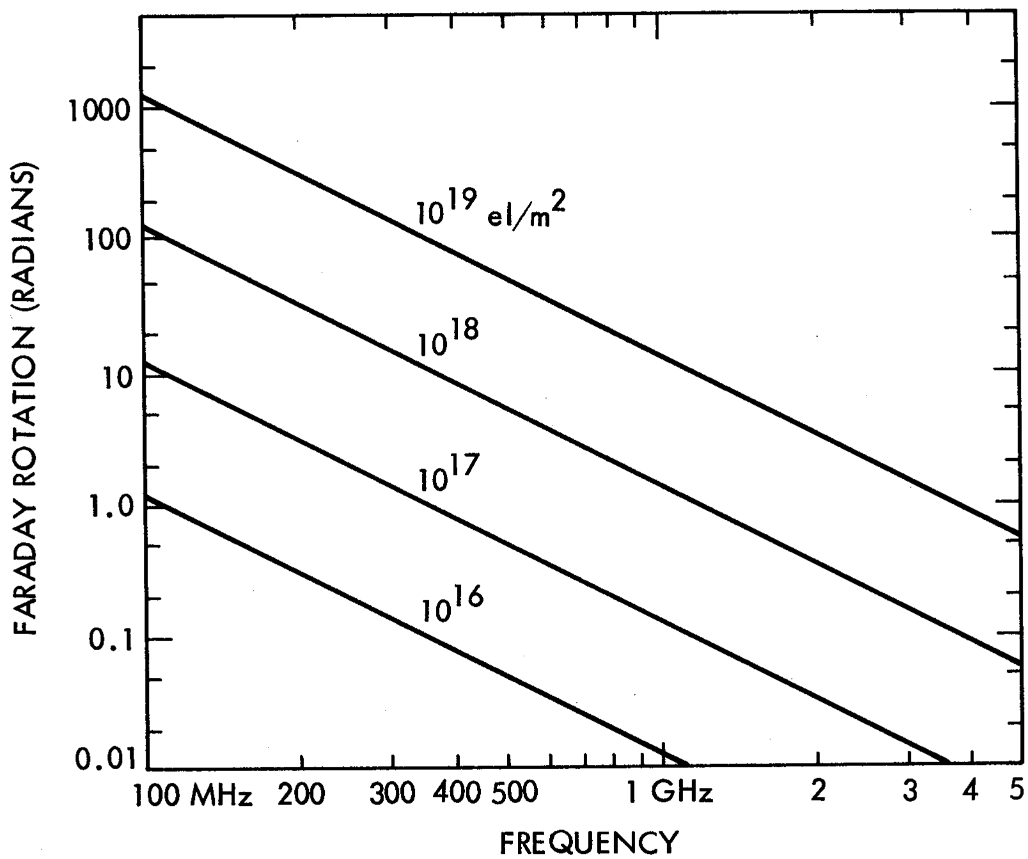

Figure 9.1. Faraday rotation as a function of ionospheric TEC and frequency (Klobuchar, 1978).

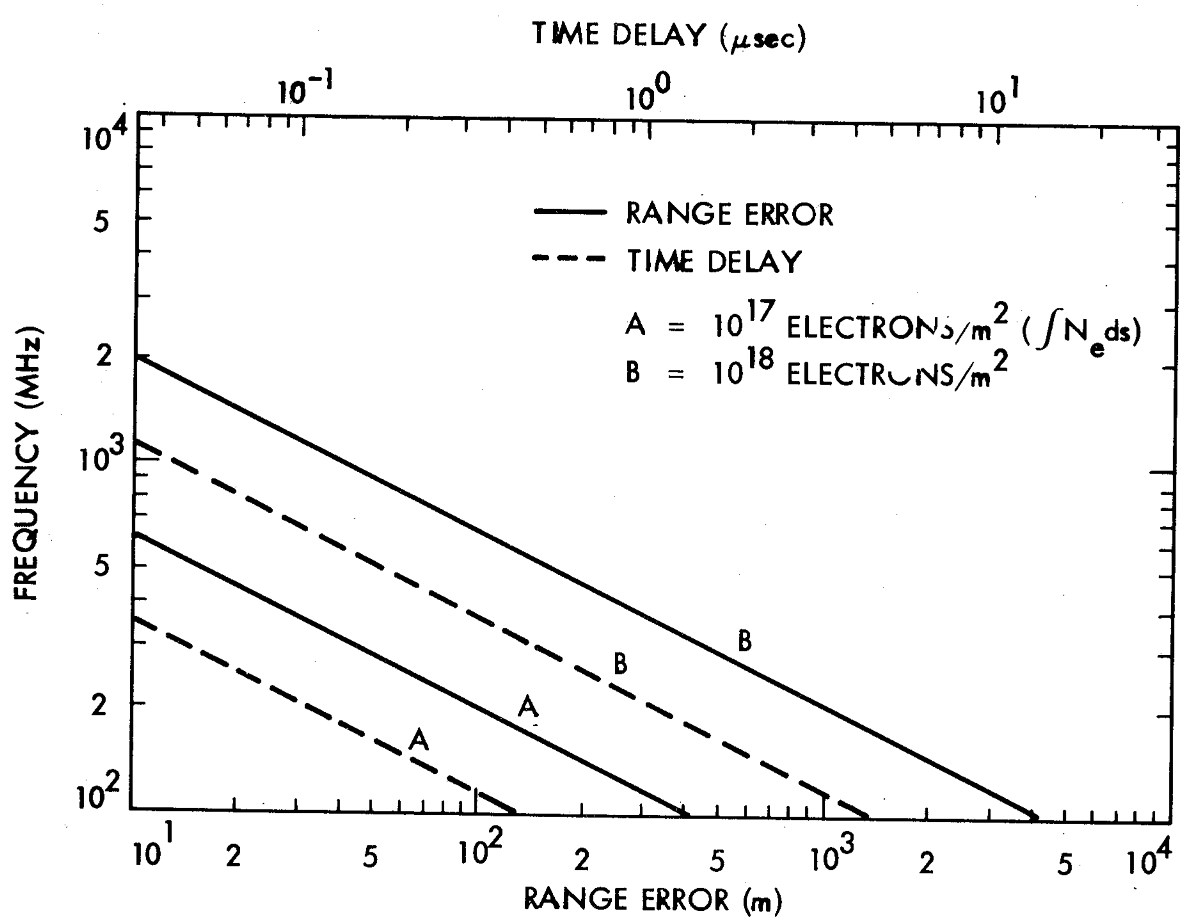

Figure 9.2. Ionospheric range error and time delay for a one-way path (Millman, 1980).

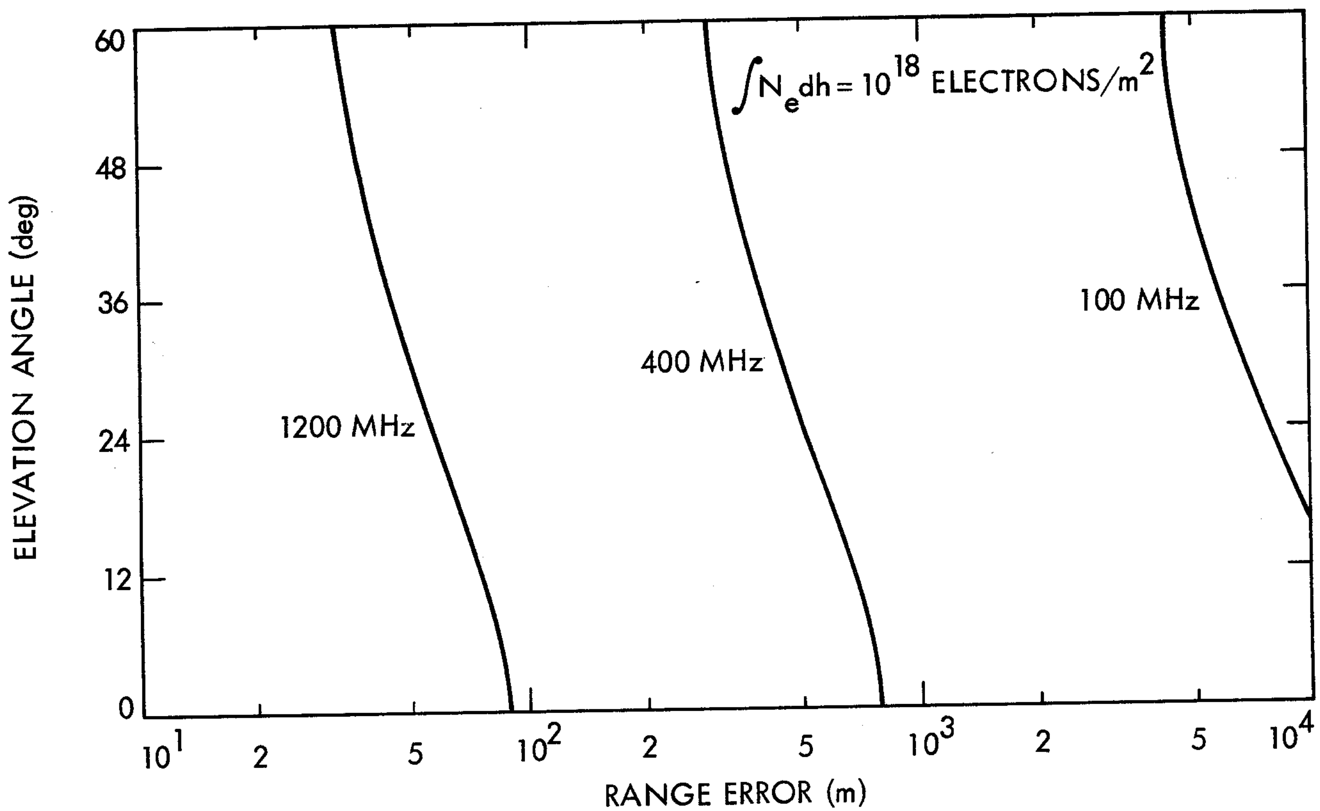

Figure 9.3. Ionospheric range error as a function of elevation angle and frequency (Millman, 1980).

9.2.2.4 Doppler Frequency

Frequency f and phase ϕ are related by $f = (1/2\pi)\ (d\phi/dt)$, and the Doppler shift in frequency f_D associated with a change in phase due to variation of TEC with time is given by

$$f_D = \frac{1.34 \times 10^{-7}}{f} \frac{d(TEC)}{dt} \qquad \text{Hz} \qquad (9.12)$$

The average Doppler frequency during a time interval or count time T_c in which TEC changes by Δ(TEC) is given by

$$f_D = \frac{1.34 \times 10^{-7}}{f} \frac{\Delta(TEC)}{T_c} \qquad \text{Hz} \qquad (9.13)$$

9.2.2.5 Dispersion

The rate of change of time delay with frequency, referred to as time-delay dispersion, is

$$\frac{dt}{df} = -\frac{2.68 \times 10^{-7}}{f^3}\ TEC \qquad \text{s/Hz} \qquad (9.14)$$

Applied to a pulse of length τ for which the associated bandwidth $\Delta f = 1/\tau$, the difference in time delay Δt between the two extreme frequencies of the pulse is given by

$$\Delta t = -\frac{2.68 \times 10^{-7}}{f^3}\ \Delta f\ (TEC) \qquad \text{s} \qquad (9.15)$$

The effect of dispersion on a pulse propagating through the ionosphere is to decrease the amplitude, increase the length, and introduce frequency modulation (Millman, 1980). Whether the effects are of significance or not depends on the values of f, Δf, and TEC.

9.2.2.6 Refractive Bending

It develops that the refractive bending or change in direction of a ray traversing the ionosphere is proportional to TEC also. The expression given by Millman and Reinsmith (1974) for the elevation

C-5

angle error $\Delta\theta$ for a satellite for which the range R is considerably larger than $r_o \sin \theta_o$, where r_o is earth radius and θ_o is elevation angle, is

$$\Delta\theta = (\cos \theta_o / 2h_i)\, \Delta R \qquad \text{rad} \qquad (9.16)$$

The quantity h_i is the height where the median electron content occurs and is generally between 300 and 450 km. As ΔR is the range error along the path and is proportional to TEC, $\Delta\theta$ is also proportional to TEC.

As irregularities in electron density such as those caused by TID's move across the line of sight and cause variations in TEC, the variations are reflected in ΔR and $\Delta\theta$.

9.2.2.7 Prediction and Measurement of TEC

TEC along a path is highly variable and difficult to predict accurately, but advance estimates or predictions of TEC may be needed for system planning and in system operations. Techniques are available for measuring TEC and these will be mentioned shortly, but their cost may preclude their use in some cases.

For some purposes it may be sufficient to estimate the maximum Faraday rotation or excess range delay that may be encountered. To obtain this estimate one may assume a maximum TEC of 10^{18} $e\ell/m^2$ for a one-way zenith path (CCIR, 1986a). At night the value of TEC may drop to about one eigth of the maximum value. Figure 9.3 illustrates how effects proportional to TEC will tend to vary as a function of elevation angle θ in the range from 0 deg to 60 deg. When the value of TEC is given without qualification it normally refers to the zenith value, but the content along a slant path is often what is wanted. This value is commonly assumed to be the zenith value multiplied by the secant of the zenith angle χ at an ionospheric height h somewhat above that of the F layer maximum, thus taking into account the preponderence of ionization on the topside of the layer. A relation giving the zenith angle χ in terms of the elevation angle θ of the path at the surface is

$$\chi = \sin^{-1}\left(\frac{r_o}{r_o + h} \cos \theta\right) \qquad (9.17)$$

where r_o is the Earth's radius and h is ionospheric height, commonly 300 to 400 km. For example if $\theta = 30$ deg and h = 350 km

$$\chi = \sin^{-1}\left(\frac{6371}{6371 + 350}(0.866)\right) = 55.18^{o}$$

As a result sec $\chi = 1.75$ and TEC for the slant path equals about 1.75 times the value for a zenith path.

The problem of predicting time delay due to TEC was considered carefully by Klobuchar and the working group of which he was the leader (Klobuchar and Working Group, 1979) at the Solar-Terrestrial Predictions Workshop Program in Boulder in 1979. It was concluded that monthly median values of TEC could be predicted to within an rms deviation of 20 to 25 percent in the daytime and 30 to 35 percent at night but that geomagnetic activity causes about a 25 percent deviation from the median values. For highest accuracy in TEC, real-time or near-real-time data are needed. A service is available for registered SELDADS users that provides hourly TEC values from satellite data. SELDADS is an operational, real-time, solar-terrestial-environment monitoring system. Further information about SELDADS and the TEC data that it can provide can be obtained by writing to the Chief Forecaster, Space Environment Services Center, R432, National Oceanic and Atmospheric Adminstration, 325 Broadway, Boulder, CO 80303.

One means for obtaining real-time data on ionospheric TEC is to measure the Faraday rotation of signals from beacons on satellites. In addition to the ionospheric TEC, the total TEC along a path to a satellite or space vehicle may include a contribution from the plasmasphere that is about 15 percent of the ionospheric TEC by day and 50 percent by night (Klobuchar and Working Group, 1979). Measurements of time delay at two frequencies can provide the value of the total TEC along a path. As discussed more fully in Sec. 2.3.1, the total TEC is given in that case by Eq. (2.38) which is repeated below.

$$TEC = \frac{\delta t\ c}{40.3}\ \frac{f_1^2 f_2^2}{f_1^2 - f_2^2}$$

The quantities f_1 and f_2 are the two frequencies, c is the velocity of light, and δt is the difference in the time delays $(\Delta t_2 - \Delta t_1)$ at the two frequencies.

Example 9.2 Effects Dependent on TEC

To illustrate the effects of the total electron content (TEC), frequencies of 870 MHz and 2.3 GHz, a TEC value of 10^{18} el/m^2, and a longitudinal component of the Earth's magnetic field B_L of 0.38 B will be utilized.

1. Faraday Rotation

<u>870 MHz, 10^{18} el/m^2, 0.38 G = 3.8×10^{-5} Wb/m^2</u>

$$\phi = \frac{2.36 \times 10^4 B_L \text{ (TEC)}}{f^2} = \frac{2.36 \times 10^4 (3.8 \times 10^{-5})(10^{18})}{(8.7 \times 10^8)^2}$$

$$= 1.17 \text{ rad} = 67.6^\circ$$

<u>2.3 GHz, 10^{18} el/m^2, 3.8×10^{-5} Wb/m^2</u>

$$\phi = \left(\frac{8.7 \times 10^8}{2.3 \times 10^9}\right)^2 67.6^\circ = 9.67^\circ$$

2. Time and Range Delay (one-way transmission)

<u>870 MHz, 10^{18} el/m^2</u>

$$\Delta R = \frac{40.3 \text{ (TEC)}}{f^2} = \frac{40.3 (10^{18})}{f^2} = 53.24 \text{ m}$$

$$\Delta t = \frac{53.24}{2.9979 \times 10^8} = 1.78 \times 10^{-7} \text{ s} = 0.178\ \mu\text{s}$$

<u>2.3 GHz, 10^{18} el/m^2</u>

$$\Delta R = (8.7 \times 10^8/2.3 \times 10^9)^2 \ (53.24) = 7.62 \text{ m}$$

$$\Delta t = \frac{7.62}{2.9979 \times 10^8} = 0.0254\ \mu s$$

3. Phase Advance (one-way transmission)

<u>870 MHz, 10^{18} eℓ/m^2</u>

$$\Delta\phi = \frac{8.44 \times 10^{-7}}{f}\ (\mathrm{TEC}) = \frac{8.44 \times 10^{-7}\ (10^{18})}{8.7 \times 10^8}$$

$$= 970.1 \text{ rad or } 970.1/2\pi = 154.4 \text{ cycles}$$

This very large advance in phase is of less interest than that due to a change, Δ(TEC), in TEC. Suppose that a traveling ionospheric disturbance modulates TEC by a factor of 0.01 so that $\Delta(\mathrm{TEC}) = 10^{16}$ eℓ/m^2. Then

$$\delta\phi = \frac{8.44 \times 10^{-7}}{f}\ \Delta(\mathrm{TEC}) = 9.70 \text{ rad} = 1.54 \text{ cycles} = 556^\circ$$

This still a very large change in phase.

<u>2.3 GHz, 10^{18} eℓ/m^2</u>

$$\Delta\phi = \frac{8.7 \times 10^8}{2.3 \times 10^9}\ (9.70) = 367 \text{ rad} = 54.4 \text{ cycles}$$

For modulation of TEC by a factor of 0.01

$$\delta\phi = 3.67 \text{ rad} = 0.584 \text{ cycles} = 210 \text{ deg.}$$

4. Doppler Frequency

<u>870 MHz, $\Delta(\mathrm{TEC}) = 10^{16}$ eℓ/m^2 in 100 s</u>

$$f_D = \frac{1.34 \times 10^{-7}}{f}\ \frac{\Delta(\mathrm{TEC})}{T_c} = \frac{1.34 \times 10^{-7}\ (10^{16})}{8.7 \times 10^8\ (100)}$$

$$= 0.015 \text{ Hz}$$

2.3 GHz, $\Delta(\mathrm{TEC}) = 10^{16}$ el/m^2 in 100 s

$$f_D = \frac{8.7 \times 10^8}{2.3 \times 10^9} (0.015) = 0.0057 \text{ Hz}$$

5. Dispersion

870 MHz, TEC = 10^{18} el/m^2, Δf = 50 MHz

This example applies to the propagation of 2.0×10^{-2} μs pulses through the ionosphere, assuming a system bandwidth Δf of 50 MHz with $\Delta f = 1/\tau$ where τ is pulse width.

$$|\Delta t| = \frac{2.68 \times 10^{-7}}{f^3} \Delta f \ (\mathrm{TEC}) = \frac{2.68 \times 10^{-7} (5 \times 10^7) 10^{18}}{(8.7 \times 10^8)^3}$$

$$|\Delta t| = 2.2 \times 10^{-8} \text{ s} = 2.2 \times 10^{-2} \ \mu\text{s} = 22 \text{ ns}$$

The time dispersion is seen to be slightly greater than the pulse width. Thus the dispersion may limit the bit rate (data rate for digital transmission) to something less than 50 Mbps.

2.3 GHz, TEC = 10^{18} el/m^2, Δf = 50 MHz

$$|\Delta t| = \left(\frac{8.7 \times 10^8}{2.3 \times 10^9}\right)^3 (2.2 \times 10^{-2}) = 1.19 \times 10^{-3} \ \mu\text{s} = 1.19 \text{ ns}$$

A data rate of 50 Mbps appears to be quite feasible at a frequency of 2.3 GHz.

6. Elevation Angle Error, $\Delta\theta$

870 MHz, 10^{18} el/m^2

$$\Delta\theta = \frac{\cos \theta_o}{2 h_i} \Delta R$$

In part 2, a range delay ΔR of 53.24 m was determined for this frequency and TEC. Assuming 400 km for h_i and arbitrarily taking θ_o to be 5 deg,

$$\Delta\theta = \frac{0.996}{2\,(4 \times 10^5)}\,(53.24)$$

$$= 6.6 \times 10^{-5} \text{ rad} = 0.066 \text{ mrad}$$

<u>2.3 GHz, 10^{18} el/m^2</u>

$$\Delta\theta = \frac{0.996}{2\,(4 \times 10^5)}\,(7.62)$$

$$= 0.0095 \text{ mrad}$$

9.2.3 Ionospheric Scintillation

Scintillation is most severe in the equatorial region within ± 20 deg of the magnetic equator and at high latitudes, where two regions of peak scintillation activity have been reported. One corresponds to the auroral oval, and one is over the polar cap above 80 deg of geomagnetic latitude. In the equatorial zone, scintillation is higher in the region of the equatorial anomaly from about 15 deg to 20 deg north and south of the magnetic equator than near the equator itself. Between the equatorial and high-latitude regions are the middle latitudes where activity is less intense. In all sectors pronounced nighttime maxima occur. The general pattern is as shown in Fig. 9.4. A review of the global morphology of ionospheric scintillation has been provided by Aarons (1982). Some data concerning scintillation levels are shown in Table 9.2 for the low frequencies of 137 and 254 MHz for which scintillation tends to be intense. At Ascension Island in the equatorial anomaly, 27 dB peak-to-peak fading was recorded at 1.54 GHz compared to 7 to 9 dB at Huancayo and Natal near the magnetic equator during the sunspot peak in 1979 and 1980 (Aarons et al., 1981). Further information about scintillation in the equatorial anomaly has been provided by Mullen et al. (1985).

Significant scintillation has been recorded in even the 4 and 6 GHz bands at equatorial latitudes. In one case involving transmission on a 6 GHz uplink and a 4 GHz downlink, fading reached 8 dB peak-to-peak (Aarons, 1982). Examples of scintillation fading on 6 GHz links are shown in Fig. 2.16.

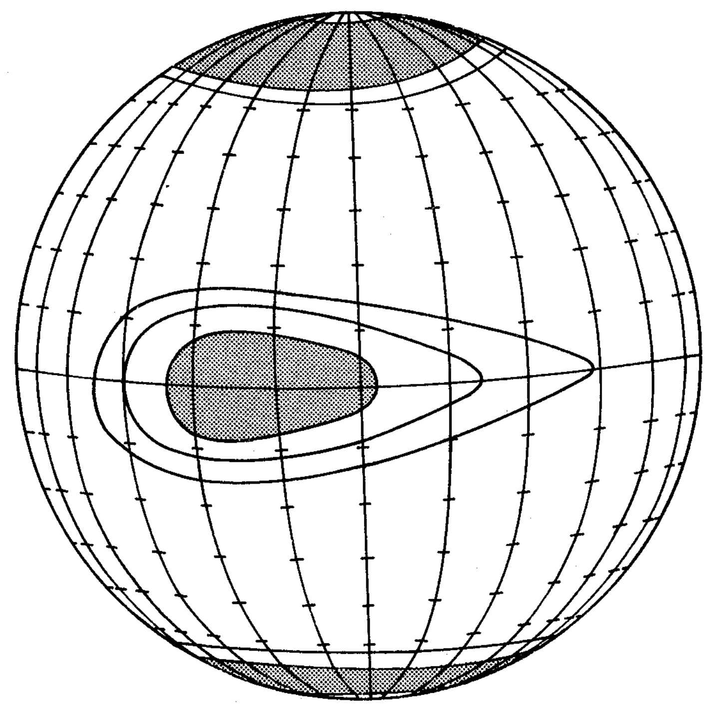

Figure 9.4. Pattern of occurrence of ionospheric scintillation (CCIR, 1986a).

Although scintillation at middle latitudes is generally not as intense as at equatorial and high latitudes, some cases of severe scintillation have been recorded. During a magnetic storm on March 22. 1979, peak-to-peak scintillation of 18, 10, 15, and 3.5 dB were recorded at 136 MHz and 1.7, 4, and 12 GHz, respectively, on different paths in and around Japan (Minakoshi et al., 1981). Also Karasawa et al. (1985) observed fluctuations sometimes exceeding 30 dB peak-to-peak on signals passing over the Indian Ocean at an elevation angle of 17.3 deg.

Considerable data have been accumulated on ionospheric scintillation, and the values quoted here give a rough idea of what margins may be needed to protect against ionospheric scintillation. Table 9.3 gives values of fade depths at midlatitudes (CCIR,1986a). The data have commonly been presented as peak-to-peak values, and in the case of the 8 dB figure mentioned for 6 GHz-4GHz links not

Table 9.2 Percentage of occurrence of scintillation (CCIR, 1982, 1986a). (a) ≥ 10 dB peak to peak, equatorial latitudes

Location	Frequency	Day	Night
		(400-1600 LT)	(1600-400 LT)
Huancayo, Peru	137 MHz	3	14
	254 MHz	2	7
		(600-1800 LT)	(1800-600 LT)
Accra, Ghana	137 MHz	0.4	14

(b) ≥ 12 dB peak to peak at 137 MHz, subauroral and auroral lat.

Location	K_p	Day (500-1700 LT)	Night (1700-500 LT)
Sagamore Hill, MA	0 to 3+	0	1.4
	> 3+	0.1	2
Goose Bay, Labrador	0 to 3+	0.1	1.8
	> 3+	1.6	6.8
Narssarssuaq, Greenl.	0 to 3+	2.9	18
		19	45

(c) ≥ 10 dB peak to peak at 254 MHz, auroral latitudes

Location	K_p	Day (600-1800 LT)	Night (1800-600 LT)
Goose Bay, Labrador	0 to 3+	0.1	0.1
	> 3+	0.3	1.2
Narssarssuaq, Greenl.	0 to 3+	0.1	0.9
		2.6	8.4

LT: Local Time

much more than half of the the 8 dB range appeared to involve a signal decrease. The needed margin may thus well be less than the peak-to-peak value. The increase in signal level, however, may in some cases present a problem of overload in itself.

A WBMOD empirical computer model of global scintillation has been prepared by Fremouw and co-workers over a period of years. This model has been described in the review paper by Aarons (1982) and in more detail by Fremouw (1982). Persons wishing to pursue the application of this model to the estimation of ionospheric scintillation may contact Dr. Edward J. Fremouw, Physical Dynamics, Inc., P.O. Box 3027, Bellevue, Washington 98009. A program employing ten frequencies between 137 and 2891 MHz for recording scintillation at equatorial and auroral latitudes was described by Fremouw et al. (1978), and early results of the HiLat mission for obtaining data on the spatial and temporal variation of amplitude and phase scintillation at high latitudes have also been described by Fremouw et al. (1985).

Table 9.3 Distribution of Mid-Latitude Fade Depths in dB due to Ionospheric Scintillation (CCIR, 1982).

Percent of Time	Frequency (MHz)			
Exceeded	100	200	500	1000
1.0	15.9	1.5	0.2	0.1
0.5	9.3	2.3	0.4	0.1
0.2	16.6	4.2	0.7	0.2
0.1	25.0	6.2	1.0	0.3

9.3 TROPOSPHERIC CLEAR-AIR EFFECTS

9.3.1 Introduction

Clear-air effects on propagation are influenced strongly by the elevation angle of the path. For elevation angles above about 10 deg and for frequencies below about 10 GHz, the effects on communication satellite operations tend to be slight. For elevation angles of only a few degrees, the effects may be severe. The low-elevation-angle effects have long been familiar to persons concerned with terrestrial line-of-sight paths, for which margins up to about 45 dB may be utilized to combat atmospheric multipath fading. For downlinks from satellites, it is difficult to supply large margins and it has been generally assumed that it would not be necessary to do so because large elevation angles would normally be utilized for satellite communications. It turns out, however, that in a number of situations it is desirable to be able to utilize satellites at low elevation angles. The problems of low-angle propagation are well illustrated in a paper on measurements of 1.5 GHz MARISAT signals (Fang, Tseng, and Calvit, 1982). It was reported that MARISAT services were not available for paths having elevation angles below 10 deg because of severe signal degradation. Reflections from the sea surface must have contributed to the problem, but atmospheric effects surely played a major role also.

The time delay due to the atmosphere may be important for navigation, ranging, and time-transfer purposes. The excess range delay caused by the ionosphere on earth-space transmissions can be determined and taken into account by transmitting two different frequencies but that technique cannot be applied to the troposphere as the tropospheric index of refraction does not vary with frequency at radio frequencies.

9.3.2 Refraction and Multipath Fading

The variation of the index of refraction of the troposphere with height causes ray paths to experience bending, which results in errors in measurements of elevation angle. For paths extending to maximum heights of 80 km, as in Table 9.4, the values of elevation angle error are different from the bending values. The amount of bending can be calculated on the basis of an assumed or known index of refraction profile, and then elevation angle error can be calculated. For a much longer path to a geostationary satellite,

Table 9.4 Ray Parameters for a Standard Atmosphere[a,b] (Crane, 1976).

Initial Elev. Angle (deg)	Height (km)	Range (km)	Bending (mdeg)	Elev.-Angle Error (mdeg)	Range Error (m)
0.0	0.1	41.2	97.2	48.5	12.63
	1.0	131.1	297.9	152.8	38.79
	5.0	289.3	551.2	310.1	74.17
	25.0	623.2	719.5	498.4	101.0
	80.0	1081.1	725.4	594.2	103.8
5.0	0.1	1.1	2.6	1.3	0.34
	2.0	11.4	25.1	12.9	3.28
	5.0	55.2	91.7	52.4	12.51
	25.0	241.1	176.7	126.3	24.41
	80.0	609.0	181.0	159.0	24.96
50.0	0.1	0.1	0.2	0.1	0.04
	1.0	1.3	1.9	1.0	0.38
	5.0	6.5	7.0	4.0	1.47
	25.0	32.6	14.3	10.3	3.05
	80.0	104.0	14.8	13.4	3.13

[a]U.S. Standard Atmosphere Supplements, 1966, Environmental Sci. Serv. Administration, Dept. of Commerce, Washington, DC (1966).

[b]Sissenwine, N., D.D. Grantham, and H.A. Salmela, AFCRL-68-0556, Air Force Cambridge Res. Lab., Bedford, MA (Oct. 1968).

Table 9.5 Ray Bending Values (CCIR,1986b).

Elevation angle	Average bending	
	Polar continental	Tropical maritime
1°	0.45°	0.65°
2°	0.32°	0.47°
4°	0.21°	0.27°
10°	0.10°	0.14°

however, one can calculate values for bending, such as those displayed in Table 9.5, and take the corresponding elevation-angle error values to be the same as the bending values, no further calculation being needed.

Atmospheric multipath fading is a serious problem for very-low-elevation-angle paths, whether terrestrial or earth-space. The amount of fading is best determined by experimental data for the particular path, and the margin to be utilized for fading depends on the grade of service needed. An effort is made here to distinguish between refractive multipath fading and tropospheric scintillation, but the distinction is not always made clearly in the literature nor is it always possible to distinguish the two phenomena in practice. Atmospheric multipath fading is generally restricted to angles less than 10 deg and is most serious for angles up to only a few degrees. It is considered to result from large-scale changes in refractivity and involves relatively long fading periods, generally from about 10 s to a few minutes. Scintillation results from the smaller-scale structure of turbulence and clouds and has short periods in the order of a second and less. Though most intense for low elevation angles, it does not decrease as rapidly with increasing elevation angle as multipath fading. Tropospheric multipath fading tends to be insensitive to frequency over the microwave frequency range. It is often associated with the occurrence of temperature inversions and disappears when the temperature inversion is destroyed by the passage of cyclonic storms (Flock, 1960).

Although sometimes referred to as scintillation, the fading observed at 4 and 6 GHz in the Canadian Arctic at an elevation angle of one deg (Strickland et al., 1977) is undoubtedly atmospheric multipath fading. The margins judged to be required for such operation for three values of reliability or availability are shown in Table 9.6. The refractivity in the Arctic tends to be less than in other sections of the world, perhaps excluding desert areas, and similar or higher margins would probably be required elsewhere for the same elevation angle. On a path in Hawaii at the slightly larger elevation angle of 2.5 deg, Thompson et al. (1975) observed fading of 20 dB.

Table 9.6 Six GHz Link Margins in dB for Tropospheric Fading at Eureka, Ellesmere Island, Canada, Elevation Angle One Degree (Strickland et al., 1977).

Time Duration	Reliability (percent)		
	90	99	99.9
Worst two hours	8.0	18.0	28.0
Worst summer day	6.8	15.5	24.5
Worst summer week	5.4	13.0	22.0
Worst month, July	3.8	10.8	20.3

9.3.3 Tropospheric Scintillation

The term tropospheric scintillation is used here to refer to generally low-amplitude, rapid variations in signal intensity with periods typically around one second. Such scintillation tends to be associated with small-scale structure such as that of turbulence and clouds. The amplitude variance due to scintillation has been modeled as a function of frequency and elevation angle (Ippolito, Kaul, and Wallace, 1983). The results of this analysis show that scintillation amplitude increases with frequency and decreases with elevation angle (Fig. 9.5).

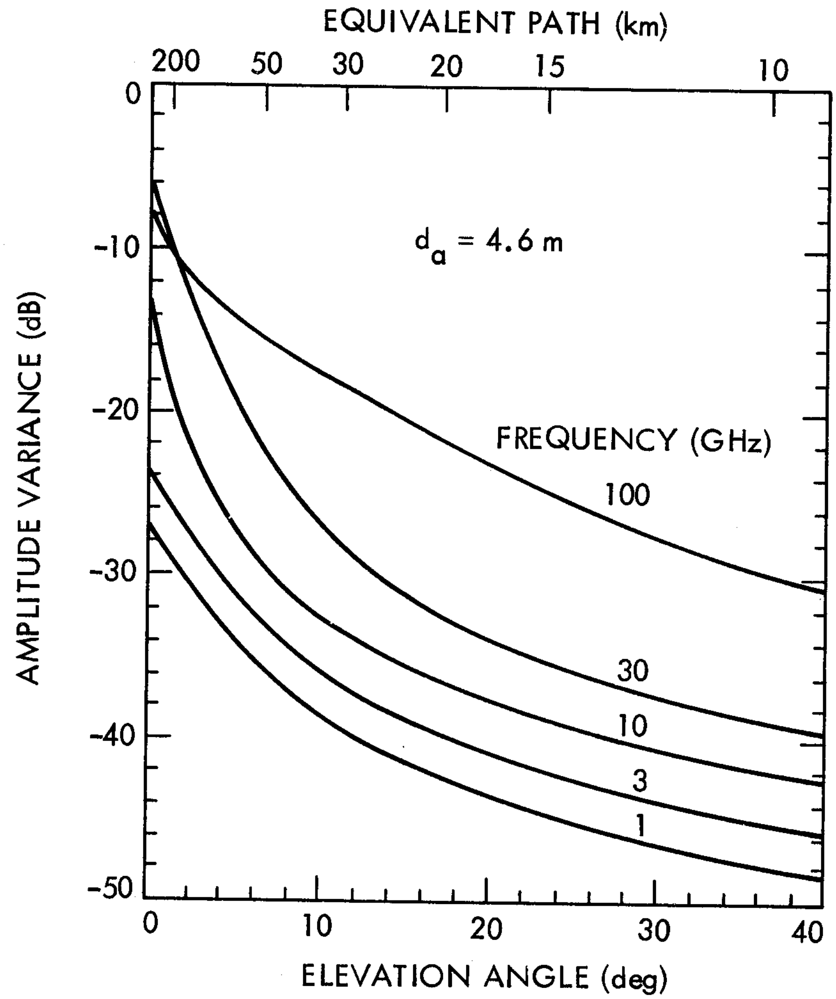

Figure 9.5. Amplitude variance for a 4.6 m diameter aperture for 1 to 100 GHz (Ippolito, Kaul, and Wallace, 1983).

Example 9.3 Tropospheric Refraction

Tropospheric refraction may result in elevation-angle error, ducting, and/or multipath fading. The material of this Sec. 9.3 and Chap. 3 include illustrative values of elevation-angle error and multipath fading, but it is difficult to compose suitable quantitative numerical calculations relating to these effects. All are functions of the index of refraction profile. Calculation of refractivity N is illustrated in this example.

The refractivity of the troposphere is described by the following relation [Eq. (3.2)].

$$N = \frac{77.6\,p}{T} + \frac{3.73 \times 10^5\,e}{T^2}$$

where $N = (n - 1) \times 10^6$ with n the index of refraction, p the total pressure in mb, e the partial pressure of water vapor in mb, and T the temperature in kelvins. Values of N that would apply to Denver, Colorado for the pressure of a standard atmosphere and a surface temperature of 20 deg C will now be calculated for water vapor specified in two ways. First a water vapor density of 7.5 g/m^3 is assumed, and secondly a relative humidity of 60 percent is assumed.

For the U.S. Standard Atmosphere, the pressure p at an altitude of 1600 m (1 mile) is 835 mb, compared to 1013 mb at sea level. The temperature of 20 deg C corresponds to a temperature in kelvins of 273 + 20 = 293 K.

1. Water vapor density $\rho = 7.5$ g/m^3

Using Eq. (3.5), $e = \frac{\rho T}{216.5} = \frac{(7.5)\,(293)}{216.5} = 10.15$ mb

$$N = \frac{77.6\,(835)}{293} + \frac{3.73 \times 10^5\,(10.15)}{(293)^2} = 222.1 + 44.1$$

$$N = 265.2$$

2. Relative humidity (R.H.) = 60 percent

From Table 3.1 for T = 20° C, e_s, the saturation water vapor pressure equals 23.4 mb.

$$e = e_s\,(\text{R.H.}) = (23.4)\,(0.60) = 14.04 \text{ mb}$$

$$N = \frac{77.6\,(835)}{293} + \frac{3.73 \times 10^5\,(14.04)}{(293)^2} = 222.1 + 61.0$$

$$N = 282.1$$

The above values of N are rather low because of the reduced pressure at the altitude of Denver. For the same water vapor contents of 7.5 g/m³ and 60 percent relative humidity at 20 deg C but the sea level pressure of 1013 mb, the corresponding values of N are 313.5 and 330.5 respectively. To illustrate what is probably the maximum value of N that might be encountered consider the temperature of 34 deg C and a partial pressure of water vapor of 53.2 mb, values recorded at Sharjah, Saudi Arabia. For this case

$$N = \frac{77.6\ (1013)}{307} + \frac{3.73 \times 10^5\ (53.2)}{(307)^2} = 256.1 + 210.5$$

$$N = 466.6$$

It is the variation of N with height that has the greatest effect on wave propagation, a decrease of 157 N/km being sufficient to cause trapping or ducting of a wave launched at an elevation angle of zero degrees. Still higher rates of decrease can trap waves having elevation angles slightly greater than zero degrees. An expression provided by Bean and Dutton (1966), namely

$$\frac{\Delta n}{\Delta r} = -\left(\frac{1}{r_o} + \frac{\theta_p^2}{2\,h_a}\right)$$

allows determining that for a decrease of 300 N/km ($\Delta n/\Delta r = -0.000300$) in a layer of thickness h_a of 0.1 km at the Earth's surface, taking r_o as 6370 km,

$$\theta_p = 5.3 \text{ mrad} = 0.3 \text{ deg}$$

The angle θ_p is the penetration angle. Rays having smaller values are subject to ducting.

9.3.4 Defocusing

Bending of rays is proportional to dN/dh, the variation of refractivity N with height (Sec. 3.2), and when dN/dh itself varies with height rays at different heights experience different amounts of bending. As a result the rays become more widely separated than previously and signal intensity is reduced. Figure 8.5 shows the attenuation due to defocusing as a function of elevation angle and ΔN, the decrease in refractivity in the first km above the surface. Figure 9.6 shows the defocusing loss in a different way. Here the loss corresponding to the average of many index of refraction profiles and the standard deviation of the loss are shown as a function of elevation angle. The results were obtained at Albany, New York and are representative of an inland continential location.

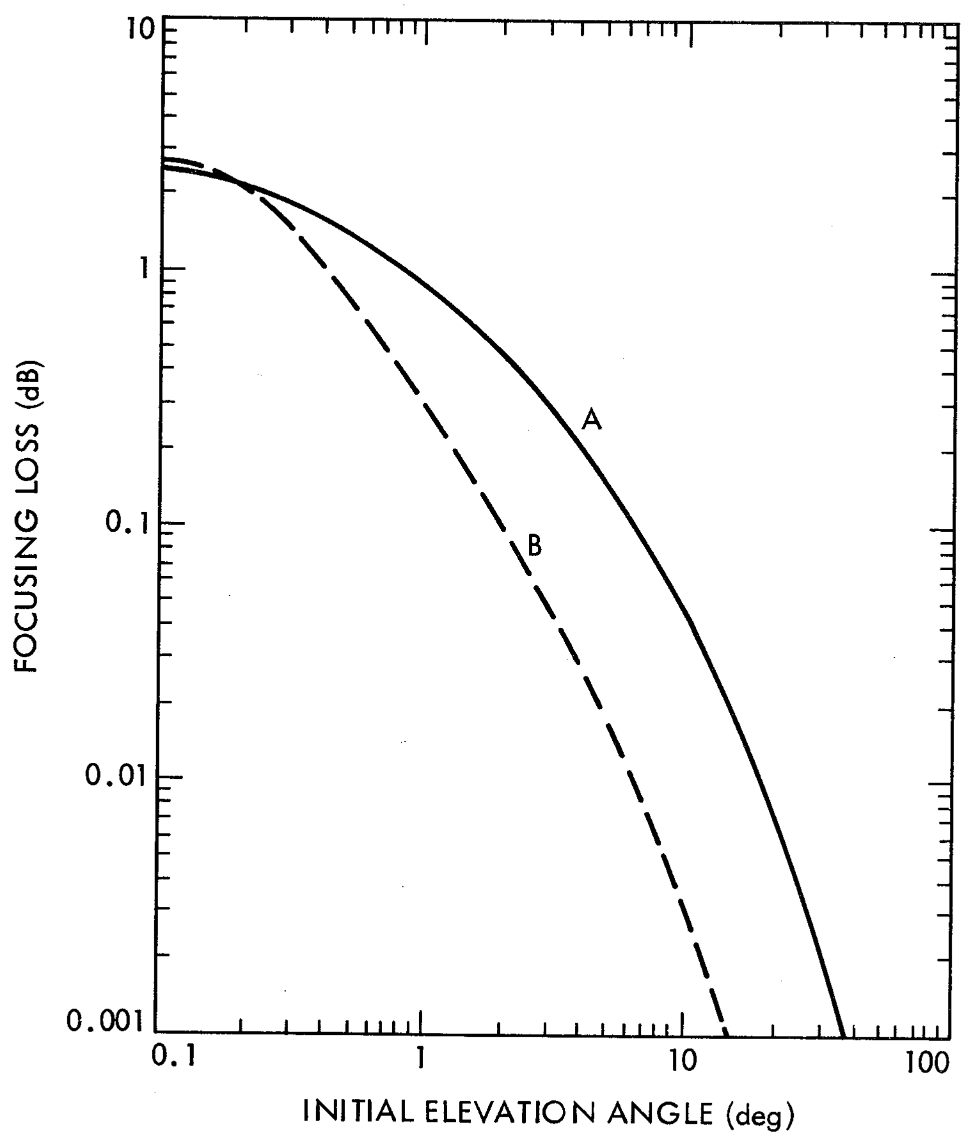

Figure 9.6. Average focusing loss (A) and standard deviation about the average (B) (CCIR, 1986b).

9.3.5 Gaseous Attenuation

The attenuation constants for oxygen and water vapor are shown in Fig. 3.10 for sea-level pressure, a temperature of 15 deg C, and a water vapor density of 7.5 g/m^3. At 10 GHz, the attenuation for oxygen is about 0.007 dB/km, and it decreases only slowly to about 0.005 dB/km at 1 GHz. For water vapor the value is only about 0.006 dB/km at 10 GHz, and the attenuation drops rapidly below 10 GHz. The total vertical one-way attenuation due to the gaseous constituents of the atmosphere from sea level to the top of the atmosphere for a water vapor density of 7.5 g/m^3 is shown in Fig. 3.11. For 10 GHz the value is nearly 0.06 dB. For 10 GHz and a height of 4 km, CCIR Report 719 for 1978 showed a value slightly over 0.02 dB for the total zenith attenuation.

In treatments of coordination distance, as in Chap. 8, it is usually considered that attenuation due to water vapor can be neglected below 10 GHz but that attenuation due to oxygen should be included. For coordination distance analysis, the recommended values of water vapor density range from 1 to 5 g/m^3. Use of these lower densities is conservative when considering interference and gives lower attenuation, of course, than for 7.5 g/m^3.

Analytical expressions for the attenuation constants due to oxygen and water vapor are also given in Chap. 3 [Eqs. (3.20) and (3.21)], and expressions are also given for the total attenuation [Eqs. (3.22) and (3.23)]. Nonlinear effects that complicate the analysis for water vapor densities of 12 g/m^3 and higher are presently being studied.

9.3.6 Excess Time and Range Delay

The excess time and range delays for propagation of signals through the Earth's atmosphere consist of components caused by the ionosphere and by the troposphere. The delay due to the ionosphere was considered in Sec. 9.2.2. Time delay Δt and range delay ΔR are related by $\Delta R = c\ \Delta t$, where c is the velocity of light in a vacuum, about 2.9979×10^8 m/s. The discussion in this section is in terms of ΔR.

The excess tropospheric range delay can be separated into the delay due to dry air ΔR_d and the delay due to water vapor ΔR_w or, somewhat more conveniently, it can be separated into ΔR_1 and ΔR_2

corresponding to the two terms of the expression for the refractivity of the troposphere (Sec. 3.7; Flock, Slobin, and Smith, 1982). The equation for N is

$$N = \frac{77.6\,p}{T} + \frac{3.73 \times 10^5\,e}{T^2} \tag{9.18}$$

The range delay ΔR_1 for a vertical path due to the first term of Eq. (9.18) is given by

$$\Delta R_1 = 10^{-6} \int N_1\,dh = 10^{-6} \int \frac{77.6\,p}{T}\,dh = 2.757 \times 10^{-3}\,p_o \text{ m} \tag{9.19}$$

for a latitude of about 45^o (only slightly different elsewhere) where p_o is total surface pressure in mb. For p_o = 1013 mb, the approximate value for sea level, ΔR_1 = 2.31 m. The total pressure $p = p_d + e$ where p_d is the pressure of dry air and e is the partial pressure of water vapor. As p_d is much larger than e, ΔR_1 is largely but not entirely due to dry air. Hopfield (1971) has determined that ΔR_1 can be determined to an accuracy of 0.2 percent or about 0.5 cm by measuring p_o.

It is shown in Sec. 3.7 that ΔR_2 for a vertical path is given by

$$\Delta R_2 = 10^{-6} \int N_2\,dh = 1.731 \times 10^{-3} \int \frac{\rho}{T}\,dh \tag{9.20}$$

where ρ is the density of water vapor in g/m^3. Water vapor density ρ in g/m^3 and water vapor pressure e in mb are related by ρ = (e 216.5)/T where T is in kelvins as in Eq. (9.18). Determining a value for ΔR_2 requires information on ρ and T as a function of height. As ρ is highly variable and difficult to predict from surface parameters, water vapor is responsible for a larger error in range than is dry air even through the magnitude of ΔR_2 is typically only about 10 cm for ρ = 7.5 g/m^3 at the surface. By the use of radiometer techniques, however, ΔR_2 can be determined to an accuracy of possibly 0.5 cm (Sec. 3.7).

Table 9.4 includes values of total excess tropospheric range delay for paths to 80 km at several different elevation angles.

Example 9.4 Tropospheric range delay

To illustrate the magnitude of excess range delay due to the troposphere, consider first a zenith path at Denver , Colorado where the surface pressure for a standard atmosphere is 835 mb. From Eq. (9.19) the typical delay corresponding to the first term of the expression for N is

$$\Delta R_1 = 2.2757 \times 10^{-3} \, p_o = 1.90 \text{ m}$$

A more reliable value at a particular time could be obtained by using the measured value of p_o at that time rather than the value for a standard atmosphere. For a relative humidity of 60 percent and other conditions likewise as in Example 9.3, the delay corresponding to the second term of the expression for N could be obtained approximately by first calculating the value of N_2 by use of

$$N_2 = \frac{3.73 \times 10^5 \, (14.04)}{(293)^2} = 61.00$$

Then assuming an exponential decrease of N_2 with a scale height of 2 km

$$\Delta R_2 = 10^{-6} \int 61.00 \, e^{-h/2000} \, dh = 10^{-6} \, (61.00) \, (2000)$$

$$\Delta R_2 = 12.2 \text{ cm}$$

The total excess delay ΔR for a zenith path would then be

$$\Delta R = \Delta R_1 + \Delta R_2 = 2.02 \text{ m}$$

For a path at an elevation angle of 30 deg, the corresponding delay would be 2.02/sin 30 deg = 4.04 m. The calculation of ΔR_2 is illustrative only, and the most accurate determination of ΔR_2 requires information about the actual value of N_2 as a function of height above the surface or the use of radiometer techniques (Sec. 3.7).

9.4 ATTENUATION AND DEPOLARIZATION CAUSED BY PRECIPITATION

9.4.1 Introduction

Attenuation caused by rain increases with frequency throughout the microwave range and has sometimes been considered to be important only for frequencies above 10 GHz. However, while it is true that attenuation decreases rapidly with decreasing frequency below 10 GHz, values of attenuation are nevertheless potentially troublesome for frequencies of 8 GHz or lower. In addition the attenuation due to rain is accompanied by an increase in antenna noise temperature which further degrades the carrier power-to-noise ratio (Sec.9.7).

Depolarization due to rain is caused by differences in attenuation and phase shift of electric-field-intensity components that are parallel to the major and minor axes of rain drops, which are roughly spheroidal in form. The most favorable condition for these differences to be high is for the absolute values to be high. Thus depolarization tends to be most severe when attenuation is high, and it might be expected that as attenuation is low for frequencies below 8 GHz depolarization would also be low. Attenuation at 4 GHz, for example, is only about 0.05 dB/km for a rain rate of 35 mm/h. Depolarization does tend to decrease with decreasing frequency, but it does so less rapidly than attenuation because differential phase shift as well as differential attenuation contributes to depolarization, and differential phase shift is relatively high for frequencies below 10 GHz. (Phase shift is proportional to the real part of the effective index of refraction of a medium, and this value is relatively high below 10 GHz as shown in Fig. 4.3.) It thus develops that depolarization due to rain may be important for frequencies of 4 GHz or lower.

Scatter of electromagnetic waves by rain is significant for frequencies of 1.5 GHz or lower, as the intense echoes from rain on L-band radar displays indicate. Such scatter in a potential source of interference (Chap. 8).

Basic concepts and definitions concerning the propagation effects of rain were presented in Chap. 4. Consideration is directed here to procedures for estimating the magnitude of the effects and to numerical examples.

9.4.2 Estimation of Attenuation Due to Rain: Step-by-step Procedure.

In the design of telecommunication links, data on propagation effects are needed in statistical form in order to provide as much assurance as possible that a certain signal level will be available for a specified percentage of time. A sufficient data base is not available for all propagation effects to allow link design on this basis, but a considerable effort has been devoted to the development of satisfactory data bases and models to account for the effects of rain in this way.

If satisfactory statistical data on rain rate or attenuation due to rain are available for the particular location in question they should be used. Lin (1977) and Lee (1979) have described procedures for obtaining the needed rain rate statistics from data supplied by the National Climatic Data Center in the United States. Lacking the information needed to proceed on the basis of local weather data or not wishing to formulate statistical data from Weather Service records, use can be made of models that have been developed for rain rate and attenuation due to rain. The steps to be taken in estimating attenuation are listed below. The application of the modified 1982 CCIR model is emphasized. Other models are described in Sec. 4.3.3.

1. Estimate Rain Rate

A first step in obtaining a value of attenuation due to rain is to estimate the rain rate R that is exceeded for the percentage or percentages of time of interest. The small percentage of 0.01 corresponding to 53 minutes per year is commonly the value that is utilized. Even if interest lies in, or includes, other percentages, the modified 1982 CCIR procedure calls for determining the attenuation for a percentage of 0.01 initially. For estimating R, use should be made of statistical data for the particular location, if satisfactory data are available, or of several models described in Sec. 4.3.3. Prominent among these is the 1980 Global Model by Crane (1980a). Figure 4.8 shows the rain-rate regions of the world according to this model, and Figs. 4.9 and 9.7 show rain-rate regions of the United States in more detail. The rain-rate values for these regions are given in Table 9.7.

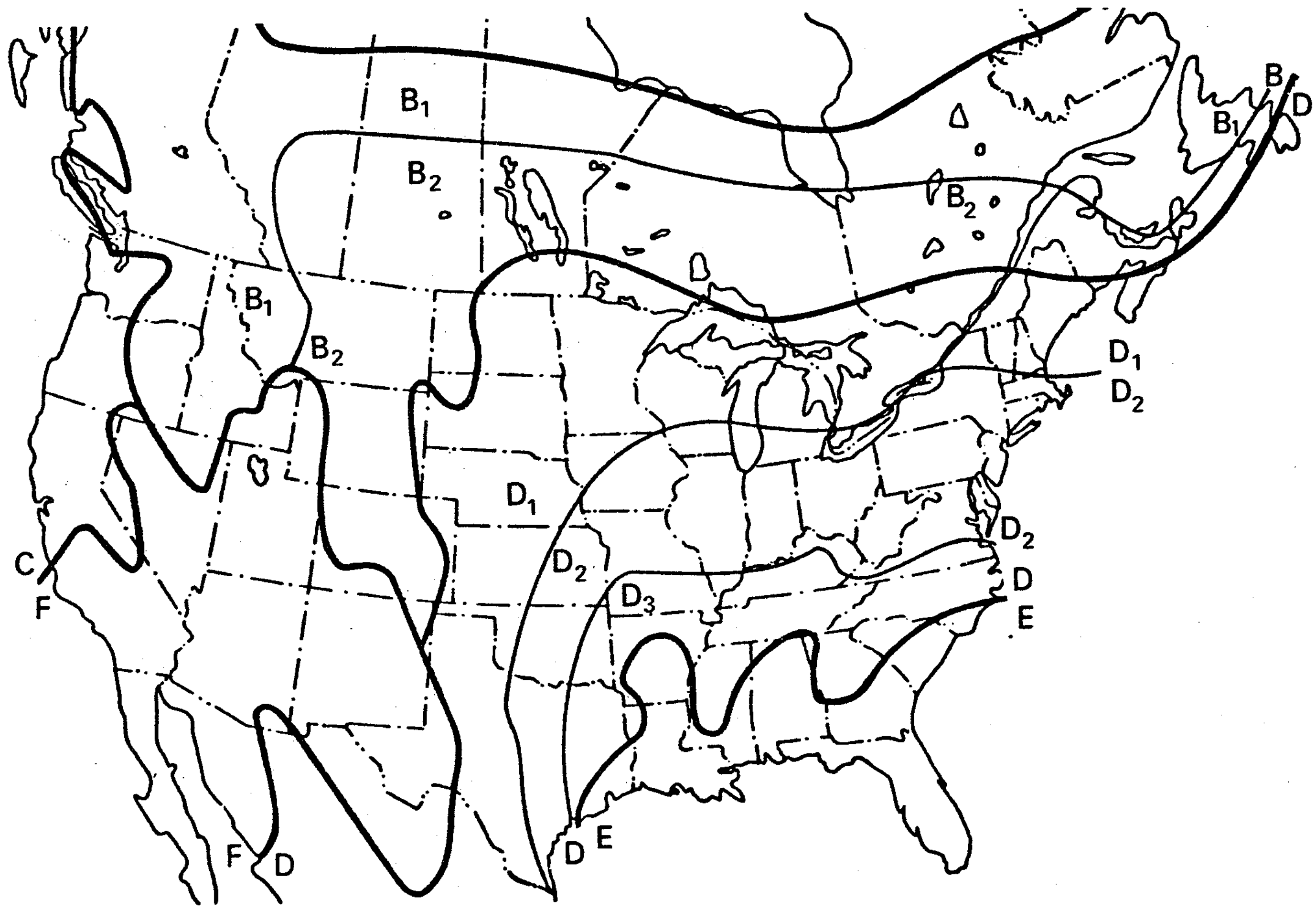

Figure 9.7. Rain-rate regions for conterminous United States and southern Canada (Crane, 1980b).

Table 9.7 Point Rain-Rate Distribution Values (mm/h) Versus Percent of Year Rain Rate is Exceeded (Crane, 1980b).

Percent of Year	RAIN CLIMATE REGION												Minutes per Year	Hours per Year
	A	B_1	B	B_2	C	D_1	$D=D_2$	D_3	E	F	G	H		
0.001	28.5	45	57.5	70	78	90	108	126	165	66	185	253	5.26	0.09
0.002	21	34	44	54	62	72	89	106	144	51	157	220.5	10.5	0.18
0.005	13.5	22	28.5	35	41	50	64.5	80.5	118	34	120.5	178	26.3	0.44
0.01	10.0	15.5	19.5	23.5	28	35.5	49	63	98	23	94	147	52.6	0.88
0.02	7.0	11.0	13.5	16	18	24	35	48	78	15	72	119	105	1.75
0.05	4.0	6.4	8.0	9.5	11	14.5	22	32	52	8.3	47	86.5	263	4.38
0.1	2.5	4.2	5.2	6.1	7.2	9.8	14.5	22	35	5.2	32	64	526	8.77
0.2	1.5	2.8	3.4	4.0	4.8	6.4	9.5	14.5	21	3.1	21.8	43.5	1052	17.5
0.5	0.7	1.5	1.9	2.3	2.7	3.6	5.2	7.8	10.6	1.4	12.2	22.5	2630	43.8
1.0	0.4	1.0	1.3	1.5	1.8	2.2	3.0	4.7	6.0	0.7	8.0	12.0	5260	87.7
2.0	0.1	0.5	0.7	0.8	1.1	1.2	1.5	1.9	2.9	0.2	5.0	5.2	10520	175
5.0	0.0	0.2	0.3	0.3	0.5	0.0	0.0	0.0	0.5	0.0	1.8	1.2	26298	438

The modified 1982 CCIR model uses similar but somewhat different rain-rate regions (CCIR, 1986c). These are shown in Figs. 4.13-4.15, and the corresponding rain-rate values are given in Table 4.5. Figure 4.10 shows the CCIR regions for Canada, as modified by Segal (1986), and we recommend using these for Canada whether otherwise following the CCIR model or not. Contours of rain rate exceeded for 0.01 percent of the time according to the modified 1982 CCIR model are reproduced here as Figs. 9.8-9.10. Table 4.5 gives rain rates exceeded for percentages other than 0.01, and attenuations for the other percentages were calculated independently for continental climates in the original 1982 model. The present CCIR procedure, however, is to calculate the attenuation for a percentage of 0.01 and to modify the value determined in this way if an attenuation for another percentage is desired.

The large-scale world-wide or continent-wide maps of rain-rate regions are extremely valuable but suffer from lack of detail. This statement is especially applicable to the western United States where large variations in rain rate occur within short distances. Rain rates on opposite sides of mountain ranges, for example, are often drastically different. As pointed out in CCIR Report 563-3, (CCIR, 1986c) additional data are needed to improve the accuracy and resolution of the information on rain rates. A considerable amount of data on the effects of rain has been accumulated for the eastern United States and is reflected in Fig. 9.7. For the United States, we recommend using the rain-rate regions of Fig. 9.7 and the values of Table 9.7. For Canada we favor the modified CCIR regions of Fig. 4.10 and the values of Table 4.5. For the rest of the world, we favor the regions and values of the modified 1982 CCIR model. (Figs. 4.13-4.15 and Table 4.5 or Figs. 9.8-9.10 for a percentage of occurrence of 0.01).

2. Determine Attenuation Constant Corresponding to Rain Rate

For the rain rate R determined in step 1, find the corresponding attenuation constant α_p by use of an expression of the form of $\alpha_p = aR^b$. Values of the coefficients of a and b, based on the assumption of spherical drops, have been provided by Olsen, Rogers, and Hodge (1978) and their values for frequencies of 15 GHz and lower are reproduced as Table 4.2. A trend exists, however, to account for

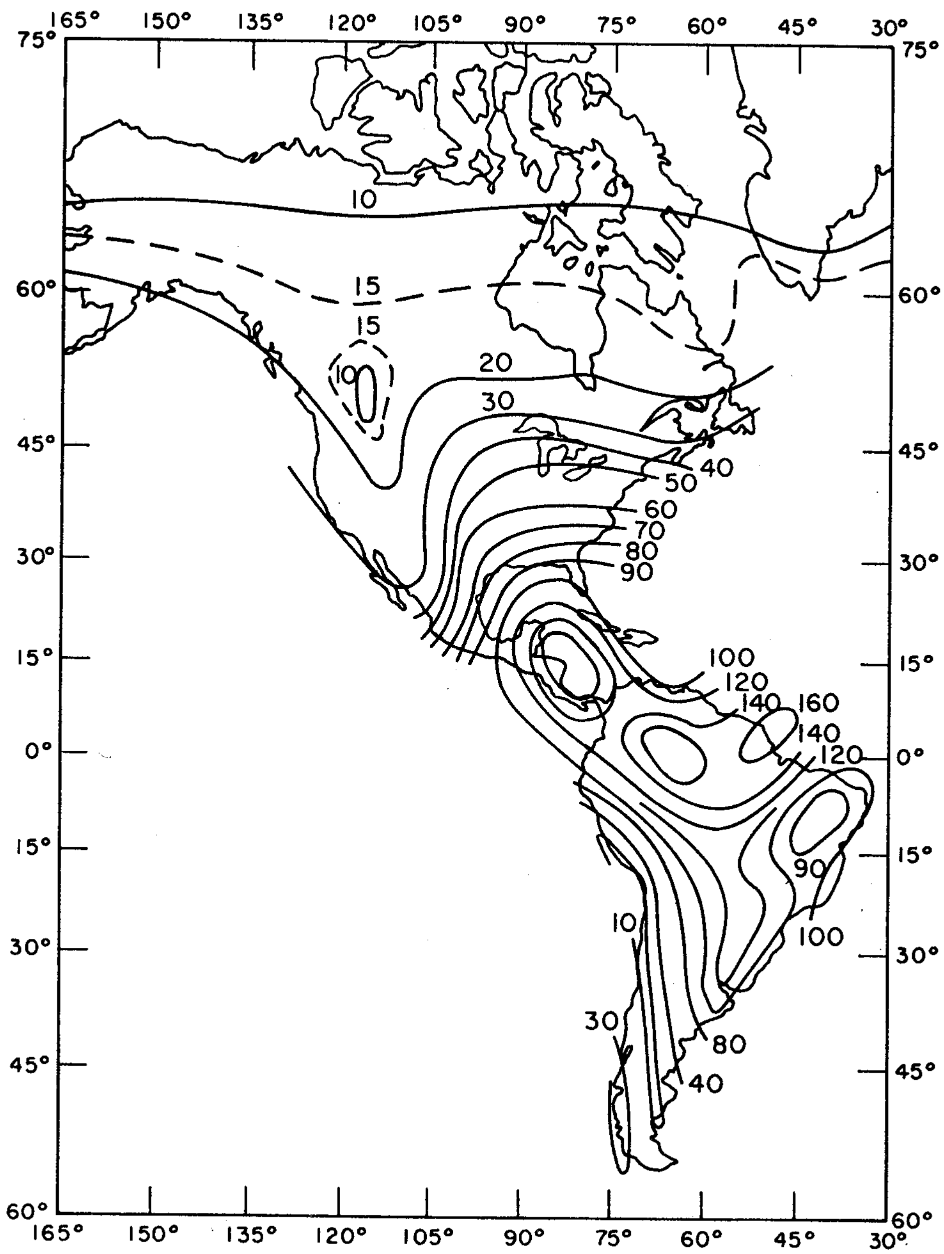

Figure 9.8. Contours of rain rates (mm/h) exceeded for 0.01 percent of the time, the Americas (CCIR,1986c).

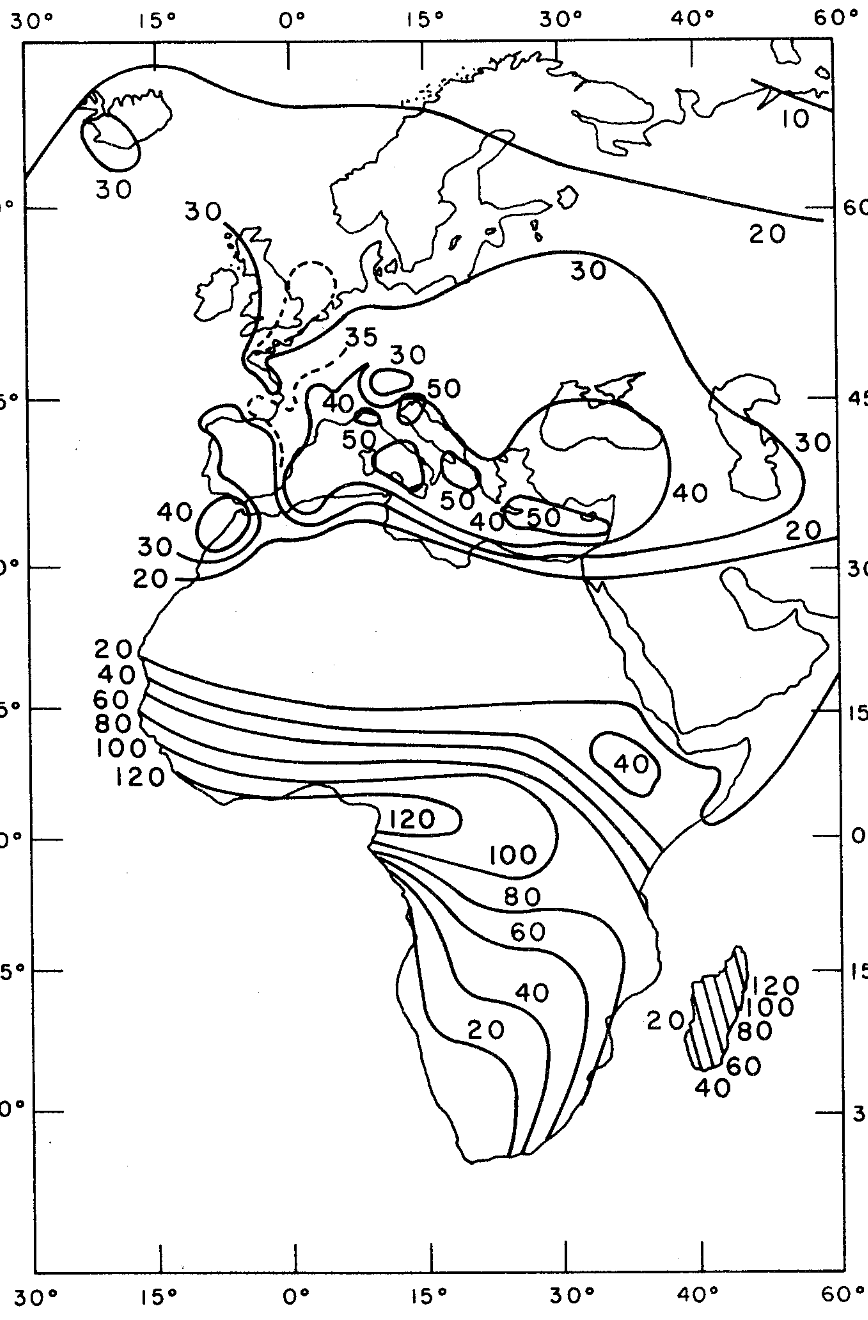

Figure 9.9. Contours of rain rates (mm/h) exceeded for 0.01 percent of the time, Europe and Africa (CCIR, 1986c).

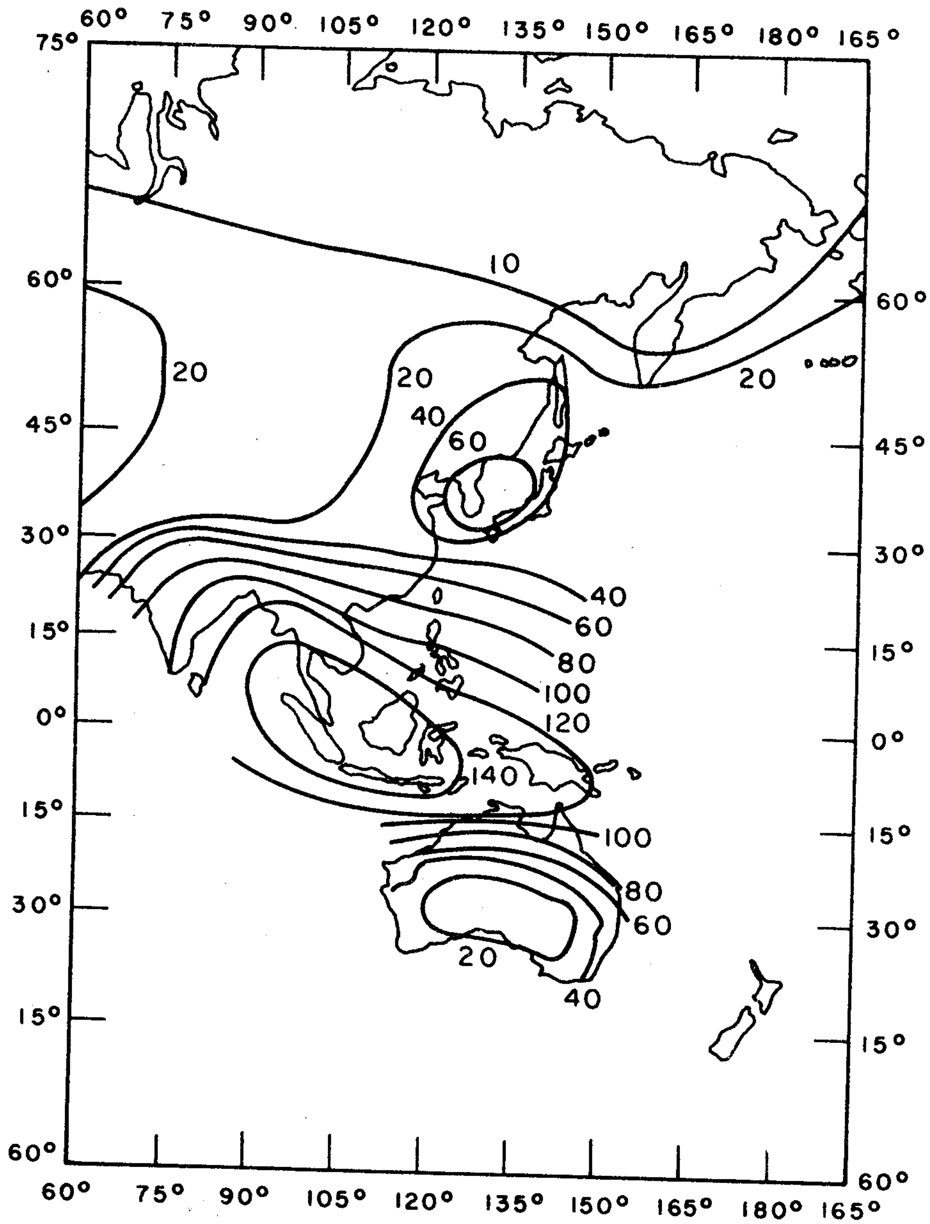

Figure 9.10. Contours of rain rates (mm/h) exceeded for 0.01 percent of the time, Asia and Oceania (CCIR, 1986c).

the non-spherical shape of raindrops and to therefore distinguish between horizontal and vertical linear polarization and circular polarization. Values of a and b for the two linear polarizations are given for a limited number of frequencies in Table 9.8 (CCIR, 1986d). Then for arbitrary linear polarization and for circular polarization values of a and b (a_c and b_c) are given by

$$a_c = [a_h + a_v + (a_h - a_v) \cos^2\theta \cos 2\tau] /2 \qquad (9.21)$$

$$b_c = [a_h b_h + a_v b_v + (a_h b_h - a_v b_v) \cos^2\theta \cos 2\tau] /2a_c \qquad (9.22)$$

where h and v refer to horizontal and vertical polarization, θ is the elevation angle of the path, and τ is the polarization tilt angle of a linearly polarized wave (see Sec. 9.4.3.2). For circular polarization τ can be taken to be 45 deg, and it can be seen that Eqs. (9.21) and (9.22) simplify considerably in that case.

Other means are available to obtain values of α_p as a function of frequency and rain rate. Figures 4.3b and 4.5, for example, can be used for this purpose with α_p given by $(2\pi/\lambda)\ m_i$ if Fig. 4.3b is used. As in some cases these figures provide only an approximate value because of the way they are plotted, they are perhaps best used as a rough check on the values obtained by using $\alpha = aR^b$.

3. Determine Path Length L and Horizontal Projection D

In addition to the attenuation constant, α, in dB/km, information on the path length L through rain is needed to determine total attenuation along the path. Rain is essentially confined to the region below the height of the 0 deg isotherm. In the previous edition of this handbook, the curves of Fig. 4.7, especially the dotted modification of the curve for the percentage of 0.01 for latitudes below 40 deg, were featured. The latest CCIR procedure, however, is to use Eq. (9.23) for the height extent H of rain for latitudes ϕ of 36 deg or greater and for a time percentage of 0.01 (CCIR, 1986e).

$$H = 4.0 - 0.075\ (\phi - 36^\circ) \quad \text{km} \qquad (9.23)$$

For latitudes less than 36 deg, H is taken to be 4.0 km.

Table 9.8 The Coefficients a and b for Calculating Attenuation for Horizontal and Vertical Polarization (CCIR, 1986d).

f (GHz)	a_h	a_v	b_h	b_v
1	0.0000387	0.0000352	0.912	0.880
2	0.000154	0.000138	0.963	0.923
4	0.000650	0.000591	1.121	1.075
6	0.00175	0.00155	1.308	1.265
8	0.00454	0.00395	1.327	1.310
10	0.0101	0.00887	1.276	1.264
12	0.0188	0.0168	1.217	1.200
15	0.0367	0.0335	1.154	1.128

For elevation angles above 10 deg, determine the length L of the path through rain by use of

$$L = \frac{H}{\sin\theta} = \frac{H_o - H_g}{\sin\theta} \quad \text{km} \tag{9.24}$$

where θ is elevation angle, H_g is the height above sea level of the surface, H_o is the height of the 0 deg C isotherm, and $H = H_o - H_g$. For elevation angles less than 10 deg, the path length L can be determined from

$$L = \frac{2\,H}{\left(\sin^2\theta + \frac{2H}{k\,r_o}\right)^{1/2} + \sin\theta} \quad \text{km} \tag{9.25}$$

where kr_o is the effective radius of the Earth (Sec. 3.2) and can be taken to be 8500 km for $k = 4/3$ in the absence of contrary information. For determining D, the horizontal projection of L, use $D = L \cos \theta$.

4. Path Reduction Factor; Effective Path Length

The average rain rate along a path through rain tends to differ from the rain rate at a particular point. For high values of rain rate at a point, the average rate tends to be less, as intense rain is generally restricted to localized areas. This problem has been approached by determining a path reduction factor which can be viewed as modifying the value of R to obtain an effective value or as modifying L to obtain an effective path length.

Following the modified CCIR procedure (CCIR, 1986e), one determines the path reduction factor r_p for a probability of 0.01 percent from

$$r_p = \frac{1}{1 + 0.045\,D} \tag{9.26}$$

where D is the horizontal projection of the path length L. Previously different coefficients of D were used for rain rates exceeded for different percentages of time, but, as mentioned under step 1, the latest procedure is to make the calculation of attenuation for 0.01 percent and to modify the value so determined to obtain attenuations for other percentages. Also the previous form was $90/(90 + 4D)$, but if numerator and denominator of this expression are divided by 90 an expression very close to that of Eq. (9.26) results.

5. Calculate Attenuation

Having determined the values of α_p, L, and r_p for a percentage of 0.01, attenuation A in dB can be calculated, using the modified CCIR model, from the simple relation

$$A = \alpha_p L r_p \quad \text{dB} \tag{9.27}$$

Attenuations equaled or exceeded for percentages p other than 0.01 percent can be found from the attenuation $A_{0.01}$ for 0.01 percent by use of

$$A_p = A_{0.01}\, 0.12\, p^{-(0.546 + 0.043 \log p)} \tag{9.28}$$

Previously the recommendation was to use Fig. 4.12 or its algebraic equivalent for the same purpose as Eq. (9.28).

It should be kept in mind that attenuation due to rain is accompanied by an increase in system noise temperature. Thus the degradation in signal-to-noise ratio due to rain is more severe than that caused by attenuation alone, especially for low-noise systems. Section 9.7 and Chap. 7 are devoted to the subject of noise.

Example 9.5 Attenuation Due to Rain

For an example of attenuation caused by rain, we find attenuation values applicable in western Kansas at a latitude of 40 deg at a frequency of 8.5 GHz.

1. Figure 9.7 shows western Kansas to be in region D_1 of the 1980

Global Model, and Table 9.7 shows the rain exceeded for 0.01 percent of the time to be 35.5 mm/h.

2. To determine applicable attenuation constants, use

$$\alpha_p = a(f)\, R^{b(f)}$$

with constants a and b from Table 9.9, using interpolation between values for 8 and 10 GHz. Values of the constants will be determined for horizontal, vertical, and circular polarizations, using Eqs. (9.21) and (9.22) for circular polarization.

The values of a and b for 8.0 GHz and 10.0 GHz and linearly interpolated values for 8.5 GHz are as follows:

f (GHz)	a_h	a_v	b_h	b_v	a_c	b_c
8	0.00454	0.00395	1.33	1.31		
10	0.1010	0.00887	1.28	1.26		
8.5	0.00593	0.00518	1.32	1.30	0.00556	1.31

Use of the a and b entries result in values of α_p in dB/km of 0.660 for horizontal polarization, 0.537 for vertical polarization, and 0.597 for circular polarization.

3. For determining path length L and horizontal projection D use

$$H = 4.0 - 0.075 \; (\phi - 36^{o}) \quad \text{km}$$

For $\phi = 40^{o}$, H = 3.7 km. To determine L and D information on elevation angle is needed. For purposes of illustration, the elevation angle is arbitrarily taken to be 42 deg. Then

$$L = \frac{H}{\sin\theta} = \frac{3.7}{0.669} = 5.53 \text{ km}$$

and

$$D = L\cos\theta = (5.53) \; (0.743) = 4.11 \text{ km}$$

4. The path reduction factor r_p for a probability of 0.01 is given by

$$r_p = \frac{1}{1 + 0.045\,D} = \frac{1}{1 + 0.185} = 0.844$$

5. Total attenuation values A for p = 0.01 are calculated by using $A = \alpha_p L r_p$. For example

$$A_h = (0.660) \; (5.53) \; (0.844) = 3.08 \text{ dB}$$

where A_h is the attenuation for horizontal polarization. Values for vertical and circular polarization, A_v and A_c respectively, are

$$A_v = 2.51 \text{ dB}$$

$$A_c = 2.79 \text{ dB}$$

The value for circular polarization is intermediate between values for horizontal and vertical polarization.

For circular polarization but for the rain rate exceeded for 0.1 percent of the time the attenuation $A_{0.1}$ is given by

$$A_{0.1} = A_{0.01} \; (0.12) \; p^{-(0.546 + 0.043 \log p)}$$

$$A_{0.1} = 2.79\ (0.12)\ 0.1^{-(0.546 + 0.043 \log 0.1)}$$
$$= 2.79\ (0.12)\ (3.184)$$
$$= 1.06 \text{ dB}$$

The value of attenuation exceeded for 0.1 percent of the time is smaller than that exceeded for 0.01 percent of the time.

9.4.3 Depolarization

9.4.3.1 Introduction

The degree of depolarization may be described in two principal ways. The terms cross polarization discrimination (XPD) and depolarization or cross polarization (D) have an inverse relation. The quantity XPD was defined by Eq. (4.32) as 20 log (E_{11}/E_{12}) where E_{11} is the copolarized or wanted signal and E_{12} is the cross polarized or unwanted signal which may have been produced by a process of depolarization. The term depolarization, however, may be used to represent 20 log (E_{12}/E_{11}). It can be noted that a high value of XPD, for example 40 dB, represents a favorable condition corresponding to a small value of D, namely −40 dB. Also the low value of XPD of 10 dB for example represents an unfavorable condition corresponding to the high value of D of −10 dB.

For frequencies below about 10 GHz we favor the analysis by Chu (1980) for which depolarization D is given for circular polarization by

$$D_{cir}(\text{dB}) = 20 \log \left[0.5 \left[(\Delta\alpha_o)^2 + (\Delta\beta_o)^2 \right]^{1/2} L \cos^2\theta \, e^{-2\sigma^2} \right] \tag{9.29}$$

For linear polarization, D is given by

$$D_{lin}(\text{dB}) = D_{cir}(\text{dB}) + 10 \log \left[0.5 \left(1 - \cos 4\tau \, e^{-8\sigma_m^2}\right)\right] \pm \Delta A'/2 \tag{9.30}$$

In the above expressions $[(\Delta\alpha_o)^2 + (\Delta\beta_o)^2]^{1/2}$ is the square root of the sum of the squares of the differential attenuation and phase constants (Fig. 9.11), L is the path length through rain, θ is the elevation angle of the path, and τ is the tilt angle from the horizontal of the electric field intensity of the linearly polarized wave. The quantity σ is the standard deviation of the raindrop canting angle ϕ, measured from the horizontal, along a path at a particular instant of time. As a conservative design procedure σ can be set equal to zero. The quantity σ_m is the standard deviation in radians of the mean raindrop canting angle ϕ_m from path to path and storm to storm. If ϕ_m is expressed in degrees, $8\ \sigma_m^2$ can be replaced by $\kappa_m^2 = 0.0024\ \sigma_m^2$ with 5 deg a suitable value for σ_m. The quantity $\Delta A'$ is given by

$$\Delta A' = 5 \log (|\alpha_v|^2/|\alpha_h|^2)$$

where α_v and α_h are attenuation constants for vertically and horizontally polarized waves. The sign of $\pm\Delta A'$ should be chosen to give the lowest value of D for quasivertical polarization. In Eq. (9.30) the logarithm of a quantity less than unity is indicated and this logarithm is negative. Thus a linearly polarized wave has a smaller value of depolarization D than a circularly polarized wave. Equation (9.29) shows that depolarization decreases with increasing elevation angle. That polarization should decrease with increasing elevation angle can be understood by considering the outline of raindrops as seen from the direction of incident waves at $\theta = 0$ deg and at $\theta = 90$ deg. From the 0 deg direction the drops appear to have an elliptical shape, while from 90 deg the outline is circular. The elliptical cross section is conducive to depolarization, but the symmetrical circular cross section is not.

At frequencies above about 8 or 10 GHz, cross-polarization discrimination (XPD), the reciprocal of D, can be expressed in the form of U - V log A where A is attenuation in dB (CCIR, 1986e, 1986f). The basis for this form is developed in Sec. 4.4. We prefer to emphasize the application of Eqs. (9.29) and (9.30), however, as these are applicable over a large range of frequencies both above and below 10 GHz.

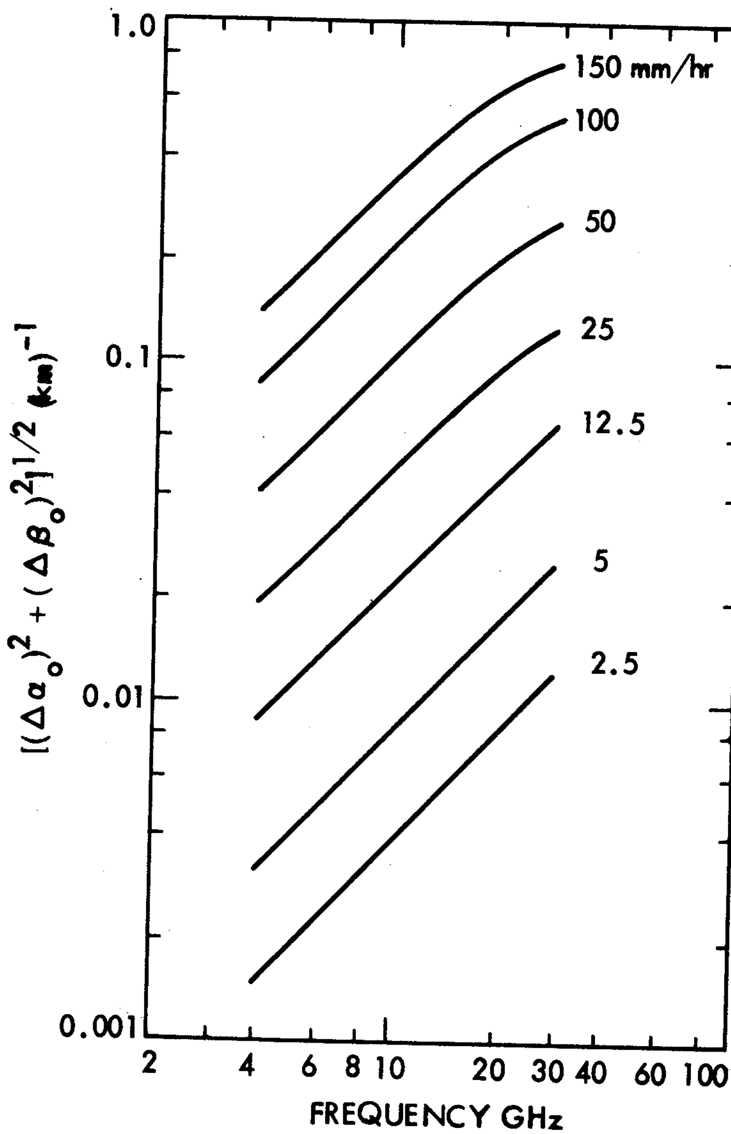

Figure 9.11. Calculated differential propagation constant at an elevation angle of zero degrees as a function of frequency for various rain rates (Chu, 1980).

Example 9.6 Depolarization at 8 GHz

This example compares depolarization for circularly and horizontal linearly polarized waves at a frequency of 8 GHz, an elevation angle of 42 deg, a latitude of 40 deg, and a rain rate of 50 mm/h. For this purpose, substitute the applicable values into Eqs. (9.29) and (9.30). From Fig. 9.11 for 8 GHz and 50 mm/h, a value of about 0.08 is found for the square root appearing in Eq. (9.29). In Example 9.5, for the same latitude and elevation angle, the path length L was found to be 5.53 km. Thus after substitution of values, Eq. (9.29) becomes

$$D_{cir}(\text{dB}) = 20 \log [\,(0.5)\,(0.08)\,(5.53)\,(0.552)\,]$$
$$= 20 \log [\,0.122\,] = -18.27 \text{ dB}$$

Taking the tilt angle τ of Eq. (9.30) as 0 deg for horizontal polarization and using a value of 5 deg for σ_m results in

$$D_{lin}(\text{dB}) = -18.27 + 10 \log [\,0.5\,(1 - \cos 0^{o}\, e^{-0.0024\,(25)}\,)]$$
$$= -18.27 + 10 \log [0.5\,(1 - e^{-0.06})] = -37.11 \text{ dB}$$

The quantity $\Delta A'/2$ was neglected above. If included the value of D_{lin}(dB) turns out to be -36.61 dB. The depolarization is considerably smaller for the linearly polarized wave than for the circularly polarized wave. If the elevation angle of the path is reduced to 20 deg, the path length L becomes 10.3 km and $\cos^2\theta$ changes from 0.552 to 0.88 with the result that D_{cir} degrades from -18.27 dB to -8.37 dB.

9.4.3.3 Depolarization due to ice particles

Clouds above the 0 deg C isotherm consist at least in part of ice particles. These have a variety of shapes but are asymmetric and when they have a preferred orientation may cause depolarization not accompanied by appreciable attenuation (Bostian and Allnut, 1979; Cox, 1981). The depolarization in this case is produced primarily by differential phase shift. Rapid changes in depolarization due to ice particles have been correlated with lightning strokes (Howell, 1977; McEwan et al., 1977). The relative amounts of rain and ice depolarization vary considerably with location and weather. When attenuation is high, depolarization is due primarily to rain, but when depolarization is accompanied by only low values of attenuation a larger amount of the depolarization may be due to ice, except at the lower frequencies for which this handbook is aimed where depolarization may be primarily caused by differential phase shift even in the absence of ice. Chu (1980) has suggested the simple procedure of adding 2 dB to the depolarization caused by rain alone (subtracting 2 dB from XPD) in order to account for the effects of ice particles. Elsewhere it has been stated that an allowance of 2 dB may be sufficient for North America but that a value as much as 4 or 5 dB may be needed for the maritime climate of northwestern Europe (CCIR, 1986e).

9.4.3.4 Extrapolation of Data From One Path to Another

The analysis by Chu (1980) outlined in Sec. 9.4.3.2 and treated somewhat more fully in Sec. 4.4, allows extrapolation of depolarization D from one path to another having a different rain rate, frequency,. elevation angle, and polarization. For this purpose Chu uses

$$D_1(\mathrm{dB}) - D_2(\mathrm{dB}) = P_1 - P_2$$

$$+ 20 \log \left[\frac{[(\Delta\alpha_1)^2 + (\Delta\beta_1)^2]^{1/2} \cos^2\theta_1 \, L_1}{[(\Delta\alpha_2)^2 + (\Delta\beta_2)^2]^{1/2} \cos^2\theta_2 \, L_2} \right] \qquad (9.31)$$

where the P's represent polarization factors which are zero for circular polarization and for linear polarization are given by

$$P = 10 \log [\, 0.5 \,(1 - \cos 4\tau \, e^{-8\sigma_m})] \pm \Delta A'/2 \qquad (9.32)$$

The quantities L_1 and L_2 are the two path lengths through rain. The factors appearing in Eqs. (9.31) and (9.32) have the same meanings as in Eqs. (9.29) and (9.30) and take account of the same difference between linear and circular polarization.

Figure 9.12 shows the application of the procedure outlined to comparison of depolarization at 4 GHz for linearly polarized transmissions on a path with an elevation angle of 38.6 deg in New

Jersey with depolarization on a path with an elevation angle of 9 deg in Japan where circular depolarization was employed.

Further information on the low values of XPD (high values of D) which may be encountered at the low elevation angles utilized on some 4 GHz earth-space paths from Japan is shown in Fig. 9.13 (Kobayashi, 1976). Low values of XPD have also been reported by Taur (1974) at 4 GHz on paths terminating at Washington, DC and having higher elevation angles.

Example 9.7 Comparison of Depolarization for Different Paths

The application of Eq. (9.32) to the comparison of depolarization on two different paths will now be illustrated. Let Station 1 have an elevation angle of 10 deg and circular polarization. Let Station 2 have an elevation angle of 40 deg and quasivertical polarization with a tilt angle τ of 75 deg. Assume that both stations operate at 4 GHz, that Station 2 is reported to have a depolarization of −30 dB, and that it is desired to determine the depolarization of Station 1. The comparison will be made for the same rain rate of 35 mm/h at both stations. Station 1 can be expected to have a higher depolarization (less favorable for frequency sharing) than Station 2 so that $D_1 - D_2$ should be positive.

As Station 1 has circular polarization, P_1 is zero. [See Eqs. (9.29) and (9.30).] The principal term of P_2 is

$$10 \log[0.5(1 - \cos 4\tau\, e^{-8\sigma_m^2})] = 10 \log[0.5(1 - \cos 300^\circ\, 0.942)]$$

$$= -5.77 \text{ dB}$$

where the exponential term has the same value as in Example 9.6. By using values of a_H, a_V, b_H, and b_V from Table 9.9 it is determined that $\Delta A/2$ is 1.19. Therefore

$$P_1 - P_2 = 0 - (-5.77 - 1.19) = 6.96$$

Considering next the second term of Eq. (9.31), the propagation constants are the same if the same rain rate is assumed and the difference in depolarization due to this term is

$$20 \log \left(\frac{\cos^2\theta_1\, L_1}{\cos^2\theta_2\, L_2} \right) = 20 \log \left(\frac{\cos^2 10^\circ\, (1/\sin 10^\circ)}{\cos^2 40^\circ\, (1/\sin 40^\circ)} \right)$$

$$= 15.73$$

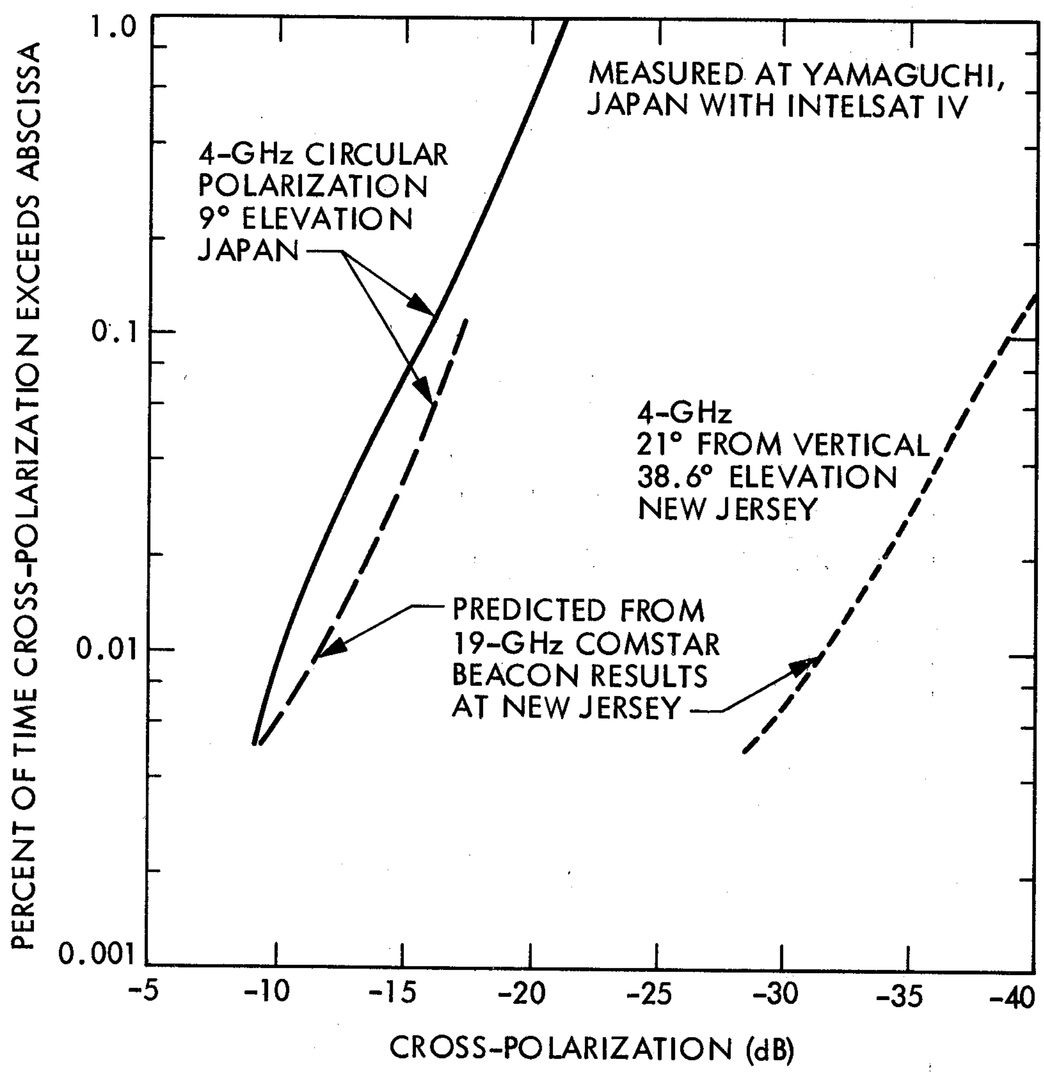

Figure 9.12. Comparison between measured 4 GHz circularly polarized INTELSAT IV depolarization statistics at 9 deg elevation angle and prediction from COMSTAR measurements (Chu, 1980).

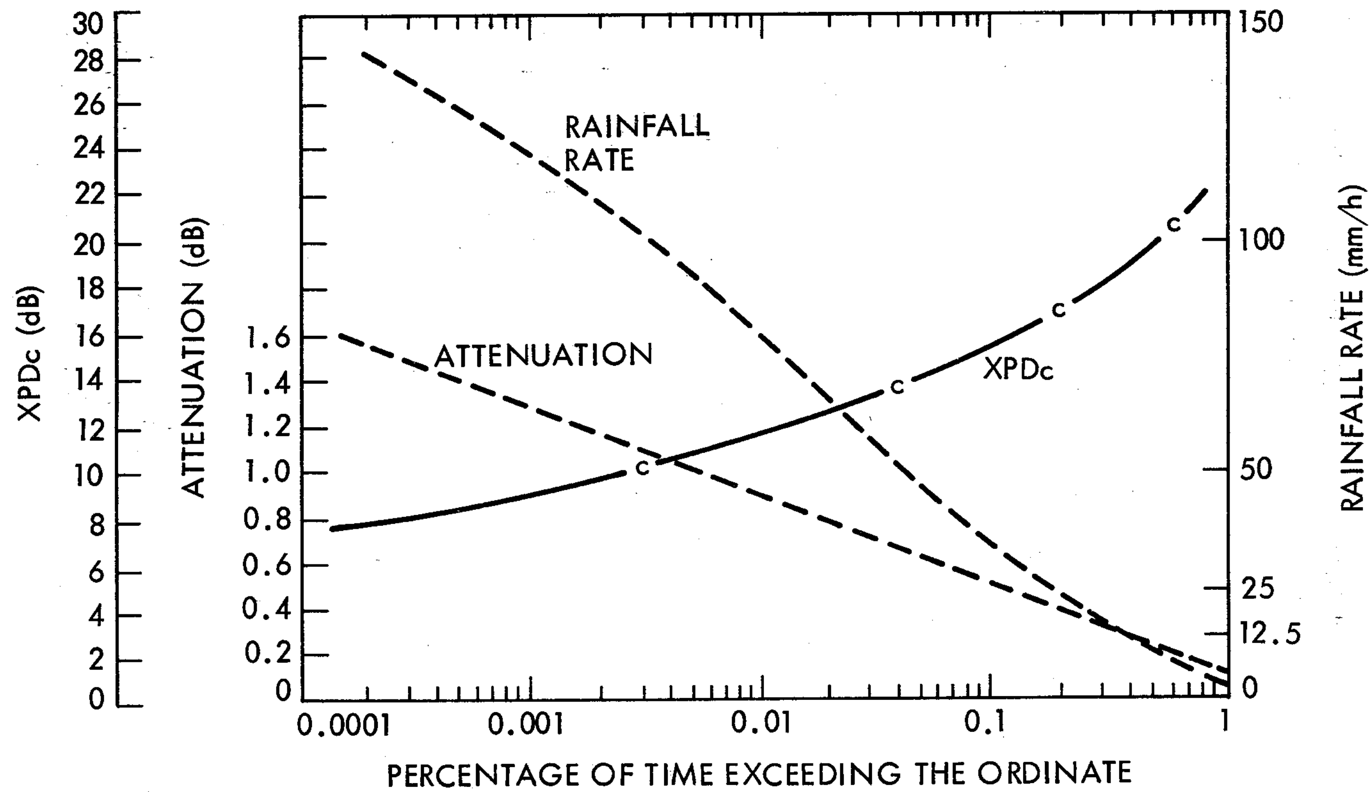

Figure 9.13. Pre-estimation of XPD on a satellite communication circuit, 4 GHz, 8 deg elevation angle, circular polarization, Yamaguchi station (Kobayashi, 1976).

Thus

$$(D_1)_{dB} - (D_2)_{dB} = 6.96 + 15.73 = 22.69 \text{ dB}$$

and

$$(D_1)_{dB} - (-30) = 22.69$$

$$(D_1)_{dB} = 22.69 - 30 = -7.31 \text{ dB}$$

To take account of different frequencies or rain rates use can be made of Fig. 9.11. For example if Station 2 operated at 8 GHz with the same depolarization of −30 dB, but Station 1 remained at 4 GHz, the ratio of propagation constants of Eq. (9.31) would be roughly 1/2 and in place of 15.73 for the second term of Eq. (9.31) one would have about 9.7. Then $(D_1)_{dB}$ would be about −13.3.

Note that whereas Station 2 was known to operate with a depolarization of −30 dB (XPD of +30 dB), Station 1, at the same frequency and rain rate in the original case considered but having a different path, was predicted to have the clearly unsatisfactory D value of −7.3 dB (XPD of +7.3 dB).

9.5 EFFECTS OF CLOUDS, DUST, AND VEGETATION

Attenuation due to clouds is normally no greater than 0.5 dB for a vertical path for frequencies of 10 GHz and less. For the same conditions otherwise, the attenuation would be 1 dB for an elevation angle of 30 deg and 2.88 dB for an elevation angle of 10 deg if the attenuation were 0.5 dB for a vertical path. As every dB of attenuation may be important, clouds may be of significance for frequencies as low as 10 GHz and somewhat lower, as well as for higher frequencies for which the attenuation is greater. Also as was indicated for the case of rain, dissipative attenuation is accompanied by an increase in noise and both effects contribute to a degradation in signal-to-noise ratio. Section 9.7 and Chap. 7 specify and discuss further the relation between attenuation and noise. Table 7.1 gives attenuation and noise temperature values for 12 different cloud models.

Although effects due to clouds do not become as intense as those due to rain, they occur for larger percentages of time. For operations for which propagation impairments occurring for relatively high percentages of the time, such as 1 to 10 percent or greater, are pertinent (rather than or in addition to small percentages such as 0.01), the effects of clouds assume the greatest relative importance. In a study of effects of clouds by Slobin (1982), the United States has been divided into 15 regions shown in Fig. 9.14. For these regions data on cumulative distributions of zenith atmospheric noise temperatures due to clouds have been provided. Figure 9.15 shows such distributions for 5 of the 15 regions.

Only very limited data on attenuation due to sand and dust are available. For earth stations in desert areas where serious sand or dust storms occur, an allowance of 1 dB for attenuation due to sand and dust on an earth-space path may be advisable.

Section 5.3 includes some background material on the effects of vegatation on propagation, primarily from one point on the Earth's surface to another. An empirical expression developed by Weissberger for attenuation due to small groves of trees has the form, as simplified in CCIR Report 236-6, of

$$A_{dB} = 0.20\, f^{0.3}\, d^{0.6} \tag{9.33}$$

with frequency f in MHz and distance d in meters. Recent data on attenuation on simulated earth-space paths are given in Chap. 6 and commented on briefly in the following Sec. 9.6.

9.6 PROPAGATION EFFECTS ON MOBILE SYSTEMS

Propagation effects on earth-space paths utilized for communication with land vehicles, ships, and aircraft include specular reflection, diffuse scatter, and shadowing by vegetation. Example 9.8 deals with reflection coefficients for reflection of linear and circularly polarized waves. Studies carried out by simulating conditions on earth-space paths have shown the importance of shadowing by trees, including even single trees. Attenuation values are generally higher for these paths than the values given by the empirical expression of Sec. 9.5 which was developed for ground-to-ground paths. A sizeable margin of over 10 dB may be advisable for attenuation due to roadside trees (Sec. 6.4). Interstate highways have wider cleared areas and tend to be less afffected than two-lane roads or parkways. Attenuation is encountered, however, when driving through underpasses. Recently

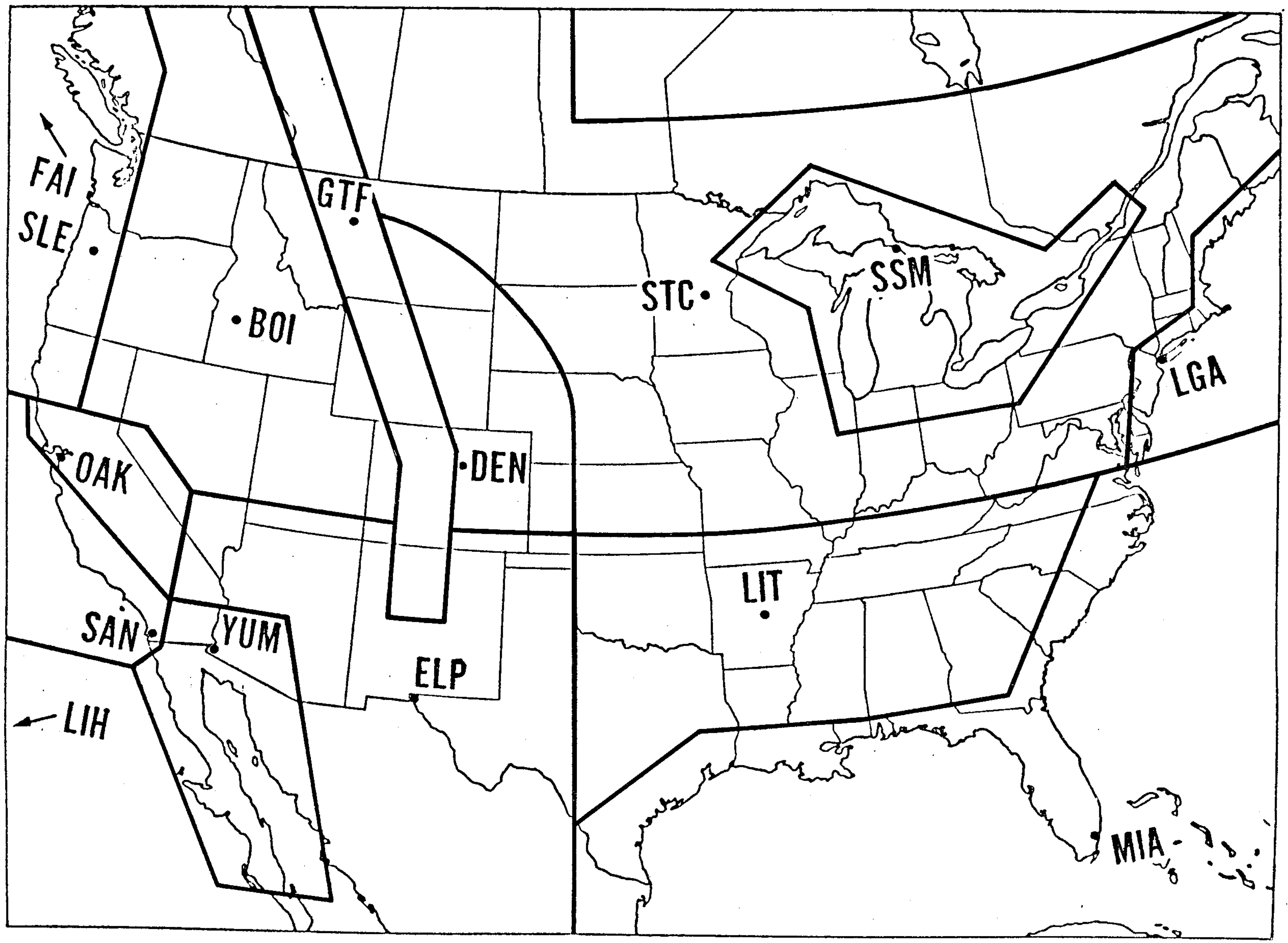

Figure 9.14. Cloud regions of the United States (Slobin, 1982).

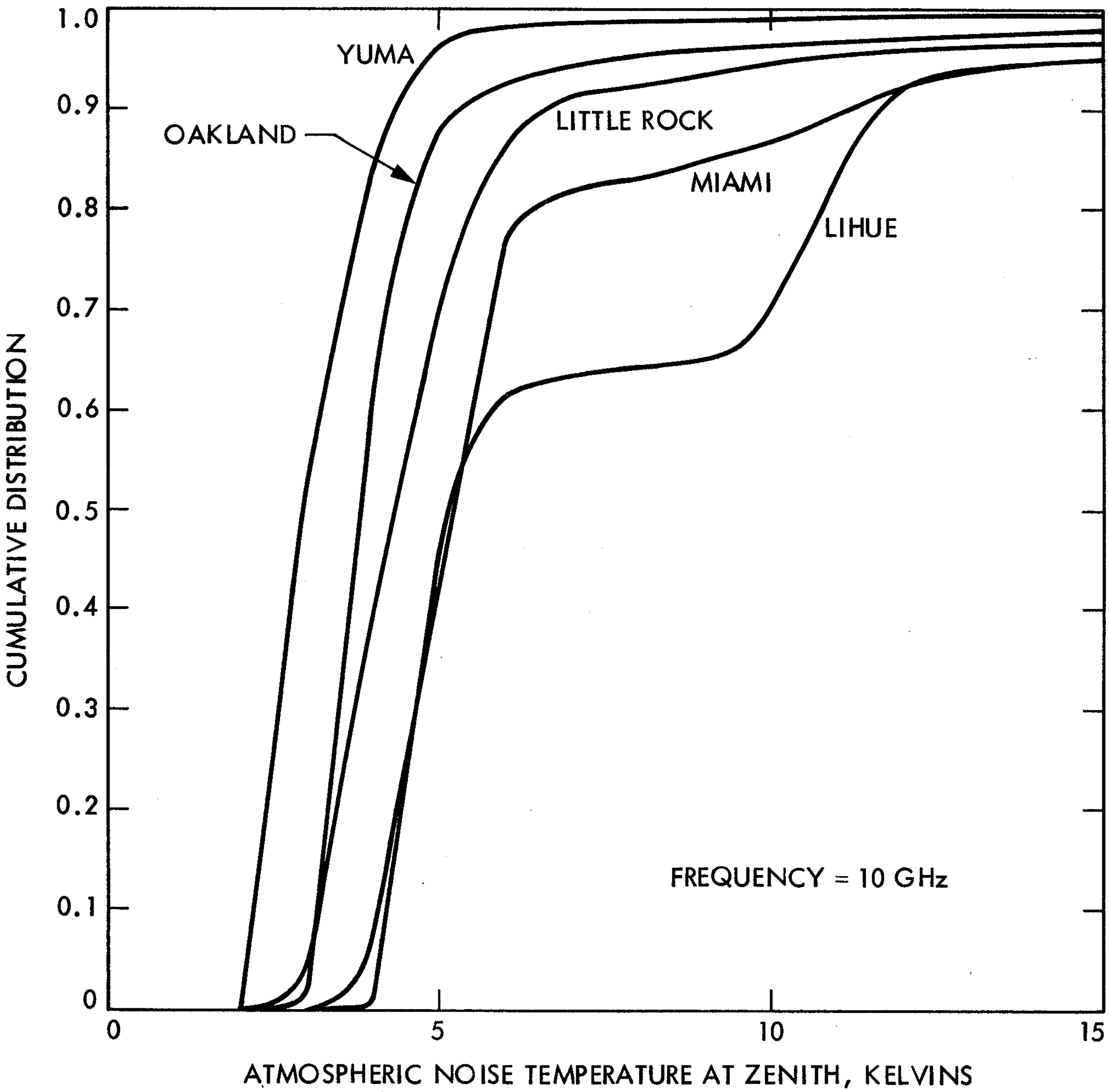

Figure 9.15. Total-year cumulative distributions of zenith atmospheric noise temperature for five regions at 10 GHz (Slobin, 1982).

reported studies by Vogel, Torrence, Goldhirsh, and Rowland (1987) in Colorado show only very small effects from reflections from canyon walls. Interesting periodic signal fades were recorded due to reflection from roadside power-line poles in open country.

Example 9.8 Reception of Signals from Geostationary Satellites by Land-Mobile Receivers.

The transmission of circularly polarized waves at a frequency of 1000 MHz is featured in this example. Calculations are made for two elevation angles, 10 deg and 30 deg. Possible ionospheric effects are neglected, but ionospheric scintillation would need to be taken into account at low latitudes. Average ground (relative dielectric constant $K = 15$ and conductivity $\sigma = 0.005$ mhos/m) is assumed. Calculations are included for $h_s = 0.1$ m, where h_s is the rms height of irregularities, and for a perfectly smooth surface for which $h_s = 0$.

Notation:

ρ_h, ρ_v are smooth-earth reflection coefficients for horizontal and vertical polarization. They are calculated by using Eqs. (6.14), (6.15).

ρ_c, ρ_x are smooth-earth reflection coefficients for the copolarized and crosspolarized components of the reflected wave and are given by Eqs. (6.18) and (6.19).

ρ_s is a surface roughness factor given by Eq. (6.28).

ρ_{cs}, ρ_{xs} are rough-surface reflection coefficients defined by

$$\rho_{cs} = \rho_c \rho_s \text{ and } \rho_{xs} = \rho_x \rho_s$$

ρ_d is a diffuse reflection coefficient.

θ is elevation angle.

g_{cr} is the relative (normalized) voltage gain of the receiving antenna for the co-polarized component of the reflected wave.

g_{xr} is the relative voltage gain for the cross-polarized component of the reflected wave.

The surface roughness factor ρ_s is given by

$$\rho_s = e^{-(\Delta\phi)^2/2}\, I_0[(\Delta\phi)^2/2]$$

with

$$\Delta\phi = 4\pi\,(h_s/\lambda)\sin\theta$$

<u>Specular Reflection: Elevation Angle $\theta = 10^\circ$</u>

Use of Eqs. (6.14) and (6.15) gives a value for ρ_h of −0.91 and a value for ρ_v of −0.18. Then

$$\rho_c = (\rho_h + \rho_v)/2 = (-0.91 - 0.18)/2 = -0.55$$

$$\rho_x = (\rho_h - \rho_v)/2 = (-0.91 + 0.18)/2 = -0.37$$

$$\rho_s = 0.783 \text{ for } h_s = 0.1 \text{ m}$$

$$\rho_{cs} = (0.783)\,(-0.55) = -0.431$$

$$\rho_{xs} = (0.783)\,(-0.37) = -0.290$$

The incident wave has only pure right or left circular polarization, but the reflected wave has a combination of both types with the original polarization dominant. Interest here is in the combination of the direct wave and the components of the specularly reflected wave. Account must be taken of the normalized voltage gains g_{cr} and g_{xr} of the receiving antenna as a function of angle from that of the direct ray. The angle of the reflected rays differs from that of the direct ray by 2θ where θ is elevation angle. If the gains of the receiving antenna are known as a function of angle, they should be used. Here it is arbitrarily assumed that the gain g_{cr} for the copolarized reflected wave, differing by 20 deg from that of the direct wave, is 3 dB down from that for the direct wave, while the gain g_{xr} is 9 dB down. Then the relative magnitude of the total signal can be expected to fall within the limits of

$$1 \pm [\,|g_{cr}(20^\circ)|\;|\rho_{cs}| + |g_{cr}(20^\circ)|\;|\rho_{xs}|\,] = 1 \pm 0.407$$

which corresponds to a variation, relative to the signal for the direct wave alone, of +2.96 to −4.53 dB.

The value for a perfectly smooth earth is obtained by using ρ_c and ρ_x instead of ρ_{cs} and ρ_{xs}. The limits of the normalized field intensity in this case are 1 ± 0.519 or +3.63 to −6.35 dB.

Specular Reflection; Elevation Angle $\theta = 30^\circ$

The reflection coefficients for horizontal and vertical polarization in this case are −0.77 and +0.33, respectively. The Brewster angle [angle of minimum reflection coefficient as given by Eq. (6.15)] is $\tan^{-1} 1/(K_2)^{1/2} = \tan^{-1} 1/(15)^{1/2} = 14.48$ deg in this case. The elevation angles of 10 and 30 deg are on opposite sides of the Brewster angle and the sign of the reflection coefficient for vertical polarization is different on the two sides. The result is that ρ_x now becomes larger than ρ_c as indicated by

$$\rho_c = (\rho_h + \rho_v)/2 = -0.22$$

$$\rho_x = (\rho_h - \rho_v)/2 = -0.55$$

The roughness factor ρ_s for 30 deg is smaller than for 10 deg. In particular

$$\rho_s = 0.290$$

so that

$$\rho_{cs} = (0.290)\ (-0.22) = -0.064$$

$$\rho_{xs} = (0.290)\ (-0.55) = -0.160$$

Although antennas are designed to have much larger gain for the copolarized wave than for the crosspolarized wave for the center of the main beam (boresight), their gains at a large angle from the center may be about the same. For the present case, it is assumed that both g_{cr} and g_{xr} are 10 dB down from the gain at the center of the beam. For this condition and still for $h_s = 0.1$ m, the total normalized signal should fall within the limits of

$$1 \pm g_r(60^\circ)\ [|\rho_{cs}| + |\rho_{xs}|] = 1 \pm 0.070 \text{ or } +0.59 \text{ to } -0.63 \text{ dB}$$

For a perfectly smooth earth, the corresponding values are +1.89 to -2.42 dB.

The fading is only about 2.4 dB for a smooth earth. Now assume that g_r(60 deg) = 1. That is, assume that the normalized gain at an angle of 60 deg from boresight is the same as on boresight. The result for a smooth earth is that the total signal variation falls in the range of 1 ± 0.77 or +4.95 to -12.8 dB. The values are not realistic but are mentioned to show the importance of antenna discrimination in minimizing the role of multipath effects in mobile communication. With discrimination of 10 dB for both the copolarized and crosspolarized wave components, fading is reduced from 12.8 dB to 2.4 dB for the case of a smooth earth.

Returning to the case of surface roughness, specular reflection decreases and diffuse scatter increases as roughness increases. The combination of specular reflection and diffuse scatter tends to be described by the Rician distribution, shown in Fig. 6.11 as function of diffuse reflection coefficient ρ_d. Fading due to shadowing by vegetation or otherwise, however, follows the log-normal distribution. Fading on simulated earth-space paths tends to show a combination of Rician and log-normal fading (Fig. 6.16). The phenomena of specular reflection and diffuse scatter need to be understood and taken into account, but shadowing by vegetation has come to assume a dominant role in consideration of what margins are needed in land-mobile satellite service.

9.7 RADIO NOISE

9.7.1 Basic Relations

The system noise temperature, T_{sys}, and the noise temperature, T_s, of Fig. 9.16 are given by

$$T_{sys} = T_A + (\ell_a - 1)T_o + \ell_a T_R \tag{9.34}$$

and

$$T_s = T_A g_a + (1 - g_a)T_o + T_R \tag{9.35}$$

In these equations, T_A is the antenna noise temperature, T_o is the attenuator temperature, normally taken as 290 K, and T_R is the receiver noise temperature. The factor g_a is the attenuator "gain" and has a maximum value of one; the factor ℓ_a equals $1/g_a$ and has a minimum value of one. If there is no attenuation, $T_{sys} = T_s = T_A + T_R$.

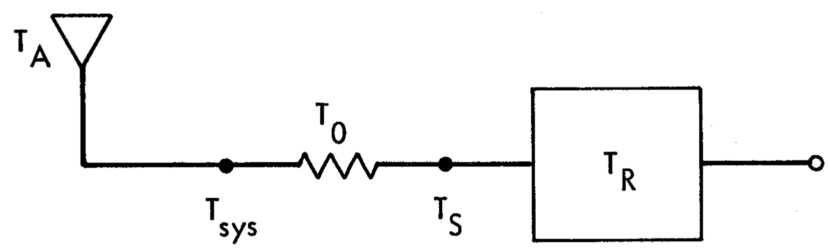

Figure 9.16. Noise temperatures of a receiving system.

The brightness temperature T_b, recorded when observing a noise source T_s through an absorbing region having an intrinsic temperature T_i and causing an attenuation represented by $e^{-\tau}$ is given by

$$T_b = T_s e^{-\tau} + T_i (1 - e^{-\tau}) \tag{9.36}$$

Note that g_a and $e^{-\tau}$ are alternative ways of representing attenuation and that if $T_R = 0$, Eqs. (9.35) and (9.36) are identical in form. Attenuation in an attenuator is represented here by g_a and that in the atmosphere is represented by $e^{-\tau}$. In both cases attenuation is encountered and thermal noise is generated in an absorbing medium.

In the case of an earth station receiving system, T_A may be approximately equal to T_b. That is, the antenna noise may be primarily that due to an absorbing region along the path plus perhaps noise of distant origin that is attenuated by the absorbing region. Actually other noise sources, such as terrestrial noise picked up by the antenna sidelobes and backlobe make at least a small contribution to to T_A as well. In some situations the value of the term T_s may be negligible and

$$T_b = T_i\,(1 - e^{-\tau}) \tag{9.37}$$

Also absorption may be negligible in some cases and then $T_b = T_A = T_s$.

Consider that a signal is propagating through an absorbing region, for example a region where rain is falling. The signal is attenuated by a factor of $e^{-\tau}$ or by A_{dB} where $A_{dB} = 4.34\ \tau$. Also the antenna receives noise given by Eq. (9.37). Values of T_i have been determined and found to range mostly from 260 to 290 K. The degradation in signal-to-noise ratio, C/X, compared to the case when no absorption occurs along the path is given by

$$\Delta(C/X)_{dB} = A_{dB} + 10 \log (T_2/T_1) = A_{dB} + 10 \log [(T_1 + T_b)/T_1] \tag{9.38}$$

where T_1 is the system noise temperature in the absence of the absorbing region and $T_2 = T_1 + T_b$ is the temperature in the presence of the absorbing region.

The concept presented here applies regardless of what the absorptive attenuation is due to (rain, clouds, or atmospheric gases). Note that the magnitude of $10 \log (T_2/T_1)$ with $T_2 = T_1 + T_b$ depends on the relative magnitudes of T_1 and T_b. If T_1 is large, a given value of T_b tends to cause a relatively small change in T_2/T_1, but if T_1 is small the same value of T_b causes a larger change in T_2/T_1. For low-noise systems and for attenuations up to about 10 dB, the degradation in the C/X ratio due to noise may be larger than that due to attenuation (Fig. 9.17).

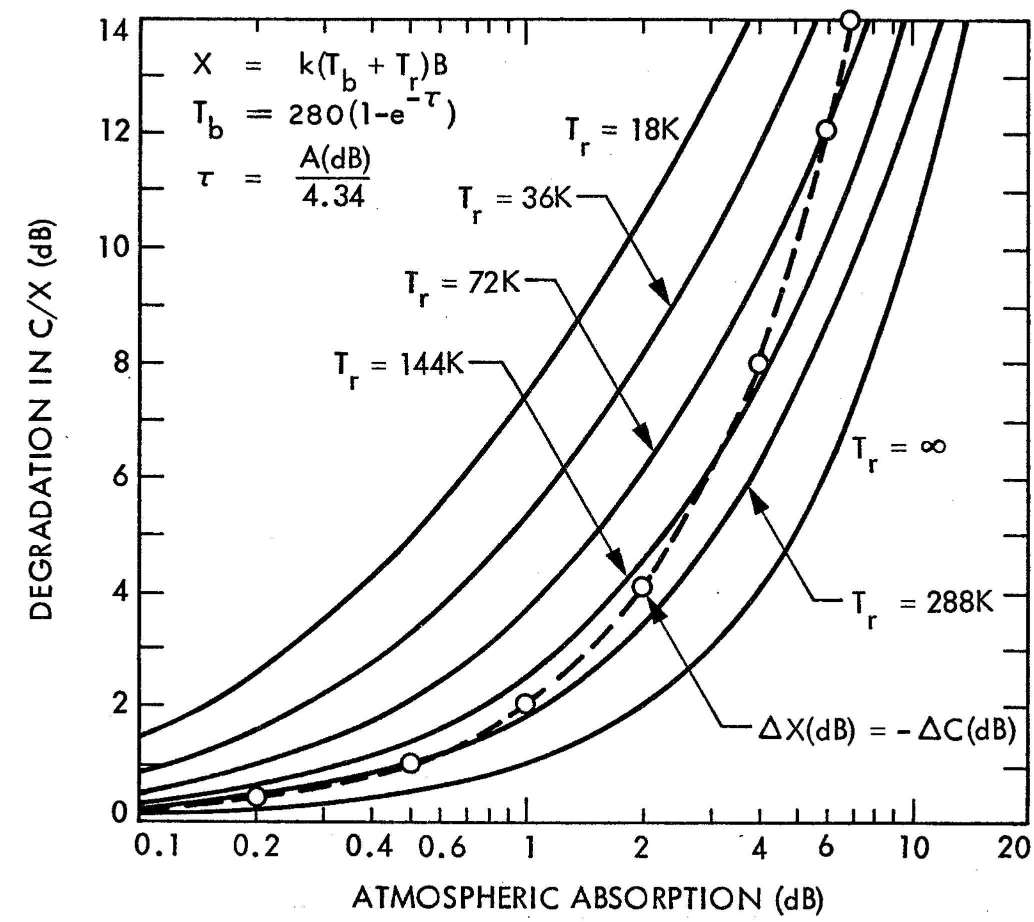

Figure 9.17. Degradation in signal-to-noise ratio (C/X) versus atmospheric absorption, for various values of T_1 (with T_1 equal to T_r).

9.7.2. Noise Sources

9.7.2.1 Extraterrestrial Noise

In the lower decade of the frequency range of this handbook from 100 MHz to 1000 MHz (1 GHz), extraterrestrial (cosmic) noise is the dominant type of noise. Atmospheric thermal noise dominates above 10 GHz, and the frequency range from 1 to 10 GHz has the least noise of natural origin of the radio-frequency spectrum.

The most intense extraterrestrial radio noise sources other than the Sun are non-thermal and have positive spectral indices, which means that their noise powers increase with wavelength and decrease with frequency. Figure 7.11 shows radio emission from that part of the celestial sphere of interest to satellite operations employing the geostationary orbit (declination angles from +8.7 to -8.7 deg) and includes data for larger declination angles as well. The plot is in celestial coordinates with declination angle δ measured from the celestial equator which is an extension into space of the Earth's equator. Declination angles of ± 8.7 deg correspond to the highest possible latitudes (± 81.3 deg) which can be used for communication with geostationary satellites. For an earth station in the northern hemisphere at a latitude of θ', the extraterrestrial noise received is that from a strip of sky behind the satellite having a declination angle δ given by

$$\delta = -\tan^{-1}\left(\frac{\sin\theta'}{6.6 - \cos\theta'}\right) \tag{9.39}$$

and equals -6.3 deg for $\theta' = 40$ deg. The fraction within the brackets of Eq. (9.39) is a ratio of distances measured in earth radii, geostationary satellites being at 6.6 earth radii from the center of the Earth. By examination of Fig. 7.11 (or a better original version) and from the accompanying discussion of Chap. 7, it can be determined that the maximum noise temperature at 250 MHz for an earth station at a latitude of 40 deg that is communicating with a geostationary satellite is 850 K. For other frequencies an equivalent blackbody temperature T can be determined by assuming that T varies as f^{-2+n} where n is the spectral index and can be taken as 0.75 as in Sec. 7.3.4 (Smith, 1982a). In adddition, for microwave frequencies, the microwave background temperature of 2.7 K should be included in T_b, the total brightness temperature. Thus for a microwave frequency f_i

$$T_b(f_i) = T_b(f_o)\,(f_i/f_o)^{-2.75} + 2.7\text{ K} \tag{9.40}$$

with f_o equal to 250 MHz.

9.7.2.2 Atmospheric Thermal Noise

Thermal noise generated by the atmospheric gases, clouds, and rain is related to attenuation in these same media by Eqs. (9.36) and (9.37) of Sec. 9.7.1. Knowledge of attenuations and the intrinsic temperatures of the media allow estimation of noise temperatures.

Detailed analyses of the attenuation and noise due to gases (Smith, 1981, 1982b) and clouds (Slobin , 1981, 1982) have been prepared. Values of attenuation due to gases are shown in Fig. 3.11 and discussed in Sec. 9.3. Table 5.3 provides some data on attenuation and atmospheric thermal noise due to clouds, and Table 7.1 presents more detailed information on the same topics. For many purposes the attenuation and noise due to the gases can be neglected for frequencies of 10 GHz and lower, but for low-angle paths and for coordination-area analyses the effects of oxygen may need to be taken into account. As discussed in Sec. 9.5, the effects of clouds may be of some significance for frequencies of 10 GHz and somewhat lower.

9.7.2.3 Terrestrial Noise

In the past it has commonly been assumed that, for the uplink to a satellite, the receiving antenna points at the ground and therefore should be assigned a noise temperature of 290 K. However, analysis of the problem by Njoku and Smith (1985) has shown that the noise temperature may be considerably lower, especially at frequencies of 10 GHz and lower, as shown in Fig. 7.14. The receiving antenna of a downlink from a satellite points at the sky but nevertheless picks up at least a small amount of terrestrial noise, ranging from one or a few degrees for a very-high-quality antenna to tens of degrees or more.

Example 9.8 Decrease in Signal-to-Noise Ratio Caused by Absorbing Region

a. Consider a receiving system with a system noise temperature $T_{sys} = T_1 = 100$ K in the absence of attenuation along the transmission path. Assume then that an attenuation of 1 dB occurs along the path in an absorbing region where the intrinsic temperature is 280 K. Because of the absorbing region T_{sys} increases to a new value T_2. The temperature T_2 and the total decrease in signal-to-noise ratio will now be calculated. The relation between τ of $T_b = T_i(1 - e^{-\tau})$ and attenuation A is

$$\tau = A_{dB}/4.34$$

For this case, $\tau = 1/4.34 = 0.23$ and $e^{-\tau} = 0.794$. Thus

$$T_b = 280\ (1 - 0.794) = 57.6\ \text{K}$$

and from Eq. (9.38)

$$\Delta(C/X)_{dB} = 1 + 10 \log \frac{100 + 57.6}{100}$$

$$= 1 + 1.98 = 2.98\ \text{dB}$$

b. Next let $T_1 = 25$ K, with other conditions the same as in part a.

$$\Delta(C/X)_{dB} = 1 + 10 \log \frac{25 + 57.6}{25}$$

$$= 1 + 5.19 = 6.19\ \text{dB}$$

The total decrease in C/X is over six times that due to attenuation.

c. For the attenuation due to rain of 2.79 dB, found for circular polarization in Example 9.5, with $T_1 = 100$ K,

$$\tau = 2.79/4.34 = 0.643 \text{ and } e^{-\tau} = 0.525$$

$$T_b = 280(1 - 0.525) = 132.78\ \text{K}$$

$$\Delta(C/X)_{dB} = 2.49 + 10 \log \frac{100 + 132.78}{100}$$

$$= 2.79 + 3.67 = 6.45\ \text{dB}$$

REFERENCES

Aarons, J., H.E. Whitney, E. Mackenzie, and S. Basu, "Microwave equatorial scintillation intensity during solar maximum," Radio Sci., vol. 10, pp. 939-945, Sept.-Oct. 1981.

Aarons, J., "Global morphology of ionospheric scintillations," Proc. IEEE, vol. 70, pp. 360-378, April 1982.

Bean, B.R. and E.J. Dutton, Radio Meteorology. Washington, DC: Supt. of Documents, U.S. Gov't Printing Office, 1966.

Bostian, C.W. and J.E. Allnut, "Ice-crystal depolarization on satellite-earth microwave radio paths," Proc. IEEE, vol. 126, p. 951, 1979.

CCIR, Report 263-5, 1982. [Earlier version of CCIR (1986a)].

CCIR, "Ionospheric effects upon earth-space propagation," Report 263-6, Vol. VI, Propagation in Ionized Media, Recommendations and Reports of the CCIR, 1986. Geneva: Int. Telecomm. Union, 1986a.

CCIR, "Effects of large-scale tropospheric refraction on radiowave propagation," Report 718-2, Vol. V, Propagation in Non-ionized Media, Recommendations and Reports of the CCIR, 1986. Geneva: Int. Telecomm. Union, 1986b.

CCIR, "Radiometeorological data," Report 563-3, Vol. V, Propagation in Non-ionized Media, Recommendations and Reports of the CCIR, 1986. Geneva: Int. Telecomm. Union, 1986c.

CCIR, "Attenuation by hydrometeors, in particular precipitation, and other atmospheric particles," Report 721-2, Vol. V, Propagation in Non-ionized Media, Recommendations and Reports of the CCIR, 1986. Geneva: Int. Telecomm. Union, 1986d.

CCIR, "Propagation data required for space telecommunication systems," Report 564-3, Vol. V, Propagation in Non-ionized Media, Recommendations and Reports of the CCIR, 1986. Geneva: Int. Telecomm. Union, 1986e.

CCIR, "Cross-polarization due to the atmosphere," Report 722-2, Vol.V, Propagation in Non-ionized Media, Recommendations and Reports of the CCIR, 1986. Geneva: Int. Telecomm. Union, 1986f.

Chu, T.S., "Microwave depolarization of an earth-space path," Bell System Tech. Jour., vol. 59, pp. 987-1007, July-Aug. 1980.

Cox, D.C., "Depolarization of radio waves by atmospheric hydrometeors in earth-space paths: a review," Radio Sci., vol. 16, pp. 781-812, Sept.-Oct, 1981.

Crane, R.K., "Refraction effects in the neutral atmosphere," in Methods of Experimental Physics, Vol. 12, Astrophysics, Part B: Radio Telescopes (M.L. Meeks, ed.), pp. 186-200. New York: Academic Press, 1976.

Crane, R.K., "Prediction of attenuation by rain," IEEE Trans. Commun., vol. COM-28, pp. 1717-1733, Sept. 1980a.

Crane, R.K., "Earth-space and terrestrial microwave propagation - estimation of rain attenuation with the global model," ERT Tech. Report P-A414-TR, prepared for NASA, Oct. 1980b.

Davies, K., Ionospheric Radio Propagation. Washington, DC: Sup. of Documents, U.S. Gov't Printing Office, 1965.

Davies, K., "Recent progress in satellite radio beacon studies with particular emphasis on the ATS-6 radio beacon experiment," Space Sci. Rev., vol. 25, pp. 357-430, April 1980.

Dawson, E. and L.R. Newitt, "The magnetic poles of the Earth," J. Geomag. Geoelectr., vol. 34, no. 4, pp. 225-240, 1982.

Fang, D.J., F.T. Tseng, and T.O. Calvit, "A low elevation angle propagation measurement of 1.5-GHz satellite signals in the Gulf of Mexico," IEEE Trans. Antennas Propagat., vol. AP-30, pp. 10-15, Jan. 1982.

Flock, W.L., "Propagation at 36,000 Mc in the Los Angeles basin," IRE Trans. Antennas Propagat., vol AP-8, pp. 235-241, May 1960.

Flock, W.L., S.D. Slobin, and E.K. Smith, "Propagation effects on radio range and noise in earth-space telecommunications," Radio Sci., vol. 17, pp 1411-1424, Nov.-Dec. 1982.

Fremouw, E.J., "A computer model of high-latitude scintillation," 82-0150, Tech. Papers, Aerospace Sci. Meeting, Orlando, FL, Jan. 11-14, 1982, 9 pp. New York: AIAA, 1982.

Fremouw, E.J. et al., "The HiLat satellite mission," Radio Sci., vol. 20, pp. 416-424, May-June 1985.

Hopfield, H.S., "Tropospheric effect on electromagnetically measured range: prediction from surface weather data," Radio Sci., vol. 6, pp. 357-367, March 1971.

Howell, R.G., "Cross-polar phase variations at 20 and 30 GHz on a satellite-earth path," Electr. Lett., vol. 13, pp. 405-406, 1977.

Ippolito, L.J., R.D. Kaul, and R.G. Wallace, Propagation Effects Handbook for Satellite Systems Design, A Summary of Propagation Impairments on 10 to 100 GHz Satellite Links With Techniques for System Design, NASA Reference Pub. 1082(03), Washington, DC: NASA Headquarter, 1983.

Karasawa, Y., K. Yasukawa, and M. Yamada, "Ionospheric scintillation measurements at 1.5 GHz in mid-latitude region," Radio Sci., vol. 20, pp. 543-551, May-June 1985.

Klobuchar, J.A. (leader) and Working Group, B. "Transionospheric propagation predictions," in R.F. Donnelly (ed.), Vol. 2: Working Group Reports and Reviews of Solar-Terrestrial Predictions Proceedings,, Boulder, CO: Environmental Research Labs., NOAA, 1979.

Kobayashi, T., "Pre-estimation of cross-polarization discrimination due to rain," J. Radio Res. Labs. (Japan), vol.23, pp. 47-64, March 1976.

Lee, M.C. et al., "Depolarization of VHF geostationary satellite signals near the equatorial anomaly crests," Radio Sci., vol. 17, pp.399-409, March-April 1982.

Lee, W.C.Y., "An approximate method for obtaining rain statistics for use in signal attenuation estimating," IEEE Trans. Antennas Propagat., vol. AP-27, pp.407-413, May 1979.

Malin, S.R.C. and D.R. Barraclough, "An algorithm for synthesizing the geostationary field," Comput. Geosci., vol. 7, No. 4, pp. 401-405, 1981.

McEwan, N.J. et al., "Crosspolarization from high altitude hydrometeors on a 20 GHz satellite radio path," Electronics Lett., vol. 13, pp.13-14, 1977.

Millman, G.H. and G.M. Reinsmith, An Analysis of the Incoherent Scatter Faraday Rotation Technique for Ionospheric Propagation Error Correction (R 74EMH2). Syracuse, NY: General Electric, Feb. 1974.

Millman, G.H., Ionospheric Electron Content Effects on Earth-Space Radio Propagation (R80EMH11). Syracuse, NY: General Electric, Dec. 1980.

Minakoshi, H. et al., "Severe ionospheric scintillation associated with magnetic storm on March 22, 1979," J. Radio Res. Labs. (Japan), vol. 28, pp. 1-9, March-July 1981.

Mullen, J.P. et al., "UHF/GHz scintillation observed at Ascension Island from 1980 through 1982," Radio Sci., vol. 20, pp. 357-365, May-June 1985.

Njoko, E.G. and E.K. Smith, "MIcrowave antenna temperature of the earth from geostationary orbit," Radio Sci., vol. 20, pp. 591-599, May-June 1985.

Olsen, R.L., D.V. Rogers, and D.B. Hodge, "The aR^b relation in the calculation of rain attenuation," IEEE Trans. Antennas Propagat., vol. AP-26, pp. 318-329. March 1978.

Segal, B, "The influence of raingauge integration time on measured rainfall-intensity distribution functions," J. Atmospheric Oceanic Tech., vol. 3, Dec. 1986.

Slobin, S.D., Microwave Noise Temperature and Attenuation of Clouds at Frequencies Below 50 GHz, JPL Pub. 81-46. Pasadena, CA: Jet Propulsion Lab., 1981.

Slobin, S.D., "Microwave noise temperature and attenuation of clouds: statistics of these effects ar various sites in the United States, Alaska, and Hawaii," Radio Sci., vol. 17, pp. 1443-1454, Nov.-Dec. 1982.

Smith, E.K., "Centimeter and millimeter wave attenuation and brightness temperature due to atmospheric oxygen and water vapor," Radio Sci., vol. 17, pp. 1455-1464, Nov.-Dec. 1982.

Strickland, J.I., R.I. Olsen, and H.L. Werstivk, "Measurements on low angle fading in the Canadian Arctic," Ann. Telecomm., vol. 32, pp. 530-535, 1977.

Taur, R.R., "Rain depolarization measurements on a satellite-earth propagation path at 4 GHz," IEEE Trans. Antennas Propagat., vol. 23, pp. 854-858, Nov. 1975.

Thompson, M.C., L.E. Wood, H.B. Janes, and D. Smith, "Phase and amplitude scintillations in the 10 to 40 GHz band," IEEE Trans. Antennas Propagat., vol. AP-23, pp. 792-797, Nov. 1975.

Titheridge, J.E., "Determination of ionospheric electron content from the Faraday rotation of geostationary satellite signals," Planet. Space Sci., vol. 20, pp. 353-369, 1972.

Vogel, W.J., G.W. Torrence, J. Goldhirsh, and J.R. Rowland, "Propagation considerations for land mobile satellite service: signal characteristics in mountainous terrain at UHF and L band," National Radio Science Meeting (URSI), 12-15 Jan. 1987, Boulder, CO.

APPENDIX 9.1

DETERMINATION OF B_L USING DIPOLE MODEL

In this appendix, a procedure is described for determining a value of B_L for estimating Faraday rotation as a function of ionospheric TEC. The procedure can be applied to any ionospheric height; we use a height of 400 km in the absence of information pointing to a different choice. For a particular earth-station location and path, the geographic latitude and longitude of the intersection of the path with the 400-km height level can be determined by the use of spherical triginometry.

The dipole model may be described by assuming a scalar magnetic potential V given by $V = -M (\cos \theta)/r^2$, where M is dipole magnetic moment, θ is the angle measured from the dipole axis, and r is the distance from the center of the Earth. Then $\mathbf{F} = -\nabla V$, where **F** is the total magnetic flux density vector and has a vertical component Z given by $Z = \partial V/\partial r = 2M (\cos \theta)/r^3$ and a horizontal component H given by $H = (1/r)\, \partial V/\partial \theta = M (\sin \theta)/r^3$. The dipole axis should ideally pass through the observed north and south magnetic dip poles but their positions, which vary with time, are not directly opposite from each other or consistent with a purely dipole field. The north magnetic pole is near Ellef Ringnes Island in the Canadian arctic. The axis of the dipole model that best approximates the observed field overall intersects the Earth's surface at a different location, namely the north geomagnetic pole. The north geomagnetic pole is in Greenland, very close to the northwest coast. Its postion was taken to be 78.3 deg N and 69 deg W in 1965 (Davies, 1965). In a 1982 paper on the magnetic poles of the Earth, Dawson and Newitt (1982) give values of 78.8 deg N and 70.9 deg W.

Rather than specifying a value for M, the magnetic moment, the expression for Z and H can be given in terms of B_o, the magnetic flux density at the Earth's surface at the geomagnetic equator. The expressions then become

$$Z = 2 B_o (a/r)^3 \cos \theta \tag{A9.1}$$

and

$$H = B_o (a/r)^3 \sin \theta \tag{A9.2}$$

with

$$F = (H^2 + Z^2)^{1/2} \tag{A9.3}$$

where a is the Earth's radius (mean value about 6371 km). Substituting the expression for H and Z into Eq. (A9.3), it becomes

$$\begin{aligned} F &= B_o\,(a/r)^3\,(\sin^2\theta + 4\cos^2\theta)^{1/2} \\ &= B_o\,(a/r)^3\,(\sin^2\theta + 3\cos^2\theta + 1 - \sin^2\theta)^{1/2} \\ &= B_o\,(a/r)^3\,(1 + 3\cos^2\theta)^{1/2} \end{aligned} \tag{A9.4}$$

Equations (A9.1), (A9.2), and (A9.4) refer to the angle θ measured from the polar axis, but for some purposes it is more convenient to use the magnetic latitude θ', which is measured from the magnetic equator. In terms of latitude θ', the expressions become

$$Z = 2\,B_o\,(a/r)^3 \sin\theta' \tag{A9.5}$$

$$H = B_o\,(a/r)^3 \cos\theta' \tag{A9.6}$$

$$F = B_o\,(a/r)^3\,(1 + 3\sin^2\theta')^{1/2} \tag{A9.7}$$

If in Eq. (A9.7) F is held constant, it develops that the radial coordinate r corresponding to a particular value of F is given by

$$r = (B_o/F)^{1/3}\,a\,(1 + \sin^2\theta')^{1/6} \tag{A9.8}$$

The quantity F represents the magnitude of the total magnetic flux density. To obtain a plot showing the direction of the magnetic flux density vector (showing magnetic flux lines), note that the direction of the vector at a particular point is as indicated by

$$\frac{dr}{r\,d\theta} = \frac{Z}{H} \tag{A9.9}$$

where an increment of length along a field line, $d\ell$, has a component dr in the radial direction and a component $rd\theta$ in the horizontal direction. Rearranging Eq. (A9.9) leads to

$$dr/r = (Z/H)\,d\theta = 2\cot\theta\,d\theta \tag{A9.10}$$

Integrating this expression from the point on the geomagnetic equator where $r = ka$ to $r = r$ and from $\theta = \pi/2$ to θ

$$\int_{ka}^{r} \frac{dr}{r} = \int_{\pi/2}^{\theta} 2 \cot \theta \, d\theta$$

and

$$\ln (r/ka) = 2 \ln \sin \theta = \ln \sin^2\theta$$

from which

$$r = ka \sin^2\theta \qquad \text{(A9.11)}$$

or, in terms of latitude θ'

$$r = ka \cos^2\theta' \qquad \text{(A9.12)}$$

Note that a particular field line that crosses the equator at $r = ka$ will intersect the Earth's surface at $\cos \theta' = (1/k)^{1/2}$.

An additional parameter describing the Earth's magnetic field is the dip angle I which can be determined from

$$\tan I = Z/H = 2 \cot \theta = 2 \tan \theta' \qquad \text{(A9.13)}$$

To estimate the value of B_L for a particular path, one needs to determine the geographic coordinates of the point where the path intersects the 400-km height level. To make this determination, use can be made of Fig. A9.1 which is like Fig. 1.1 but with an additional radial line passing through the 400 km intercept at Z′. Also ψ of Fig. 1.1 is at its minimum value of 90 deg in Fig. A9.1.

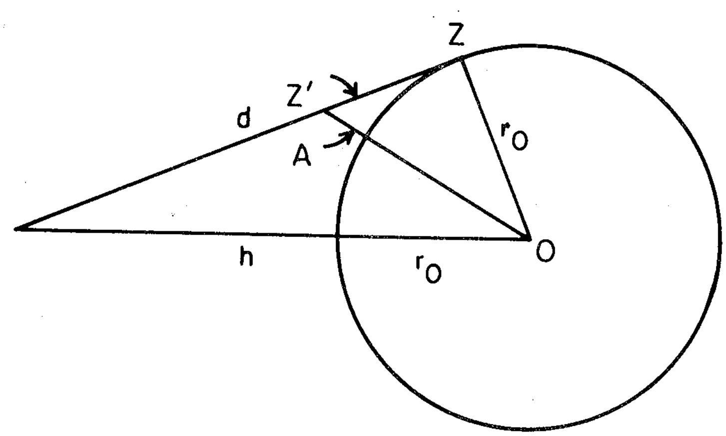

Figure A9.1. Geometry for determination of Z′.

The law of sines can be applied to the triangle ZZ′O resulting in

$$\frac{\sin\psi}{r_o + 400} = \frac{\sin A}{r_o} = \frac{\sin[\,180^o - \psi - (Z - Z')]}{r_o} \tag{A9.14}$$

The angle ψ can be calculated by use of Eqs. (1.13) and (1.15) and then Z', the only remaining unknown in Eq. (A9.14) , can be determined. If the satellite and earth station are at the same longitude, Z is the latitude of the earth station and Z' is the latitude of the 400-km intercept. If the satellite and earth station are not on the same longitude, both the latitude and longitude of Z' are different from those of Z. The latitude and longitude of Z' can be determined by referring to spherical triangles like those of Fig. 1.2, a reference triangle showing Z and a smaller triangle for Z', with Z' a shorter distance from the subsatellite point than Z. In particular one can use

$$\sin\phi' = \sin Z' \sin\alpha \tag{A9.15}$$

and

$$\sin\theta' = \tan\phi' \cot\alpha \tag{A9.16}$$

where α is determined by use of Eq. (1.17). Note that the two triangles are like two plane triangles in that the angle α is the same for both. Also note the θ' is latitude, an angle measured from the equator, whereas ϕ' is an angle measured from the subsatellite point and not longitude but a difference in longitude.

Having the geographic coordinates of the earth station, the 400-km intercept, and the satellite, one can obtain the corresponding geomagnetic coordinates by use of

$$\sin\theta'_m = \sin\theta'_g \sin\theta'_p + \cos\theta'_g \cos\theta'_p \cos(\phi_g - \phi_p) \tag{A9.17}$$

and

$$\sin\phi_m = \frac{\cos\theta'_g \sin(\phi_g - \phi_p)}{\cos\theta'_m} \tag{A9.18}$$

where the primes represent latitudinal quantities, θ'_m is the magnetic latitude of the location of interest, θ'_g is its geographic latitude, θ'_p is the geographic latitude of the north geomagnetic pole, ϕ_m is the magnetic longitude of the location of interest, ϕ_g is its geographic longitude, and ϕ_p is the geographic longitude of the north geographic pole.

Having expressed all quantities in magnetic coordinates [previously the subscript m was not used but Eqs. (A9.1) to (A9.13) are all in magnetic coordinates], one can obtain vector representations of d, the path from the earth station to the satellite and F, the total geomagnetic field at the 400-km intercept. One can then determine the angle between the magnetic field and the path at 400 km by using

$$Fd \cos \theta_B = \mathbf{F} \cdot \mathbf{d} \tag{A9.19}$$

where θ_B is the angle desired and $\mathbf{F} \cdot \mathbf{d}$ is the scalar dot product of vectors. The magnetic field F and the locations of the satellite (S) and the earth station (G) can be most conveniently described in spherical coordinates initially, but to find $\mathbf{d} = \mathbf{S} - \mathbf{G}$ and to take the dot product they are converted to rectangular coordinates by use of

$$\mathbf{a}_r = \sin\theta \cos\phi \, \mathbf{a}_x + \sin\theta \sin\phi \, \mathbf{a}_y + \cos\theta \, \mathbf{a}_z \tag{A9.20}$$

$$\mathbf{a}_\theta = \cos\theta \cos\phi \, \mathbf{a}_x + \cos\theta \sin\phi \, \mathbf{a}_y - \sin\theta \, \mathbf{a}_z \tag{A9.21}$$

for F and

$$x = r \sin\theta \cos\phi \tag{A9.22}$$

$$y = r \sin\theta \sin\phi \tag{A9.23}$$

$$z = r \cos\theta \tag{A9.24}$$

for the locations of the earth station and satellite. Note that in these expression θ is colatitude, the polar angle of spherical coordinates, rather than latitude θ'. Once the magnitude of F and the angle θ_B are known, one has B_L from

$$B_L = F \cos \theta_B \tag{A9.25}$$

CHAPTER 10

SPACE-COMMUNICATIONS SYSTEMS DESIGN

10.1 INTRODUCTION

10.1.1 Performance Requirements

The role of propagation phenomena in earth-space telecommunications system design is illustrated in this final chapter, and it appears desirable to include some related considerations about systems as well. The propagation loss L and system noise temperature T_{sys}, introduced in Chap. 1, appear in the link power budget equation, and reference to system design in this chapter refers primarily to link budgets. In earlier chapters, including Chap. 9, Estimation of Propagation Impairments, this handbook treats the additional topics of time and range delay, phase and Doppler frequency, and refractive bending. Also Chap. 8 is devoted to propagation effects on interference and determination of coordination area.

The system designer may have the function of meeting system requirements posed by the user, but in the process of attempting to do so it may develop that the requirements present problems and may need to be modified. The design of a complicated system like a telecommunications system is largely an iterative process, starting with a preliminary design, rather than a true synthesis. The amount of readily available information dealing specifically with system design is limited, but a useful treatment of the subject has been provided by Ippolito, Kaul, and Wallace (1983) in the final chapter of NASA Reference Publication 1082(03) for the design of systems operating at frequencies from 10 to 100 GHz.

Some minimum signal-to-noise ratio is needed for satisfactory operation of a telecommunications system, and information must be available or a decision must be reached in some way as to what this value is. [We will use C/X generally as in Eq. (1.6) for this ratio but certain related designations may be used instead in particular cases]. Because of the characteristics of the propagation medium, C/X tends to be a random variable and, as it is usually impractical to design a system so that C/X never drops below any particular level, a specification should normally be made of the permissable percentage of time for which C/X may be below the specified level. This specification defines the signal availability, namely the percentage of time that a specified C/X ratio should be available. Alternatively, or additionally, a specification may be made concerning outage, for example the mean outage duration, the time until the next outage, etc. In some cases the statistical nature of the phenomena affecting C/X may not be known, and it may not be possible to design a system to have a specified availability or outage characteristic. In such cases, one may nevertheless need to estimate the margins that should be provided for the phenomena under consideration as best one can. For example, a margin of so many dB must be allotted in some cases to take account of ionospheric scintillation even though a satisfactory statistical description of the scintillation may not be available.

10.1.2 Digital Systems

For digital systems performance is generally measured in terms of the bit error rate (BER), and the BER is a function of the energy-per-bit to noise-power-density ratio E_b/N_o. (When referring specifically to digital systems, we will use N_o in place of the X_o of Chap. 1 and elsewhere). The energy per bit E_b is related to carrier power C by $E_bR = C$, where R is the information rate in bits per second. Therefore

$$E_b/N_o = C/(N_oR) \tag{10.1}$$

Also

$$\frac{E_b}{N_o}\frac{R}{B} = \frac{C}{X} \tag{10.2}$$

Equation (10.2) shows that if bandwidth B equals bit rate R, $E_b/N_o = C/X$. The ratio R/B depends on the type of modulation and coding used. For uncoded binary phase-shift modulation (BFSK) employing phase values of 0 deg and 180 deg, B may be equal to R. For uncoded quadriphase modulation (QFSK) employing phase values of 0, 90, 180, and 270 deg, the bandwidth B may be only half the bit rate, as for each phase there are two corresponding bits (Feher, 1983; Freeman, 1981). Coding of digital transmissions is used as a means of minimizing errors or to reduce the needed E_b/N_o ratio and therefore the power C needed for a fixed BER. Coding involves adding redundant symbols to an information symbol sequence and requires additional bandwidth beyond that of the original uncoded signal. The ratio of the number of information bearing symbols to the total number is known as the rate of the code and has values such as 3/4, 2/3, etc., with 1/3 usually being the minimum value of the rate that is used. The two principal types of error-correcting codes are block codes and convolutional codes (Feher, 1983; Pratt and Bostian, 1986). FEC (forward-error-correction) codes have application to ameliorating the effect of attenuation due to rain, for example (Ippolito, 1986). When using coding in this way, a small amount of system capacity may be held in reserve and allocated as needed for links experiencing attenuation. The link data rate remains constant when following this procedure, the additional capacity being used for coding, or additional coding. Although block codes may be used in some cases, convolutional codes have the advantages for satellite communications of ease of implementation and availability of attractive decoding schemes (Van Trees, 1979). Convolutional coding and Viterbi decoding (Heller and Jacobs, 1971) are an effective combination. The performance of a Viterbi decoder depends upon the rate R, the number K of consecutive information bits encoded (e.g. 4, 6, or 8), the levels of quantization Q (1 to 8), and path length (e.g. 8, 16, or 32 bit). Figure 10.1 shows illustrative plots of BER versus E_b/N_o for convolutional coding and Viterbi decoding and for no coding.

10.1.3 Analog Systems

The allowable noise in analog systems used for voice communications may be specified in pW0p, standing for noise power in picowatts (pW) at a point of zero relative level (0) with psophometric weighting (p) utilized. We consider here how the system designer, given the permissable value of pW0p, can determine the corresponding C/X ratio.

In Recommendation 353-5, the CCIR (1986a) advises that the noise power at a point of zero relative level in any telephone channel used in FDM-FM (frequency division multiplex-frequency modulation) telephony in the fixed satellite service should not exceed the following values:

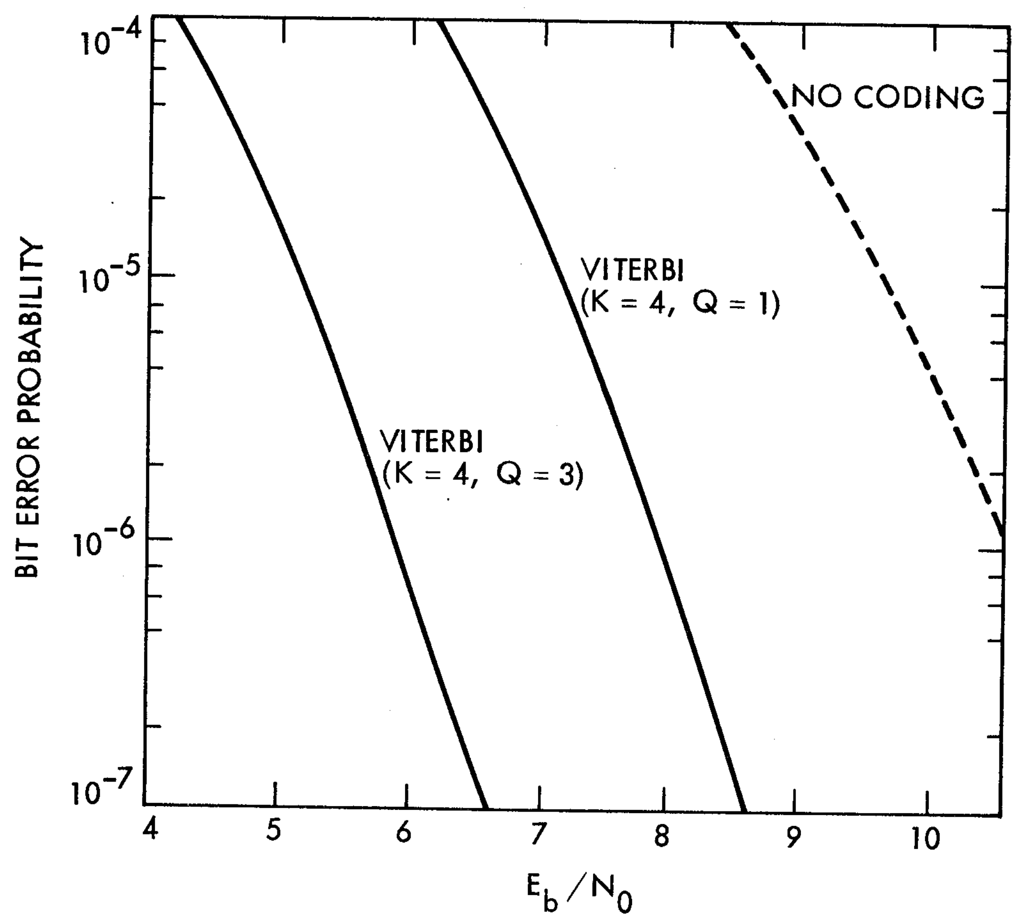

Figure 10.1. Bit error rate versus E_b/N_o (Van Trees, 1979).

10,000 pW0p for psophometrically-weighted one-minute mean power for more than 20 percent of any month

50,000 pW0p for psophometrically-weighted one-minute mean power for more than 0.3 percent of any month

1,000,000 pW0 for unweighted power (with an integration time of 5 ms) for more than 0.01 percent of any year

For RF levels above the FM threshold (commonly 10 dB above the noise level), the noise expressed in pW0p can be related to carrier power by (GTE, 1972)

$$10 \log pW0p = -C_{dBm} - 48.6 + F_{dB} - 20 \log (\Delta f/f_{ch}) \quad (10.3)$$

where F is the receiver noise figure, Δf is the peak frequency deviation of the channel for a signal of 0 test tone level, and f_{ch} is the center frequency occupied by the channel in the baseband.

Solving for C_{dBm} and then subtracting $10 \log kT = 10 \log kT_o + F_{dB} = -174$ dBm $+ F_{dB}$ for $T_o = 290$ K, yields

$$(C/X_o)_{dB} = (C/kT)_{dB} = 125.4 - 20 \log (\Delta f/f_{ch}) - 10 \log pW0p \quad (10.4)$$

For determining C/X, use $X = X_oB$ where B is bandwidth. Values of $20 \log (\Delta f/f_{ch})$ are given in GTE (1972) as -1.82 dB for an 120-channel system with emphasis, -9.2 for a 300-channel system with emphasis, etc.

10.1.4 Allocation of Noise and Signal-to-Noise Ratio

A communication satellite system consisting of an uplink and a downlink is subject to thermal noise generated in the uplink and downlink, to intermodulation noise generated in the satellite transponder in an FDMA system, and to interfering signals which may be received on the uplink or downlink or both. Considering all the individual noise sources to be additive at the downlink receiver input terminal, the ratio of carrier power C to total noise power density $(X_o)_T$ is given by

$$\frac{C}{(X_o)_T} = \frac{C}{(X_o)_U + (X_o)_D + (X_o)_{IM} + (X_o)_I} \tag{10.5}$$

where $(X_o)_D$ is generated in the downlink, $(X_o)_{IM}$ represents intermodulation noise, and $(X_o)_I$ represents interference. The quantity $(X_o)_U$ is derived from but is not equal to the noise $(X'_o)_U$ at the satellite (uplink) receiver input terminal. The relation between the two quantities is $(X_o)_U = (X_o)_U\, g/L_t$ where g is gain of the satellite transponder and L_t is the total downlink loss factor, defined so as to be greater than unity. Starting from Eq. (10.5), it can be shown by algebraic manipulation that

$$\frac{1}{(C/X_o)_T} = \frac{1}{(C/X_o)_U} + \frac{1}{(C/X_o)_D} + \frac{1}{(C/X_o)_{IM}} + \frac{1}{(C/X_o)_I} \tag{10.6}$$

The ratio $(C/X_o)_T$ appears at the downlink receiver input terminal; the ratio $(C/X_o)_D$ would be observed at this location if the input signal for the downlink was noiseless and interference was negligible. If one knows the values of all of the terms of Eq. (10.6) but one, that unknown quantity can be determined from Eq. (10.6).

The allowable noise of 10,000 pW0p is separated in the INTELSAT system noise budget into the three major categories shown below.

Space segment	8,000 pW0p
Earth stations	1,000 pW0p
Terrestrial interference	1,000 pW0p
Total noise	10,000 pW0p

Noise allotted to the space segment includes noise generated in the uplink and downlink, intermodulation noise generated in the satellite transponder, and interference other than terrestrial interference.

10.2 DIVERSITY RECEPTION

Diversity reception of several types, most prominently site diversity, space diversity, and frequency diversity, may be advantageous for particular applications. For satellite communications site diversity can be used to reduce the effect of attenuation due to rain. Site diversity takes advantage of the fact that high rain rates tend to occur only over areas of limited extent. For example, the probability that rain rates greater than 50 mm/h will occur jointly at two locations 20 km apart is reported to be about 1/15th the probability that the rate will occur at one location (Miya, 1981). Most interest in site diversity is directed to frequencies above 10 GHz for which attenuation due to rain is most severe (Ippolito, Kaul, and Wallace, 1983). For terrestrial line-of-sight paths, space and frequency diversity are used to combat fading due to atmospheric multipath and reflections from surfaces (GTE, 1972). The form of space diversity most commonly used involves vertical separation of two receiving antennas on the same tower.

The performance of a diversity system can be characterized by diversity gain and diversity advantage, which are shown in Fig. 10.2. Diversity gain is the difference, for the same percentage of time, between the attenuation exceeded on a single path and that exceeded jointly on two paths to two sites. Diversity advantage is defined as the ratio of the percentage of time that a given attenuation is exceeded on a single path to that exceeded jointly on two paths.

Site diversity to minimize the effects of attenuation due to rain may be useful for critical applications at frequencies below 10 GHz but must be weighed against the alternative of providing a margin to cover the expected attenuation. For the higher attenuations that tend to occur at higher frequencies, the advantage is more apt to be on the side of site diversity. Likewise, site diversity may be helpful on low-angle paths where atmospheric multipath or reflections from sea or land surfaces are a problem. An example of this type is provided by the Canadian arctic where, in the 6/4 GHz band, a site diversity system involving two receiving sites is expected to reduce the required propagation margin from 20 to 8 dB (Mimis and Smalley, 1982).

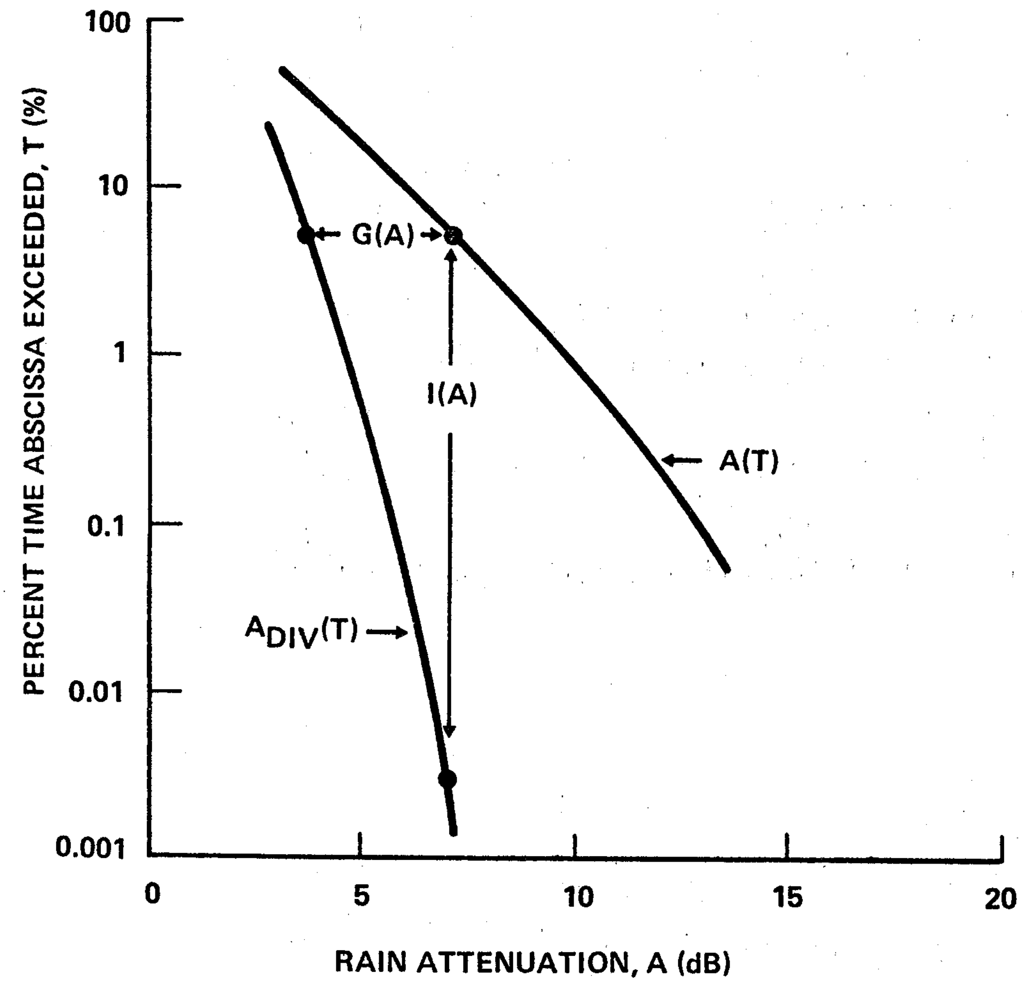

Figure 10.2. Definition of diversity gain G(A) and diversity advantage I(A). The curve A(T) represents performance when only one path is employed, while $A_{DIV}(T)$ represents performance when two paths are employed in a diversity system (Ippolito, Kaul, and Wallace, 1983).

10.3 TELECOMMUNICATION LINK BUDGETS

The link power budget equation gives the received signal-to-noise ratio in terms of all the various parameters that affect it. Two of these, loss factor L and system noise temperature T_{sys}, tend to be random variables. The object of system design is to ensure a satisfactory signal-to-noise ratio for a specified high percentage of time. The equation can be written in terms of $C/X_o = (C/kT_{sys})$ where C is carrier power (W) and k is Boltzmann's constant (1.38×10^{-23} J/K). This ratio C/X_o is the carrier power to noise density ratio, as X_o is the power per Hz. To obtain C/X from C/X_o, one can simply divide by B, the bandwidth in Hz. The quantity C/X_o was introduced in Chap. 1 where it was first written in the form of

$$\frac{C}{X_o} = \frac{C}{kT_{sys}} = \frac{EIRP\ G_R}{L\, L_{FS}\, k\, T_{sys}} \tag{10.7}$$

where EIRP stands for effective isotropic radiated power, G_R is the gain of the receiving antenna, L is a loss factor greater than unity if truly representing a loss, and L_{FS} is the free space basic transmission loss. The propagation medium plays a major role in determining L and T_{sys}. In carrying out satellite telecommunication systems design, attention must be given to both the uplink and the downlink; they both affect the C/X_o ratio observed at the downlink receiver input terminal.

For applying Eq. (10.7), we separate EIRP into the product of P_T and G_T and convert to decibel values as is customary, with the result that

$$\begin{aligned}(C/X_o)_{dB} = {} & (P_T)_{dB} + (G_T)_{dB} + (G_R)_{dB} - L_{dB} \\ & - (L_{FS})_{dB} - k_{dBW} - (T_{sys})_{dB}\end{aligned} \tag{10.8}$$

where for k we actually use Boltzmann's constant k times 1 K times 1 Hz to obtain a quantity in dBW. Then T_{sys} and bandwidth B when it is utilized are treated as nondimensional. But G_R and T_{sys} are often combined into one term which is considered a figure of merit. Using this combination and also reverting back to EIRP

$$(C/X_o)_{dB} = (EIRP)_{dB} + (G_R/T_{sys})_{dB} - L_{dB} - (L_{FS})_{dB} - k_{dBW} \tag{10.9}$$

The treatment of telecommunication link power budgets here is primarily by example. The first example, 10.1, illustrates some of the basic types of calculations pertinent to link budgets, and the second example deals with a hypothetical system operating at 8.5/8.0 GHz. Following examples deal with particular systems using values quoted in the literature.

Example 10.1 System Concepts

1. System Noise Temperature, T_{sys}

The system noise temperature T_{sys} is a measure of noise power as X_o, the noise power per Hz, equals kT_{sys} where k is Boltzmann's constant (1.38×10^{-23} J/K). Also X, the total noise power, equals X_o times bandwidth B. System noise temperature is defined at the antenna terminal of a receiving system as shown in Fig. 10.3, which shows an antenna having a noise temperature of T_A, a lossy transmission line at the standard reference temperature T_o (commonly taken as 290 K), and a receiver having a noise temperature of T_R.

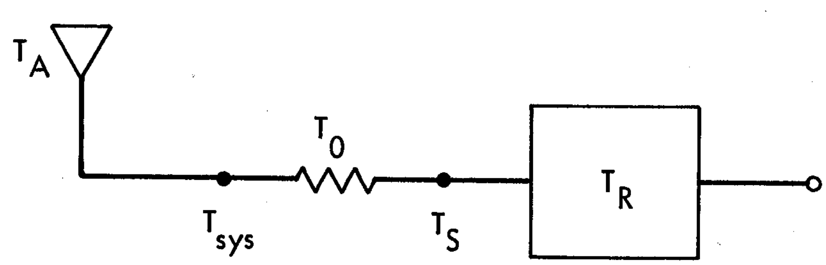

Figure 10.3. Receiving system, showing location of T_{sys}.

For the receiving system of Fig. 10.3, T_{sys} is given by

$$T_{sys} = T_A + (\ell_a - 1)T_o + \ell_a T_R$$

To illustrate the calculation of T_{sys}, let T_R equal 100 K and T_A = 50 K, and consider that the transmission line has a loss of 1 dB. In the expression for T_{sys}, $\ell_a = 1/g_a$ where g_a is less than unity and is the power "gain " of the transmission line, considering it as a lossy attenuator. The relation between g_a and attenuation A in dB is

$$-A_{dB} = 10 \log g_a$$

and for A = 1

$$-1 = 10 \log g_a, \quad g_a = 0.794, \quad \ell_a = 1/g_a = 1.26$$

Substituting values into the expression for T_{sys}

$$\begin{aligned} T_{sys} &= 50 + (1.26 - 1)\ 290 + 1.26\ (100) \\ &= 50 \quad + \quad 75.4 \quad + 1.26 \\ &= 251.4 \text{ K} \end{aligned}$$

Note that if there were no attenuation between the antenna and receiver, g_a and ℓ_a would equal unity and T_{sys} would equal $T_A + T_R$ = 150 K.

The noise power density X_o corresponding to T_{sys} = 251.4 K is given by

$$X_o = kT_{sys} = (1.38 \times 10^{-23})\ (251.4) = 3.47 \times 10^{-21} \text{ W}$$

and

$$(X_o)_{dB} = 10 \log (3.47 \times 10^{-21}) = -204.6 \text{ dBW}$$

Also

$$(X_o)_{dBm} = -174.6 \text{ dBm}$$

The quantity X_o is 204.6 dB below one watt (W) and 174.6 dB below one milliwatt (mW).

2. Antenna gain, G

The gain of an antenna having an effective aperture area, A_{eff}, is given by

$$G = (4\pi A_{eff})/\lambda^2$$

where λ is wavelength. The effective area for the antenna aperture considered here equals the geometric area times an efficiency factor κ which generally falls between about 0.5 and 0.7 or higher. To illustrate the calculation of G consider a frequency of 3 GHz, a paraboloidal antenna having a diameter of 3 m, and an efficiency factor of 0.54. The wavelength $\lambda \simeq 3 \times 10^8/(3 \times 10^9) = 0.1$ m and

$$A_{eff} = (\pi d^2/4)\ \kappa = \pi(9/4)\ (0.54) = 3.817\ m^2$$

Thus

$$G = 4\pi\ (3.817)/0.01 = 4{,}797$$

$$G_{dB} = 10 \log G = 36.8$$

3. Distance and elevation angle of geostationary satellite

Consider an earth receiving station at 65 deg N and a geostationary satellite on the same meridian. The distance d betweeen the station and the satellite is given by Eq. (1.13).

$$d^2 = r_o^2 + (h + r_o)^2 - 2r_o\ (h + r_o) \cos \theta'$$

where r_o is the earth radius, h is the height of the satellite above the Earth, and θ' is latitude (65 deg in this example). Thus

$$d^2 = (6378)^2 + (35786 + 6378)^2 - 2(6378)(35786 + 6378) \cos 65^o$$

$$d = 39{,}889.6 \text{ km}$$

To determine the elevation angle θ, the following expression can be solved for ψ which equals the elevation angle θ plus 90 deg.

$$(h + r_o)^2 = d^2 + r_o^2 - 2\ r_o d \cos \psi$$

$$(42{,}164)^2 = (39.889.6)^2 + (6378)^2 - 2(6378)(39{,}889.6) \cos \psi$$

$$\cos \psi = -0.2868, \quad \psi = 106.67^o$$

$$\theta = 106.67^o - 90^o = 16.67^o$$

If the earth station were displaced by 10 deg from the longitude of the satellite then in place of $\cos\theta' = \cos 65$ deg $= 0.4226$ one would use $\cos 65$ deg $\cos 10$ deg $= 0.4162$. The result would be that $d = 39{,}932$ km and $\theta = 16.24$ deg. If the difference in longitude were 20 deg, the distance would be 40,060 km and the elevation angle would be 15.0 deg.

Example 10.2 Link Power Budget Equation for Hypothetical 8.5/8.0 GHz System

For an example of a link power budget, consider a hypothetical analog system using 8.5 GHz for the uplink and 8.0 GHz for the downlink. The system has a performance objective of 99.99 percent availability in an environment in which a rain rate of 35mm/h is exceeded for 0.01 percent of the time. The elevation angle of the path is taken as 42 deg which allows using the results of Example 9.5 for attenuation due to rain. An earth-station antenna which would be suitable for a portable system is considered.

The distance d to the satellite corresponding to the elevation angle of 42 deg can be found from Eq. (1.15), namely

$$(h + r_o)^2 = d^2 + r_o^2 - 2r_o\, d \cos\psi$$

with $\psi = 42$ deg + 90 deg = 132 deg, and turns out to be about 37,600 km. Ordinarily one would start with a particular location to find the value of d and then find ψ, but here we have determined a value of d consistent with an elevation angle of 42 deg. Knowing d, $(L_{FS})_{dB}$, the free space loss can be determined from

$$(L_{FS})_{dB} = 20 \log (4\pi d/\lambda)$$

and is found to be 202.55 dB for 8.5 GHz and 202.02 dB for 8.0 GHz.

To formulate a link equation, some initial assumptions must be made about the equipment to be utilized, the required C/X ratio, the bandwidth, etc. The initial assumptions may need to be modified later. We assume a minimum overall or composite C/X ratio of 10 dB, a bandwidth B of 5 MHz, a 3-m earth-station antenna having an efficiency factor of 0.54, $T_{sys} = 300$ K for the earth station, and $G/T_{sys} = -10$ dB for the satellite.

Allowance is made for a carrier-to-interference ratio of 18 dB, as well as for thermal noise on the uplink and downlink. The C/X ratios for the uplink and downlink could be chosen to be equal, but it is easier to supply relatively high power for the uplink so a somewhat higher C/X ratio is chosen for it. The combination of $(C/X)_U = 15$ dB for the uplink, $(C/X)_D = 13$ dB for the downlink, and 18 dB for C/I gives an overall or composite ratio of 10.11 dB, thus satisfying the requirement of 10 dB. As ordinary numbers, the four ratios are 31.62, 19.95, 63.10, and 10.25, corresponding to 15, 13, 18, and 10.11 dB respectively, consistent with Eq. (10.6) without a contribution for intermodulation noise. The applicable equation is

$$1/(C/X)_T = 1/(C/X)_U + 1/(C/X)_D + 1/(C/X)_I$$

Substituting numbers

$$1/10.247 = 1/31.623 + 1/19.953 + 1/63.096$$

<u>Uplink (8.5 GHz)</u>

Attenuation due to rain is taken to be 2.49 dB (from Example 9.5), gaseous attenuation is assumed to be 0.1 dB, and the pointing error loss is taken as 0.3 dB. The gain of the transmitting antenna is calculated from $G_T = 4\pi A_{eff}/\lambda^2$ (Example 10.1, Sec.2) to be 38,558 or 45.86 dB. At this stage the needed transmitter power P_T can be determined by rearranging Eq. (10.9) to give

$$(EIRP)_{dBW} = (C/X_o)_{dB} + (L_{FS})_{dB} + L_{dB} + k_{dBW} - (G_R/T_{sys})_{dB}$$

where

$$(C/X_o)_{dB} = (C/X)_{dB} + B_{dB}$$

The bandwidth B is 5 MHz and $B_{dB} = 67$ dB. Thus

$$(C/X)_{dB} = 15 + 67 = 82 \text{ dB}$$

Substituting numbers into the equation for EIRP.

$$(EIRP)_{dBW} = 82 + 202.55 + 2.89 - 228.6 + 10 = 68.84 \text{ dBW}$$

where

$$(EIRP)_{dBW} = (P_T)_{dBW} + (G_T)_{dB}$$

so that

$$(P_T)_{dBW} = 68.84 - 45.86 = 22.98 \text{ dBW} \simeq 200 \text{ W}$$

The various system parameters are summarized in Table 10.1.

Table 10.1A Uplink (8.5 GHz).

Transmitter Power, P_T	22.98 dBW (200 W)	
Antenna Gain. G_T	45.86 dB	
EIRP		68.84 dBW
Free Space Loss, L_{FS}		202.55 dB
Losses, L		
Attenuation from rain	2.49 dB	
Gaseous attenuation	0.1 dB	
Pointing error	0.3 dB	
Total		2.89 dB
Satellite G_R/T_{sys}		-10 dB
C/X		15 dB
C/X_o		82 dB

Downlink (8.0 GHz)

The gain of the receiving antenna for the downlink (same antenna as for the uplink) is calculated to be 34,159 or 45.34 dB. The system noise temperature T_{sys} is taken to be 300 K or 24.77 dB above 1 K in the absence of attenuation due to rain, and the G_R/T_{sys} ratio is thus 45.34 - 24.77 = 20.57 dB. The assumed rain rate of 35 mm/h introduces an attenuation of 2.092 dB and an additional contribution to the antenna noise temperature given by

$$T_b = 280\ (1 - e^{-\tau}) = 280\ (1 - e^{-2.09/4.34}) = 107.1 \text{ K}$$

The total degradation in C/X due to rain is then given by

$$(C/X)_{dB} = 2.092 + 10 \log [\,(107.1 + 300)/300]$$
$$= 2.092 + 1.325 = 3.42 \text{ dB}$$

Gaseous attenuation of 0.1 dB and a pointing error loss of 0.3 dB are assumed. Solving for EIRP and P_T in the same way as for the uplink

$$(EIRP)_{dBW} = (C/X_o)_{dB} + B_{dB} + (L_{FS})_{dB} + L_{dB} + k_{dBW} - (G_R/T_{sys})_{dB}$$
$$= 13 + 67 + 202.02 + 3.82 - 228.6 - 20.57$$
$$= 36.67 \text{ dBW}$$

At this point it is necessary to have information on or to make an assumption about the gain of the transmitting antenna. Taking this gain G_T as 24 dB, the transmitter power P_T is given by

$$(P_T)_{dBW} = 36.67 - 24 = 12.67 \text{ dBW} \simeq 20 \text{ W}$$

System parameters are summarized in Table 10.1B.

Table 10.1B Downlink (8.0 GHz).

Transmitter Power, P_T	13 dBW (20 W)	
Antenna Gain, G_T	24 dB	
EIRP		37 dBW
Free Space Loss, L_{FS}		202.02 dB
Losses, L		
Attenuation due to rain	2.09 dB	
Gaseous attenuation	0.1 dB	
Pointing error	0.3 dB	
Total loss		2.49 dB

(continued on p. 10-17)

Antenna Gain, G_R	45.34 dB	
T_{sys}	24.77 dB (300 K)	
G_R/T_{sys}		20.57 dB
Increase in noise due to rain		1.32 dB
C/X		13 dB
C/X_o		80 dB

Example 10.3 Initial LMSS System

As an example in the UHF band, we consider an initial design for a Land Mobile Satellite System (LMSS) (Naderi, 1982). This system was planned for an 806-890 MHz allotment for satellite-mobile and mobile-satellite links and the S band for satellite-base station and base station-satellite links. As mentioned at the end of Sec. 1.2, the FCC authorized use of only the L band for land-mobile service in its decision of July 28, 1986, but the original design (uplink at 826 MHz and downlink at 871 MHz) nevertheless serves as an illustration of design, and we retain it in this second edition. At the time of writing, no L-band frequencies have actuallly been assigned nor have licenses for operation been issued.

For the UHF links, a design was prepared for a large (55-m) multibeam (87-beam) offset-reflector antenna on the satellite with separate beams formed by the use of 134 microstrip-patch feed elements excited in clusters of 7. The 87 beams would provide coverage of the entire conterminous 48 states of the United States. An original concept was that the satellite system would be compatible with cellular mobile radiotelephone service, but developments have not proceeded in that direction. At UHF, 95 voice channels would have been available per beam, each requiring a 10.2 kHz bandwidth with a 15 kHz channel separation and a total bandwidth per beam of 10 MHz. It was recognized, however, that the initial systems would have a much smaller number of beams and channels. The satellite-to-mobile link, initially planned for operation at 871 MHz, is the most critical of the links, and the power budget for this link is shown in Table 10.2A.

Downlink (871 MHz)

The required total or overall C/X ratio is taken to be 10 dB, and the system must be able to function with a C/I (carrier-to-interference ratio) of 17 dB   Analysis of intermodulation noise indicates that a 25 dB carrier-to-intermodulation noise ratio is expected. To initiate the link design process, a 20 dB $(C/X)_U$ ratio (carrier-to-thermal noise ratio for the uplink) is assumed. Using the relation of Eq. (10.6) but applying it to $C/X = C/(X_oB)$, it is determined that $(C/X)_D$ for the downlink must be 11.8 dB in order for the carrier-to-overall-noise ratio to be 10 dB (line 1). For designing the links, the process begins with the carrier-to-noise requirement at the receiver terminal and progresses backwards to find the needed transmitter power.

A number of the losses shown in Table 10.2A are equipmental in nature or due to the fact that the system is a mobile system. For example, a 4 dB loss is shown to account for a mobile receiver not being at the center of a beam but at a point of minimum signal (line 14). Also losses of 2 dB and 1 dB represent pointing losses for the mobile and satellite antennas respectively (lines 15 and 16). The mobile antenna has a maximum gain of only 5 dB and a correspondingly large beamwidth but the antenna may not always be pointed towards the satellite as the mobile moves uphill and downhill, etc. The satellite antenna has a pointing stability of 0.04 deg but at a point at the edge of the coverage area of a beam a pointing error of 0.04 deg could cause a loss of 1 dB.

For system noise temperature, the use of such a large antenna beamwidth for the mobile receiver indicates a minimum antenna temperature of 290 K. In addition it is considered that the LMSS must provide satisfactory performance in suburban areas where man-made noise would be encountered. A value of antenna temperature of 1.6 times 290 K or 464 K as suggested in the ITT handbook (ITT, 1968) is used for this reason (line 4). Taking into account also a receiver noise figure of 2 dB and 2.25 dB for input circuit losses gives a T_{sys} of 991 K or about 30 dB (relative to 1 K).

For propagation losses, the following considerations apply. At UHF frequencies, attenuation and depolarization due to precipitation are negligible. Circular polarization is used, and Faraday rotation is not a factor. Ionospheric scintillation is most severe at equatorial and auroral latitudes, and the design is for the conterminous 48 states. Table 9.3 gives data for mid-latitude fading due to ionospheric scintillation. The smallest percentage of time shown in the table is 0.1, for which the fade depth is 1 dB for 500 MHz and 0.3 dB for 1000 MHz. Thus the 800-900 MHz range is sufficiently high that scintillation effects should not be severe, and taking into account that a two percent probability of system overload was assumed an allowance for scintillation was not not included among the losses. For service at the lower latitudes of Hawaii, for example, an allowance would probably needed. Also observations of peak-to-peak scintillations of 18, 10, 15, and 3.5 dB at 136 MHz and 1.7, 4, and 14 GHz, respectively, in and around Japan (Minakoshi et al., 1981), indicate that ionospheric scintillation may need to be taken into account in some system designs at temperate latitudes if a high grade of service is required.

Mobile observations are subject to fading due to multipath propagation involving specular reflection from the Earth's surface or structures. Also, as specular reflection decreases due to surface roughness, diffuse scatter may become important. On the basis of measurements made by use of the ATS-6 satellite, a 5 dB margin for multipath effects was utilized in the original LMSS design. However, subsequent measurements (Sec. 6.4) have indicated that shadowing due to trees is a serious effect, and emphasis has shifted from multipath effects to shadowing. A margin of at least 10 dB would be needed to ameliorate effects of shadowing by trees.

Uplink (826 MHz)

For the uplink operating at 826 MHz, many of the same considerations apply. A 20 dB $(C/X)_U$ ratio at the satellite was assumed at the outset. This ratio is achieved by using a mobile antenna gain of 5 dB and a transmitter power per channel of 2.45 W or 3.9 dBW. The system noise temperature (line 4) is 580 K rather than 991 K. A principal reason for the difference is that the mobile receiver is assumed to operate in a 464 K noise environment whereas the satellite receiver is assumed to receive radiation from the Earth at 290 K. A fading allowance of 10 dB or more, rather than 5 dB, would actually be needed for shadowing, as on the downlink.

Table 10.2A LMSS Satellite-to- Mobile Link Budget.

Line	Parameter	Value	Comment
1	Downlink C/X	11.8 dB	At mobile receiver
2	IF Bandwidth, 10.2 kHz	40.1 dB	Channel spacing 15 kHz
3	C/X_o	51.9 dB	(1) + (2)
4	T_{sys} (991 K)	30.0 dB	464 K suburban noise, 2 dB receiver
5	Boltzmann's constant	-228.6 dB	
6	Misc. receiver loss	2.0 dB	
7	Needed received power	-147.7 dBW	(3) + (4) + (5) + (6)
8	Mobile antenna gain	5.0 dB	$G/T_{sys} = -25$ dB
9	Free space loss (f = 871 MHz)	182.8 dB	182.5 to 183.2 dB over U.S.
10	Transmitting antenna gain, G_T	50.0 dB	
11	Transmitting circuit losses	1 dB	
12	Control signal power	1 dB	
13	Fading (multipath)	5 dB	10 dB or more with shadowing
14	Edge of coverage	4 dB	
15	Mobile pointing loss	2 dB	
16	Satellite pointing loss	1 dB	
17	Scanning loss	0.5 dB	
18	Required transmitter power per channel	-2.2 dBW (0.6 W)	(7) - (8 + 10) + (9 + 11 through 17)
19	Average transmitter power per channel	-6.2 dBW (0.24 W)	40 percent voice activity factor

Table 10.2B LMSS Mobile-to-Satellite Link Budget.

Line	Parameter	Value	Comment
1	Uplink C/X	20.0 dB	At satellite receiver
2	IF bandwidth	40.1 dB	
3	C/X_o	60.1 dB	(1) + (2)
4	T_{sys} (580 K)	27.7 dB	290 K Earth, 2 dB receiver
5	Boltzmann's constant	-228.6 dBW	
6	Misc. receiver loss	1 dB	
7	Needed received power	-139.8 dBW	(3) + (4) + (5) + (6)
8	Satellite antenna gain	49.7 dB	G/T = 22 dB
9	Free space loss (f = 826 MHz)	182.4 dB	182.0 to 182.7 over U.S.
10	Transmitting antenna gain, G_T	5 dB	
11	Transmitting circuit losses	2.5 dB	
12	Control signal power	1 dB	
13	Fading (multipath)	5 dB	10 dB or more with shadowing
14	Edge of coverage	4 dB	
15	Mobile pointing loss	2 dB	
16	Satellite pointing loss	1 dB	
17	Scanning loss	0.5 dB	
18	Required transmitter power per channel	3.9 dBW (2.45 W)	

Example 10.4 Maritime Mobile System

This example involves L-band operation for the uplink from a ship to a MARISAT satellite and C-band operation for the downlink from the satellite to a ground station. The system parameters utilized in the example and shown in Tables 10.3A and 10.4B are taken from a paper dealing with application of the MARISAT system to the transmission of seismic data at 56 kbps from a ship or seismic vessel, with losses taken into account (Calvit and Heitman, 1981). Since the date of this paper, the INMARISAT system has replaced the original MARISAT system (Sec. 6.5).

Table 10.3A Ship to Satellite Uplink (1.6405 GHz)>

Transmitter Power, P_T	15.7 dBW	
Diplexer/Feed Loss	0.6 dB	
Antenna Gain, G_T	23.5 dB	
EIRP		38.6 dBW
Free Space Loss, L_{FS}		188.6 dB
Losses, L		
Wet Radome	0.5 dB	
Polarization Coupling	0.2 dB	
Atmospheric absorption	0.4 dB	
Total		1.1 dB
Satellite G_R/T_{sys}		-15.9 dB
C/N_o (carrier power to noise density ratio in digital system)		61.6 dB

The values in the table are consistent with Eq. (10.9), namely

$$(EIRP)_{dBW} - (L_{FS})_{dB} - L_{dB} - k_{dBW} + (G_R/T_{sys})_{dB} = (C/X)_{dB}$$

as can be checked by numerical sustitution, giving

$$38.6 \quad - 188.6 \ - 1.1 - (-228.6) - 15.9 \quad = 61.6$$

Next consider Table 10.3B for the downlink

Table 10.3B Satellite to Shore Station Downlink (4.197 GHz).

Satellite EIRP		2 dBW
Free Space Loss, L_{FS}		196.9 dB
Losses, L		
Atmospheric Absorption	0.3 dB	
Rain Attenuation	1.2 dB	
Polarization Coupling	0.4 dB	
Total		1.2 dB
Increase in T_{sys} Due to Rain		1.2 dB
Shore Station G_R/T_{sys}		33 dB
C/N_o		64.3 dB

Overall C/N_o Ratio

The overall or composite C/N_o value, neglecting interference, is found from

$$\frac{1}{(C/N_o)_T} = \frac{1}{(C/N_o)_U} + \frac{1}{(C/N_o)_D}$$

in which $(C/N_o)_U = 10^{6.16} = 1.445 \times 10^6$ and $(C/N_o)_D = 10^{6.43} = 2.96 \times 10^6$. The resulting value of $(C/N_o)_T$ is 9.333×10^5 or 59.7 dB.

The E_b/N_o ratio can then be found from $E_b/N_o = C/(N_oR)$ where R is the data rate, namely 56 kbps in this case. Carrying out the calculation in decibels, $10 \log (5.6 \times 10^4) = 47.5$ dB and

$$(E_b/N_o)_{dB} = 59.7 - 47.5 = 12.2 \text{ dB}$$

which is a satisfactory value, as it was determined that a bit error rate (BER) of better than 1×10^{-5} can be acheived with an E_b/N_o ratio above 5 to 6 dB.

A film of water on antenna or radome has the potential for creating a loss, and a loss of 0.5 dB was assigned for the condition of a wet radome on the uplink. A loss of 0.4 dB was assigned for atmospheric absorption on the uplink, at about 1.6 GHz. At this frequency, true absorption of this magnitude is improbable, but a reduction in signal amplitude of this magnitude associated with ionospheric scintillation could very likely occur. For the downlink at about 4.2 GHz, a generous allowance of 0.3 dB is provided for atmospheric absorption, 0.5 dB is assigned for attenuation due to rain, and 1.2 dB is assigned for the increase in noise due to rain. The basis for the rain effects is not stated but they correspond to intense rain such as might be exceeded in region D_3 of the United States for 0.01 percent of the time (63 mm/h) or slightly higher. A greater margin would be needed at 1.6 GHz for ionospheric scintillation at equatorial latitudes, and a larger margin would probably be needed for the degradation in signal-to-noise ratio on paths at elevation angles below 10 deg. It appears that the system actually had a larger margin than that specifically assigned. A practical consideration in shipboard operations is that ships are subject to large values of pitch and roll in high seas, and these motions can result in degradation in performance unless the antenna platform is extremely well stabilized. Also, as stated in Sec. 6.5 where maritime mobile systems are considered, fading problems are likely to be encountered at low elevation angles. Ohmori and Miura (1983) have described the use of a four-terminal hybrid combiner for use in overcoming this problem when using circular polarization and low-gain antennas which have low discrimination against specular reflection from the sea surface.

Example 10.5 Westar V

Westar V serves as an example of a C-band system, with the uplink operating at 6 GHz and the downlink operating at 4 GHz (Piraino and Schoen, 1982). Tables 10.4A and 10.4B give some of the parameters for the uplink and downlink. The system is a digital system having a bit error rate of 1×10^{-6} as a performance objective without encoding and 1×10^{-11} when rate-7/8 convolutional forward-error-correction (FEC) encoding is employed. The overall E_b/N_o required to meet these objectives is stated to be

14.5 dB. The various contributions to this ratio are 22.9 dB for the uplink, 18.6 dB for the downlink, 24.3 dB for adjacent satellite interference, 20.1 dB for cross-polarized transponders, and 23.0 dB for interference from terrestrial microwave systems. When these quantities are taken into account in a relation like that of Eq. (10.6), which is written in terms of ordinary numbers rather than decibel values, an overall E_b/N_o value of 14.3 dB (close to 14.5 dB) is obtained. The calculation is summarized in Table 10.4A.

Table 10.4A E_b/N_o Values for Westar V.

Category	dB	Numerical	Reciprocal
Uplink	22.9	194.984	0.00512861
Downlink	18.6	72.4436	0.0138038
Adjacent Sat.	24.3	269.153	0.00371535
Cross Pol.	20.1	102.329	0.00977237
Terrestrial	23.0	199.526	0.00501187
Overall (Total)	14.3	26.7171	0.0374320

Uplink (6 GHz)

Table 10.4B 6 GHz Uplink Budget.

Earth Station EIRP	79.0 dBW
Free Space Loss, L_{FS}	200.1 dB
Atmospheric Absorption	0.1 dB
Rain Attenuation	0.4 dB
Wind Effect on Antenna	0.3 dB
Transponder G_R/T_{sys}	-6.0 dB

The values of the table are consistent with Eq. (10.9), repeated below.

$$(C/N_o)_{dB} = (EIRP)_{dB} - (L_{FS})_{dB} - L_{dB} - k_{dBW} + (G_R/T_{sys})_{dB}$$

Substituting numbers

$$(C/N_o)_{dB} = 79.0 \quad - 200.1 \quad - 0.8 - (-228.6) - 6.0 = 100.7$$

Converting to $(E_b/N_o)_{dB}$ by subtracting R_{dB} with R, the bit rate being 60 Mbps,

$$(E_bN_o)_{dB} = (C/N_oR)_{dB} = 100.7 - 10 \log (6 \times 10^7)$$

$$= 100.7 - 77.8 = 22.9 \text{ dB}$$

<u>Downlink (4 GHz)</u>

Table 10.4C 4 GHz Downlink Budget.

Transmitter EIRP	33.3 dBW
Free Space Loss, L_{FS}	196.6 dB
Atmospheric Absorption	0.1 dB
Rain Attenuation	0.1 dB
Wind Effect on Antenna	0.2 dB
Increase in T_{sys} due to Rain	0.3 dB
Earth Station G_R/T_{sys}	31.8 dB

Substituting numbers into Eq. (10.() as was done following Table 10.4B,

$$(C/N_o)_{dB} = 33.3 - 196.6 - 0.7 - (-228.6) + 31.8 = 96.4$$

$$(E_b/N_o)_{dB} = 96.4 - 77.8 = 18.6 \text{ dB}$$

In the numerical relation, 0.7 represents the sum of atmospheric absorption, rain attenuation, wind effect on antenna, and increase in noise due to rain.

For both the uplink and downlink, the small reasonable allowance of 0.1 dB is made for atmospheric absorption. An allowance of 0.4 dB is made for rain attenuation on the uplink at 6 GHz and 0.1 dB for rain attenuation plus 0.3 dB for noise due to rain is assigned for the downlink. The basis for the attenuation values is not given, but the values are reasonable though less than those for the rain rate of 35 mm/h considered in Example 9.5. Effects due to rain at these frequencies are small but should still be included in the link equations.

10.4 A GRAPHICAL MARGIN-DESIGN PROCEDURE

Insight into choosing suitable uplink and downlink margins in the presence of rain can be obtained by use of a graphical procedure described by Calo, Schiff, and Staras (1978). Consider first Fig. 10.4 in which the curve illustrates the combination of uplink and downlink C/X ratios which can provide the needed total or composite C/X ratio (10 dB in this case) in the absence of rain. Equal C/X values of 13 dB for the uplink and downlink, for example, can provide the composite value of 10 dB.

Now consider how the curve would need to be modified for the presence of rain on the uplink of a TDMA (time-division-multiple-access) system. Numerical values will be used for purposes of illustration. If 3 dB of attenuation is expected to be encountered, with a probability of p percent of being exceeded where p is consistent with performance objectives, the original curve of Fig. 10.4 can be moved to the right by 3 dB in order to provide a margin of 3 dB for the uplink. In addition the output power of the satellite repeater, which serves as the transmitter power for the downlink, will have been reduced but, because of the nonlinear characteristic of traveling-wave tubes, by not necessarily the same amount as the reduction in input power. Assuming the reduction is 2 dB, the original curve can be moved upwards to compensate by 2 dB, corresponding to increasing the downlink power and therefore the downlink C/X ratio by 2 dB. In Fig. 10.5, the curve of Fig. 10.4 is redrawn and labeled A and the curve obtained by an upward movement of 2 dB and movement to the right of 3 dB is labeled as B. Next consider rain causing attenuation of 3 dB on the uplink. Whereas the receiving antenna of the uplink is commonly assumed to receive noise corresponding to 290 K from the Earth (but see Fig.

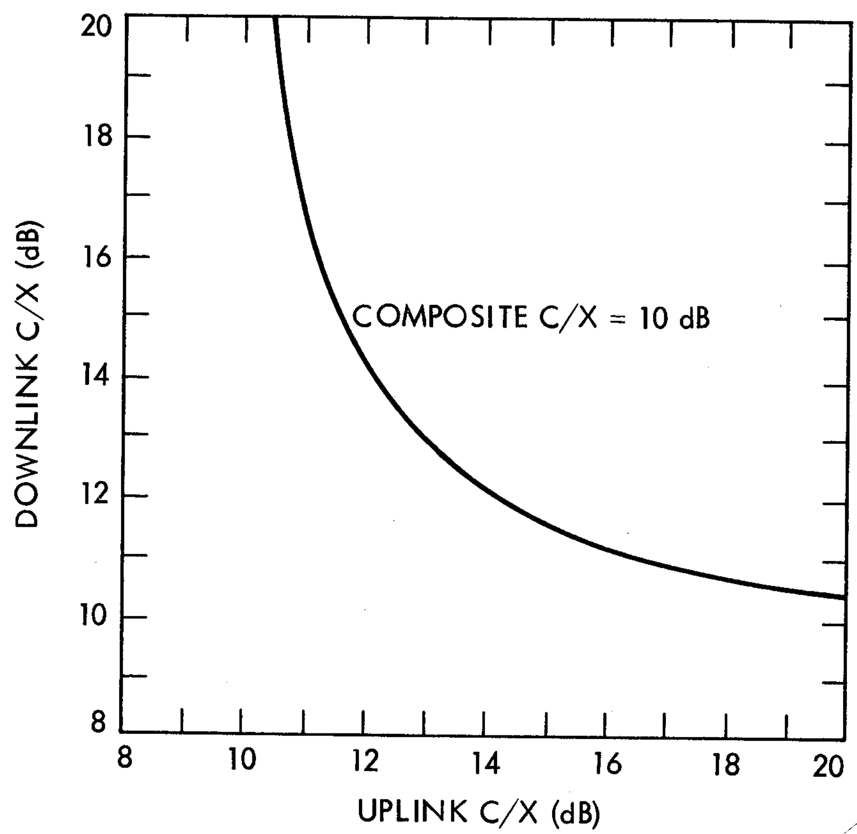

Figure 10.4. Values of downlink and uplink C/X ratios that give a composite ratio of 10 dB in the absence of attenuation.

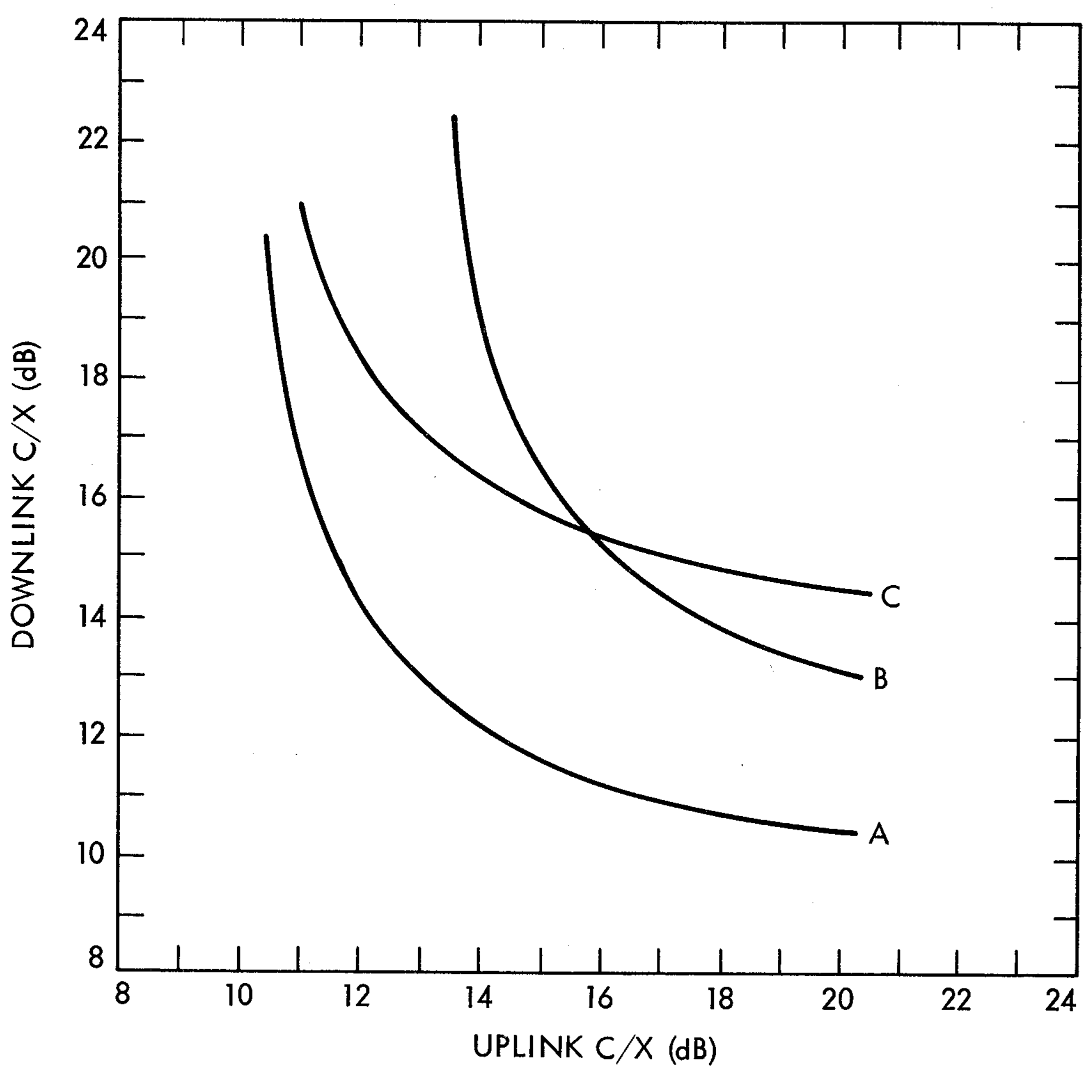

Figure 10.5. Illustration of graphical procedure for determining downlink and uplink C/X ratios such that the composite ratio will be satisfactory when propagation impairments caused by rain are encountered.

7.14), whether there is rain or not, the receiving antenna of the downlink receives additional noise when there is rain along the path. Take the increase in noise to be 2 dB so that the total degradation in C/X ratio for the downlink is 4 dB. To compensate for this degradation, the original curve A can be moved upwards by 4 dB to form curve C which therefore includes a margin of 4 dB. The point where curves B and C intersect now corresponds to C/X values providing sufficient margins to accommodate simultaneous rain causing attenuations as indicated for both the uplink and downlink. Assuming the probabilities of such rain rates are independent, however, the accommodation is now for all but 2p percent of the time rather than for all but p percent. Although the point of intersection of curves B and C may give suitable C/X values for the uplink and downlink, it may be desirable to choose a point slightly to the right along curve C so that C/X for the uplink is slightly higher than previously for the uplink than for the downlink.

10.5 COVERAGE AREA

It may be necessary in system design to provide for service over a given, possibly extensive, geographical area rather than for only a particular earth station. The relation betwen the service or coverage area, A_{cov}, and system parameters, including C/X_o, is shown in Eq. (1.11), from which k and other numerical factors were eliminated. The relation is repeated below but with k and κ_{ant}, the antenna efficieny factor, reinserted

$$A_{cov}(C/X_o) \simeq \frac{P_T A_R \kappa_{ant}}{k\, T_{sys}\, L} \tag{10.10}$$

The relation is still shown as only an approximation for a reason to be explained in the course of deriving the expression. To derive Eq. (10.10) one can start with Eq. (10.7). In this expression make the substitutions $L_{FS} = (4\pi d/\lambda)^2$, $G_R = 4\pi A_R/\lambda^2$, and $G_T = \kappa_{ant} 4\pi/\Omega_A$ where A_R is the effective area of the receiving antenna and Ω_A is the solid angle of the transmitting antenna beam. Note that $4\pi/\Omega_A$, with Ω_A in rad^2 or steradians, represents antenna directivity by definition and that directivity times antenna efficiency equals gain. After making these substitutions the resulting expression for C/X_o is

$$(C/X_o) = \frac{P_T \kappa_{ant} A_R}{\Omega_A d^2 L k T_{sys}} \tag{10.11}$$

By definition the solid angle Ω_A subtended at a point by an area $A_\perp$ that is perpendicular to the line of sight from the point at a distance d is given by

$$\Omega_A = \frac{A_\perp}{d^2} = \frac{\int \mathbf{a}_r \cdot d\mathbf{S}}{d^2} \tag{10.12}$$

If $A_\perp$ is identified as A_{cov} and Ω_A of Eq. (10.11) is set equal to A_{cov}/d^2, Eq. (10.10) is obtained. The equation is an approximation and possible a rough one because A_{cov} is not strictly perpendicular to the line of sight except in the vicinity of the subsatellite point. But if that limitation is taken into account, Eq. (10.10) shows correctly that, with other parameters held constant, it takes more power to provide coverage over a large area than over a smaller area.

Contours of constant EIRP and G_R/T_{sys} for Westar IV and V are shown in Figs. 10.6 and 10.7, respectively. These satellites provide coverage over the entire United States, with an EIRP for downlink transmission at 4 GHz of 34 dBW for the adjacent 48 states and with smaller values of EIRP for Alaska, Hawaii, and Puerto Rico. Fig. 10.7 shows that G_R/T_{sys} for the uplink at 6 GHz has a value of −6.0 dB for the adjacent 48 states.

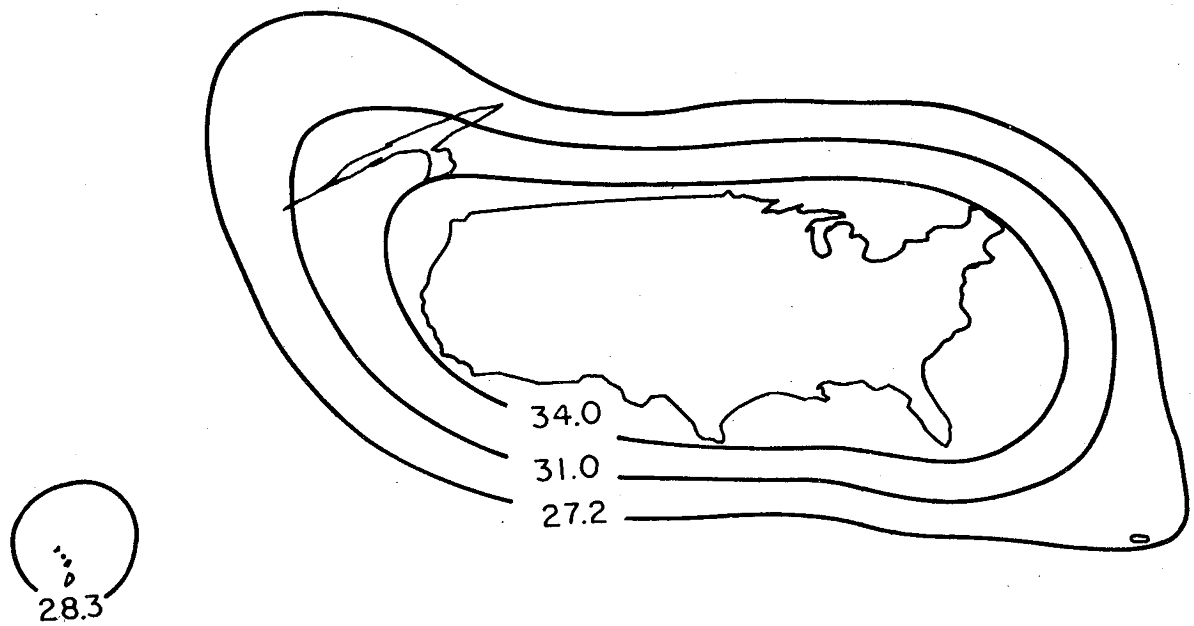

Figure 10.6. EIRP contours for Westar IV and V at 4 GHz.

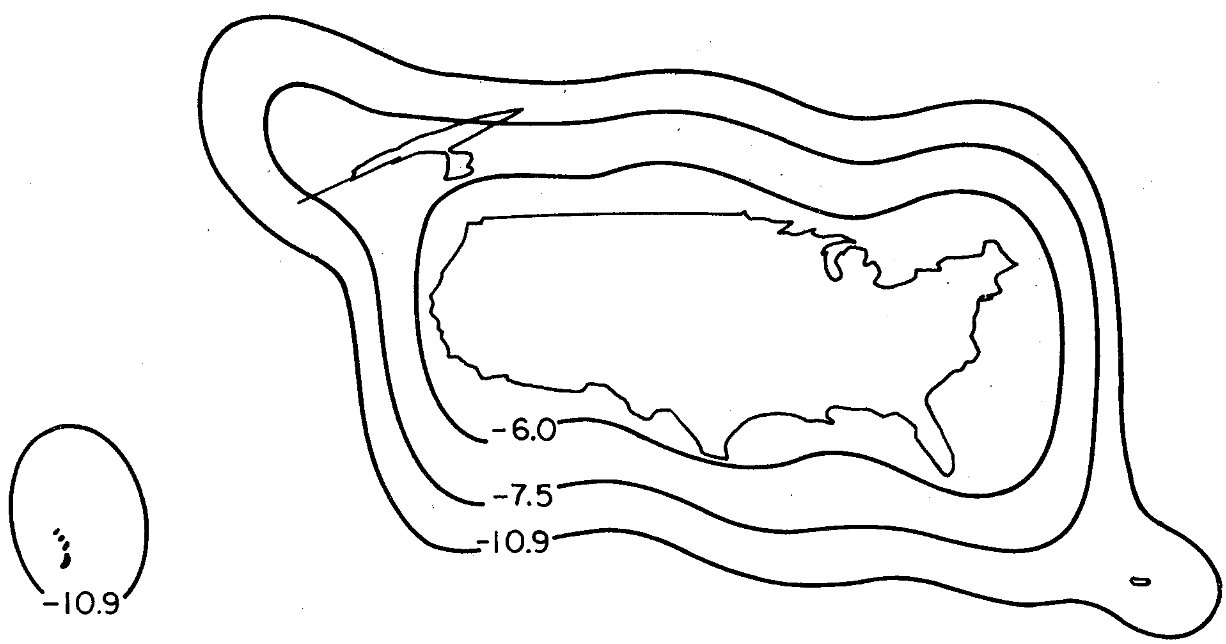

Figure 10.7. Contours of $G_R T_{sys}$ for Westar IV and V at 6 GHz.

c - 6

10.6 COMPANDED SSB SYSTEMS

As mentioned in Sec. 6.3.3., companded single-sideband systems (SSB systems) use spectrum efficiently and have an advantage with respect to signal-to-noise ratio for analog audio signals. The interest in that section was in the use of a pilot tone for reducing the unwanted amplitude and phase modulation introduced by fading. Companded systems involve the use of a compressor at the transmitter and an expandor at the receiver. These compress and expand the dynamic range of the signal. A zero level is unaffected by the compression and expansion, but signals having greater or smaller amplitudes are affected. Compression generally reduces the dynamic range to one half of the original range, and expansion by a factor of two than restores the signal to its original range (Fig. 10.8). In a noiseless system, this would be the only effect; the receiver-output signal would simply be the same as the transmitter-input signal. In a practical noisy system, however, the signal-to-noise ratio at the receiver input is considerably less than that at the transmitter output. Assume that the noise level at the receiver input in gaps between syllables, words, and sentences is -25 dB relative to the zero reference level. After expansion, however, the corresponding noise level is -50 dB. Thus companding produces an improvement in the subjective or apparent signal-to-noise ratio. The word "apparent" is used because the improvement cannot be measured by instruments but is apparent to the listener. It is rather difficult to decide what value to assign to this improvement. Values in the range from about 6 to 16 dB have been seriously considered, and the present trend appears to be to use values of about 10 or possibly slightly greater.

Another characteristic of the companding process is that average power level is increased by compression with respect to that of the input audio signal. To obtain a quantitative estimate of the amount of increase, use can be made, both before and after compression, of

$$L = L_s + 0.1125\,\sigma^2 + 10 \log \tau \qquad (10.13)$$

(Bell Tel. Labs., 1971; Jonnalagadda and Schiff, 1984). In this expression L is the average talker power, σ is the standard deviation of active speech power, and τ is the duty factor of speech. L_s is the mean power of a distribution of talkers. L and L_s differ because the normal distribution for which L_S is the mean is a distribution in dB values, whereas L is the average of the corresponding distribution of actual power. To illustrate the increase in power let L_S = -20 dBm0 and σ = 4.8 dB at the compressor input. Also letting $\tau = 0.35$ and $L = L_1$

$$L_1 = -20 + 0.115\,(4.8)^2 + 10 \log 0.35$$

$$= -21.9 \text{ dBm0}$$

After compression, however, the average talker level is given by

$$L_2 = -10 + 0.115\,(2.4)^2 + 10 \log 0.35$$

$$= -13.9 \text{ dBm0}$$

Using X to stand for the increase in power level

$$X = -13.9 - (-21.9) = 8 \text{ dB}$$

Performance of such systems can be analyzed in terms of test-tone to noise-power ratio, T_T/N, for a 0-dBm0 signal at the receiver input, after transmission over a radio-frequency link. This ratio can be expressed in terms of signal-to-noise ratio S/N, the companding improvement ratio A, and the levels L_1 and L_2 by (Jonnalagadda, 1982)

$$T_T/N = S/N + A - (L_1 + X) = S/N + A - L_2 \qquad (10.14)$$

The value of T_T/N is generally required to be 51 dB. Using 51 for T_T/N, 12 for A, and the values for L_1 and L_2 given above

$$51 = S/N + 12 - (-21.9 + 8) = S/N + 12 + 13.9$$

and the necessary S/N ratio is 25.1 dB. If a companding advantage of 12 is truly applicable, the S/N ratio can be 12 dB less than it would otherwise need to be. To justify the above expression for T_T/N , it needs to be recognized that T_T/N must be 51 dB for a 0-dBm0 signal whereas the actual signal level of this example is -13.9 dBm0 (13.9 dB below that for a 0-dBm0 signal). Assuming the system to be satisfactory if T_T/N is 51 dB for a 0-dBm0 signal means that it is also satisfactory for S/N to be lower by 13.9 dB for a −13.9 dBm0 signal. The two factors of A and $-L_2$ result in a value of 25.1 dB being satisfactory for S/N.

The value of L_1 of −21.9 dBm0 used above is lower than what has been the CCIR recommended value of −15 dBm0 because recent studies of average talker level have shown the level to be lower (Jonnalagadda, 1982). If psophometric weighting is utilized a factor of w dB (with w = 2.5 dB) can be added with the result that the needed value of S/N is reduced further to 22.6 dB for A = 12. In that case the subjectively perceived signal-to-noise ratio is higher by A + w = 12 + 2.5 = 14.5 dB than S/N.

SSB satellite systems are subject to intermodulation noise, which is developed in the transmitting amplifiers of satellites. The newer solid-state power amplifiers (SSPA) are more nearly linear and thus generate less intermodulation noise than traveling-wave-tube amplifiers (TWTA). Analysis for an uplink can be carried out in terms of flux density ϕ at the satellite where

$$\phi = \frac{(EIRP)_e}{4\pi d^2} \tag{10.15}$$

with $(EIRP)_e$ referring to the earth station EIRP and d the distance from the earth station to the satellite. A saturation flux density ϕ_{sat} (the flux density that saturates the satellite amplifier) is specified by the manufacturer but to reduce intermodulation noise the amplifier may be operated with a lower density ϕ where

$$(\phi)_{dBW/m^2} = (\phi_{sat})_{dBW/m^2} + IBO_{dB} \tag{10.16}$$

where IBO stands for input backoff and is negative as ϕ is less than ϕ_{sat}. If the input signal is reduced below the saturation level, the output signal is also reduced. That is, the output signal is also backed off, but the amount of output backoff is not necessarily the same as the amount of input backoff. The difference between the output backoff OBO and in the input backoff IBO equals a "gain" G_a. Thus

$$(OBO)_{dB} - (IBO)_{dB} = (G_a)_{dB} \tag{10.17}$$

An expression for S/N in an uplink channel, in terms of ϕ and considering only thermal noise, is

$$(S/N)_{dB} = \phi_{dBW/m^2} - 10 \log n + 10 \log (\lambda^2/4\pi) + (G_s/T_{sys})_{dB} - 10 \log b - 10 \log k \qquad (10.18)$$

The expression is similar to that of Eq. (1.8), but here for an audio channel we use S/N rather than C/X. Also the factor of d squared and one factor of 4π of

$$(L_{FS})_{dB} = 10 \log (4\pi d/\lambda)^2$$

have been included in ϕ, leaving a factor of $10 \log (\lambda^2/4\pi)$ in the equation. For B_{dB} of Eq. (1.8) there is $10 \log b$ where b is the bandwidth of an audio channel, commonly 3000 Hz. Also a $10 \log n$ term, where n is the number of channels, is included to take account of the fact that the total power included in ϕ is distributed over n channels. The quantity G_s is the gain of the receiving antenna on the satellite. If ϕ of Eq. (10.18) is recognized as being equal to $\phi_{sat} + I_{BO}$, the equation has the form of

$$(S/N)_{dB} = (\phi_{sat})_{dBW/m^2} + (I_{BO})_{dB} - \log n + 10 \log(\lambda^2/4\pi) + (G/T_{sys})_{dB} - 10 \log b - 10 \log k \qquad (10.19)$$

Equation (10.19) is given by Jonnalagadda (1982) for the uplink from a ground station to a satellite. He then proceeds to consider intermodulation noise and external interference, including that from adjacent transponders of the same satellite that are designed to be cross polarized but become depolarized to a degree because of Faraday rotation or propagation though precipitation. External interference from adjacent satellites is aggravated by the fact that satellites may be spaced only 2 deg apart in the geostationary orbit. To keep such adjacent-satellite interference within bounds, earth-station uplink antenna gains must be no greater than $32 - 25 \log\theta$ with θ the angle from the center of the main beam in deg, for $\theta \geq 1$ deg. For the downlink the corresponding relation is $29 - 25 \log\theta$.

A similar analysis for a downlink results in

$$(S/N)_{dB} = (EIRP)_{dBW} + (OBO)_{dB} - 10 \log n - (L_{FS})_{dB} + (G_e/T_{sys})_{dB} - 10 \log b - 10 \log k \quad (10.20)$$

Effort has been devoted to accommodating as many as 6000 audio channels in a 36 MHz transponder by use of SSB, and a paper used in preparation of this section by Jonnalagadda (1982) was devoted to this topic. This type of application has apparently not met with success because of power limitations in 6/4 GHz service, interference considerations, etc., and this approach is understood to have been dropped. A number of the 12 companies that have applied for licenses to provide satellite land-mobile service, however, have planned to use SSB in their first-generation systems. This application appears to be practical and is a major reason for treating SSB here. A change may be made in later-generation systems, however, to digital transmission.

10.7 APPLICATIONS OF SPREAD-SPRECTRUM SYSTEMS

Some basic concepts of spread-spectrum systems were introduced in Sec. 6.3.5, and attention is given now to possible applications of such systems. Spread-spectrum systems provide a degree of immunity from interference and jamming and their low power densities in W/m^2 contribute to a low probability of intercept. For these reasons as well as relative freedom from multipath effects, spread-spectrum systems have been employed quite extensively in military applications. Considerable interest is now being shown in applications for nonmilitary purposes as well (Utlaut, 1978; CCIR, 1986b; Cooper and Nettleton, 1983; IEEE, 1983). Docket 81-413 of the Federal Communications Commission called for comments on proposed authorization for spread-spectrum systems and an IEEE Communications Society panel prepared a statement about spread-spectrum systems and some of the responses that had already been received to the docket (IEEE, 1983). The statement of the Communications Society does not promote or condemn any particular application and is a careful analysis of possible applications.

The subject of the relative spectral efficiences of spread-spectrum and other systems is complex. Cooper and Nettleton (1978) asserted that, for cellular mobile systems employing small cells for which frequency-division multiple access (FDMA) systems and spread-spectrum systems are interference limited, spread-spectrum systems employing differential phase shift keying (DPSK) can achieve greater user densities by a considerable factor than FDMA systems. Developments regarding the relative spectral efficiencies of the various systems have reviewed by Yue (1983), using efficiency as defined by

$$\eta_m = U\ (30\ \text{kHz})/W \qquad (10.21)$$

witn η_m the efficiency of an m cell system, U the average number of users per cell, and W the bandwidth for one-way tranmission. If only a single cell is considered, the efficiency of an FM system with channel spacing of 30 kHz is unity (100 percent) when defined in this way. In a multicell system, however, this efficiency must be reduced by the reuse factor (which takes into account that adjacent cells can not use the same frequency because of mutual interference considerations). Taking the reuse factor as 12, η_m for FDMA is reduced to 8.3 percent. An analysis by Yue (1982) showed a spectral efficiency of 8.4 percent for the DPSK technique of Cooper and Nettleton. Goodman et al. (1980) reported that an efficiency of 35.7 percent should be possible by use of multiple level frequency shift keying (MFSK), and Viterbi (1978) reported the possibility of efficiencies up to 37.5 percent by use of a processing transponder on a satellite. Use of on-board processing, although introducing some complication into a satellite, has important advantages (Pelton, 1984) and satellites of the future are expected to make considerable use of it (Evans, 1986). Signals may be reduced to baseband on a processing satellite. Yue (1983) concluded that it had not been demonstrated that FH/CDMA was more spectrally efficient than FDMA. The reverse would also seem to be true. Yue indicated that other practical considerations concerning spread-spectrum, including cost, needed to be resolved before a commercial system could be implemented.

An interesting point about the comparison between broad and narrow band channels has been made by Costas (1959) and considered further by Utlaut (1978). Costas showed that the relative communication capacities of broadband channels, C_B, and narrowband channels, C_N, are given by

$$C_B/C_N = 1/[\alpha\,(S/N)_{min}] \qquad (10.22)$$

where α is the fraction of time each station is transmitting and $(S/N)_{min}$ is the minimum signal-to-noise ratio that can be tolerated. The comparison applies to the case for which the broadband users occupy an entire bandwidth whereas for narrowband operation the same bandwidth is broken into a number of narrowband channels. When α is small, C_B tends to be significantly larger than C_N. Utlaut (1978) used as an example the case for which a 3 MHz bandwidth is separated into 1000 channels of 3 kHz for narrowband operation. He considered two grades of service, one percent and seven percent, meaning that one in a hundred or one in fourteen attempts at establishing communication fail on the first attempt because all channels are occupied. The results are summarized in Table 10.5. For C_B, each user occupies the entire bandwidth.

Table 10.5 Capacities of Broad and Narrow Band Systems (C_B, C_N)

C_B or C_N	Grade of Service	Capacity (Erlangs)
C_N	1/100	10
C_B	1/100	84.1
C_N	1/14	80
C_B	1/14	98.99

This interesting example shows a clear advantage for the broadband system, but caution must be exercised in drawing broad conclusions. It does seem reasonable to conclude that the most favorable cases for employing spread-spectrum systems will be those for which α of Eq. (10.22) is small. In other words, lightly used systems appear to offer the best prospects. Applications which the IEEE panel (IEEE, 1983) looked on most favorably included low-power-density applications and multiple access systems with many low-duty-cycle users.

The Global Positioning System (GPS) uses spread spectrum for positioning (Sec. 6.7), and spread spectrum has also been used for satellite communications. Prominent in this respect is the TDRSS (Tracking and Data Relay Satellite System) which provides for transmitting commands to and receiving data from low-orbiting satellites by means of the TDRS satellites (Holmes, 1978; Goddard, 1980). The configuration for using a TDRS satellite is shown in Fig. 10.8. Forward and return links from the ground terminal through the TDRS satellite to the user spacecraft at S band and Ku band use the direct-sequence pseudonoise spread-spectrum technique. The multiple access return link can accommodate 20 users at data rates up to 50 kbps. Return single access service at S band can provide data rates to 12 Mbps, and single access return service at Ku band can provide data rates to 300 Mbps but in this case spread spectrum is not used. An important factor in deciding to use spread spectrum was the need to keep power density levels low at the Earth's surface.

The Equatorial Communications Company (Parker, 1984) uses a combination of VSAT (Very-Small-Aperture-Terminal) and spread-spectrum technologies. Data transmission is carried out in the 6 and 4 GHz bands by using antennas 1.2 or 0.6 m in diameter. The broad beamwidth of such small receiving antennas allows them to receive interfering signals from satellites close to the satellite that it is intended to be operating with. Signals from five satellites spaced two deg apart, for example, could be received by a 0.6 m antenna having a beamwidth of nine deg. The use of spread spectrum employing code division multiple access, however, allows successfull operation under such conditions. One hundred parties can use the same channel at the same time and, if a duty cycle of 0.01 is assumed for the users, 10,000 assignments can be made to one channel though 1,000 to 5,000 is more typical (Parker, 1986).

Other satellite applications of spread spectrum that are reported include SAMSARS (Satellite Aided Maritime Search and Rescue System) and TATS (Tactical Tranmissions System), described by Proakis (1983, pp. 594, 595). SAMSARS was described in the 1982 version of CCIR Report 761. The same report for 1986 (CCIR, 1986) has much interesting material on other systems for facilitating maritime rescue. A domestic Japanese mobile satellite system that is under development is reported to be using FH spread spectrum.

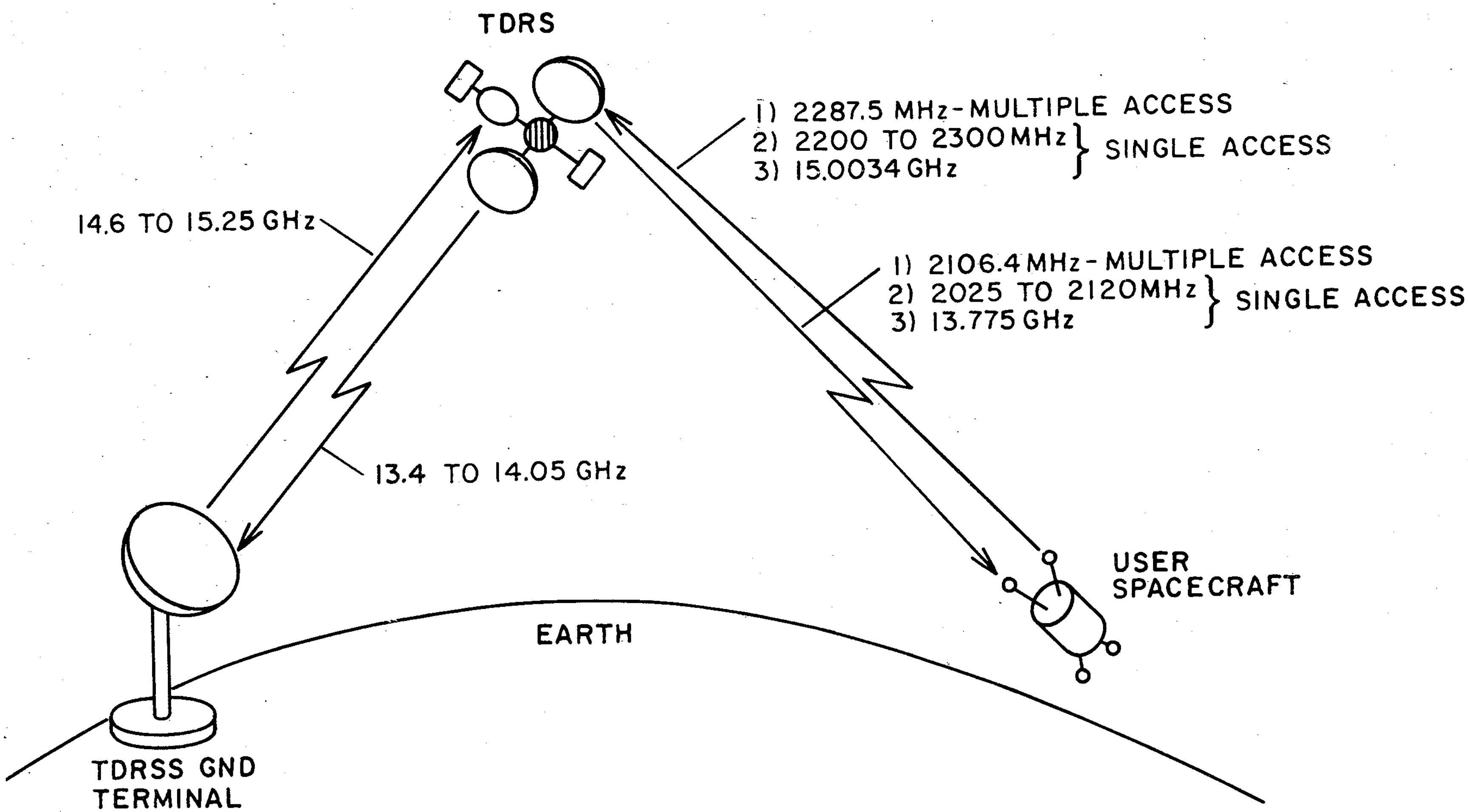

Figure 10.8. Telecommunication links of Tracking and Data Relay Satellite System (TDRSS).

10.6 CONCLUSION

The emphasis of this handbook is on propagation effects, but the intent has been to relate propagation to the closely related subject of earth-space link design rather than to treat propagation as an isolated, academic topic of its own. Some remarks on trends and potential developments in satellite communications follow. Increasing attention is likely to be given to effects at higher frequencies, up to perhaps 94 GHz, but we concentrate on the 100 MHz to 10 GHz range of this handbook. In this frequency range, the propagation effects of interest in the future may not be much different than those of today, but the associated satellite link parameters are likely to show a trend that takes account of the increasing importance of small earth stations.

During the first two decades of satellite operations, satellites had a near monoply of new long-distance telecommunication service, but fiber optics has made major advances in recent years. The view is taken here that satellite and fiber optic systems are largely complementary, but they will probably be in competition on some high-capacity point-to-point links such as those across the Atlantic. Trends in future satellite systems, taking account of the role of fiber optics, have been discussed by Evans (1986). The INTELSAT system, presently involving about 110 countries, originally acheived interconnectivity by employing broad satellite antenna beams which provided coverage over wide areas. The earth stations required for this mode of operation, however, use very large, expensive antennas. The trend in the future is expected to be to use multiple spot beams, on-board switching, and higher transmitter powers on satellites for interconnectivity. The earth stations that will used for such systems can in many cases be small and low in cost. The term VSAT, standing for Very Small Aperture Terminal, is now applied to such earth stations. Antenna diameters may be very small, like 1.2 or 0.6 m for 6/4 GHz systems. The corresponding beamwidths will be large, and the earth stations will tend to be subject to interference from, or cause interference to, satellites spaced as little as two deg from the satellite the system is designed to operate with. It was mentioned in Sec. 6.7 that the use of spread spectrum is one means to alleviate this problem.

Numbers of active satellite transponders used for various traffic types, as measured by the FCC in March 1986, summarized in Satellite Week, and repeated by Inglis (1986) are shown in Table 10.6. It appears unlikely that many of the transponder usages listed, other than for heavy-route voice service, will be affected very greatly by optical fibers.

Table 10.6 Estimated Usage of Active Transponders by Traffic Type

Traffic Type	C-Band	K-Band	Total
Television			
Cable TV	68	1	69
Broadcast	43	17	60
Closed Circuit	9	3	12
Radio	5	0	5
Voice			
Heavy Route	7	0	7
Light Route	37	0	37
Private Networks	39	1	40
Data (Private Networks)	72	29	101

The 1 GHz to 10 GHz range that is included in the coverage of this handbook is an ideal frequency range from the propagation and noise viewpoints, but propagation effects still need to be taken into account and may possibly be severe in some cases. Ionospheric scintillation may be serious, especially at frequencies of about 1.5 GHz and lower, within about 20 deg of the equator. Excess range delay due to the ionosphere and troposphere are important to range measurements, and increasing accuracy is demanded for geodetic applications and programs like TOPEX (Ocean Topography Experiment, Sec. 6.7). The ionospheric delay can be determined by using two transmitted frequencies (Sec. 2.3.1) or eliminated by going to a sufficiently high frequency, but tropospheric effects tend to be more serious at high frequencies. The use of water vapor radiometers is needed to obtain the highest accuracy for the excess range delay due to the troposphere (Sec. 3.7).

Effects of rain are most intense at frequencies above 10 GHz, but attenuation, depolarization, thermal noise, and scatter as a source of interference are all significant below 10 GHz. Specular reflection and diffuse scatter may be problems for land and maritime satellite mobile systems, but shadowing by trees has become prominent as the major problem for land-mobile systems (Sec. 6.4).

It is desirable to treat the propagation impairments satistically. This type of approach has been quite well developed for attenuation due to rain but is less well developed for other impairments. In the latter cases, it may be necessary to rely to a considerable extent on operational experience and representative values that have been reported. Some more nearly complete analyses, however, have been made. Bantin and Lyons (1978) in their statistical analysis of propagation effects in northern and southern Canada included rain attenuation, ionospheric scintillation, tropospheric scintillation (including multipath fading), gaseous attenuation, and pointing error due to wind.

REFERENCES

Bantin, C.C. and R.G. Lyons, "The evaluation of satellite link availability," IEEE Trans. Commun., vol. COM-26, pp. 847-853, June 1978.

Bell Telephone Laboratories, Transmission Systems for Communications, 4th Ed. Holmdel, NJ: Bell Labs., 1971.

Calo, S.B., L. Schiff, and H. Staras, "Effects of rain on multiple access transmission of data via satellite," Record, IEEE 1978 Int. Communications Conf., Toronto, pp. 30.1.1-6.

Calvit, T.O. and L.B. Heitman, "High-speed satellite data transmission of maritime seismic data," Tech. Papers, Communication Satellite Systems Conf., 8th, Orlando, FL, April 20-24, 1980, pp. 714-722. New York: AIAA, 1980.

CCIR, "Allowable noise power in the hypothetical reference circuit for frequency-division mulitplex telephony in the fixed satellite service," Recommendation 353-5, Vol. IV, Fixed Service Using Communication Satellites, Recommendations and Reports of the CCIR, 1986. Geneva: Int. Telecomm. Union, 1986a.

CCIR, "Spread spectrum techniques," Report 651-2 in Vol. I, Spectrum Utilization and Monitoring, Recommendations and Reports of the CCIR, 1986. Geneva: Int. Telecomm. Union, 1986b.

CCIR, "Technical and operating characteristics of distress systems in the maritime mobile-satellite service," Report 761-2 in Vol. VIII, Mobile Services, Recommendations and Reports of the CCIR, 1986. Geneva: Int. Telecomm. Union, 1986c.

Cooper, G.R. and R.W. Nettleton, "A spread-spectrum technique for high-capacity mobile communication," IEEE Trans. Veh. Technol., vol. VT-27, pp. 264-275, Nov. 1978.

Cooper, G.R. and R.W. Nettleton, "Cellular mobile technology: the great multiplier," IEEE Spectrum, vol. 20, pp. 30-37, June 1983.

Costas, J.P., "Poisson, Shannon, and the radio amateur," Proc. IRE, vol. 47, pp. 2058-2068, Dec. 1959.

Evans, J.V., "Twenty years of international satellite communication," Radio Sci., vol. 21, pp. 647-664, July-Aug. 1986.

Feher, K., Digital Communications, Satellite/Earth Station Engineering. Englewood Cliffs, NJ: Prentice-Hall, 1983.

Freeman, R.L., Telecommunication Transmission Handbook, 2nd Ed. New York: Wiley, 1981.

Goddard Space Flight Center, Tracking and Data Relay Satellite System (TDRSS) User's Guide, Revision 4, Goddard Space Flight Center, Greenbelt, MD, Jan. 1980.

Goodman, D.J., P.S. Henry, and V.K. Prabhu, "Frequency-hopped multilevel FSK for mobile radio," Bell Syst. Tech. J., vol. 59, pp. 1257-1275, Sept. 1980.

GTE Lenkurt, Engineering Considerations for Microwave Communication Systems. San Carlos, CA: GTE Lenkurt, Inc., 1972.

Heller, J.A. and I.W. Jacobs, "Viterbi decoding for satellite and space communications," IEEE Trans. Commun. Technol., vol. COM-19, pp. 835-848, Oct. 1971. Also in Van Trees (1979).

Holmes, W.M., "NASA's tracking and data relay satellite system," IEEE Commun. Mag., Sept. 1978.

IEEE (Communication Society), "Before the Federal Communications Commission, Washington, DC 20554, General Docket No. 81-413," IEEE Comm. Mag., vol. 21, pp. 59-63, March 1983.

Inglis, A.F., "The United States satellite industry - an overview," Proceedings FIBRESAT 86, pp. 73-81, Vancouver, BC, Sept. 9-12, 1986.

Ippolito, L.J., R.D. Kaul, and R.G. Wallace, Propagation Effects Handbook for Satelllte Systems Design, A Summary of Propagation Impairments on 10 to 100 GHz Satellite Links with Techniques for System Design, NASA Reference Pub. 1082(03). Washington, DC: NASA Headquarters, 1983.

Ippolito, L.J., Radiowave Propagation in Satellite Communications. New York: Van Nostrand Reinhold, 1986.

ITT, Reference Data for Radio Engineers, 5th Ed. Indianapolis: Howard W. Sams & Co., 1968.

Jonnalagadda, K., "Single sideband, amplitude modulated, satellite voice communication system having 6000 channels per transponder," RCA Rev., vol. 43, pp. 464-488, Sept. 1982.

Jonnalagadda, K. and L. Schiff, "Improvements in capacity of analog voice multiplex systems carried by satellite," Proc. IEEE, vol. 72, pp. 1537-1547, Nov. 1984.

Mimis, V. and A. Smalley, "Low elevation angle site diversity satellite communications for the Canadian arctic," Record, IEEE 1982 Int. Commun. Conf., Philadelphia, PA, June 13-17, 1982, pp. 4A.4.1-5.

Minakoshi, H. et al., "Severe ionospheric scintillation associated with magnetic storm on March 22, 1979," J. Radio Res. Labs. (Japan), vol. 28, pp. 1-9, March/July 1981.

Miya, K., Satellite Communications Technology. KDD Bldg. 3-2, Nishi-Shinjuku 2-chome, Shinjuku, Tokyo 160, Japan, 1981.

Naderi, F. (ed,), Land Mobile Satellite Service (LMSS), Part II: Tech. Report, JPL Publ. 82-19. Pasadena, CA: Jet Propulsion Lab., 1982.

Ohmori, S. and S. Miura, "A fading reduction method for maritime satellite communications," IEEE Trans. Antennas Propagat., vol. AP-31, pp. 184-187, Jan. 1983.

Parker, E.B., "Micro earth stations as personal computer accessories," Proc. IEEE, vol. 72, pp. 1526-1531, Nov. 1984.

Parker, E.B., "Micro earth station satellite networks and economic development," Proceedings FIBRESAT 86, pp. 122-125, Vancouver, BC, Sept. 9-12, 1986.

Pelton, J.N., "Satellite telenets: a techno-economic assessment of major trends for the future," Proc. IEEE, vol. 72, pp. 1445-1456, Nov. 1984.

Piraino, S.M. and A.P. Schoen, "CITISATCOM: Citicorp's digital satellite network," 82-0513, Technical Papers, Communications Satellite Systems Conf., 9th, San Diego, CA, March 7-11. 1982, pp. 309-404. New York: AIAA, 1982.

Pratt, T. and C.W. Bostian, Satellite Communications. New York: Wiley, 1986.

Proakis, J.G., Digital Communications. New York: McGraw-Hill, 1983.

Utlaut, W.F., "Spread-spectrum principles and possible application to spectrum allocation," Telecomm. J., vol. 45, pp. 20-32, Jan. 1978.

Van Trees, H.L. (ed.), Satellite Communications. New York: IEEE Press, 1979.

Viterbi, A.J., "A processing satellite transponder for multiple access by low-rate users," Proc. Fourth Int. Conf. on Digital Satellite Communications, Montreal, Quebec, Oct. 1978.

Yue, O., "Maximum likelihood combining for noncoherent and differentially coherent frequency-hopping, multiple-access systems," IEEE Trans. Inform. Theory, vol. IT-28, pp. 631-639, July 1982.

Yue, O., "Spread spectrum mobile radio, 1977-1982," IEEE Trans. Veh. Technol., vol. VT-32, pp. 98-105, Feb. 1983.

NASA
National Aeronautics and Space Administration

Report Documentation Page

1. Report No.	2. Government Accession No.	3. Recipient's Catalog No.
NASA RP-1108(02)		

4. Title and Subtitle	5. Report Date
Propagation Effects on Satellite Systems at Frequencies Below 10 GHz - A Handbook for Satellite Systems Design Second Edition	December 1987
	6. Performing Organization Code

7. Author(s)	8. Performing Organization Report No.
Warren L. Flock	
	10. Work Unit No.
9. Performing Organization Name and Address	11. Contract or Grant No.
University of Colorado Department of Electrical Engineering Boulder, CO 80309	NAS7-100; 956249 (JPL)
12. Sponsoring Agency Name and Address	13. Type of Report and Period Covered
National Aeronautics and Space Administration Washington, DC 20546	Reference Publication (Second Edition)
	14. Sponsoring Agency Code

15. Supplementary Notes

16. Abstract

Frequencies below 10 GHz continue to be used for a large fraction of satellite service, and new applications, including mobile satellite service and the global positioning system, use frequencies below 10 GHz. As frequency decreases below 10 GHz, attenuation due to precipitation and gases decreases and ionospheric efforts increase. Thus the ionosphere, which can be largely neglected above 10 GHz, receives major attention in this handbook. Although attenuation and depolarization due to rain are less severe below 10 GHz than above, they are nevertheless still important and constitute another major topic. The handbook emphasizes the propagation effects on satellite communications but material that is pertinent to radio navigation and positioning systems and deep-space telecommunications is included as well. Chapter 1 through 7 describe the various propagation impairments, and Chapter 9 is devoted to the estimation or calculation of the magnitudes of these effects for use in system design. Chapter 10 covers link power budget equations and the role of propagation effects in these equations. Chapter 8 deals with the complex subject of interference between space and terrestrial systems. The second edition of this handbook supersedes the first.

17. Key Words (Suggested by Author(s))	18. Distribution Statement
Microwave Propagation, Slant path satellite communications systems ionosphere propagation effects, troposphere propagation effects, VHF, UHF, SHF propagation, radio noise	Unclassified - Unlimited Subject Category 32

19. Security Classif. (of this report)	20. Security Classif. (of this page)	21. No. of pages	22. Price
Unclassified	Unclassified	506	A22

NASA FORM 1626 OCT 86

☆ U.S. GOVERNMENT PRINTING OFFICE: 1988—526-064/61809

National Aeronautics and
Space Administration
Code NTT-4

Washington, D.C.
20546-0001

Official Business
Penalty for Private Use, $300

NASA

National Aeronautics and
Space Administration

Washington, D.C.
20546

SPECIAL FOURTH CLASS MAIL
BOOK

Postage and Fees Paid
National Aeronautics and
Space Administration
NASA-451

Official Business
Penalty for Private Use $300

U.S. MAIL

L2 001 RP-1108-2 871214S090569A
NASA
SCIEN & TECH INFO FACILITY
ACCESSIONING DEPT
P O BOX 8757 BWI ARPRT
BALTIMORE MD 21240

NASA

POSTMASTER: If Undeliverable (Section 158
Postal Manual) Do Not Return